Eur Radiol (2009) 19 (Suppl 4): S765–S974
DOI 10.1007/s00330-009-1569-1

Fifth International Congress on MR-Mammography 24–26 September 2009, Jena, Germany

Organization: Prof. Dr. med. Dipl.-Chem. Werner A. Kaiser
Institute of Diagnostic and Interventional Radiology
Friedrich-Schiller University, Jena, Germany

INVITED PAPERS

Diffusion Weighted Imaging—Useful in all kinds of lesions? A systematic review

Pascal A.T. Baltzer[1], Matthias Dietzel[1], Tibor Vag[1], Mieczyslaw Gajda[2], Oumar Camara[3] and Werner A. Kaiser[1]
[1]AG MR-Mammographie, Institute of Diagnostic and Interventional Radiology; [2]Institute of Pathology; [3]Clinic of Gynecology, University Hospital of the Friedrich Schiller University Jena

Introduction

Diffusion weighted imaging (DWI) is increasingly recognized as a promising and—with limitations—quantitative method for differential diagnosis of enhancing lesions in MR-mammography, also referred to as breast MRI. The basic concept is to assess the random motion of water molecules in vivo, referred to as diffusion. This is achieved by inserting opposite directed motion probing gradients into a pulse sequence compensating for each other. Diffusion processes between these gradients lead to incomplete rephasing of moving spins. The consequence is a diffusion dependent signal decrease. By acquisition of at least two diffusion weightings, mean quantitative diffusivity, referred to as apparent diffusion coefficient (ADC), can be calculated. The diffusion weighting described by the *b*-value depends on timing and amplitude of the diffusion gradients and is expressed by s/mm^2. In general, DWI techniques are faster than dynamic contrast enhanced MRI. Consequently, they can be easily added to a standard breast MR imaging protocol. Reports so far showed high diagnostic accuracy of quantitative mean diffusivity or apparent diffusion coefficient (ADC) values [1–11]. As DWI does not require any contrast agent to be injected, it possibly could be of value as a standalone technique in severely ill patients, not being able to tolerate a long examination. Furthermore, in patients with impaired renal function, the risk of nephrogenic systemic fibrosis (NSF) would be avoided [12]. However, before such an approach could be introduced into clinical routine, a possible incremental value of contrast free breast MRI over conventional methods has to be validated. Alternatively, a comparable intra-individual accuracy between contrast free breast MRI and contrast enhanced MRI has to be proven.

This systematic review was performed in order to evaluate lesion visibility and reported values of diffusion weighted imaging for differential diagnosis and, furthermore, to compare reported ADC values for benign and malignant tissues. Limitations, technical aspects as well as biological influences on DWI are discussed.

Methods of Literature Review and Analysis

The articles eligible for this systematic review were retrieved searching Pubmed and Medline databases from 2002 until 2009 by means of following keywords: breast, MRI, DCE–MRI, MR-mammography, DWI, ADC, diffusion, sensitivity and specificity. Studies on monitoring of primary systemic therapy were omitted as this review focused on differential diagnosis between benign and malignant breast lesions. Thus 18 investigations were identified [1–11, 13–19]. Eligible for further analysis were all breast MRI investigations focusing on diffusion weighted Echo Planar Imaging (EPI) techniques using high *b*-values> 500 s/mm^2. The articles were searched for reported mean ADC values in benign and malignant subgroups as well as information about lesion visibility on DWI images as well as sensitivity and specificity of ADC measurements. Papers without precise methodological information on lesion number and subgroups were omitted. Data from different studies was compared using chi-square and t-Test as well as standardized mean difference (SMD) statistics for continuous measures including 95% confidence intervals (CI). Statistical analysis was performed using Excel 2007 and MedCalc 9.4.2.0.<

Results

Lesion visibility

Investigations concentrating on lesion visibility in DWI compared to contrast enhanced breast MRI detected 89–100% of all lesions [1, 2, 16, 18], a good lesion visibility was given in 89%–95.3% [1, 18]. Less visible lesions were reported being either small or benign without further details given.

Sensitivity and Specificity of ADC measurements

Following the selection criteria above, sensitivity and specificity were reported in ten studies. Two investigations by Woodhams et al. were omitted [9, 19] as an overlap of investigated lesions with [7] could not be excluded from the materials and methods sections of the cited papers. The latter publication was included as it was the report with the highest number of included lesions. Except the investigation by Woodhams et al., Receiver Operating Characteristics (ROC) analysis, plotting sensitivity against 1-specificity values for successive thresholds of the measured ADC values was reported in all studies in order to identify optimal cutoff values. Cutoff values ranged between 1.1–1.6 mm^2/s with most investigators choosing values between 1.1–1.3 mm^2/s [1, 2, 6, 10, 17]. Reported sensitivity values ranged from 80.9%–93% (figure 1) and specificity values from 39.2%–88% (figure 2). *T*-test revealed significant (P<0.05) differences between the study of Woodhams et al. compared to some investigations regarding sensitivity [3, 6, 10] and to

all investigations regarding specificity. Results of the other investigations did not differ significantly ($P>0.05$). Analogous to Receiver Operating Characteristics (ROC) reported Sensitivity values of the analyzed investigations are plotted against reported 1-specificity values in figure 3. The work by Woodhams et al. [7], applying a different threshold is clearly located on the same ROC curve as the diagnostic parameters of the other evaluated investigations.

Reported ADC values in benign and malignant lesions

Mean diffusivity for malignant lesions has been reported between 0.89–1.22 mm^2/s with a total mean (897 lesions) of 1.05±0.26 (SD) mm^2/s [2, 6–9, 16–19]. Higher diffusivity levels have been found in mucinous carcinoma. In this subgroup, Hatakenaka et al. [3] showed ADC values of 2.11±0.18 mm^2/s (four cases) while Woodhams et al. [8] reported ADC values of 1.8±0.4 mm^2/s (15 cases). Ductal carcinoma in situ (DCIS) show somewhat higher diffusivity compared to mean invasive carcinomata with ADC values between 1.0–1.6 mm^2/s, total mean (79 lesions) 1.22±0.20 (SD) mm^2/s [1, 5, 6, 8, 9, 16, 17]. According to SMD statistics, all cited investigations found significant differences between DCIS and invasive cancer (figure 4). On the other hand, mean diffusivity of benign lesions has been reported between 1.3–1.6 mm^2/s with a total mean (257 lesions) of 1.52±0.36 (SD) mm^2/s. Reported subgroups showing lower ADC values were fibrocystic disease (1.2–1.6 mm^2/s [7, 8]), fibrosis and scars (1.13±0.23 mm^2/s [7]) and papilloma (1.1–1.3 mm^2/s [7, 8]). According to SMD statistics, major differences between benign and malignant lesions were found in all studies. Furthermore, the majority of all studies reported medium to large differences between benign lesions and DCIS (figure 5 and figure 6).

Discussion

Investigations on DWI of the breast so far mainly focused on ADC measurements in order to differentiate between benign and malignant lesions. SMD analysis of reported mean ADC values indicates major diffusivity differences between benign and malignant lesions. This fact is reflected in the reported high sensitivity and specificity values. Following the investigation of Yabuuchi et al. [10], low ADC values are an independent and important predictor for differential diagnosis of enhancing mass lesions in the breast. Except for the cited study, knowledge on the diagnostic value of ADC values in comparison with standard morphologic and dynamic descriptors is limited. In a recent investigation carried out in our institution, quantitative diffusivity measurements showed high but nonetheless clearly inferior diagnostic parameters compared with routine MR-mammography rated by the radiologist [1]. Clearly, further study is needed to verify, if there is indeed an incremental value of DWI measurements in the breast compared to dynamic contrast enhanced MRI. Following the principle of DWI, that is visualization and quantification of the random motion of molecules, this technique is able to analyze tissue microstructure in vivo. Compared to contrast enhanced techniques, showing the vasculature and perfusion, this new approach on tissue characteristics may well add diagnostic information exceeding simple means of differential diagnosis. Several authors have described an inverse correlation between tumor cellularity and ADC values [2, 3, 8]. Further associations with proliferation rate and tumor aggressiveness may be assumed. Analogous to brain imaging, abscess forming inflammations can be easily differentiated from tumor necrosis according to our experience. ADC values of noninvasive malignant lesions (DCIS) were found significant higher compared to invasive cancers but lower compared to benign lesions, underlining their biological less aggressive but malignant nature. However, several benign lesion subgroups show a remarkable overlap with malignant lesions and vice versa. Mucinous carcinoma, being characterized by extracellular mucus without a higher degree of cellularity has been reported to show high ADC values [3, 8]. Further information like irregular margins is needed for reliable diagnosis. Fibrocystic disease, characterized by varying degrees of fibrosis and proliferation can show ADC values in the range of malignant lesions [3, 8]. According to Woodhams et al. and own unpublished data, papilloma may show relatively low ADC values [7, 8].

In order to use DWI as a standalone technique, further, e.g. morphologic lesion descriptors should be considered in order to achieve reliable diagnoses. An initial investigation on exclusively malignant lesions showed a high sensitivity for a contrast free diagnostic approach combining DWI and STIR imaging [14]. Breast lesions have to be detected before they can be evaluated for differential diagnosis. Studies so far reported lower to equal lesion detection rates using DWI compared to dynamic contrast enhanced MRI [1, 2, 16, 18]. Regarding the technique utilized, the Half Fourier Acquired Turbo Spin Echo (HASTE) sequence provides lower susceptibility artifacts but also a lower lesion visibility [1, 4]. Because of its sensitivity to chemical shift artifacts, the mostly used Echo Planar Imaging (EPI) sequence has to be combined with a fat saturation technique. Basically, fat saturation can be achieved by chemical shift selective (CHESS) pulses, short tau inversion recovery (STIR) and water excitation techniques. Spectral fat saturation requires a homogenous magnetic field distribution in order to obtain diagnostic useful images. According to our experience, automated frequency adjustments can mistake methylene and water peak in patients with fatty breasts (ACR I and II). This failure leads to diagnostic useless images but may be avoided by manual frequency adjustments. Kazama et al. reported its occurrence in 44%, 14 out of 32 cases [13]. Signal to Noise Ratio (SNR) in STIR-DWI images is lower compared to CHESS-DWI images. Consequently, a lower lesion visibility was found in a direct comparison [18]. Homogeneous fat saturation with a high SNR can be achieved by the water excitation technique (personal communication with Rolf Janka, Radiologisches Institut, University hospital Erlangen, Germany and Christian Geppert, Siemens Health Care, Erlangen, Germany). A further limitation which has to be discussed is the rather low spatial resolution of DWI due to SNR limitations. More than 90% of all lesions analyzed in the cited investigations exceeded 1 cm, mean lesion sizes ranged between 1.7 and 3.6 cm [1–3, 5, 6, 9, 16–18]. In an initial intra-individual comparison of DWI on 1.5T vs. 3T, Matsuoka et al. found an improved visualization of lesions below 10 mm at 3T, enabling a higher spatial resolution [15]. According to the ACR BIRADS lexicon, pathological growth conditions in the breast can be described as solid mass or non solid non-mass [20]. As non-mass lesions can form large but non compact lesions, these are more likely to lead to a lesser restriction of diffusion processes compared to solid tumors. In an own investigation, we found a limited ability of ADC measurements to differentiate between benign and malignant non-mass lesions. ADC values of the malignant lesions (DCIS exclusively) were in the range of benign lesions. Our findings somewhat differ from the reported ADC values for DCIS lesions. As other reports did not differentiate between mass and non-mass growth patterns, at least a part of these lesions may have been solid tumors. Further investigation is needed to estimate the diagnostic potential in non-mass lesions.

Conclusion

The literature on DWI of the breast agrees on the capability of DWI to visualize and differentiate breast lesions. However, uncertainty remains on the capability of DWI to assess lesions below 10 mm in

diameter. Furthermore, the value of DWI in non-mass lesions remains elusive. One initial report suggests a diagnostic value of ADC measurements in comparison with other lesion descriptors. Yet, an incremental value of DWI compared with routine dynamic contrast enhanced MR-mammography has not been proven. As to the possibility to use DWI as a standalone technique for breast imaging, no valid investigations including benign and malignant lesions and having a representative standard of reference have been published. Although an inverse correlation between tumor cellularity and ADC values was found, no correlations with pathologic prognostic factors are available so far.

Acknowledgement
The authors would like to thank the following persons for their technical and scientific support as well as personal advice (alphabetical order): Dr. Beatrix Fey, Ines Krumbein, Dr. Juliane Schelhorn

References

1. Baltzer PAT, Renz DM, Herrmann KH, et al. (2009) Diffusion Weighted Imaging (DWI) in MR-Mammography (MRM). A Clinical Comparison of Echo Planar Imaging (EPI) and Half-Fourier Single-Shot Turbo Spin Echo (HASTE) diffusion techniques. Eur Radiol 19:1612–1620.
2. Guo Y, Cai YQ, Cai ZL, et al. (2002) Differentiation of clinically benign and malignant breast lesions using diffusion-weighted imaging. J Magn Reson Imaging 16:172–178.
3. Hatakenaka M, Soeda H, Yabuuchi H, et al. (2008) Apparent diffusion coefficients of breast tumors: clinical application. Magn Reson Med Sci 7:23–29.
4. Kinoshita T, Yashiro N, Ihara N, et al. (2002) Diffusion-weighted half-Fourier single-shot turbo spin echo imaging in breast tumors: differentiation of invasive ductal carcinoma from fibroadenoma. Journal of Computer Assisted Tomography 26:1042–1046.
5. Kuroki Y, Nasu K, Kuroki S, et al. (2004) Diffusion-weighted imaging of breast cancer with the sensitivity encoding technique: analysis of the apparent diffusion coefficient value. Magn Reson Med Sci 3:79–85.
6. Marini C, Iacconi C, Giannelli M, et al. (2007) Quantitative diffusion-weighted MR imaging in the differential diagnosis of breast lesion. Eur Radiol 17:2646–2655.
7. Woodhams R, Hata H, Iwabuchi K, et al. (2006) Is Diffusion weighted imaging helpful for differentiating benign from malignant lesions? Eur Radiol 16:E98–99.
8. Woodhams R, Kakita S, Hata H, et al. (2009) Diffusion-weighted imaging of mucinous carcinoma of the breast: evaluation of apparent diffusion coefficient and signal intensity in correlation with histologic findings. Ajr 193:260–266.
9. Woodhams R, Matsunaga K, Iwabuchi K, et al. (2005) Diffusion-weighted imaging of malignant breast tumors: the usefulness of apparent diffusion coefficient (ADC) value and ADC map for the detection of malignant breast tumors and evaluation of cancer extension. Journal of computer assisted tomography 29:644–649.
10. Yabuuchi H, Matsuo Y, Okafuji T, et al. (2008) Enhanced mass on contrast-enhanced breast MR imaging: Lesion characterization using combination of dynamic contrast-enhanced and diffusion-weighted MR images. J Magn Reson Imaging 28:1157–1165.
11. Luo JD, Liu YY, Zhang XL, et al. (2007) [Application of diffusion weighted magnetic resonance imaging to differential diagnosis of breast diseases]. Ai zheng = Aizheng = Chinese Journal of Cancer 26:168–171.
12. Agarwal R, Brunelli SM, Williams K, et al. (2008) Gadolinium-based contrast agents and nephrogenic systemic fibrosis: a systematic review and meta-analysis. Nephrol Dial Transplant.
13. Kazama T, Nasu K, Kuroki Y, et al. (2009) Comparison of diffusion-weighted images using short inversion time inversion recovery or chemical shift selective pulse as fat suppression in patients with breast cancer. Japanese Journal of Radiology 27:163–167.
14. Kuroki-Suzuki S, Kuroki Y, Nasu K, et al. (2007) Detecting breast cancer with non-contrast MR imaging: combining diffusion-weighted and STIR imaging. Magn Reson Med Sci 6:21–27.
15. Matsuoka A, Minato M, Harada M, et al. (2008) Comparison of 3.0-and 1.5-tesla diffusion-weighted imaging in the visibility of breast cancer. Radiation Medicine 26:15–20.
16. Park MJ, Cha ES, Kang BJ, et al. (2007) The role of diffusion-weighted imaging and the apparent diffusion coefficient (ADC) values for breast tumors. Korean J Radiol 8:390–396.
17. Rubesova E, Grell AS, De Maertelaer V, et al. (2006) Quantitative diffusion imaging in breast cancer: a clinical prospective study. J Magn Reson Imaging 24:319–324.
18. Wenkel E, Geppert C, Schulz-Wendtland R, et al. (2007) Diffusion weighted imaging in breast MRI: comparison of two different pulse sequences. Academic radiology 14:1077–1083.
19. Woodhams R, Matsunaga K, Kan S, et al. (2005) ADC mapping of benign and malignant breast tumors. Magn Reson Med Sci 4:35–42.
20. Ikeda DM, Hylton NM, Kuhl CK, et al. (2003) MRI Breast Imaging Reporting And Data System Atlas. 1 ed. Reston: American College of Radiology.

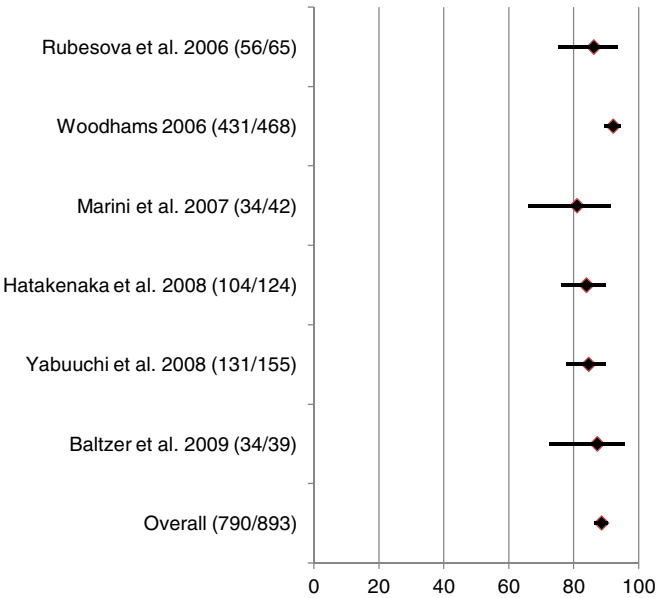

Figure 1: Sensitivity values (rectangles) and their 95% confidence intervals (lines) for the evaluated studies.

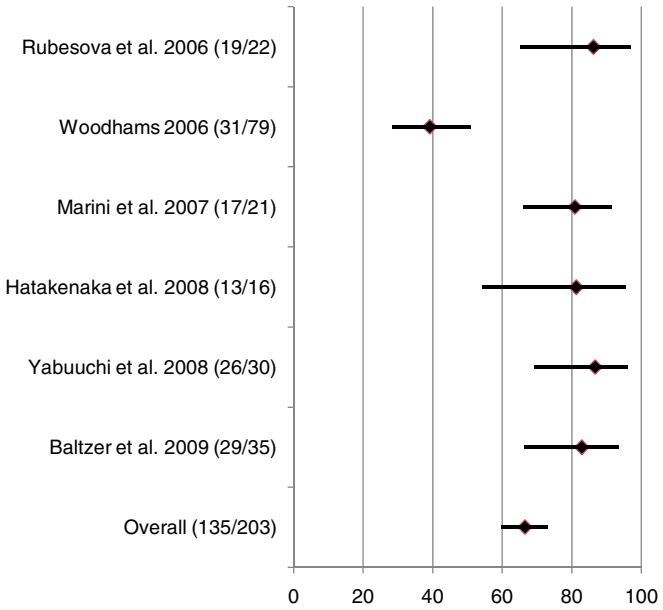

Figure 2: Specificity values (rectangles) and their 95% confidence intervals (lines) for the evaluated studies.

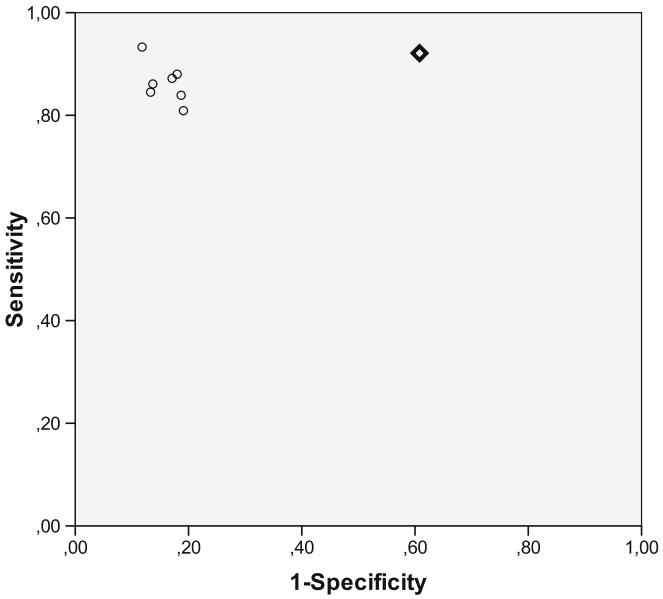

Figure 3: Sensitivity against 1-specificity plot. Note the diagnostic parameters of the majority of evaluated investigations in the upper left corner (sensitivity and specificity values >80%). The rectangle indicates the results of Woodhams et al. 2006. Higher sensitivity and lower specificity are due to a higher cutoff value for ADC measurements and fit well within a theoretical ROC curve.

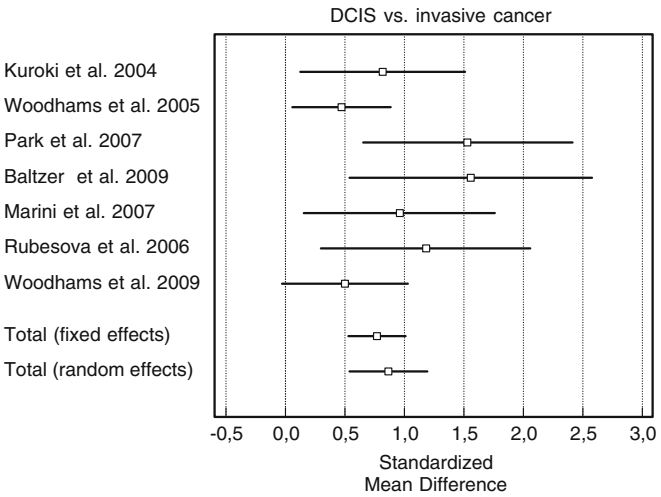

Figure 4: Forest plot of standardized mean differences for of DCIS vs. invasive cancer. Heterogeneity testing revealed $P=0.14$, therefore fixed effects model results can be considered.

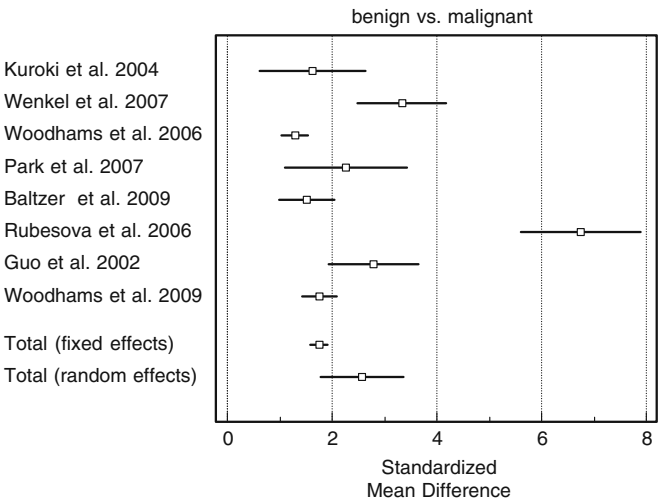

Figure 5: Forest plot of standardized mean differences for of benign vs. malignant lesions. Heterogeneity testing showed $P<0.0001$, therefore the random effects model results should be considered.

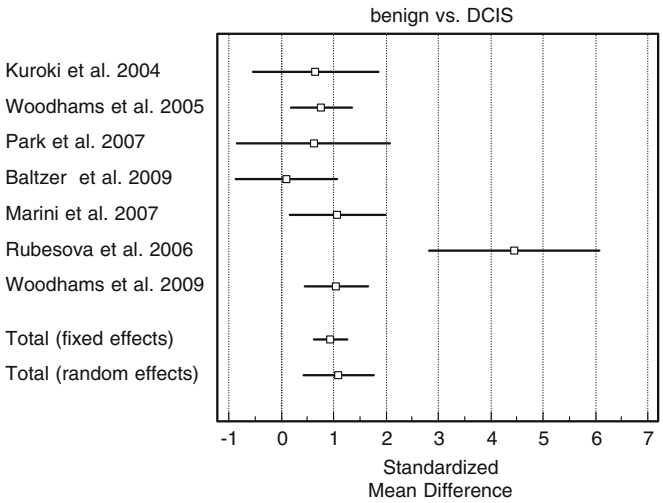

Figure 6: Forest plot of standardized mean differences for of benign vs. DCIS lesions. Heterogeneity testing showed P=0.0005, therefore the random effects model results should be considered.

Effect of different contrast agents on the results of spectroscopy—Are some agents better than others?

Pascal A.T. Baltzer[1], Alexander Gussew[2], Reinhard Rzanny[2], Matthias Dietzel[1], Tibor Vag[1], Mieczyslaw Gajda[3], Oumar Camara[4], Jürgen R. Reichenbach[2], Werner A. Kaiser[1]

[1]AG MR-Mammographie, Institute of Diagnostic and Interventional Radiology, Friedrich Schiller University Jena; [2]Medical Physics Group, Institute of Diagnostic and Interventional Radiology, Friedrich Schiller University Jena; [3]Institute of Pathology, Friedrich Schiller University Jena; [4]Clinic of Gynecology, Friedrich Schiller University Jena

Purpose

Proton MR spectroscopy (MRS) is able to noninvasively assess molecular tissue characteristics *in vivo* [1–3]. The presence of choline is attributed to an increased cellular membrane turnover in tissue and is considered to be a biomarker for malignant breast disease. Assuming that malignant tissues contain higher levels of choline compared to benign proliferative diseases, a simple differential diagnostic approach is to assess either qualitatively or quantitatively the total choline compound amplitude around 3.23 ppm [1, 2]. Recent experimental research reported a decrease in choline amplitudes following administration of ionic compared to neutral gadolinium based contrast agents [4]. Consequently, these findings may severely impact clinical MRS of the breast, insofar as a contrast agent related decrease of choline not only influences quantification but also affects the sensitivity of qualitative choline detection. Therefore, this prospective cohort study was performed to identify a possible impact of ionic compared to nonionic MR contrast agents on qualitative choline detection as well as quantification in clinical MRS of the breast.

Methods and Materials

Two patient cohorts were examined by standardized MR mammography (1.5 T Siemens AVANTO using the breast matrix coil, T1w FLASH 2D dynamic scans before and after contrast agent injection, T2w TSE, TIRM), one receiving gadopentetate-dimeglumine (group A, ionic), the other gadodiamide (group B, neutral), administered by an automated injector (Medrad, Spectris) with a dose of 0.1 mmol/kg and flow rate of 3 ml/second. Following manual shimming, MRS was performed with a single voxel PRESS sequence (SVS-PRESS, TR 2000, TE 270, 128 averages, outer volume suppression, reduced water suppression, acquisition time: 4:14 min). The acquired breast spectra were post-processed and analyzed by using the non commercial MRUI software 2.2 (http://www.mrui.uab.es/). First, positive choline resonances were identified visually at approximately 3.23 ppm using the water (4.73 ppm) or the lipid methylene peak (1.3 ppm) as reference. The observer was blinded regarding imaging results as well as any clinical information. Identified peaks in malignant lesions were quantified using the AMARES algorithm [5]. To consider the influence of voxel size and voxel position, estimated choline signal intensities (peak area) were corrected by dividing the intensity by the voxel volume $(V_{Voxel} = (a \times b \times c)/1000)$ and the coil sensitivity factor (S) $(Cho_{corrected} = Cho_{estimated}/(S \times V_{Voxel}))$. Data analysis was performed by using Microsoft Excel 2007 and SPSS 17.0. A two-sided exact Mann–Whitney U test was used to compare both groups at a significance level of α=5%.

Results

63 spectra in 62 patients (A: n=34; B: n=29; 43 malignant, 20 benign) were investigated. Mean water line widths (FWHH, full width at half high) were 14.2±3.7 Hz (A) and 16.1±8.9 Hz (B) without significant difference between both groups (P=0.693). A choline peak was identified in 14 of 24 malignant lesions in group A (58.3%, 95% *CI* 36.7–77.9%) and in 14 of 19 malignant lesions in group B (73.7%, 95% *CI* 48.8–82.0%). Choline was also detected in one benign lesion in group A. Median values and interquartile ranges (*IQR*) for the normalized choline signal intensities (Cho_{corr}) were determined as 37.8 (A, *IQR*: 29.2) and 51.4 (B, *IQR*: 18.0). The differences between the groups were statistically significant (P=0.008). Mean tumour diameters (29.1±15.4 mm in A; 35.6±17.5 mm in B) and mean gradings (2.46±0.66 in A; 2.21±0.58 in B) did not differ significantly between the groups (P=0.269 and P=0.292, respectively).

Discussion

In this study, we were able to identify significantly lower choline signal intensities in patients receiving an ionic (gadopentetate dimeglumine) compared to patients receiving a non-ionic (gadodiamide) contrast agent. In agreement with previous experimental findings, these preliminary results suggest a negative influence of the ionic contrast agent on choline measurements in the breast. Since to date intravenous contrast agent injection is mandatory to identify malignant breast disease by exploiting the high sensitivity of MR-mammography to cancer associated neoangiogenesis, enabling the detection of tumours down to 3 mm in size [6, 7], our findings are of clinical importance because MRS is mostly acquired after contrast agent administration [4]. Interaction of the contrast agent with choline can, thus, cause false negative findings. Furthermore, comparisons between quantitative studies should be performed with care and should take into account potential contrast agent related bias. As this investigation was conducted in a clinical setting, some limitations exist. Although tumour grading and diameter did not differ significantly between both patient cohorts, patient number and study design do not allow for ruling out all biological differences between both groups. Regarding technical influences, we corrected the estimated choline signal intensities with respect to voxel size and position. All examinations were performed using the same equipment and measurement parameters. No significant differences regarding the quality of manual shimming were found between both groups. As no pre-contrast MRS measurements were performed, it was not possible to assess any intra-

individual influence of the contrast agents. Previous investigations suggest varying influences on choline estimations depending on the contrast agent as well as on the time interval between contrast agent injection and MRS examination [4, 8].

Conclusion

Our preliminary results suggest administration of a non-ionic contrast agent to avoid possible false negative findings in breast MRS. Contrast agent related influences on MRS results should be considered when performing quantitative metabolite assessments or study comparisons.

References

1. Haddadin IS, McIntosh A, Meisamy S, et al. (2007) Metabolite quantification and high-field MRS in breast cancer. NMR in Biomedicine 22:65–76.
2. Mountford C, Ramadan S, Stanwell P, et al. (2008) Proton MRS of the breast in the clinical setting. NMR in Biomedicine 22:54–64.
3. Tse GM, Yeung DK, King AD, et al. (2007) In vivo proton magnetic resonance spectroscopy of breast lesions: an update. Breast cancer research and treatment 104:249–255.
4. Lenkinski RE, Wang X, Elian M, et al. (2009) Interaction of gadolinium-based MR contrast agents with choline: implications for MR spectroscopy (MRS) of the breast. Magn Reson Med 61:1286–1292.
5. Vanhamme L, van den Boogaart A, Van Huffel S (1997) Improved method for accurate and efficient quantification of MRS data with use of prior knowledge. J Magn Reson 129:35–43.
6. Kaiser WA, Zeitler E (1989) MR imaging of the breast: fast imaging sequences with and without Gd-DTPA. Preliminary observations. Radiology 170:681–686.
7. Kuhl C (2007) The current status of breast MR imaging. Part I. Choice of technique, image interpretation, diagnostic accuracy, and transfer to clinical practice. Radiology 244:356–378.
8. Madhu B, Robinson SP, Howe FA, et al. (2008) Effect of Gd-DTPA-BMA on choline signals of HT29 tumors detected by in vivo 1H MRS. J Magn Reson Imaging 28:1201–1208.

Whole body imaging: technique and workflow

Pascal A.T. Baltzer, Matthias Dietzel, Tibor Vag, Hans-Joachim Mentzel, Werner A. Kaiser
Institute of Diagnostic and Interventional Radiology, University Hospital of the Friedrich Schiller University Jena

In Germany, according to the S3-guidelines, distant metastasis screening in newly diagnosed breast cancer includes ultrasound examination of the abdomen, an X-ray examination of the thorax, as well as bone scintigraphy. Only in case of suspicious findings, further imaging methods (i.e. CT, PET-CT, and MRI) are applied, routinely. Basically, breast cancer is able to metastasize in any body region. The main sites for metastasis are bone, liver and brain. Use of more sophisticated imaging modalities increases costs, but is highly likely to improve diagnostic accuracy of distant staging.

Modern multi-channel whole body MRI (WB-MRI) scanners are feasible to screen for metastases from head to toe in a reasonable time period below one hour. The diagnostic accuracy of WB-MRI for bone and organ metastases matches and even exceeds that of PET-CT. Furthermore, radiation exposure can be avoided and there are no extra costs for tracer substances.

Applying WB-MRI for metastasis screening is a major challenge for clinical workflow. Easily, several thousand images are produced, having to be interpreted by the radiologist, correctly. Especially small lesions for instance costal metastases are prone to be missed. Such mistakes can be avoided by choosing the optimal imaging sequence for target pathology: Some organs (e.g. liver) require dynamic contrast enhanced imaging as well as multiple breath holds to achieve optimal accuracy, while others require dedicated examination (e.g. brain). Moreover, WB-MRI requires the patient to be enclosed by multiple coils, a fact which is likely to cause claustrophobia and limits the acceptable examination time. Examination time is further limited by workflow requirements with the necessity of a clinically practicable imaging time.

We propose a breast cancer metastasis screening WB-MRI protocol based on T1w-TSE and TIRM sequences, including dedicated imaging of thorax and upper abdomen (multiple breath hold TIRM and dynamic contrast enhanced T1w-VIBE), brain (FLAIR, contrast enhanced T1w-SE) as well as bones (T1w-TSE in 2 plains, TIRM, contrast enhanced T1w-VIBE) and lymph nodes (TIRM, contrast enhanced T1w-VIBE). The complete imaging protocol requires between 35–40 min (c.f. table 1). It is feasible to be performed also in sick patients. It showed promising initial results in breast cancer patients with and w/o known distant metastases. Insufficient cooperation regarding breath holds could be compensated by triggered image acquisitions on the price of prolonging the examination.

Table 1: Imaging protocol for breast cancer metastasis screening.

Weighting	Sequence	Orientation	Region	Approx. time (min.)
T2	**HASTE-TIRM**	**CORONAL**	Whole body	3
T1	TSE			8
T2	TSE TIRM	AXIAL	Head & neck	8
			Thorax (bh)	
			Abdomen (bh)	
			Pelvis	
T1	TSE	SAGITTAL	Whole spine	4
T2	FLAIR	AXIAL	Brain	3
T1+CA	VIBE	CORONAL	Whole body including dynamic abdominal imaging	5
T1+CA	SE	AXIAL	Brain	3

bh: breath hold

MR-mammography: High Sensitivity and Low Specificity—still valid?

M. Benndorf, P. A. T. Baltzer, M. Gajda, W. A. Kaiser
University Hospital of the Friedrich Schiller University Jena, Germany

Introduction

Magnet-resonance-mammography (MRM) is known to be the most sensitive imaging modality for the detection of invasive breast cancer. Despite this, critics of MRM often bring up the argument of the technique's low specificity against its broader use in clinical routine. In recent years, plenty of research has been conducted to assess the diagnostic accuracy of MRM in various clinical settings. Each and every study published before showed the superior sensitivity of MRM (with sensitivities between 71% and 100%). Specificity of MRM was superior compared with the specificity of conventional imaging modalities (i.e. X-ray-mammography (XRM) and ultrasound) in some studies, while other studies showed contradictory results. All studies performed so far regarded preselected cohorts, depending on the respective indication for MRM. Commonly accepted indications for MRM are preoperative staging, control of chemotherapy, patients with breast implants as well as unclear findings in conventional imaging modalities. We therefore wanted to retrospectively assess the diagnostic accuracy of MRM if all patients are regarded that were consecutively examined in our university hospital, irrespective of their reason for referral.

Methods and Materials

Bilateral MRM examinations of 342 patients were enrolled in this ethical review board approved study. The cohort was recruited consecutively between January, 2005 and April, 2006. Contrast enhanced MRM was performed in each case. The radiologists evaluating the MRI examinations were not specialized but trained in MRM (with around 200 MRMs performed at the beginning of the study period). The mean age of the patients was 54.4 years at the time of MRM. The cohort included three male patients (0.8%).

Negative findings were validated by means of follow-up examinations. In our case, MRI, XRM, ultrasound or clinical follow-up were regarded as sufficient for follow-up examinations. For the verification of positive findings the histopathological examination was regarded the gold standard. If a malignant neoplasm was detected more than 1 year after the initial MRM (rated as benign), the examination was regarded to be true negative.

We chose the single breast the study subject. This was due to the fact that the majority of XRM studies regard the single mammography and we wanted our results to be comparable with this kind of study. Overall, 736 breasts were examined by MRM. This is more than twice the number of patients because some patients were examined twice during the study period. We calculated 95% confidence intervals from the normally approximated binomial distribution.

Results

Indications for MRM were the following (regarding the single breast, $n=736$): unclear XRM: 131 (17.8%), suspect XRM: 86 (11.7%), suspect only in ultrasound, unsuspect XRM: 40 (5.4%), suspect galactography: 1 (0.1%), tumour-aftercare: 213 (28.9%), control MRI (previously unsuspicious): 93 (12.6%), examined because other breast was of interest: 154 (20.9%), retrospectively not determinable: 18 (2.4%). Negative findings were followed-up with a median time of 26.6± 7.5 (SD) months. The loss-to-follow-up was 8.4% (follow-up examinations were available for 676 of all examined 736 breasts). Table 1 shows the contingency table for the diagnostic results of MRM.

Table 1: Contingency table for the diagnostic results of MRM

	Malignant lesion (following results of pathological examination)		Count
MRM	Yes	No	
Malignant	125	33	158
Benign	4	514	518
Count	129	547	676

Following these results, sensitivity was 96.9% (93.9%–99.9%), specificity was 94.0% (92.0%–96.0%), the positive predictive value (PPV) was 79.1% (72.8%–85.4%) and the negative predictive value (NPV) was 99.3% (98.4%–100.0%). Overall, 129 malignant neoplasms were detected in the study population. They were comprised of 85 invasive ductal carcinomata, 19 invasive lobular carcinomata, nine DCIS lesions, three lymphomata, one mixed type carcinoma, one case of Paget's disease, one sarcoma, one tubular carcinoma, one medullary carcinoma, one mucinous carcinoma, one inflammatory carcinoma as well as six carcinomata not classified.

The four false negative findings in MRM were comprised of two DCIS lesions sized 1.8 mm and 2 mm, respectively, one invasive lobular carcinoma sized 2 mm and the case of Paget's disease. The latter was diagnosed 6 months after the initial MRM. For malignant lesions larger than 2 mm in size, the sensitivity of MRM is therefore 99.7%.

Conclusions

MRM presents as a highly sensitive and specific technique for the detection of invasive breast cancer. However, our results are only valid for a non-screening population like the described one. Furthermore, caution should be given to the herein calculated predictive values—they also are applicable only on the non-screening setting. This is because predictive values depend critically on the prevalence of the disease among the cohort studied.

Non-cancer enhancement of lumpectomy sites beyond 18 months

Eva C. Gombos, MD and Robyn L. Birdwell, MD FACR
Brigham & Women's Hospital, Department of Radiology, Boston, USA

Background Information

The standard of care for women with early-stage breast cancer (stage I and II) is breast-conserving therapy (BCT), consisting of lumpectomy and whole-breast irradiation. While the risk of local recurrences is reported as 1–2% or more per year after treatment; there is evidence that detection of recurrence in the early stage improves relative survival [1–3]. Post-therapeutic changes often limit accurate analysis of conventional imaging techniques (i.e. mammography and sonography) [4,5]. Breast magnetic resonance (MR) imaging has been shown to differentiate benign posttreatment changes of fibrosis from tumor recurrence, and non-enhancing areas have a high negative predictive value for malignancy [6,7]. MR demonstrates areas of increased vascularity rather than density of tissue or deformity alone, thus offering benefits over mammography. The time interval for when MRI should first be used after BCT has been questioned. Use of MR was discouraged for up to 12–18 months after treatment because of post-treatment inflammatory changes that were thought to hamper identification of residual or recurrent breast cancer [8–10]. However, a more recent report suggested that confounding early radiation-induced changes on MR should only

occur up to 3 months after treatment [11]. Intense enhancement of a radiated lumpectomy site can be seen beyond 18-months post-therapy, however this is not yet commonly accepted [10, 12].
Our purpose is to demonstrate benign MR enhancement patterns, not associated with recurrent cancer, at the lumpectomy site following BCT with special attention to cases where enhancement continued beyond 18 months.

Technique
MR examinations were performed on a 1.5-T MR device (Signa HDx 1.5 T, GE Healthcare), using an InVivo 7 channel, dedicated breast surface coils (MRI Devices, InVivo Research) with the patient in the prone position on the dedicated breast coil. Institutional standard dynamic contrast-enhanced protocol was used, including fast three-plane localizer sequence, sagittal T2-weighted FSE fat saturated and axial T1-weighted non-fat suppressed FSPGR sequences followed by VIBRANT (Volume Imaging for Breast Assessment) dynamic series consisting of one acquisition before and four after an intravenous bolus injection of 20 ml gadolinium dimeglumine (Magnevist; Schering). Each dynamic volume had 2–3 mm thick sections, with an acquisition matrix of 256×224×224 and temporal resolution of approximately 1 min 30 s per dynamic run. A late axial T1-weighted FSPGR post-contrast fat saturated sequence was also routinely obtained. In addition to fat saturation, image subtraction was performed off-line after the actual imaging session.

Interpretation
MR studies were reviewed according to the American College of Radiology (ACR) BI-RADS® guidelines [13]. If the MR showed enhancement at the lumpectomy site, the enhancement was reviewed for location of the enhancement in relation to the lumpectomy site and type of enhancing finding (mass vs. nonmasslike enhancement [NMLE]) was recorded. Intensity of enhancement was determined by radiologist's visual observation of the presence of signal on post-contrast or subtraction.

Persistent enhancement after 18 months
As we reported previously, in a considerable percentage of cases (12%) we found persistent enhancement at >18 months (average 34 months, range 19–147 months) at the lumpectomy site without recurrent cancer with the longest post-treatment follow-up time interval being 12 years post therapy [12]. Independent re-evaluation of the enhancing lumpectomy sites typically showed a focal area of persistent NMLE at the lumpectomy site. In some cases, obvious fat necrosis was seen and best diagnosed on T1WI as hyperintensity in the center of the enhancement at the lumpectomy site (Figure 1.).

Mass enhancement at the lumpectomy site
Cysts and hematomas are usually diagnosed on T2-weighted images as hyperintense masses and typically do not enhance. Posttreatment fibrosis is often identified as slow persistent enhancement within the region of the lumpectomy site. Scar tissue may appear as mass with rapid enhancement and even washout (Figure 2.). The possibility of recurrence must be considered and biopsy should be recommended to determine histology in such cases. Recurrent cancers usually exhibit strong initial enhancement and washout in the delayed images, and may demonstrate rim enhancement or heterogeneous internal enhancement. MR is highly sensitive in the identification of recurrent malignancy and as with primary cancer, can detect multifocality of the recurrent cancer (Figure 3).

Non mass like (NMLE) enhancement at the lumpectomy site
Non-specific focal area of persistent NMLE at the lumpectomy site is considered very likely to be benign and appropriate for a 12-month MR follow-up. There are occasions when a, short interval 6 month follow-up may be recommended.
Because of the limitations within the BI-RADS lexicon specific to lumpectomy site descriptors, we found that "postlumpectomy changes" with slow initial and persistent delayed enhancement was the most frequent enhancement pattern descriptor found in our cases. Also used was the BIRADS descriptor "NMLE at the lumpectomy site". Both descriptors were associated with final assessments of either BIRADS 2 or 3.

Conclusions
The evolution of scar into a non-enhancing, relatively avascular fibrotic area may take much longer than 18 months, depending on the degree of inflammation. In a considerable percentage of cases there may be persistent enhancement at >18 months at the lumpectomy site without recurrent cancer.

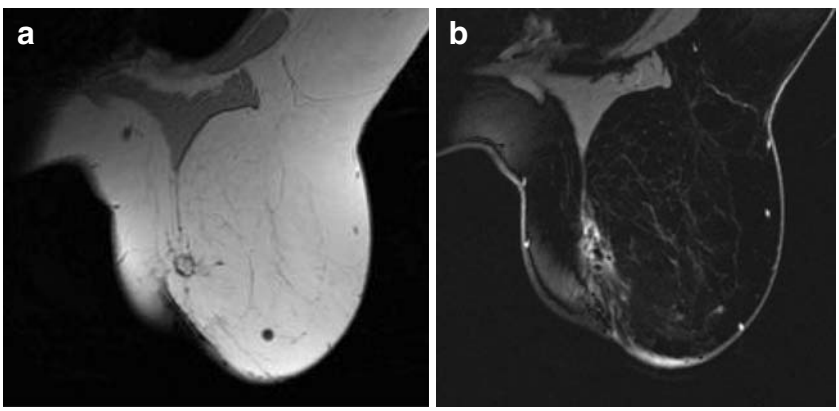

Figure 1. This is a 55 year old patient with a history of right lumpectomy. Unilateral right breast MRI was ordered with the statement of pain in the right axilla.
A. Axial non fat suppressed MR image shows fat intensity within an irregular area at the lumpectomy site.
B. Delayed postcontrast image shows persistent enhancement with contrast.
This findings are consistent with fat necrosis at the lumpectomy site and was interpreted as benign, appropriate for annual follow up. The findings are stable now after 3 years.

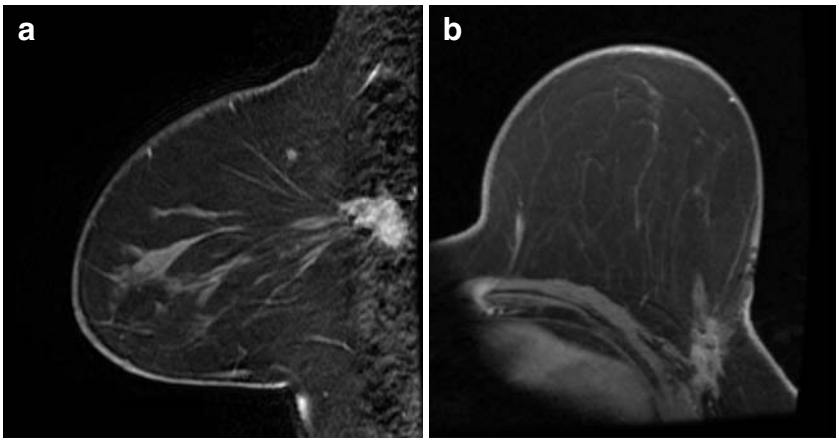

Figure 2. A 55 year old asymptomatic woman 4 years after LUOQ lumpectomy for IDC and DCIS.
A. Sagittal MR image shows rapidly enhancing, irregular mass at the lumpectomy site.
B. Delayed image shows washout of the contrast but less mass-like appearance.
Excisional biopsy showed breast tissue with dense fibrosis (scar), calcifications, and a giant cell reaction; typical posttreatment histopathological findings.

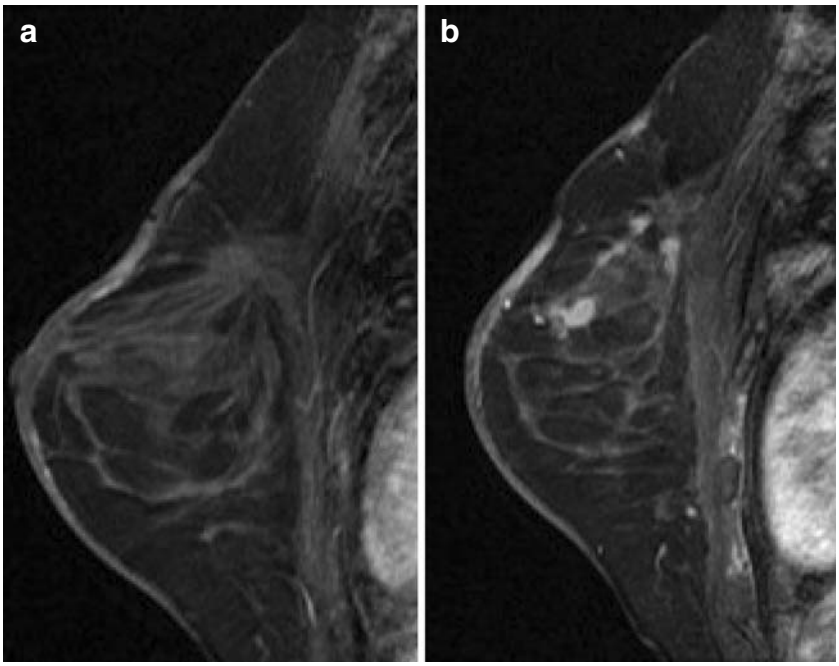

Figure 3. This is a 39 year old woman 2 years after LUOQ lumpectomy for poorly differentiated ER/PR negative, 3+ HER2/NEU IDC, presented with palpable abnormality.
A. Sagittal MR image shows the expected architectural distortion at the lumpectomy bed.
B. Multiple rapidly enhancing, irregular masses are seen adjacent to the lumpectomy site.
US guided biopsy adjacent to the scar showed grade 3 IDC, histologically identical to her original tumor. Subsequent restaging showed anterior mediastinal lymph nodes and a pericardial soft tissue nodule consistent with metastases. Her disease unfortunately progressed while on adjuvant Herceptin therapy. She was lost for follow up 1 year ago.

References

1. Voogd AC, van Tiehoven G, Peterse HL, et al. Local recurrence after breast conservation therapy for early stage breast carcinoma: detection, treatment, and outcome in 266 patients. Dutch Study Group on local recurrence after breast conservation (BORST). Cancer 1999; 85:437–466.

2. Heittaner P, Miettinen M, Makinen J. Survival after first recurrence in breast cancer. Eur J Cancer Clin Oncol 1986; 22:913–919.

3. Nomura Y, Tsutsui S, Murakami S, Takenaka Y. Prognostic impact of second cancer on the survival of early breast cancer patients. Int J Oncol 1999; 14:1103–1109.

4. Hassell PR, Olivotto IA, Mueller HA, Kingston GW, Basco VE. Early breast cancer: detection of recurrence after conservative surgery and radiation therapy. Radiology 1990; 176: 731–5.
5. Locker AP, Hanley P, Wilson AR et al. Mammography in the pre-operative assessment and post-operative surveillance of patients treated by excision and radiotherapy for primary breast cancer. Clin. Radiol. 1990; 41: 388–91.
6. Preda, L., Villa, G., Rizzo, S., Bazzi, L., Origgi, D., Cassano, E., and Bellomi, M., 2006, Magnetic resonance mammography in the evaluation of recurrence at the prior lumpectomy site after conservative surgery and radiotherapy: Breast Cancer Res., v. 8, p. R53.
7. Viehweg, P., Heinig, A., Lampe, D., Buchmann, J., and Heywang-Kobrunner, S. H., 1998, Retrospective analysis for evaluation of the value of contrast-enhanced MRI in patients treated with breast conservative therapy: MAGMA, v. 7, p. 141–152.
8. Fischer U, Vosshenrich R, Kopka L, Kahlen O, Grabbe E. [Contrast medium assisted dynamic MR-mammography after diagnostic and therapeutic interventions on the breast] Bildgebung 1996; 63: 94–100.
9. Drew PJ, Kerin MJ, Turnbull LW et al. Routine screening for local recurrence following breast-conserving therapy for cancer with dynamic contrast-enhanced magnetic resonance imaging of the breast. Ann.Surg.Oncol. 1998; 5: 265–70.
10. Heywang-Kobrunner SH, Schlegel A, Beck R et al. Contrast-enhanced MRI of the breast after limited surgery and radiation therapy. J.Comput.Assist.Tomogr. 1993; 17: 891–900.
11. Morakkabati N, Leutner CC, Schmiedel A, Schild HH, Kuhl CK. Breast MR imaging during or soon after radiation therapy. Radiology 2003; 229: 893–901.
12. Magnetic resonance imaging of the breast following conservative therapy for breast cancer. 4th International Congress on MR-Mammography, 28–30 September 2006, Jena, Germany, abstract published in European Radiology Supplements, Volume 16, Supplement 5 / September, 2006
13. Ikeda D. *ACR Breast Imaging Reporting and Database System, Breast Imaging Atlas*. 4th ed.. edn. Reston,VA, American College of Radiology, 2003.

Invasive lobular carcinoma

Boetes, Carla
Department of Radiology, Radboud University Nijmegen, Medical Centre, Nijmegen, The Netherlands

Invasive lobular carcinoma (ILC): is the second most frequent type of breast malignances and accounts for 10% to 15% of all cancers.
More than in invasive ductal carcinoma (IDC) there is multifocality and multicentricity.
The last decades the incidence of ILC has increased due to the use of hormonal replacement therapy.
At presentation most patients are a bit older than in IDC. Furthermore the mean tumor size at presentation is slightly larger than in IDC.
The clinical presentation can be the same as in IDC, a palpable mass.
On mammography it has than the same features as IDC, namely a spiculated mass.
However the findings both on clinical examination and mammography can be more subtle.
There might be a vague area of the thickening or induration without clear margins on physical examination. The findings on mammography in this type of ILC are also subtle. On mammography there may be an area of architectural disturbance or an asymmetric density, but sometimes there is even no abnormality seen on mammography.
Histopathology shows in the classical form small uniform cells that invade the stroma in a single file pattern ("Indian file").
Also sometimes tumor cells infiltrate the breast tissue in an insidious way giving no desmoplastic reaction.
Mitotic activity is rare and the classical form of ILC (and also lobular carcinoma in situ) is E-cadherin negative.
On pathology there are different types of ILC.
The first one is the solid type. In this type the tumor cells are growing in a confluent sheet with hardly any normal stroma. On mammography this type shows as a spiculated mass. The second type is the alveolar type. Here the tumor grows in nests of 20 or more cells. These nests are separated from each other by fibrous septa.
The third type is the tubulolobular variant. Here the tumor cells invade the stroma in linear strands and this is the classical growth pattern.
On mammography this is seen as an area of architectural distortion or an asymmetric density, however sometimes no abnormality is seen.
The last type is the pleomorphic variant. In this type the neoplastic cells are larger and show more nuclear variation.
The classical ILC is estrogen and progesteron receptor positive and HER −2/neu negative. However the pleomorphic type can be HER −2/neu positive.
The pattern of metastases in ILC is different from IDC. Metastases go in particular to the bone, peritoneal surface, retroperitoneum, gastrointestinal tract and the reproductive organs.
The survival of especially small ILC is better than IDC. The only exception is the pleomorphic type. This type has a very poor prognosis.
Magnetic resonance imaging (MRI) plays an important role in the imaging of ILC.
Dependent on the type of ILC a distinction between mass-like and non-mass-like tumors can be made. The solid type of ILC will show on mammography a spiculated mass and the same will be seen on US and MRI.
The other types of ILC will show on MRI either also architectural distortion (even on plane T1 weighted images) or regional or segmental enhancement.
Kinetics of ILC tend to show delayed maximum enhancement and wash-out is not as often as in IDC.
Correlation in size of ILC compared to histology is best performed with MRI.
Also multifocality and multicentricity is best evaluated with MRI. In about 32% of the ILC casus there is multifocality or multicentricity detected on MRI.
In about 7% of the patients there are malignant findings in the contralateral breast detected by MRI.
In conclusion it can be stated that CE-MRI is the best way to evaluate ILC, for tumor size, multifocality and multicentricity but especially for the contralateral size.

Value of MRI in screening

Boetes, Carla
Department of Radiology, Radboud University Nijmegen, Medical Centre, Nijmegen, The Netherlands

The standard care for breast cancer screening among women over the age of 40 years is mammography.
However sensitivity of mammography on women with a high glandular density is low.
For women, who have an increased risk for getting breast cancer mammography alone is not sufficient for detecting breast cancer in an early stage.

There are three categories of women who are at increased risk for getting breast cancer:

1. women with a proven gene mutation
2. women with a family history of getting breast cancer
3. women with a personal history

ad. 1: Gene mutation
The most known gene mutations are BRCA1 and BRCA2 mutation carriers. BRCA1 tumors are often receptor negative and in about 70% of the cases grade 3. BRCA1 carriers and there family members have also an increased risk for getting ovarian cancer and male carriers for prostate cancer. There is a suggestion that the BRCA1 carriers also have a slightly increased risk for colonic cancer.
BRCA2 cancers behave more like sporadic cancers and can be receptor positive.
BRCA2 carriers are slightly older than BRCA1 carriers at the moment of detecting breast cancer. BRCA2 carriers are also associated with an increased life time risk of about 6% of male breast cancer.
About 15% of all male breast cancers are BRCA2 carriers. BRCA2 carriers are also associated with an elevated risk for the development of other cancers like prostate cancer, pancreatic cancer, non-Hodgkin lymphoma and bladder cancer.
Other known gene mutation carriers who have an increased risk for breast cancer are:
Li-Fraumeni. These mutation carriers have a high risk for developing soft tissue sarcoma during childhood but also osteosarcoma and brain tumors. Nearly 30% of the malignances arise before the age of 15.
Breast cancer is detected at a very young age, about 22–35 years. It is in about 25% of the cases bilateral and in 11% of the cases breast cancer is associated with other malignances.
Ataxia-Telangiectasia (ATM). ATM has a predisposition to develop leukaemia and lymphoma. Patients with ATM have also cerebellar ataxia and immune deficiency. These patients have a 4 fold increased risk for breast cancer.
Cowden Disease shows benign proliferation of the gastrointestinal tract, mucosa, thyroid. Patients with Cowden disease have at least a 50% life time risk for developing breast cancer.

ad. 2: Family history.
Female patients who are a first degree relative of BRCA carriers but not tested need to be screened with MRI. If women have a life time risk for getting breast cancer of 20% or more according several models that estimate the life time risk based on family history, in combination with other risk factors like reproductive history or prior breast biopsies, they should also be evaluated with a yearly MRI.

ad. 3: Personal history.
There are clinical factors associated with a substantial breast cancer risk. Women with a history of (non) Hodgkin lymphoma and thoracic irradiation between the age of 10 to 30 have a significantly increased risk 15 to 30 years after the irradiation, to develop breast cancer.
Lobular carcinoma in situ (LCIS) and atypical lobular hyperplasia (ALH) have a life time risk ranging from 10% to 20%. The invasive cancers are in most cases invasive lobular cancers and are detected more than 15 years after the original diagnosis of LCIS. They can be ipsi- or contralateral.
Atypical ductal hyperplasia is part of a continuum of ductal proliferative disease from ductal hyperplasia to ductal carcinoma in situ (DCIS). This group of women have a five fold increased risk for getting breast cancer.

All these above mentioned categories of women should be evaluated yearly with both mammography and MRI.
In many studies the value of MRI has been proved with a mean sensitivity of MRI for breast cancer of about 85% and a sensitivity of mammography of 35%.
However in these studies the specificity of MRI was about 92% and of mammography more than 98%.
In conclusion it can be stated that MRI of the breast plays an important role in screening women with an increased risk for getting breast cancer. However it is important to improve specificity of MRI.

MRI/MRS of Breast Cancer: Why do we measure total choline and how do we do breast spectroscopy?

Patrick J. Bolan, Ph. D., Assistant Professor
Center for Magnetic Resonance Research, Department of Radiology, University of Minnesota Medical School, Minneapolis MN 55419, USA

Introduction
Magnetic resonance mammography is rapidly increasing in clinical usage. Due to its high sensitivity, MR mammography is now widely used for high-risk screening, but it is also used for diagnosis, monitoring response to treatment, and determining extent of disease. MR spectroscopy (MRS) of the breast is developing into a useful adjust examination. Breast MRS gives information about the metabolic content of a lesion in contrast to the anatomical and vascular information provided by dynamic contrast-enhanced MRI. This paper will provide a brief summary of the motivation for performing breast MRS and a description of the methods used to perform these examinations.

Motivation—Why measure total choline?
Most MR spectra acquired from the human breast show both water and lipid resonances, which originate from the pathological lesion and surrounding adipose and fibroglandular tissues. Spectra often also show a small resonance centered at 3.2 ppm that is typically called a *total choline* peak, commonly abbreviated *tCho*. *Ex vivo* and *in vitro* studies have shown that this peak is attributable to several metabolites, including phosphocholine (PCho), glycerophosphocholine (GPC), free choline, taurine, myo-inositol, phosphoethanolamine, and glucose (1; 2). At field strengths up to 4 T, these resonances generally appear as a single broad peak, which is termed *total choline* to reflect that the choline-containing compounds are the dominant constituents.
A number of studies have demonstrated that this tCho resonance has a greater intensity and is easier to detect in cancers than normal tissues and benign lesions (3–9; 1; 10–13). *Ex vivo* and *in vitro* studies have also shown that it is primarily high concentrations of PCho that leads to the elevated tCho in cancers, whereas in normal breast tissues the predominant resonance is GPC (2; 14; 15). Notably, it has been shown that the tCho peak that can be detected in the normal fibroglandular tissue of some healthy subjects is shifted in frequency due to the different ratios of contributing metabolites (11). The source of the elevation in PCho concentration is still under investigation. It has been proposed that the elevated PCho is due to increases in activity of choline kinase and phospholipases, and upregulated choline transport (16–18). Additionally, the increased *in vivo* signal may be due to higher cell density in cancers, as suggested by the lower apparent diffusion coefficients measured in malignant lesions (19–21).

While these underlying mechanisms are not fully understood, an elevated tCho peak is generally considered a biomarker of elevated metabolic processes and is characteristic of malignancy. This biomarker has been shown to be clinically useful in diagnosing suspicious lesions and in evaluating early response to chemotherapy (5; 22; 23).

Methods—How to perform breast spectroscopy

Measuring tCho with breast MRS is greatly dependent on the reception sensitivity of the MR scanner. For typical physiological concentrations, the intensity of the tCho signal is approximately 10,000 times less that that of the water signal that is used for imaging. Because of this, the quality of MRS data is much more dependent on scanner sensitivity than MRI, and therefore benefits greatly from increased field strengths and close-fitting breast receive coils.

The two general types of pulse sequences used for breast MRS are single-voxel spectroscopy (SVS) and spectroscopic imaging (SI) techniques. In SVS, the MR operator prescribes a rectangular volume (a *voxel*) in the region of interest. Using a localization sequence such as PRESS or STEAM, a spectroscopic signal from inside the voxel is acquired, and all signals from outside the voxel are eliminated. All of the important system calibrations, such as pulse powers, frequency, and B0 shimming, can be carefully optimized for the SVS voxel region, which greatly improves spectral quality. However, the voxel must be prescribed at the time of the scan, and this requires some expertise to perform quickly and consistently.

Spectroscopic imaging methods, in contrast, acquire a grid of spectra, covering a large region of the breast. This can be done by exciting a slice and performing 2D phase encoding, or by exciting a slab and using 3D phase encoding. This approach has the advantage of covering a larger region and giving information about spatial variation. Both SVS and SI methods have the same measurement sensitivity, but SI has some technical limitations: the system calibrations must be optimized over the larger region, lipid artifact suppression is more difficult, localization precision is lower, and quantitative analyses are more complicated. Nevertheless SI of the breast is an active area of ongoing research (24; 25).

Several methods have been used for analyzing breast spectra. Many studies have used qualitative interpretation of spectra to evaluate whether or not a tCho resonance is present. This approach treats tCho as a simple tumor biomarker: if present (or has an SNR greater than a fixed threshold) it indicates that a lesion is more likely to be malignant. The underlying assumption in this approach is that if the PCho concentration is elevated, it is more likely that a tCho resonance will be detected. Numerous research groups have demonstrated this approach is reproducible and clinically valuable (reviewed in Katz-Brull et al. (4)).

A limitation of this "detection" approach is that the sensitivity of a breast MRS measurement can vary between subjects and between sites. The sensitivity depends on numerous factors that are not always controlled: voxel size, field strength, receive coil sensitivity, adipose tissue content, accurate flip angle calibration, and number of averages all impact the signal-to-noise of the tCho resonance. Other analysis techniques aim to correct for these confounding factors and estimate the underlying concentration of the tCho metabolites. These *quantitative* methods use either an external MR signal (26) or the water signal from the voxel of interest (27) to compensate for variable measurement sensitivities. Both approaches are feasible but require careful consideration of biasing factors such as water T2 variation (28) and receive coil sensitivity profiles.

Conclusion

Magnetic resonance spectroscopy measurements of tCho in breast cancers can give metabolic information that complements breast MRI and improves the clinical utility of the overall MR examination. Currently, breast MRS is predominately used in research institutions, and further developments are required in order to bring methods for quantitative analyses and spectroscopic imaging into the routine clinical setting. With future improvements in methods and coils, breast MR spectroscopy can develop into a valuable and routine diagnostic tool.

Acknowledgements

NIH Grant CA120509

References

1. Gribbestad IS, Sitter B, Lundgren S, Krane J, Axelson D. Metabolite composition in breast tumors examined by proton nuclear magnetic resonance spectroscopy. Anticancer Res. 1999 Jun;19 (3A):1737–1746.

2. Sitter B, Ursula Sonnewald, Manfred Spraul, Hans E. Fjösne, Ingrid S. Gribbestad. High-resolution magic angle spinning MRS of breast cancer tissue. NMR in Biomedicine. 2002;15(5):327–337.

3. Kvistad KA, Bakken IJ, Gribbestad IS, Ehrnholm B, Lundgren S, Fjøsne HE, et al. Characterization of neoplastic and normal human breast tissues with in vivo (1)H MR spectroscopy. J Magn Reson Imaging. 1999 Aug;10(2):159–164.

4. Katz-Brull R, Lavin PT, Lenkinski RE. Clinical utility of proton magnetic resonance spectroscopy in characterizing breast lesions. J. Natl. Cancer Inst. 2002 Aug 21;94(16):1197–1203.

5. Jagannathan NR, Kumar M, Seenu V, Coshic O, Dwivedi SN, Julka PK, et al. Evaluation of total choline from in-vivo volume localized proton MR spectroscopy and its response to neoadjuvant chemotherapy in locally advanced breast cancer. Br. J. Cancer. 2001 Apr 20;84(8):1016–1022.

6. Yeung DK, Cheung HS, Tse GM. Human breast lesions: characterization with contrast-enhanced in vivo proton MR spectroscopy—initial results. Radiology. 2001 Jul;220(1):40–46.

7. Roebuck JR, Cecil KM, Schnall MD, Lenkinski RE. Human breast lesions: characterization with proton MR spectroscopy. Radiology. 1998 Oct;209(1):269–275.

8. Gribbestad IS, Singstad TE, Nilsen G, Fjøsne HE, Engan T, Haugen OA, et al. In vivo 1H MRS of normal breast and breast tumors using a dedicated double breast coil. J Magn Reson Imaging. 1998 Dec;8(6):1191–1197.

9. Kim J, Park S, Lee HM, Lee Y, Sung N, Chung D, et al. In vivo 1H-MRS evaluation of malignant and benign breast diseases. Breast. 2003 Jun;12(3):179–182.

10. Bartella L, Morris EA, Dershaw DD, Liberman L, Thakur SB, Moskowitz C, et al. Proton MR spectroscopy with choline peak as malignancy marker improves positive predictive value for breast cancer diagnosis: preliminary study. Radiology. 2006 Jun;239(3):686–692.

11. Stanwell P, Gluch L, Clark D, Tomanek B, Baker L, Giuffrè B, et al. Specificity of choline metabolites for in vivo diagnosis of breast cancer using 1H MRS at 1.5 T. Eur Radiol. 2005 May;15(5):1037–1043.

12. Cecil KM, Schnall MD, Siegelman ES, Lenkinski RE. The evaluation of human breast lesions with magnetic resonance imaging and proton magnetic resonance spectroscopy. Breast Cancer Res. Treat. 2001 Jul;68(1):45–54.

13. Meisamy S, Bolan PJ, Baker EH, Pollema MG, Le CT, Kelcz F, et al. Adding in vivo quantitative 1H MR spectroscopy to improve diagnostic accuracy of breast MR imaging: preliminary results of observer performance study at 4.0 T. Radiology. 2005 Aug;236(2):465–475.

14. Aboagye EO, Bhujwalla ZM. Malignant transformation alters membrane choline phospholipid metabolism of human mammary epithelial cells. Cancer Res. 1999 Jan 1;59(1):80–84.
15. Podo F. Tumour phospholipid metabolism. NMR Biomed. 1999 Nov;12(7):413–439.
16. Eliyahu G, Tamar Kreizman, Hadassa Degani. Phosphocholine as a biomarker of breast cancer: Molecular and biochemical studies. International Journal of Cancer. 2007;120(8):1721–1730.
17. Glunde K, Jie C, Bhujwalla ZM. Molecular causes of the aberrant choline phospholipid metabolism in breast cancer. Cancer Res. 2004 Jun 15;64(12):4270–4276.
18. Ramírez de Molina A, Rodríguez-González A, Lacal JC. From Ras signalling to ChoK inhibitors: a further advance in anticancer drug design. Cancer Lett. 2004 Apr 8;206(2):137–148.
19. Corum CA, McIntosh AD, Bolan PJ, Nelson M, Snyder AL, Powell NJ, et al. Feasibility of single-voxel MRS measurement of apparent diffusion coefficient of water in breast tumors. Magn Reson Med. 2009 May;61(5):1232–1237.
20. Guo Y, Cai Y, Cai Z, Gao Y, An N, Ma L, et al. Differentiation of clinically benign and malignant breast lesions using diffusion-weighted imaging. J Magn Reson Imaging. 2002 Aug;16(2):172–178.
21. Partridge SC, McKinnon GC, Henry RG, Hylton NM. Menstrual cycle variation of apparent diffusion coefficients measured in the normal breast using MRI. Journal of Magnetic Resonance Imaging. 2001;14(4):
22. Meisamy S, Bolan PJ, Baker EH, Bliss RL, Gulbahce E, Everson LI, et al. Neoadjuvant chemotherapy of locally advanced breast cancer: predicting response with in vivo (1)H MR spectroscopy—a pilot study at 4 T. Radiology. 2004 Nov;233(2):424–431.
23. Baek HM, Chen JH, Nie K, Yu HJ, Bahri S, Mehta RS, et al. Predicting Pathologic Response to Neoadjuvant Chemotherapy in Breast Cancer by Using MR Imaging and Quantitative 1H MR Spectroscopy. Radiology. 2009;251(3):653.
24. Jacobs MA, Barker PB, Bottomley PA, Bhujwalla Z, Bluemke DA. Proton magnetic resonance spectroscopic imaging of human breast cancer: a preliminary study. J Magn Reson Imaging. 2004 Jan;19(1):68–75.
25. Baek H, Chen J, Yu HJ, Mehta R, Nalcioglu O, Su M. Detection of choline signal in human breast lesions with chemical-shift imaging. J Magn Reson Imaging. 2008 May;27(5):1114–1121.
26. Bakken IJ, Gribbestad IS, Singstad TE, Kvistad KA. External standard method for the in vivo quantification of choline-containing compounds in breast tumors by proton MR spectroscopy at 1.5 Tesla. Magn Reson Med. 2001 Jul;46(1):189–192.
27. Bolan PJ, Meisamy S, Baker EH, Lin J, Emory T, Nelson M, et al. In vivo quantification of choline compounds in the breast with 1H MR spectroscopy. Magn Reson Med. 2003 Dec;50(6):1134–1143.
28. Tan PC, Pickles MD, Lowry M, Manton DJ, Turnbull LW. Lesion T(2) relaxation times and volumes predict the response of malignant breast lesions to neoadjuvant chemotherapy. Magn Reson Imaging. 2008 Jan;26(1):26–34.

Use of single voxel choline MR spectroscopy to determine which MR suspicious breast lesions require biopsy

Sandra Brennan, Sunitha Thakur, Elizabeth Morris, Laura Liberman, Hedvig Hricak, D. David Dershaw
Department of Radiology, Memorial Sloan-Kettering Cancer Center, 1275 York Ave, New York, NY 10065, USA.
This study was funded by a Department of Defense, U.S. Army Medical Research Grant, (W81XWH-04-1-0568).

Introduction

Magnetic resonance imaging is playing an increasingly important role in the clinical setting [1–3]. Although the American Cancer Society has recommended annual screening breast MRI for women with >20–25% lifetime breast cancer risk, the relatively low specificity of MRI can generate many benign biopsies. Hydrogen 1 (^{1}H) MR spectroscopy has been studied as a potential adjunct to breast MRI [4]. Proton MR Spectroscopy (^{1}H MRS) may improve the positive predictive value (PPV) of breast MRI, sparing some benign biopsies, while maintaining sensitivity in breast cancer diagnosis. While ^{1}H MRS is FDA approved and widely used in the brain and prostate its use in breast is still investigational.

The diagnostic value of ^{1}H MRS in cancer is based on the detection of elevated levels of choline compounds, which are markers of active tumor [5]. Several studies have shown that neoplastic breast tissue contains elevated levels of total choline-containing compounds (tCho) [6–7]. These compounds have methyl protons which resonate at a chemical shift of 3.2 ppm [8]. This includes contributions from choline, phosphocholine, glycerophosphocholine, myoinositol, and taurine [8–9].

Technical Background

Single-voxel (i.e. one single box volume of interest) technique (SVS) is most commonly used in the breast. This technique is limited to evaluating one lesion at a time and lesions should be at least 1 cc in size as smaller voxels yield large errors in tCho measurements. Magnetic resonance spectroscopic imaging (MRSI) or multi voxel MR spectroscopy provides information about the spatial distribution of metabolites, which is useful for studying multiple lesions. Both qualitative and quantitative approaches have been used but the majority of ^{1}H MR spectroscopic studies are based on the detection of the choline peak or its signal-to-noise ratio (SNR) [10].

Differentiating benign from malignant lesions

Several in vivo ^{1}H MRS studies have been done in an effort to improve differentiation between benign and malignant breast lesions [4, 8, 10, 11]. There are reported sensitivities of 70–100% and specificity of 67–100% on 1.5 T scanners. In our study we prospectively evaluate the diagnostic performance of 1H MRS in breast lesions with pathologic correlation, to determine the ability of MRS in differentiating malignant from benign lesions.

Materials and Methods

We enrolled a total of 146 patients to the protocol. A total of 37 patients were excluded from the study. Thirteen patients withdrew consent, one patient was not registered to the protocol, one incorrect patient was consented and the voxel was misplaced in 2 patients. Spectroscopy was not performed in 20 patients due to time constraints/interference with clinical procedure n=7, cancelled procedure n=2, terminated procedure n=2, allergic reaction to contrast n=1, lesion not suitable n=8 (no lesion seen/failed to enhance n=6, clip n=1, too small n=1). There were a total of 109 patients, which were evaluable for the protocol. The median age of the eligible patients was 48 with a range of 26–73. All women had a suspicious mass or biopsy-proven breast lesion (cancer or benign) measuring >1 cm on MRI. Single-voxel MRS data were collected from a single box volume which encompassed the lesion with a scanning time of approximately 10 min. MRS, interpreted blinded to pathology, was defined as positive if signal-to-noise ratio of the choline resonance peak was >2, negative otherwise. Lesions were prospectively classified as BI-RADS Category 2 (benign, proven by

prior biopsy), 4 (suspicious), 5 (highly suggestive of malignancy), or 6 (proven cancer). The MRI, MRS, and pathology findings were correlated. Statistical analysis was performed.

Results

One hundred and nine patients with 110 lesions were imaged. The median MRI voxel size was 2.6 cc (range 0.4–27). Cancer was present in 0/7 (0%) BI-RADS 2, 9/30 (30%) BI-RADS 4, 3/4 (75%) BI-RADS 5, and 69/69 (100%) BI-RADS 6, lesions. A choline peak was present in 76/81 (94%) cancers vs. 2 (7%) of 29 benign lesions. Overall, the sensitivity of MRS was 94% (76/81), specificity 93% (27/29), positive predictive value (PPV) 97% (76/78), negative predictive value 84% (27/32), and accuracy 94% (103/110). Five of the 81 cancers had no choline peak (MRS "false-negatives"). Factors accounting for the five false-negative cases included: susceptibility artifact from localizing clips placed at the time of biopsy (n=3), poor shimming with broad lipid peak which may have obscured the choline peak (n=1), and signal degradation due to motion artifact from breathing due to close proximity of a lesion to the chest wall (n=1). Two (7%) of 29 benign lesions had a choline peak (MRS "false positives"). Histologic findings in these two false-positive cases, both BI-RADS 4 lesions, were desmoid tumor (n=1) and lobular carcinoma in situ (n=1). For the 30 BI-RADS 4 lesions, if biopsy had only been performed in lesions with a choline peak at MRS, the PPV would have significantly increased from 30% (9/30) to 82% (9/11). Biopsy would have been spared in 19/30 (63%) women with BI-RADS 4 lesions and in 19/21 (90%) women with BI-RADS 4 lesions that were benign, without missing any of the cancers.

Conclusion

1H MRS can significantly improve the PPV of biopsy recommendations based on breast MRI. Our data suggest that incorporating MRS into the management algorithm for BI-RADS Category 4 lesions would maintain high sensitivity in the diagnosis of breast cancer while sparing most benign biopsies. These results compare favorably with results from prior studies.

References

1. Liberman L. Breast cancer screening with MRI: what are the data for patients at high risk? N Engl J Med 2004; 351:497–500.
2. Morris EA, Liberman L, Ballon DJ, et al. MRI of occult breast carcinoma in a high-risk population. AJR AM J Roentgenol 2003; 181:619–626.
3. Robson ME, Offit K. Breast MRI for women with hereditary cancer risk. JAMA 2004; 292:1368–1370.
4. Bartella L, Morris EA, Dershaw DD, et al. Proton MR spectroscopy with Choline Peak as Malignancy Marker Improves Positive Predictive Value for Breast Cancer Diagnosis: Preliminary Study. Radiology 2006; 239:686–692.
5. Negendank W. Studies of human tumors by MRS: a review. NMR Biomed 1992; 5:303–324.
6. Mackinnon WB, Barry PA, Malycha PL, et al. Fine Needle biopsy specimens of benign breast lesions distinguished from invasive cancer ex vivo with proton MR spectroscopy. Radiology 1997; 204:661–666.
7. Aboagye EO, Bhujwalla ZM. Malignant transformation alters membrane choline phospholipid metabolism of human mammary epithelial cells. Cancer Res 1999; 59:80–84.
8. Bolan PJ, Meisamy S, Baker EH, et al. In vivo quantification of choline compounds in the breast with 1H MR spectroscopy. Magn Reson Med 2003; 50(6):1134–43.
9. Stanwell P, Gluch L, Clark D, et al. Specificity of choline metabolites for in vivo diagnosis of breast cancer using 1H MRS at 1.5 T. Eur Radiol 2005; 15: 1037–1043.
10. Huang W, Fisher PR, Dulaimy K, Tudorica LA, et al. Detection of breast malignancy; diagnostic MR protocol for improved specificity. Radiology 2004; 232:585–591.
11. Tse GM, Heung HS, Pang LM, et al. Characterization of lesions of the breast with proton MR spectroscopy: comparison of carcinomas, benign lesions, and phyllodes tumors. AJR AM J Roentgenol 2003; 181:1267–1272.

MR-Mammography in breast reconstructions—potentials and pitfalls

Ellyete de Oliveira Canella
Instituto Nacional de Câncer, Rio de Janeiro, Brasil; Rede Labs D'Or, Rio de Janeiro, Brasil

1. Introduction

Despite improvements in the early detection of breast cancer, making it possible to identify lesions of small sizes and allowing conservative treatment, many patients are still submitted to nonconservative treatments with mastectomy.

The mastectomy is indicated in some types of carcinoma *in situ* and in situations where there is an absolute contra indication for conservative treatment as in multicentric disease, extensive tumors, when it is impossible to assure free margins in surgery, contra indication of radiotherapy, due to pregnancy or collagen disease, in previous radiotherapy in the mammary region and in cases when the esthetic outcome will certainly not be satisfactory.

The mastectomy represents a mutilation, which causes loss of body identity and low self-esteem, leading to emotional disturbances, and generally associated depression, that directly influence social and family relations. The opportunity of mammary reconstruction, with psychotherapeutic support, permits a woman to recover her self-esteem [2].

In the reconstructed breast, the challenge of the radiologist is to make the differential diagnosis between post-treatment changes and disease recurrence. With this objective, magnetic resonance imaging represents an exam of great potential, however; it is necessary that the radiologist knows the changes caused by each surgery and the magnetic resonance imaging findings.

2. Potential of magnetic resonance imaging

Considering that in the reconstructed breast exists the possibility of disease recurrence, which varies between 3–5% [3, 4], and that bilateral cancer is found in 4% [5] of the cases, magnetic resonance imaging represents an important exam in the evaluation of these patients.

For diagnostic purposes, if disease recurrence is suspected and when clinical exams, mammography and ultrasound are not conclusive, magnetic resonance imaging is indicated due to its capacity to differentiate between fibrosis and recurrence, an ability that has already been studied in conservative surgeries with radiotherapy [6, 7]. The diagnosis of suspect lesions in the magnetic resonance imaging, although it always needs histological diagnosis, many times represents the possibility of an earlier surgical approach, thus avoiding progression of the disease. To exclude the possibility of recurrence using magnetic resonance imaging means preserving the esthetic result, preserving the patient emotionally, eliminating the risk resulting from invasive methods and reduction of costs.

For screening [8], magnetic resonance imaging can detect recurrence in the reconstructed breast [9] and also in the contra-lateral breast [5]. Although there is not a consensus in the literature regarding the impact on survival, magnetic resonance imaging can be utilized as an adjunct to mammography.
In addition the above indications, magnetic resonance imaging represents an important tool in the diagnosis of complications in breasts reconstructed with implants [4].

3. Types of mastectomies
A mastectomy is the removal of the whole breast, which can be associated or not with surgical treatment of the axillary region.

3.1. Halstead radical mastectomy
This technique consists of the removal of the breast, including the skin and areolar-papillary complex, the pectoralis major muscle, preserving the clavicular portion, the small pectoral muscle and the lymph nodes of levels I, II, and III of the axillary region [1].
It currently represents the most mutilating surgery for the treatment of breast cancer and is only performed in specific cases, when besides the mammary lesion, there exists an extensive infiltration of the pectoral muscle and damage to axillary lymph nodes.
In the magnetic resonance imaging, the changes resulting from the Halstead radical mastectomy are the absence of the breast and of the pectoral muscles, which can be identified in the axial plane (Figure 1).

3.2. Modified radical mastectomy
The modified radical mastectomy has two variations: Patey technique and Madden technique [1]. In both procedures the breast is removed including the skin and areolar-papillary complex and the lymph nodes of levels I, II, and III of the axillary region. In the Patey technique there is the preservation of the pectoralis major muscle and the removal of the small pectoral muscle. In the Madden technique there is the preservation of both pectoral muscles.
If there is no infiltration of the pectoral musculature, the modified radical mastectomy has the same indications of the Halstead surgery and represents a technique of choice when radical treatment is considered, as the preservation of the pectoralis major muscle causes less deformity, facilitating the reconstruction of the breast and lesser functional limitation of the upper member.
In the magnetic resonance imaging, the changes resulting from modified radical mastectomy are also well identified in the axial plane, being the absence of the breast and the presence only of the pectoralis major muscle in the Patey surgery (Figure 2), and the presence of both pectoral muscles in the Madden surgery (Figure 3).

3.3. Total mastectomy or simple mastectomy
This surgery consists in the removal of the breast, including the skin and areolar-papillary complex, without approaching the axillary region.
Initially this was indicated in the treatment of ductal carcinoma in situ, however; currently it has been substituted by the skin sparing mastectomies (see item 3.4). It is still performed with a palliative purpose, to avoid the local evolution of the disease, in the stages IV or in the presence of an ulcerated tumor.
The magnetic resonance imaging findings related to simple mastectomy represents the absence of the breast and the preserved axillary region.

3.4. Skin sparing mastectomy
Consists in the removal of the and the areolar-papillary complex, sparing the remaining cutaneous covering.
In some cases of small tumors that are distant from the nipple, the skin and areolar-papillary complex sparing mastectomy can be performed and only the glandular portion of the breast is removed and all of the other structures are preserved.
The skin sparing mastectomy can be associated with the axillary treatment, and currently, represents the technique of choice when there is no possibility of a conservative treatment, however; it should only be performed together with immediate breast reconstruction [10, 11].
In the magnetic resonance imaging, the change resulting from the skin sparing mastectomy are associated with the type of breast reconstruction and the type of axillary surgery, observing also the preservation of the skin (Figure 4).

4. Axillary surgery
In the treatment of breast cancer, the objective of axillary approach is to perform the surgical staging of the axillary region and indicate the complementary therapy, representing an important prognostic factor. It can be associated with a simple mastectomy or with a skin sparing mastectomy.
The axilla approach can be radical or not radical, based on the biopsy of the sentinel lymph node.

4.1. Radical approach
This represents the removal of the axillary lymph nodes of levels I, II, and III [1] it can be done by the Halstead, Patey or Madden techniques. Currently the removal of the axillary lymph nodes is performed only in cases in which the biopsy of the sentinel lymph node is positive, and preferably, by the Madden technique.
In the magnetic resonance imaging of the breast, the type of axillary surgery utilized can be well observed in the axial plan, as already shown in the Figures 1, 2, and 3.

4.2. Sentinel lymph node biopsy
The sentinel lymph node is the first lymph node to receive lymphatic drainage from the tumor. The injection of a radiopharmaceutical or blue dye are used to identify the sentinel lymph node.
When the biopsy of the sentinel lymph node is positive, the removal of the axillary lymph nodes is indicated. When the sentinel lymph node biopsy is negative, it is considered that spreading of the disease to the other lymph nodes did not occur, and axillary dissection is not performed.
The sentinel lymph node biopsy represents an important advance in the surgical treatment of breast cancer, as it avoids the damaging effects of axillary dissection [12] and currently is the technique of choice of axillary approach, in association with conservative surgery, simple mastectomy or skin sparing mastectomy.
In the magnetic resonance imaging, the changes caused by the sentinel lymph node biopsy are minimal, since the muscles are preserved and the lymph nodes are present, observing only a discrete architectural distortion in the axillary region.

5. Types of breast reconstruction
In regards to the opportunity, the breast reconstruction can be immediate or late, the choice being determined by the analysis of several factors, such as the type of mastectomy, the staging of the disease, the clinical conditions and the patient's will.
Immediate and late reconstruction cause the same changes in the magnetic resonance imaging, being important the knowledge of the time between the reconstruction and the exam.
Regarding the type, the reconstruction can be autologous, heterologous or combination of both. In autologous reconstruction tissues from the patient are utilized (tranverse *rectus abdominis* myocuta-

neous flap, *latissimus dorsi* flap or tissue from other origin). In the heterologous reconstruction implants are utilized and tissues expanders that can be permanent or temporary. The choice of the type of reconstruction will depend mainly on the type of mastectomy and of the patient's condition (clinical condition, biotype, previous abdominal surgeries, smoking habits).
In the magnetic resonance imaging, each surgical technique has a specific characteristic, according to the description in the following items.

5.1. Reconstruction with tranverse rectus abdominis myocutaneous flap
A very common technique done with tranverse *rectus abdominis* myocutaneous flap (TRAM), allowing the extraction of a reasonable quantity of tissue for the breast reconstruction [4]. This flap is vascularized by superior epigastric vessels, it may be uni or bipedicle, utilizing one or both *rectus abdominis* and is migrated to the thorax through a subcutaneous tunnel. Simultaneously, an abdominoplasty is performed and the abdominal weakness is repaired with crystalline polypropylene. In the TRAM reconstruction, microsurgery techniques may also be used [13, 14, 15], through specific anastomosis, with the objective of increasing the vascularization, reducing the possibility of flap necrosis (supercharged TRAM) or with the objective of reducing the damage in the donating area (free TRAM).
In the magnetic resonance imaging, the pediculated TRAM has a characteristic aspect, with the reconstructed breast totally adipose and identification of the *rectus abdominis* muscle in the posterior portion (Figure 5).

5.2. Reconstruction with latissimus dorsi flap
It also represents a very utilized technique, principally when it is impossible to utilize the TRAM. The flap is composed of skin, a subcutaneous fat tissue and *latissimus dorsi* muscle [16], mainly vascularized by the toracodorsal artery. The migration of the flap to the thorax is done diagonally, by means also of a subcutaneous tunnel, with the distal extremity pointed towards the sternum. As it is a less robust flap, it needs a volume complement with the utilization of a silicon implant, which is placed between the flap and the pectoralis major muscle.
In magnetic resonance imaging the *latissimus dorsi* flap, together with or without the silicon implant, has a characteristic aspect, with the identification of the muscle from the lateral portion of the thorax to the reconstructed breast (Figure 6).

5.3. Reconstruction with tissue of other origin
These are less frequent techniques, utilizing the contra lateral breast tissue or epiplon, both with a poor esthetic result, and is only used when it is not possible to perform the other techniques.
With the utilization of the contra lateral breast tissue, the presence of parenchyma in the reconstructed breast is observed in the magnetic resonance imaging with a significant architectural distortion (Figure 7).
With the utilization of the epiplon, the reconstructed breast is observed in the magnetic resonance imaging filled with fat tissue and generally with small volume (Figure 8).

5.4. Reconstruction with implants
The utilization of implants is also an alternative for breast reconstruction [17].
In radical and simple mastectomies, the removal of the skin does not allow immediate inclusion of the implant. In these cases, during the same surgical period, an expander is included, that through the gradual filling with saline solution, produces distension of the skin and depending on the type, are later substituted by silicon implants or remain after expansion.
The expanders may have a magnetic incorporated or remote valves. In the expanders with an incorporated valve, it is embedded in the expander and there is a necessity of using a magnetic device to locate it, before the injection of the saline solution. The expanders with an incorporated valve block the acquisition of the image, as they create a signal drop off.
In the expanders with a remote valve, a flexible thin tube connects the expander to the valve, which is covered by a metallic material and can be placed in a location different of the expander. The expanders with a remote valve, permit the acquisition of the image, as they create a small signal drop off at the location of the valve. According to the current standards, the expanders are considered unsafe for use in magnetic resonance, due to the possibility of local damage of the incorporated valves and movement of the remote valves.
The expanders that can remain after the skin expansion have double lumen, an external of silicon and an internal filled with a saline solution, allowing expansion to the desired volume. A thin flexible tube joins the internal lumen to the valve, that is placed in a different site and both, tube and valve, are removed after obtaining the desired volume. This type of expander is considered safe for use in magnetic resonance after the removal of the valve (Figure 9).
In the case of skin sparing mastectomies, the implant can be inserted during the same surgical procedure, without the necessity of skin expansion (Figure 10).
Through the analysis of implants, in esthetical surgeries as well as reconstructive surgeries, magnetic resonance imaging permits characterizing the implant (type, number, location, symmetry) and helps in the diagnostic of the complications (fluid collection, position shifting, deformation, rupture and shrinking).

6. Differential diagnosis between post-treatment changes and disease recurrence
In order to do the differential diagnosis between post-treatment changes and disease recurrence it is necessary to analyze the all the factors that may influence the imaging.

6.1. Healing phases
There are three phases of healing: inflammation, proliferation, and maturation [19]. Although each phase has its own characteristics, they overlap each other in the process of healing and lesser the damage, quick and simpler is the recovery.
The inflammation phase lasts 4 days, depending on the extent of the wound and the nature of the aggressive agent. It is characterized by the reaction of the vascularized tissue to an aggressive agent with liquid and blood cell loss to the interstice. The damaged tissue release chemical mediators that cause vasodilatation and increase the permeability of the vessels. During this phase, occurs a haemostatic reaction to impede the exit of blood from the vessels and a cellular reaction to clean the wound, through leucocysts, lymphocytes and macrophages. As it is a very early phase, rarely is it indicated to perform magnetic resonance imaging during this period, but if it is performed, due to the intense inflammatory reaction there may be enhancement in the surgical site.

The proliferation phase lasts 5 to 20 days, but can extend itself for months. It is characterized by angiogenesis and production of collagen by the fibroblasts, filling the wound by a granular tissue. In the reconstructive surgeries, rarely is magnetic resonance imaging indicated in this phase, in virtue of it also being an early phase. However, if the exam is performed, enhancement in the surgical site is expected, due to the intense proliferative activity.
The maturation phase starts on the 21st day and may last years. It is characterized by the growth of the ephitelial cells to reestablish the continuity of the covering. The process of maturation is made more evident by the change of color of the scar, which changes from red to pink, and later to pearly white. If magnetic resonance imaging is performed during this phase, it is also possible to occur enhancement in the surgery site, with variable intensity. As recommended in the literature, to avoid false positives, the ideal situation is that the exam be performed after 6 months of surgery, as the healing process is expected to be complete at then end of this period.

6.2. Evolution of the changes

Edema, fluid collection, fat necrosis and fibrosis are commonly found in operated breasts [16, 20, 21].
The edema is a result of normal fluid accumulation in the interstitial space. In the case of surgery, the edema is inflammatory, representing the organism's defense process, where there is an increase in the permeability of the blood vessels allowing the arrival of specialized cells to eliminate external aggressors and to repair the damaged tissue. The edema may affect the whole breast and cause skin thickening. With magnetic resonance imaging, the edema spread out in the breast can be observed as hyper intense in T2 images. The skin thickening is well evidenced in the sequences weighted in T2 with fat suppression, without enhancement or with a low intensity enhancement in the dynamic study (Figure 11). In relation to the evolution, the edema is intense in the initial phase after the surgery, regresses slowly and is expected to disappear in 6 months. Tumours infiltrating the breast also cause skin thickening and diffuse edema but have a progressive character in relation to time and exhibit more intense heterogeneous enhancement that may be associated with other lesions of the breast [4, 22].
The most common fluid collections in breast surgery are hematoma and seroma. When they have a large volume, they require surgical drainage, but when of small size they may pass clinically unnoticed and be only detected in the image exams. The hematoma generally happens early, has an acute beginning and may represent complication from the surgical procedure. In the magnetic resonance imaging, the hematoma has a variable signal in the sequences weighted in T1 and T2 without fat suppression, in accordance with the evolution of the hemoglobin. In operated breasts, it generally is found in subacute or chronic phase, with a high-intermediary signal in T1 and low signal in T2. The seroma is a result of the accumulation of blood and residue cells, lipolysis and lymphatic fluid. It appears early, in variable quantity and is expected to be absorbed over time, but the process may last months and years [23]. In magnetic resonance imaging, the seroma has a variable sign in the sequences weighted in T1 and T2, in accordance to the predominance of components. If there is a predominance of blood, it may be the evidence of the same evolution of a intensity sign of hematoma. If there is predominance of one of the components, the behavior of other liquids is observed in relation to the intensity signal (Figure 12). By the intensity sign in the magnetic resonance imaging, hematomas e seromas do not cause problems in the differential diagnosis of disease recurrence in reconstructed breasts.
Fat necrosis a special type of necrosis that occurs after breast trauma, due to external leaking of lipolytic enzymes to the fat tissue, causing rupture and liquefaction of the fat cells. This process causes an inflammatory reaction similar to a foreign body, with the accumulation of macrophages and tends to be chronic, with duration of more than 3 months. In magnetic resonance imaging, fat necrosis has a variable appearance, in accordance with the degree of the fat liquefaction. Generally it appears irregular, with signs of fat (possibly with a level) [24], surrounded by fibrosis and with variable enhancement around the lesion, due to the inflammatory process. The presence of fat into the lesion reduces the possibility of recurrence (Figure 13). The fat necrosis can also present itself as a solid irregular mass without a central area of fat and with enhancement of variable intensity, simulating a recurrence [4] and representing a significant cause of false positive (Figure 14).
The fibrosis occurs when, there is no adequate organization during the wound repair [25]. In the image exams, the fibrosis presents itself as an irregular or spiculated mass [4], making the differential diagnosis relating to recurrence difficult. In the magnetic resonance imaging, the fibrosis has a low signal intensity in the sequences weighted in T2 without fat suppression, without enhancement or with a low intensity enhancement, slowly and progressive, in accordance with the phase in which the exam is performed.

6.3. Radiotherapy

Radiotherapy is not a required adjuvant treatment after breast reconstruction, but it is indicated in some cases, as for example: in the immediate breast reconstructions in patients with tumors T3 and T4 or if there is more than 50% of metastatic involvement in the axillary lymph nodes and in the skin sparing mastectomies when there is residual disease without possibility of excision. Radiotherapy causes dilation and vessel damage, leading to neovascularization, has cumulative and progressive effects, potentializing the changes from the surgery. In irradiated breasts the edema is longer lasting, establishing itself or regressing within 3 years [26, 27], the fluid collections has reduced absorption and may last for years. The enhancement induce by radiotherapy does not form mass, and tends to be regional or diffuse, with variable intensity and velocity. It is common to occur during the first 8 months after radiotherapy, tends to regress between 10 to 18 months and is insignificant in 93% of the cases after 18 months.

6.4. Recurrence disease

In reconstructed breasts, the recurrence can manifest itself by mass or non-mass lesion, both generally away from the flap. In the majority of lesions, the enhancement pattern tends to be heterogeneous or peripheral, fast and presents washout (Figure 15) [28]. Magnetic resonance imaging can also detect recurrence of the chest wall [29, 30], which manifests itself by an infiltrating mass.

7. Final considerations

The analysis of the reconstructed breast represents fundamental elements for diagnosis between the changes resulting from the surgery and recurrence: the knowledge about the surgical techniques, the correlation of findings considering the time since the surgery and the radiotherapy, the location of the lesion and the enhancement pattern where the analysis of all elements is recommended.

Acknowledgements: I would like to express my gratitude to Carlos Alberto Jaimovich, Clarissa Canella Moraes do Carmo, Eric Bevan Muller and Luis Antonio de Andrade Mendonça for their assistance.

8. References

1. Franco JM, Santos RA, Müller P, Malfacini SS (1997) Reconstrução mamária imediata. In: Franco JM Mastologia Formação do especialista, 1st edn. Atheneu, Rio de Janeiro, pp 251–258.
2. Jaimovich CA (2001) Reconstrução mamária pós-mastectomia com expansores e implantes de silicone mais poliuretano. In: Ribeiro RC, Saltz R Cirurgia da mama estética e reconstrutiva, 1st edn. Revinter, Rio de Janeiro, pp 123–139.
3. Howard MA, Pólo K, Pusic AL et al (2006) Breast cancer local recurrence after mastectomy and TRAM flap reconstruction: incidence and treatment option. Plast Reconstr Surg 117(5):1381–1386.
4. Devon RK, Rosen MA, Mies C et al (2004). Breast reconstruction with a transverse rectus abdominis myocutaneous flap: spectrum of normal and abnormal MR imaging findings. Radiographics 24:1287–1299.
5. Lehman CD, Blume JD, Thickman D et al (2005) Added cancer yield of MRI in screening the contralateral breast of women recently diagnosed with breast cancer: results from the International Breast Magnetic Resonance Consortium (IBMC) trial. J Surg Oncol 92 (1):9–15.
6. Gorechlad JW, McCabe EB, Higgins JH et al (2008) Screening for recurrences in patients treated with breast-conserving surgery: is there a role for MRI? Ann Surg Oncol 15(6):1703–1709.
7. Preda L, Villa G, Rizzo S et al (2006) Magnetic resonance mammography in the evaluation of recurrence at the prior lumpectomy site after conservative surgery and radiotherapy. Breast Cancer Res 8(5):R53.
8. Saslow D, Boetes C, Burke W et al (2007) American Cancer Society guidelines for breast screening with MRI as an adjunct to mammography. CA Cancer J Clin 57: 75–89.
9. Stralman K, Mollerup CL, Kristoffersen US, Elberg JJ (2008) Long-term outcome after mastectomy with immediate breast reconstruction. Acta Oncol 47(4):704–708.
10. Fersis N, Hoenig A, Relakis K, Pinis S, Wallwiener D (2004) Skin-sparing mastectomy and immediate breast reconstruction: incidence of recurrence in patients with invasive breast cancer. Breast 13(6):488–493.
11. Omranipour R, Bobin JY, Esouyeh M (2008) Skin Sparing Mastectomy and Immediate Breast Reconstruction (SSMIR) for early breast cancer: eight years single institution experience. World J Surg Oncol 27(6):43.
12. Kootstra J, Hoekstra-Weebers JE, Rietman H et al (2008) Quality of life after sentinel lymph node biopsy or axillary lymph node dissection in stage I/II breast cancer patients: a prospective longitudinal study. Ann Surg Oncol; 15(9): 2533–41,
13. Viterbo F, Icibaci A (2001) Princípios de microcirurgia relacionados a reconstrução mamária. In: Ribeiro RC, Saltz R Cirurgia da mama estética e reconstrutiva, 1st edn. Revinter, Rio de Janeiro, pp 195–200.
14. Nohira K, Yamamoto Y, Shintomi Y (2001) Retalho miocutâneo do reto do abdome com fluxo aumentado através de microanastomose vascular (supercharged). In: Ribeiro RC, Saltz R Cirurgia da mama estética e reconstrutiva, 1st edn. Revinter, Rio de Janeiro, pp 201–210.
15. Chernyak V, Rozenblit AM, Greenspun DT et al (2009) Breast reconstruction with deep inferior epigastric artery perforator flap: 3.0-T gadolinium-enhanced MR imaging for preoperative localization of abdominal wall perforators. Radiology 250(2):417–424.
16. Abdalla HM, Shalaan MA, Fouad FA, Elsayed AA (2006) Immediate breast reconstruction with expander assisted latissimus dorsi flap after skin sparing mastectomy. J Egypt Natl Canc Inst 18 (2):134–140.
17. Middleton MS (1997) Breast implant classification. In: Gorczyca DP, Brenner RJ The augmented breast, 1st edn. Thieme Medical, New York, pp 28–44.
18. Shellock FG (2001) Breast tissue expanders and implants. In: MRI safety. Avaible via http://www.mrisafety.com/list_search.asp. Accessed 12 Jul 2009.
19. Gragnani A, Keira SM, Hochman B, Ferreira LM (2007) Cicatrização, fibroplasia e fatores de crescimento. In: Ferreira LM, Schor N Cirurgia Plástica. Guias de Medicina ambulatorial e hospitalar, 1st edn. Manole, São Paulo, pp 49–53.
20. Kang BJ, Jung JI, Park C et al (2005) Breast MRI findings after modified radical mastectomy and transverse rectus abdominis myocutaneous flap in patients with breast cancer. J Magn Reson Imaging 21(6):784–791.
21. Rieber A, Schramm K, Helms G et al (2002) Breast-conserving surgery and autogenous tissue reconstruction in patients with breast cancer: efficacy of MRI of the breast in the detection of recurrent disease. Eur Radiol 13(4):780–787.
22. Kaiser WA (2007) Signs in MR-Mammography, 1st edn. Springer, New York, pp 82–83.
23. Oliveira VM, Roveda Junior D, Lucas FB et al (2007) Late seroma after breast augmentation with silicone prostheses: a case report. Breast J 13(4):421–423.
24. Kaiser WA (2007) Signs in MR-Mammography, 1st edn. Springer, New York, pp 186–187.
25. Krishnamurthy R, Whitman GJ, Stelling CB, Kushwaha AC (1999) Mammographic findings after breast conservation therapy. Radiographics 19:53–62.
26. Kaiser WA (2007) Signs in MR-Mammography, 1st edn. Springer, New York, pp 260–261.
27. Padhani AR, Yarnold J, Regan J, Husband JE (2003) Dynamic MRI of breast hardness following radiation treatment. J Magn Reson Imaging 17(4):427–434.
28. Kaplan JB, Dershaw DD (2004) Posttherapeutic magnetic resonance imaging. In: Morris EA, Liberman L (ed) Breast MRI, 1st edn. Springer, New York, pp 227–237.
29. Yilmaz MH, Esen G, Ayarcan Y et al (2007) The role of US and MR imaging in detecting local chest wall tumor recurrence after mastectomy. Diagn Interv Radiol 13(1):13–18.
30. Morris EA, Schwartz LH, Drotman MB et al (2000) Evaluation of pectoralis major muscle in patients with posterior breast tumors on breast MR images: early experience. Radiology 214(1):67–72.

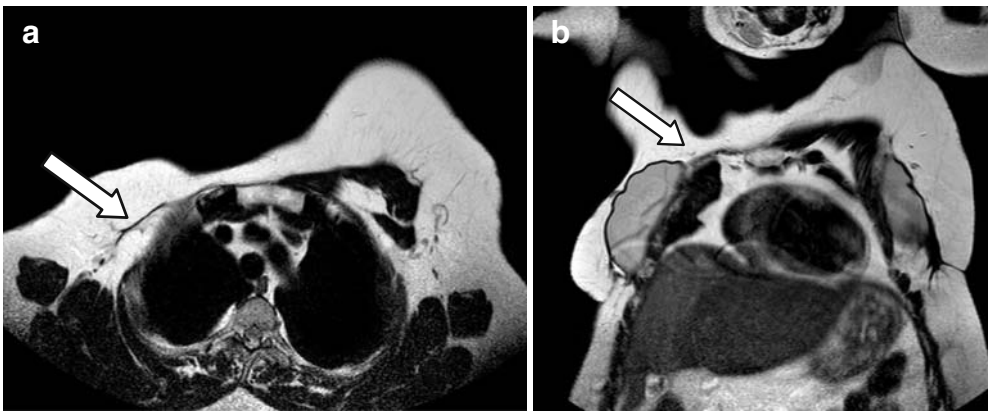

Figure 1—Case number 8544 of February 13th, 2009; 58 year-old patient, Halstead radical right mastectomy in 1996, reconstruction with implants in 2008; T2-weighted sequences in the sagittal (A) and coronal (B) plans showing the abscence of the right pectoralis muscles (white arrows).

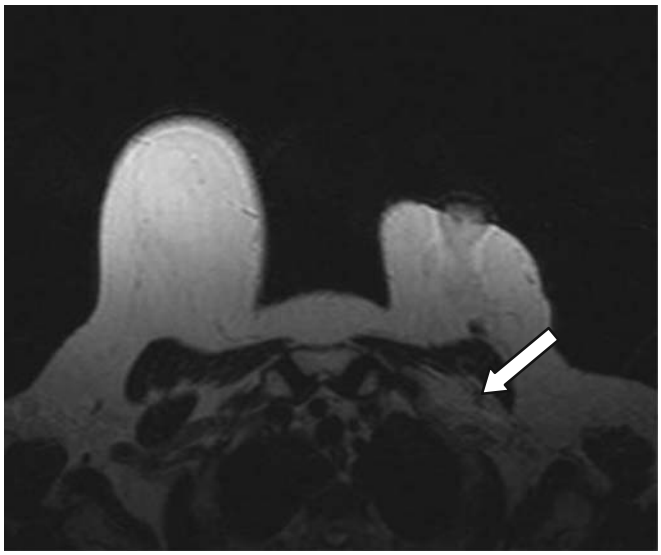

Figure 2—Case number 3313 of April 25th, 2005; 56 year-old patient, left radical mastectomy in 2003, reconstruction with TRAM flap after 6 months; T2-weighted sequence in the transverse plan showing the absence of the left pectoralis minor muscle (white arrow).

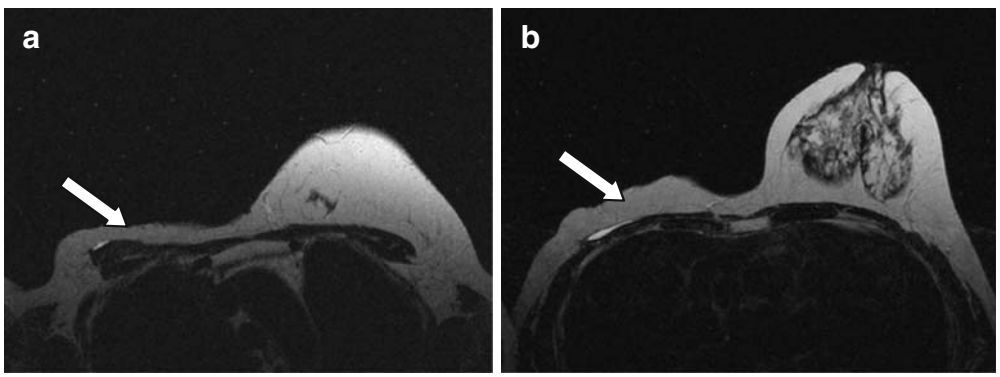

Figure 3—Case number 9105 of May 28th, 2009; 57 year-old patient, right radical mastectomy and radiotherapy in 2006; T2-weighted sequences in the axial plan showing (white arrows) the presence of both pectoralis muscles (A) and the absence of the right breast (B).

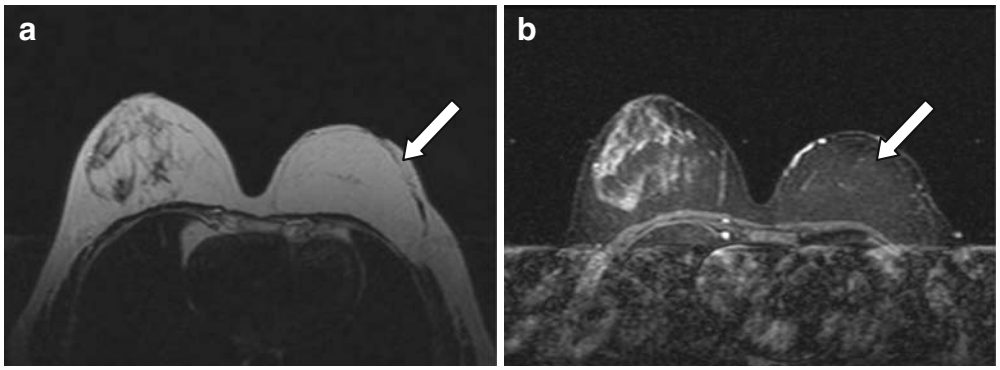

Figure 4—Case number 2818 of October 25th, 2004; 53 year-old patient, right skin sparing mastectomy and reconstruction with TRAM flap in 2002; T2-weighted sequences with (A) and without (B) fat suppression in the axial plan showing the skin and the subcutaneous fat tissue of the left breast (white arrows).

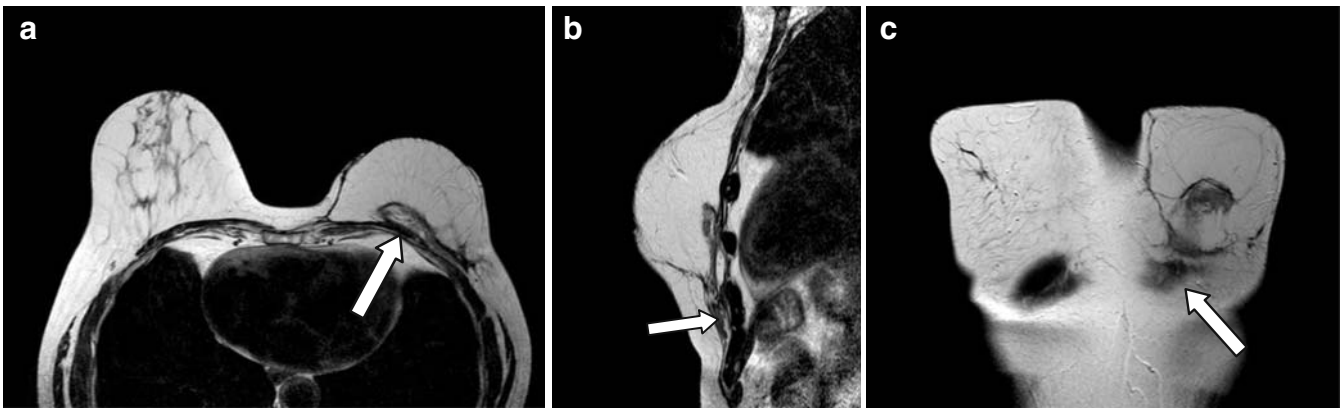

Figure 5—Case number 8640 of March 12th, 2009; 58 year-old patient, left skin sparing mastectomy and TRAM reconstruction flap in 2007; T2-weighted sequences in the transverse (A), sagittal (B) and coronal (C) plans showing the *rectus abdominis* muscle in the posterior portion of the reconstructed breast (white arrows).

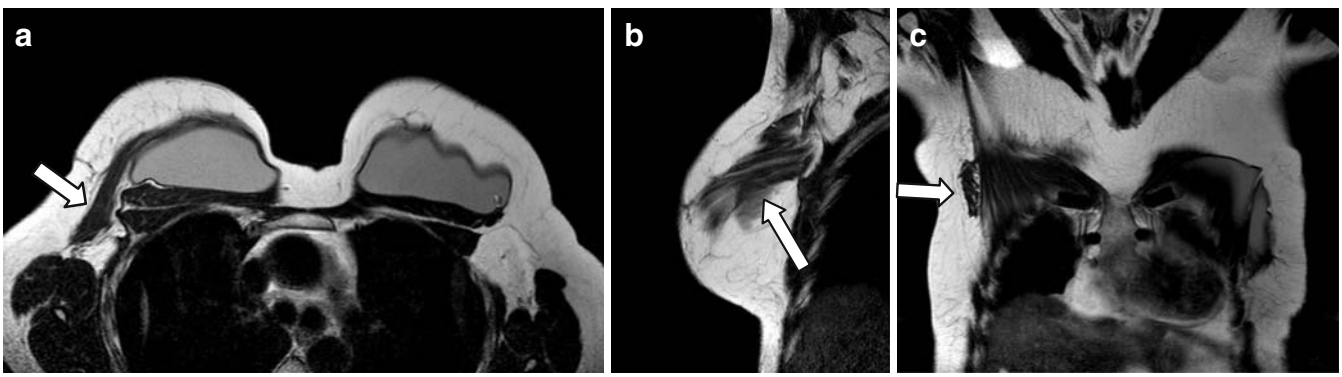

Figure 6—Case number 8726 of March 26th, 2009; 48 year-old patient, left radical mastectomy, breast reconstruction with *latissimus dorsi* flap and implants in 2005; T2-weighted sequences in the transverse (A), sagittal (B) and coronal (C) plans showing the *latissimus dorsi* muscle in the lateral portion of the chest wall (white arrows).

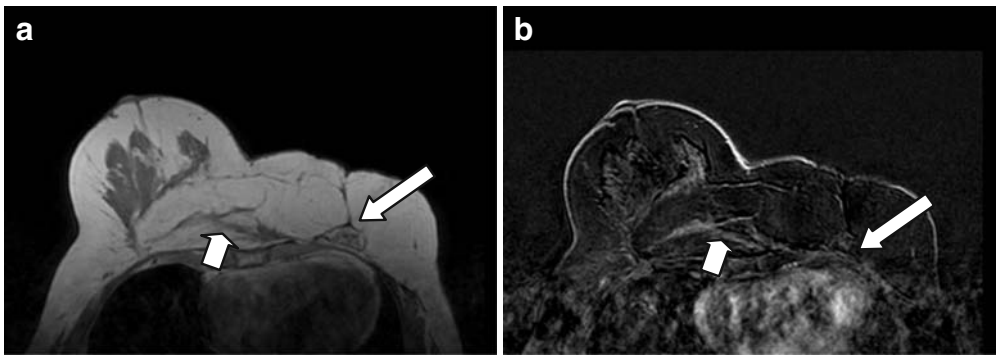

Figure 7—Case number 5334 of December 27th, 2006; 64 year-old patient, left radical mastectomy in 1984; breast reconstruction with the contra lateral breast in 1997; dynamic study before the Gadolineum injection (A) and subtraction (B) in the transverse plan showing the enhancement of the breast tissue (small white arrows); note the *rectus abdominis muscle* (big white arrows).

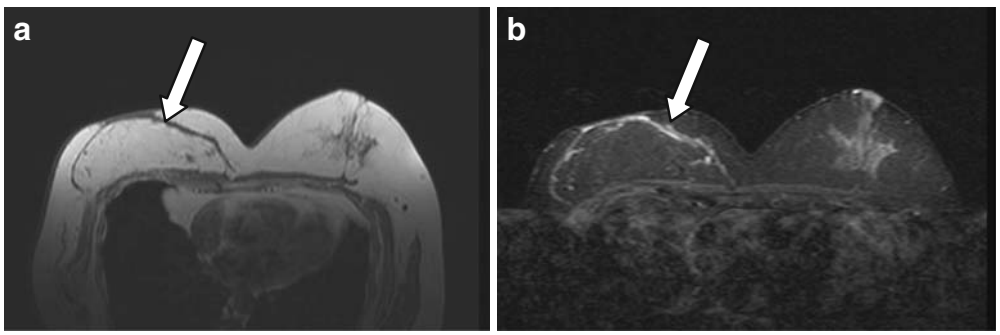

Figure 8—Case number 3131 of February 14th, 2005; 57 year-old patient, right mastectomy in 1997 and reconstruction with epiplon in 1997; T2-weighted sequences without fat suppression (A) and with fat suppression (B) in the transverse plan showing the reconstructed breast with epiplon (white arrows).

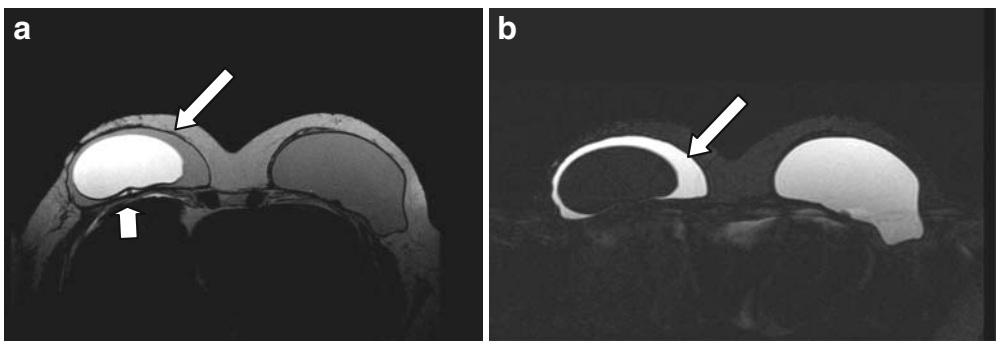

Figure 9—Case number 8020 of October 29th, 2008; 55 year-old patient, right mastectomy in 2003; reconstruction with double lumen expander in 2003; implant in the left breast in 2008; T2-weighted (A) and "silicone only" (B) sequences in the transverse plan showing the double lumen expanders bilaterally (white arrows); note the flexible tube remaining after complete filling in A (small white arrow).

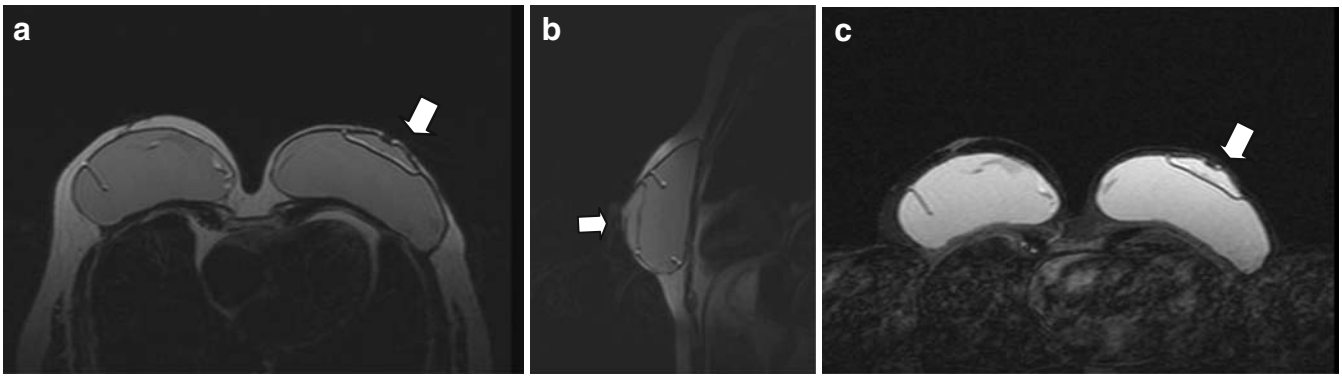

Figure 10—Case number 3951 of November 23th, 2005; 51 year-old patient, left radical mastectomy in 2002 and breast reconstruction with expander in 2003; the expander was changed by two implants on the left side and one was included on the right side; T2-weighted sequences in the transverse (A) and sagittal (B) plans, and T2-weighted sequences with fat suppression in coronal (C) plan showing the left breast reconstruction with 2 implants, the smallest specific for the nipple reconstruction (white arrows).

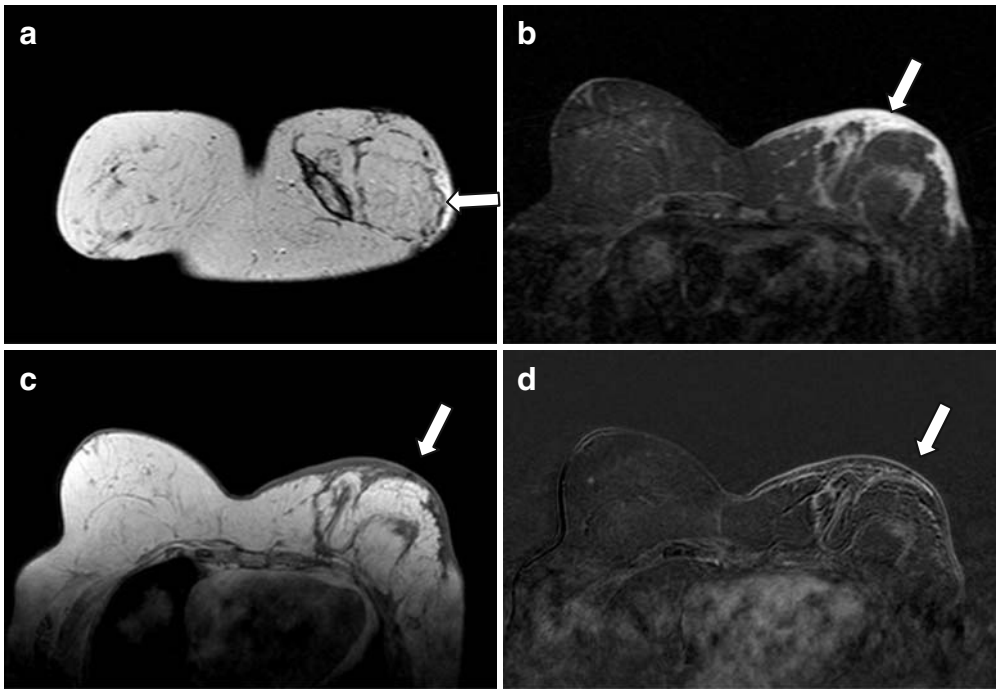

Figure 11—Case number 8735 of March 26th, 2009; 77 year-old patient, left skin sparing with *latissimus dorsi* flap and implant reconstruction in November 2008; T2-weighted sequences in coronal plan (A), T2-weighted sequence with fat saturation (B), dynamic study before the Gadolinium injection (C) and subtraction (D) in the transverse plans showing the edema (white arrows in A, B and C) and the low intensity enhancement due to the recent surgery (white arrow D).

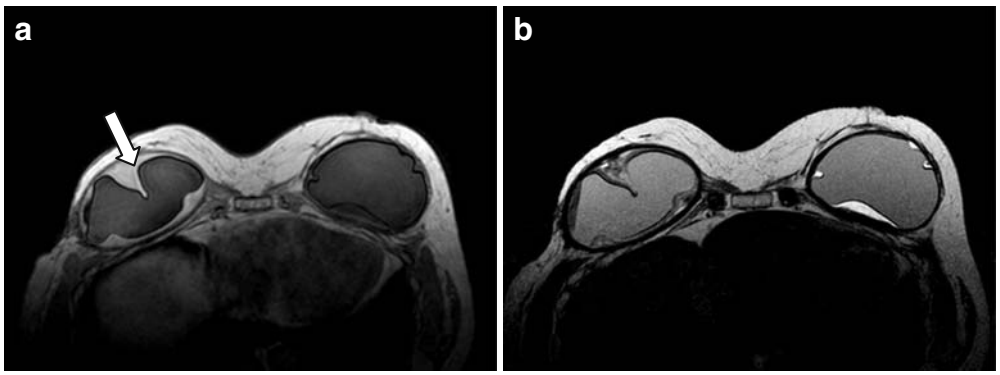

Figure 12—Case number 8689 of March 19th, 2009; 60 year-old patient, right skin sparing mastectomy and bilateral implants in 1997; T1 (A) and T2-weighted (B) sequences in the transverse plan showing fluid collection around the implants; note also blood on the right side with the high intensity sign in A (white arrow).

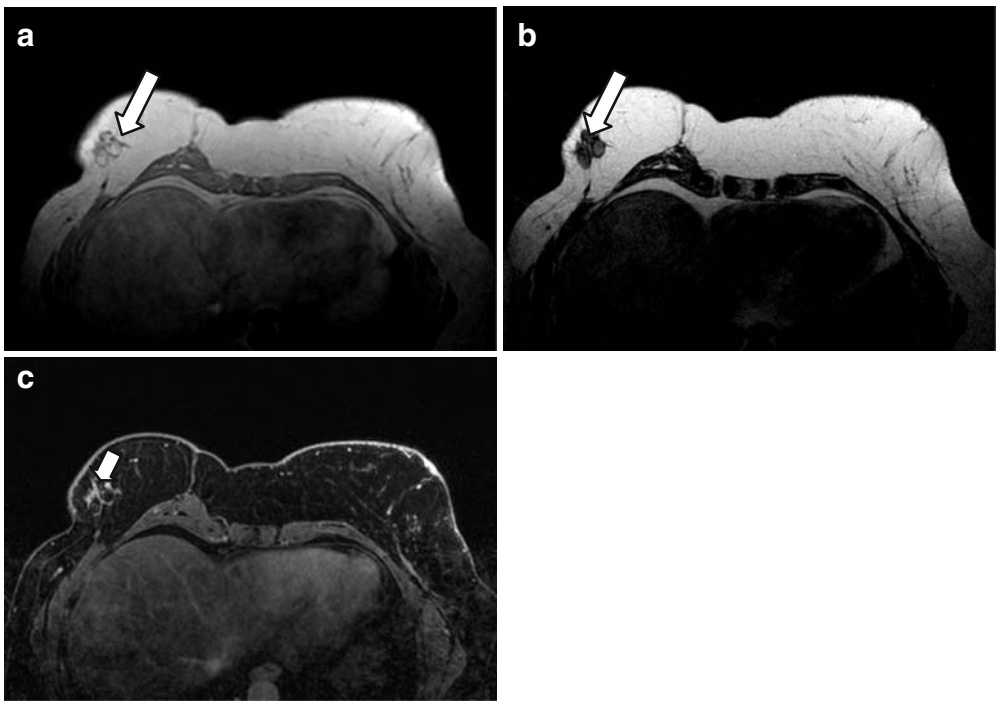

Figure 13—Case number 8901 of April 27th, 2009; 50 year-old patient, right radical mastectomy and breast reconstruction with TRAM flap in 2006; T1 (A), T2-weighted (B) and T1-weighted with fat suppression (C) sequences in the transverse plan showing fat necrosis (white arrows); note the characteristic intensity sign of fat necrosis in C (small white arrow).

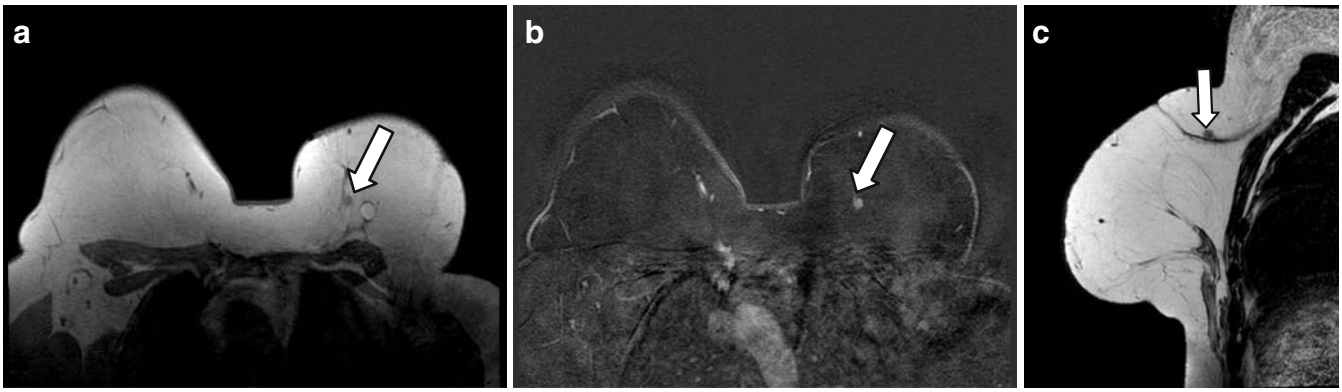

Figure 14—Case number 8861 of April 20th, 2009; 37 year-old patient, left radical mastectomy in 2003 and breast reconstruction with TRAM flap in 2004; dynamic study before the Gadolinium injection (A), subtraction (B) in the transverse plan and T2-weighted sequence in the sagittal plan (C) showing an enhancement mass away from the flap, confirmed as fat necrosis (white arrows); note the atypical pattern of the fat necrosis without central fat tissue representing pitfall.

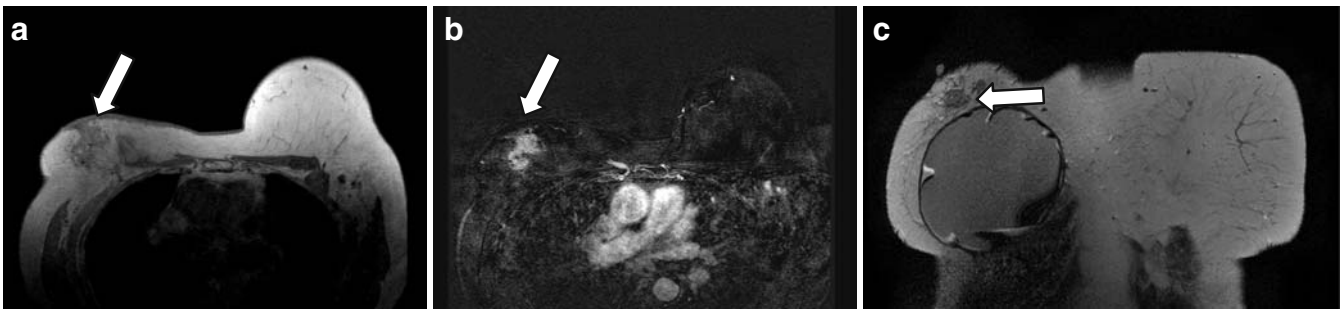

Figure 15—Case number 8131 of November 17th, 2008; 70 year-old patient, right radical mastectomy in 1999 and breast reconstruction with expansor changed for implant in 2003; dynamic study before the Gadolinium injection (A), subtraction (B) in the transverse plan and T2-weighted sequence in the coronal plan (C) showing an enhancement mass in the breast reconstruction suggesting recurrence disease (white arrows).

The use of high relaxivity contrast agents for breast MR in imaging

Luca A. Carbonaro, Nicola Verardi, Francesco Sardanelli
Università degli Studi di Milano, Dipartimento di Scienze Medico-Chirurgiche, IRCCS Policlinico San Donato, Via Morandi 30, 20097 San Donato Milanese, Milan, Italy

1. Introduction

The first applications of magnetic resonance imaging (MRI) to the breast with classic T1-, proton density, or T2-weighted sequences were disappointed. This scenario changed dramatically with the introduction of intravenously administered paramagnetic Gd-based contrast agents (GBCAs) [1].

The neoangiogenesis related to the tumor growth determines an increased vascularity (more and larger vessels) with increased permeability (up to eightfold the normal parenchyma). This affects the behavior of GBCAs: breast tumors (especially malignancies) show contrast enhancement higher than that of normal gland parenchyma. Moreover, an increased interstitial space (up to three-fivefold the normal parenchyma) works as a large distribution space for the contrast agent [2].

In this article, after illustrating the difference in chemical and pharmacokinetic properties of the mainly used GBCAs, we discuss the applications, advantages, limitations and new possibilities of high relaxivity contrast agents for breast MRI.

2. Gd-based contrast agents for breast MRI

The non-selective GBCAs used for clinical breast MRI (Table 1) are characterized by two-compartment pharmacokinetics, i.e. they exhibit a linear relation between dose and tissue concentration due to an extracellular (intravascular↔interstitial) biodistribution, without accumulation in target organs or crossing through cell membranes [3].

Extracellular GBACs are formed by chelation of gadolinium to organic ligands. Chelation serves to eliminate heavy metal toxicity by preventing the cellular uptake of free gadolinium ion Gd3+ which has high toxicity. Chelation maintains the biodistribution of GBCAs within the extracellular space and enhances renal filtration, resulting in a biological half life of approximately 1.5–2.0 h in patients with normal renal function.

There are two structurally distinct categories of GBCAs: the macrocyclic molecules where Gd3+ is caged in the preorganized cavity of the ligand and linear molecules. The stability of the molecule depends on its kinetic, thermodynamic, and conditional stability. These parameters are not only related to the molecular structure, although macrocyclic GBCAs have a higher stability than linear GBCAs. Because of their relatively low stability, the pharmaceutical solutions of linear nonionic gadolinium complexes (gadodiamide and gadoversetamide) include excess chelate to ensure the absence of toxic free Gd3+ cations in the pharmaceutical solutions [4]

The recommended dose of GBCAs for the majority of clinical indications is 0.1 mmol/kg of body weight and the recommended injection rate is 2–3 ml/s (0.5 mmol/ml) [5,6]. All nonspecific Gd-based contrast agents are available in a concentration of 0.5 mmol/ml except gadobutrol which is available in a concentration of 1.0 mmol/ml.

Nonspecific extracellular Gd-based contrast agents (gadopentetate, gadoterate, gadodiamide, gadoteridol, gadobutrol) have pharmacokinetics similar to those of iodinated contrast agents and are excreted almost exclusively by passive glomerular filtration through the kidneys, without secretion nor reabsorption. In patients with normal renal function about 98% of these agents are excreted within 24 h of injection [7].

3. Gadobenate dimeglumine as a high relaxivity agent

MRI efficacy of GBCAs is not determined just by their pharmacokinetic properties but also by their magnetic properties, described by their r1- and r2-relaxivities. All the nonselective GBCAs have different structures and properties [8] but have similar r1-relaxivity values of approximately 4.2–5.3 L $mmol^{-1}$ s^{-1} at 1.5 T [9] (see Table 1) and produce similar contrast enhancement when administered at the same dose.

Gadobenate dimeglumine (Gd-BOPTA) is an octodentate chelate of the paramagnetic ion gadolinium, whose aromatic tail can interact with several small hydrophobic pockets on the human serum albumin [10]. This leads to a transient, noncovalent, weak protein binding to serum albumin that allows a biliary excretion 2–4% [11]. sufficient for a long lasting enhancement of the normal liver parenchyma. Moreover, this binding has proven to be generally useful for better delineate malignant lesions taking advantage of the pathologic concentration of serum albumin in human tissue with abnormal vascular permeability, i.e., inflammation or angiogenesis associated with tumor growth [12]. In fact, in certain tumors, endothelial fenestration can become quite large (up to 30–70 nm) allowing extravasation of relatively big proteins as serum albumin [13].

The weak and transient interaction of gadobenate dimeglumine with serum albumin results in a slowing of the tumbling rate of the Gd complex, which allows for a longer rotational correlation time with inner shell water protons in adjacent tissues [14]. This means shorter T1, T2, and T2* relaxation time constants that produce higher signal enhancement on T1-weighted MR images and signal loss on T2-and T2*-weighted MR images (one exception is short inversion time inversion recovery (STIR) sequences with gadolinium accumulation leading to signal loss as a result of T1 shortening) [4]. Thus, gadobenate dimeglumine is a high relaxivity contrast agent because it possesses r1-relaxivity values of approximately 6.7 L $mmol^{-1}$ s^{-1} at 1.5 T [9].

4. The high relaxivity approach for breast MRI

In the intervening 20 years, most breast MR studies have been performed with agents such as gadopentate dimeglumine (Gd-DTPA), gadodiamide (Gd-DTPA-BMA), or gadoteridol (Gd-HP-DO3A).

In 2003, the efficacy and safety of Gd-BOPTA in breast MR were clearly demonstrated in a European multicentric dose-finding study of 189 patients with known or suspected breast cancer [15]. In this study, patients were randomized to 4 different groups: Gd-BOPTA, 0.05 mmol/kg (n=48); Gd-BOPTA, 0.1 mmol/kg (n=47); Gd-BOPTA, 0.2 mmol/kg (n=47); Gd-DTPA, 0.1 mmol/kg (n=47). MR imaging was performed using a standard technique (coronal 3D T1-weighted images before and 2, 4, 6 and 8 min after intravenous injection of contrast agent at 2 ml/s, followed by a 10–20 ml saline flush). MR images were evaluated for lesion presence and characteristics by two independent off-site observers blinded to the patients' identities and study group assignments. On the basis of the single-observer sensitivities for detecting breast lesions (number of lesions detected at MR versus number of lesions diagnosed at biopsy or surgery × 100) on unenhanced images, on contrast-enhanced images and for the combined dataset of unenhanced and enhanced images, the single dose (0.1 mmol/kg) of Gd-BOPTA was considered to be at least equal to, if not superior to, the single dose of Gd-DTPA. Furthermore, there was no gain in sensitivity with higher doses of Gd-BOPTA. When different doses of Gd-BOPTA were compared, the number of false-positive interpretations was greater at the double dose (0.2 mmol/kg) than at the single dose (0.1 mmol/kg) of Gd-BOPTA. The authors concluded that the single dose of Gd-BOPTA was optimal for gadolinium-enhanced breast MR imaging. When the results for both observers were combined, the sensitivity and accuracy of diagnosis for the single dose of Gd-BOPTA were superior while the specificity was slightly lower than that of a single dose of Gd-DTPA. The lower specificity for Gd-BOPTA may be explained by the fact that the group of 47 women imaged at 0.1 mmol/kg Gd-BOPTA had more benign lesions (20 versus 13) and more fibroadenomas (8 versus 0) than the 47 age-matched women imaged with a similar dose of Gd-DTPA.

In order to overcome the bias of a nonuniform disease distribution among the treatment arms, as observed by Hylton [16], Pediconi et al. published an intraindividual study on 26 consecutive women suspected of having breast cancer on the basis of conventional mammography and sonography [17]. Each patient underwent two identical MR examinations at 1.5 T, separated by more than 48 h but less than 72 h. A T1-weighted three-dimensional gradient-echo sequence was used, and images were acquired before and at 0, 2, 4, 6, and 8 min after injection of gadopentetate dimeglumine or gadobenate dimeglumine at an identical flow rate of 2 ml/s. The administration of Gd-based contrast agent was randomized in order to get 13 patients administered gadobenate dimeglumine as the first contrast agent and gadopentetate dimeglumine as the second and 13 patients administered with inverse order. Separate and combined assessment of unenhanced, contrast-enhanced, and subtracted images was performed blindly by two readers in consensus. The surgery was performed not later than one month after the second MR examination. Follow-up of lesions diagnosed as benign was performed with both mammography and MR imaging at intervals of 12–18 months after initial diagnosis. MR mammography with gadobenate dimeglumine depicted significantly more lesions (45 of 46) than did that with gadopentetate dimeglumine (36 of 46), and detected lesions were significantly more conspicuous with gadobenate dimeglumine. Confidence for characterization was significantly greater with gadobenate dimeglumine. Comparison of the contrast agents for their ability to help identify malignant lesions revealed significant superiority for gadobenate dimeglumine: Sensitivity, specificity, positive predictive value, negative predictive value, and overall accuracy for malignant lesion identification were, respectively, 94.7%, 100%, 100%, 80.0%, and 95.6% with gadobenate dimeglumine and 76.3%, 100%, 100%, 47.1%, and 80.4% with gadopentetate dimeglumine.

This study was then confirmed by the same group from Rome in 2008 on a larger number of patients (47 women) with 78 pathologically-proven lesions [18]. Overall, 75/78 (96.2%) lesions were detected on breast MRI after gadobenate dimeglumine administration versus 62/78 (79%) detected on MRI after gadopentetate dimeglumine administration. The principal benefit of gadobenate dimeglumine was for the detection of the 50 malignant lesions: 49 (98%) were detected after gadobenate dimeglumine compared

with only 38 (76%) seen after gadopentetate dimeglumine. The malignant lesion not detected after gadobenate dimeglumine was a small (≤5 mm) DCIS in a patient with two DCIS lesions confirmed after lumpectomy. Significantly better diagnostic performance was noted with gadobenate dimeglumine than with gadopentetate dimeglumine, respectively, for sensitivity (98.0% vs 76.0%), accuracy (88.5% vs 69.2%), PPV (86.0% vs 76.0%), and NPV (95.2% vs 57.1).

The resulting increased conspicuity not only improves the confidence for characterization of lesions, but also the detection of small malignant foci with poor neoangiogenesis, achieving a higher sensitivity.

5. Effect of breast MRI on surgical decision-making

A large number of published studies are highly concordant in finding that breast MR is the most sensitive imaging technique currently available for local breast cancer staging [5]. The fact that contrast-enhanced breast MRI impacts on therapy planning in patients with a newly diagnosed breast cancer has been described in several works with a mean change of surgical treatment in about 19.4% of patients in a recent meta-analysis [19]. The impact of preoperative MRI on disease-free or overall survival is still matter of debate. The results of two randomized studies are awaited.

Using gadobenate dimeglumine as a GBCA, Pediconi et al [20] studied a series of 164 women with 175 breast lesions considered suspicious or highly suspicious (BI-RADS IV–V) for malignancy with conventional imaging. Contrast-enhanced MR revealed 51 additional lesions in 34/164 patients; multifocal and multicentric cancer was detected in seven and four additional patients, respectively. Contralateral foci in 21 additional patients and pectoral muscle infiltration in two additional patients were found. On a total of 226 lesions detected on MRI, 211 were determined to be malignancy and 15 non-malignant at histologic evaluation. The 51 lesions missed on mammography/ultrasound compared to contrast-enhanced MR comprised 47 that were histologically confirmed to be malignant and four that were confirmed to be non-malignant. Because of the inclusion criteria of the study, no lesion detected on mammography/ultrasound was considered a true negative result. The values for sensitivity, accuracy and PPV of mammography/ultrasound for the identification of malignant lesions were 77.3%, 72.1%, and 91.4%, respectively. The values for sensitivity, accuracy and PPV of breast MRI for the identification of malignant lesions were 100%, 93.4%, 93.4%, respectively. The potential impact of breast MRI on surgical decision-making was thereafter evaluated for each patient. Breast MRI was considered to accurately suggest the appropriateness of breast conservation in cases in which the breast MR images clearly demonstrated the respectability of the lesion and in which breast MRI was the only imaging modality able to do so. Breast MRI was considered to accurately suggest the necessity of a mastectomy in cases in which the MR images clearly showed more extensive disease than otherwise suspected from conventional mammography or ultrasound. A final assessment of the impact of contrast enhancement breast MRI on surgical decision-making was made based on the number of patients whose management was altered because of additional information available on breast MRI relative to mammography and/or ultrasound. Patient management was altered for 32/164 (19.5%) patients as a result of gadobenate dimeglumine-enhanced breast MRI.

Another recent prospective study evaluated the accuracy of gadobenate dimeglumine-enhanced breast MRI for depiction of synchronous contralateral breast cancer in patients with newly diagnosed unilateral breast cancer or high-risk lesions [21]. One hundred eighteen consecutive women (mean age, 52 years) with unilateral breast cancer or high-risk lesions and negative findings in the contralateral breast at physical examination, ultrasonography, and conventional mammography underwent gadobenate dimeglumine-enhanced 1.5-T MR mammography. A transverse three-dimensional T1-weighted gradient-echo dynamic sequence was performed before the administration of contrast agent, followed by repeat performance of this same sequence at 0, 2, 4, 6, and 8 min after the administration of 0.1 mmol/kg of contrast agent. MR images were interpreted by two breast imaging specialists in consensus who assigned a score from 0 to 5 by using the BI-RADS scale for suspicion of malignancy. All lesions that were detected with conventional techniques and/or contrast-enhanced MR mammography and were classified as BI-RADS category 4 or 5 were evaluated histologically after biopsy or surgical resection. Contrast-enhanced MR mammography revealed 28 contralateral lesions in 28 (24%) of 118 patients. Twenty-four lesions were detected in patients with dense breasts (BIRADS breast density category III or IV). Lesions in eight (29%) of 28 patients were BI-RADS category 4 and patients underwent biopsy. The remaining 20 lesions (71%) were BIRADS category 5 and these patients underwent surgery. At histological analysis, 22 lesions (18.6% overall) were confirmed as malignant; six lesions were fibroadenomas. No false-negative lesions were detected, considering a follow-up for 12–24 months with conventional mammography, high-frequency-transducer US, or contrast-enhanced MR mammography. The sensitivity, specificity, accuracy, and positive and negative predictive values of contrast-enhanced MR mammography for depiction of malignant or high-risk contralateral lesions were 100%, 94%, 95%, 79%, and 100%, respectively.

The rate of contralateral malignant lesions (18.6%) detected with MRI and not seen at mammography and high-frequency-transducer US was higher than the rate from 3% to 5% reported by other studies [22, 23, 24, 25]. However, we do not know how much of this high rate is due to a selection of patients with a higher probability of contralateral cancer and how much is due to a higher sensitivity of gadobenate dimeglumine.

6. Gadobenate Dimeglumine-enhanced dynamic breast MR Imaging: do we need higher thresholds for initial enhancement evaluation?

Quantitative evaluation of signal intensity–time curves revealed significantly greater lesion enhancement with gadobenate dimeglumine at an equivalent dose of 0.1 mmol/kg of bodyweight when compared with that produced by gadopentetate dimeglumine [17].

The higher contrast enhancement of breast lesions obtained using Gd-BOPTA was also evaluated to define a tailored initial enhancement threshold in a preliminary report of our institution [26]. Thirty-four patients with 36 lesions (28 malignant, 8 benign) underwent dynamic (resolution 120 seconds) 3D FLASH with Gd-BOPTA (0.1 mmol/kg). A multifactorial score system based on lesion shape (round/oval/lobular=0; linear/dendritic/stellate=1), margins (well-defined=0; ill-defined=1), enhancement pattern (homogeneous=0; inhomogeneous=1; rim sign=2), enhancement time course (continuous=0; plateau=1; wash-out=2), and initial enhancement with standard threshold, (<50%=0; 50-to-100%=1; >100%=2) or adjusted threshold (<100%=0; 100-to-240%=1; >240%=2) was used. For both thresholds, a 0-to-3 score was considered benign and a 4-to-8 score malignant. The initial enhancement was >100% for 33/36 (92%) lesions (26/28 malignant, 7/8 benign). For 17 of these 33 lesions the initial enhancement was >240% (16/26 malignant, 1/7 benign). The score for malignant lesions was 5.89±1.34 with standard threshold and 5.50±1.53 with adjusted threshold (p=0.003)

for benign lesions 4.00±1.93 and 3.25±1.75 (p=0.028), respectively. The standard threshold gave 96% sensitivity, 13% specificity, 79% positive predictive value, 50% negative predictive value and 78% accuracy. The same data for the adjusted threshold were 96%, 75%, 93%, 86%, and 92%, respectively.

The same evaluation was performed with a larger number of patients and lesions (especially a higher rate benign:malignant) and presented as oral presentation at RSNA meeting 2009 [27]. Sixty-eight patients with 73 breast lesions (21 benign and 51 malignant) underwent dynamic breast 1.5-T MR imaging with 0.1 mmol/kg of gadobenate dimeglumine. The initial enhancement for benign lesions was 141±65% (mean±standard deviation), while for malignant lesions it was 210±80%. There were used the same criteria of Sardanelli et al. [26] except that the adjusted thresholds were set at values of 180% and 240% for initial increase of signal intensity. Specificity increased from 38% with standard thresholds to 71% with adjusted thresholds (gain of 33%; P=.016). Sensitivity was 100% for both thresholds positive predictive value 80% and 90%, negative predictive value 100% and 100%, and accuracy 82% and 92%, respectively.

We concluded that breast lesion characterization with Gd-BOPTA, due to its high T1-relaxivity, requires a higher initial enhancement threshold than that used with conventional Gd-chelates in order to improve specificity, predictive values and accuracy.

7. Gadobenate dimeglumine as a vascular agent in breast MRI

A better specificity has been investigated not only with the modification of well known parameters but also with the evaluation of new features of breast MR imaging.

The performance of Gd-BOPTA as a vascular contrast agent in breast MR was reported in 2005 [28]. A total of 95 patients with known or suspected breast cancer were randomized to receive 0.05 (n=24), 0.1 (n=24), or 0.2 (n=24) mmol/kg of Gd-BOPTA or 0.1 mmol/kg Gd-DTPA (n=23). Coronal 3D-T1w-GE images were acquired before and 2 min after contrast injection. Two blinded readers assigned by consensus a 0-to-3 score to vascular maps obtained by maximum intensity projection (MIP) reconstruction of subtracted images. The number and conspicuity of the vascular structures on the volume representation were considered. Global variability analysis revealed the presence of significant intergroup differences (p=0.018). At direct comparison, significant differences were observed between Gd-BOPTA at 0.05 mmol/kg and Gd-DTPA at 0.1 mmol/kg (p=0.044), between Gd-BOPTA at 0.1 mmol/kg and Gd-DTPA at 0.1 mmol/kg (p=0.009), and between Gd-BOPTA at 0.2 mmol/kg and Gd-DTPA at 0.1 mmol/kg (p=0.002). Significant differences between the Gd-BOPTA groups were not observed. We concluded that Gd-BOPTA permits the acquisition of high quality MR breast vascular maps at doses as low as 0.05 mmol/kg [28].

Based on the anecdotic observations of more numerous and conspicuous vessels in a breast with malignancy, compared to the contralateral breast, we investigated whether asymmetry of breast vascular maps was predictive of cancer. To this end, we evaluated the MIP maps in 69 women with known or suspected breast cancer studied with Gd-BOPTA at 0.05, 0.1, or 0.2 mmol/kg. MIP maps obtained from subtracted images were evaluated off-site by two observers blinded to the patients' identities and study group assignments. We considered the symmetry or asymmetry of the vascular map, in relation to the diagnosis made after surgical excision or core biopsy. Among the 69 patients, two had bilateral cancer and symmetric vascular maps. The remaining 67 patients were diagnosed with invasive ductal carcinoma (n=41), invasive lobular carcinoma (n=4), invasive ductal-lobular carcinoma (n=3), invasive tubular carcinoma (n=2), and benign neoplasms (n=17). The vascular maps for these 67 patients were asymmetric in 47 cases and symmetric in 20 cases. An association between one-side increased vascular maps and ipsilateral invasive cancer was found in 88% of cases (44 of 50 patients with monolateral cancer) while its absence was noted half cases in 82% (14 of 17 patients without malignancy). The overall accuracy was therefore 87% (58 of 67 patients). The positive predictive value was 94% (44 of 47 patients with asymmetric maps), while the negative predictive value was 70% (14 of 20 patients) and accuracy was 87% (58 of 67 patients). Although ipsilateral vascular prevalence in association with cancer was previously studied exclusively with gadopentetate dimeglumine [29,30], greater overall accuracy was achieved in our study. Interesting improvement of specificity breast MRI were obtained for the same vascular score by Schmitz et al using the 1-molar gadobutrol (0.1 mmol/kg) at 3.0 T [31].

8. Performance of gadobenate dimeglumine for low field breast MRI

Gadobenate dimeglumine was used by us for a small study of 18 claustrophobic or oversized patients on a 0.2-T open magnet with a body coil [32]. Of 397 consecutive patients undergoing breast MR over a 31-month timeframe, 379 (95.5%) were evaluated at 1.5-T with a dedicated bilateral breast coil according the international indications [33]. Due to claustrophobia (n=15) or large body size (n=3), 18 (4.5%) patients could not be evaluated on a 1.5 T magnet used for routine breast MRI, so they were evaluated on a 0.2-T open magnet with a body coil. A three-dimensional dynamic T1-weighted gradient-echo sequence (94-s time resolution) was acquired after intravenous injection of gadobenate dimeglumine at 0.1 mmol/kg bodyweight. The standard of reference comprised pathological examination after surgical excision for 16 lesions scored BI-RADS 3-to-5 and negative follow-up for seven lesions scored BI-RADS 1 or 2. Diagnostic MR image quality was achieved for 20/23 lesions in 15/18 patients. Three lesions (two invasive cancers and a cyst) were not assessed due to patient movement and considered as two false negatives and one false positive. Thus, an 86% sensitivity [13/15; 95% confidence interval (CI): 70%–100%], an 87% specificity (7/8; 95% CI: 65%–100%) and an 87% accuracy (20/23; 95% CI: 73%–100%) were obtained. The intraclass correlation coefficient between MR and pathologic lesion size was 0.845.

Although higher field strength is preferred because of better fat suppression and decreased motion artifacts [33], the possibility to achieve a sufficient diagnostic performance using Gd-BOPTA for breast imaging even in low-field open magnets may allow claustrophobic or oversized women not to be excluded from breast MR imaging.

9. Interaction of GBCAs with choline peak at proton MR spectroscopy

Magnetic resonance spectroscopy (MRS) can improve the specificity of breast MR examination by the detection of the peak of total choline-containing compound (tCho) at 3.2 ppm [34,35,36]. The majority of the in vivo MRS studies were performed using single-voxel methods, where the lesion is first visualized on the postcontrast study and the MRS voxel positioned accordingly. It has been suggested that the charge of the agent is important since choline is a positively-charged molecule at neutral pH and in solution can form a weak complex with negatively-charged gadolinium chelates [37]. The situation in vivo may be complicated by the fact that choline must come into direct contact with the contrast agent in order to form a complex. The formation of this complex can lead to shortening of the relaxation times of the methyl protons of Cho through the electron–nuclear dipole interaction. In a recent study, Lenkinski examined the effects of six Gd-based contrast agents on the tCho peak in phantoms and in a rat model

for breast cancer. They showed that use of ionic chelates (gadopentetate dimeglumine, gadobenate dimeglumine, and gadoterate meglumine) decrease the area of the tCho peak by about 40% leading to an underestimation of the levels of Choline present in human breast cancers, while the neutral chelates (gadodiamide, gadoversetamide, and gadoteridol) had little or no effect [38].
Thus, a possible drawback of the use of gadobenate dimeglumine for breast MRI is the potential reduction of tCho peak from malignant lesions. However, this possibility should be investigated in vivo on humans.

10. Safety in the use of gadobenate dimeglumine for breast MRI

No significant difference between gadobenate dimeglumine and gadopentetate dimeglumine as GBCAs for breast MRI was observed regarding the incidence of adverse events, including also minimal events like pain at the site of injection (12.7% for all Gd-BOPTA groups combined vs. 14.9% in the Gd-DTPA group) [15].
Discussing of adverse effect of GBCAs we must not forget the increasing evidence of the association between nephrogenic systemic fibrosis (NSF) and exposure to GBCAs [39]. It shows that nephrogenic systemic fibrosis can develop after exposure to more than one type of these agents in patients who have acute and transient renal failure. One proposed trigger for NSF is transmetallation of the gadolinium chelate whereby free gadolinium ion is released from the chelate in exchange for endogenous metals (such as zinc, copper and calcium) with subsequent binding to human tissue [40].
Broome et al [41] recently published a thorough analysis and summary of the medical literature on this matter: as of February 1, 2008, there were 186 biopsy-proven cases of NSF published in the peer-reviewed literature with the following unconfounded associations: 157 cases for gadodiamide, eight for gadopentetate dimeglumine, three cases for gadoversetamide, and 18 cases for unspecified GBCAs. A further four NSF cases were confounded with more than one GBCA, while five additional cases were not associated with any GBCA.
Identification of patients at risk should be carried out in order to minimize the risk of developing NSF [42]. Another strategy to be combined with risk assessment is dose reduction. In fact, although it is probably shifted in either direction by patient-level factors, it is possible that a dose–response curve exists [43].
Gadobenate dimeglumine has been proved to posses the greater contrast efficacy for lower concentrations [44]. This opens the possibility to perform breast MRI with half the usual dose of 0.1 mmol/kg in particular cases. In figure 2 we show the case of a 54 year old-woman with a pathological diagnosed invasive lobular carcinoma who had gromelural filtration rate (GFR) equal to 55 ml/min candidates to breast MR imaging for pre-surgical staging. The examination was performed in May 2008, during a 6-month period of time when we did not administrate intravenous Gd-contrast agents to patients with GFR ≤60 ml/min according to internal rules of our institution. Although the we used only 0.05 mmol/kg, images were clearly diagnostic for a unifocal mass enhancement with diameter of 21 mm. Also the asymmetric vascular maps were well defined, showing as additional feature the feeding vessels. It was also possible to evaluate the altered and suspicious morphology of an axillary lymph node (at pathology 4/15 lymph nodes were positive for tumor metastasis).

11. Conclusion

In conclusion, the high relaxivity approach for breast MRI seems to be characterized by an excellent safety profile and high diagnostic performance with only possible negative influence on proton MRS.

References

1. Heywang SH, Hahn D, Schmidt H, et al (1986) MRI of the breast using gadolinium–DTPA. J Comput Assist Tomogr 10:199–204
2. Heywang-Kobrunner SH, Beck R (1995) Contrast-enhanced MRI of the breast. 2nd ed. Springer-Verlag, Berlin
3. Sardanelli F, Iozzelli A, Fausto A (2002) Contrast agents and temporal resolution in breast MR imaging. J Exp Clin Cancer Res 21 (3 Suppl):69–75
4. Bellin MF, Van Der Molen AJ (2008) Extracellular gadolinium-based contrast media: an overview. Eur J Radiol 66(2):160–7
5. Kuhl CK. Current status of breast MR imaging. Part 1 (2007) Choice of technique, image interpretation, diagnostic accuracy, and transfer to clinical practice. Radiology 244:672–691
6. Sardanelli F, Giuseppetti GM, Canavese G, et al (2008) Indications for breast magnetic resonance imaging. Consensus document "Attualità in senologia", Florence 2007. Radiol Med 113(8):1085–95
7. Tweedle MF,Wedeking P, Krishan K (1995) Biodistribution of radiolabeled, formulated gadopentetate, gadoteridol, gadoterate, and gadodiamide in mice and rats. Invest Radiol 30:372–80
8. Kirchin MA, Runge VM (2003) Contrast agents for magnetic resonance imaging: safety update. Top Magn Reson Imaging 14 (5):426–35
9. Rohrer M, Bauer H, Mintorovitch J, Requardt M, Weinmann HJ (2005) Comparison of magnetic properties of MRI contrast media solutions at different magnetic field strengths. Invest Radiol 40(11):715–24
10. Giesel FL, von Tengg-Kobligk H, Wilkinson ID, Siegler P, von der Lieth CW, Frank M, Lodemann KP, Essig M (2006) Influence of human serum albumin on longitudinal and transverse relaxation rates (r1 and r2) of magnetic resonance contrast agents. Invest Radiol 41 (3):222–8
11. Spinazzi A, Lorusso V, Pirovano G, Kirchin M (1999) Safety, tolerance, biodistribution and MR imaging enhancement of the liver with Gd-BOPTA: results of clinical pharmacologic and pilot imaging studies in non-patient and patient volunteers. Acad Radiol;6:282–91
12. Cavagna FM, Maggioni F, Castelli PM, et al (1997) Gadolinium chelates with weak binding to serum proteins. A new class of high-efficiency, general purpose contrast agents for magnetic resonance imaging. Invest Radiol 32(12):780–96
13. McDonald DM, Choyke PL (2003) Imaging of angiogenesis: from microscope to clinic. Nat Med 9:713–725
14. Banci L, Bertini I, Luchinat C (1991) Nuclear and Electron Relaxation. VCH Verlagsgesellschaft mbH, Weinheim
15. Knopp RH, Dujovne CA, Le Beaut A, et al (2003) Evaluation of the efficacy, safety, and tolerability of ezetimibe in primary hypercholesterolaemia: a pooled analysis from two controlled phase III clinical studies. Int J Clin Pract 57(5):363–8
16. Hylton NM (2003) Evaluation of gadobenate dimeglumine for contrast-enhanced MRI of the breast. AJR Am J Roentgenol 181 (3):677–8
17. Pediconi F, Catalano C, Occhiato R, et al. (2005) Breast lesion detection and characterization at contrast-enhanced MR mammography: gadobenate dimeglumine versus gadopentetate dimeglumine. Radiology 237(1):45–56
18. Pediconi F, Catalano C, Padula S, Roselli A, Dominelli V, Cagioli S, Kirchin MA, Pirovano G, Passariello R (2008) Contrast-enhanced MR mammography: improved lesion detection and differentiation with gadobenate dimeglumine. AJR Am J Roentgenol 191(5):1339–46
19. Houssami N, Ciatto S, Macaskill P, et al (2008) L. Accuracy and surgical impact of magnetic resonance imaging in breast cancer staging: systematic review and meta-analysis in detection of multifocal and multicentric cancer. J Clin Oncol. 2008 Jul 1;26 (19):3248–58

20. Pediconi F, Catalano C, Padula S, Roselli A, Moriconi E, Dominelli V, Pronio AM, Kirchin MA, Passariello R (2007) Contrast-enhanced magnetic resonance mammography: does it affect surgical decision-making in patients with breast cancer? Breast Cancer Res Treat 106(1):65–74
21. Pediconi F, Catalano C, Roselli A, Padula S, Altomari F, Moriconi E, Pronio AM, Kirchin MA, Passariello R (2007) Contrast-enhanced MR mammography for evaluation of the contralateral breast in patients with diagnosed unilateral breast cancer or high-risk lesions. Radiology 243(3):670–80
22. Lee SG, Orel SG, Woo IJ, et al (2003) MR imaging screening of the contralateral breast in patients with newly diagnosed breast cancer: preliminary results. Radiology 226: 773–778
23. Liberman L, Morris EA, Kim CM, et al (2003) MR imaging findings in the contralateral breast of women with recently diagnosed breast cancer. AJR Am J Roentgenol 180: 333–331
24. Lehman CD, Gatsonis C, Kuhl CK, et al (2007) MRI evaluation of the contralateral breast in women with recently diagnosed breast cancer. N Engl J Med 356:1295–1303
25. Schell AM, Rosenkranz K, Lewis PJ (2009) Role of breast MRI in the preoperative evaluation of patients with newly diagnosed breast cancer. AJR Am J Roentgenol 192(5):1438–44
26. Sardanelli F, Fausto A, Esseridou A, Di Leo G, Kirchin MA (2008) Gadobenate dimeglumine as a contrast agent for dynamic breast magnetic resonance imaging: effect of higher initial enhancement thresholds on diagnostic performance. Invest Radiol. 43(4):236–42
27. Carbonaro LA, Verardi N, Pedretti S, Di Leo G, Sardanelli F (2008) Gadobenate dimeglumine as a contrast agent for dynamic breast MRI: effect of higher initial enhancement thresholds on diagnostic performance. Scientific Session 94th Scientific and Annual Meeting of RSNA
28. Sardanelli F, Iozzelli A, Fausto A, Carriero A, Kirchin MA (2005) Gadobenate dimeglumine-enhanced MR imaging breast vascular maps: association between invasive cancer and ipsilateral increased vascularity. Radiology 235:791–797
29. Mahfouz AE, Sherif H, Saad A, Taupitz M, Filimonow S, Kivelitz D, Hamm B (2001) Gadolinium-enhanced MR angiography of the breast: is breast cancer associated with ipsilateral higher vascularity? Eur Radiol 11:965–969
30. Carriero A, Ambrossini R, Mattei PA, Angelucci D, Bonomo L (2002) Magnetic resonance of the breast: correlation between enhancement patterns and microvessel density in malignant tumors. J Exp Clin Cancer Res 21(3 Suppl):83–7
31. Schmitz AC, Peters NH, Veldhuis WB, et al. (2008) Contrast-enhanced 3.0-T breast MRI for characterization of breast lesions: increased specificity by using vascular maps. Eur Radiol 18(2):355–64
32. Calabrese M, Brizzi D, Carbonaro L, Chiaramondia M, Kirchin MA, Sardanelli F (2006) Contrast-enhanced breast MR imaging of claustrophobic or oversized patients using an open low-field magnet. Radiol Med 114(2):267–85
33. American College of Radiology (2004) ACR practice guideline for the performance of magnetic resonance imaging (MRI) of the breast. In: Practice guidelines and technical standards Reston, VA. See also: www.acr.org/s_acr/bin.asp?CID=549&DID=17775&DOC=FILE.PDF
34. Katz-Brull R, Lavin PT, Lenkinski RE. (2002) Clinical utility of proton magnetic resonance spectroscopy in characterizing breast lesions. J Natl Cancer Inst 21;94(16):1197–203.
35. Bartella L, Thakur SB, Morris EA, et al (2007) Enhancing nonmass lesions in the breast: evaluation with proton (1H) MR spectroscopy. Radiology 245(1):80–7
36. Sardanelli F, Fausto A, Di Leo G, et al (2009)In vivo proton MR spectroscopy of the breast using the total choline peak integral as a marker of malignancy. AJR Am J Roentgenol 192(6):1608–17
37. Smith JK, Kwock L, Castillo M (2000) Effects of contrast material on single volume proton MR spectroscopy. AJNR Am J Neuroradiol 21: 1084–1089
38. Lenkinski RE, Wang X, Elian M, Goldberg SN (2009) Interaction of gadolinium-based MR contrast agents with choline: implications for MR spectroscopy (MRS) of the breast. Magn Reson Med 61(6):1286–92
39. Wertman R, Altun E, Martin DR, et al (2008) Risk of nephrogenic systemic fibrosis: evaluation of gadolinium chelate contrast agents at four American universities. Radiology. 2008 Sep;248(3):799–806
40. Grobner T (2006) Gadolinium—a specific trigger for the development of nephrogenic fibrosing dermopathy and nephrogenic systemic fibrosis? Nephrol Dial Transplant 21:1104–108. Erratum in: Nephrol Dial Transplant 21:1745
41. Broome DR (2008) Nephrogenic systemic fibrosis associated with gadolinium based contrast agents: a summary of the medical literature reporting. Eur J Radiol 66(2):230–4
42. van der Molen AJ (2008) Nephrogenic systemic fibrosis and the role of gadolinium contrast media. J Med Imaging Radiat Oncol 52 (4):339–50
43. Shabana WM, Cohan RH, Ellis JH, et al (2008) Nephrogenic systemic fibrosis: a report of 29 cases. AJR Am J Roentgenol 190 (3):736–41
44. Pintaske J, Martirosian P, Graf H, Erb G, et al (2006) Relaxivity of Gadopentetate Dimeglumine (Magnevist), Gadobutrol (Gadovist), and Gadobenate Dimeglumine (MultiHance) in human blood plasma at 0.2, 1.5, and 3 Tesla. Invest Radiol 41(3):213–21. Erratum in: Invest Radiol 41(12):859.

Figure 1. Presurgical MRI examination of a 54-year old woman, with invasive lobular carcinoma proven at vacuum assisted biopsy, performed with half of a standard dose (0.05 mmol/kg) of Gd-BOPTA. The maximum intensity reconstruction of the first enhanced sequence shows a unifocal mass enhancement with diameter of 21 mm. Note the well defined feeding vessels (with asymmetric vascular map) and the highly suspicious axillary lymph node (at pathology 4/15 lymph nodes were positive for tumor metastasis).

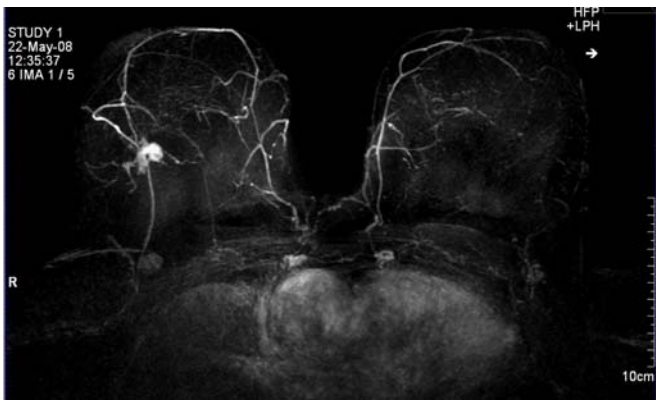

Table 1 Physicochemical characteristics of gadolinium-based contrast agents

Generic name	Gadopentetate dimeglumine	Gadoterate meglumine	Gadoteridol	Gadodiamide	Gadobutrol	Gadoversetamide	Gadobenate dimeglumine
Brand name	Magnevist®	Dotarem®	ProHance®	Omniscan®	Gadovist®	OptiMARK®	MultiHance®
Acronym	Gd-DTPA	Gd-DOTA	Gd-HP-DO3A	Gd-DTPA-BMA	Gd-BTDO3A	Gd-DTPA-BMEA	Gd-BOPTA
Manufacturer	Bayer Schering Pharma	Guerbet	Bracco	GE Healthcare	Bayer Schering Pharma	Tyco	Bracco
Characteristic	0.5 mol/L	0.5 mol/L	0.5 mol/L	0.5 mol/L	1.0 mol/L	0.5 mol/L	0.5 mol/L
Molecular structure	Linear	Cyclic	Cyclic	Linear	Cyclic	Linear	Linear
Charge	Ionic	Ionic	Nonionic	Nonionic	Nonionic	Nonionic	Ionic
Thermodynamic stability constant (log*K*eq)	22.5	25.8	23.8	16.9	21.8	16.6	22.6
Osmolality (Osm/kg)	1.96	1.35	0.63	0.78	1.39	1.11	1.97
Viscosity (mPa s at 37 ◦C)	2.9	2.0	1.3	1.4	4.96	2.0	5.3
r1-relaxivity (L/mmol s−1) in plasma at 1.5 T[a]	4.1	3.6	4.1	4.3	5.2	4.7	6.7
*T*1/2	10 min	9 h, 60 h, >1 month	3 h	35 s	90 min	18 h	80–120 min

[a]Values obtained from Rohrer M et al. [9]
[b]CNS: central nervous system.
Table data extract from Bellin MF et al. [4]

Freehand, non-grid vacuum core biopsies. A preliminary analysis of 500 biopsies.

Bruce L. Daniel MD[1], Gloria Hwang, MD[2], Jennifer Kao MD[3], Debra M. Ikeda MD[4]
Correspondence author[1]
[1]Associate Professor of Radiology, Stanford University, 300 Pasteur Drive, Room H1307, Stanford, CA, 94305, SA, bdaniel@stanford.edu, 650-725-1812, 650-723-1909 [Fax]
[2]Assistant Professor of Radiology, Stanford University, glhwang@stanford.edu, Yung Do, MD, Department of Radiology, Stanford University, yung_do1@yahoo.com
[3]Department of Radiology, Stanford University, Stanford, CA, 94305, USA, 650-723-8462, drkao@stanford.edu
[4]Director, Breast Imaging, Department of Radiology, Stanford University, Stanford, CA, 94305, USA, 650-723-8462

Introduction

Minimally invasive core needle biopsy sampling of enhancing abnormalities detected on breast MRI streamlines the surgical management of breast disease. When MRI core biopsy results are benign, it avoids surgical biopsy. When MRI core biopsy reveals invasive carcinoma, it replaces excisional biopsy with lumpectomy and axillary nodal sampling. In general, large gauge vacuum-needle methods have become the standard for breast core needle biopsy because the larger samples provide more definitive histologic diagnosis.

Vacuum large core needle biopsy (LCNB) was first reported under MRI guidance by Heywang-Köbrunner et al. [1, 2] using a method that employed a custom external positioner to place an MRI-compatible "substitute" needle into a tract in the compressed breast. The tract was then used for vacuum biopsy outside the magnet. Currently, most biopsies employ a plastic sheath that is initially placed into the compressed breast under MRI-guidance using a grid or positioning device. Vacuum biopsy is performed through the sheath outside the magnet [3, 4, 5].

A limitation of grids and positioners is the assumption that the biopsy needle tip does not deflect and that the target does not move when the needle is inserted. We have previously reported methods for freehand MRI-guided breast interventions, including pre-operative needle localization [6, 7, 8] and spring-loaded core needle biopsy [8, 9] in which interactive imaging and needle advancement are alternated to provide direct image-guidance of the needle being inserted to the enhancing target even if it moves. In this paper, we report our experience performing freehand MRI-guided vacuum core needle biopsy.

Methods

Biopsy Method. Freehand MRI-guided vacuum core needle biopsy was adapted from previously reported methods for freehand core needle biopsy [8, 9, 10]. All patients had diagnostic MRI performed at least 1 day prior to the procedure. Un-enhanced T1-weighted diagnostic MRI images were scrutinized in comparison with axial reformations of water-specific T1-weighted high-resolution spoiled gradient echo contrast-enhanced images of the breast to identify the architecture of the fibroglandular tissue at the target site.

MRI-guided biopsies were usually performed in a 0.5T vertically open scanner (Signa-SP, GE Healthcare, Milwaukee, WI) using an open transmit-receive quadrature breast coil (custom OBC coil, Invivo Inc, Waukesha, WI). Four biopsies in 3 patients were performed on a conventional 1.5 T closed bore scanner (HD-Excite, GE Healthcare, Milwaukee, WI) using an eight-channel coil (HD Vibrant breast array coil, GE Healthcare, Milwaukee, WI) using the same method, because the 0.5 T scanner was not functioning. The following steps comprised the biopsy procedure:

1. *Scan* the portion of the breast containing the target, with a fiducial marker (IZI Medical, Baltimore, Md) place on the skin over the approximate location of the target using un-enhanced multislice axial T1-weighted fast-spin echo imaging (TR/TE/etl 350/13/4) through.

2. *Identify* the location of the target on the initial un-enhanced T1-weighted images by comparing the architecture of the breast with the corresponding architecture seen on the preceding diagnostic exam. Decide the optimal needle trajectory, and measure the distance from the desired skin entry site to the fiducial.
3. *Prepare* the biopsy site by mark it with a pen, removing the fiducial, sterilizing the breast with either povidone/iodine solution or alcohol/chlorhexadine solution, and attaching a sterile fenestrated drape to the skin entry site. Anesthetize the skin and the first ~2–3 cm of the anticipated sheath trajectory with 1% lidocaine infiltration. Make a 3 mm skin incision with an MRI-compatible scalpel.
4. *Advance* a 9 g MRI-compatible sheath (Suros Atec, Hologic Inc, Bedford, MA) approximately 1–2 cm through the breast along the desired trajectory using the non-magnetic trocar. Keep the side port of the sheath to continuous vacuum to prevent introduction of air (that can cause susceptibility artifacts on MR images) during exchanges of the trocar with other devices. Replace the trocar with the MRI-compatible plastic obdurator, inserted so that the tip of the obdurator is at the tip of the sheath.
5. *Image* the sheath in the breast and the target location with ~5–7 Axial T1 FSE images. If anesthetic or procedure-related hemorrhage disrupt landmarks, consider non-fat-suppressed T2-weighted FSE image, in which the high signal from anesthetic and blood become bright like fat, returning the breast to its original appearance.
6. *Repeat* steps 4 & 5 until targeting is complete based on breast architecture. The optimal final sheath position is traversing the target, and ending about 1–2 cm beyond the target. If additional anesthesia is required, insert a "skinny" 22 g needle inserted through the sheath, into the tissue beyond the sheath tip and infiltrate with 1% Lidocaine. In our practice we also infiltrate the target site only with ~1 cc 0.75% Bupivicaine or longer acting anesthesia.
7. *Image* the target with water-selective T1-weighted multi-slice images in axial and sagittal planes through the distal sheath and target locations before and after intravenous bolus administration of 0.1 mmol/kg Gd-DTPA (Magnevist, Bayer Healthcare). At 0.5 T we use 3-Point Dixon gradient echo scans for water-selective images (TR/TE/FA 175/13/80°). At 1.5 T we use fat-suppressed T1-FSE (TR/TE/ETL: <150 ms/minimum full TE/4).
8. *Sample* the target by using the 9 g biopsy device (Suros MRI Atec, Hologic Inc, Bedford, MA). After inserting the biopsy device, withdraw the sheath an appropriate distance to leave the biopsy device bowl centered in the target, as measured on axial images of the sheath and target. Use the perpendicular sagittal images to determine which way to direct the sample bowl. If the enhancing target is more than 1 cm from the sheath, reposition the sheath and trocar and repeat step 7.
9. *Deploy* an MRI compatible marker at the biopsy site via the sheath. Image the marker location with fast un-enhanced T1-weighted 2D spoiled gradient-echo images
10. *Manually compress* the biopsy site for 15 min after removing the sheath and marker deployment system, to achieve hemostasis. Apply sterile dressing.
11. *Radiograph* the breast to document marker placement.

Overall this method differs from more widely practiced grid biopsy approaches in several ways:

- Breast compression is not used. The interactive image-guidance approach compensates for target motion intrinsically, rather that trying to prevent it. This maximizes patient comfort, and maximizes enhancement of target lesions. We do, however, use the medial compression plate as a "back-stop" to keep the breast from swinging during the procedure.
- A variety of approaches are possible:
  - i Prone patient—Angled lateral approach. The most common approach.
  - ii. Prone patient—Angled medial approach. Usually performed by placing the breast in the opposite breast coil aperture, and lifting the opposite breast out of the way. Can be performed by reaching through the inside of the coil.
  - iii. Decubitus patient—Vertical medial approach to the dependent breast supported by the patient cradle. Use pair surface coils—a flat coil under the side of the patient, and a loop coil over the medial aspect of the dependent breast. Useful for patients with sternal or back pain that precludes prone positioning.
  - iv. Supine patient—Medial approach. Useful for parasternal lesions.
  - v. Supine patient—Antero-lateral approach. Useful for lesions in the axillary tail close to the chest wall, and for superficial lesions overlying implants.
- Initial needle placement is performed using breast architecture on unenhanced images. This saves the brief period of a few minutes when targets are most reliably visualized immediately after contrast injection, for the most critical part of the procedure—imaging the target vis-à-vis the sheath tip. This also means that biopsy is rarely cancelled for "non-visualization" of target enhancement. We usually perform biopsy of the target area based on architecture even if the target is not well seen, since the needle is already there.
- Vacuum is continuously applied to the sheath to prevent hematoma formation and minimize air injection into the breast.
- The patient remains in the magnet for all steps of the procedure, unless it is performed on a closed bore system, in which case the patient is pulled out of the magnet for a few seconds for each manipulation.

Study Design. A retrospective review of all our core biopsy cases between 7/15/03 and 12/31/2007 was performed according to a protocol approved by our institutions human subjects panel that was exempt from requirement for individual patient consent. The cut-off date was chosen to allow at least 1 year for potential follow-up of non-operatively managed lesions. Data collected included indication for initial MRI, results of initial MRI, details of the MRI-guided biopsy procedure include approach, number of samples removed, and any complications, and results of any relevant follow-up of the target abnormality including pathology from subsequent excisions or re-biopsies, appearance of the target on follow-up MRI scans, all available subsequent imaging finding, and clinic notes, with a particular note made of any subsequent tumor diagnoses at the target locations that would imply a false-negative biopsy occurred. A "final diagnosis" was determined for each lesion based on the follow-up data, if possible. A diagnosis of invasive carcinoma on core biopsy alone was considered "final" even if the patient was subsequently lost to follow-up because the had their cancer treated at another facility (we assumed there were no false-positive pathologic diagnoses of invasive carcinoma).

Analysis. Biopsy results were classified as Benign, High Risk (including atypical ductal hyperplasia (ADH), atypical lobular hyperplasia (ALH), flat epithelial atypia (FEA), lobular carcinoma

in situ (LCIS), intraductal papilloma, and radial scar), Malignant (*i.e.* ductal carcinoma *in situ*) and Invasive (including invasive ductal carcinoma, infiltrating lobular carcinoma, invasive tubular carcinoma, mucinous carcinoma, medullary carcinoma and lymphoma).
A sub-analysis was performed on all lesions with follow-up to determine false negative rates, discordance rates, and underestimation rates. At time of this submission, this analysis, which includes trying to track down outcome in patients who transferred care to other institutions, etc, remains in progress. Preliminary results only are presented.

Results

Overall, biopsy was performed of 500 sites in 400 breasts in 382 procedures in 368 patients. Of the 382 procedures, 364 were unilateral, and 18 were bilateral. A single site was sampled in 279 procedures. Two sites were sampled in 91 procedures. Three sites were sampled in nine procedures. Four sites were sampled in three procedures. No biopsies were cancelled due to non-visualization of the target. Reported procedural complications included ten hematomas, one of which was large (5 cm) and was managed by surgical aspiration. Two patients reported significant pain with trocar insertion, and in one, the procedure was terminated due to pain. This patient was removed from the study. One vaso-vagal reaction occurred and was successfully managed with IV fluid resuscitation only. Four patients had delayed post-procedural bleeding that was self limited and managed by re-dressing the wound. Once case was converted to spring-loaded biopsy due to poor sample yield, likely due to mechanical failure or operator error.
The vast majority of cases used a prone-lateral approach. A medial approach was used in 42 cases. An anterior approach was used in six. A supine medical or lateral approach was also used in several cases. The distribution of core biopsy diagnoses of lesions sampled by freehand MRI-guided vacuum core needle biopsy is compared to previous published reports using grid/positioner -based approaches in Table 1.

Comparison of study results with published large studies of MRI-guided large core vacuum biopsy

Study	Other benign	High risk	DCIS	Invasive	Total sampled	Canceled for non-visualization
Perlet et al. [2]	221 (66%)	29 (9%)	47 (14%)	37 (11%)	334	52 (13%)
Liberman et al. [5]	61 (64%)	10 (11%)	13 (14%)	11 (12%)	95	14 (14%)
Han et al. [12]	69 (46%)	21 (14%)	15 (13%)	24 (16%)	150	22 (13%)
This study	356 (71%)	64 (13%)	34 (7%)	46 (9%)	500	0 (0%)

The core biopsy diagnoses of the subset of lesions with follow-up information is compared with the final diagnosis in Table 2:

Core biopsy diagnosis	Final diagnosis, at subsequent excision or imaging and clinical follow-up					
	Lost to follow-up	Benign by follow-up	Benign at excision	High risk	DCIS	Invasive
Benign [incomplete data]	[11]	[n/a]	[26]	[3]	[0]	[5]
High risk	16	6	12	23	5	2
DCIS	9			4	17	4
Invasive						46

Discussion

Overall, the prevalence of malignancy (both DCIS and Invasive) in our cohort is slightly lower than in other studies. This probably reflects the overall more conservative nature of Radiologist's in our practice. Analysis is also in progress to determine if the indication for MRI is different in our cohort. It is also likely that because we did not cancel biopsies due to lack of enhancement (as occurred in other studies) this diluted the sample population with more benign lesions. Lastly, we cannot entirely exclude that differences biopsy procedure accuracy could affect this discrepancy. The proportion of DCIS compared to invasive carcinoma is similar to previous studies.
The prevalence of high risk lesions is also very similar to other studies. Within those lesions, however, the rate at which malignancy was underestimated is less that other studies [11] only seven of 42 (17%) cases with documented surgical follow-up. Still, this prevalence is high enough that biopsy remains recommended for core biopsies yielding high risk results.
Data to definitively measure the false negative rate for freehand MRI-guided core biopsy is this study is still being collected. However, the preliminary results indicate that five invasive carcinomas were found at sites where core biopsies had been performed with benign results. At least two cases were suspected at the time of the procedure and

immediate excision was recommended because the core biopsy result was discordant. This rate of discordance (2/500) is similar or slightly less that reported for grid-based biopsy [13]. One site had *both* an invasive carcinoma and a fibroadenoma excised, where the original core biopsy revealed only fibroadenoma. It is unclear whether the fibroadenoma, or the invasive carcinoma corresponded to the target that was originally identified for biopsy. In two cases, the carcinoma was detected one or more years later, and was felt to be an *interval* carcinoma, not a pre-existing carcinoma that was missed.

The major limitation of this study is that the follow-up data has not been completely collected for sites that were either not excised, or that were excised at other hospitals. Other limitations include the fact that follow-up pathology reports from subsequent surgeries do not always report findings at sites of previous benign biopsies, especially if they are not in the vicinity of the dominant tumor. Finally, the data presented so far do not stratify results based on the size or imaging characteristics of the target.

Overall, the flexibility of the approach, including angled approaches that can target lesions near the chest wall, nipple, and over implants, and anterior approaches for far lateral lesions, and para-sternal lesions make freehand biopsy an attractive alternative for difficult lesions. The method has potential to become nearly as easy as Ultrasound-guided core biopsy, provided once MRI-visible vacuum core biopsy devices become commercially available [14].

References

1. Heywang-Köbrunner SH, Heinig A, Schaumlöffel U, Viehweg P, Buchmann J, Lampe D, Spielmann R. MR-guided percutaneous excisional and incisional biopsy of breast lesions. Eur Radiol. 1999;9 (8):1656–65.

2. Perlet C, Heinig A, Prat X, Casselman J, Baath L, Sittek H, Stets C, Lamarque J, Anderson I, Schneider P, Taourel P, Reiser M, Heywang-Köbrunner SH. Multicenter study for the evaluation of a dedicated biopsy device for MR-guided vacuum biopsy of the breast. Eur Radiol. 2002 Jun;12(6):1463–70. Epub 2002 Apr 24.

3. Liberman L, Morris EA, Dershaw DD, Thornton CM, Van Zee KJ, Tan LK. Fast MRI-guided vacuum-assisted breast biopsy: initial experience. AJR Am J Roentgenol. 2003 Nov;181(5):1283–93.

4. Clinical experience with MRI-guided vacuum-assisted breast biopsy. Lehman CD, Deperi ER, Peacock S, McDonough MD, Demartini WB, Shook J. AJR Am J Roentgenol. 2005 Jun;184 (6):1782–7.

5. Liberman L, Bracero N, Morris E, Thornton C, Dershaw DD. MRI-guided 9-gauge vacuum-assisted breast biopsy: initial clinical experience. AJR Am J Roentgenol. 2005 Jul;185(1):183–93.

6. Daniel BL. Intraprocedural magnetic resonance imaging-guided interventions in the breast. Top Magn Reson Imaging. 2000 Jun;11 (3):184–90.

7. Daniel BL, Birdwell RL, Ikeda DM, Jeffrey SS, Black JW, Block WF, Sawyer-Glover AM, Glover GH, Herfkens RJ. Breast lesion localization: a freehand, interactive MR imaging-guided technique. Radiology 1998 May;207(2):455–63.

8. Van den Bosch MAAJ, Daniel BL, Pal S, Knowels KW, Birdwell RL, Jeffrey SS, Ikeda DM. MRI-guided needle localization of suspicious breast lesions: results of a freehand technique. Eur Radiol 2006; 16: 1811–1817.

9. Daniel BL, Birdwekk RL, Butts K, Nowels KW, Ikeda DM, Heiss S, Cooper CR, Jeffrey SSJ, Dirbas FM, Herfkens RJ. Freehand iMRI-Guided Large-Gauge Core Needle Biopsy: A New Minimally Invasive Technique for Diagnosis of Enhancing Breast Lesions. J Magn Reson Imaging 2001;13:896–902.

10. Schneider JP, Schulz T, Horn LC, Leinung S, Schmidt F, Kahn T. MR-guided percutaneous core biopsy of small breast lesions: first experience with a vertically open 0.5T scanner. J Magn Reson Imaging. 2002 Apr;15(4):374–85.

11. Liberman L, Holland AE, Marjan D, Murray MP, Bartella L, Morris EA, Dershaw DD, Wynn RT. Underestimation of atypical ductal hyperplasia at MRI-guided 9-gauge vacuum-assisted breast biopsy. AJR Am J Roentgenol. 2007 Mar;188(3):684–90.

12. Han BK, Schnall MD, Orel SG, Rosen M. Outcome of MRI-guided Breast Biopsy. AJR 2008; 191:1798–1804.

13. Lee JM, Kaplan JB, Murray MP, et al. Imaging-Histologic Discordance at MRI-Guided 9-Gauge Vacuum-Assisted Breast Biopsy. AJR 2007;189:852–59.

14. Daniel BL, Freeman LJ, Pyzoha JM, McCoy TD, Birdwell RL, Bouley DM, Movius B, Hibner JA. An MRI-compatible semiautomated vacuum-assisted breast biopsy system: initial feasibility study. J Magn Reson Imaging. 2005 May;21(5):637–44.

Figure 1. Positioning for prone freehand vacuum core biopsy. The patient lies on an open breast coil (Custom OBC, MRI-Devices/ Invivo Inc, Waukesha, WI) in the 0.5 T vertically open scanner (Signa-SP, GE Healthcare, Milwaukee, WI).

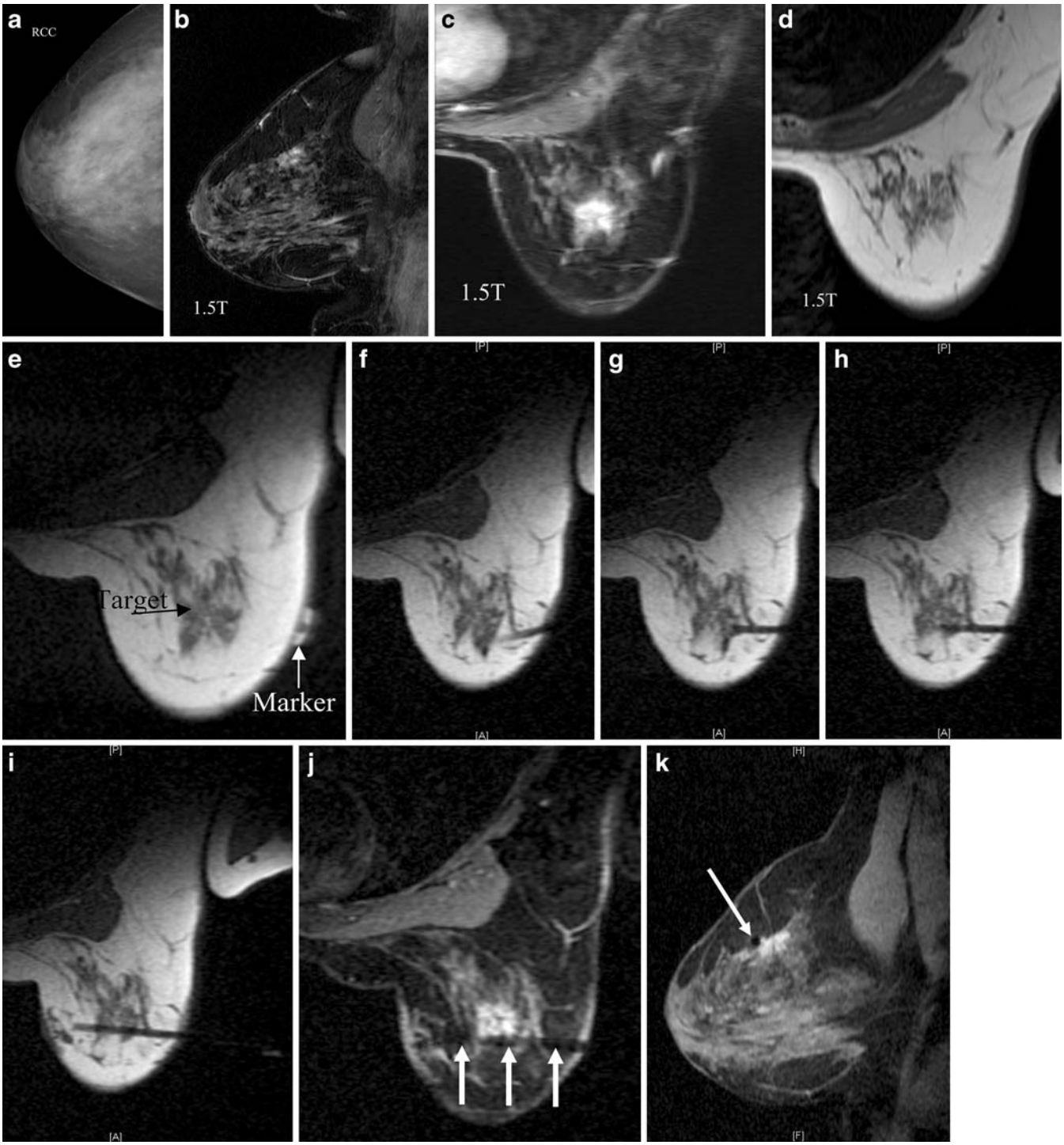

Figure 2. Method for freehand 9 gauge core vacuum assisted MRI-guided biopsy. A 48 y/o woman presented with vague microcalcifications on a screening right CC mammograph (Figure 2a). X-ray stereotactic vacuum core biopsy of the 9:00 o'clock and 6:00 o'clock calcifications revealed only fibrocystic change and atypia. Diagnostic MRI revealed a non-palpable, suspicious spiculated enhancing mass in the 12:00 o'clock position that was not seen by sonography (Figure 2b, Sagittal contrast-enhanced water-selective T1-weighted 3D spoiled gradient-echo sequence). Axial reformations (Figure 2c) were compared with initial unenhanced T1 images (Figure 2d) to determine the fibroglandular architecture of the target. On the day of biopsy, initial scanning with a marker over the breast was used to select the skin entry site (arrow, Figure 2e). After sterile prep, and infiltration with local 1% lidocaine, a 9 g MRI-compatible sheath was inserted freehand. Interactive images were used to guide incremental advancements of the sheath past the target (Figures 2F–2I). Contrast-enhanced axial images (Figure 2J) and sagittal images (Figure 2K) were used to measure how far back to pull the sheath to reveal the target in the sample chamber, and which radial directions to direct vacuum sampling. Histopathology revealed invasive ductal carcinoma and ductal carcinoma *in situ*. Lumpectomy confirmed a 1.5 cm invasive ductal carcinoma with 2.1 cm ductal carcinoma *in situ*.

Figure 3. Positioning for prone freehand vacuum core biopsy. The patient lies on an open breast coil (Custom OBC, MRI-Devices/ Invivo Inc, Waukesha, WI) in the 0.5 T vertically open scanner (Signa-SP, GE Healthcare, Milwaukee, WI).

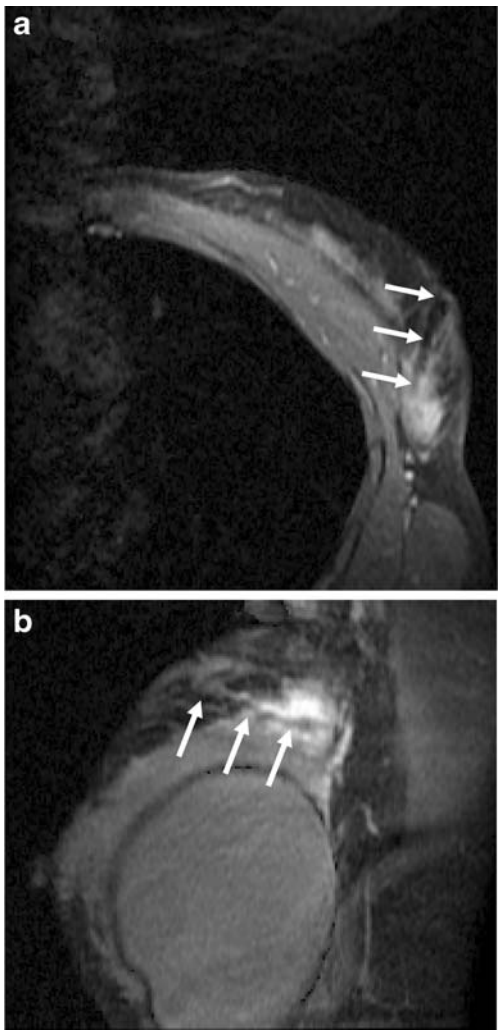

◀Figure 4. Anterior Supine Approach in a 41 y/o woman who had a staging MRI for contralateral DCIS and invasive ductal carcinoma. Axial (Figure 4a) and Sagittal (Figure 4b) water-selective 3-point Dixon contrast-enhanced Gradient Echo MR images reveal the biopsy sheath approaching the extreme posterior/lateral aspect of the breast from anteriorly so as to avoid the underlying chest wall and nearby implant. Histopathology revealed benign breast parenchyma. Follow-up MRI's over 4 years show gradually decreasing enhancement in this area that ultimately vanished, confirming benignancy.

Small foci in MR: What should we do? Neglect, follow, excise? A retrospective analysis of 19 small foci compared with 19 typical MRI-detected mammographically occult lesions.

Bruce L. Daniel MD[1], Maurice van den Bosch, MD, PhD[2], Hargreaves, Brain A, Ph.D.[3], Jennifer Kao MD[4], Debra M. Ikeda MD[5]
Correspondence Author[1]
[1]Associate Professor of Radiology, Stanford University, 300 Pasteur Drive, Room H1307, Stanford, CA, 94305, USA, bdaniel@stanford.edu, 650-725-1812, 650-723-1909 [Fax]
[2]Department of Radiology, Room E.01.132, University Medical Center Utrecht, Heidelberglaan 100, 3584 CX Utrecht, The Netherlands, E: m.a.vandenbosch@umcutrecht.nl, P: +31887556689
[3]Lucas MRS/I Center, Stanford University, Stanford, CA, 94305, 650-498-5368, bah@stanford.edu,
[4]Department of Radiology, Stanford University, Stanford, CA, 94305, USA, 650-723-8462, drkao@stanford.edu
[5]Director, Breast Imaging, Department of Radiology, Stanford University, Stanford, CA, 94305, USA, 650-723-8462

Introduction

The goal of breast imaging is to detect cancer at the earliest possible size before it presents clinically. By detecting cancers at the smallest size, treatment can be initiated with the highest likelihood of preventing recurrence and avoiding metastasis. In addition, reliable detection at smaller sizes could theoretically lengthen the surveillance interval require between imaging exams. Magnetic Resonance Imaging, which has a resolution of 1–2 mm or less, and which detects mammographically occult breast cancer by virtue of its contrast enhancement should be ideally suited to detect very small enhancing foci of cancer, defined by the ACR BIRADS Breast MRI Lexicon [1] as enhancing lesions ≤5 mm in size. In practice, however, foci are a dilemma. The prevalence of malignancy among foci <5 mm in a study by Liberman *et al.* was so low, only 3% (one in 37), that the authors concluded that biopsy of foci is rarely indicated.

We recently reported our analysis of small foci [3] taken from our study of MRI wire-localized lesions [4] and noted a prevalence of malignancy of 37% [11/30]. The purpose of this study was to determine *why* the small foci in our population were targeted for biopsy, and whether there were any clinical, morphologic or dynamic imaging features that are especially important for identifying cancer among small lesions compared to more typical MRI-detected lesions.

Methods

Study Design. A retrospective case-controlled study was performed. The "study" cohort included patients with small enhancing foci identified in our previous analysis [3, 4]. The "control" cohort consisted of patients whose ages matched the "study" patients with typical MRI-detected lesions that were removed during the same period (2004–2006) and were larger that 5 mm in size on imaging. This study was performed in accordance with protocol approved by our institutional human subjects panel.

Scanning Technique. All exams were performed using a 1.5T MR Scanner with high performance gradients (Echospeed or HD Excite, GE Healthcare, Milwaukee, WI) using a dedicated phased-array prone breast coil (four-channel OBC coil, or seven-channel breast coil by In Vivo/MRI Devices Inc, Waukesha, WI). Scans were performed using a standard unilateral protocol that includes that includes pre-and post-contrast high spatial resolution images immediately before and after rapid dynamic 3D images performed during bolus injection of 0.1 mmol/kg Gd-DTPA [5]: The rapid dynamic 3D imaging was performed with a 3D "stack-or-spirals" sequence that includes water-selective spectro-spatial pulses that prevent fat signal and minimize off resonance blurring [5] (TR/TE/FA/#interleaves: 38 ms/12.3 ms/40°/20 Voxel size 1.1×1.1×6 mm, bulk motion correction applied in reconstruction of raw data). Dynamic 3D spiral "post-contrast" images were also performed at the end of the study to improve detection of contrast "wash-out". The high-spatial resolution images were performed with a 3D spoiled gradient-echo sequence with water-selective spectro-spatial excitation. Elliptical centric phase encoding was used so that the brightness of structures in the image is dominated by their signal intensity at the start of the 6 min 35 s scan (3DSSMT [6], TR/TE/FA: 33 ms/9 ms/50°, Voxel size: 0.4×1.0×1.5 mm). The elliptical centric phase encoding preserves brightness among early enhancing structures, especially cancers, even though the sequence does not start until after dynamic imaging of initial contrast uptake, approximately 1:40 min after contrast arrived at the breast.

Image analysis Images from subsequent MRI-guided biopsy and pre-operative wire localization procedures were used to determine the exact location of the enhancing lesions in the breast on original diagnostic MR images. These lesions were then retrospectively reviewed by two board-certified radiologists with over 5 years of experience reading breast MRI who were blinded to the pathologic diagnosis, and who were instructed to focus only on the target lesion. Morphology was scored using MRI-BIRADS lexicon terminology, even though they were smaller that 5 mm, because the purpose of this study was to determine if MR imaging features can assess the risk of malignancy in small foci. In addition to specific features, the radiologists were asked to score their overall level of suspicion based on the lesion's morphology, using a modified BIRADS scale that includes 4a, 4b, and 4c categories. Dynamic imaging was analyzed from region-of-interest drawn around the perimeter of the lesions using Functool (GE Healthcare, Milwaukee, WI), and classified by percent enhancement at 1 min. The shape of the dynamic enhancement curve was classified according to the scheme of Daniel et al. [7]. The radiologist's overall assessment was also scored using the modified BIRADS scale. Clinical data was recorded independently by a third radiologist, and included the presence or absence of known tumor in the same breast, the indication for the scan, and overall breast density and degree of background enhancement.

Statistical Analysis 95% confidence intervals were calculated. ROC analysis was used to determine the compare the diagnostic accuracy of various criteria among small foci in the "study" cohort and with the more typical "control" lesions. Individual proportions were compared using Z tests and were considered significantly different at a p value of ≤0.05.

Preliminary Results

Overall 19 "study" lesions (<5 mm lesions) were identified in 18 patients from our original report that had complete imaging studies available for formal retrospective reanalysis and review. The "control" cohort consisted of 19 lesions untreated, mammographically occult lesions that were biopsied (either by MRI core biopsy or MRI wire-localized surgical biopsy) during the same period, in 19 patients whose ages were at most 1 year different from individual corresponding "study" patients. The indication for MRI was similar between the two groups, as shown in Table 1. Co-existent cancer in the same breast (a.k.a. the *ipsilateral staging* indication) was slightly more common among patients with "study" foci, than among control patients (28% vs. 16% respectively). An un-diagnosed clinical or imaging abnormality (a.k.a. the *Diagnosis* indication) was slightly more common among "control" patients than patients with "study" foci (33% vs. 22%).

Indication for MRI	"Study"	"Control"
Screening	4 (22%)	4 (21%)
Diagnosis	6 (33%)	8 (42%)
Staging—ipsilateral breast	5 (28%)	3 (16%)
Staging—contralateral breast	3 (17%)	4 (21%)

Eight of 19 "study" foci were malignant (42%) [0.20–0.67]. Only four of 19 "control" lesions were malignant (21%) [0.06–0.45]. The types of malignancies were also similar in the study group (three invasive ductal, two infiltrating lobular, one invasive tubular, and two ductal carcinoma *in situ*) compared with the control group (three invasive ductal, one ductal carcinoma *in situ*). Pathology revealed only two discrete masses among the 11 benign "study" foci (one papilloma, one lymph node). There were eight discrete masses among the 15 benign "control" lesions (three fibroadenoma, two papilloma, one hemangioma, one lymph node).

Selected differences between the reader's assessment of "study" and "control" lesions are presented in Table 2. Results for each reader are presented on separate lines, together with Z-score test statistics for comparison of unpaired proportions and two-tailed p-value and significance at a <0.05% threshold.

Diagnostic criteria	"Study"	"Control"	Z	2-tailed P value
Mass	19/19 (100%)	13/18 (72%)	2.01	0.045
	16/19 (84%)	8/19 (42%)	2.35	0.019
Round or oval shape	10/19 (63%)	2/16 (13%)	2.12	0.033
	14/19 (78%)	3/18 (17%)	3.15	0.002
Smooth or macrolobulated margins	11/19 (58%)	7/14 (50%)	0.05	0.964 ns
	18/19 (95%)	8/17 (47%)	2.77	0.006
Rim enhancement	4/19 (21%)	2/19 (11%)	0.49	0.628 ns
	4/19 (21%)	2/19 (11%)	0.49	0.628 ns
Morphology BIRADS 1, 2, 3 or 4a	15/19 (79%)	10/19 (53%)	1.35	0.178 ns
	15/16 (94%)	13/18 (72%)	0.49	0.626 ns
DCE curve with rapid enhancement (type III, IV, V)	14/19 (74%)	9/19 (47%)	1.31	0.191 ns
	12/19 (63%)	7/19 (37%)	1.34	0.180 ns

An example of a malignant focus identified by MRI is shown in Figure 1:

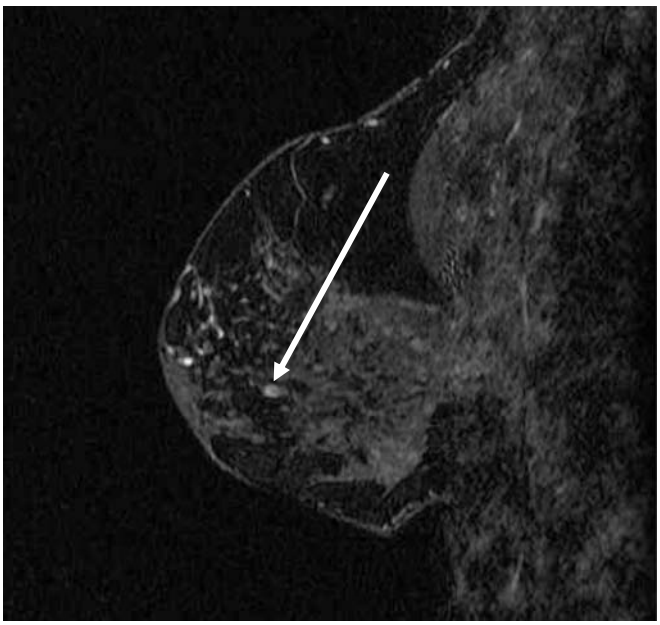

Figure 1. Invasive ductal carcinoma, 3 mm in diameter. This lesion was incidentally detected in a 51 y/o woman who presented for staging MRI of a tumor elsewhere in the breast [not shown]. Note suspicious rim enhancement. Dynamic imaging also showed rapid initial contrast uptake followed by early transition to a plateau of signal intensity.

Statistically significant comparisons of the diagnostic accuracy of various interpretation criteria between "study" foci and "control" lesions was limited by small sample size in each group. No consistent differences in the shape of the ROC curves for the lesion morphology BIRADs score, we noted. No consistent differences in the shape of the ROC curves derived from the classification of the dynamic contrast uptake curves of the lesions were noted between "study" foci and "control" lesions. However, the "operating point" or balance of sensitivity and specificity at a given interpretation threshold varied between the two groups. This is due to the differences in overall rate at which those criteria were applied by the readers to each group shown in table 2.

Discussion

The significantly higher prevalence of malignancy in our "study" foci (42%) compared to the low prevalence published by other investigators (3%) implies that only very high-risk foci were selected for MRI-guided wire-localized excision at our institution (since only biopsy-proven lesions were analyzed in this study).

One strategy to increase the prevalence of malignancy among foci being selected for excision is to concentrate on foci that occur in the same breast as a known malignancy because foci in these breasts are more likely to be malignant. While their was a trend toward a greater number of patients with known ipsilateral cancer in our "study" group (five, compared with three in the control group) this is clearly not enough to explain the very high yield of malignancy in our "study" cohort.

Another strategy to increase the yield of malignancy among foci is to apply interpretation criteria based on lesion morphology and dynamic contrast uptake. The trend that rim enhancement, and rapid initial contrast uptake were more prevalent among our "study" foci suggest that these factors may have been used to identify these foci for biopsy. The ability of the two radiologists to reliably identify these two features affirms the value of our interleaved diagnostic scanning protocol that interposes high spatial-resolution imaging between dynamic imaging of initial contrast uptake and dynamic imaging of wash-out. Water-selective rapid dynamic imaging of rapid initial contrast uptake was particularly critical for identifying small foci that required biopsy. This is in contrast to published results in larger lesions, where dynamic imaging has less diagnostic impact [8].

Of interest is the observation that the "study" foci were frequently round or oval masses with smooth or macrolobulated borders. This was a trend for one radiologist reviewer, and was statistically significant for the other (see table). These criteria are usually considered indicators of relatively benignancy among more typical sized breast lesions. Our data suggests these morphologic features should not be used to categorically dismiss small foci as benign.

The lack of substantial differences among the ROC curves for the "study" foci compared to "control" lesions suggests that the usual breast MRI interpretation criteria can be as successfully applied to foci as they are to larger masses, provided scan technique is adequate. However, this study had very limited power to investigate diagnostic accuracy, because only biopsy-proven lesions were included in the sample. Thus the sample is biased and includes relatively few lesions with a benign appearance that would not precipitate biopsy according to normal interpretation criteria.

Practice recommendations are difficult to infer based on this limited size study. However clearly not all enhancing foci deserve biopsy. Based on the results of our study, the approach at our institution is to look carefully at all foci encountered. Biopsy is contemplated most frequently if the focus is an isolated, dominant finding, if it occurs in a breast with a very high risk of malignancy such as the same breast as a known un-treated tumor. Finally, features, such as rim enhancement, and especially rapid initial contrast uptake are used to select those foci that may merit biopsy; other criteria including smooth margins or round or oval shape are ignored because they are frequently present in many malignant foci.

Overall this study is limited by being a retrospective design with a small sample size, and by the preliminary nature of the study. Future studies in larger numbers of patients are in progress to confirm these results, and enable more rigorous policy recommendations.

References

1. Tardivon AA, Athanasiou A, Thibault F, El Khoury C. Breast imaging and reporting data system (BIRADS): magnetic resonance imaging. Eur J Radiol. 2007 Feb;61(2):212–5. Epub 2006 Dec 4.

2. Liberman L, Mason G, Morris EA, Dershaw DD. Does size matter? Positive predictive value of MRI—detected breast lesions as a function of lesion size. AJR 2006; 186:426–430.

3. Van Den Bosch, MAAJ, Ikeda DM, Daniel BL. Does Size Matter? Likelihood of Cancer in MRI-Detected Lesions Less Than 5 mmMRI-guided needle localization and surgical small breast lesions. AJR 2007; 188:W571 0361-803X/07/1886-W571.

4. Van den Bosch MAAJ, Daniel BL, Pals S, et al. MRI-guided needle localization of suspicious breast lesions: results of a freehand technique. Eur Radiol 2006; 16:1811–1817.

5. Agoston AT, Daniel BL, Herfkens RJ, Ikeda DM, Birdwell RL, Heiss SG, Sawyer-Glover AM. Intensity-modulated parametric mapping for simultaneous display of rapid dynamic and high-spatial-resolution breast MR imaging data. Radiographics. 2001 Jan–Feb;21(1):217–26.

6. Yen YF, Han KF, Daniel BL, Heiss S, Birdwell RL, Herfkens RJ, Sawyer-Glover AM, Glover GH. Dynamic breast MRI with spiral trajectories: 3D versus 2D. J Magn Reson Imaging. 2000 Apr;11 (4):351–9.
7. Leong CS, Daniel BL, Herfkens RJ, Birdwell RL, Jeffrey SS, Ikeda DM, Sawyer-Glover AM, Glover GH. Characterization of breast lesion morphology with delayed 3DSSMT: an adjunct to dynamic breast MRI. J Magn Reson Imaging. 2000 Feb;11(2):87–96.
8. Schnall MD, Blume J, Bluemke DA, DeAngelis GA, DeBruhl N, Harms S, Heywang-Köbrunner SH, Hylton N, Kuhl CK, Pisano ED, Causer P, Schnitt SJ, Thickman D, Stelling CB, Weatherall PT, Lehman C, Gatsonis CA. Diagnostic architectural and dynamic features at breast MR imaging: multicenter study. Radiology. 2006 Jan;238(1):42–53.

Angiogenesis and Lymphangiogenesis in Breast Cancer: In vivo Fluorescence and MRI Investigations

Dadiani M, Badikhi D, Margalit R, Seger D, Degani H.
Weizmann Institute of Science, Rehovot, ISRAEL

All tumors reach early in their development a stage where their continuous progression depends on their capacity to recruit and form a network of blood vessels. The induction of angiogenesis is therefore a rate-limiting step in tumor progression and has been intensively addressed in the last two decades by many investigators (1,2). Tumor angiogenesis, most often leads to the development of a microvascular system with distinct structural and functional features. The capillaries form a disorganized system, tortuous, dilated, with discontinuous walls and fenestrated endothelial lining (3). Consequently, blood flow in some tumor regions is impaired and delivery of nutrients and oxygen is inefficient. In addition, the high vascular permeability of tumor capillaries and impaired drainage of fluid by the lymphatic system lead to water accumulation in the tissue and increased interstitial fluid pressure (IFP). Under high IFP conditions, the distribution of blood borne molecules in the tumor is dominated by convection from high IFP regions in the tumor to its boundaries with low IFP (4,5). This phenomenon presents a physical drug resistance mechanism.

The new capillaries formed in tumors can also provide an escape route for cells' dissemination and metastasis. Tumor cells can intravasate by direct tissue invasion, through the blood circulation or trough the lymphatic system. Because the lymphatic system is optimally suited for the entry and transport of cells, it has many advantages over the blood circulation as a transport route for metastasizing tumor cells. The smallest lymphatic vessels are much larger than blood capillaries, and lymphatic flow is orders of magnitude slower (6). Dissemination of cells occurs at the level of lymphatic capillaries which are devoid of a continuous basement membrane and pericytes, typical of blood capillaries. This entry of tumor cells into lymphatics can be a passive process (7). The latter concept suggests that tumor cells are washed into lymphatics along with interstitial fluid and proteins. However, whether the invasion process is active or passive and what are the initial forces that affect cell transport into the lymphatics remain open questions. We hypothesize that high IFP facilitates the probability of detached tumor cells to be washed into the lymphatics in the tumor's periphery and hence, promote metastasis (6).

We have investigated the above hypothesis correlating IFP with lymphatic velocities and with lymph node metastasis in MDA-MB-231 tumors stably transfected with red fluorescence protein as previously described (8) and implanted in the mammary of SCID mice. By inoculating 2.5×10^6 and 5×10^6 cells we obtained slow-growing and fast growing tumors, respectively, which also corresponded to the time of the onset of lymph node metastasis. For fluorescence imaging of the lymphatic vessels we used FITC-dextran, intradermally injected into the tumor's periphery (2 μl of 10 mg/ml). Velocities of lymphatic flow pulses, and the appearance of spontaneous metastasis, were followed during 2–8 weeks post inoculation. The images were recorded *in vivo*, non-invasively, using a stereo-microscope and a CCD camera as previously described (8). Lymphatic flow velocities were calculated from the lymphatic repulsion frequency (9). The fluorescent signal from adjacent lymphatic segments was plotted and the mean distance between the peaks of the lymphatic pulses, was used to calculate the velocity as demonstrated in Figure 1.

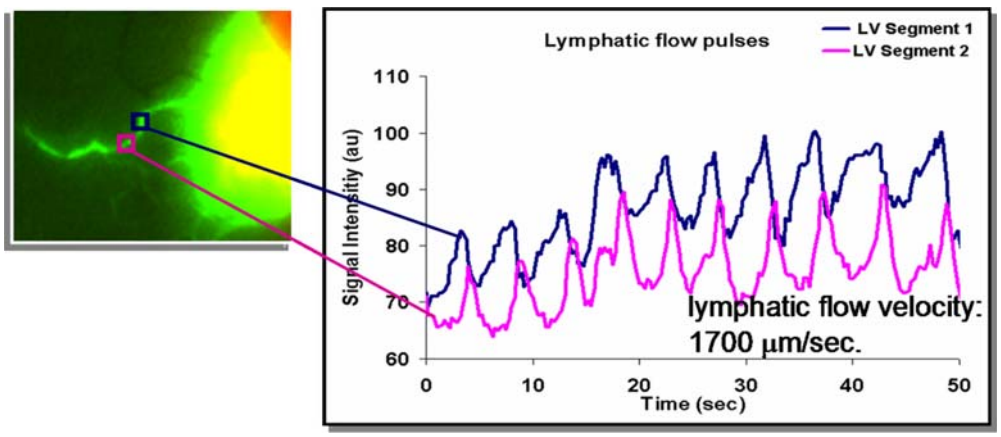

Figure 1. Signal intensity from two adjacent lymphatic segments (each segment is 0.15 mm in length and the distance between the segments is 1 mm). The shift in the peaks of the repulses served to calculate the velocity of the lymphatic flow (time reached for the fluorescent marker to reach from segment 1 to segment 2).

We found that in the fast growing tumors (5×10^6 cells), already at week 3 after cell implantation, the lymphatic flow was fast, whereas in the slow growing tumors (2.5×10^6 cells), the velocities of lymphatic flow were slow until 5 weeks post inoculation. These results correlated with the onset of metastases to the lymph nodes; metastasis occurred earlier in mice bearing a fast growing tumor than in mice bearing a slow growing tumor. In all mice, metastases were observed only after fast lymphatic drainage was detected in the same mouse.

In the late stages of tumor growth (8–9 weeks), when very high lymphatic flow velocities were measured in both tumor groups, we observed red fluorescent cells in the lymphatic vessels. In lymphatic vessels filled with cancer cells, the lymphatic flow decreased and the FITC-dextran was unable to drain through the lymph vessels.

The preliminary results suggested that there is a correlation between the elevation of the lymphatic drainage from the area surrounding the tumor and the onset of metastases to the lymph nodes. Based on the presence of high IFP within these tumors and on the above correlation we propose that this hyper pressure provided a major driving force for tumor cell dissemination into the lymphatic system and facilitated metastasis. Further *in vivo* studies of IFP level by MRI (10, 11), lymphatic flow by Fluorescence imaging, extent of metastasis, as well as the application of drugs that reduce IFP (11) would help clarifying whether the unique physical properties of tumors' vasculature leading to high IFP facilitate lymphatic metastasis.

Taking advantage of the prior knowledge of the presence and extent of lymph node metastases achieved by fluorescence microscopy we embarked on developing dynamic contrast enhanced MRI in order to identify distinct patterns of enhancement in lymph node metastasis. Administration of the contrast-agent, GdDTPA, was designed to first enter intravenously to the blood circulation and indicate enhancement in blood capillaries and then to reveal lymphatic drainage from the extracellular compartment into the lymphatic vessels and into the lymph nodes. To that end we designed a hybrid infusion protocol consisting of a bolus injection followed by a slow infusion to reach steady state contrast agent concentration. Applying the hybrid infusion protocol enabled us to first enhance the blood vessels (rapid bolus injection) and then visualize the drainage through the lymph node (slow infusion at steady state). During the bolus injection there was a rapid entry of the contrast agent to the blood circulation, enhancing mainly the hilus area in the lymph node. Then, during the infusion, the interstitial concentration reached steady state, and the drainage through the lymphatic system entered via afferent lymphatic vessels through the subcapsular sinus.

Images were acquired with a 4.7 T Biospec spectrometer (Bruker). Gd-DTPA was infused with a bolus dose (0.4 mmol/kg) followed by slow infusion (0.015 mmol/kg*min) for 100 min. A multislice 3D gradient echo sequence was acquired before and during the infusion with TR/TE of 18.3/4.3 ms, a flip angle of 30°, four averages and acquisition time of 2.5 min at very high spatial resolution: $0.12\times0.23\times0.5$ mm^3

The enhancement pattern following contrast-agent infusion is shown in figure 2 for a normal lymph node (A) and metastatic lymph node (B). Analysis of these series showed that in normal lymph nodes of naïve mice, the contrast agent entered the blood vessels and immediately enhanced the hilus region. After reaching a steady state GdDTPA concentration in the plasma and the interstitial spaces through out the body, the interstitial fluid was drained via the lymphatic vessels, leading to the enhancement of the entire lymph node within 25 min. On the other hand, in the metastatic lymph nodes, the immediate entry into the hilus from the blood circulation was followed by enhancement of a peripheral rim, caused by entrance from afferent lymph flow, but inner regions within the node were not enhanced as in the normal lymph node. Interestingly, MRI lymphography with a dendrimer-based paramagnetic contrast agent also showed no filling of the contrast agent in the metastatic lymph node (12).

Histopathology of the involved lymph nodes revealed the localization of tumor cells which correlated with the enhanced ring in the lymph node rim observed by MRI (Figure 2). This congruence suggested that tumor cells occupying the sinuses in the lymph node, where the lymphatic fluid enters, blocked extravasation of the contrast-agent throughout the entire lymph node, thus interfering with the normal lymph flow.

The tumor model in mice, that we have used, mimics the metastatic process in humans, starting with detachment from the primary tumor and entering the blood or lymphatic system. Although SCID mice has only small rudimentary lymph node consisting of reticuloendothelial (phagocytic) cells, the overall architecture of the lymphatic node is conserved, with subcapsular sinus, efferent and afferent lymphatic flow and blood circulation. The lymphatic dissemination in our model initiated in the subcapsular sinus and then spread to the entire lymph node, replacing the whole lymphatic tissue. The same pattern of initial spread of cancer cells to the lymph nodes is frequently seen in carcinomas in the clinic (13,14). Thus, the mechanism and methodologies presented inhere may serve as a basis for further clinical investigations.

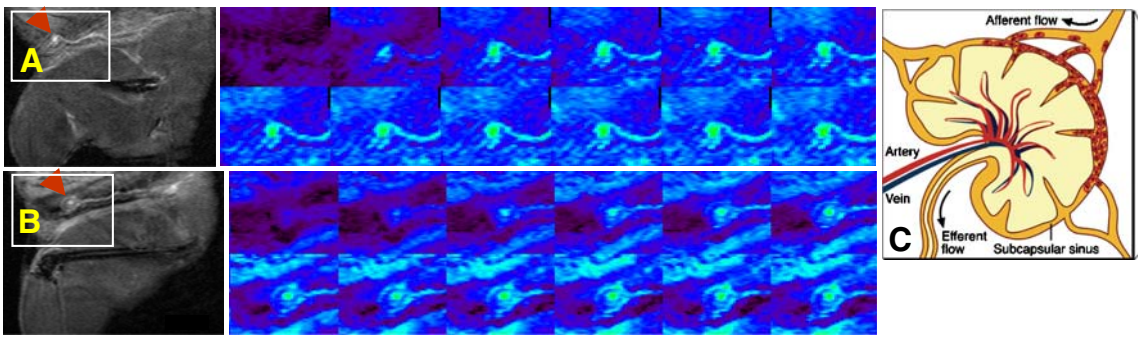

Figure 2: Enhancement pattern of normal and metastatic lymph node by DCE-MRI
A. T1 weighted image post contrast and a series of 12 sequential MRI images (enhancement is color coded) of a normal lymph node, pre (1st image) and post GdDTPA administration using the hybrid bolus/slow infusion protocol. Temporal resolution: 2.5 min. Spatial resolution: $0.12\times0.23\times0.5$ mm^3
B. T1 weighted image post contrast and a series of 12 sequential MRI images of metastatic lymph node recorded as described in A. The enhanced lymph node is marked with red arrow. The squared region was demonstrated in the dynamic

References
1. Folkman J. Fundamental concepts of the angiogenic process. Curr Mol Med 2003;3:643–51.
2. McDonald DM, Choyke PL. Imaging of angiogenesis: from microscope to clinic. Nat Med 2003;9:713–25.
3. Carmeliet P, Jain RK. Angiogenesis in cancer and other diseases. Nature 2000;407:249–57.
4. Jain RK. Transport of molecules in the tumor interstitium: a review. Cancer Res 1987;47:3039–51.
5. Heldin CH, Rubin K, Pietras K, Ostman A, 2004. High interstitial fluid pressure—an obstacle in cancer therapy. Nat. Rev. Cancer 2004;4: 806–813.
6. Swartz MA, Skobe M. Lymphatic function, lymphangiogenesis, and cancer metastasis. Microsc Res Tech 2001;55:92–9.
7. Pepper MS, Tille JC, Nisato R, Skobe M. Lymphangiogenesis and tumor metastasis. Cell Tissue Res 2003;314:167–77.
8. Dadiani M, Kalchenko V, Yosepovich A, Margalit R, Hassid Y, Degani H, Seger D. Real-Time Imaging of Lymphogenic Metastasis in Orthotopic Human Breast Cancer. Cancer Res 2006; 66: 8037–41.
9. Kwon S, Sevick–Muraca EM, Noninvasive Quantitative Imaging of Lymph Function in Mice. Lymphatic Research and Biology 2007; 5: 219–231.
10. Hassid Y, Furman-Haran E, Margalit R, Eilam R, Degani H. Noninvasive magnetic resonance imaging of transport and interstitial fluid pressure in ectopic human lung tumors. Cancer Res. 2006 Apr 15;66:4159–66.
11. Hassid Y, Eyal E, Margalit R, Furman-Haran E, Degani H. Non-invasive imaging of barriers to drug delivery in tumors. Microvasc Res. 2008 Aug;76:94–103.
12. Kobayashi H, Kawamoto S, Sakai Y*, et al.* Lymphatic drainage imaging of breast cancer in mice by micro-magnetic resonance lymphangiography using a nano-size paramagnetic contrast agent. J Natl Cancer Inst 2004;96:703–8.
13. Carr I. Lymphatic metastasis. Cancer Metastasis Rev 1983;2:307–17.
14. Sleeman JP. The lymph node as a bridgehead in the metastatic dissemination of tumors. Recent Results Cancer Res 2000;157:55–81.

Hormonal Regulation of Breast Cancer Vasculature: Molecular and Functional Studies

M. Dadiani, D. Seger, D. Badikhi, T. Kreizmann, R. Margalit R Eilam and H. Degani
Weizmann Institute of Science, Rehovot, ISRAEL

Breast cancer has a striking dependence upon steroid hormones, particularly estrogen and progesterone, in its onset, development, progression and metastasis (1). Hormonal regulation of breast cancer is, therefore, a fundamental research topic with immense clinical implications. The idea of endocrine therapy was put forward more than 100 years ago, when Beaston G. showed a remission of metastatic breast cancer followed removal of the ovaries. Later on, the ovarian released estrogen was shown to be involved in the stimulation of breast cancer growth, through interaction with a specific estrogen receptor (ER) (2 and references cited therein). More recently it was found that there are two distinct estrogen receptors ERalpha and the newly discovered ERbeta. Both bind 17beta-estradiol with high affinity and interact with classical estrogen response elements in a similar fashion. However, there are also major differences between their tissue distribution and their transcriptional activities (3). The discovery of ERalpha paved the way for the development of anti-estrogen therapy with ER blockers as well as estrogen synthesis inhibitors (4, 5). The level of ERs and of the progesterone receptor (PgR) are dominant prognostic factors and serve to select patients for endocrine therapy, however, not all breast cancers with positive levels of ER and even PgR are endocrine-responsive, and even those cancers will eventually become resistant to anti-estrogen treatment (5, 6).

Although it has been recognized for decades that breast cancer is hormonal-dependent, only lately attention has been drawn to the role of estrogen in the process of angiogenesis and vasculature function in breast cancer. Multiple lines of evidence indicate that estrogen regulates angiogenesis in breast cancer, predominantly via the regulation of vascular endothelial growth factor (VEGF) (7–9). However, the molecular mechanisms and the detailed regulation in vivo remain unclear (9). Recent studies also indicated that VEGF expression levels are also controlled by c-Myc (10, 11) and that c-Myc is essential for angiogenesis (12). Other studies have revealed that c-Myc plays a central role in the angiogenic switch in tumors (11, 13). It has been also shown that estrogen activate c-Myc expression in ERalpha-positive human breast cancer cells and act as a mediator of estrogen effects on cell growth (14). We, therefore, investigated the role of c-Myc in estrogen regulation of VEGF and of the vascular function in breast cancer cells and tumors using molecular techniques and magnetic resonance imaging methods. In order to differentiate between estrogen upregulation of c-Myc through ERα and induction of c-Myc alone we concentrated on investigating MCF7 human breast cells, stably transfected with a tetracycline-inducible (tet-on/tet-off) c-*myc* gene–MCF7-35im (15). We also confirmed the results in MCF7 wild-type cells.

Methods of molecular biology were applied *in vitro*, quantifying mRNA and protein levels including a detailed time course of estrogen induced changes in the expression levels of ERalpha. ERbeta, c-Myc, and VEGF. The studies of tumors derived from the MCF7-35im cells growing in the mammary tissue of SCID mice included histopathology and immunohistochemistry characterization of *ex vivo* specimens, as well as *in vivo* studies of the vascular perfusion function by dynamic contrast enhanced MRI using experimental parameters and model based image analysis as previously described (16).

We found a typical time dependent, transient induction of c-Myc and VEGF transcription by estrogen in parallel to ERalpha degradation with no significant involvement of ERbeta. Silencing of c-Myc activity by siRNA reduced the estrogenic time-dependent induction of VEGF. However, short term, estrogen-independent overexpression of c-Myc was not sufficient to induce VEGF. Indeed, a co-binding of c-Myc and ERalpha on the VEGF promoter in chromatin immunoprecipitation experiments illuminated the role of c-Myc in estrogen induction of VEGF. Based on these results we concluded that estrogen induction of c-Myc is necessary for the transient stimulation of VEGF transcription. The co-binding of c-Myc and the activated estrogen receptor on the VEGF promoter present a novel mechanism for estrogen regulation of VEGF (Figure 1).

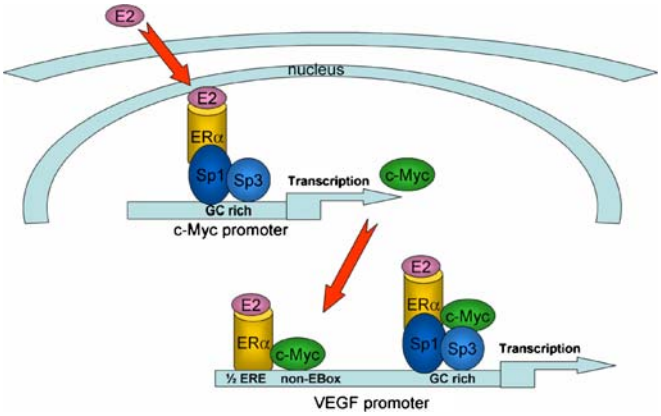

Figure 1 Schematic drawing of the mechanism of c-Myc-mediated induction of VEGF by estrogen: estrogen (E2) stimulates c-Myc transcription through recruitment of Sp proteins to the c-Myc promoter. Then, c-Myc and the ERalpha–E2 complex co-bind on the VEGF promoter, 1.5 kb upstream of the transcription start site, inducing VEGF transcription. VEGF can be also induced through interaction with Sp proteins in the GC region on the VEGF promoter.

Further cell culture studies that mimic the conditions in tumors, characterizing VEGF and c-Myc expression levels, as well as *in vivo* studies revealed that chronic treatment with estrogen, as well as long term upregulation of c-Myc induced a smaller increase in the level of VEGF as compared to the transient in *vitro* induction**,** but regulated steady gene expression levels of VEGF. The results also revealed differences between acute, transient *in vitro* regulation and chronic *in vivo* regulation, highlighting the complexity of estrogen regulation in the unstable microenvironment of tumors. Investigating the effects of hypoxic conditions *in vitro* served to explain the differences and suggested a sequence of events that provided a complemented picture of estrogen regulation of VEGF.

Additional dynamic contrast enhanced MRI studies enabled us to correlate hormonal regulation of VEGF with the function of the microcapillary network. Specifically, we found that the values of the transcapillary transfer constants, which are determined by the microcapillary permeability factor, correlate with VEGF levels. Estrogen treatment of the tumors over 20 days resulted in sustained levels of VEGF and in a stable capillary permeability factor promoting tumor progression. Estrogen-withdrawal (EWD) led to an increase in the level of VEGF expression and of the capillary permeability factor. Increased permeability factor were also detected in these tumors upon tamoxifen treatment (17, 18). Although VEGF expression level in cell cultures decreased upon removal of estrogen, it increased in the tumors, most likely due to the induction of hypoxic conditions which strongly upregulate VEGF expression. The dominant role of hypoxia in upregulating VEGF described and the induction of hypoxia following tamoxifen (19) strongly supports this hypothesis.

Figure 2 provides a summary of the results of the *in vitro* and *in vivo* experiments and demonstrates the need to account for the temporal effects and influence of the microenvironment conditions on estrogen induced changes.

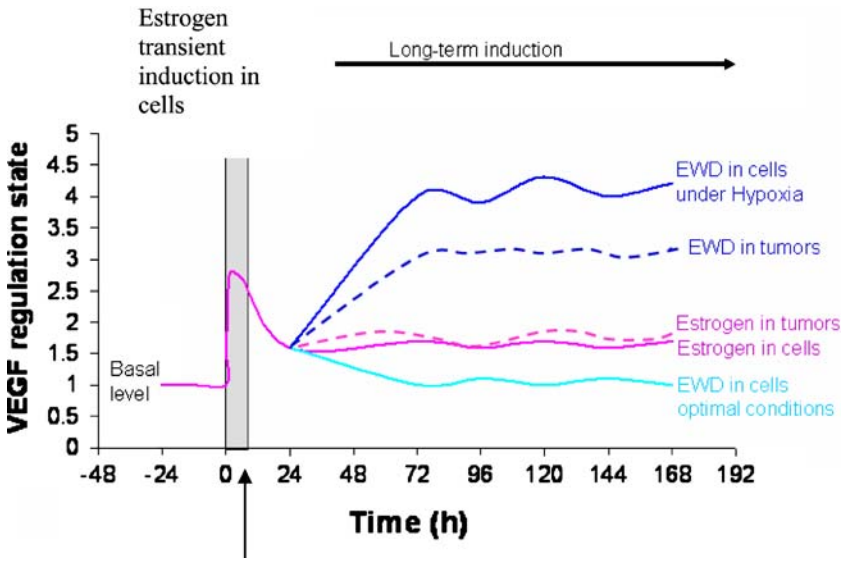

Figure 2 Summary of the time courses of VEGF expression levels in human breast cancer cells *in vitro* and tumors *in vivo*, regulated by acute estrogen treatment (cells) and estrogen chronic (long term) treatment and withdrawal (cells and tumors) under optimal conditions and hypoxic conditions. The changes in VEGF levels were calculated from the actual results obtained from western PCR and immunohistochemistry results. EWD—withdrawal of estrogen

In summary, our findings illuminate the critical role of c-Myc in estrogen regulation of VEGF and angiogenesis in breast cancer, and further suggest that sustained high levels of c-Myc alone can partially mimic estrogen regulation of breast cancer angiogenesis. The results also revealed the difference between the transient estrogen regulation *in vitro* and the chronic estrogen regulation *in vivo*, highlighting the complexity of this regulation in the unstable microenvironment of tumors.

References

1. Osborne CK and Schiff R. Estrogen-receptor biology: continuing progress and therapeutic implications. J Clin Oncol 2005; 23, 1616–22.
2. Jensen EV, Jordan VC. The estrogen receptor: a model for molecular medicine, Clin Cancer Res 2003, 9:1980–1989.
3. Koehler KF, Helguero LA, Haldosen L-A, Warner M, Gustafsson J-A. Reflection on the Discovery and Significance of Estrogen Receptorbeta. Endocrine Reviews 2005, 26:465–478
4. Ali S, Coombes RC. Endocrine-responsive breast cancer and strategies for combating resistance. Nat Rev Cancer 2002; 2:101–12.
5. MacGregor JI, Jordan VC. Basic guide to the mechanisms of antiestrogen action. Pharmacol. Rev 1998; 50:151–96.
6. WL McGuire, Hormone receptors: Their role in predicting prognosis and response to endocrine therapy. Semin. Oncol. 1978; 5: 428–33.
7. Djonov V, Andres AC, Ziemiecki A. Vascular remodelling during the normal and malignant life cycle of the mammary gland. Microsc Res Tech 2001;52:182–9.
8 . Hyder SM. Sex-steroid regulation of vascular endothelial growth factor in breast cancer. Endocr Relat Cancer 2006;13:667–87.
9 Losordo DW, Isner JM. Estrogen and angiogenesis: A review. Arterioscler Thromb Vasc Biol 2001; 21:6–12.
10. Barr LF, Campbell SE, Diette GB, Gabrielson, EW, Kim S, Shim H, and Dang, CV. c-Myc suppresses the tumorigenicity of lung cancer cells and down-regulates vascular endothelial growth factor expression. Cancer Res 2000; 60: 143–149.
11. Knies-Bamforth UE, Fox SB, Poulsom R, Evan GI, Harris AL. c-Myc interacts with hypoxia to induce angiogenesis in vivo by a vascular endothelial growth factor-dependent mechanism. Cancer Res 2004; 64: 6563–6570.
12. Baudino TA, McKay C, Pendeville-Samain H, Nilsson JA, Maclean KH, White, E L, Davis AC, Ihle JN, Cleveland JL. (2002). c-Myc is essential for vasculogenesis and angiogenesis during development and tumor progression. Genes Dev 16, 2530–2543.
13. Shchors K, Shchors E, Rostker F, Lawlor ER, Brown-Swigart L, Evan GI. The Myc-dependent angiogenic switch in tumors is mediated by interleukin 1beta. Genes Dev 2006; 20: 2527–2538.
14. Musgrove EA, Sergio CM, Loi S, Inman CK, Anderson LR, Alles MC, Pinese M, Caldon CE, Schütte J, Gardiner-Garden M, Ormandy CJ, McArthur G, Butt AJ, Sutherland RL. Identification of functional networks of estrogen-and c-Myc-responsive genes and their relationship to response to tamoxifen therapy in breast cancer. PLoS One. 2008; 3(8): e2987.
15. Venditti M, Iwasiow B, Orr FW, and Shiu RP. C-myc gene expression alone is sufficient to confer resistance to antiestrogen in human breast cancer cells. Int J Cancer 2002; 99: 35–42.
16. Dadiani M, Margalit R, Sela N, Degani H. High-resolution magnetic resonance imaging of disparities in the transcapillary transfer rates in orthotopically inoculated invasive breast tumors. Cancer Res 2004; 64:3155–61.
17. Bogin L, and Degani H. Hormonal regulation of VEGF in orthotopic MCF7 human breast cancer. Cancer Res 2002; 62, 1948–1951.
18. Furman-Haran E, Grobgeld D, and Degani H. Dynamic contrast-enhanced imaging and analysis at high spatial resolution of MCF7 human breast tumors. J Magn Reson 1997; 128:161–171.
19. Evan SM, Koch CJ, Laughlin KM, Jenkins WT, Van Winkle T, and Wilson D F. Tamoxifen induces hypoxia in MCF-7 xenografts. Cancer Res 1997;57: 5155–5161.

Combination of Signs—Diagnosing Tumor Grading?

Matthias Dietzel MD[1], Pascal A.T. Baltzer MD[1], Tibor Vag MD/PhD[1], Aimee B. Herzog MD[1], Tobias Gröschel[1], Mieczyslaw Gajda MD[2], Oumar Camara MD[3], Werner A. Kaiser MD/MSc[1]

[1]Institute of Diagnostic and Interventional Radiology, Friedrich-Schiller-University Jena, Erlanger Allee 101, D-07740 Jena, Germany; [2]Institute of Pathology, Friedrich-Schiller-University Jena, Ziegelmühlenweg 1, D-07740 Jena, Germany; [3]Clinic of Gynecology, Friedrich-Schiller-University Jena, Bachstr. 18, D-07740 Jena, Germany

Corresponding Author:
Matthias Dietzel, MD, Institute of Diagnostic and Interventional Radiology, Friedrich-Schiller-University Jena, Erlanger Allee 101, D-07740 Jena, Phone: +49-3641-9324928, Fax: +49-3641-9324832, E-mail: matthias.dietzel@med.uni-jena.de

Introduction

Grading of invasive breast cancer is a standard and independent prognostic factor classifying tumor aggressiveness (8, 9, 11). Epidemiological studies demonstrate strong association of both breast cancer-specific survival and disease-free survival with Grading (2, 8). Most evidence for the use of MR-Mammography (MRM) has been accumulated for differential diagnosis of suspect breast lesions and preoperative staging (1, 7, 10). Yet, there is also increasing evidence that descriptors in MRM might accurately classify Grading (4, 6). To our knowledge there are no large series >300 patients addressing the correlation of MRM vs. Grading. Therefore, this prospective cohort study was designed to

1. *Assess* dynamic and morphologic profiles in invasive breast cancers using a detailed set of 17 previously published descriptors in a standard protocol
2. *Correlate* these single descriptors with Grading
3. *Evaluate* a statistical model for the estimation of Grading using all descriptors combined

Methods

399 invasive breast cancers were included into this prospective IRB approved study. Standardized protocol and study design was applied (T1w-FLASH; 0.1 mmol/kgBW Gd-DTPA; T2w-TSE). Recent surgery, core biopsy, chemotherapy or radiation therapy of the breast were exclusion criteria. Standard of reference was histological verification and Grading according to Elston-Eillis (2).

In every lesion 17 previously published descriptors were assessed by expert readers (>500 MRM), which were unaware of histopathological outcome, but knew patients history (3, 5).

Subgroups of G1 (*n*: 49), G2 (*n*: 193) and G3 cancers (*n*: 157) were created. Prevalence of each descriptor was correlated with Grading (Crosstabs, Chi-Square-test). Overall diagnostic accuracy to correlate invasive breast cancer with Grading was identified using binary logistic regression (LRA) and ROC-analysis.

Results

399 patients with 399 invasive cancers were included into the dataset (mean age: 59.7 years; CI: 58.5–60.8; range: 25–87 years; SD: 11.9 years).

Prevalence of homogenous internal enhancement was inversely correlated with Grading (G1: 24.5%; G3: 5.1%; *P*: 0.003). Most significant correlation with Grading was identified regarding edema (*P*:<0.0001).

Classification of Grading was possible using LRA in all subclasses (P:<0.0001). Highest potential could be observed to differentiate G1 from G3 cancers (AUC: 0.895). Lowest accuracy was observed, if focus was set on differentiation of G3 vs. G2 lesions (AUC: 0.733).

Conclusion

This prospective cohort study of 399 invasive breast cancers with surgicopathological verification identified significant correlation of morphologic and dynamic descriptors in MR-Mammography with histopathological Grading. Our results illustrate the importance of combined assessment of multiple descriptors to accurately correlate morphologic and dynamic profiles with tumor Grading. As Grading represents a major prognostic factor in breast cancer, MR-Mammography could be used to estimate prognosis.

Acknowledgement

We'd like to thank our Team of MR-Physicists: Prof. Reichenbach and Dr. Herrmann.

This study was only possible due to the help and huge enthusiasm of our MR-Technicians (in alphabetical order): H. Hartmann, A. Heyer, C. Kipker, C. Nyffenegger, I. Krumbein, M. Hammer, P. Loob, M. Pohl, K. Prast and T. Rehm to mention only a few.

Finally, we'd like M. Hoppert for their help to prepare the manuscript for publication.

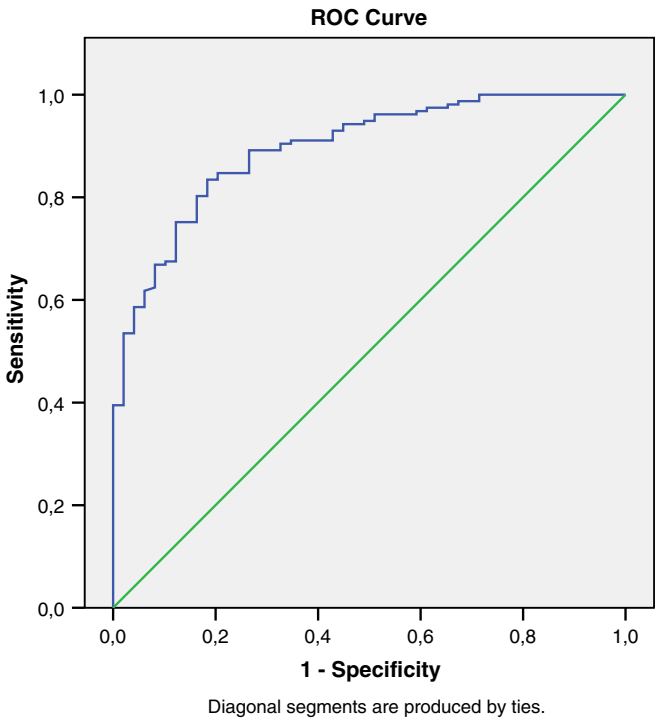

Figure 1: Receiver operating characteristic curve to differentiate well differentiated (G1) from poorly differentiated invasive breast cancer (G3) using 17 predefined descriptors in MR-Mammography. Thin line: zero-hypothesis (Area=0.5).

References

1. DeMartini W, Lehman C. A review of current evidence-based clinical applications for breast magnetic resonance imaging. Top Magn Reson Imaging 2008; 19:143–150.

2. Elston CW, Ellis IO. Pathological prognostic factors in breast cancer. I. The value of histological grade in breast cancer: experience from a large study with long-term follow-up. Histopathology 1991; 19:403–410.

3. Kaiser WA. Signs in MR-Mammography. Berlin, Heidelberg, New York: Springer, 2007.

4. Lee SH, Cho N, Kim SJ, et al. Correlation between high resolution dynamic MR features and prognostic factors in breast cancer. Korean J Radiol 2008; 9:10–18.

5. Malich A, Fischer DR, Wurdinger S, et al. Potential MRI interpretation model: differentiation of benign from malignant breast masses. AJR Am J Roentgenol 2005; 185:964–970.

6. Montemurro F, Martincich L, Sarotto I, et al. Relationship between DCE-MRI morphological and functional features and histopathological characteristics of breast cancer. Eur Radiol 2007; 17:1490–1497.

7. Peters NH, Borel Rinkes IH, Zuithoff NP, Mali WP, Moons KG, Peeters PH. Meta-analysis of MR imaging in the diagnosis of breast lesions. Radiology 2008; 246:116–124.

8. Rakha EA, El-Sayed ME, Lee AH, et al. Prognostic significance of Nottingham histologic grade in invasive breast carcinoma. J Clin Oncol 2008; 26:3153–3158.

9. Rakha EA, El-Sayed ME, Menon S, Green AR, Lee AH, Ellis IO. Histologic grading is an independent prognostic factor in invasive lobular carcinoma of the breast. Breast Cancer Res Treat 2008; 111:121–127.

10. Schnall MD, Blume J, Bluemke DA, et al. Diagnostic architectural and dynamic features at breast MR imaging: multicenter study. Radiology 2006; 238:42–53.

11. Zhang JZ, Petushi S, Regli WC, Garcia FU, Breen DE. A study of shape distributions for estimating histologic grade. Conf Proc IEEE Eng Med Biol Soc 2008; 2008:1200–1205.

Combined staging in one step: MR-Mammography and Whole-body MR

Matthias Dietzel MD[1], Pascal A.T. Baltzer MD, Tibor Vag MD/PhD[1], Werner A. Kaiser MD/MSc[1]

[1]Institute of Diagnostic and Interventional Radiology, Friedrich-Schiller-University Jena, Erlanger Allee 101, D-07740 Jena, Germany

[2]Institute of Pathology, Friedrich-Schiller-University Jena, Ziegelmühlenweg 1, D-07740 Jena, Germany

[3]Clinic of Gynecology, Friedrich-Schiller-University Jena, Bachstr. 18, D-07740 Jena, Germany

Corresponding Author:

Matthias Dietzel, MD, Institute of Diagnostic and Interventional Radiology, Friedrich-Schiller-University Jena, Erlanger Allee 101, D-07740 Jena, Phone: +49-3641-9324928, Fax: +49-3641-9324832, E-mail: matthias.dietzel@med.uni-jena.de

Background

Accurate staging of breast cancer is essential to appropriately choose the best therapeutic options and to adequately assess prognosis of the

patients. Different from most other malignant human tumors, three steps for adequate staging are necessary:

1. **Local staging**: Assessment of the primary tumor and its geometric boundaries. Furthermore, evaluation of multifocal or multicentric as well as contralateral disease.
2. **Regional staging**: Evaluation of axillary lymph nodes is routinely done in invasive carcinomas after surgical dissection. According to current data the "Sentinel concept" represents an alternative to complete dissection of axilla.
3. **Distant staging**: Invasive breast cancer is a highly aggressive disease. Metastases are frequently observed with predilection of bone, liver, lung and brain. Depending on guidelines different tests are recommended to screen for incidental metastases at initial diagnosis.

Depending on several factors such as results of loco-regional Staging, the following tests are most widely used in clinical routine to give a few examples:

Organ	Modality
Liver	US, CT, MRI
Bone	Scintigraphy
Lung	CT, MRI
Brain	CT, MRI

Most current concepts do not address MRI for distant whole body staging, as there is still little data on this issue. However, fast evolving techniques provide excellent sequences for fast and accurate staging in whole body imaging.

Teaching point

This talk will give an overview over the current data regarding local staging vs. breast MRI. In a second part focus will be set on regional and distant staging. Starting with a survey on the current literature the limitations of knowledge will be discussed. Subsequently, the current technical options for whole body imaging at one step will be addressed. Using this approach a conventional breast MRI is combined with a whole body staging at one scanning session within a reasonable time period. A possible protocol will be presented and clinical examples will be demonstrated to illustrate this charming approach. Finally, comparison with conventional distant staging will be discussed.

The Hook sign for differential diagnosis of malignant from benign lesions in magnetic resonance mammography

Matthias Dietzel MD[1], Pascal A.T. Baltzer MD, Tibor Vag MD/PhD[1], Aimee Herzog MD[1], Tobias Gröschel[1], Mieczyslaw Gajda MD[2], Oumar Camara MD[3], Werner A. Kaiser MD/MSc[1]

[1]Institute of Diagnostic and Interventional Radiology, Friedrich-Schiller-University Jena, Erlanger Allee 101, D-07740 Jena, Germany

[2]Institute of Pathology, Friedrich-Schiller-University Jena, Ziegelmühlenweg 1, D-07740 Jena, Germany

[3]Clinic of Gynecology, Friedrich-Schiller-University Jena, Bachstr. 18, D-07740 Jena, Germany

Corresponding Author:

Matthias Dietzel, MD, Institute of Diagnostic and Interventional Radiology, Friedrich-Schiller-University Jena, Erlanger Allee 101, D-07740 Jena, Phone: +49-3641-9324928, Fax: +49-3641-9324832, E-mail: matthias.dietzel@med.uni-jena.de

Background

In the past years central focus of clinical research in MR-Mammography (MRM) was improvement of specificity. Due to the abundance of information, there is room for extension of the current MRI BI-RADS®-lexicon. This is why additional descriptors have been described. One of these is Hook sign (HS). To our knowledge neither detailed statistical analysis, nor evaluation of subgroups has been published so far. Accordingly, this clinical investigation of was designed to

1. *evaluate* HS in a large prospective cohort study,
2. *assess* association between HS and tumor size,
3. *correlate* prevalence of HS and histopathological outcome and to
4. *analyze* the correlation between HS and grading of invasive carcinomas.

Methods

This study was approved by the local ethical committee. 1,084 consecutive lesions with histological verification after MR-Mammography were included in this study (no prior manipulations of the breast before MRM). T2w-TSE images and dynamic contrast enhanced series of T1-weighted images were acquired using standardized examination protocols (B: 1.5 T). HS was positive, if a hook like spiculated dendrite connecting the lesion with the pectoral muscle could be visualized. Examinations were rated by experienced observers ($n>500$). Prevalence of HS was correlated with histological diagnosis, Grading and size (Chi-square test; Confidence-Intervals).

Results:

HS was significantly associated with malignancy ($p<0.001$), providing high specificity and positive predictive value (96.1% and 93.1%). Malignant lesions >20 mm presented significantly more often HS ($p<0.001$). HS was characteristic of invasive cancers and rare in preinvasive malignomas ($p<0.001$). Prevalence of HS didn't differ between invasive lobular and ductal carcinomas (n.s.). There was no correlation between HS and the Grading of invasive carcinomas.

Conclusion:

Hook sign (HS) is still a new descriptor in MRM. It can be used to interpret MR Mammograms in a standard protocol and there is no need for extra scanning time or hardware. We could demonstrate the potential of HS to differentiate benign from malignant breast lesions in MRM with high specificity (96.8%) and PPV (93.1%). Analysis of subgroups revealed the potential to accurately characterize invasive breast carcinomas, even if the cancer was well differentiated. Hook sign was particularly useful in the evaluation of advanced lesions.

Surgical applications of breast MRI: Is it really useful?

Professor Philip J Drew

Professor of Breast Surgery, Hull York Medical School, Director/ Consultant Oncoplastic Breast Surgeon; Mermaid Breast Unit, Royal Cornwall Hospitals, Treliske, Cornwall, UK

Since I began my research with Professor Turnbull in Hull, UK, on the surgical application of breast MRI the early 1990's there has been a dramatic increase in the use of breast MRI in the surgical clinic. Amongst other things we are now using breast MRI for the detection

of multi-focal disease, surgical planning for breast conserving therapy, monitoring response to neo-adjuvant chemotherapy and screening. Research has largely been driven by radiologists seeking a more accurate diagnostic modality for the evaluation of breast cancer. The implications of this technology for surgical practice and the patients' concerned have not been evaluated in such a rigorous fashion, leading to conflicting views within the global surgical community. Indeed the utilisation of the information provided to surgeons by radiologists reporting breast MRI varies between mainland Europe, the UK and the USA, leading to differing claims for its clinical effectiveness. It is certainly the case that the available data has recently been presented in arguments both for and against the use of breast MRI in routine surgical practice. In most surgical practice there is still a "technology gap" between the quality of the information generated by breast MRI and the methods a surgeon can use to interpret the information. In presenting a surgical review of the data I will endeavour to highlight these problems and encourage debate on how best to involve radiologists, surgeons and patients so that breast MRI can be used effectively to improve clinical outcomes.

Advanced second-look ultrasound of MR detected lesions with fusion imaging

Fausto A[1], Preziosa A[2], Gruden M[1], Gaburro L[2], Crisci M[1] and Rizzatto G[1]
[1]Diagnostic Imaging, St. John of God Hospital, Viale Fatebenefratelli, 34-34170 Gorizia, Italy; [2]Ultrasound imaging, GE Healthcare, Via Galeno, 36-20156 Milan, Italy

Keywords: Breast neoplasm · Ultrasound · Magnetic resonance · Fusion imaging· Diagnosis

Introduction

Many studies have demonstrated how contrast-enhanced magnetic resonance (MR) imaging is more sensitive to detect breast cancer compared to mammography and ultrasound (US) [1–3]. Worldwide experts have published indications, guidelines and recommendations to obtain the best achievable result in diagnosing breast cancer, throughout risk factor stratification, detailed technique and lexicon description [4–6]. However, high rate of benign lesions at pathology obtained with MR-guided biopsy, i.e. lesions occult to mammography and US but with suspicious characters, shows MR lack of positive predictive value for breast cancer even in experienced settings [7].
New sequences are proposed to increase MR specificity prior to biopsy [8]; however a cutting edge technique seems to be the second evaluation with US of additional or unexpected MR lesions. Previous experiences described a sort of malignancy probability when US correlation is found [9–10]. However, a noteworthy number of breast cancers were found in the group without US correlation; moreover, the impact of this operator-dependent technique in proving objectively US-MR correlation still remains unknown.
Nowadays US technology developments allow to integrate new tools to breast US imaging: MR volume navigation (VNav), fusion imaging and elastography.
Aim of this paper is to show how an advanced second-look US with VNav and fusion imaging can be obtained increasing techniques correlation.

Risk evaluation

From a theoretical point of view, any MR lesion could be classified according to morphology, dynamics [11, 12] and signs [13, 14]. However, if we consider drugs intake, hormonal status, previous therapy (surgery, radiation and chemotherapy), and risk factors (genetic and familial predisposition to breast cancer), the same appearance should be differently classified [15–17].
Succeeding procedures are mainly based on ACR BI-RADS score [18]. However some inherent limitations should be considered in choosing the approach for final diagnosis. Breast hypertrophy, scan technique [19] and lesion position and dimension [7, 20] could theoretically limit US–MR correlation and detection reducing biopsy performance [7]. An example can be found in a retrospective study showing a very low percentage of cancer in MR enhancing foci smaller than 5 mm in diameter [21]. Therefore, a cost effectiveness balance is often made mainly based on available facilities, radiologist's skills and risk evaluation.

Advances in US technology

US with VNav for breast imaging is a new technology (LOGIQ E9, GE Healthcare) in which a magnetic tracking system is used to determine the relative position of a pair of freehand sensors versus a fixed transmitter using a defined operating volume. In particular, an electromagnetic transmitter is positioned near the subject under examination and two electromagnetic sensors are mounted on a 6–15 MHz linear transducer' bracket. Both, transmitter and sensors, are connected to a position-sensing unit embedded in the US scanner allowing to track probe position and orientation within the electromagnetic field. Live US image is coregistered to a breast MR volume, previously acquired and loaded into the US system, by coupling at least three pair of points. After US–MR coregistration, VNav software reconstructs a real time multiplanar MR image of the corresponding live US image that can be displayed side-by-side or in a blended overlaying format.
In addition to live B-mode and Color-Flow images, it is possible to perform real time manual US elastography for target lesions during US with VNav. Elastography is a technique depicting tissue stiffness by analyzing US signals before and after a gentle manual tissue compression and relaxation made with the US probe. The resulting color mapped image is displayed in a blended overlaying B-mode format for a user-selected region of interest. All images and video clips generated can be stored and/or printed.

Technical aspects for US–MR coregistration

Due to breast volume distortion, three softgel capsules of natural d-alpha-tocopherol (Vitamin E, 400 UI, Smart Nutrition Ltd.) are positioned over a corresponding black or blue surgical skin marker (product #26-001 or #26-016B, DeRoyal Industries Inc.). Each skin marker is drawn as large as capsule dimensions and subjectively positioned at 9, 12 and 3 o'clock radially to the nipple. Each capsule is fixed with a polyolefin single coated surgical tape (product #1527-0, 3M Health Care) during MR examination and removed at the end. Skin markers are covered with a transparent dressing (product #1623W, 3M Health Care) to prevent its alteration before US exam. MR examinations is performed on a 1.5 T MR scanner (Achieva, Philips Healthcare) as follows: three-dimensional turbo field echo sequence with T1-weighted high resolution isotropic examination volume and spectral attenuated inversion recovery fat suppression (THRIVE SPAIR), 200 axial 1-mm partitions (TR/TE=4.7/2.3 ms; flip angle=10°; field of view=420 mm; matrix=330×420 mm; time 8′30″) with 120-s time resolution; one precontrast and three postcontrast phases, after automated intravenous administration (2 ml/s) of 0.05 mmol/kg of Gd-BOPTA (Multihance, Bracco Diagnostics Inc.) followed by a flush of 20 ml saline solution using a cubital vein (30 ml if dorsal metacarpal vein was used). Supine position with upper extremities extended using double synergy body

coil with SENSivity Encoding (SENSE) covering both breasts is used. Breast compression is minimized using a dedicated mattress and two straps.
MR exams are uploaded on a dedicated postprocessing console (MR Extended WorkSpace, Philips Healthcare) for image evaluation. Native postcontrast sequence of the first or second dynamic phase with or without colors coded pixels describing wash-in and wash-out enhancement for fixed threshold are collected. Digital versatile disk rewritable (DVD+RW) or universal serial bus (USB) is used to store MR volume data.
US imaging is performed in supine position similar to that maintained during MR exam. US scanner system is configured with VNav and high-frequency linear transducer is used after uploading MR volume data and coupling three points as previously described.

Personal experience
Feasibility, accuracy and reproducibility of US with VNav were evaluated by two independent experienced radiologists, in a random fashion, by measuring twice five point-to-probe distances in five healthy volunteers using points of reference (three skin markers, nipple, and internal mammary artery). Time to obtain VNav was recorded. McNemar test and Bland–Altman plot were used for statistical analysis. In all subjects VNav was obtained. Time to obtain VNav was 10±2 and 9±4 minutes (p=n.s.). A total of 100 point-to-probe distances were measured. For each radiologist, point-to-probe distance mean and SD were 0.6±0.5 cm, 0.5±0.3 cm and 0.6±0.4 cm and 0.4±0.3 cm (p=n.s.), respectively.
From February 2nd to April 18th, 73 MR examinations were performed on a 1.5 T MR scanner (Achieva, Philips Healthcare) in prone position using SENSE breast coil, seven elements, as follows: three-dimensional turbo field echo sequence with T1-weighted high resolution isotropic voxel, 150–190 coronal 1-mm partitions with 120-s time resolution using a time interval depending on sequence acquisition time; dynamic evaluation was obtained with one precontrast and four postcontrast phases, after automated intravenous administration (2 ml/s) of 0.05 mmol/kg of Gd-BOPTA (Multihance, Bracco Diagnostics Inc.) followed by a flush of 20 ml saline solution using a cubital vein (30 ml if dorsal metacarpal vein was used).
Seven patients with additional lesion or uncertain findings underwent, after at least 1 h wait, a supine breast MR exam and markers positioning, as previously described. Two independent experienced radiologists performed second-look US without and with VNav to investigate the clinical valued of this new tool. Pathologic examination was standard of reference. McNemar and Sign test were used for statistical analysis.
Out of six patients, eight additional lesions were detected both on prone and supine position breast MR. Pathologic examination showed one IDC, one ILC, one relapse of breast lymphoma, one DCIS, one benign gland tissue, one fibrocystic changes and two sclerosing adenosis. Additional lesions mean and SD were 0.6± 0.2 cm in diameter. A 87% (7/8) detection rate was found using second look US with VNav and only 25% (2/8) without (p=0.018). Second look US with and without VNav sensitivity was 75% (3/4) and 50% (2/4) without; specificity 50% (1/2) and 60% (3/5), respectively (p=n.s.). Both radiologists missed a DCIS of 0.9 cm in diameter pathologically proved with MR-guided biopsy.

Conclusion
According to our first experience, US with VNav can be obtained with acceptable level of accuracy and elevated values of intra-and interobserver agreement. Advanced second-look US with VNav seems to show a significant higher detection rate for only MR detected lesions without differences in diagnostic values, probably related to the small number of cases.
However, this new tool its easy to apply, well-integrated and could be a way to reduce US operator-dependent weight on US–MR lesion correlation.

Acknowledgments
We want to thank Emilio Scarabò, Marco Culot, Alessandro Morena, Sonia Figar, Cristina Furlan, Antonia Muzic, Mike Washburn, Markus Marquart, Yelena Tsymbalenko, Zhe Wu, Laura Taroni, and Kirstin Laconte for their untiring support.

References
1. Sardanelli F, Giuseppetti GM, Panizza P, et al. (2004) Sensitivity of MRI versus mammography for detecting foci of multifocal, multicentric breast cancer in fatty and dense breasts using the whole-breast pathologic examination as a gold standard. AJR Am J Roentgenol 183:1149–1157
2. Kuhl CK, Schrading S, Leutner CC, et al. (2005) Mammography, breast ultrasound, and magnetic resonance imaging for surveillance of women at high familial risk for breast cancer. J Clin Oncol 23:8469–8476
3. Sardanelli F, Podo F, D'Agnolo G, et al. (2007) Multicenter comparative multimodality surveillance of women at genetic-familial high risk for breast cancer (HIBCRIT study): interim results. Radiology 242:698–715
4. Sardanelli F, Giuseppetti GM, Canavese G, et al. (2008) Indications for breast magnetic resonance imaging. Consensus document "Attualità in senologia", Florence 2007. Radiol Med 113:1085–1095
5. Mann RM, Kuhl CK, Kinkel K, Boetes (C. 2008) Breast MRI: guidelines from the European Society of Breast Imaging. Eur Radiol 18:1307–1318
6. Smith RA, Cokkinides V, Brawley OW. (2009) Cancer screening in the United States, 2009: a review of current American Cancer Society guidelines and issues in cancer screening. CA Cancer J Clin 59:27–41
7. Perlet C, Heywang-Kobrunner SH, Heinig A, et al. (2006) Magnetic resonance-guided, vacuum-assisted breast biopsy: results from a European multicenter study of 538 lesions. Cancer 106:982–999
8. Sinha S, Sinha U. (2009) Recent advances in breast MRI and MRS. NMR Biomed. 22:3–16
9. LaTrenta LR, Menell JF, Morris EA, et al. (2003) Breast lesions detected with MR imaging: utility and histopathologic importance of identification with US. Radiology 227:856–861
10. Shin JH, Han BK, Choe YH, Ko K, Choi N. (2007) Targeted ultrasound for MR-detected lesions in breast cancer patients. Korean J Radiol 8:475–483
11. Baum FT, Fischer U, Vosshenrich R, Grabbe EH (2002) Classification of hypervascularized lesions in CE MR imaging of the breast. Eur Radiol 12:1087–1092
12. Schnall MD, Blume J, Bluemke DA, et al. (2006) Diagnostic architectural and dynamic features at breast MR imaging: multicentric study. Radiology 238:42–53
13. Fischer DR, Baltzer P, Malich A, et al. (2004) Is the "blooming sign" a promising additional tool to determine malignancy in MR mammography? Eur Radiol 14:394–401

14. Fischer DR, Wurdinger S, Boettcher J, Malich A, Kaiser WA. (2005) Further signs in the evaluation of magnetic resonance mammography: a retrospective study. Invest Radiol 2005;40:430–435
15. Kuhl CK, Mielcareck P, Klaschik S, et al. (1999) Dynamic breast MR imaging: are signal intensity time course data useful for differential diagnosis of enhancing lesions? Radiology 211:101–110
16. Coulthard A, Potterton AJ (2000) Pitfalls of breast MRI. Br J Radiol 73:665–671
17. Kinkel K, Hylton NM (2001) Challenges to interpretation of breast MRI. J Magn Reson Imaging136:821–829
18. American College of Radiology. (2003) Breast imaging reporting and data system (BI-RADS™) ultrasound. Reston, Va: American College of Radiology. Available at: http://www.acr.org/SecondaryMainMenuCategories/quality_safety/BIRADSAtlas/BIRADSAtlasexcerptedtext/BIRADSUltrasoundFirstEdition.aspx Accessed July 16, 2009.
19. Skaane P, Sauer T. (1999) Ultrasonography of malignant breast neoplasms. Analysis of carcinomas missed as tumor Acta Radiol 40:376–382
20. Panizza P, De Cobelli F, De Gaspari A, et al. (2003) MR-guided stereotactic breast biopsy: technical aspects and preliminary results Radiol Med 106:232–244
21. Liberman L, Mason G, Morris EA, et al. (2006) Does size matter? Positive predictive value of MRI-detected breast lesions as a function of lesion size. AJR Am J Roentgenol 186:426–430

Figure 1. A 36 years old woman with previous left breast skin spearing mastectomy (for 6 cm ductal carcinoma in situ) and subglandular silicon-gel implant insertion of the right breast, for volume compensation, is presented. High-frequency linear transducer with two electromagnetic sensors mounted on bracket' probe are showed during US with MR volume navigation (VNav) scan of the right breast. The others two skin markers are visible at 9 and 12 o'clock.

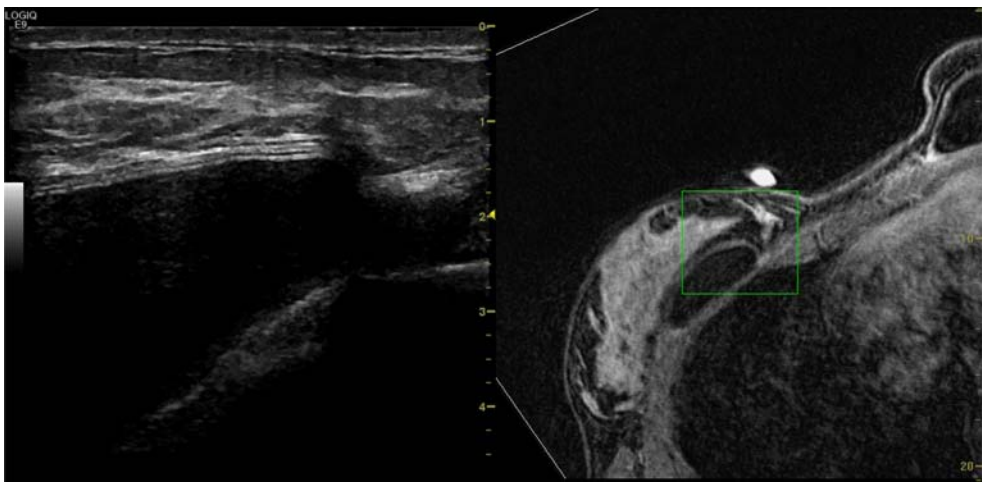

Figure 2 US scan (left side) with the corresponding multiplanar reconstructed MR image (right side) are shown at the same level in Figure 1. The green box represents US scanned area on MR image. Below the capsule at the confluence of internal quadrants—the round high signal intensity over the skin—a suspicious 1.4 cm enhancing MR lesion is depicted, BI-RADS 4. Medially to the lesion the subglandular implant shell is visible as well. On US image, is difficult to recognize any lesion near implant shell. At pathology, obtained with US guided biopsy with VNav, a sclerosing adenosis lesion was demonstrated.

The role of MRI in patients undergoing neoadjuvant chemotherapy: should sentinel lymph node biopsy be performed when MRI findings are negative?

Elisabetta De Matteis[1], Laura Cortesi[1], Annarita Pecchi[2], Rachele Battista[2], Barbara Canossi[2], Claudia Cirilli[1], Massimo Federico[1]
[1]Dipartimento di Oncologia ed Ematologia, Università di Modena e Reggio Emilia; [2]Dipartimento Integrato dei Servizi Diagnostici e per Immagini, Università di Modena e Reggio Emilia
Corresponding author:
Massimo Federico, MD, Oncologia Medica II, Dipartimento di Oncologia ed Ematologia, Centro Oncologico Modenese, Università di Modena e Reggio Emilia, Policlinico—Via del Pozzo 71, 41100 Modena, Italy.
Phone +39-059-4224547; Fax +39-059-4224549; e-mail: federico@unimore.it

Abstract
Over the past decade, neoadjuvant chemotherapy (NACT) has become an appealing option for the management of patients with locally advanced breast cancer and is now also being offered to many patients with early-stage disease. The aim of our study was to assess the ability of MRI to determine nodal status after NACT and to explore if MRI may help to decide between axillary dissection and sentinel node biopsy. This retrospective study included women, diagnosed with locally advanced or large operable breast cancer between 2004 and 2007 in the province of Modena. A total of 48 breast cancer patients were included, who received NACT and were studied by MRI before and after treatment. The sensitivity, specificity, and accuracy of MRI in defining the disease status of the primary tumour were 86% (95% CI: 0.74–0.97), 83% (95% CI: 0.63–1.02), and 85% (95% CI: 0.75–0.95), respectively, for a positive predictive value (PPV) of 97% (95% C.I.: 0.91–1.03) and a negative predictive value (NPV) of 45% (95% C.I.: 0.20–0.70). The sensitivity, specificity, and accuracy of MRI in predicting axillary status was 60%, 86%, and 75%, respectively. These results suggest that a more conservative surgical approach can be offered to patients with locally advanced breast cancer who achieve a satisfactory response with NACT.

Keywords: breast cancer, MRI, neoadjuvant chemotherapy, nodal status

Introduction
Mammography (MM), ultrasound (US), and magnetic resonance imaging (MRI) are currently the three most valuable diagnostic modalities for breast examination. Several studies suggest MRI is more accurate than any other imaging technique in preoperative assessment [1] following neoadjuvant chemotherapy (NACT). Over the past decade, NACT has become an appealing option for management of patients with locally advanced breast cancer and is now also being offered to many patients with early-stage disease. In breast cancer treatment, NACT is similar to adjuvant therapy in terms of disease free and overall survival [2]. Moreover, NACT increases the chance of conservative surgery, which when combined with radiation therapy, guarantees overall survival and disease free survival rates similar to those achieved by mastectomy [3]. In addition, several patients not suitable for surgery at diagnosis may eventually undergo surgery with success due to downstaging of the tumour. Moreover, NACT can also identify patients with chemosensitive disease who are likely to have a favourable outcome, and conversely, those for whom additional treatment may be necessary [4,5]. In any case, accurate assessment of tumour size and location is necessary for planning the most appropriate surgical management [6].

MRI has the unique ability to recognize chemotherapy-induced changes—mainly necrosis and fibrosis—that are otherwise difficult to assess [7]. Due to its ability to distinguish between fibrous and vascularized tissue, MRI is more accurate than X-ray mammography and ultrasound in assessing residual disease although it has been reported that MRI usually overestimates large lesions and underestimates small ones [8,9]. Several studies compared the accuracy of clinical examination, mammography, ultrasound, and MRI in the assessment of final response. They found volumetric-MRI was capable of predicting both the degree of cancer response to NACT at an early stage of treatment and the rate of disease recurrence at the end of treatment [10–13].
Lymph node status is one of the most relevant prognostic factors in breast cancer patients [14,15]. Knowledge of lymph node status is of paramount importance for assessing the regional extent of the disease and for choosing the appropriate treatment [16–19]. In patients undergoing NACT, the standard surgical treatment consists of residual breast tumour resection and axillary node dissection [20]. However after NACT, 50% to 60% of patients have negative lymph nodes status [21]. The correct identification of these patients could lead to more conservative therapy [22,23], i.e. a sentinel lymph node biopsy (SNLB) could determine if the sentinel lymph node is involved and if axillary dissection is necessary.
The aim of our study was to retrospectively assess the ability of MRI in determining nodal status after NACT and to explore if MRI may help decide if axillary dissection is necessary or if sentinel node biopsy should be performed.

Materials and methods
Patients and treatment
The study population was retrieved from the Modena Cancer Registry database and consisted of 2891 women residents in the province of Modena, diagnosed with breast cancer between 2004 and 2007. During this period, 197 women (6.8%) were treated with NACT. Among them, 75 (38.1%) were also investigated with MRI. For this study, we considered only those 48 women (61.5%) investigated with MRI before and after chemotherapy. Forty-four patients were treated with anthracycline-based treatment, associated with taxanes in 30 instances. The remaining four patients were treated with different combinations of drugs. Breast cancer was diagnosed by core needle biopsy before NACT.

Disease assessment
US Examination
US examinations were performed by radiologists with at least 10 years of experience in breast imaging. Both breasts were systematically examined by a radiologist who reported the findings using the five-point Breast Imaging Reporting and Data System (BI-RADS) scale. Transducers with a frequency of 10 MHz or greater were used.

Mammographic Examination
Bilateral two-view mammography (unilateral in women who previously had undergone one-breast mastectomy) was performed with screen-film units with a rotating anode, a 0.3–0.1-mm focus, a focus-film distance of 55 cm or greater, homogeneous breast compression, a mobile grid, and automatic exposure control. Standard mediolateral oblique and craniocaudal projections were acquired. Further dedicated mammograms (i.e., magnification, spot compression, or other additional views) were obtained when necessary. Images from mammographic examinations were evaluated by one reader, with at least 10 years of experience in breast

imaging and findings were classified using BI-RADS. The density pattern was classified according to two categories: breasts with more than 50% of the breast occupied by fibroglandular density as determined by the mean of the two mammographic views and breasts with 50% or less of the breast occupied by fibroglandular density as determined by the mean of the two mammographic views.

Contrast-enhanced MR Imaging

Contrast-enhanced MR imaging was performed at 1.5 T. Dedicated synchronous breast coils were used for bilateral studies (or unilateral studies when a mastectomy had previously been performed) with the patient in the prone position. The examination was planned on the 7th–21st day of the menstrual cycle in premenopausal women, but without scheduling limitations in postmenopausal women. A long venous catheter access was obtained using a plastic cannula in a cubital vein. After localizing scout views were obtained, a contrast-enhanced dynamic three-dimensional T1-weighted spoiled gradient-echo sequence was performed in the transverse or coronal plane. The parameters were as follows: repetition time, 13 ms or less; flip angle, 20°–30°; partition thickness, 3 mm or smaller; number of partitions, 40–128 (to cover both breasts entirely); and acquisition time, not longer than 120 s. The field of view and image matrix were combined to obtain a pixel size of 1.4 mm or less. An unenhanced sequence was performed before contrast agent injection. Then, 0.1 mmol/kg of one of the commercially available gadolinium chelates was intravenously administered at the rate of 2 mL/s using an automatic injector. Injection was followed by a flush with 20 mL of saline. The number of contrast-enhanced sequences, typically five with a temporal resolution not longer than of 120 s, was sufficient to obtain dynamic information during at least the first 6 min after contrast agent injection. Temporal subtraction (enhanced minus unenhanced images) was always performed for the first, second, and last contrast-enhanced sequences. A maximum intensity projection algorithm was applied for the first and second contrast-enhanced sequences. Signal intensity–time and the percentage of enhancement–time dynamic curves were obtained for targeted small regions of interest positioned on the areas of homogeneous maximal enhancement within the enhancing lesion.

Tumour response assessment

Response after NACT was defined according to RECIST criteria [20]; tumor size was measured by MRI, MM, and US scan (USS) at baseline and upon completion of chemotherapy. Complete response (CR) was defined as a complete vanishing of the tumour, partial response (PR) as a decrease of the sum of the longest axes of all individual lesions by more than 30%, progressive disease (PD) as an increase of this sum by more than 20%, and the remainder were classified as stable disease (SD). Complete pathological response was defined as the absence of any invasive component or the exclusive presence of intraductal components.

Results

From 2004 to 2007, a total of 48 breast cancer patients aged between 33 and 84 years (median age 52 years) received NACT and were studied by MRI before and after treatment. Twenty-six (54%) were pre-menopausal and 22 (46%) post-menopausal. According to TNM classification, 15 (31%), 16 (34%), and 17 (35%) patients were in clinical stage IIA, IIB, and III, respectively. Patients' characteristics at baseline are summarized in Table 1. Tumour size, as assessed by different imaging modalities, is described in Table 2. Tumour size measured by MRI was greater than or equal to 5.1 cm in 12 (25%) patients, 2.1 to 5.0 cm in 34 (70.8%) patients, and less than or equal to 2.0 cm in 1 (2.1%) patient. Tumour characteristics after NACT are summarized in Table 3.

TUMOUR RESPONSE TO NACT

After NACT, tumour size as assessed by different imaging modalities is described in Table 4. According to RECIST criteria, 10 (21%) CRs, 22 (46%) PRs, and 15 (31%) stable or progressive diseases were classified by MRI. Overall, there were six false negative and one false positive MRI readings; three false negatives and five false positives by MM; and three false negatives and three false positives by US. Thus, the sensitivity, specificity, and accuracy of MRI were 86% (95% CI: 0.74–0.97), 83% (95% CI: 0.63–1.02), and 85% (95% CI: 0.75–0.95), respectively, for a positive predictive value (PPV) of 97% (95% C.I.: 0.91–1.03) and a negative predictive value (NPV) of 45% (95% C.I.: 0.20–0.70). MM sensitivity, specificity, and accuracy were 92% (95% CI: 0.83–1.01), 29% (95% CI: 0.05–0.52), and 82% (95% CI: 0.71–0.93), respectively, for a PPV of 87% (95% C.I.: 0.75–0.98) and a NPV of 40% (95% C.I.: 0.15–0.65). USS sensitivity, specificity, and accuracy were 92% (95% CI: 0.83–1.0), 57% (95% CI: 0.31–0.84), and 87% (95% CI: 0.77–0.96), respectively, for a PPV of 92% (95% C.I.: 0.83–1.01) and a NPV of 57% (95% C.I.: 0.32–0.82) (Table 5).

LYMPH NODE RESPONSE TO NACT

MRI findings after NACT were suggestive of residual axillary lymph node involvement in 16 (33.3%) cases. However, pathologic examination revealed the presence of residual disease in twenty cases, including 12 true positive and eight false negative cases. Table 6 summarizes discordances between MRI and pathologic findings. Overall, the sensitivity, specificity, and accuracy of MRI were 60%, 86%, and 75%, respectively. However, two of eight false negative cases were represented by micrometastatic disease in an otherwise normal sized lymph node (less than 1 cm in diameter). If we consider these two cases as true negatives by imaging, then the sensitivity, specificity, and accuracy of MRI were 66%, 87%, and 79% respectively. In the remaining six false cases, the lymph node diameter assessed by MRI was between 7 and 21 mm.

Discussion

The availability of newer and effective treatment strategies has favoured the use of NACT as an initial therapy for locally advanced or large operable breast cancer. As a consequence, concern has emerged on the necessity of routine axillary lymph node dissection after NACT in this group of patients, especially when both clinical and imaging examinations suggest an absence of axillary nodal involvement. Thus, accuracy in identifying the presence or absence of residual disease in breasts and axilla after NACT may be of help for choosing the more appropriate, and possibly conservative, surgical approach. For tumours located within the breast, different studies have shown MRI is associated with a higher rate of accuracy than traditional techniques (mammography and ultrasound) [24–25], mostly due to its ability to discriminate between fibrosis and tumour vascularisation [26]. In our study, the accuracy, sensitivity, and specificity of MRI in defining the disease status of the primary tumour compared favourably with literature data. Moreover, we tried to assess the accuracy of MRI in determining the disease status of the axillary nodes. The sensitivity, specificity, and accuracy in predicting axillary status were 60%, 86%, and 75%, respectively. Although eight false negatives were found, two had only micrometastatic involvement. And only a few cases had more than three involved nodes. Recently, Hsiang et al. published their findings on the ability

of dynamic contrast enhanced MRI to predict nodal status in a group of 46 patients with locally advanced breast cancer treated with NACT. They found the status of the primary tumour was predictive of axillary nodal status, suggesting that sentinel lymph node sampling is warranted in patients with negative MRI findings [27]. Our results compare favourably with those of Hsiang and suggest that a more conservative surgical approach can be offered to patients with locally advanced breast cancer who achieve a satisfactory response with NACT. Of course, considering the relevance of morbidity associated with axillary dissection and the risks of underestimating disease extension and consequent appropriate therapies, well designed prospective clinical trials are warranted in this field.

References

1. Esserman L., Hylton N., Yassa L., Barclay J., Frankel S. and Sickles E., Utility of magnetic resonance imaging in the management of breast cancer: evidence for improved preoperative staging, J Clin Oncol 17 (1) (1999), pp. 110–119.
2. Mauri D, Pavlidis N, Ioannidis JP. J Natl Cancer Inst. 2005 Jun 1;97(11):858; author reply 858–9. Neoadjuvant versus adjuvant systemic treatment in breast cancer: a meta-analysis.
3. Fisher B., Anderson S. and Bryant J. et al., Twenty-year follow-up of a randomized trial comparing total mastectomy, lumpectomy, and lumpectomy plus irradiation for the treatment of invasive breast cancer, N Engl J Med 347 (16) (2002), pp. 1233–1241.
4. Feldman LD, Hortobagyi GN, Buzdar AU, Ames FC, Blumenschein GR (1986) Pathological assessment of response to induction chemotherapy in breast cancer. Cancer Res 46: 2578–2581.
5. Singletary SE, Allred C, Ashley P, Bassett LW, Berry D, Bland KI, Borgen PI, Clark G, Edge SB, Hayes DF, Hughes LL, Hutter RV, Morrow M, Page DL, Recht A, Theriault RL, Thor A, Weaver DL, Wieand HS, Greene FL (2002) Revision of the American joint committee on cancer staging system for breast cancer. J Clin Oncol 20: 3628–3636.
6. Garimella V.et al., Recurrence rates after DCE-MRI image guided planning for breast conserving surgery following neoadjuvant chemotherapy for locally advanced breast cancer patients, Eur J Surg Oncol 33 (2) (2007), pp. 157–161.
7. Newman LA, Pernick NL, Adsay V, et al: Histopathologic evidence of tumor regression in the axillary lymph nodes of patients treated with preoperative chemotherapy correlates with breast cancer outcome. Ann Surg Oncol 10:734–739, 2003.
8. Partridge S.C., Gibbs J.E., Lu Y., Esserman L.J., Sudilovsky D. and Hylton N.M., Accuracy of MR imaging for revealing residual breast cancer in patients who have undergone neoadjuvant chemotherapy, Am J Roentgenol 179 (5) (2002), pp. 1193–1199.
9. Londero V., Bazzocchi M. and Del Frate C. et al., Locally advanced breast cancer: comparison of mammography, sonography and MR imaging in evaluation of residual disease in women receiving neoadjuvant chemotherapy, Eur Radiology 14 (8) (2004), pp. 1371–1379.
10. Therasse P., Arbuck S.G. and Eisenhauer E.A. et al., New guidelines to evaluate the response to treatment in solid tumors. European Organization for Research and Treatment of Cancer, National Cancer Institute of the United States, National Cancer Institute of Canada, J Natl Cancer Inst 92 (3) (2000), pp. 205–216.
11. Belli P, Costantini M, Malaspina C et al. MRI accuracy in residual disease evaluation in breast cancer patients treated with neoadjuvant chemotherapy. Clin Radiol 2006;61:946–953.
12. Montemurro F, Martincich L, De Rosa G, et al. Dynamic contrast-enhanced MRI and sonography in patients receiving primary chemotherapy for breast cancer. Eur Radiol 2005;15:1224–1233.
13. Pickles M., Martin Lowry et al. Role of dynamic contrast enhanced MRI in monitoring early response of locally advanced breast cancer to neoadjuvant chemotherapy. Breast Cancer Res Treat 2005;91:1–10.
14. National Institutes of Health, NIH consensus conference on the treatment of early-stage breast cancer, JAMA **265** (1991), pp. 391–395.
15. Pierga J.Y., Mouret E. and Dieras V. et al., Prognostic value of persistent node involvement after neoadjuvant chemotherapy in patients with operable breast cancer, Br J Cancer 83 (2000), pp. 1480–1487.
16. Mustafa I.A., Cole B., Wanebo H.J.,. Bland K.I and Chang H.R., The impact of histopathology on nodal metastases in minimal breast cancer, Arch Surg 132 (1997), pp. 384–391.
17. White R.E., Vezeridis M.P., Konstadoulakis A., Cole B.F., Wanebo H.J. and Bland K.I., Therapeutic options and results for the management of minimally invasive carcinoma of the breast: influence of axillary dissection for treatment of T1a and T1b lesions, J Am Coll Surg 183 (1996), pp. 575–582.
18. March D.E., Wechsler R.J., Kurtz A.B., Rosenberg A.L. and Needleman L., CT-pathologic correlation of axillary lymph nodes in breast carcinoma, J Comput Assist Tomogr 15 (1991), pp. 440–444.
19. Newman LA et al. Histopathologic evidence of tumor regression in the axillary lymph nodes of patients treated with preoperative chemotherapy correlates with breast cancer outcome. Annals of Surgical Oncology 10:734–739 (2003).
20. Thomas A, Ohlinger R, Hauschild M, et al: Options and limits of surgery after pre-operative chemotherapy in breast cancer. Anticancer Res 26:1677–1682, 2006.
21. Bear HD, Anderson S, Brown A, et al: The effect on tumor response of adding sequential preoperative docetaxel to preoperative doxorubicin and cyclophosphamide: Preliminary results from National Surgical Adjuvant Breast and Bowel Project Protocol B-27. J Clin Oncol 21:4165–4174, 2003.
22. Newman EA, Sabel MS, Nees AV, et al: Sentinel lymph node biopsy performed after neoadjuvant chemotherapy is accurate in patients with documented node-positive breast cancer at presentation. Ann Surg Oncol 14:2946–2952, 2007.
23. Cocconi G., Di Blasio B., Alberti G., Bisagni G., Botti E. and Peracchia G., Problems in evaluating response of primary breast cancer to systemic therapy, Breast Cancer Res Treat 4 (4) (1984), pp. 309–313.
24. Steele JRC. The axillary lymph nodes in breast cancer. Seven years on. J Royal Coll Surg Edinb 1983; 28:282–91
25.Kalisher L. Xeroradiography of axillary lymph node disease. Radiology 1975; 114: 67–71
26. Stomper PC, Winston JS, Herman S, Klippenstein DL, Arredondo MA, Blumenson LE. Angiogenesis and dynamic MR imaging gadolinium enhancement of malignant and benign breast lesions. Breast Cancer Res Treat. 1997 Aug;45(1):39–46
27. Hsiang DJ et al. Predicting nodal status using dynamic contrast-enhanced magnetic resonance imaging in patients with locally advanced breast cancer undergoing neoadjuvant chemotherapy with and without sequential trastuzumab. Arch Surg. 2007 Sep;142 (9):855–61; discussion 860–1

Table 1 Patients characteristics at baseline

	Population *(n= 48)*	
Characteristic	*N*	%
Age, years		
Median	52	
Range	33–84	
Menopausal status		
Premenopausal	26	54
Postmenopausal	22	46
Histology		
Invasive ductal carcinoma	41	85.4
Invasive lobular carcinoma	6	12.5
Mixed ductal and lobular	1	2.1
Estrogen Receptor status		
Positive	34	70.8
Negative	14	29.2
Progesteron receptor status		
Positive	29	60.4
Negative	19	39.6
Mib-1		
≤20	16	33.3
>20	32	66.7
Her2		
Positive	11	23
Negative	37	77
Pre-chemotherapy clinical/pathologic stage		
IIA	15	31
IIB	16	34
IIIA	9	19
IIIB	5	10
IIIC	3	6
Grading		
2	6	12.5
3	41	83.3
Unknown	1	4.2
Lesion site		
QSE	20	41.7
QII	2	4.2
QSI	8	16.7
QS	11	22.9
Lesions between two quadrants	3	6.2
Central	4	8.3
Chemotherapy		
FEC	14	29.2
FEC+TAX	30	62.4
Other	4	8.4

Table 2 Tumor size pre-NACT

Diagnostic modalities	**≤ 2.0 cm**	**2.1–50 cm**	**≥ 5.1 cm**	**Not measureable***	**MTD**
	N(%)	**N(%)**	**N(%)**	**N(%)**	
USS	8 (16.5)	35 (72.8)	2 (4.2)	3 (6.5)	29.13
MM	8 (16.6)	33 (68.8)	4 (8.3)	3 (6.3)	33.71
MRI	1 (2.1)	34 (70.8)	12 (25)	1 (2.1)^	43.85

Abbreviation: USS, ultrasound; MM, mammography; MRI, Magnetic Resonance Imaging
MTD: median tumour diameter
* *imaging not evaluable or not measurable*
^Carcinomatous Mastitis

Table 3 Characteristics of patients after NACT

	Population (n=48)	
Characteristic	*n*	%
Ductal carcinoma in situ	16	33.3
Estrogen Receptor status		
Positive	37	77.1
Negative	11	22.9
Progesteron receptor status		
Positive	32	66.7
Negative	16	33.3
Ki 67		
≤20	21	43.7
>20	27	56.3
Her2status		
Positive	11	23
Negative	37	77
Grading		
2	7	14.6
3	34	70.8
Not performed (CR)	7	14.6
Pathological Lymph node status		
Negative	27	56.2
Positive	21	43.8
Pathologic stage		
NED/CR	7	14.6
I	14	29.1
IIA	7	14.6
IIB	4	8.3
IIIA	10	20.9
IIIB	1	2.1
IIIC	5	10.4

Table 4 Tumor size post NACT

Diagnostic modalities	≤ 2.0 cm N(%)	2.1–50 cm N(%)	≥ 5.1 cm N(%)	Not measureable* N(%)	MTD
USS	35 (72.9)	11 (22.9)		2 (4.2)	14.3
MM	26 (54.1)	15 (31.3)	4 (8.3)	3 (6.3)	22.7
MRI	29 (60.4)	15 (31.3)	4 (8.3)		20.56
Pathological size	30 (62.5)	16 (33.3)	2 (4.2)		18.27

Abbreviation: USS, ultrasound; MM, mammography; MRI, Magnetic Resonance Imaging
MTD, median tumour diameter
** imaging not evaluable or not measurable*

Table 5 MRI, MM and USS evaluation of primary tumor response to NACT

MRI post NACT[a]	Tumor Pathologic Response		
	positive	negative	Total
positive	36	1	**37**
negative	6	5	**11**
Total	**42**	**6**	**48**
MM post NACT[b]			
positive	35	5	**40**
negative	3	2	**5**
Total	**38**	**7**	**45**
USS post NACT[c]			
positive	37	3	**40**
negative	3	4	**7**
Total	**40**	**7**	**47**

[a]Sensitivity, 86% (95% CI:0.74–0.97); specificity 83% (95% CI:0.63–1.02); accuracy 85% (95% CI:0.75–0.95); positive predictive value (PPV) 97% (95% C.I.:0.91–1.03); negative predictive value (NPV) 45% (95% C.I.:0.20–0.70)
[b]Sensitivity, 92% (95% CI:0.83–1.01), specificity ,29%(95% CI:0.05–0.52) , accuracy 82% (95% CI:0.71–0.93); positive predictive value 87% (95% CI:0.75–0.98); negative predictive value 40% (95% CI:0.15–0.65);
[c]Sensitivity 92% (95% CI:0.83–1.0 , specificity 57%(95% CI:0.31–0.83) and accuracy 87% (95% CI:0.77–0.96); positive predictive value 92% (95% CI:0.83–0.1.01); negative predictive value 57%(95% CI:0.32–0.82)

Table 6 MRI assessment of axillary nodal status post NACT[a]

MRI post NACT	Axillary Lymph Node Pathologic Response		
	positive	Negative	Total
positive	12	4	**16**
Negative	8*	24	**32**
Total	**20**	**28**	**48**

[a]Sensitivity was 60% (95% CI:0.43–0.76); specificity, 86% (95% CI:0.68–1.04); and accuracy 75% (95% CI:0.63–0.87); VPP 75% (95% CI:0.60–0.90); VPN 75% (95% CI:0.53–0.97)
** 2 were micrometastasis*

Breast Ultrasound in the era of MRI: A new paradigm shift?

Bruno D. Fornage, M.D.
Professor of Radiology and Surgical Oncology, The University of Texas M. D. Anderson Cancer Center, Houston, Texas, USA

MRI can detect invasive as well as noninvasive breast carcinomas that are mammographically, sonographically, and clinically occult, thereby improving the detection and diagnosis of breast cancer. Indications for breast MRI include screening (of the high-risk population and of the contralateral breast), diagnosing (e.g., problem-solving equivocal mammograms, sonograms, or physical examination results, nipple discharge, or metastatic axillary node with unknown primary), staging of a newly diagnosed breast cancer, and evaluating response to neoadjuvant chemotherapy. In the last 3 decades, sonography (US) has been used extensively in those applications (except screening) and has become the standard for guiding needle biopsies of breast masses. However, the superiority of MRI in the demonstration of minute cancers is reshaping the role of US in the evaluation of breast diseases in general and breast cancer in particular.

Screening of women at high risk for breast cancer

Because many cancers in young women at high risk for breast cancer are interval cancers that are not detected during the course of annual screening,[1] adding US or MRI to mammography and screening more frequently is a valid strategy for detecting breast cancer early among such women. Multiple studies have shown that the sensitivity of MRI in the early detection of breast cancer in women with BRCA1 or BRCA2 mutation is superior to that of physical examination, mammography, and US.[2,3] In a multinational study of high-risk populations, the sensitivity of MRI in detecting breast cancer ranged from 77% to 100%, whereas that of US ranged from 16% to 40%.[4] In another multicenter study, the sensitivity of MRI in detecting invasive cancer, preinvasive cancer, and premalignant lesions during surveillance of women at high risk for breast cancer ranged from 71% to 100%, whereas that of US ranged from 25% to 59%. Of note is the fact that the specificities of US and MRI were similar, both lower than that of mammography.[5]

Screening MRI is recommended for women with an approximately 20–25% or greater lifetime risk of breast cancer, including women with a strong family history of breast or ovarian cancer and women previously treated for Hodgkin disease. Subpopulations for which the available data are insufficient to recommend for or against screening include women with a personal history of breast cancer, carcinoma in situ, atypical hyperplasia, and extremely dense breasts on mammography.[4]

However, when MRI is unavailable or supplementing it is desirable, US can be used for screening, especially in young women with mammographically dense breasts, although one must keep in mind that US will miss carcinomas appearing as microcalcifications alone (e.g., DCIS) and therefore will miss those cancers that have the best chance for cure. Another rarely addressed technical limitation of breast US is the large size of the breast examined. It is no surprise that screening programs using breast US have already been implemented in East Asia where the average volume of the breast is smaller than that in other areas of the world. However, except in the very young, US and MRI should always be used as a supplement to—never a replacement for—mammography, whose superiority in detecting microcalcifications remains unchallenged.

Large-scale studies will aim at defining the appropriate subpopulation(s) of women for whom the benefits from supplemental screening with US may outweigh the risks and costs of the procedure. In the

ACRIN 6666 study, women at elevated risk of breast cancer who had at least heterogeneously dense breast tissue in at least one quadrant were recruited from 21 sites. The diagnostic yield for mammography was 7.6 per 1,000 women screened (20 of 2,637), which increased to 11.8 per 1,000 (31 of 2637) for combined mammography plus US; the supplemental yield was 4.2 per 1,000 women screened.[6]

It is now obvious that MRI depicts most cancers (invasive lobular ones in particular) better and more reliably than US does (Figure1). However, because few centers can perform MRI-guided breast biopsies and because US-guided biopsy of a mass seen on US is easier and faster than MRI-guided biopsy,[7,8] lesions detected by MRI (whether they were initially examined—and missed—with US or not) are routinely subjected to a "second-look" US examination; if lesions are now visible on US, they are sampled with US-guided biopsy.

Diagnostic applications of breast MRI

As a problem-solving tool in the setting of an equivocal mammogram, sonogram, or physical examination, MRI has shown an exquisite sensitivity, close to 100% for invasive ductal carcinoma. However, this is achieved at the cost of 21% to 35% false-positive results, and only approximately 20% of MRI-detected lesions recommended for biopsy prove to be malignant.[9] Benign lesions that enhance on MRI and are potential false positives include fibroadenomas, fat necrosis, fibrocystic changes, and even normal breast tissue (Figure 2).

MRI is very sensitive in demonstrating papillary lesions and may be used as an additional diagnostic tool to evaluate nipple discharges when ductography and US results remain equivocal.

In women with axillary node metastasis and an unknown primary tumor, MRI can detect the primary tumor with sensitivity of 94%, specificity of 94% to 100%, and an estimated positive predictive value of 90%.[10] MRI appears to be more sensitive than US, although the second-look US examination succeeds in retrieving the lesion in most patients in whom US results were reported as negative initially.[11]

It is not clear in which diagnostic application(s) MRI will (cost-effectively) replace US. Today, in women with "busy breasts" and "hard-to-scan" breasts, MRI offers the needed relief to both sonographers and patients.

Staging of newly diagnosed breast cancer

At M. D. Anderson Cancer Center, we have used US extensively in the past two decades to refine the local and regional staging of breast cancer.[12] MRI appears to be more accurate than US in delineating the exact margins of cancer, although with a substantial risk of overestimation.[13] It is definitely superior to US in patients with invasive lobular cancer.

In the detection of additional foci of malignancy (i.e., multifocal and multicentric disease), MRI has proven to be accurate, detecting additional foci of cancer in 14.5% of patients and changing the clinical management in 19.7% of cases.[14]

Because of the risk that false-positive findings will lead to unnecessary mastectomy, MRI-detected additional foci of suspected malignancy should be confirmed pathologically, which may be a problem in case of multiple lesions. Because real-time US guidance for needle biopsy is more accurate, faster, and less traumatic than MRI-guided biopsy, US is often used after MRI to confirm and document the presence of additional malignant foci, which will affect the local staging.

Although MRI is superior to US in evaluating the local extent of cancer, US remains unsurpassed in the evaluation of the lymphatic spread because US can evaluate more nodal basins (e.g., supraclavicular fossa and low neck) than MRI can, and it can confirm the status of an indeterminate node within minutes via US-guided fine-needle aspiration.

Monitoring of response to therapy

MRI is used by some authors to evaluate the response of breast cancer to neoadjuvant chemotherapy. However, US is also capable of monitoring the volume changes of the tumor, although this may be difficult in invasive lobular cancers and in those tumors that break into pieces during chemotherapy. We have successfully used US for that purpose at M. D. Anderson in the last two decades. US is faster than MRI, can provide the clinician and patient with the percentage decrease in volume within minutes, and is far less expensive than MRI (keeping in mind that the test is done at least twice—before and after treatment).

In conclusion, US is no longer the most sensitive detector of breast masses and MRI is the best screening tool to use in high-risk populations. Preoperative staging of breast cancer can be done with US and it is not clear which patients should undergo a preoperative staging MRI examination (probably, patients with invasive lobular cancer), the cost-effectiveness of such an examination being unknown. In the assessment of the lymphatic spread of breast cancer, US has the advantages of examining more nodal basins than MRI and to confirm or rule out a lymph node metastasis within minutes via an US-guided FNA.

US remains the only real-time cross-sectional imaging modality, and it retains its status as best imaging modality for guiding needle biopsies and intervention. US is also the only imaging modality available in the OR, and it can be used to localize nonpalpable masses.[15]

References

1. Brekelmans CT, Seynaeve C, Bartels CC, et al. Effectiveness of breast cancer surveillance in BRCA1/2 gene mutation carriers and women with high familial risk. J Clin Oncol 2001;19:924–30.
2. Warner E, Plewes DB, Hill KA, et al. Surveillance of BRCA1 and BRCA2 mutation carriers with magnetic resonance imaging, ultrasound, mammography, and clinical breast examination. JAMA 2004;292:1317–25.
3. Kriege M, Brekelmans CT, Boetes C, et al. Efficacy of MRI and mammography for breast-cancer screening in women with a familial or genetic predisposition. N Engl J Med 2004;351:427–37.
4. Saslow D, Boetes C, Burke W, et al. American Cancer Society guidelines for breast screening with MRI as an adjunct to mammography. CA Cancer J Clin 2007;57:75–89.
5. Riedl CC, Ponhold L, Flöry D, et al. Magnetic resonance imaging of the breast improves detection of invasive cancer, preinvasive cancer, and premalignant lesions during surveillance of women at high risk for breast cancer. Clin Cancer Res 2007;13:6144–52.
6. Berg WA, Blume JD, Cormack JB, et al, and the ACRIN 6666 Investigators. Combined screening with ultrasound and mammography vs mammography alone in women at elevated risk of breast cancer. JAMA 2008;299:2151–63.
7. Fornage BD. Sonographically guided needle biopsy of nonpalpable breast lesions. J Clin Ultrasound 1999;27:385–98.
8. Fornage BD, Sneige N, Edeiken BS. Interventional breast sonography. Eur J Radiol 2002;42:17–31.
9. Orel S. Who should have breast MRI evaluation? J Clin Oncol 2008;26:703–11.

10. Van Goethem M, Tjalma W, Schelfout I, et al. Magnetic resonance imaging in breast cancer. Eur J Surg Oncol 2006;32:901–10.
11. Ko EY, Han BK, Shin JH, et al. Breast MRI for evaluating patients with metastatic axillary lymph node and initially negative mammography and sonography. Korean J Radiol 2007;8:382–9.
12. Fornage BD, Edeiken-Monroe BS. Breast sonography. In: Breast Cancer, M. D. Anderson Cancer Care Series, 2nd edition. Hunt KK, Robb GL, Strom EA, Ueno NT, eds. Springer, New York, 2008, pp 121–161.
13. Uematsu T, Yuen S, Kasami M, et al. Comparison of magnetic resonance imaging, multidetector row computed tomography, ultrasonography, and mammography for tumor extension of breast cancer. Breast Cancer Res Treat 2008;112:461–74.
14. Dao TN, Lamont JP, Knox SM. Clinical utility of breast magnetic resonance imaging in patients presenting with primary breast cancer. Proc (Bayl Univ Med Cent) 2007;20:227–30.
15. Fornage BD, Ross MI, Singletary SE, et al. Localization of impalpable breast masses: value of sonography in the operating room and scanning of excised specimens. AJR Am J Roentgenol 1994;163:569–73.

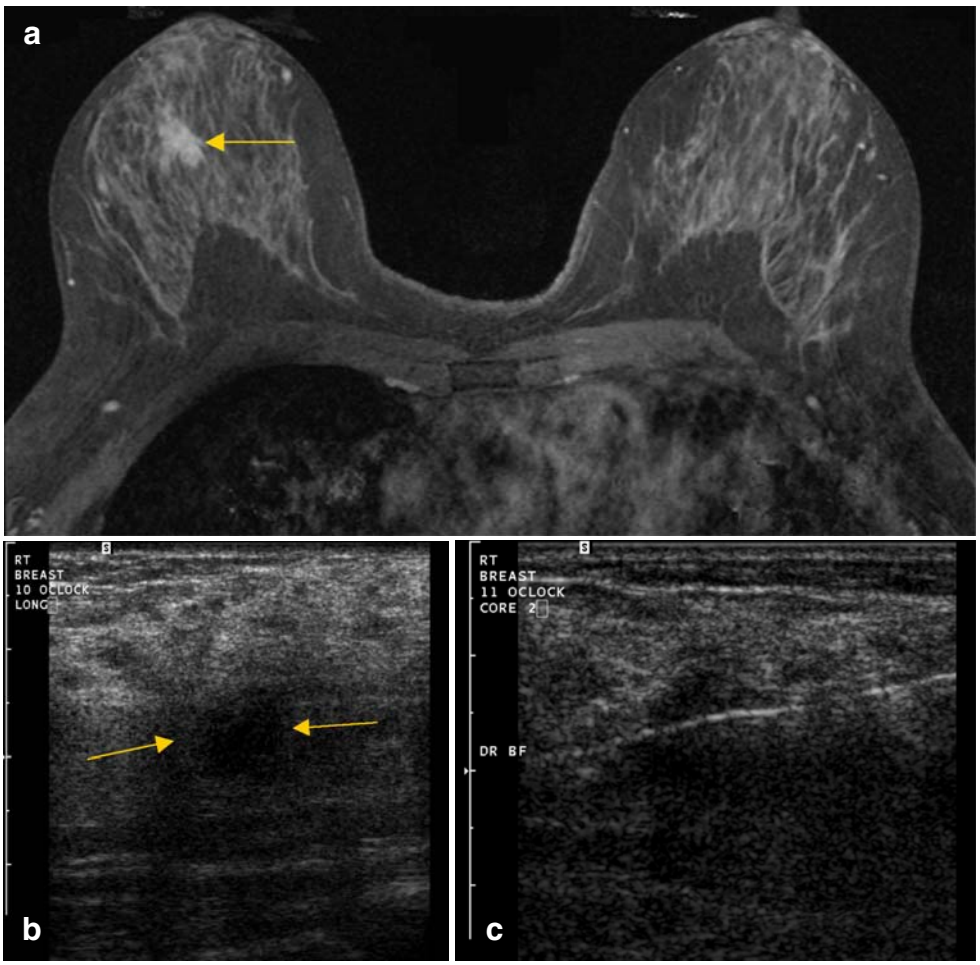

Figure 1

Invasive lobular cancer detected by MRI screening in a woman with BRCA mutation.

1. MRI scan shows clearly a mass in the right breast that is suggestive of cancer.
2. Sonogram shows only a poorly defined mass (arrows) in the region of the lesion visualized on MRI.
3. Sonogram obtained during the US-guided core-needle biopsy shows the cutting needle traversing the mass.

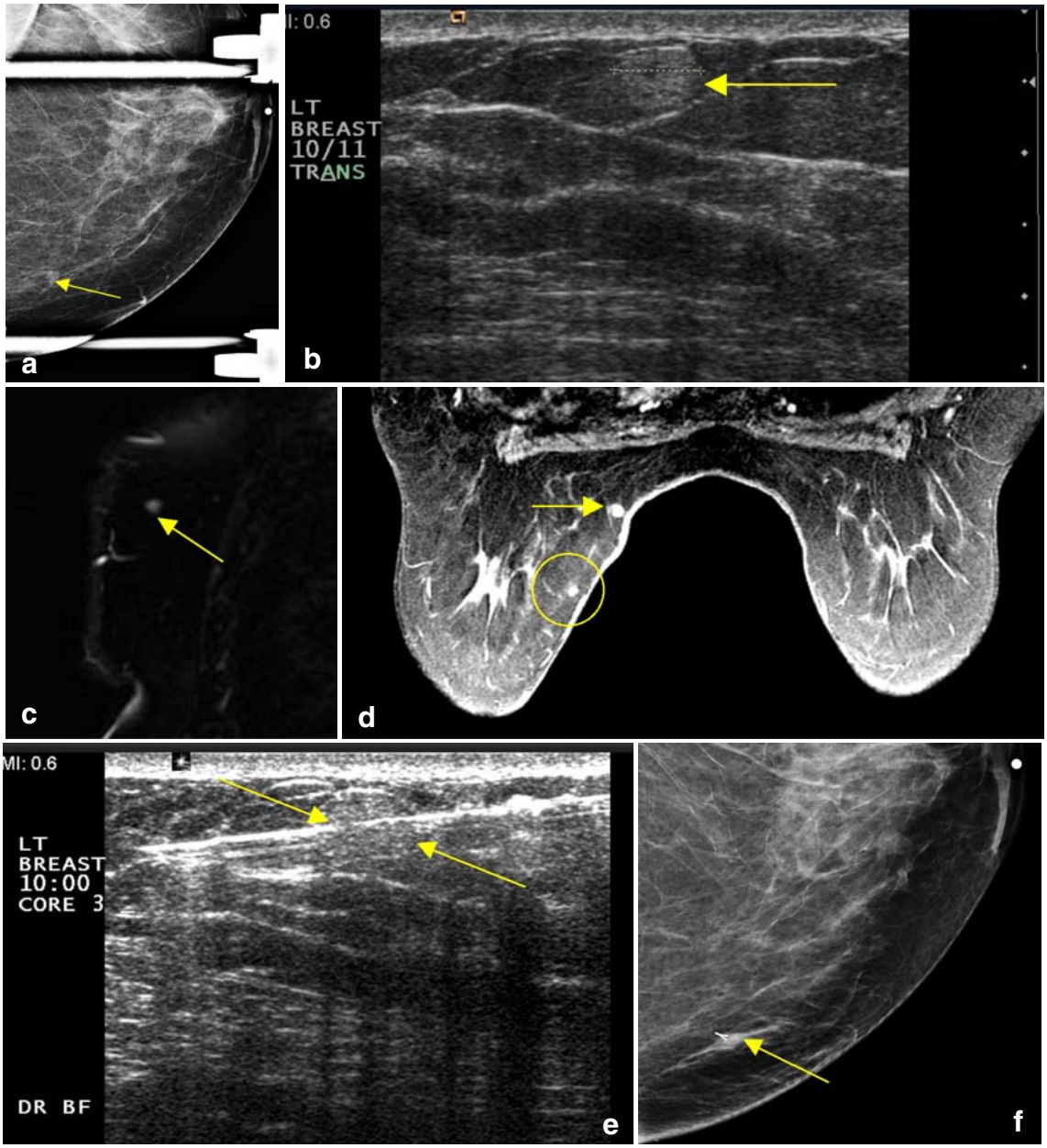

Figure 2

New 0.6-cm mass on annual screening mammograms in a 69-year-old woman.

A. Diagnostic mammogram of the left breast confirms a new suspicious 0.6-cm mass (arrow); it has indistinct margins and is located at 10 o'clock, 10 cm from the nipple.
B. Patient was referred for an US-guided needle biopsy. Sonogram of the area of concern shows only a small subcutaneous echogenic mass (arrow) described as a lipoma with no evidence of cancer. A similar but even smaller subcutaneous nodule was also identified along the same radius but closer to the nipple; it was also described as a minute lipoma (not shown). An MRI of the breast was recommended.
C. Sagittal T2-weighted image shows the hyperintense nodule (arrow).
D. Axial T1-weighted postcontrast image shows a 0.6-cm enhancing nodule (arrow) in the 10 o'clock position 10 cm from the nipple. Note the second, smaller, similar lesion (open circle) closer to the nipple, which correlated with the second benign-appearing lesion visualized on US.
E. Second-look US examination confirmed the initial US findings and the absence of any mass sonographically suggestive of cancer. Sonogram obtained during the US-guided core-needle biopsy of the echogenic lesion shows the needle traversing the target lesion (arrows).

F. Postprocedural mammogram shows the biopsy clip (arrow) within the mammographically visualized nodule. Pathologic examination revealed fibroadipose tissue infiltrated by angiomatous proliferation with scattered microthrombi in small vessels consistent with a benign angiolipoma.

The EUSOMA breast MRI recommendations working group—sufficient?

Fiona J Gilbert
Aberdeen Biomedical Imaging Centre, University of Aberdeen, Aberdeen, UK

Introduction

The European Society of Breast Cancer Specialists (EUSOMA) committee agreed that there was a need to produce consensus evidence based recommendations for undertaking clinical breast MRI in Europe. Experts from different disciplines were identified from across Europe and invited to contribute to this workshop. The expert group comprised more than twenty European participants including radiologists, surgeons, oncologists, radiotherapists, pathologists, epidemiologists and geneticists. This workshop was supported by the EUSOMA secretariat who organised the literature review and organised the consensus meeting in Milan, October 2008. Four topics were identified and two chairpersons appointed for each topic. The chairs' responsibility was to sift the literature and identify key publications and produce a draft document for their topic. The chairperson led the discussion on each topic in the focussed sessions and then presented the conclusions to the whole group at the plenary session for consensus decisions. MRI technique was discussed by the whole group at a plenary session. The four main topics were 1. screening women at high risk; 2. pre-operative staging (including the contralateral breast); 3. evaluation of response to neo-adjuvant chemotherapy including hormone therapy; 4. other indications : inconclusive findings at conventional imaging, imaging after conserving therapy, Carcinoma of Unknown Primary syndrome, nipple discharge, implants.

General recommendations

The group supported breast MRI being undertaken in centres performing conventional breast imaging in order to ensure that the technique was not being performed in isolation and that there was access to breast guided biopsy. Machines with field strength <1 T were not supported and dedicated bilateral multichannel breast coils should be used. Bilateral high spatial resolution imaging should be undertaken with either T2 with or without fat saturation or STIR or SPIR sequence. Bilateral T1W 2D or 3D gradient echo dynamic sequence, with or without fat saturation, of high spatial resolution, ideally 1 mm^2 with slice thickness <3 mm, with each acquisition <120 s. Single dose contrast (0.1 mmol/kg) was recommended in order to minimise background parenchymal enhancement. The examination should be undertaken in the second week of the menstrual cycle and HRT should ideally be stopped 4 weeks before the examination.

All strongly enhancing lesions >5 mm should be analysed. A standardised reporting system such as MR imaging Breast Imaging Reporting and Data System (BI-RADS) lexicon or equivalent. There was insufficient evidence to recommend the routine use of breast MR CAD.

Screening high risk women

There evidence in favour of the use of MRI for the screening of high risk women especially those with a family history or a proven or suspected genetic risk or who have had previous mantle radiotherapy for Hodgkin's disease. However it was felt that in those women with lower risk related to other risk factors (for example previous invasive carcinoma or DCIS, LCIS, ADH, papilloma) there is insufficient evidence for recommending annual MRI screening. Women who were having a prophylactic mastectomy should have a pre-operative MRI to ascertain whether she already has cancer. Referral to a cancer family clinic or to a clinical genetic service for counselling and genetic testing was considered important.

Pre-operative staging (including the contralateral breast)

There is a large body of evidence suggesting that MRI is more sensitive in the assessment of tumor size, detection of multifocal and multicentre cancers than mammography or ultrasound. MRI will detect additional disease in the same breast and to a smaller extent (3–4%) in the contralateral breast. This is especially the case for lobular cancer. Although MRI is able to detect some ductal carcinoma in situ (DCIS) and extensive intraductal component (EIC) results from different studies vary with some over-estimating extent and others under-estimating size. A meta-analysis of 19 studies showed a 7.0% increase in mastectomies due to malignant disease and 1.1% due to benign changes with 5.8% wider excisions due to malignant disease and 5.5% due to benign lesions. However, so far, no clear evidence exists proving that preoperative MRI is beneficial concerning final outcome. Existing data cannot exclude a benefit for subgroups. The results of two randomized controlled trials are awaited. Pragmatically the group recommended pre-operative MRI in women with newly diagnosed with a lobular invasive cancer, at high-risk for breast cancer, <60 years of age with discrepancy in size >1 cm between mammography and ultrasound with expected impact on treatment decision. The eligibility for partial breast irradiation was also considered. Additional lesions seen only on MRI should be confirmed by biopsy.

Evaluation of response to neo-adjuvant chemotherapy including hormone therapy

A number of studies showed the diagnostic accuracy of MRI to assess the response to neo-adjuvant chemotherapy to be better than that of clinical breast examination, mammography, or ultrasound. The r value of correlation between residual tumour size at MRI and pathology was reported to be from 0.65 to 0.98. Several studies showed the MRI ability to predict the tumour response to neo-adjuvant chemotherapy. The ultimate benefit on survival in patients monitored with breast MRI in the adjuvant setting is not yet established. There was consensus that a baseline breast MR examination should be performed before the first course of neo-adjuvant chemotherapy and that the final examination should take place 2 weeks after the final chemotherapy at least 2 weeks before surgery. It was noted that residual disease may have very low contrast enhancement. Where there is poor response MRI may not add any additional information.

Other indications

In presence of localised metastatic disease (typically, axillary lymphadenopathy) and negative conventional imaging, breast MR imaging is indicated. There is no evidence for a role of MR imaging in CUP with extensive disease and poor prognosis. There was no consensus as to the place of MRI in nipple discharge. MR is known to have a high sensitivity for recurrence and is recognised as an accurate technique for differentiating surgical scarring from recurrent tumour. MR imaging is more accurate than conventional imaging for assessing implant integrity and for evaluating the breast tissue around and behind the implant.

Conclusion

A full document co-authored by all the participants of the Eusoma working group is being prepared. Full details of the guidance together with the evidence and levels of evidence will be published and presented at the Jena meeting.

Molecular and Functional Imaging of Breast Cancer—New Advantages

Kristine Glunde, Ph.D.
Radiology Department, The Johns Hopkins University, School of Medicine, Baltimore, USA

Advances in molecular biology, synthetic chemistry, and visualization techniques have created molecular-functional imaging capabilities that are finding applications in basic, preclinical, and translational breast cancer research. Molecular imaging techniques include imaging gene expression, receptors, signaling pathways, apoptosis, multi-drug resistance, and the extracellular matrix. Functional imaging can assess angiogenesis, hypoxia, and metabolism. Imaging has traditionally played an important role in breast cancer diagnosis and monitoring treatment response. However, noninvasively visualizing molecules and molecular pathways and relating these to function makes multi-modality molecular imaging an exciting and powerful means for studying a multifaceted disease such as cancer. An overview of recent advances in molecular and functional breast cancer imaging achieved in the Johns Hopkins University (JHU) *In Vivo* Cellular and Molecular Imaging Center (ICMIC) will be given in this talk.

One research focus of the ICMIC program has been hypoxia as it is one of the hallmarks of tumors, and triggers multiple signaling cascades that significantly impact upon biological outcomes including angiogenesis, selection for resistance to apoptosis, resistance to radiation and chemotherapy, and increased invasion and metastasis. These hypoxic regions that arise from inadequate blood supply of tumors have a heterogeneous spatial distribution. Understanding and characterizing the hypoxic response of tumors is therefore critically important and requires approaches that can evaluate the complexity as well as the spatial distribution of the response. A combined Magnetic Resonance Spectroscopic Imaging (MRSI), optical imaging, and Mass Spectrometric Imaging (MSI) approach will be presented that can unravel hypoxia-driven signaling pathways in the breast tumor microenvironment.

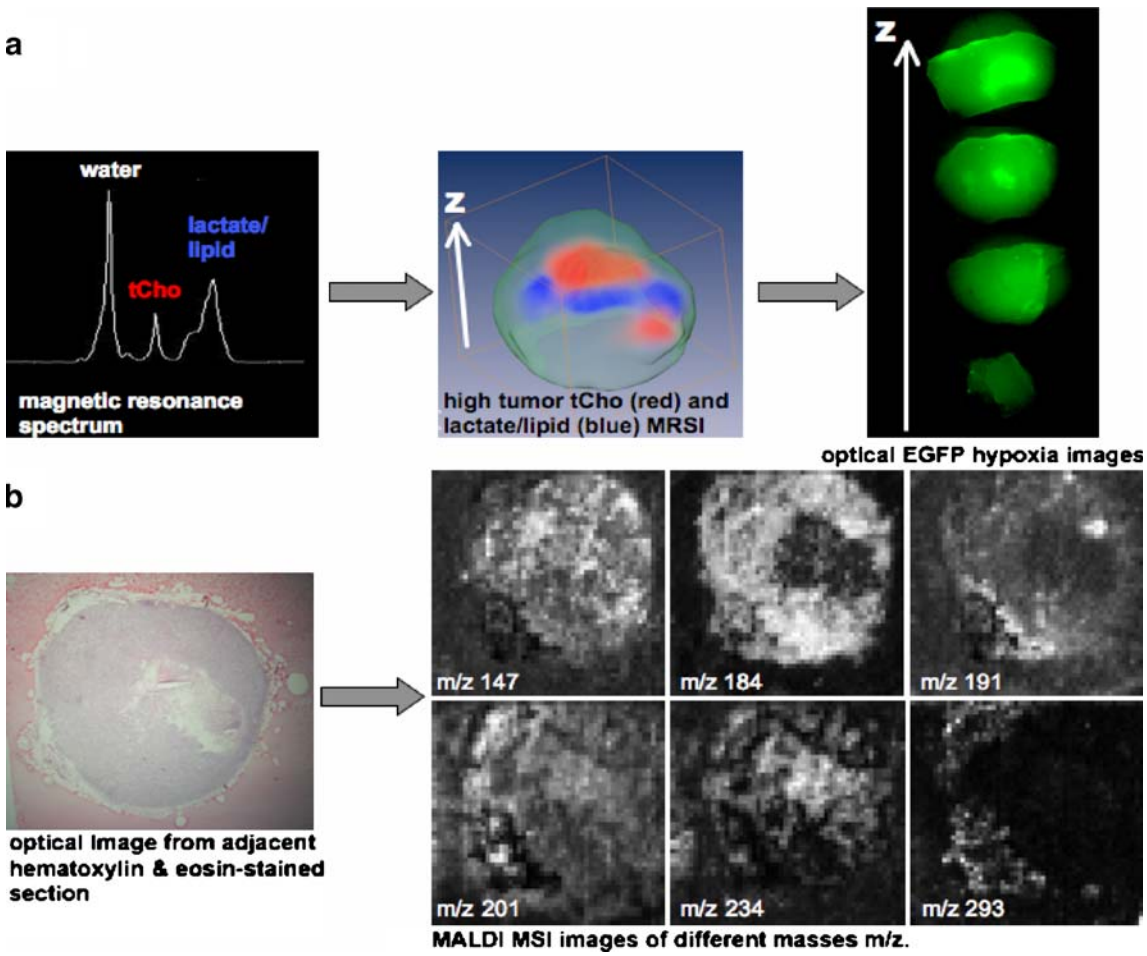

Figure 1: *(a) 3D MRSI demonstrating the distribution of high total choline-containing compounds (tCho) displayed in red and high lactate/lipid displayed in blue corresponding to the ex vivo hypoxia maps of EGFP-fluorescing hypoxic tumor regions. tCho colocalizes with hypoxic regions. (b) MALDI MSI images of several m/z demonstrate the heterogeneous distribution of these small molecules in viable tumor regions detected in the corresponding hematoxylin & eosin-stained section.*

Breast tumors contain multiple physiologically distinct microenvironments, such as hypoxic and/or extracellular acidic regions. Tumor hypoxia correlates with poor clinical outcome, confers radio-and chemoresistance, and triggers cancer invasion and metastasis through hypoxia-inducible factor (HIF)-1 alpha-mediated gene regulation. We combined *in vivo* detection of metabolites such as total choline (tCho) with *ex vivo* detection of hypoxia and newly discovered small molecules and proteins. 3D magnetic resonance spectroscopic imaging (MRSI) was used to detect metabolites *in vivo*. Fluorescence microscopy of human MDA-MB-231 breast tumor xenografts stably expressing enhanced green fluorescent protein (EGFP) under the control of multiple hypoxia response elements measured hypoxic tumor regions. Matrix Assisted Laser Dissociation Ionization (MALDI) Mass Spectrometric Imaging (MSI) was employed to provide molecular information directly on tissue sections to determine the spatial distribution of biomolecules in these human breast tumor xenografts. We studied small molecules as well as proteins in the range between 0–20,000 m/z. MRSI as well as MSI revealed high levels of total choline (Figure 1a) in hypoxic EGFP-fluorescing regions, and phosphocholine, which is m/z 184 (Figure 1b), in viable hypoxic tumor regions. Necrotic and hypoxic tumor regions showed a markedly different molecular and metabolic profile compared to other regions (Figure 1b). MSI detected the spatial distribution of multiple different species of biomolecules, which can be related to the corresponding MRSI and optical imaging data sets (Figure 1b). These metabolic and molecular 3D distributions can in the future be used to differentiate distinct microenvironmental regions in breast tumors, and provide insight in the molecular processes in hypoxic regions. This work was supported by NIH R01 CA134695.

High-resolution MAS MRS of breast cancer biopsies—different approaches

Beathe Sitter, Tone F. Bathen and Ingrid S. Gribbestad
Department of Circulation and Medical Imaging, Norwegian University of Science and Technology (NTNU), Trondheim, Norway
Corresponding Author:
Beathe Sitter, e-mail: beathe.sitter@ntnu.no, Phone: +47 73 55 13 53, Fax: +47 73 86 77 08

Introduction

More than one million new cases of breast cancers are diagnosed each year globally, which makes it the cancer form with the highest incidence and mortality of all malignant diseases among women [1]. Histopathological evaluation of the tumor and lymph node status are the basis for the patient treatment plan. However, breast cancer patients with identical clinical and histopathological cancer diagnosis can have distinct different outcomes. The high numbers of affected women and the variable and often poor response to chemotherapy require increased knowledge about breast tumor biology and improved diagnostic and predictive tools.

Numerous studies have proven MR spectroscopic profiling as a promising tool in cancer diagnosis and treatment monitoring, for instance for brain [2], prostate [3] and breast cancer [4,5]. The choline metabolites choline, phosphocholine (PCho) and glycerophosphocholine (GPC), have gained a lot of interest in MR studies of cancer as their metabolism appear to be altered in malignant cells [6]. High levels of PCho is associated with increased malignancy in breast cancer cells [7,8] and higher drug sensitivity [9]. Detailed metabolic descriptions of tissue samples from breast tumors can provide this type of information and contribute to increase the understanding of tumor biology in patients. High resolution magic angle spinning magnetic resonance spectroscopy (HR MAS MRS) can provide quantitative metabolite identification with minimal sample preparation and keeping the sample intact after analysis [10]. Metabolomics describes the metabolism in a single biological sample and correlate these metabolomic profiles with known physiological or pathological states. Metabolic phenotypes can probably be useful in a wide range of applications; from identification of molecular subclasses of diagnostic value, to more basic studies of metabolic processes in cells. Large datasets require powerful tools for effective analysis of the data, and multivariate analysis is evolving as the method of choice, as it is reduces the complexity of data and tests scientific hypotheses. MR metabolomics may contribute to establish a more detailed breast tumor portrait, by defining specific fingerprints reflecting diagnostic status or therapeutic response. It is of vital importance to identify the factors causing these fingerprints, which can become biomarkers to be used in the clinic. Our HR MAS MRS studies of breast cancer biopsies have been performed using two different, yet closely linked, approaches. Firstly, we have aimed for a detailed picture of tissue metabolites in order to increase the understanding of breast tumor biology. Tissue metabolites have been quantified and the findings have been combined with histopathology and gene expressions of the same tissue samples. Secondly, we have established a protocol for fast and simple analysis, with the purpose to develop a clinical tool to aid in a more individualized breast cancer treatment. Different studies on fresh-frozen samples from our biobank (600 patients) have been performed correlating MR spectral profiles to clinical parameters with predictive qualities, predicting long-term health status based on spectral profiles and correlating MR spectral profiles with treatment response.

Materials and Methods

The information obtained from tissue using HR MAS MRS depends on the study design, from collection and storage to extraction of information from the resulting spectra. In addition, care must be taken to preserve the samples for subsequent analysis. Excised tissue is no longer under the enzymatic control of the body, and storing, additives, MAS conditions and temperature affect the extent of these reactions. Samples are usually frozen immediately after excision and kept cold through the experiments. Additives (buffer, D_2O and similar) will extract molecules from the tissue, and spinning rates will have influence on the preservation of sample for further analysis, like histopathology. The options for spectral acquisitions are numerous. One-dimensional spectra with water suppression and spin-echo filtering of broad resonances are most widely applied [10]. It is of key importance to follow the same protocol for all samples throughout the study.

In breast cancer studies described here, experiments have been performed at a Bruker AVANCE DRX600 (Bruker BioSpin GmbH, Germany). Tissue size has been approximately 16 mg in average, and we have used two different sample preparation protocols. Samples have been kept cold through the sample preparation procedure and added PBS-D_2O with TSP for field-lock and chemical shift referencing. In the first protocol applied with Teflon inserts for the MAS rotors, we added a fixed amount (40 µl) buffer in excess, and monitored the amount of buffer that was lost in rotor assembly [5]. In the later protocol applied with the disposable and leak-proof kel-F inserts, 3 µl of buffer is added with the sample, and no buffer is lost in the assembling procedure [11]. Samples were spun at 5 kHz and kept at 4°C. Typically two types of experiments have been acquired. A one-dimensional single pulse experiment with water suppression

allow for acquisition of all MR-visible metabolites in the tissue. One-dimensional spin-echo experiments suppress broad signals with short T_2, which leads to reduced signals from lipids and macromolecules, and relatively increased signals from small molecular weight metabolites with longer T_2. Quantification of metabolites has either been performed based on the single-pulse experiment and TSP concentrations, or by a third experiment with electronic signal for referencing (ERETIC). For MR metabolomic studies, spectra have been analyzed by several different multivariate methods. Principal component analysis (PCA) has been applied for variable reduction and pattern recognition. It is an unsupervised dimension reduction technique, and provides an overview of the patterns in the data, both between samples and between metabolites. Principal least squares regression (PLS) has been used to obtain classification of samples. PLS is the regression extension of PCA, and is a supervised multivariate approach, useful for prediction and classification purposes. Other supervised multivariate methods we have applied are probabilistic neural network (PNN) and Bayesian Belief Networks (BBN).

Results and Discussion

Differencing breast cancer tissue from non-involved

The metabolic composition in breast cancer tissue is distinctively different from non-involved breast tissue [4,5]. Sitter *et al.* [5] compared peak intensity ratios of choline compounds in tumor samples (n=76) and adjacent non-involved tissue from the same patients (n=9). The ratios GPC/PCho and GPC/Cho were significantly lower in tumor samples compared to non-involved, whereas PCho/Cho was higher in tumors. Bathen *et al.* [4] analyzed breast tissue using PCA on spectra from 91 breast cancers and 48 non-involved samples from the same patients. The result was a near-complete separation of breast cancer and non-involved tissue based on the three first principal components representing 80% of the dataset variations.

Breast cancer biology

Metabolites in breast cancers (n=70) have been quantified for comparisons of tissue spectra from patients with different diagnosis, lymph node status and tumor size [5]. No differences were found related to diagnosis (histological type and grading), whereas choline and glycine concentrations were higher in tumors larger than 2 cm compared with smaller tumors, and a trend of higher *myo*-inositol was found in tissue from lymph node-positive patients compared to node-negative. Metabolite estimates were influenced by the percentage of tumor cells in the investigated specimens. In a recent study [10], tissue metabolites were quantified in samples from patients with clinically predicted poor prognosis (n=16, tumor size >2 cm, axillary lymph node metastasis, negative for estrogen or progesterone receptors) and good prognosis (n=13, tumor size <2 cm, no findings of metastasis in the axillary lymph nodes and positive for estrogen and progesterone receptors). Tissue metabolic concentrations were not different for these two groups of patients, with the exception of possibly higher glycine concentration in samples from patients with poor prognosis (1.9 μmol/g) compared to those with good (1.1 μmol/g, p=0.067). We did find that tissue concentrations of β-glucose correlated to proliferation index (MIB-1) with a negative correlation factor (−0.45, p=0.015), consistent with increased energy demand in proliferating tumor cells. We also found that combined information about more than one metabolite, either in ratios or by metabolic profiles analyzed by PCA, correlated to patients' prognoses and health status 5 years after surgery.

With the aim of increased understanding of breast tumor biology, metabolic information and gene expression data from breast cancers have been combined [12,13]. In our first approach [13], tissue samples were collected from breast cancer patients (>5% tumor cells, n=41), and two samples from each patient were analyzed by HR MAS. One of these samples was further analyzed by histopathology, whereas the other was extracted for RNA. The obtained RNA was labeled and hybridized to Human Whole Genome Oligo Microarrays (Agilent), and totally 32 good quality arrays were obtained. The average ratios of signals in corresponding spectra (n=32) from choline compounds were found to be 0.72 for GPC/PCho, 1.89 for GPC/choline and 3.28 for PCho/choline, implying relatively high levels of PCho and low levels of choline. We compared choline metabolic ratios to the expression levels of genes associated to synthesis and degradation of phospholipids, in particular genes related to cholines and phospolipases. Ratios of choline signals from MAS spectra correlated significantly (p<0.05) to the mRNA expression levels of 10 of the 49 cholines associated genes, and to 24 of the 89 phospholipases associated genes. The mRNA expression levels for four of the phospholipase A2 and three phospholipase C had weak but significant positive correlations to the ratios GPC/choline or PCho/choline. The mRNA expression levels of choline kinase a correlated positively to the PCho/choline ratios. These first studies have shown that metabolic and genetic information could be measured in the same breast cancer tissue, and that it is possible to correlate metabolic levels to gene expression of proteins regulating specific pathways.

This study has been extended, and combined metabolic and gene expression information have been obtained from 48 patients [12]. All 48 samples were classified into one of five intrinsic subgroups based on gene expression [14,15]. The majority were classified as luminal A, which is the largest subgroup of breast cancers. The luminal A subgroup is associated with positive ER status and relatively good prognosis, but a certain fraction of patients with this type of cancer have a poor outcome. By applying an inclusion criterion of at least 5% tumor tissue from histopathology, 31 luminal A samples were selected for further analyses. The spectral region (4.7–1.4 ppm) of HR MAS spin echo spectra served as input for hierarchical clustering and multidimensional scaling, which led to the definition of two subgroups of luminal A, named luminal A1 and A2. Lipid signals are important metabolic differences between the two luminal A groups. Gene Set Analysis of the gene expression data show that the luminal A1 subgroup with higher lipid signals is associated with myeloid cell differentiation and luminal A2 is associated with biosynthesis of steroids. The combination of metabolic and genetic profiling showed a potential to reveal more refined subgroups of breast cancer. The clinical value of the transcriptional differences between the two groups will be investigated in a different breast cancer gene expression microarray dataset with long term follow up.

Correlation to clinical predictive factors

The metabolic profiles of breast cancer tissues have been explored for qualities that correlate to clinical prognostic factors like tumor size, lymph node status and hormone receptor status [5]. PCA was performed using parts of breast tissue spectra (n=85) which included signals from which included signals from glucose, lactate, creatine, *myo*-inositol, glycine, taurine, GPC, PCho and choline (Figure 1). The first principal component was influenced by the percentage of tumor cells, whereas higher principal components indicated a possible prediction of spread to axillary lymph nodes. Including only spectra from samples with no fat tissue from patients with invasive ductal carcinomas (n=37), led to a significant clustering of

samples from patients with and without spread to the axillary lymph nodes. Increased taurine and reduced glycine appeared to be the major metabolic difference in breast tumors from patient with axillary spread compared to those without.

Different multivariate methods were applied to classify breast tumor samples (n=91) with respect to the clinical predictive factors hormone receptor, lymphatic spread and grading [4]. Models were established and validated, and blind sample testing showed that hormone status was well predicted by both PNN and PLS (11 of 12 correct), lymphatic spread was best predicted by PLS (eight of 12), whereas PLS-UVE PNN was the best approach for predicting grade (nine of 12 correct).

A larger dataset was later analyzed in order to further characterize and classify samples with respect to histopathological grading, lymph node status and estrogen receptor status [16]. Samples from tumor (n=286, more than 5% tumor) and adjacent non-involved tissue (n=50, confirmed by histopathology) from breast cancer patients were analyzed by HR MAS MRS. The spectral region between 3.2–3.3 ppm, including resonances from taurine, GPC, PCho and choline was used as input for PLS performed with mean-centering and full cross-validation. There was a trend of higher GPC/PCho (0.83) in tumors from patients with negative lymph node status compared to patients with lymphatic spread (0.68, p=0.097). In a subset of these samples (excluding samples from patients who had received neo-adjuvant therapy and samples with fat tissue), choline profiles of estrogen receptor (ER) positive tumors (N=165) were found to be different from ER negative (N=24). PCho/Cho was lower in ER negative tumor tissue compared to ER positive and PLS provided classification of ER status (Figure 2). Six significant PCs were retained in the model, and the MR predicted versus the clinically measured ER status was significantly correlated both for calibration (r=0.67, p<0.01) and validation (r=0.48, p<0.01).

The ability of MR metabolomics to predict lymphatic spread and ER status of breast cancer patients has been further explored [17]. HR MAS spectra were obtained from tumor samples (with at least 5% tumor cells) from breast cancer patients diagnosed with invasive ductal carcinoma. For prediction of lymphatic spread and ER status datasets of 167 spectra (119 patients: 67 lymph node status negative and 52 positive, mean age: 61 years) and 163 spectra (116 patients: 25 ER negative and 91 positive, mean age: 61 years) were analyzed using PLS and BBN. The score values for PC1 and PC2 obtained from PLS were significantly different for positive and negative patients for both prognostic factors (p<0.01). The MR predicted versus clinically measured status was significantly correlated both for lymphatic spread (rcalibration=0.42, rvalidation=0.25) and ER status (rcalibration=0.71, rvalidation=0.53) (p<0.001). Prediction of blind samples by BBN gave better results for the prediction of both lymphatic spread and ER status, possibly because BBN can detect nonlinear relationships between variables. This study suggests that both lymphatic spread and ER status can be predicted by MR metabolomics. The findings in these four studies [4,5,16,17] all show that breast cancer metabolic profiles correlate to clinically established prognostic factors and thereby should have the potential for predicting outcome for breast cancer patients.

Predicting long-term survival

The feasibility of MR determined metabolic phenotype to predict long term breast cancer survival has been explored [18]. Samples were excised from patients diagnosed with invasive ductal carcinomas who had not received any treatment before the operation. After HR MAS MRS analysis, a pathologist scored the relative areas of normal and neoplastic epithelial elements and only spectra from biopsies with at least 5% tumor-content were included. The final dataset consisted of spectra from 40 patients, where 32 patients survived four years (represented by 38 spectra), and eight patients (represented by nine spectra) who had deceased within 4 years after surgery. PLS regression was performed relating the selected spectral region (2.9–4.7 ppm) to survival 4 years after surgery. Three significant PCs were retained in the model, and the MR predicted versus the clinical known survival was significantly correlated, both for calibration (r=0.77, p<0.01) and validation (r=0.48, p<0.01). Spectra from patients still alive after 4 years were associated with lower levels of PCho, glycine and lactate, and higher levels of glucose and taurine.

The analysis of these data were later refined using Support Vector Machine [19]. (SVM parameters: normalized polynomial kernel of degree=2; no data normalization; leave-one-out generalization error estimate; sequential minimal optimization algorithm; and C=1,000). The actual versus the SVM predicted correct survival status for 37 of the 38 spectra from patients who survived four years after surgery, whereas eight of the nine spectra from patients who died within four years were correctly predicted. This preliminary investigation suggests that MR determined metabolic phenotype may have a potential in prediction of long term breast cancer survival. Further validation, including more samples and blind testing will be necessary.

Correlating metabolic profile to response to treatment

Metabolic profiles seem to predict treatment response and patient outcome, found by evaluating quantitative changes in the level and composition of the choline containing metabolites (tCho) prior to and after treatment [20]. In this study, 33 patients with locally advanced breast cancer (TNM-stages T1–T3) were treated weekly with doxorubicin. Patients with a >50% reduction in tumor volume were considered responders (n=12), while patients with a <50% reduction or <25% increase in tumor volume were designated non-responders (n=21). Tissue specimens (16.9±5.1 mg) were obtained from open surgical biopsy before starting on chemotherapy (n=33) and during main surgery (n=33). Spin-echo spectra and spectra with ERETIC for quantification were recorded. The spin-echo spectra (1.4–1.6 ppm and 2.9–4.7 ppm) of the biopsies excised prior to treatment were related to clinical response by PLS.

The PLS led to a definition of four sub-groups with different total choline profiles. Spectra representing four responders and five non-responders clustered in two separate groups in accordance with treatment response. The remaining spectra from responders (n=8) and non-responders (n=16) formed a third cluster. Tissue concentration of GPC in sample excised prior to treatment were higher in patients who were healthy 5 years after surgery compared to those who deceased or experienced recurring cancer. We also found that GPC more often had decreased after treatment in those patients who were healthy 5 years after surgery. Although further studies are needed to validate these data, our study suggests that quantitative changes in different choline profiles may be related to breast cancer treatment response.

The possible value of the choline compounds to predict treatment response has also been evaluated by *in vivo* MRS of breast cancer patients before (n=22) and during (n=12) neo-adjuvant chemotherapy, and by HR MAS of core biopsies prior to chemotherapy (n=11) [21]. Total choline was detected in 15 of the 22 spectra recorded prior to treatment. Choline could also be detected in six (two responders and four non-responders) of the 12 *in vivo* spectra recorded during treatment 1 day before second cycle of chemotherapy. The six spectra with undetectable levels of choline were all from responders. These

results are consistent with previous reported findings [22]. Concentrations of total choline compounds in core-needle biopsies taken prior to start of treatment was not different for good response (n=6, [tCho]=3.05±3.97 mmol/g tissue) compared to poor response (n=5, [tCho]=1.76±2.96 mmol/g tissue) patients. However, the spectral profiles obtained from core-needle biopsies showed similar choline profiles as the biopsies prior to treatment in the study by Cao *et al.* [20] with respect to response to treatment. These results indicate that total choline are being reduced with efficient chemotherapy, and that the choline metabolic profile can predict response to treatment.

Conclusion

Metabolic phenotyping of breast cancer using HR MAS MRS has demonstrated distinct patterns correlating to clinical and histopathological findings, and a possible prediction of patient outcome. In particular choline compounds, glycine, taurine and lactate have shown biomarker qualities. An important finding is that metabolic profiles seem to predict treatment response and patient outcome.

References

1. Parkin DM, Bray F, Ferlay J, Pisani P (2001) Estimating the world cancer burden: Globocan 2000. Int J Cancer 94: 153–156.
2. Martinez-Bisbal MC, Marti-Bonmati L, Piquer J, Revert A, Ferrer P, Llacer JL, Piotto M, Assemat O, Celda B (2004) 1H and 13C HR-MAS spectroscopy of intact biopsy samples ex vivo and in vivo 1H MRS study of human high grade gliomas. NMR Biomed 17: 191–205.
3. Swanson MG, Vigneron DB, Tabatabai ZL, Males RG, Schmitt L, Carroll PR, James JK, Hurd RE, Kurhanewicz J (2003) Proton HR-MAS spectroscopy and quantitative pathologic analysis of MRI/3D-MRSI-targeted postsurgical prostate tissues. Magn Reson Med 50: 944–954.
4. Bathen TF, Jensen LR, Sitter B, Fjosne HE, Halgunset J, Axelson DE, Gribbestad IS, Lundgren S (2007) MR-determined metabolic phenotype of breast cancer in prediction of lymphatic spread, grade, and hormone status. Breast Cancer Res Treat 104: 181–189.
5. Sitter B, Lundgren S, Bathen TF, Halgunset J, Fjosne HE, Gribbestad IS (2006) Comparison of HR MAS MR spectroscopic profiles of breast cancer tissue with clinical parameters. NMR Biomed 19: 30–40.
6. Ackerstaff E, Glunde K, Bhujwalla ZM (2003) Choline phospholipid metabolism: A target in cancer cells? J Cell Biochem 90: 525–533.
7. Aboagye EO, Bhujwalla ZM (1999) Malignant transformation alters membrane choline phospholipid metabolism of human mammary epithelial cells. Cancer Res 59: 80–84.
8. Singer S, Souza K, Thilly WG (1995) Pyruvate utilization, phosphocholine and adenosine triphosphate (ATP) are markers of human breast tumor progression: a 31P-and 13C-nuclear magnetic resonance (NMR) spectroscopy study. Cancer Res 55: 5140–5145.
9. Kaplan O, van Zijl PC, Cohen JS (1990) Information from combined 1H and 31P NMR studies of cell extracts: differences in metabolism between drug-sensitive and drug-resistant MCF-7 human breast cancer cells. Biochem Biophys Res Commun 169: 383–390.
10. Sitter, B., Bathen, T., Tessem, M.-B., and Gribbestad, I. S. High-resolution magic angle spinning (HR MAS) MR spectroscopy in metabolic characterization of human cancer. Progress in Nuclear Magnetic Resonance Spectroscopy 54, 239–254. 2009.
11. Sitter B, Bathen T, Singstad T, Fjosne HE, Lundgren S, Halgunset J, Gribbestad IS (2009) Quantification of metabolites in breast cancer patients with different clinical prognosis using HR MAS MR spectroscopy. NMR Biomed Submitted.
12. Borgan, E., Sitter, B., Bathen, T., Lundgren, S., Johnsen, H., Lingjærde, O. C., Sørlie, T., Børresen-Dale, A.-L., and Gribbestad, I. S. Combining data from HR MAS MR spectroscopy and gene expression can refine the subclassification of breast cancer. ISMRM 17th Scientific Meeting & Exhibition Apr. 18 2009
13. Sitter, B., Johnsen, H., Bathen, T., Lundgren, S., Fjøsne, H. E., Halgunset, J., Børresen-Dale, A.-L., and Gribbestad, I. S. Combined HR MAS MR spectroscopy and gene expression of breast cancer tissue. Joint Annual Meeting ISMRM-ESMRMB May 19 2007
14. Perou CM, Sorlie T, Eisen MB, van de RM, Jeffrey SS, Rees CA, Pollack JR, Ross DT, Johnsen H, Akslen LA, Fluge O, Pergamenschikov A, Williams C, Zhu SX, Lonning PE, Borresen-Dale AL, Brown PO, Botstein D (2000) Molecular portraits of human breast tumours. Nature 406: 747–752.
15. Sorlie T, Perou CM, Tibshirani R, Aas T, Geisler S, Johnsen H, Hastie T, Eisen MB, van de RM, Jeffrey SS, Thorsen T, Quist H, Matese JC, Brown PO, Botstein D, Eystein LP, Borresen-Dale AL (2001) Gene expression patterns of breast carcinomas distinguish tumor subclasses with clinical implications. Proc Natl Acad Sci USA 98: 10869–10874.
16. Sitter, B., Bathen, T., Grinde, M. T., Fjøsne, H. E., Halgunset, J., Lundgren, S., and Gribbestad, I. S. Choline profiles of breast cancer correlate to clinical tumor characteristics. ISMRM 16th Scientific Meeting & Exhibition May 3 2008
17. Giskeødegård, G. F., Lundgren, S., Sitter, B., Fjøsne, H. E., Halgunset, J., Axelson, D., Gribbestad, I. S., and Bathen, T. Classification and prediction of prognostic factors of breast cancer patients by MR metabolism. ISMRM 17th Scientific Meeting & Exhibition May 18 2009
18. Bathen, T., Sitter, B., Fjøsne, H. E., Axelson, D., Lundgren, S., and Gribbestad, I. S. MR-determined metabolic phenotype—a possible tool for prediction of long term survival in breast cancer. Joint annual meeting ISMRM–ESMRMB May 19 2007
19. Bathen, T., Sitter, B., Fjøsne, H. E., Axelson, D., Lundgren, S., and Gribbestad, I. S. Prediction of long term breast cancer survival using MR metabolomics. ISMRM 16th Scientific Meeting & Exhibition May 3 2008
20. Cao, M. D., Sitter, B., Bathen, T., Lønning, P. E., Lundgren, S., and Gribbestad, I. S. Choline metabolites as biomarkers for predicting response to neoadjuvant chemotherapy in local advanced breast cancer patients. ISMRM 17th Scientific Meeting & Exhibition Apr. 18 2009
21. Heldahl, M. G., Sitter, B., Bathen, T., Cao, M. D., Lundgren, S., and Gribbestad, I. S. In vivo and ex vivo choline metabolite profiles as biomarkers for treatment response in locally advanced breast cancer. ISMRM 17th Scientific Meeting & Exhibition Apr. 18 9 A.D.
22. Meisamy S, Bolan PJ, Baker EH, Bliss RL, Gulbahce E, Everson LI, Nelson MT, Emory TH, Tuttle TM, Yee D, Garwood M (2004) Neoadjuvant chemotherapy of locally advanced breast cancer: predicting response with in vivo (1)H MR spectroscopy—a pilot study at 4 T. Radiol 233: 424–431.

Figure Legends
Figure 1

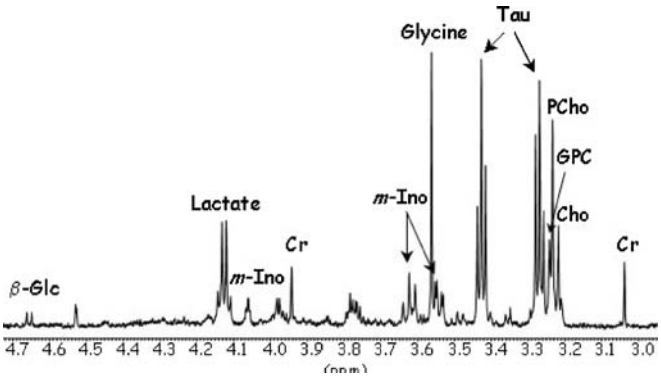

Figure 1

Part of spin-echo acquired HR MAS spectrum of breast cancer sample showing the spectral region used as input for PCA: 4.7 to 2.9 ppm. Abbreviations in spectral assignments: β-Glc; β-glucose, *m*-Ino; *myo*-inositol, Cr; creatine, Tau; taurine, GPC; glycerophosphocholine, PCho; phosphocholine and Cho; choline.

Figure 2

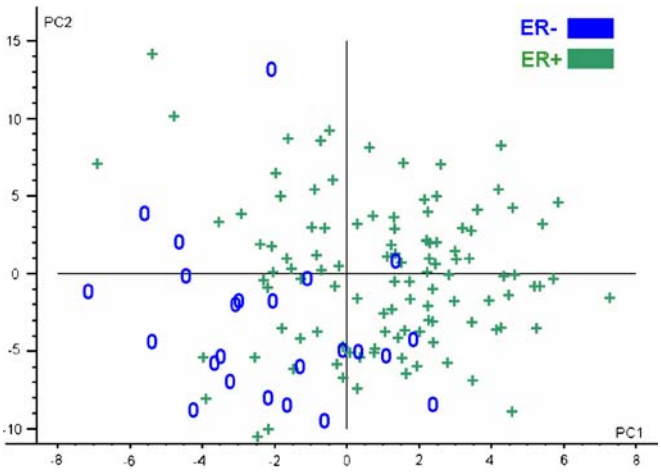

Figure 2

Score plot of the first two principal components from PLS of choline region from spectra from patients who were positive (N=165) and negative (N=24) with respect to estrogen receptors.

Is there a correlation between DCE-MRI and survival?

Line R Jensen[1], Mariann G Heldahl[1], Pål E. Goa[2], Steinar Lundgren[1,3] and Ingrid S Gribbestad[1*]
[1]Department of Circulation and Medical Imaging, Norwegian University of Science and Technology (NTNU), Trondheim, Norway
[2]Department of Medical Imaging and [3]Department of Oncology, St. Olavs University Hospital, Trondheim, Norway

*Corresponding author:
Ingrid S. Gribbestad, PhD, e-mail: ingrid.s.gribbestad@ntnu.no, Phone: +47 73 86 38 44, Fax: +47 73 55 13 50

Introduction

Treatment of breast cancer has during recent years moved to more individualized therapies, aiming to give each patient optimal treatment for their disease. This challenging task relies on good predictive and prognostic markers that provide information on tumour aggressiveness, treatment response and survival. Prognostic factors used in clinical treatment planning include metastatic axillary lymph nodes, tumour size and grade, oestrogen and progesterone receptor status, proliferation markers and HER-2/neu over expression. However, patients with similar tumour characteristics respond different to treatment. The response to breast cancer chemotherapy is correlated with long-term survival, although studies have demonstrated different responses and survival rates (1). This indicates that the present prognostic indicators based on patient group studies need additional biomarkers to be true on an individual patient basis. Therefore, identification of surrogates that early predicts therapeutic effect and give prognostic information would be valuable for individually tailored patient treatments.

Several MRI studies of breast cancer have investigated tumour properties and correlated MRI to tumour characteristics and treatment response. DCE-MRI has been shown to detect short-term treatment response in breast tumours undergoing neoadjuvant therapy (2, 3). Contrast enhancement kinetics is dependent on neovasculature in tumours, usually consisting of chaotic, highly permeable, and heterogeneous blood vessels. Hawighorst et al. demonstrated that DCE-MRI parameters correlated with both micro vessel density (MVD) and vascular endothelial growth factor (VEGF), both of which are markers for neoangiogenesis (4). The same properties may contribute to assessment of disease free and overall survival. However, only a few studies have correlated MRI-derived parameters to long-term patient outcome. DCE-MRI parameters have been correlated with survival and local recurrence after therapy in high-grade glioma, small-cell lung cancer, cervical cancer, and breast cancer, with promising results for the prediction of clinical outcome (5–9).

The purpose of this study was to investigate if DCE-MRI data obtained prior to neoadjuvant chemotherapy could provide prognostic information in locally advanced breast cancer patients using multiple analytical approaches.

Methods

Patients with locally advanced breast cancer undergoing neoadjuvant therapy at St Olavs Hospital, Trondheim, Norway, were examined with MRI at the time of diagnosis before therapy was initiated. As a part of the clinical MRI examination, DCE-MRI data were acquired on a 1.5 Tesla system with a T1-weighted 3D spoiled gradient echo sequence in the sagittal plane (TR/TE/α: 9 ms/3.8 ms/30°). The sequence was repeated eight to nine times with 1 min temporal resolution, and a dose of 0.1 mmol/kg gadodiamide injected after 2–3 pre-contrast frames. All image postprocessing was performed using in-house software developed in Matlab 7.5 (Mathworks, Natick, MA, USA). Regions of interest (ROI) were drawn manually around the enhancing lesion in the postcontrast subtracted MR images.

A cohort of DCE-MRI data from 24 patients were analysed, and tumour volume, relative signal intensity (RSI) after two minutes, and area under the curve (AUC) from the pre contrast images to the sixth frame were calculated. Furthermore, multivariate analysis methods were applied to both the analysis parameters and the enhancement curves, as described in Johansen et al (10). The results were correlated to 5 years overall survival.

An extended cohort of 32 patients was evaluated further for enhancement characteristics. The DCE-MRI enhancement curves from each tumour voxel were classified according to curve types; type I (persistent, the signal intensity increases over the entire dynamic study, defined as >10% increase), type II (plateau, initial increase of signal intensity followed by a plateau, defined as ≤10% change) and type III (washout, rapid increase in the signal intensity followed immediately by a washout, defined as >10% decrease) (11, 12), and the volumes of each enhancement type were calculated. The tumour volumes were then correlated to survival data[13].

Results

After 5 years, 14 of the 24 patients were still alive. The mean RSI was significantly lower for patients surviving longer than 5 years (Figure 1). Similarly, by use of multivariate analyses, the AUC skew and kurtosis were found to be important parameters for separating patients surviving less than or more than 5 years. Finally, the enhancement curves were used as input in multivariate analysis to predict survival with a sensitivity and specificity ranging from 80%–92%. The total tumour volume and the mean AUC value tended to be lower for patients surviving more than 5 years, although not significant.

In the second study, 20 of the 32 patients were still alive after 5 years. The total tumour volume together with the volume of type III curves were most important for differentiating patients surviving more or less than 5 years (Figure 1). Using both total volume and volume of washout characteristics yielded a sensitivity and specificity of 0.75 and 0.85 for detecting patients surviving less than 5 years. Using total volume alone gave a sensitivity and specificity of 0.75 and 0.70. DCE-MRI images for two patients with different tumour characteristics as analyzed with curve types is presented in Figure 2.

Discussion

All the studies published on DCE-MRI and survival reports a correlation between contrast enhancement parameters and survival (Table 1). Generally, patients with large tumours and high degree of contrast enhancement will be expected to have a shorter overall survival than the rest of the patient cohort. Furthermore, high volume of tumour with type III enhancement characteristics is also correlated to a poorer prognosis. The present study confirmed the previous findings by Pickles et al. (9), where both tumour volume and enhancement parameters were found to correlate to overall survival (Table 1). This study included more patients and higher temporal resolution, but was otherwise similar to the present study. In the study by Boné et al., patients with primary malignancy were included and examined pre-operatively, resulting in a different patient population than the other studies. However, despite poor temporal resolution (6 min), the findings were similar showing high contrast enhancement and larger tumour volumes for patients with shorter survival.

The MRI examinations in these studies are carried out at the time of diagnosis, before therapy is initiated. The tumours are then treated with a combination of chemotherapy, surgery, hormonal therapy, and radiation therapy. However, the tumour characteristics at the time of diagnosis are used as basis for evaluating patient prognosis. Furthermore, most of the tumour progression has happened before the patient's cancer disease is detected. One of the most important steps in this tumour progression is the neoangiogenic switch. When the tumour adapts the ability to initiate neoangiogenesis, the blood supply is enhanced and one important premise for metastatic ability is "ensured". In vivo measurements of the angiogenic conditions in tumours could thus contribute to each patients prognosis.

DCE-MRI is an indirect method for measuring perfusion in tumours, and numerous methods have been applied to assess physiologic relevant parameters. Usually, this requires a set of assumptions to implement pharmacokinetic models that apply to the data. Only the study by Pickles et al has implemented such methods, however, the derived parameters were not significant when correlated to survival (9). One can question the need for these methods if simple calculations, e.g. relative increase in signal intensity, are correlated to survival.

In conclusion, the DCE-MRI studies of breast cancer presented in this paper show that there is a correlation between contrast enhancement and survival, although the results have to be verified in a larger patient population. DCE-MRI derived parameters as new biomarkers for more individualized prognostic factor must be further explored to enhance sensitivity and specificity.

References

1. Rastogi P, Anderson SJ, Bear HD, et al. Preoperative chemotherapy: updates of National Surgical Adjuvant Breast and Bowel Project Protocols B-18 and B-27. J Clin Oncol 2008; 26:778–785.

2. Manton DJ, Chaturvedi A, Hubbard A, et al. Neoadjuvant chemotherapy in breast cancer: early response prediction with quantitative MR imaging and spectroscopy. Br J Cancer 2006; 94:427–435.

3. Padhani AR, Hayes C, Assersohn L, et al. Prediction of clinicopathologic response of breast cancer to primary chemotherapy at contrast-enhanced MR imaging: initial clinical results. Radiology 2006; 239:361–374.

4. Hawighorst H, Knapstein PG, Knopp MV, et al. Uterine cervical carcinoma: comparison of standard and pharmacokinetic analysis of time–intensity curves for assessment of tumor angiogenesis and patient survival. Cancer Res 1998; 58:3598–3602.

5. Mills SJ, Patankar TA, Haroon HA, Baleriaux D, Swindell R, Jackson A. Do cerebral blood volume and contrast transfer coefficient predict prognosis in human glioma? AJNR Am J Neuroradiol 2006; 27:853–858.

6. Ohno Y, Nogami M, Higashino T, et al. Prognostic value of dynamic MR imaging for non-small-cell lung cancer patients after chemoradiotherapy. J Magn Reson Imaging 2005; 21:775–783.

7. Mayr NA, Taoka T, Yuh WT, et al. Method and timing of tumor volume measurement for outcome prediction in cervical cancer using magnetic resonance imaging. Int J Radiat Oncol Biol Phys 2002; 52:14–22.

8. Bone B, Szabo BK, Perbeck LG, Veress B, Aspelin P. Can contrast-enhanced MR imaging predict survival in breast cancer? Acta Radiol 2003; 44:373–378.
9. Pickles MD, Manton DJ, Lowry M, Turnbull LW. Prognostic value of pre-treatment DCE-MRI parameters in predicting disease free and overall survival for breast cancer patients undergoing neoadjuvant chemotherapy. Eur J Radiol 2008.
10. Johansen R, Jensen LR, Rydland J, et al. Predicting survival and early clinical response to primary chemotherapy for patients with locally advanced breast cancer using DCE-MRI. J Magn Reson Imaging 2009; 29:1300–1307.
11. Kuhl CK, Mielcareck P, Klaschik S, et al. Dynamic breast MR imaging: are signal intensity time course data useful for differential diagnosis of enhancing lesions? Radiology 1999; 211:101–110.
12. Lehman CD, Peacock S, DeMartini WB, Chen X. A new automated software system to evaluate breast MR examinations: improved specificity without decreased sensitivity. AJR Am J Roentgenol 2006; 187:51–56.
13. Heldahl MG, Bathen TF, Rydland J, Kvistad KA, Lundgren S, Gribbestad IS, and Goa PE, Prognostic value of pretreatment dynamic contrast-enhanced MR imaging in locally advanced breast cancer: Overall survival predicted from single voxel classification of signal intensity time course data, unpublished work 2009

Table 1: Overview over publications and the most important findings.

Publication	Patients	Methods	MRI parameters correlated to shorter overall survival	Logrank test
Johansen et al, 2009	Neoadjuvant chemotherapy (n=24)	Empirical parameters and multivariate analysis	High RSI	P=0.048
Heldahl et al, Unpublished 2009	Neoadjuvant chemotherapy (n=32)	Empirical parameters	Large tumour volume	P=0.011
			High volume of type III curves	P=0.0023‡
Boné et al. 2003	Primary malignancy (n=50)	Empirical parameters	High early contrast enhancement ratio	P=0.016
			Large tumour volume	P<0.0001
Pickles et al, 2008	Neoadjuvant chemotherapy (n=54)	Pharmacokinetical and empirical parameters	Large tumour volume	P=0.021
			High enhancement index	P=0.012
			High initial slope	P=0.012
			High AUC	P=0.014

‡ Logrank test for both volumes combined

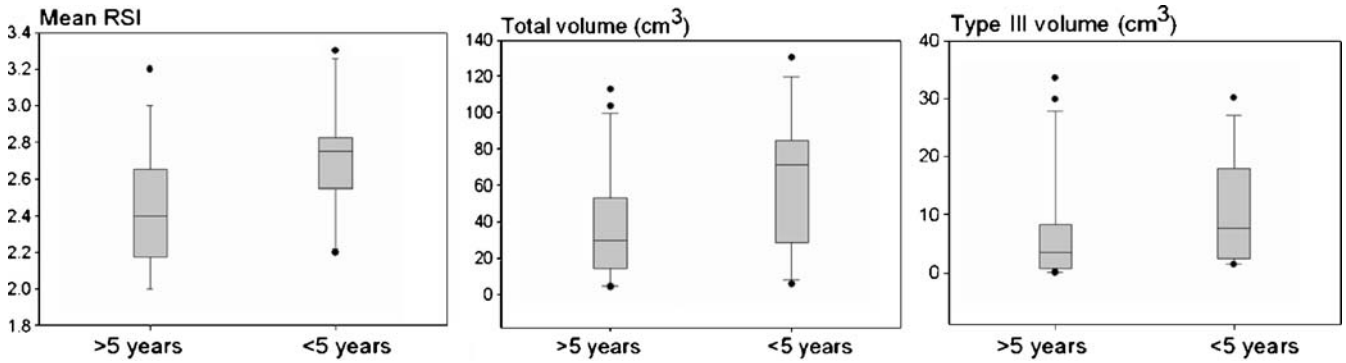

Figure 1: DCE-MRI parameters for patients surviving more or less than 5 years. From left, mean RSI from 24 patients (p=0.048, t-test), the total volume and type III volume for 32 patients (p=0.039 and p=0.21). Boxes represents 25th percentile, median and 75th percentile, whiskers represents 10th and 90th percentile.

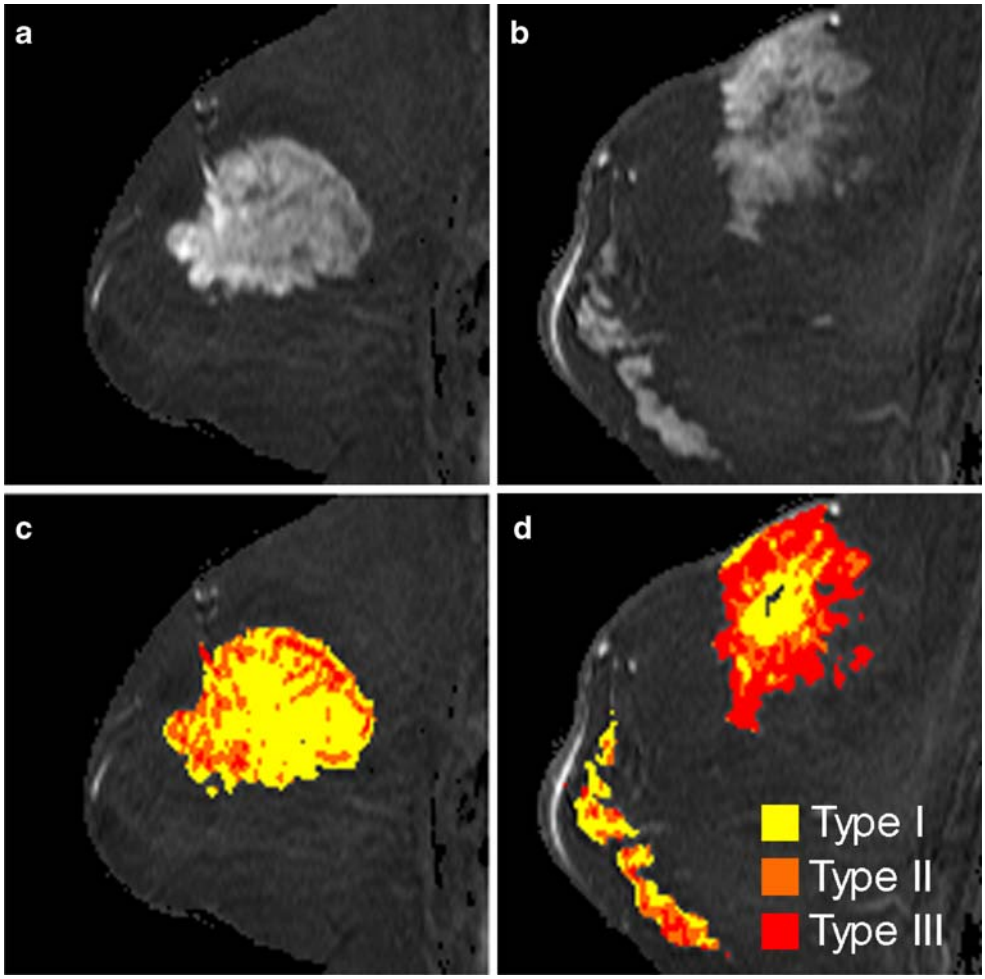

Figure 2: Subtraction images from patients surviving longer than (a) and less than (b) 5 years after time of diagnosis. The tumour size is similar in the two patients, however evaluating the enhancement curves reveals a smaller volume of type III curves for the patient surviving longer than five years (c), compared to the patient with shorter survival (d).

The stem cells of the mammary gland and breast cancer

Prof. Dr. Bernd Groner
Georg Speyer Haus, Institute for Biomedical Research, Paul Ehrlich Str. 42, 60596 Frankfurt, Germany

The perpetual renewal of tissues and organs is driven by resident stem cells and progenitors. These cells guarantee tissue maintenance and regeneration after injury or involution. Most tissues and organs contain small populations of primitive stem cells and progenitors. These cells play a major role in the developing fetus and contribute to the generation of tissues and organs. Stem cells are positioned on top of the cellular hierarchy and give rise to progenitors with more restricted lineage potential. The stem cells can divide and self-renew to generate daughter stem cells or they can differentiate into a variety of mature cell types.

The stem cell hypothesis has been extrapolated to tumour tissues and the postulation of stem cells has many attractive conceptual and practical implications. Cancer cells are distinguished by multiple mutations which alter their cell cycle regulation, their sensitivity to apoptotic signals and their life span. Since stem cells persist within the organism for long periods of time, they have the potential to accumulate genetic damages and propagate them to their daughter stem cells and their downstream progenitors. Many tumours comprise minor populations of tumour-initiating cells, cells able to reconstitute a tumour upon transplantation; these cells have been called cancer stem cells (CSCs). CSCs share characteristics of normal stem cells, i.e. they can self-renew and they can give rise to heterogeneous cell populations within a tumour and maintain the tumour mass. They are also more resistant to chemotherapeutic drugs and radiotherapy than their progenitors and thus represent a cellular reservoir for tumour recurrence. CSCs can be derived directly from mutational events in stem cells which confer proliferative properties or they can result from mutations in progenitor cells which provide them with self renewal capacity. Both pathways might be used and result in tumours with different pathological properties. The characterisation of the signalling pathways which provide self renewal properties to CSCs and the targeted interference with limiting signal transduction components offer a promising new therapeutic approach for the treatment of cancer.

Targeted tumour therapy relies on genetic and biochemical distinctions between normal and tumour cells. The identification of specific signalling pathways and signalling components active in CSCs opens new possibilities for therapeutic exploitation. CSCs could possibly be targeted and these agents might improve conventional treatment

results. CSCs, however, initially have properties which make them more resilient towards therapy. They are more resistant to chemotherapy and ionizing radiation. New therapeutic agents which target the genuine stem cell properties have to be designed.
The presence and the molecular characteristics of CSC have interesting implications for the understanding of tumour aetiology, the response to treatment and the development of novel therapeutics. If CSC are more resistant to conventional chemotherapeutic drugs and radiation than the majority of the cells present in solid tumours, and if they are the source of residual cells which cause recurrence of tumour growth after therapy, strategies and targeted drugs have to be designed which are preferentially aimed at their communication with their microenvironment and their eradication. The targets of such drugs could be components of the pathways which maintain breast cancer stem cells, such as the Notch, hedgehog, and Wnt pathways. Since many of these components are not susceptible to conventional drug action, new classes of drugs might have to be discovered and developed.

Overcoming artifacts and distortions of DWI of the breast

Daniel Güllmar
Medical Physics Group, Institute of Diagnostic and Interventional Radiology, University Hospital Jena, Germany

Over the past years it was shown that MR diffusion weighted imaging of the breast can add valuable information in order to distinguish between malignant and benign lesions. Especially the apparent diffusion coefficient (ADC) allows differentiating compartments with different cellular structures, since ADC in biological tissue depends largely on the presence of micro structural barriers to diffusion, like cell membranes and macromolecules. Several studies [1–3] have shown, that an ADC threshold of 1.2 μm^2/ms can be used to classify breast lesions, since the mean ADC of malignant lesions was found to be 0.95–1.2 μm^2/ms and the mean ADC of benign lesions is 1.5–1.6 μm^2/ms. The diffusion imaging technique has been primarily used to study the central nervous system because many technical issues complicate the used of DWI outside the brain. Especially artifacts due to susceptibility and physiologic motion which occur inherently with echo-planar imaging (EPI) amplify, if EPI is applied outside the brain. In recent years, however, new developments in EPI techniques and scanner hardware have made DWI of the abdomen and breast feasible. A more general improvement is the availability of parallel acquisition. Using more than one receiver coils and appropriate reconstruction techniques like GRAPPA or SENSE, one is able to reduce the read-out train and thus the accumulation of phase errors due to local inhomogeneities. For this reason the use of parallel imaging techniques with DWI is advisable in any case. Additionally, the application of parallel imaging enables to increase the spatial resolution of the images, which indeed increases scan time, however, additionally lowers the sensitivity to local inhomogeneities (susceptibility). Unfortunately, with increasing acceleration factor the SNR of the acquired images decreases and thus the SNR of the estimated ADC maps. Thus, averaging is necessary which increases the scan time. Additionally, an optimal b-value has to be selected in order to increase the SNR of the estimated ADC maps. The optimal b-value can be derived by defining the diffusion coefficient of interest and using the formalism, which was proposed by Kingsley et al. [4] stating that in case of isotropic diffusion, the optimal b-value is determined by $b\text{-}value = 1.278/ADC$. If we select the proposed ADC threshold of 1.2 μm^2/ms as value of interest, the optimal b-value is according to the formalism 1065 s/mm^2. If a higher b-value is selected to focus more on the exact determination of the malignant lesions with ADC values of 0.95–1.2 μm^2/ms, one has to take into account, that regions with higher ADC values (like in benign lesions) are usually underdetermined with high b-values. A second major issue in diffusion weighted breast imaging is fat suppression. Standard DW-EPI sequences are equipped with fat suppression features which are typically based on chemical-shift-selective pulses (CHESS) [5] or spectrally selective fat suppression (SPIR), however, these techniques often seems to fail in properly suppression of fat tissue as proposed by Stadlbauer et al. [6]. They state that these fat suppression techniques encounter difficulties in the determination of the resonance frequency of water as the reference frequency, especially of tissues with high fat content, such as in the breasts of elderly women. Stadlbauer et al. also applied a technique called diffusion weighted imaging with background body signal suppression (DWIBS) to breast DWI, which was first introduced by Takahara et al. [7]. DWIBS is a DWI method that uses a short TI inversion recovery (STIR)–echo planar imaging (EPI) sequence and free breathing to screen for malignancies in the whole body. Free breathing and a high number of averages (ten or more) reduces the fat signals, since the motion of fat tissue is observed as coherent motion and thus not sensitive to the diffusion sensitizing gradients in contrast to the incoherent motion of water molecules. One general drawback of DWIBS is the correct quantification of ADC. Because of the allowance of respiratory motion in DWIBS, slice levels of images obtained with different b-values may not be identical [8]. Thus, ADC measurements of moving organs in DWIBS is different from conventional (breath hold or respiratory triggered) DWI as shown by Stadlbauer et al. [6] and makes DWIBS images of moving organs more suitable for visual non quantitative evaluation than quantitative analysis. Other sequence techniques like Propeller MRI [9], which was also successful applied with diffusion weighting [10], can additionally reduce susceptibility artifacts and is suitable to be combined with DWIBS.

1. Guo Y, Cai YQ, Cai ZL, Gao YG, An NY, Ma L, Mahankali S, Gao JH. Differentiation of clinically benign and malignant breast lesions using diffusion-weighted imaging. J Magn Reson Imaging. 2002 Aug;16(2):172–8.
2. Marini C, Iacconi C, Giannelli M, Cilotti A, Moretti M, Bartolozzi C. Quantitative diffusion-weighted MR imaging in the differential diagnosis of breast lesion. Eur Radiol. 2007 Oct;17(10):2646–55.
3. Rubesova E, Grell AS, De Maertelaer V, Metens T, Chao SL, Lemort M. Quantitative diffusion imaging in breast cancer: a clinical prospective study. J Magn Reson Imaging. 2006 Aug;24(2):319–24.
4. P. Kingsley, Concepts in Magnetic Resonance Part A, Volume 28A, Issue 2, Date: March 2006, Pages: 101–179
5. Matthaei D, Frahm J, Haase A, Schuster R, Bomsdorf H. Chemical-shift-selective magnetic-resonance imaging of avascular necrosis of the femoral head. Lancet. 1985 Feb 16; 1(8425):370–1.
6. Stadlbauer A, Bernt R, Gruber S, Bogner W, Pinker K, van der Riet W, Haller J, Salomonowitz E. Diffusion-weighted MR imaging with background body signal suppression (DWIBS) for the diagnosis of malignant and benign breast lesions. Eur Radiol. 2009 May 5
7. Takahara T, Imai Y, Yamashita T, Yasuda S, Nasu S, Van Cauteren M. Diffusion weighted whole body imaging with background body signal suppression (DWIBS): technical improvement using free breathing, STIR and high resolution 3D display. Radiat Med. 2004 Jul–Aug;22(4):275–82.

8. Kwee TC, Takahara T, Ochiai R, Nievelstein RA, Luijten PR. Diffusion-weighted whole-body imaging with background body signal suppression (DWIBS): features and potential applications in oncology. Eur Radiol. 2008 Sep;18(9):1937–52.
9. Pipe JG. Motion correction with PROPELLER MRI: application to head motion and free-breathing cardiac imaging. Magn Reson Med. 1999 Nov;42(5):963–9.
10. Forbes KP, Pipe JG, Karis JP, Heiserman JE. Improved image quality and detection of acute cerebral infarction with PROPELLER diffusion-weighted MR imaging. Radiology. 2002 Nov;225(2):551–5.

Breast MR at 3T and Beyond: Is it Necessary?

Brian A. Hargreaves
Department of Radiology, Stanford University, Stanford, USA, *bah@stanford.edu*

Introduction

While the majority of clinical MRI scanners operate at field strengths of 1.5 T or lower, 3.0 T systems are increasingly common in clinical practice, while higher-field systems, particularly at 7.0 T are being investigated. The primary benefits of increased field strength are higher signal-to-noise ratio (SNR) and greater spectral selectivity. However, there are numerous challenges of imaging at higher field strengths, as well as protocol adjustments that must be made in order for routine clinical scanning at 3.0 T and higher. Although breast MRI at 3.0 T is becoming more common, there are few articles comparing it to breast MRI at 1.5 T [1, 2]. This article describes the expected benefits and challenges of high field (3.0 T and higher) breast imaging.

Physics

This section reviews the fairly well-known MR physics of scanning with increased field strengths.

Polarization and SNR

Since polarization is roughly proportional to field strength, increasing field strength is one potential way to overcome SNR limitations of SNR. Since SNR is proportional to voxel volume, the increased SNR is critical in order achieve high spatial resolution. Furthermore, higher field scanning will reduce the SNR limits of higher parallel imaging acceleration.

Coils

The gains in SNR attributed to high-field scanning typically assume similar coil performance at different field strengths. However, the decreased wavelengths at 3.0 T and higher become a significant challenge to coil design, and some SNR loss may result.

Spectral selectivity

Since resonant frequency is proportional to field strength, higher-field scanning allows better resolution of spectral components. This is an obvious benefit to MR spectroscopy, where twice the spectral resolution can be achieved in the same acquisition time. However, it also shortens the duration of spectrally-selective pulses used for fat suppression or water-only excitation. Furthermore, T2* effects are enhanced at higher field strengths, potentially offering other contrast mechanisms such as BOLD or SWI [3, 4]. A negative effect of high field imaging is that off resonance effects (chemical-shift induced, susceptibility induced, or from static field inhomogeneities) increase proportionally with field strength, and can cause artifacts that depend on the pulse sequence and parameters.

Relaxation and Relaxivity

An important consideration in protocol optimization is the range of tissue relaxation times at different fields [5]. T1 times generally increase with field strength, while T2 should stay roughly constant. (Note that T2 and T2* times should not be confused, as the latter decrease with increasing field strength.) Furthermore, the relaxivity of contrast agents decrease as field strength increases. Although increased T1 often results in reduced signal at 3.0 T compared with 1.5 T, the greater T1 variation can improve T1 contrast. Overall, protocols must be adjusted to maximize the contrast-to-noise ratio (CNR).

RF Power Deposition

RF power deposition or specific absorbed radiation (SAR) increases with field strength, which can force longer repetition times, longer echo spacings, or fewer slices in spin echo sequences. Although reduced flip angle echo trains help to address SAR limits, the result can be varied contrast, typically with T1 contamination in T2-weighted images. Although SAR limits can also be addressed by using smaller transmit/receive coils, these are not common for breast imaging.

RF Inhomogeneity

The increased RF frequency, and shorter wavelength, at higher fields leads to dielectric effects that tend to attenuate the transmit amplitude nearer the surface. Overall this results in a spatial variation of the flip angle, which can cause shading in images as well as variation of contrast. Specifically this variation can be a problem for DCE breast imaging at 3.0 T, as it can lead to reduced visualization of contrast enhancement in otherwise high-quality images [6].

Breast MRI Applications

The following section outlines how the above physical effects are expected to affect specific breast MRI pulse sequences.

General Benefits

The increased SNR is generally a great benefit to breast imaging, particularly as it allows higher spatial resolution, which is important for visualization of lesion size, shape, borders and heterogeneity. Increased spectral selectivity makes fat suppression faster, so can improve pulse sequence efficiency. However, increased off-resonance effects cause more displacement in images, which is often addressed by using higher readout bandwidths (which in turn reduces SNR, though may reduce scan times).

T2-weighted MRI

T2-weighted imaging typically uses multiple spin echo sequences (FSE, TSE, RARE). Since T2 does not vary at higher fields, the echo times should not require much adjustment. However, the repetition times are usually extended in order to allow complete T1 recovery. SAR limitations may reduce the number of slices that can be achieved, or conversely, reduced refocusing flip angles may be used, which may result in more T1 contamination of contrast. Similarly, B1 variations may result in T1 contamination, but this is probably a small effect. At 3.0 T, where SAR limits have been addressed, T2-weighted imaging is generally better than at 1.5 T.

T1-weighted CE MRI

Contrast-enhanced protocols are the predominant MRI technique for assessment of breast cancer. T1-weighted sequences must be adjusted at 3T to achieve similar contrast to their 1.5 T counterparts. 2D or 3D spoiled gradient-echo sequences can be adjusted either by increasing the repetition time, decreasing the flip angle, or both. SAR is typically not a

limitation with these methods. As mentioned, RF inhomogeneity can affect contrast, though additional studies of this effect would be beneficial. The differences in relaxation rates and contrast agent relaxivity at different field strengths, combined with the sensitivity of the pulse sequence to these parameters requires careful analysis. The further challenges of studying these effects *in vivo* and in different abnormal tissue have limited comparative studies thus far.

Spectroscopy and Diffusion-Weighted MRI

Spectroscopic imaging at 3T would demand longer TR for complete T1 recovery, and consideration of T2* effects. However, in general it will benefit tremendously from increased SNR and increased spectral selectivity. Diffusion-weighted imaging (DWI) benefits from higher SNR, since the diffusion weighting inherently dephases signal. However, many DWI methods use echo-planar imaging, which is sensitive to shorter T2* and to susceptibility effects, so consideration should be made.

Susceptibility-Weighted Imaging

A recent development at high field is susceptibility weighted imaging (SWI) [4]. Using a gradient-echo sequence, the phase image is filtered, and used to weight the magnitude image. The contrast and signal in SWI both improve with field strength. SWI is potentially sensitive to calcifications in breast cancer [7], and if this is demonstrated successfully, then high-field imaging would certainly be more attractive for breast MRI.

Multinuclear MRI

Aside from hydrogen, MRI of other nuclei such as sodium [8] and carbon-13 may be of interest. Sodium MRI is very limited by SNR, so the greater polarization at high field is certainly a huge benefit. Carbon-13 is usually hyperpolarized, and may be used to image downstream metabolites. Although high field may not be necessary for SNR, it may be of great value for spectroscopic C-13 imaging. Both of these nuclei have gamma 1/4 that of water, meaning that they are less prone to T2* and susceptibility effects at high field. SAR considerations are about the same as for hydrogen, and challenges increase with field strength. B1 variations are likely to exist regardless of field, as surface coils are commonly used.

Summary

Despite numerous 3.0 T systems in clinical use for imaging of breast cancer, there have been very few studies directly comparing diagnostic accuracy between 1.5 T and 3.0 T. Although image quality in "standard" breast MR protocols typically improves at 3.0 T, subtle effects such as variation of contrast enhancement due to RF inhomogeneity or effect of reduced flip angle echo trains require more study to assess their overall impact on diagnostic accuracy. Additionally, many of the gains of using higher field strength can be made by improving receiver coil arrays, and option that should always be explored. However some more advanced breast imaging techniques such as spectroscopic imaging, multinuclear imaging or susceptibility weighted imaging certainly benefit from higher field, so that the overall impact of high-field scanning on breast MRI really depends on the role that some of these methods ultimately will play.

References

[1] Kuhl CK. Breast MR imaging at 3T. "Magn Reson Imaging Clin N Am." 2007; 15:315–320.
[2] Kuhl CK, Jost P, Morakkabati N, Zivanovic O, Schild HH, Gieseke J. Contrast-enhanced MR imaging of the breast at 3.0 and 1.5 T in the same patients: initial experience. "Radiology." 2006; 239:666–676.
[3] Ogawa S, Lee TM, Kay AR, Tank DW. Brain magnetic resonance imaging with contrast dependent on blood oxygenation. "Proc Natl Acad Sci U S A." 1990; 87:9868–9872.
[4] Haacke EM, Xu Y, Cheng YC, Reichenbach JR. Susceptibility weighted imaging (swi). "Magn Reson Med." 2004; 52:612–618.
[5] Rakow-Penner R, Daniel B, Yu H, Sawyer A, Glover GH. Relaxation times of breast tissue at 1.5T and 3T measured using IDEAL. J Magn Reson Imaging 2006; 23:87–91.
[6] Kuhl CK, Kooijman H, Gieseke J, Schild HH. Effect of B1 inhomogeneity on breast MR imaging at 3.0 T. Radiology 2007; 244:929–930.
[7] Moran C, Smith M, Kelcz F, Block W. Susceptibility weighted imaging in breast tissue: Initial experiences. In: Proceedings of the 17th Annual Meeting of ISMRM, Honolulu, 2009. p. 2128.
[8] Jacobs MA, Ouwerkerk R, Wolff AC, Stearns V, Bottomley PA, Barker PB, Argani P, Khouri N, Davidson NE, Bhujwalla ZM, Bluemke DA. Multiparametric and multinuclear magnetic resonance imaging of human breast cancer: current applications. Technol Cancer Res Treat 2004; 3:543–550.

Fast Acquisition with Parallel Imaging and Other Techniques

Brian A. Hargreaves
Department of Radiology, Stanford University, Stanford, USA, *bah@stanford.edu*

Introduction

Numerous aspects of breast MRI protocols demand fast acquisition methods. Most importantly, bilateral dynamic contrast-enhanced (DCE) scanning requires rapid scanning to achieve high spatial resolution while resolving contrast kinetics. Faster acquisition allows reduced echo train lengths in T2-weighted scans, which typically reduces image artifacts. Finally, faster scanning reduces motion artifacts in all scans, particularly in longer acquisitions such as spectroscopic imaging. Recent technical advances that improve imaging speed include faster gradient systems, parallel imaging, alternative acquisition trajectories, and faster excitation methods. Here we describe numerous acceleration methods that can be applied to different pulse sequences and protocols.

Techniques

Parallel Imaging—Coils and Geometry

Parallel imaging uses multiple receive coils (up to 32 or more) to accelerate imaging by exploiting spatial sensitivity patterns of the coils [1–3]. Generally these methods reduce the number of *phase encode* steps in the image acquisition, and require a coil geometry with sensitivity variations in this direction. In standard breast MRI, it is common to use the anterior/posterior direction for image readout to prevent cardiac motion artifacts from interfering with the signal in the breasts. This leaves the superior/inferior and left/right directions available for parallel imaging. Therefore, receive coils should be designed with maximal sensitivity variations in these directions. Additionally, coils should always be designed to maximize SNR, both to enable higher spatial resolution

imaging and to compensate for SNR lost by using parallel imaging. Numerous parallel imaging breast coil designs have been shown recently [4–6], and coil technology continues to improve.

Parallel Imaging—Reconstruction

There are numerous methods of data acquisition and reconstruction using parallel imaging. Two common approaches are sensitivity encoding (SENSE) [3] and generalized reconstruction from partially parallel acquisition (GRAPPA) [7]. GRAPPA and the so-called modified-SENSE or mSENSE both acquire calibration data within the sequence, which reduces artifacts from patient motion between calibration and scanning. Another set of self-calibrated parallel imaging approaches use averaged temporal information for parallel imaging calibration [8, 9]. These can be optimized for DCE breast MRI, where coil sensitivities do not vary much over time [10], as illustrated in Fig. 1.

Dual-Slab Imaging

There are many acceleration benefits to using two separate slab excitations for breast MRI, assuming the space between breasts can be neglected or studied in a different part of the exam protocol. Sharper slab profiles can be achieved, reducing phase-encode coverage, and cardiac motion artifacts are reduced by not exciting the heart. Restricting the volume to each breast allows interleaved slab imaging with reduced field-of-view, which is a simple and SNR-efficient acceleration method that avoids encoding the space between breasts [5]. Furthermore, slabs can be independently shimmed, which can improve fat suppression and image quality [11].

Simultaneous Dual-Slab Imaging

It is also possible to use simultaneous dual-slab excitation, with further benefits. Greater parallel imaging acceleration can be exploited across both slabs. Independent phase-modulation approaches can alter the aliasing pattern when undersampling is used [12], resulting in lower artifacts from parallel imaging. In dual-slab breast imaging these can lower the "g-factor" or noise amplification in parallel imaging [13]. Simultaneous dual-slab excitations can be applied with water-only excitation [14] or standard excitations [15].

Acquisition Trajectories

Although Cartesian scanning is by far the most common approach to MR imaging, other acquisition trajectories can provide benefits. 3D spiral imaging can reduce scan times by a factor of 3–4 in many cases, and can be combined with parallel imaging along the slab direction (Fig. 1), but requires careful off-resonance correction to avoid image blurring [16]. Undersampled projection (PR) imaging methods offer very very fast scanning with high resolution and minimal artifacts [17–19]. Undersampled PR imaging tends to produce a diffuse aliasing pattern that is less severe than in other methods. K-space weighted image contrast (KWIC) exploits central oversampling in PR to allow spatiotemporal resolution tradeoffs in *post-processing* [17, 20].

Compressed Sensing

A further approach to undersampling is compressed sensing (CS), which exploits the "compressibility" of the images to remove aliasing resulting from undersampling [21]. CS requires the use of a random sampling pattern, some knowledge of general image characteristics, and a specialized reconstruction. CS can accelerate MR images in both spatial and temporal dimensions [22], and can be combined with parallel imaging, partial Fourier imaging and other acceleration methods.

Summary

Numerous acceleration methods using parallel imaging and other techniques are changing the way clinical breast MRI will be performed. This overview has briefly described how combinations of these methods can be applied to Breast MR imaging.

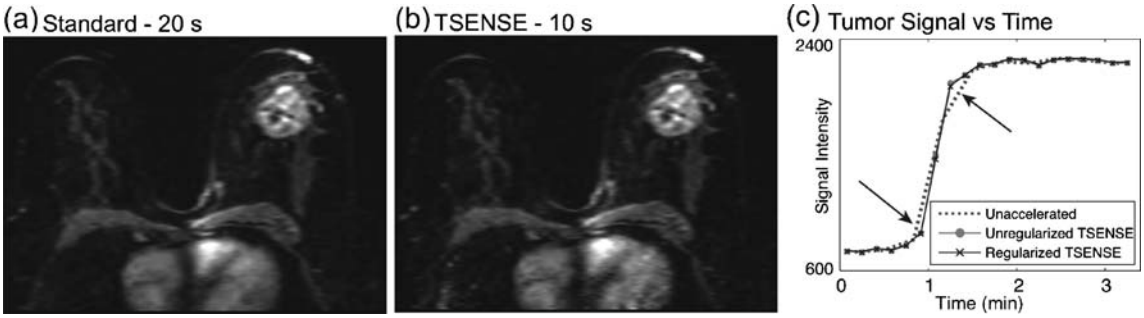

Figure 1: *Axially-reformatted images from a sagittal TSENSE accelerated acquisition using 3D spiral imaging and water-only dual-slab excitation with independent phase modulation. Standard reconstruction (a) and 2 TSENSE-accelerated images (b). Images are acquired with 32 sagittal sections (3 mm thick) across each breast (20 cm FOV), and a phase modulated excitation to reduce scan times. TSENSE is applied in the left/right direction. The accelerated images have slightly decreased SNR, but no aliasing artifact. The TSENSE signal enhancement curves show better depiction of rapid uptake with the tumor (c, arrows). The different acceleration methods shown here can be applied independently to other types of acquisition.*

References
[1] Roemer PB, Edelstein WA, Hayes CE, Souza SP, Mueller OM. The NMR phased array. Magn Reson Med 1990; 16:192–225.
[2] Sodickson DK, Manning WJ. Simultaneous acquisition of spatial harmonics (SMASH): Fast imaging with radiofrequency coil arrays. Magn Reson Med 1997; 38:591–603.
[3] Pruessmann KP, Weiger M, Scheidegger MB, Boesiger P. SENSE: Sensitivity encoding for fast MRI. Magn Reson Med 1999; 42:952–962.
[4] Ikeda T, Monzawa S, Komoto K, Aso E, Saito Y, Maeda T, Sakamoto T, Adachi S. Performance assessment of phased-array coil in breast MR imaging. Magn Reson Med Sci 2004; 3:39–43.
[5] Konyer NB, Ramsay EA, Bronskill MJ, Plewes DB. Comparison of MR imaging breast coils. Radiology 2002; 222:830–834.
[6] Giaquinto RO, McKenzie C, Sodickson DK, Grant AK, Murtagh GE, Furman RL, Swider LJ, Hardy CJ, Dumoulin CL. A 28 channel bi-lateral breast array for accelerated MR imaging. In: Proceedings of the 14th Annual Meeting of ISMRM, Seattle, 2006. p. 423.
[7] Griswold MA, Jakob PM, Heidemann RM, Nittka M, Jellus V, Wang J, Kiefer B, Haase A. Generalized autocalibrating partially parallel acquisitions (GRAPPA). Magn Reson Med 2002; 47:1202–1210.
[8] Kellman P, Epstein FH, McVeigh ER. Adaptive sensitivity encoding incorporating temporal filtering (TSENSE). Magn Reson Med 2001; 45:846–852.
[9] Breuer FA, Kellman P, Griswold MA, Jakob PM. Dynamic autocalibrated parallel imaging using temporal GRAPPA (TGRAPPA). Magn Reson Med 2005; 53:981–985.
[10] Han M, Daniel BL, Hargreaves BA. Accelerated bilateral dynamic contrast-enhanced 3d spiral breast MRI using TSENSE. J Magn Reson Imaging 2008; 28:1425–1434.
[11] Han M, Rodriguez S, Sawyer A, Daniel B, Cunningham C, Pauly J, Hargreaves B. Fat suppression with independent shims for bilateral breast MRI. In: Proceedings of the 17th Annual Meeting of ISMRM, Honolulu, 2009. p. 579.
[12] Breuer FA, Blaimer M, Heidemann RM, Mueller MF, Griswold MA, Jakob PM. Controlled aliasing in parallel imaging results in higher acceleration (CAIPIRINHA) for multi-slice imaging. Magn Reson Med 2005; 53:684–691.
[13] Han M, Hargreaves BA. Slab-phase modulation combined with parallel imaging in bilateral breast imaging. In: Proceedings of the 16th Annual Meeting of ISMRM, Toronto, 2008. p. 2730.
[14] Pauly JM, Cunningham CH, Daniel BL. Independent dual-band spectral-spatial pulses. In: Proceedings of the 11th Annual Meeting of ISMRM, Toronto, 2003. p. 966.
[15] Staroswiecki E, Pauly J, Daniel B, Hargreaves B. An on-the-fly radiofrequency pulse for bilateral excitation with independently modulated phase. In: Proceedings of the 17th Annual Meeting of ISMRM, Honolulu, 2009. p. 4506.
[16] Daniel BL, Yen YF, Glover GH, Ikeda DM, Birdwell RL, SawyerGlover AM, Black JW, Plevritis SK, Jeffrey SS, Herfkens RJ. Breast disease: dynamic spiral MR imaging. Radiology 1998; 209:499–509.
[17] Dougherty L, Isaac G, Rosen MA, Nunes LW, Moate PJ, Boston RC, Schnall MD, Song HK. High frame-rate simultaneous bilateral breast dce-MRI. Magn Reson Med 2007; 57:220–225.
[18] Chan RW, Ramsay EA, Cunningham CH, Plewes DB. Temporal stability of adaptive 3d radial MRI using multidimensional golden means. "Magn Reson Med." 2009; 61:354–363.
[19] Moran CJ, Kelcz F, Jung Y, Brodsky EK, Fain SB, Block WF. Pilot study of improved lesion characterization in breast MRI using a 3d radial balanced ssfp technique with isotropic resolution and efficient fat-water separation. "J Magn Reson Imaging." 2009; 30:135–144.
[20] Song HK, Dougherty L. Dynamic MRI with projection reconstruction and kwic processing for simultaneous high spatial and temporal resolution. Magn Reson Med 2004; 52:815–824.
[21] Donoho D. Compressed sensing. Information Theory, IEEE Transactions on 2006; 52:1289–1306.
[22] Lustig M, Donoho D, Pauly JM. Sparse MRI: The application of compressed sensing for rapid MR imaging. Magn Reson Med 2007; 58:1182–1195.

A combined high temporal and high spatial resolution 3.0 Tesla MR imaging protocol for the assessment of breast lesions: initial results

TH Helbich[1], G Grabner[1], W Bogner[1], S Gruber[1, 2], P Szomolanyi[3], S Trattnig[1, 2], G Heinz-Peer[1], Weber M[1], F Fitzal[4], U Pluschnig[5], M Rudas[6], K. Pinker [1]
[1]Department of Radiology, Medical University Vienna, Austria; [2]MR Centre of Excellence, Department of Radiology, Medical University Vienna, Austria; [3]Department of Imaging Methods, Institute of Measurement Science, Slovak Academy of Sciences, Bratislava, Slovakia; [3]Department of Radiology, Medical University Vienna, Austria; [4]Department of Surgery, Medical University Vienna, Austria; [5] Department of Internal Medicine, Division of Oncology, Medical University Vienna, Austria; [6]Clinical Institute of Pathology, Medical University Vienna, Austria

Purpose
To develop a 3.0 Tesla breast imaging protocol that combines high temporal and spatial resolution 3D MR sequences for quantitative time course and morphological analysis of breast lesions.

Materials and Methods
Thirty-four patients were included in the study (age range, 31–82; mean age, 54.3). The study protocol was approved by the Institutional Review Board and written, informed consent was obtained from all patients. The MRI protocol included: a coronal T1-weighted Volume-Interpolated-Breathhold-Examination sequence (VIBE), focused on high temporal resolution for optimal assessment of the contrast-enhancement behavior of lesions (SI 1.7 mm isotropic; TA 3.45 min for 17 measurements); a coronal T1-weighted turbo fast-low-angle-shot-3D sequence (FLASH), with water-excitation and fat-suppression, focused on high spatial resolution for morphologic analysis (SI 1 mm isotropic; TA 2 min); and a repeated coronal VIBE for detection of washout. Lesion size and morphology were assessed. ROIs for suspicious areas were manually drawn and evaluated for contrast-enhancement behavior by plotting intensity courses against time. Sensitivity and specificity with a 95% confidence interval and the negative predictive value (NPV) and

positive predictive value (PPV) were calculated. Diagnostic accuracy was assessed. The histopathological diagnoses were used as a standard of reference.

Results
Fifty-five lesions were detected in 34 patients. All malignant breast lesions were identified correctly. There were five false-positive lesions. The sensitivity of contrast-enhanced MRI of the breast at 3 T was 100%, with a 95% confidence interval (CI) of 90.6–100%. The specificity was 72.2%, with a 95% CI of 49.1–87.5%. The PPV was 0.88 and the NPV was 1. Diagnostic accuracy was 91% with a 95% CI of 80.4–96.1%.

Conclusion
Our prospective study demonstrates that the presented 3 Tesla MR imaging protocol, comprising both high temporal and high spatial resolution, enables accurate detection and assessment of breast lesions.

Diffusion-weighted MRI for differentiation of breast lesions at 3.0 Tesla: How does selection of diffusion schemes affect diagnosis?

Thomas H Helbich, MD, Wolfgang Bogner, MSc, Stephan Gruber, PhD, Katja Pinker, MD, Günther Grabner, MSc, Andreas Stadlbauer, PhD, Michael Weber, PhD, Ewald Moser, PhD, Siegfried Trattnig, MD
Department of Radiology, Medical University of Vienna , Vienna General Hospital, Waehringer Guertel 18–20, A-1090 Vienna, Austria

Purpose
To compare the diagnostic quality of different diffusion weighting schemes with regard to apparent diffusion coefficient (ADC) accuracy, ADC precision, and diffusion-weighted image (DWI) contrast-to-noise ratio (CNR) for different types of lesions and breast tissue.

Materials and Methods
Institutional Review Board approval and written, informed consent were obtained. Fifty-one patients with histopathologic correlation or follow-up were included in this study on a 3.0 Tesla MR scanner. There were 112 regions of interest (ROIs) drawn in 24 malignant, 17 benign, 20 cystic, and 51 normal tissue regions. ADC maps were calculated for combinations of ten different diffusion-weightings (b-values), ranging from 0 to 1250 s/mm^2. Differences in ADC among tissue types were evaluated. The CNR of lesions on DWI was compared for all b-values. A repeated measure ANOVA was used to assess lesion differentiation.

Results
ADC (mean±SD×10^{-3} mm^2/s) values calculated from b=50 and 850 s/mm^2 were 0.99±0.18, 1.47±0.21, 1.85±0.22, and 2.64±0.30 for malignant, benign, normal, and cystic tissue, respectively. An ADC threshold of 1.25×10^{-3} mm^2/s allowed discrimination of malignant from benign lesions with a diagnostic accuracy of 95% ($p<.001$). ADC calculations using multiple b-values were not significantly more precise than calculations using two b-values. We found an overestimation of ADC for maximum b-values of up to 1,000 s/mm^2. The best CNR for tumors was identified at 850 s/mm^2.

Conclusion
Optimum ADC determination and DWI quality at 3.0 Tesla was found for a combination of two b-values: 50 and 850 s/mm^2. This provided a high accuracy for differentiation of benign and malignant breast tumors.

Ultra-wideband technology—What is it and could it be used for breast cancer detection?

Ingrid Hilger, Dr.rer.biol.hum.[1], Christiane Geyer, Dipl.-Biol.[1], Ulrich Schwarz, Dipl.-Ing. [2], Marko Helbig, Dr.-Ing[2], Gabriella Rimkus, Dipl-Biochem. [1], Matthias Hein, Dr.rer.nat. [2], Jürgen Sachs, Dr.-Ing. [2], Werner A. Kaiser Dipl.-Chem, Dr. med. [1]
[1]Institute of Diagnostic and Interventional Radiology, University Hospital Jena, Erlanger Allee 101, D-07747 Jena; [2]Institute of Information Technology, Technische Universität Ilmenau, P.O. Box 100565, D-98684 Ilmenau
Corresponding author:
Prof. Dr. Ingrid Hilger, Institute of Diagnostic and Interventional Radiology, University Hospital Jena, AG Experimentelle Radiologie, Erlanger Allee 111, D-07747 Jena, Germany, Phone: 0049-(0)3641-9325921, Fax: 0049-3641-9325922, e-mail: ingrid.hilger@med.uni-jena.de

Abstract
The present article considers ultra-wideband (UWB) technology as a potential new modality for the image-based identification of normalites/abnormalities in the breast. We particularly describe determination of physiological signatures by sounding with electromagnetic waves of very large bandwidth and very low power, the design, simulation, measurement, and application of ultra-wideband imaging in phantoms. Extrapolations to the situation in humans will be discussed.

Introduction
Radiological breast cancer detection has progressed enormously in the last years. Due to the increased awareness of women against breast cancer together with the implementation of X-ray mammography, ultrasound, and particularly magnetic resonance mammography (MRM), incidence of breast cancer has increased with a concomitant decrease of morbidity [1, 2]. Nevertheless, there is still a need for further improvement of breast diagnostic imaging in dedicated situations. For example, best accuracy in breast cancer detection can be achieved by the use of MRM [3, 4]. However, this methodology is comparatively expensive and will presumably be restricted mainly to specific diagnostic centres. On the other hand,

the need of a simple, accurate, robust, biocompatible method, with the potential of an adequate "pre-screening" of patients, e.g. in the sense of reliable exclusion of the presence of breast cancers, would be of great benefit. We expect that these requirements could be adequately fulfilled by the use of UWB technology. Ultra-wideband sensing is nowadays mainly restricted to the technical field, concerning information, communication, and object identification purposes [5, 6]. The use in clinical applications particularly related to radiological diagnostics is lacking up to now. First steps are being done by several groups worldwide, focusing their work particularly on simulations, modelling or experimental studies of phantoms [7, 8]. Very recently, a few approaches on microwave imaging have been considered as well [9, 10]. The fundamental idea behind UWB technology comprises selective tissue identification by their inherent dielectric properties which are determined by the respective water contents. The basic technical implementation is very simple at a first glance, comprising the measurement of scattered waves at a short distance from the target. Nevertheless, a huge interaction of specific biological, technical, and physical parameters and combinations thereof should be kept under consideration as will be demonstrated in the present study.

Among the different organs and human body parts that could be potentially imaged with this technology, several aspects make particularly the breast a good candidate for first diagnostic applications. Topographically, the breast is accessible to UWB sounding, and is composed mainly of glandular and fatty tissue. Increasing incidence of breast cancer worldwide additionally favours investigations on this topic.

From the technical point of view, the particular reflection properties of electromagnetic wave packets (UWB pulses) are influenced by the dielectric boundary surfaces and interfaces, e.g. of the breast. The dielectric properties are determined by the complex dielectric permittivity $\varepsilon=\varepsilon'-j\varepsilon''$. The real part ε' quantifies the ability of the material to store electrical field energy and is tightly related to the index of refraction, $n=\sqrt{\varepsilon'}$. The imaginary part ε'' represents the dielectric absorptive losses in tissues, which often are normalized to yield the dielectric loss tangent, $\tan\delta=\varepsilon''/\varepsilon'$. Depending on the different dielectric values ε_1 and ε_2 of adjacent materials, a reflected signal will occur which is determined by the reflection coefficient: $\Gamma=\frac{\sqrt{\varepsilon_1}-\sqrt{\varepsilon_2}}{\sqrt{\varepsilon_1}+\sqrt{\varepsilon_2}}$ for perpendicular incidence of a plane wave on the material boundary.

Dielectric spectroscopy.

As a first step towards the development of UWB technology for diagnostic purposes, the interaction of electromagnetic waves with biological tissues was studied via dielectric spectroscopy using coaxial probes and antennas. By means of coaxial probes, determination of absolute dielectric values is feasible. However, measurements are restricted to a small measuring volume and penetration depth, being determined by the cross-section of a conveniently calibrated coaxial probe (see below). To particularly demonstrate the relationship between dielectric spectroscopy and water content in different tissues, *ex-vivo* UWB probing experiments were conducted. The volumetric water content c was assessed by weighing tissue samples (volume: 1 cm^3) excised directly from the respective measurement positions before and after drying (Fig. 1.). As a result, a clear correlation between the real and imaginary parts of the permittivity and the water content was observed. The data were interpolated by the use of an empirical logarithmic interpolation according to Lichtenecker-Rother [11, 12]: $\ln\varepsilon_{eff}\cong(1-c).\ln\varepsilon_{fat}+c.\ln\varepsilon_{water}$, with $\varepsilon_{fat}\cong5$ and $\varepsilon_{water}\cong80$ at f=3 GHz.

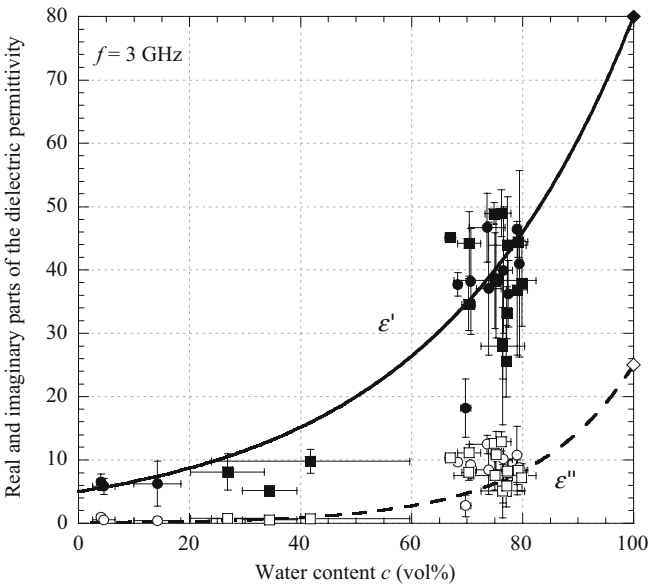

Fig. 1 Relationship between the real (filled symbols) and imaginary part (open symbols) of the dielectric permittivity and the water content for different organ tissues of pigs (squares) and cows (circles). Data are shown as mean and standard deviation of three independent experiments. From [13].

Dielectric spectroscopy seems to be sensitive enough to particularly depict structural inhomogeneities in cow udder tissue. When randomly measuring different areas, the UWB response is lower and standard deviation larger as compared to those ones selectively positioned at the glandular component (Fig. 2).

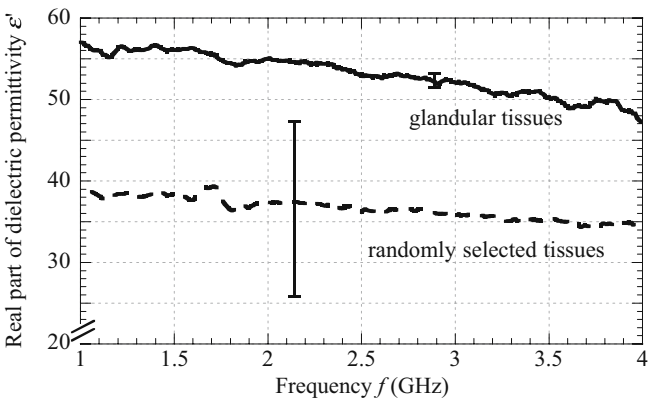

Fig. 2. Frequency dependent permittivity ε' of glandular and randomly chosen tissues of cow udders; the error bars represent typical standard deviations. From [13].

Dielectric spectroscopy of tumours in the frequency range of 1 to 4 GHz using a coaxial probe was performed as well. Permittivity of subcutaneously implanted human adenocarcinoma in living mice revealed permittivity values ε'=18 to 15 and ε''=4 to 2 for increasing frequency. Moreover, dedicated experimental conditions were considered as well. For example, squamous cell carcinoma in rabbits (VX-2 tumour, Fig. 3, tumour volume: 32 cm^3) showed an *in vivo* permittivity ε'=55 to 49, ε''=17 to 10). These values summarize

signal reflection and absorption components resulting from the presence of skin covering the tumours, tumour tissue itself and tumour vascularization in the investigated tissue sample volume. In contrast, for healthy tissues surrounding the tumour, comparatively lower permittivity values $\varepsilon'=26$ to 23, $\varepsilon''=7$ to 3 were detected, reflecting mainly the influence of skin, normal connective and fatty tissue underneath.

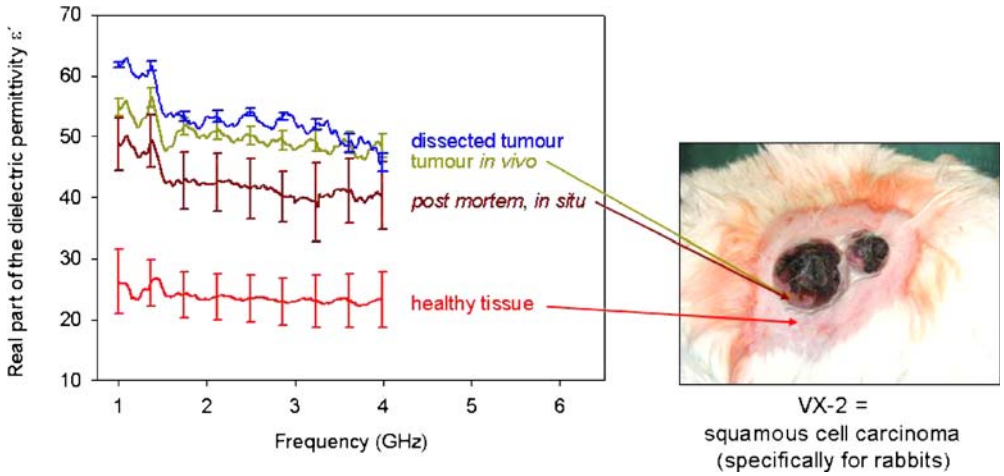

Fig. 3 Dielectric properties of tumour and normal tissues. Mean and standard deviation of at least three measurements.

Assessing the effect of blood circulation on permittivity, the same tumour was also measured *post mortem, in situ*. In this case, the permittivity values were solely determined by cancerous tissue and the skin covering the tumour. Accordingly, the dielectric properties of the tumour dropped to values between $\varepsilon'=49$ to 41, $\varepsilon''=14$ to 9. Dissected and opened tumours showed a permittivity of $\varepsilon'=62$ to 46, $\varepsilon''=22$ to 12, representing the tumour tissue itself (without the influence of skin and blood circulation). Apart from evidences related to the water contents that could be derived from the results, they clearly show how distinctly the signal reflection and adsorption components can be influenced by different tissue types and physiological parameters of the respective sample volume. These relationships will be of particular interest in regard to future processing and interpretation of signals during UWB sounding of patients.

Based on the fact that dielectric spectroscopy is not a suitable tool to generate images, antennas are interesting tools that illuminate the regions of interest from a remote distance. As opposed to coaxial probes, antennas radiate the energy in a divergent beam. The received signals contain reflection components from different tissue areas of different permittivities. Therefore, basic image capabilities of UWB sensors were assessed by the use of cylindrically shaped oil-gelatine phantoms with sequentially increasing gelatine rates (up to 80% (v/v)), modelling systematically the water content of different organic tissues. Experimentally, good agreement between the measured values for the complex permittivity values and published data was observed. Furthermore, arrangements of the same phantoms were successfully imaged by UWB sounding [14].

In the view of the implementation in the clinical practice in the long term, first risk assessments of UWB sounding were performed under controlled experimental conditions as well. By measuring the activity of cellular dehydrogenases, the viability of a human fibroblast (BJ cells) and a human breast cancer cell line (BT474 cells) was observed not to be influenced by UWB sounding (f=4.5 GHz, power=4 mW, peak voltage=0.5 V, exposure time=5–60 min). The power the cells were exposed to were equivalent to those expected to occur in patients during the diagnostic procedure. This level is approximately 1,000 times lower compared to the exposure of the human body—particularly the region around the ear—to mobile telephone devices. Therefore, exposure of the human body to the above mentioned electromagnetic fields would not lead to any adverse and undesired effects. UWB sensors utilizing ultra-low power signals as mentioned above should therefore be suitable for human medical applications.

Antennas and probes for ultra-wideband medical sensors

Dielectric spectroscopy employing coaxial probes was the initial attempt for tissue characterisation, as pointed out in the previous section. The functionality is characterized by uncomplicated handling without the need for extensive signal processing or hardware. On the other hand, the drawback is to be found in the spatial extension of the fringing fields, limiting this approach to a quasi-surface analysis. This behaviour is caused by the layout of this kind of probes, which generally consist of an abrupt termination of a coaxial waveguide. Under ideal conditions in vacuum or air, a transmitted signal is almost completely reflected back from this interface. However, fringing fields give rise to an evanescent near-field in front of the probe tip, as illustrated by Fig. 4. These field components are strongly affected by the material attached to the coaxial probe. Consequently, the complex permittivity can be extracted from the measured reflection coefficient of the probe tip.

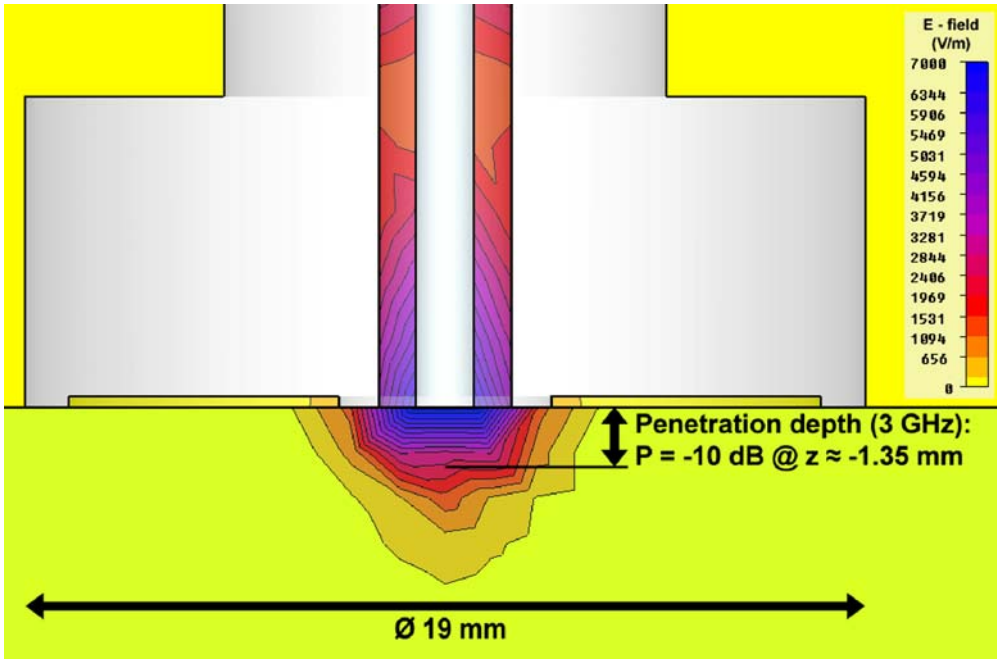

Fig. 4. Numerical simulation of an evanescent electric field distribution at 3 GHz related to a coaxial probe tip above a skin sample. The penetration depth of 1.35 mm is derived as the distance at which the field strength has dropped to about one third of its value at the surface (corresponding to a power attenuation to one tenth). The absolute scale has been set arbitrarily for numerical purposes and does not account for the low field levels applied by our M-sequence technique.

According to the numerical simulations, the non-radiated electrical field seems to decay linearly with distance, providing very small and material-independent penetration depths, as summarized in Table 1. While measurements of homogeneous samples can be expected to yield reliable information, special attention is required for the quantitative analysis of data acquired from layered or inhomogeneous materials like the breast. Thereby, the dominant contributions of the measured data are determined by the first millimetre of the sample, masking subjacent layers. Consequently, the application of a coaxial-probe based dielectric spectroscopy is limited to a one-dimensional near-surface characterization of small and homogeneous samples.

Table 1: Penetration depth in mm (definition according to the caption of Fig. 4) of the electrical field at 3 GHz computed for different samples and two different coaxial probes. Except for numerical errors in the sub-millimetre range, a constant penetration depth is observed. Ø=diameter.

Medium	Commercial coaxial probe (Ø 19 mm)	Coaxial probe (Ø 3×19 mm)
distilled water	−1.3	−3.5
human skin	−1.4	−2.9
vegetable oil	−2.2	−3.6

Since tumours may be located well below the skin, the penetration depth of the sensing signal has to be increased significantly. The most obvious measure is to replace the coaxial probe by radiating sensor elements, e.g. by antennas. Depending on the applied frequency, the radiated electromagnetic fields may penetrate the whole body.

In contrast to the evanescent fields of coaxial probes, capturing only a very small part of a sample, a radiated signal would capture an average value of an extended sample volume without the capability of spatial differentiation or depth information. Thus, special UWB measurement setups are required to facilitate an identification and localisation of different tissue structures. As indicated previously, this approach is characterized by challenges in antenna design and signal processing (see following section) as well. While two different sensor scenarios, namely remote and contact-mode measurements employing a suitable scanning technique, are currently under investigation, each of them has specific assets and drawbacks for the desired application [15]. Due to the use of a single-channel UWB-radar front-end, a synthetic aperture is required for both scenarios to facilitate a three-dimensional microwave imaging process, indicating that a single target point has to be investigated from at least three different positions for a three-dimensional rendition.

For a bistatic sensor system, simultaneously transmitting and receiving, a minimum of two antennas is required, which operate at the same time. The two different scenarios can be achieved by the use of a scan of a pair of antennas around a region of interest by a certain distance or by the use of a number of compact antenna elements under sequential operation, placed directly on the skin at the target area (Fig. 5). As the first scenario allows the use of conventional directive UWB radiators, which focus the signal towards the target, it was implemented in an initial approach. Latest results for that scenario are summarized in the following section. Due to the remote setup and multiple reflections between the antenna aperture and the skin, the measurements suffered from large clutter signals [15] (see Fig. 6 for illustration). This is in contrast with the properties of a contact-mode sensor array. However, this scenario requires very compact radiating elements with good input matching

over a broad bandwidth. Such antennas should have geometrical dimensions d much smaller the longest wavelength λ involved, e.g. λ =30 cm for f=1 GHz.

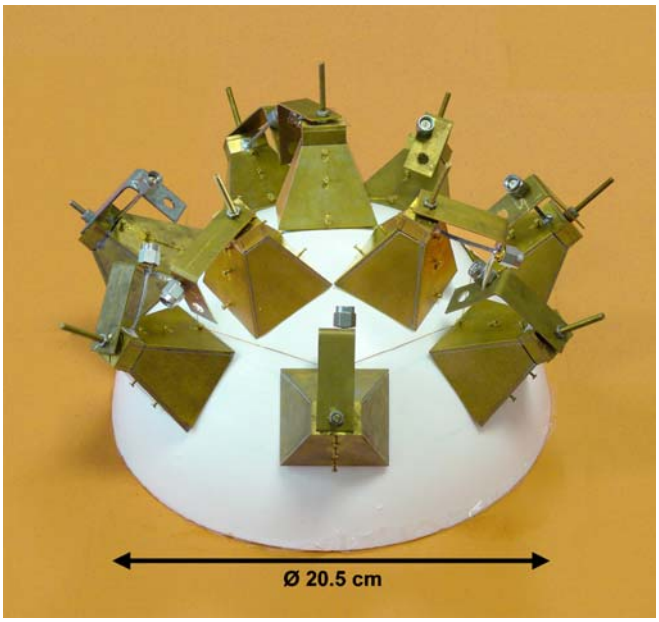

Fig. 5: Enlarged schematic breast phantom with an experimental 10-element array of compact and dielectrically matched antennas for three-dimensional microwave breast imaging.

Antennas with $d/\lambda<1$ are called electrically small antennas. Due to fundamental physical constraints, electrically small antennas reveal a poor radiation efficiency, similar to coaxial probes, and a narrow matched frequency bandwidth [13]. One opportunity to overcome these obstacles is the use of dielectric material in and around the antenna. Scaling with the square root of the real part of the permittivity, the guided wavelength λ_g and, hence, the geometrical size of the antenna can be reduced while keeping the electrical size $d/\lambda_g \approx 1$. Additionally, the dielectric material can be employed to act as a coupling medium, in order to reduce signal reflections at the dielectric interface between the antenna and the target, e.g. the human body, by matching the permittivity of the antenna to that of the target. These benefits motivated the dielectric scaling of double-ridged horn antennas. As a result, the outer geometrical dimensions of 44 mm × 40 mm of the antenna aperture, which presents the integral parameter for biomedical applications, could be reduced by almost a factor of 10 compared to a version of similar performance operating in air.
Two different dielectric materials with a permittivity of $\varepsilon' = 22 \pm 2$ have been studied for different tasks. While acetone is used for antenna measurements because of its electrical, optical, and liquid properties, a biocompatible compound of oil and gelatine is used as an antenna enclosing material for test person measurements. Figure 5 shows a first schematic arrangement of an array of dielectrically scaled antennas, arranged on a breast phantom. To achieve a still smaller size of the radiating elements, the use of ceramic-based antennas is under investigation. The solid sintered material is characterized by a high dielectric constant, low losses and a high biocompatibility, enabling target aperture dimensions of 24 mm × 24 mm and less [15]. In combination with a sophisticated signal processing, this attempt has a great potential for the detection and imaging of very small malignant targets in an ultrasound-like scenario.

UWB imaging for breast cancer detection

The basic idea for the technical implementation of ultra-wideband imaging is to expose the female breast with an electromagnetic sounding wave of very low power and to register the wave reflected from a hidden body as e.g. cancerous tissue (Fig. 6).

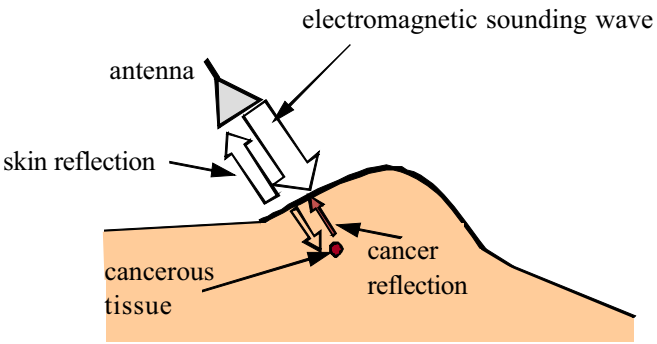

Fig. 6: Detection of hidden objects by sounding with electromagnetic waves.

If these waves are able to penetrate the object, there is some chance to visualize its internal structure. For that purpose, the frequency of the sounding wave must be as low as possible, since the human body becomes opaque, if the frequencies are too high. On the other hand, the resulting image resolution improves with increasing frequency, and accordingly bandwidth. A reasonable compromise is to work in the frequency range from about 1 to 10 GHz.
The physical basis of ultra-wideband imaging resembles ultrasound imaging which applies sound waves instead of electromagnetic ones. However, while ultrasound sensors have to be in contact with the body of investigation, this is not necessarily required for sensors based on the scattering of electromagnetic waves. However, for ultrasound as well as for ultra-wideband imaging, the visualization of a hidden object, e.g. tumour tissue, requires a defined contrast with respect to the surrounding substance. Here, this contrast is given by the difference of the electric permittivity between healthy and malignant tissue. As shown above, the biological reason of a permittivity aberration is the increased water content of malignant tissue. Since the variation of the permittivity within the propagation path of the electromagnetic waves causes reflections, the presence of abnormal tissue with increased water content can be registered outside the body as depicted in Fig. 6.
If the propagation velocity of the waves within the breast is roughly known, the depth of the cancerous target can be estimated from the roundtrip time of the scattered waves. Unfortunately, this is not enough to actually localize it, since the antennas radiate over an

extended area (see Fig 7). Hence, the measurement will merely register an integral value over the interaction volume. In order to solve this problem, the measurement has to be repeated from different locations, and accordingly, different aspect angles (as applied in ultrasound imaging too). Here again, we have the options of scanning a single sensor element or employing an array of sensors, either at a remote distance or in contact with the target under inspection.

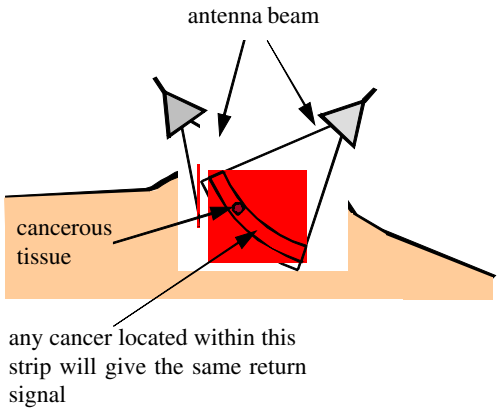

Fig. 7. Illustration of antenna behaviour and the approach to localise a point like object.

The scanning approach requires less electronic equipment, since only one sensor is in operation. But its dislocation and the manifold repetition of the measurements extends the measurement time, which is only acceptable for research purposes, for motionless surrogate phantoms. Under clinical conditions, the measurement duration should be of the order of seconds. This makes multi-element sensor arrays inevitable. For this purpose, special sensor electronics is under development [16].

The questions concerning remote versus contact-mode measurement options are still under investigation as outlined in the previous section. Both approaches have inherent advantages and disadvantages. The direct placement of the antennas onto the skin leads to better wave penetration, but it has less comfort for the patient. In contrast, the remote sensing of the breast provides better comfort and a simpler clinical work flow. Therefore, we started to investigate this measurement approach. Unfortunately, it suffers from strong reflections of the sounding waves at the skin. These signals tend to mask the backscattered waves from suspected cancerous tissue. Hence, the current work is aimed at removing the perturbing skin reflections from the measurement data by appropriate numerical techniques. This is a sophisticated task, since the structure of the backscattered waves is quite complex due to the complicated geometry of the breast. The first step towards a reasonable solution is the reconstruction of the breast surface from the sensor data. This knowledge will then be used to identify the skin reflection in the measured data and to remove it.

Data capturing is based on scanning a toroidal area enclosing the breast as depicted in Fig 8.

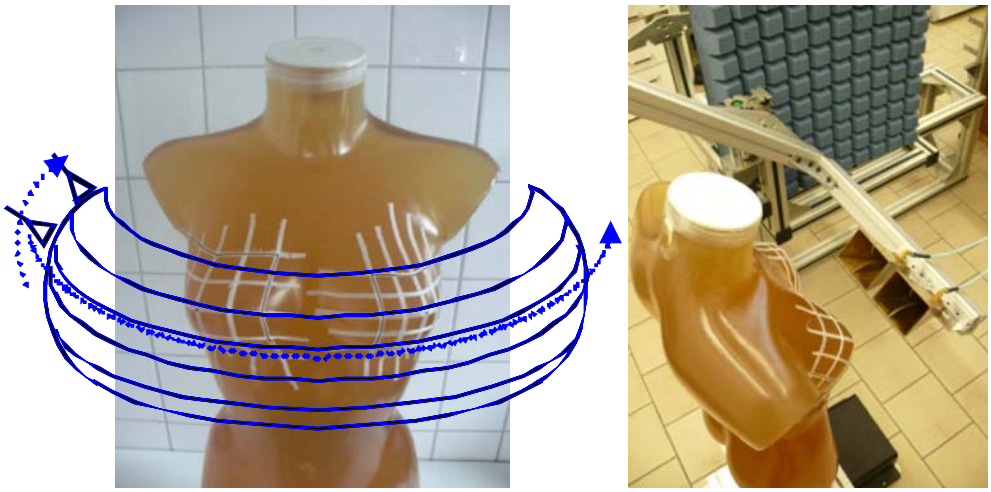

Fig. 8: Scanning approach and photograph of the experimental setup.

Subsequently, the measured data are subjected to an extended SEABED (**S**hape **E**stimation **A**lgorithm based on **B**oundary Scattering Transform and **E**xtraction of **D**irectly Scattered waves) algorithm [17, 18]. It uses super-resolution techniques leading to imaging qualities which are not attainable by classical processing approaches of UWB-data, as e.g. migration. Figure 9 gives an example for the reconstructed surface of a female torso filled with surrogate material.

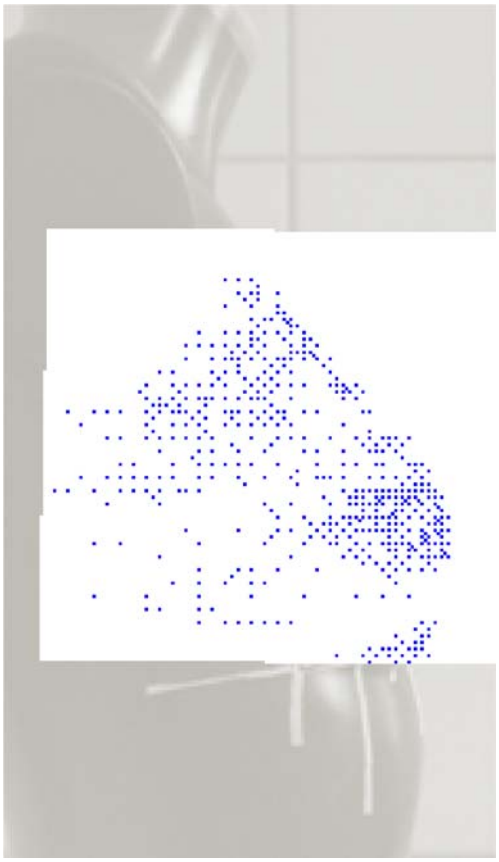

Fig. 9: Three-dimensional surface structure of a female torso. The data were acquired by the use of an UWB-sensor with 12 GHz bandwidth and processed with the expanded SEABED-algorithm.

Future work should be focused on the improvement of data quality by removing the skin reflection which will be followed by imaging the interior of the breast. For performance comparison, we will also look into the signal reconstruction using contact-mode measurements.

Conclusions

Taken together, UWB technology might have the potential to become a new modality for breast diagnostic imaging in the long term. It might probably fill the gap between distinct specifications of established diagnostic imaging techniques, comprising a valuable, non-invasive, radiation-less, easy-to-handle, and economic approach, e.g. for accurate prediction, exclusion of normal and/or malignant conditions in the breast. Extensive and challenging investigations remain necessary to manage the complexity of different technical, biological and physical aspects.

Acknowledgements

This work was supported by the German Science Foundation (DFG, SPP 1202, project ultraMEDIS (SA 1035/4-2, HE 3642/1-2, HI 689/9-2) and HaLoS (HE 1035/3-2, SA 1035/3-2)

References

1. Katalinic A, Pritzkuleit R, Waldmann A (2009). Recent Trends in Breast Cancer Incidence and Mortality in Germany. Breast Care 4:75–80.
2. Stang A, Schmutzler RK (2009). The Epidemiology and Aetiology of Female Breast Cancer. Breast Care 4:73–74.
3. Kuhl CK, Schrading S, Bieling HB, et al. (2007). MRI for diagnosis of pure ductal carcinoma in situ: a prospective observational study. Lancet 370:485–492.
4. Fischer DR, Wurdinger S, Boettcher J, et al. (2005). Further signs in the evaluation of magnetic resonance mammography: a retrospective study. Invest Radiol 40:430–435.
5. Gu X, Taylor L (2003). Ultra-wideband and its capabilities. Bt Technology Journal 21:56–66.
6. Zhuang WH, Shen XM, Bi Q (2003). Ultra-wideband wireless communications. Wireless Communications & Mobile Computing 3:663–685.
7. Davis SK, Van Veen BD, Hagness SC, et al. (2008). Breast tumor characterization based on ultrawideband microwave backscatter. IEEE Transactions on Biomedical Engineering 55:237–246.
8. Li X, Hagness SC, van Veen BD, et al. (2003). Experimental Investigation of Microwave Imaging via Space–Time Beamforming for Breast Cancer Detection. IEEE MTT-S International Microwave Symposium Digest 1:379–382.
9. Merla C, Liberti M, Apollonio F, et al. (2009) A Microwave Microdosimetric Study on Blood Cells: Estimation of Cell Membrane Permittivity and Parametric EM Analysis. 2009 International Microwave Symposium (ISM), Boston, USA, pp 1333–1336.
10. Salvador SM, Vecchi G (2009). Experimental Tests of Microwave Breast Cancer Detection on Phantoms. IEEE Transactions on Antennas and Propagation 57:1705–1712.
11. Baker Jarvis J, Janezic MD, Riddle BF, et al. (2005). Measuring the permittivity and permeability of lossy materials: Solids, liquids, metals, building materials, and negative-index materials. NIST technical note 1536.
12. Shin FG, Yeung YY, Tsui WL (1990). Symmetrization of dielectric binary mixture formulae. J Materials Science Lett 9:1002–1004.
13. Hein MA, Geyer C, Helbig M, et al. (2009). Antennas for Ultra-Wideband Medical Sensor Systems. Antennas for Ultra-Wideband Medical Sensor Systems 3rd European Conference on Antennas and Propagation (EuCAP), Berlin, Germany, pp 1868–1872.
14. Geyer C, Helbig M, Schwarz U, et al. Image-based detection of water contents in tissue-modelling phantoms by ultra-wideband sensors. RoeFo, subm.
15. Schwarz U, Helbig M, Sachs J, et al. (2009). Design and application of dielectrically scaled double-ridged horn antennas for biomedical UWB radar applications. 2009 IEEE International Conference on Ultra-Wideband, Vancouver, Canada.
16. Sachs J, Borokhovych Y, Gustat H, et al. New integrated UWB-Sensor Electronics for Array based Super-Resolution Imaging Techniques. Frequenz, subm.
17. Helbig M, Geyer C, Hein MA, et al. (2009). Improved Breast Surface Identification for UWB Microwave Imaging. World Congress of Medical Physics and Biomedical Engineering, Munich, Germany.
18. Sakamoto T, Sato T (2004). A target shape estimation algorithm for pulse radar systems based on boundary scattering transform. IEICE Transactions on Communications E87B:1357–1365.

Multiparametric and Multinuclear MRI and PET Imaging of breast cancer patients

Michael A. Jacobs Ph.D[1,2], Ronald Ouwerkerk[1], Antonio C. Wolff[2], Katarzyna Macura[1], Pedram Argani[2,3], Zaver M. Bhujwalla[1,2], Richard Wahl[1], David A. Bluemke[1], Vered Stearns[2]
[1]The Russell H. Morgan Department of Radiology and Radiological Science, [2]Sidney Kimmel Comprehensive Cancer Center. and [3]Pathology.
The Johns Hopkins University School of Medicine, Baltimore, MD 21205, and
Correspondence author:
Michael A. Jacobs, Ph.D., Department of Radiology, The Johns Hopkins University School of Medicine, Traylor Blg, Rm 217, 712 Rutland Ave, Baltimore, MD 21205, Tel: 410-955-7492, Fax: 410-614-1948
email: mikej@mri.jhu.edu

Keywords: Breast, Magnetic Resonance Imaging, Sodium MR, ^{23}Na, proton, ISODATA, Cancer

Abstract

Purpose

We initiated a prospective clinical trial to investigate the feasibility of using dynamic magnetic resonance imaging (DCE-MRI), sodium imaging (^{23}Na) and Positron Emission Tomography/computed tomography (PET/CT) before (baseline), during, and following preoperative systemic treatment (PST) for stage II III, and IV breast cancer.

Methods and Materials

Women with stage II III, or IV breast cancer received PST were studied using DCE-MRI and ^{23}Na MR images before, during, and following treatment. In addition, a subset of patients underwent additional PET/CT. PET/CT was acquired with following injection of ^{18}FDG (0.22 mCi/kg) with standard uptake value (SUV) assessment. Quantitative metrics of total sodium concentration (TSC; mM) and tumor volume were determined during treatment intervals. Patients were clinically assessed for tumor response and a pathological assessment of residual disease was conducted at surgery.

Results

Eighteen eligible women entered the trial. Fifteen women responded to therapy, including four (22%) with a complete pathological responders (pCR) and 11 (61%) with a partial pathological response (pPR). Three (17%) had stable or progressive disease (nPR). Sodium concentration significantly decreased in responders (62.8±18 to 48.8±8 mM; $p<0.01$); however, there was an increase (56.5±1.5 to 57.7±7.6) in the TSC for the non-responders. Lesion volume decreased in all groups, for responders (38%: 86±78 to 53±52 mm^3) and nPR (22%: 100±104 to 78±88 mm^3) after the first cycle. In the subset of patients ($n=6$) with PET, the SUV lean-max significantly decreased by 28% (responders) and 22% (nonresponder; $p=0.03$).

Conclusion

We have demonstrated that using multiparametric and multinuclear MR and PET imaging for monitoring PST in patients with stage II III, and IV is feasible. Total sodium concentration and SUV were significantly reduced after the first cycle of PST in responders and predictive of treatment response. Our results suggest that advanced radiological methods can monitor treatment response and may provide new surrogate radiological biomarkers for potential adaptive therapy in breast cancer patients.

Introduction

With early detection and optimal local and adjuvant systemic therapy, breast cancer is a potentially curable disease (1). While several prognostic and predictive factors are currently available to calculate odds of disease free and overall survival, new radiological metrics that help select women who are most likely to benefit from specific therapies are needed.

Since pathologic response following preoperative systemic therapy (PST) correlates with long-term outcome, PST, also referred to as primary or neoadjuvant chemotherapy is increasingly being used as a research platform for new drug investigation. Currently, only approximately 20–30% of patients who receive PST obtain complete clinical or pathological complete response (2). One potential avenue to increase the likelihood of achieving a complete response in patients is early differentiation between patients who respond to therapy from those who will not. Methods of early response determination are critical for optimal "tailoring" of treatments to individual patients.

Noninvasive imaging provides tools that could monitor PST and would be very helpful in determining treatment response are particularly attractive. Indeed, magnetic resonance imaging (MRI) and positron emission tomography/computed tomography (PET/CT) are increasingly being used as single modalities to screen and monitor response to PST. Recent studies have demonstrated the benefit of using MRI in patients with known invasive disease with detection of unknown contralateral cancers (3,4). In addition, several reports have demonstrated the ability of MRI to assist in monitoring response to treatment using dynamic contrast enhancement (DCE) imaging, and/or volumetrics (5–13). PET/CT is not currently used as a breast screening tool, but is utilized for staging and/or detecting metastasis with moderate to high sensitivity and moderate specificity in tumors (14–18). PET tracers using 2-deoxy-2-[18F]-fluoro-D-glucose (^{18}FDG), quantitative measures of glycolic activity in tumors can be measured with the Standardized Uptake Value (SUV) from PET/CT data. The combined use of these multimodality-imaging methods (MR/PET/CT) is novel and an active area of research (6,19,20). The use of advanced MR and PET/CT methods, may allow to non-invasively probing of the physical and metabolic changes in the tumor microenvironment. In this study, we systematically investigated the relationship between the changes in MR parameters and the efficacy of PST intervention in a subset breast cancer patients using multiparametric and multinuclear MR with PET/CT parameters to characterize early evaluation of response to PST within a the first cycle of treatment and correlate these parameters to histological parameters.

Clinical Subjects

Female patients ($n=18$, age range: 18–80) who had stage II, III, or IV breast cancer and were undergoing PST were enrolled in this prospective study. Patients were referred for MR evaluation of breast lesions and to monitor their treatment regimen. The patients were imaged before treatment (baseline), after the first cycle (within 14 days), and at the conclusion of PST therapy. The treating oncologist determined the chemotherapy regimen.

Clinical Response and Histological Tissue Classification

Clinical response in the breast was evaluated, and when appropriate, in the axilla, infraclavicular, supraclavicular regions, and skin. All biopsy procedures and histological tissue analysis were performed or reviewed as part of the patient's routine clinical care using standard of care criteria. Pathologic response of the primary tumor was defined at the time of surgery by a board certified breast pathologist. Immunohistochemistry values were performed to assess the status of

hormonal receptors and Her2-neu on a baseline biopsy and were repeated on the final specimens at the discretion of the pathologist. For analysis, pCR and pPR are grouped as responders and all others as non-responders. The protocol was approved by our Institutional Review Board, and informed consent was obtained from all subjects.

MR imaging protocol

Proton MR imaging: MR imaging was performed on a 1.5 T MR scanner (General Electric Med. Sys.), using a dedicated 4-channel phased array breast coil (Medrad, PA) with the patient in the prone position. MR sequences were: sagittal fat suppressed (FS) T_2WI fast spin echo $(TR/TE = 5700/102)$, and fast spoiled gradient echo (FSPGR) T_1WI $(TR/TE = 200/4.4)$ with a field of view $(FOV) = 18 - 20 \times 18 - 20cm$ (adjusted to the size of the breast), a $matrix = 256 \times 192$, slice thickness=4 mm, and a 1 mm gap. In addition, fat suppressed, three-dimensional FSPGR T_1WI $(TR/TE = 20/4$, $matrix = 512 \times 160$, slice thickness, 2 mm) pre- and post-dynamic contrast-enhanced (DCE) images were obtained after intravenous administration of 0.1 mmol/kg gadolinium contrast agent (Omniscan). The contrast agent was injected over 10 s, with MR imaging beginning immediately after completion of the injection. The contrast bolus was immediately followed by a 20 cc saline flush. Total scan time for the protocol was less than 20 min.

Sodium (23Na) MRI: For quantitative ^{23}Na MRI, subjects were positioned in a custom-made breast ^{23}Na receive surface coil. A projection imaging sequence was used with a TR of 100 ms (>3 times T_1), an ultrashort TE of 0.2 ms, and 400 μs adiabatic excitation pulses. The resolution was 6 mm isotropic (0.2 ml voxel volume), with a 22 cm FOV interpolated to 128×128 points by 64 slices (3.4 mm slice and 1.7×1.7 mm in-slice resolution (12)).

Positron Emission Tomography and Computed Tomography (PET/CT)

A subset of patients (n=6) underwent PET/CT imaging. After the patient fasted for 4 h, an intravenous (IV) access was started and a serum glucose level measured. The patient was injected with the glucose analog ^{18}FDG. The ^{18}FDG dose is calculated based on the weight (kg) of the patient as follows: Dose (mCi)=Weight (kg)× 0.22 (mCi/kg). Maximum dose is 25 mCi with weights greater than 114 kg or 250 lbs. Minimum dose is 5 mCi with weights less than 23 kg or 51 lbs. After the uptake phase, which lasts 45–60 min, the patient is positioned and near whole body images are acquired using a PET/CT unit (General Electric Discovery Light Speed).

MR Image Preprocessing and Analysis

Volume Analysis: MR image analysis was performed using a SUN T2000 server (Sun Microsystems Inc., Mountain View, CA) using the Eigentool image analysis software (Image Analysis Lab, Henry Ford Hospital, Detroit MI (21,22)).

PET: Standardized Uptake Values: Standardized uptake values (SUV) within the tumor region were obtained from areas of increased signal intensity on the PET scans. The SUV is defined as the ratio of tumor ^{18}FDG concentration (mCi/kg) to whole body concentration (injected dose divided by weight of the patient in kg) was used to assess treatment response and defined as;

$$SUV = \frac{Activity(\mu Ci/g)}{[injected\ dose(\mu Ci/g)/weight(kg)]} \quad (3)$$

where activity is obtained from the PET images, the injected dose of ^{18}FDG, and weight (kg) of the patient is used for normalization (23). In general, an SUV unit of one is considered normal, whereas, an SUV unit greater than approximately 2.5 is considered suspicious and needs clinical correlation.

Statistical Analysis

The differences between MR, ^{23}Na concentrations, SUV, and Ki-67 were tested before and after treatment using ANOVA and unpaired t-tests with a Bonferroni correction for multiple testing. Statistical significance was set at $p<0.05$.

Results

Clinical and Histopathologic Characteristics

Eighteen patients (mean, 47, range 38–60) met eligibility criteria and signed a written informed consent. Ten (66%) patients were premenopausal and eight (44%) were postmenopausal and the summary statistics of clinical parameters are shown in Table 1. At baseline, the mean Ki-67 was elevated in responders (36%± 27%) and after the first cycle, there was a 47% decrease in the Ki-67 (range=29%–20%). In the nonresponder, an increase in Ki-67 (14%; range=70%–80%; p=0.06).

Radiological Metrics

Figure 1 demonstrates the ability of DCE-MR to define the extent of disease and monitor tumor response throughout the course of treatment of a pCR patient with a T3N0M0 invasive ductal carcinoma. Figure 2 demonstrates the use of multiparametric and multinuclear imaging on the same patient and demonstrates the potential to obtain different, yet complementary information of the tumor microenvironment during therapeutic intervention. Indeed, changes in the radiological metrics of DCE-MR and ^{23}Na imaging before, during, and after treatment show not only a decrease in lesion volume as measured with DCE-MR, but also a decrease in sodium within the lesion as measured with ^{23}Na MRI, indicating that, by combining these methods, more information was obtained.

^{23}Na Sodium: We evaluated total sodium concentration at baseline, after the first treatment, and just before surgery, which reflects the metabolic and ionic status of the tumor microenvironment. Similarly the total sodium concentration (TSC) in breast tumors decreased in responders (62.8±18 to 48.8±8 mM; $p<0.01$) with an increase (56.5±1.5 to 57.7±7.6) in the TSC for the non-responders after the first cycle. However, there were decreases in the TSC during the final treatment cycles for both groups.

Proton DCE-MR: Mean DCE MR tumor volume decreased between baseline(70 cc) and the first cycle of treatment in both groups of patients, with the largest decrease in the responders (38%: 86±78 to 53±52 mm^3) and nPR (22%: 100±104 to 78±88 mm^3) after the first cycle. The volume decrease continued slightly after the end of treatment. However, there was a large variability in the size of the tumors. Intra and inter-variability volume measurements on a subset of patients demonstrated reproducibility with intra-variability measurements of 5.9±4.8% and inter-variability measurements of 9.1%±5.8 in volume measurements.

PET/CT-SUV: The SUV lean-max significantly decreased after the 1st cycle of treatment by 38% in responders (5.4 to 3.3; p=0.04) and 22% in the nonresponders (14 to 11). In addition, the SUV for all complete responders decreased by 59%. Figure 4 demonstrates the use of multimodality imaging of breast cancer.

Discussion

We provide compelling evidence using multi-modality proton and ^{23}Na MR combined with PET/CT imaging the feasibility of monitoring PST in patients with operable breast cancer in the clinical setting. Significant decreases in total sodium concentration, DCE-MR volumes, and SUV were observed in responders. Moreover, these radiological imaging changes were concurrent with decreases in proliferation index Ki-67 in the responder group with concurrent increases in the Ki-67 in nonresponders; suggesting that these radiological imaging markers of sodium and glycolic metabolism could be indicative of tissue response or lack thereof after treatment. Indeed, by combining multimodality imaging methods important biophysical information can be obtained of the tumor microenvironment beyond standard volumetric data and this information will provide a basis for multimodality radiological procedures to be utilized as surrogate biomarkers for monitoring response or lack of to therapeutic intervention. Specifically, by examining changes in sodium concentration and SUV, the complex cellular interactions that occur within the tumor microenvironment can be investigated before changes are noted using traditional response criteria, such as Response Evaluation Criteria in Solid Tumors (RECIST) and provide a platform for adaptive therapy.

In conclusion, we have demonstrated that multimodality radiological imaging is feasible for identifying and monitoring PST in breast cancer patients and these methods can provide a basis to for a comprehensive evaluation of the complex tumor microenvironment by examining the changes in morphology, sodium concentration, and glucose metabolism in response to therapy. These data serve as proof of principle and suggest the potential utility of combining these technologies to monitor PST and predict response to treatment.

Acknowledgements

We thank Lucie Bower, Dr Donald Peck, and Dr. Hamid Soltanian-Zadeh, Henry Ford Hospital, Detroit, MI for the Eigentool image analysis software used for image processing. This work was supported in part by NIH 1R01CA100184 and P50 CA103175.

References

1. Jemal A, Siegel R, Ward E, et al. Cancer statistics, 2008. CA Cancer J Clin 2008;58(2):71–96.
2. Wolff AC, Berry D, Carey LA, et al. Research issues affecting preoperative systemic therapy for operable breast cancer. J Clin Oncol 2008;26(5):806–813.
3. Lehman CD, Gatsonis C, Kuhl CK, et al. MRI evaluation of the contralateral breast in women with recently diagnosed breast cancer. N Engl J Med 2007;356(13):1295–1303.
4. Smith RA. The evolving role of MRI in the detection and evaluation of breast cancer. N Engl J Med 2007;356(13):1362–1364.
5. Gilles R, Guinebretiere JM, Toussaint C, et al. Locally advanced breast cancer: contrast-enhanced subtraction MR imaging of response to preoperative chemotherapy. Radiology 1994;191(3):633–638.
6. Chen X, Moore MO, Lehman CD, et al. Combined use of MRI and PET to monitor response and assess residual disease for locally advanced breast cancer treated with neoadjuvant chemotherapy. Acad Radiol 2004;11(10):1115–1124.
7. Jacobs MA, Ouwerkerk R, Wolff AC, et al. Multiparametric and multinuclear magnetic resonance imaging of human breast cancer: current applications. Technol Cancer Res Treat 2004;3(6):543–550.
8. Partridge SC, Gibbs JE, Lu Y, et al. MRI measurements of breast tumor volume predict response to neoadjuvant chemotherapy and recurrence-free survival. AJR Am J Roentgenol 2005;184(6):1774–1781.
9. Manton DJ, Chaturvedi A, Hubbard A, et al. Neoadjuvant chemotherapy in breast cancer: early response prediction with quantitative MR imaging and spectroscopy. Br J Cancer 2006;94(3):427–435.
10. Hylton N. MR imaging for assessment of breast cancer response to neoadjuvant chemotherapy. Magn Reson Imaging Clin N Am 2006;14(3):383–389, vii.
11. Yu HJ, Chen JH, Mehta RS, Nalcioglu O, Su MY. MRI measurements of tumor size and pharmacokinetic parameters as early predictors of response in breast cancer patients undergoing neoadjuvant anthracycline chemotherapy. J Magn Reson Imaging 2007;26(3):615–623.
12. Ouwerkerk R, Jacobs MA, Macura KJ, et al. Elevated tissue sodium concentration in malignant breast lesions detected with non-invasive (23)Na MRI. Breast Cancer Res Treat 2007;106(2):151–160.
13. Jacobs MA. Multiparametric Magnetic Resonance Imaging of Breast Cancer. Journal of the American College of Radiology 2009;6(7): 523–526.
14. Wahl RL. Positron Emission Tomography (PET): an update on applications in breast cancer. Breast Dis 1998;10(3–4):165–175.
15. Kumar R, Alavi A. Fluorodeoxyglucose-PET in the management of breast cancer. Radiol Clin North Am 2004;42(6):1113–1122, ix.
16. Kim SJ, Kim SK, Lee ES, Ro J, Kang S. Predictive value of [18F] FDG PET for pathological response of breast cancer to neo-adjuvant chemotherapy. Ann Oncol 2004;15(9):1352–1357.
17. Kelloff G, Hoffman JM, Johnson B, et al. Progress and promise of FDG-PET imaging for cancer patient management and oncologic drug development. 2005;11(8):2785–2808.
18. Tatsumi M, Cohade C, Mourtzikos KA, Fishman EK, Wahl RL. Initial experience with FDG-PET/CT in the evaluation of breast cancer. Eur J Nucl Med Mol Imaging 2006;33(3):254–262.
19. Jacobs MA, Stearns V, Wolff A, Ouwerkerk R, Bluemke DA, Wahl RL. Multimodality (MR/PET/CT) monitoring preoperative systemic therapy in operable breast cancer. Proc Intl Soc Mag Reson Med 2006;14.
20. Moy L, Ponzo F, Noz ME, et al. Improving specificity of breast MRI using prone PET and fused MRI and PET 3D volume datasets. J Nucl Med 2007;48(4):528–537.
21. Peck D, Windham J, Soltanian-Zadeh H, Roebuck J. A fast and accurate algorithm for volume determination in MRI. Med Phys 1992;19(3):599–605.
22. Jacobs MA, Knight RA, Windham JP, et al. Identification of cerebral ischemic lesions in rat using eigenimage filtered magnetic resonance imaging. Brain Research 1999;837(1–2):83–94.
23. Thie JA. Understanding the Standardized Uptake Value, Its Methods, and Implications for Usage. J Nucl Med 2004;45(9):1431–1434.

Table 1. Patient Characteristics and Treatment Response

Enrolled patients	18
Age, years	
Median	49
Range	35–68
Stage	
II	4
III	8
IV	6
Histology	
Ductal	14
Lobular	4
Mixed ductal and lobular	3
Grade	
2	4
3	8
4	6
Estrogen-receptor positive	10
Progesterone-receptor positive	7
Her2-*neu*positive	
IHC (3+)	5
FISH positive	5

Abbreviations: IHC, immunohistochemistry; FISH, fluorescence in situ hybridization.

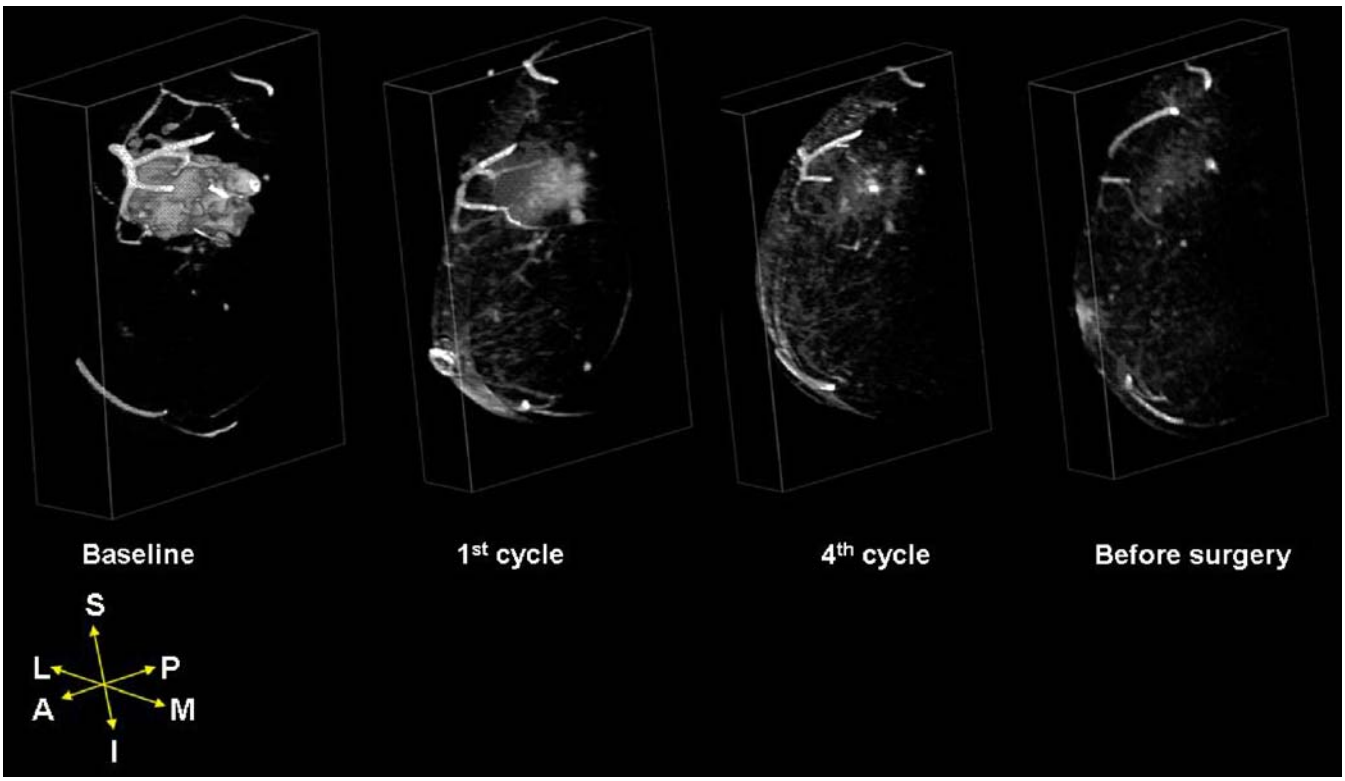

Figure 1. Representative 3D visualization of dynamic contrast-enhanced MR images after therapeutic intervention in a 54 y/o female with T3N0M0 invasive ductal carcinoma of a large operable breast lesion. There was a steady reduction in tumor volume from baseline until surgery.

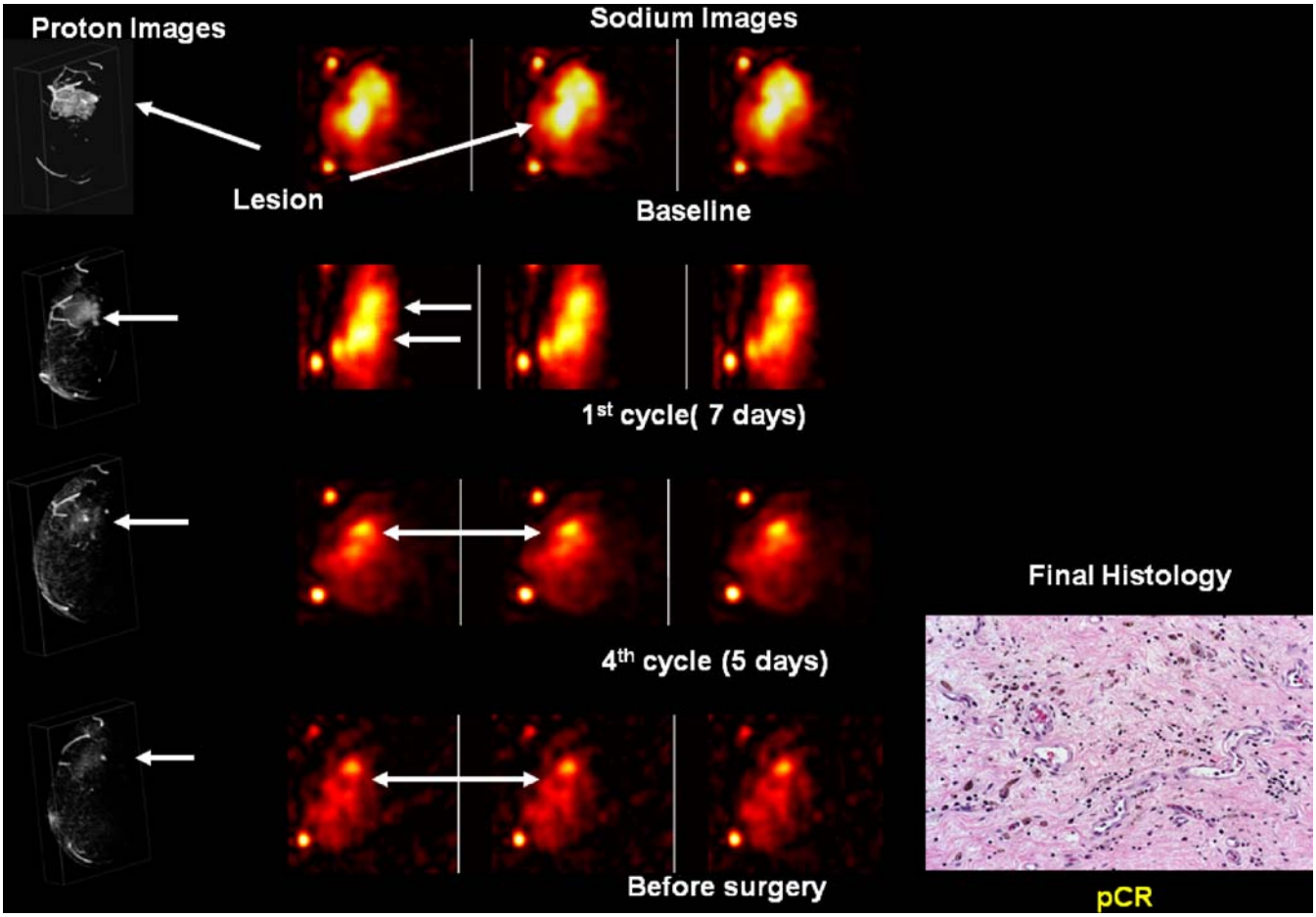

Figure 2: Demonstration of multiparametric and multinuclear MR on a 54 y/o female with T3NoM0 invasive ductal carcinoma receiving Adriamycin and cyclophosphamide followed taxotere chemotherapy. At baseline, there was a large volume of tumor with increased sodium. After treatment, there was a steady reduction in sodium concentration and tumor volumes beginning after the first cycle of treatment. At surgery, she was determined to have a complete pathological response.

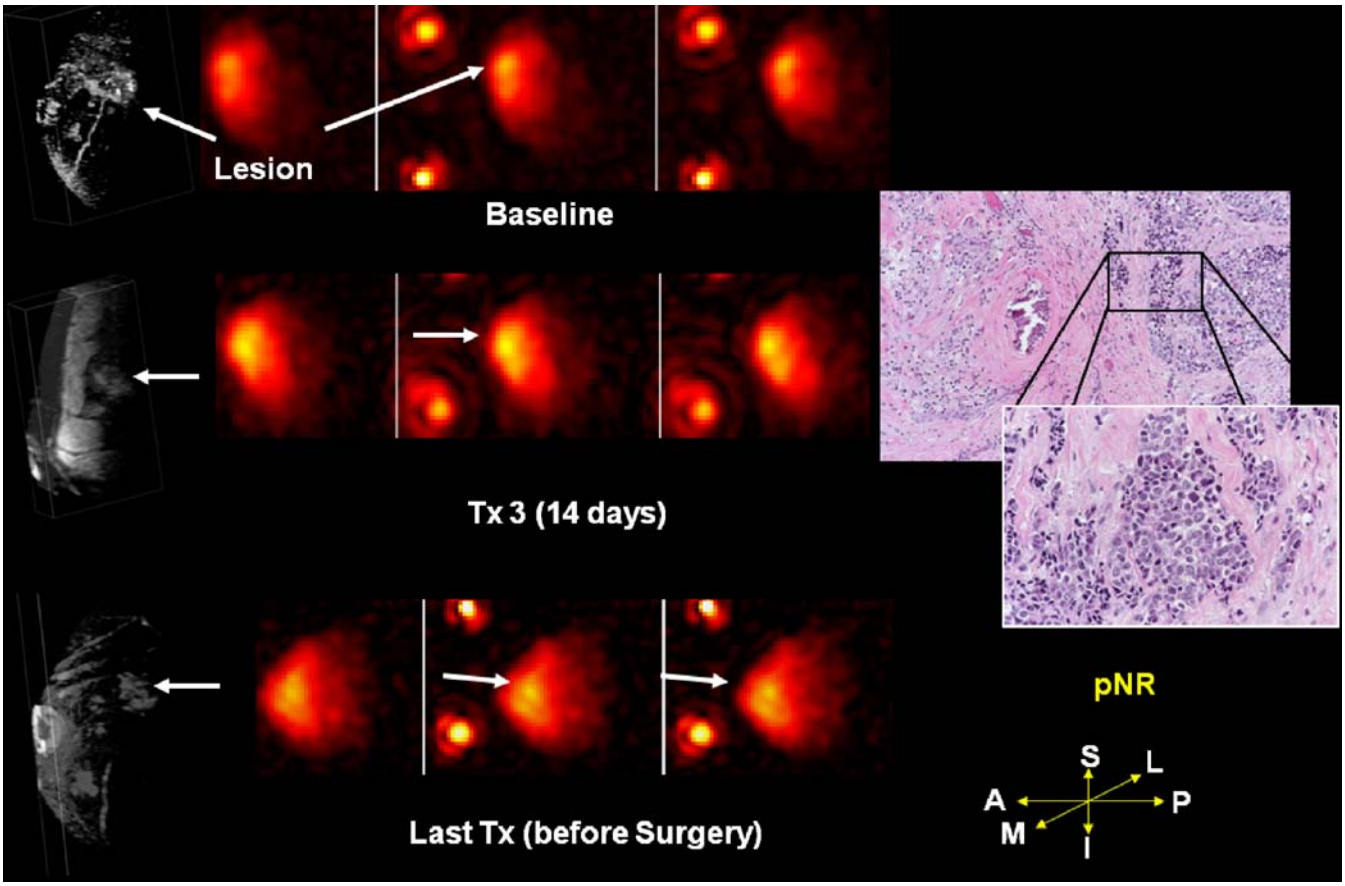

Figure 3. A representative 49 y/o postmenopausal female with cT2N1M0 invasive ductal carcinoma who was receiving preoperative chemotherapy. **Left column**: DCE-MR volumes showed little or no reduction in tumor volume after treatment. **Middle column**: similarity, there was little change in the sodium concentration and this remained constant until surgery. **Right column**: Her final pathological diagnosis was no response (pNR), with residual tumor present.

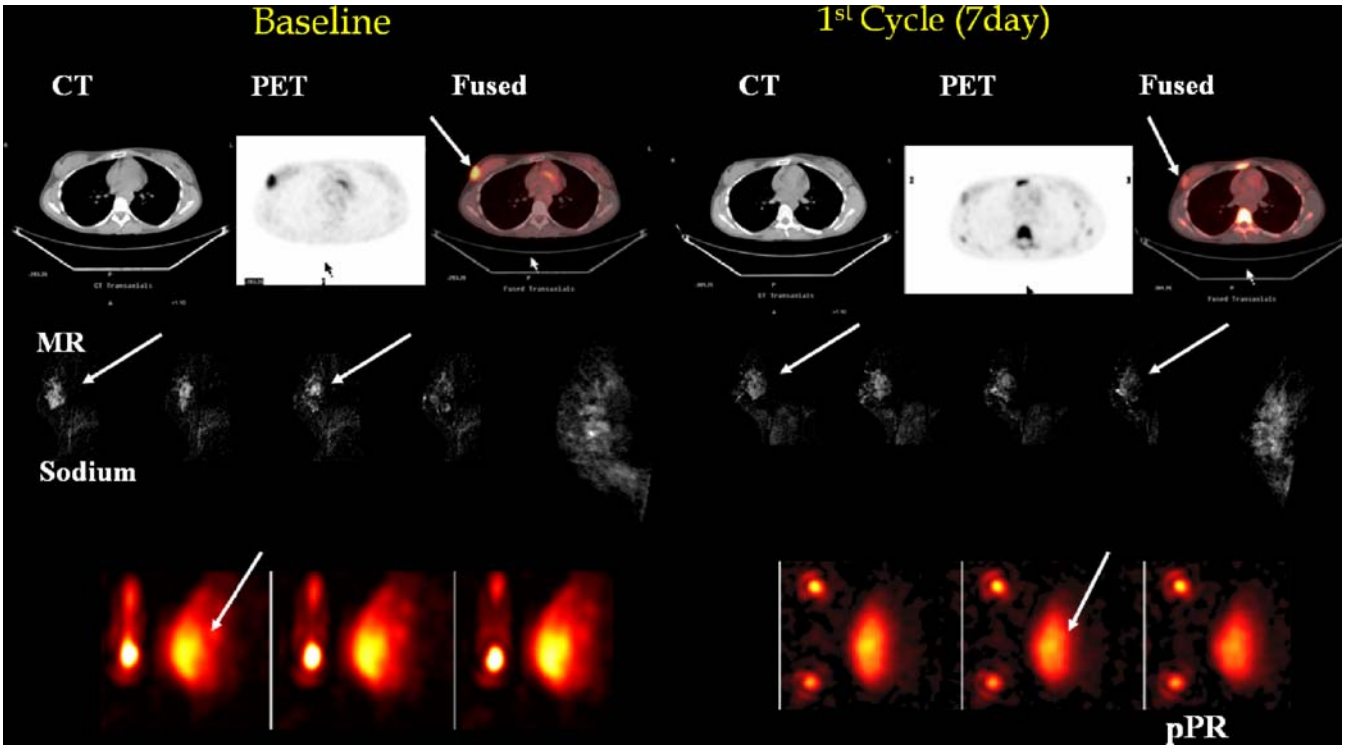

Figure 4. Combined multimodality images on a 35 y/o female. Baseline MR volume was 32 cc, which decreased to 28 cc after the first cycle (C1), and 12 cc before surgery. The sodium concentration within lesion before was 42.8 mMol, and after C1, 41 mMol. Standard Uptake Value significantly decreased from 6.7 to 3.15 after C1 as noted in the PET image.

The Ductal Obstruction Sign (DOS): Helpful in the differential diagnosis between benign and malignant lesions?

C. G.N. Kaiser[1], P.A.T. Baltzer[1], M. Dietzel[1], T. Vag[1], A. B. Herzog[1], M. Gajda[2], W.A. Kaiser[1]
[1]Institute of Diagnostic and Interventional Radiology, [2]Department of Pathology,
Friedrich-Schiller-University, Jena, Germany
Corresponding Authors:
Clemens G. N. Kaiser, Pascal A. T. Baltzer, Institute of Diagnostic and Interventional Radiology, Friedrich-Schiller-University Jena, Erlanger Allee 101, D-07740 Jena, Phone: +49-3641-9324801, Fax: +49-3641-9324802, E-mail: pascal.baltzer@med.uni-jena.de

Purpose

For years MR-Mammography (MRM) has been considered the most sensitive procedure in the detection of breast lesions.

However, low specificity was assumed even though a tremendous variety of morphological and kinetic "signs" before and after the injection of contrast medium is hidden in more than 1,000 pictures of each breast. Multiple "signs" have been described and accepted during the last years—and among these: the "duct obstruction sign", meaning the existence of wide and dilatated ducts in the gland in association with proximally located intraluminal and intraductal lesions.

Observations from clinical routine have allowed an assumptive association of papilloma and dilated ducts. However, the differential diagnostic value of this observation remained unclear.

The aim of this prospective study was to clarify the diagnostic value of the ductal obstruction sign (DOS) in the differential diagnosis of malignant or benign lesions.

Materials and Methods

Between January 2005 and October 2006, a total of 983 patients were examined in the University Hospital of Jena using MR-Mammography. All 316 female patients who underwent surgical procedures for histological clarification in the surgical department of the University of Jena were included in the study. This protocol allowed a histological correlation with MR-diagnostic results.

All patients were examined using the same standard protocols (T1-weighted gradient echo sequences before and in short intervals after the injection of Gadolinium-DTPA, as well as following T2-Turbo-Spin-Echo and STIR (Short Tau Inversion Recovery) sequences. An axial dynamic T1-weighted spoiled gradient echo sequence was used (FLASH, GRAPPA factor 2, repetition time 113 ms, echo time 5 ms, flip angle 80°, matrix 384×384 pixels, FOV 350×350 mm, slice thickness 3 mm). The contrast agent gadopentetate dimeglumine (Gd-DTPA, Magnevist, Schering, Germany) was administered after the first scan as a rapid bolus (3 ml/s), picture analysis was conducted by two MR. Mammography-experienced radiologists in consensus. The definition of ductal obstruction was hereby "wide ducts filled with fluid proximal of an enhancing lesion". Sensitivity, specificity as well as positive and negative likelihood ratio (LR+, LR−) were determined.

Results
Of the 316 patients with histological correlation 60 patients showed a ductal obstruction (19%), among which 20 were found in association with a lesion, which was histologically verified.
90% (18/20) of these 20 lesions associated with a DOS could be determined to be benign lesions; 10% (2/20) as being malignant.
83% (15/18) of the associated 18 benign lesions revealed to be papilloma, 11% (2/18) mastopathic proliferative lesions, as well as one fibroadenoma (5%). The two malignant histologies could be determined as one ductal invasive carcinoma and one ductal carcinoma in situ (DCIS).
Chi square testing ($p<0.001$) proved a highly significant relation. These results have been measured (CI=95% confidence interval): (benign lesions showing a DOS were considered as true positive findings, malignant lesions without a DOS as true negative findings). Sensitivity 15.4% (CI: 10.0%–23.0%), specificity 99.0% (CI: 96.4%–99.7%), LR+ 15.3 (CI: 3.6–64.8), LR− 0.9 (CI: 0.8–0.9) and odds ratio 17.9 (CI: 4.1–78.7)

Discussion
As a result of this study "ductal obstruction" is found to be a very helpful tool in the differentiation of small lesions once a ductal dilatation has been detected: If ductal dilatation is detected, there is a strong likelihood of a benign correlating finding in histopathology (15 times more likely a benign than a malignant lesion!).
The clear association of ductal obstruction with benign lesions, especially papillomas might lead to some hypotheses: In histopathology, papillomas typically show a continuous myoepithelial cell layer, whereas this feature is not typical for carcinoma. Papillary lesions might block intraductal liquid flow like a stone in a watercourse. In contrast, increased levels of proteolytic enzymes are a typical finding in cancer growth and progression, degrading the extracellular matrix leading to a higher permeability like a sponge.
Since ductal obstruction findings could only be discovered in 6,3% of all cases, it shows though, that DOS as a diagnostic sign can only be used as an additive parameter, that will not replace the evaluation of other kinetic or morphologic signs in the finding of a diagnosis. It should however, be definitely included in the ACR BIRADS lexicon in order to improve lesion differentiation.

High-resolution CT of the breast: A proposal?

Willi A. Kalender
Institute for Medical Physics (IMP), Henkestr. 91, 91052 Erlangen, Germany, E-Mail: willi.kalender@imp.uni-erlangen.de

Full field digital mammography (FFDM) [1–3] is based on X-ray measurements. It represents today's standard and the most widely applied imaging modality for the early detection of breast cancer. However, severe limitations with respect to its sensitivity and specificity are to be acknowledged. In consequence, many alternative approaches are under investigation at present with magnetic resonance imaging (MRI) as one of the promising candidates [4; 5]. Surprising to many, but for a number of good reasons, X-ray computed tomography (CT) has also been proposed and is presently under investigation and development as an alternative method.

Demands on breast imaging
What are the general demands? There is a general consensus that 2D projection imaging has limitations; this especially is the case for FFDM when dense breasts are to be examined. The superpositioning of structures can obscure the details of interest to a degree that a diagnostic finding is missed. Therefore, full 3D capabilities are an essential demand. Traditionally the detection and diagnosis of microcalcification clusters is one of the most important tasks; high spatial resolution on the order of 100 µm in all three dimensions appears necessary for this. Soft tissue structures shall be discerned just the same nevertheless which implies moderate demands regarding low-contrast resolution. In addition, specific information about lesion characteristics is desired; the recording of contrast medium kinetics, that is dynamic imaging capabilities, are of considerable interest as has been shown in several studies [6; 7]. Also, any modality under consideration should support intervention and therapy efforts. Patient comfort and safety are a further demand which cannot be neglected. Safety relates both to the radiation dose delivered when X-rays are involved and to the contrast medium dose being applied. Comfort mostly relates to the examination time, patient positioning and to the question if the breast is compressed or not. Also, it is of importance to image the full breast including all regions close to the chest wall and close to the axilla. These demands are briefly summarized in table 1. It is the purpose of this proposal to show that a dedicated breast CT scanner may fulfill all these demands.

Prior art
Efforts at building a dedicated CT scanner for the breast date back to the 1970s. A so-called CT mammography (CTM) scanner was promoted at the time [8; 9]. The woman was lying prone on the table with one breast at a time hanging through a hole in the table. Spatial resolution was considered inadequate for the mammographic task, and the concept was discontinued. Renewed efforts started in the early 2000s in the United States [10–13]. Standard components were mostly used for the respective prototype setups. Several limitations resulted from this. E.g., with X-ray tubes and detectors as commonly used in angiography or flat-detector CT with effective pixel sizes of 150 to 400 µm, insufficient spatial resolution was obtained. Nevertheless some of these scanners provide dynamic CT capabilities, i.e. the possibility for differentiating lesions which are enhancing either fast (malignant) or slow (benign).
This feature was also shown for standard clinical CT imaging of complete thorax cross-sections with the patient lying prone. Perrone et al. reported [7] remarkably good results for the differential diagnosis of benign and malignant lesions (figure 1). While efforts regarding dynamic CT are being continued, there is a general consensus that dedicated breast CT up to now does not allow adequate diagnosis of microcalcifications to the same degree that mammography offers [14].

Proposed concept
A new effort was started by W. Kalender in 2007 [15]. The European Union project aims at designing a dedicated breast CT scanner which is capable of achieving all goals stated in table 1; a sketch of the principal setup is shown in figure 2. Essential parts of the necessary basic measurements and simulation studies have been completed; the results confirm that the stated goals can be achieved. However, the concept necessitates the development of new technological solutions for most scanner components. For example, as an X-ray source, a tube with focus size down to 100 µm is required with the focus spot very close to one end of the tube to allow having the focus directly under the table and thereby to include the region near to the chest wall. As a detector, a highly efficient design with detector pixel sizes of 100 µm or less is required to achieve the desired high spatial resolution. Also, the number of readings per second has to be increased to allow for a high number of projections being measured during a 360° rotation in very short time. The geometry should be

similar to the typical biopsy tables which are in use today, i.e. the scanner should be small and neither require much space nor intimidate the patient.

Preliminary proof of evidence for the expected imaging performance of a respective scanner was obtained in first practical test measurements on an experimental micro CT scanner using the parameters as outlined above, in this case a focal spot size of 10 µm and a detector pixel size of 100 µm. Spatial resolution in this case was about 50 µm. Measurement results for a surgical resection specimen are shown in figure 3 to indicate the potential. Microcalcifications in a great range of sizes are displayed with high clarity; to indicate the 3D nature of the findings, three views of the volume from different perspectives are shown side by side.

Patient dose considerations

It is considered essential that patient dose associated with the projected CT scanner does not exceed the levels necessary and accepted for FFDM. Therefore, the situation was assessed in detail from the very start. In a manner similar to the assessment of image quality, the approach was based both on calculations [16] and on measurements. Average glandular dose values in the range of 2 to 5 mGy appear feasible [17; 18] which amount to the values typically found in FFDM. It is important to note that dose for dynamic scans will be significantly lower than for high-resolution scans so that the total dose of a complete examination including high-resolution microcalcification and low-resolution dynamic or functional scanning will not exceed the above estimates significantly. Accordingly, the effective or whole body-equivalent dose will be around 1 mSv or less. These values may be compared to the typical natural background radiation level of 3 mSv per year with its range given at 1 to 10 mSv.

Conclusions

Based on simulations, on preliminary experiments and on general experience with high-resolution flat-detector micro-CT it appears feasible to build a dedicated CT scanner of the breast fulfilling all the demands given in table 1. In particular, this includes the demand that dose has to be limited to the levels known for mammography. Necessary developments of respective new technological components, of algorithms and software will take time, but we expect that practical solutions for clinical testing will be available in about two years.

Acknowledgement

The author acknowledges support from the European Union Framework Programme 7 [15] for the basic studies on breast CT reported here. Special thanks go to Prof. Matthias Beckmann and his team from the Department of Gynecology of the University of Erlangen for very helpful discussions and for providing the specimen shown in fig. 3.

References

[1] Pisano ED, Yaffe MJ. Digital mammography. Radiology 2005; 234: 353–362

[2] Fischer U, Hermann K, Baum F. Digital mammography: current state and future aspects. Eur Radiol 2006; 16: 38–44

[3] Schulz-Wendtland R, Hermann K-P, Wacker T, Bautz W. Aktueller Stand und weitere Perspektiven der digitalen Mammographie. Der Radiologe 2008; 48: 324–334

[4] Kuhl CK, Schrading S, Bieling HB et al. MRI for diagnosis of pure ductal carcinoma in situ: a prospective observational study. The Lancet 2007; 370: 485–492

[5] Hall FM. The rise and impending decline of screening mammography. Radiology 2008; 247(3): 597–601

[6] Kuhl CK, Schild HH. Dynamic image interpretation of MRI of the breast. J of Magnetic Res Imaging 2000; 12: 965–974

[7] Perrone A, Lo Mele L, Sassi S et al. MDCT of the breast. Am. J. Roentgenol. 2008; 190(6): 1644–1651

[8] Chang C, Sibala J, Fritz S, Gallagher J, Dwyer S, Templeton A. Computed tomography evaluation of the breast. Am J Roentgenol 1978; 131: 459–464

[9] Gisvold JJ, Reese DF, Karsell PR. Computed tomographic mammography (CTM). Am J Roentgenol 1979; 133(6): 1143–1149

[10] Chen B, Ning R. Cone-beam volume CT breast imaging: feasibility study. Med Phys 2002; 29(5): 755–770

[11] Shaw CC, Chen L, Altunbas MC et al. Cone beam breast CT with a flat panel detector-simulation, implementation and demonstration. Engineering in Medicine and Biology Society, 27th Annual International Conference 2005. IEEE-EMBS 2005: 4461–4464

[12] Boone JM, Lindfors KK. Breast CT: potential for breast cancer screening and diagnosis. Future Oncology 2006; 2(3): 351–356

[13] Glick SJ. Breast CT. Annu. Rev. Biomed. Eng. 2007; 9(1): 501–526

[14] Lindfors KK, Boone JM, Nelson TR, Yang K, Kwan ALC, Miller DF. Dedicated breast CT: Initial clinical experience. Radiology 2008; 246(3): 725–733

[15] Kalender WA (Principal Investigator). Dedicated CT of the female breast: Feasibility, optimisation and comparison to competing imaging modalities. Project in the 7th Framework Research Project of the European Commission: Enhanced safety and efficacy in the medical uses of radiation (2008–2010); FP7-213153

[16] Deak P, van Straten M, Shrimpton PC, Zankl M, Kalender WA. Validation of a Monte Carlo tool for patient-specific dose simulations in multi-slice computed tomography. Eur Radiol 2008; 18: 759–772

[17] Vollmar S, Kalender WA. Dedicated breast CT at the same exposure level as two-view mammography: Influence of detector pixel size and focal spot size on image quality. Eur Radiol 2008; 18 (2) Suppl. 1: 208

[18] Vollmar S, Weigel M, Kalender WA. Dose distribution and image quality in CT of the breast as a function of projection angle range. In: Radiological Society of North America scientific assembly and annual meeting program. Oak Brook, III: Radiological Society of North America 2008: 544

Figure captions

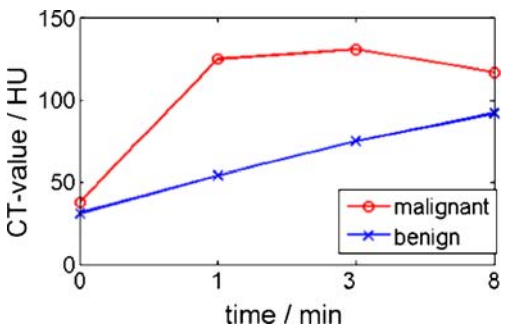

Figure 1: Dynamic clinical CT allows for differential diagnosis of benign and malignant lesions (Data reproduced from [7].). However, in that case spatial resolution and patient dose values are of the same order as in standard thoracic CT.

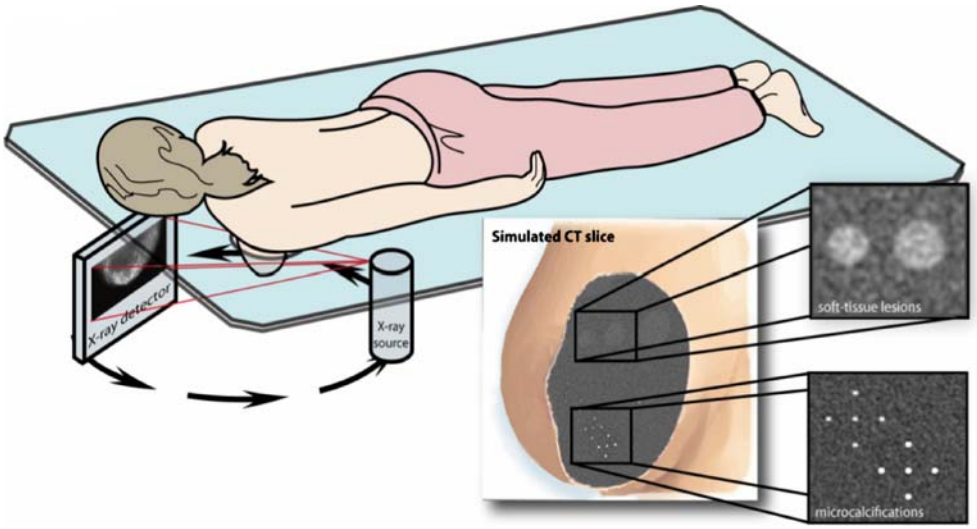

Figure 2: In dedicated breast CT, the patient will be scanned in prone position with only one breast exposed at a time with low X-ray dose. Calculations and preliminary measurements indicate that we will be able to display microcalcifications as well as or even better than in standard mammography. Soft-tissue lesions which in mammography are often obscured by overlaying tissue will be displayed clearly without an increase in dose at decreased spatial resolution. Note: The two separate inserted displays of soft tissue lesions and of microcalcifications are derived from the same, single measurement by different processing.

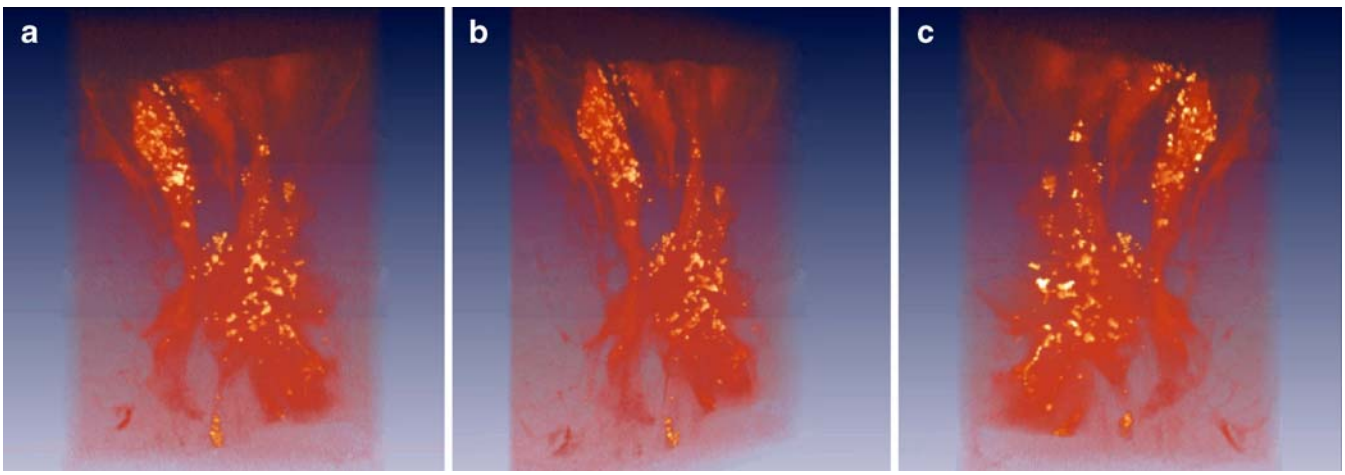

Figure 3: Experimental micro-CT allows modeling the imaging task. Scans of a breast surgical specimen at about 50 μm isotropic spatial resolution display the 3D microcalcification clusters in a quality not available in clinical imaging so far. Fig. 3a–c display three different perspectives to indicate the 3D nature of the data.

Tables

Table 1: General requirements for breast imaging

Full 3D capability
High isotropic spatial resolution of about 100 μm
Dynamic imaging capabilities (sub-minute temporal resolution)
Soft-tissue differentiation
Support of intervention and therapy efforts
Low dose of X-rays and contrast medium to the patient
Patient comfort, no breast compression

3DPR-SSFP of the Breast—Submillimeter T2-like Contrast

Frederick Kelcz, PhD, MD
Department of Radiology, University of Wisconsin, Madison, USA 53792-3252

Acknowledgements
The work presented here is the accumulated efforts of a joint collaboration between the Depts. of Radiology and Medical Physics involving the following individuals:
Catherine J. Moran, Youngkyoo Jung and Walter F. Block,

Introduction
T2 imaging has garnered little attention in the Breast MRI literature. Kuhl (1) has published one of the few publications directly addressing how T2 imaging characteristics aid radiologists in differential diagnosis of rapidly enhancing lesions. In our own practice, we have noticed that very high T2 signal is frequently a property of benign lymph nodes. These structures, even when completely normal may exhibit a type III enhancement profile (rapid contrast washin and delayed washout), typical of malignancy. Morphology of lymph nodes is distinctive—a fatty hilus and vessels entering this hilus provide confident diagnosis in the face of a worrisome enhancement profile. However, for smaller lymph nodes, especially if intramammary, confirming the morphology of a lymph node can be challenging and may lead to follow-up MRI or even MR-guided biopsy. The mismatch between the typical slice thickness used for state of the art 3D T1-weighted imaging of the breast (~2–3 mm) and the slice thickness required for good quality, yet not too lengthy T2 imaging (3–4 mm) further makes it difficult to correlate imaging findings for small lesions (4). Fibroadenomas also pose a potential problem in MR interpretation. Detection of non-enhancing internal septation and very high "cyst-like" T2 signal intensity (SI), help to determine diagnosis and avoid the need for biopsy, but again, the limited resolution of current MRI techniques may not be able to reliably depict internal septations or distinguish lesion border micro from macrolobulation.
Aside from the slice thickness limitations noted above, another current limitation of standard FSE T2 imaging is the fact that with a typical imaging time of 4 min per breast, few sites are obtaining both fat suppressed and non-fat suppressed T2 imaging. This despite the fact that Kuhl (1) did indicate that non-fat saturated T2 imaging may result in improved benign/malignant discrimination.

Physical Principles of 3DPR-SSFP
With the development of high performance gradient systems, steady State Free Precession (SSFP) imaging has emerged as an alternative contrast mechanism. The impetus for SSFP is speed of imaging and the fact that it provides T2-like contrast. Strong fat signals are always an issue with bSSFP, leading to the development of Linear Combination SSFP (LC-SSFP) (2) which provides fat/water separation. Finally 3D Radial trajectory was combined with LC-SSFP (3) which offered an optimized out and back k-space trajectory with imaging during the rewinder and prewinder phases. This method (3DPR-SSFP) offers high isotropic resolution within the timing constraints of LC-SSFP.

MR Protocol
LC-SSFP is a dual acquisition (pass) fat–water separation method. In 3DPR-SSFP, the same set of radial lines is acquired during the first and second pass with each pass lasting 2.5 min. During the first pass, π phase cycling is used while constant phase cycling is performed in the second pass. This phase cycling combined with a TR of close to 2.4 ms at 1.5 T and a center frequency halfway between water and fat allows for suppression of either the fat or water signal during reconstruction. Exams were performed on either a GE Echospeed 1.5 T scanner (General Electric Health Care, Waukesha, WI) or on a GE Twinspeed 1.5 T scanner. A GE 8-channel HD Breast coil was used in all but two cases in which a 4-channel breast coil (MRI Devices Corp., Waukesha, WI) was used to accommodate patient size. All 3DPR-SSFP and FSE acquisitions were preformed unilaterally and identical shimming was performed for the two acquisitions. For the 3DPR-SSFP exams, a 20 cm diameter spherical field of view and matrix size of 320×320×320 was chosen to match the 0.63 mm x 0.63 mm in-plane resolution of the FSE datasets at our institution. The resultant isotropic resolution of 3DPR-SSFP was 0.63 mm in all directions. TRs were 2.7–2.9 ms and flip angle was 30°. In a total scan time of 5 min, approximately 106,000 TRs were acquired, each comprised of two radial lines.
The FSE datasets were acquired following the clinical protocol at our institution as part of a pilot study (5) using the following imaging parameters: 4 mm slice thickness, 256×256 in-plane matrix (0.63×0.63 mm resolution), 16 cm–22 cm FOV, TR/TE of 5000 ms/128 ms, and total scan time of 4 minutes. The average echo train length was 14 and average number of slices was 28. Fat suppression in the FSE acquisition used standard chemical presaturation.

Looking at the 3DPR-SSFP imaging
The immediate impression, upon looking at a 3D Radial SSFP data set is that of very high spatial resolution regardless of the plane of imaging (Figure 1):

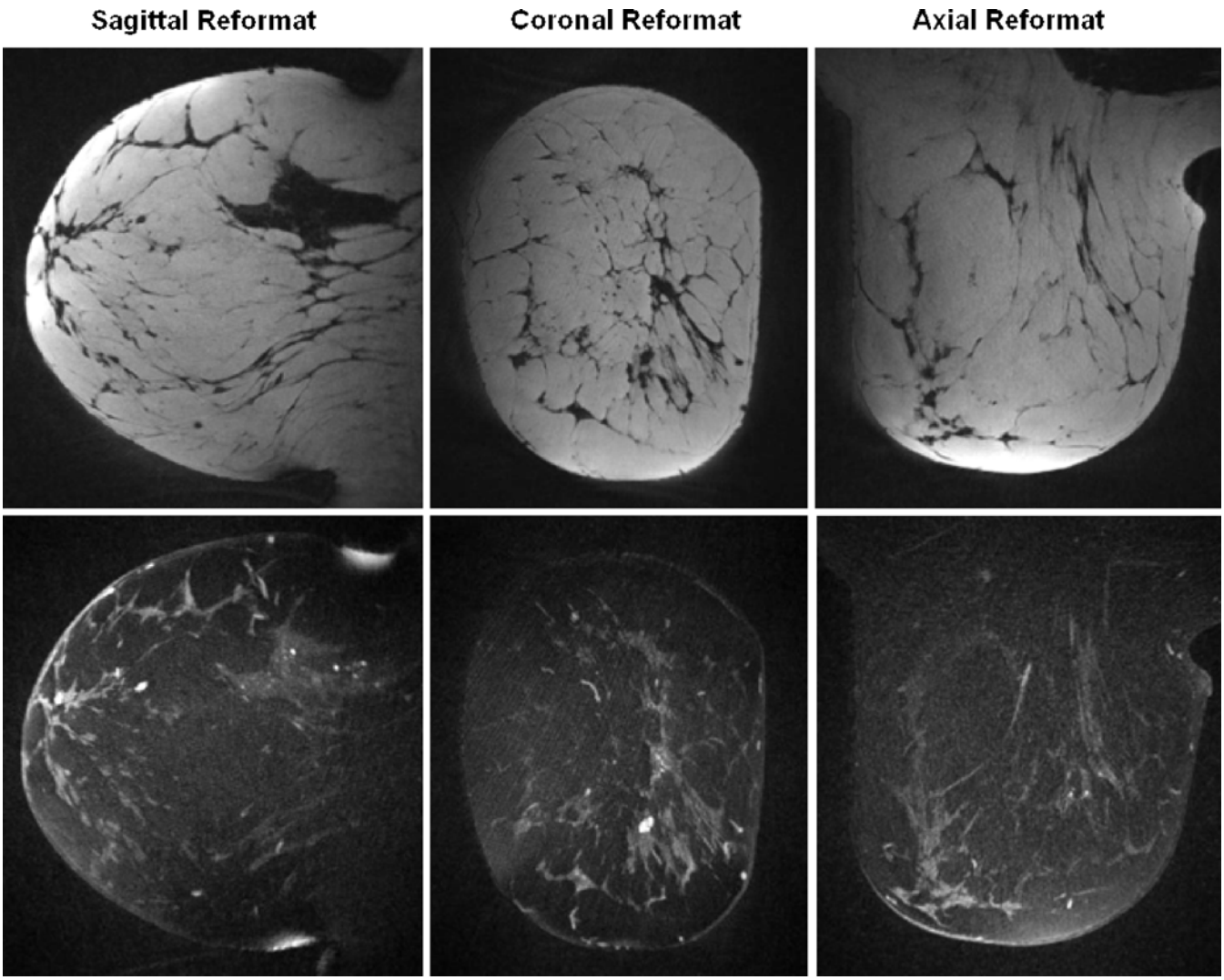

Figure 1: 3D Radial SSFP image of a normal breast displaying isotropic submillimeter resolution (pixels are 0.625 mm in each dimension) and production of fat suppressed and non-fat suppressed imaging in one 5 minute acquisition. At the time of acquisition of these images, 3D Radial SSFP was limited to single breast imaging.

"T2-like" imaging: It must be noted that the radiologist will require reorientation in that 3D Radial SSFP images do not display pure T2 weighting, but rather a weighting that depends on the ratio of T2 to T1. Thus the radiologist must be constantly on the lookout for artifactually elevation of lesion SI due to other reasons than long T2 relaxation, such as: (a) post Gd-enhanced views of an enhancing lesion, (b) pre-contrast short T1 lesions such as post bx hematoma, or proteinaceous cysts. Obviously, 3DPR SSFP imaging should be performed *prior to gadolinium contrast injection*. An example of a possible difficulty in interpretation is shown in Figure 2.

Figure 2: (a) Small focal non-enhancing lesion in the sub-aureolar region displays low central SI on conventional T2-FSE imaging with fat saturation. (b) Pre-Gd enhanced T1 weighted fat suppressed image shows a high SI lesion at this location. Taken together, a confident diagnosis of proteinaceous cyst can be made. (c) 3D Radial SSFP image show high SI lesion compared to low SI lesion seen on conventional T2-FSE imaging due to combined T1 and T2 contrast. Radiologists will have to learn new ways of looking at SSFP T2-like imaging and carefully avoid post contrast radial SSFP imaging.

High Resolution Imaging of Small Cysts: It is not unusual for benign cysts in the breast to display wall enhancement after intravenous contrast injection. However, when these cysts are very small and adjacent to each other, the individual cystic components may not be perceived and only a focus of enhancement corresponding to the unresolved cyst walls is noted. This nonspecific enhancement may result in the recommendation for follow-up MRI or even biopsy. With high resolution 3D SSFP, individual cysts are clearly resolved, resulting in increased specificity (see Figure 3)

Unexpected Benefit—visualization of fine detail on water suppressed imaging: Although fat suppression is routinely used with T2 imaging to enhance the ability of the reader to detect high T2 tissues/fluids within the fatty breast, we observed an unexpected benefit from the "free" water suppressed 3D Radial SSFP images. We found that detection of certain aspects of morphology, such as spiculation, was better seen against the white fat than on post Gd-enhanced 3D SPGR imaging. This is shown in Figure 4.

Improved correlation of lymph nodes between T2 and Gd-enhanced T1 imaging: As noted in the introduction, lymph nodes may be problematic as they normal show enhancement profiles typical of malignancy. Determination of anatomic detail is key in avoiding false positive diagnosis of a benign lymph node as a small cancer. In Figure 5, we show a comparison between an enhancing mass suggesting lymph node and comparative standard T2-FSE imaging with fat saturation and 3D SSFP T2 like imaging. The superior isotropic resolution of the latter makes the diagnosis of lymph certain.

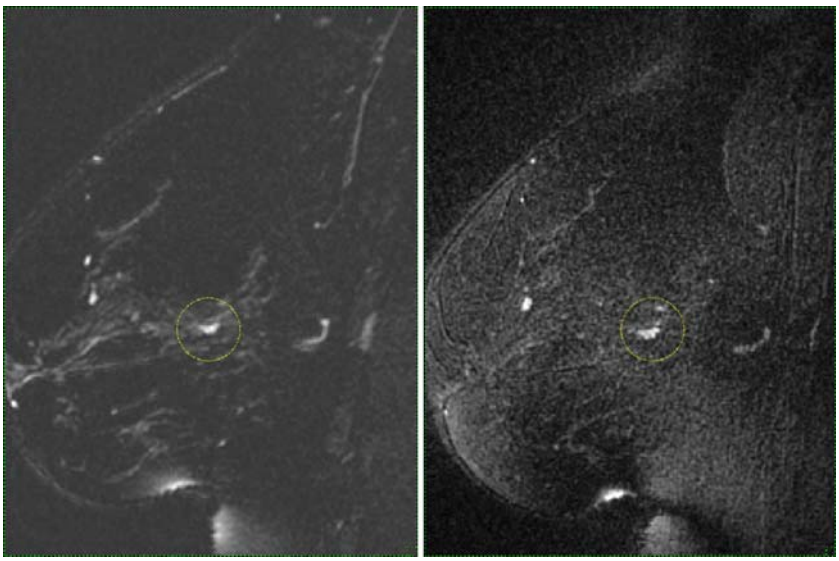

Figure 3: Patient with central cluster of tiny cysts. (a) The T2 FSE with fat saturation image doe not individually resolve the cysts, which, as explained in the text could lead to misdiagnosis of normal, but unresolved cyst wall enhancement, as an enhancing mass. (b), Image from 3D SSFP T2-like sequence definitely resolves individual cyst components, confirming the benign nature of this finding. The decreased SNR on the 3D scan is due to a voxel volume 1/5 that of the FSE exam due to thinner slices. Averaging in the slice dimension can be used, if necessary, to increase apparent SNR.

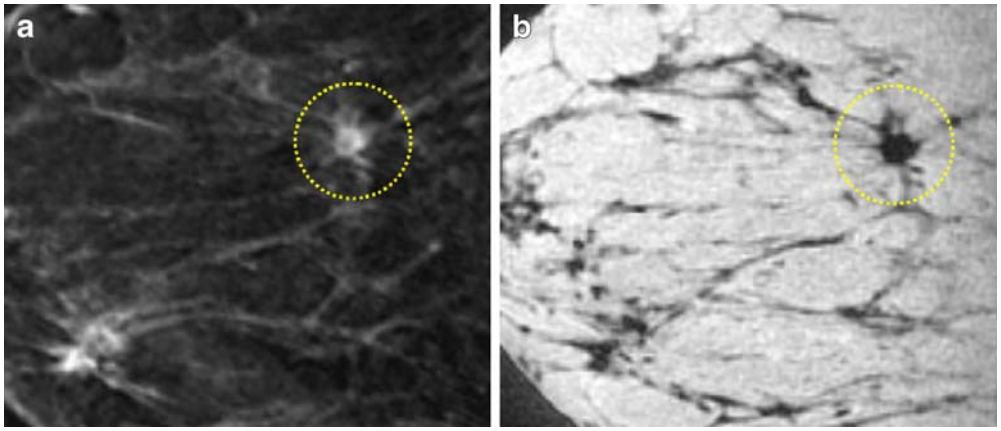

Figure 4: Patient with multifocal cancer demonstrates the value of simultaneous fat and water imaging. (a) This small spiculated enhancing lesion is relatively well seen on the post gadolinium 3D FSPGR imaging. (b) Spicules associate with the lesion are depicted with greater conspicuity on the 3D SSFP fat-separated imaging volume than on the contrast-enhanced image due to the greater contrast difference (black spicules on white fat) and higher resolution (0.625 mm pixels isotropic vs. 0.625 mm in plane×3 mm through plane) associated with this new imaging method.

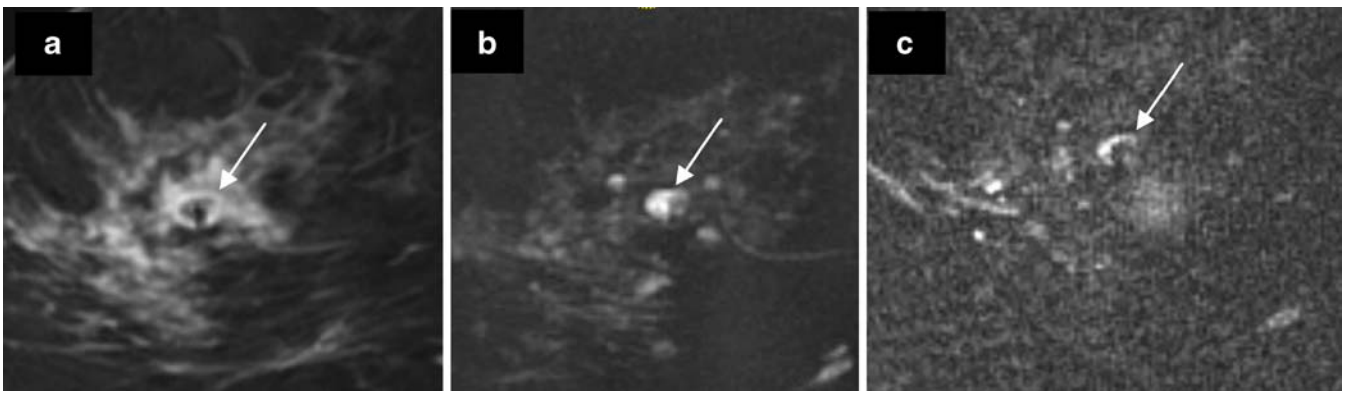

Figure 5: Patient with normal lymph node. (a) 3D FSPGR image shows oval area of enhancement with interrupted border suggesting hilum. (b) T2-FSE with fat saturation show small high SI focus likely corresponding to (a), but not obviously a lymph node. (c) 3D SSFP T2-like image with fat saturation shows obvious "C" shape type of lymph node and a small portion of the entering hilar vessel, thus permitting more definitive assignment of result in (a) to a benign category.

References

1. Kuhl CK, Klaschik S, Mielcarek P, Gieseke J, Wardelmann E, Schild HH. Do T2-weighted pulse sequences help with the differential diagnosis of enhancing lesions in dynamic breast MRI? J Magn Reson Imaging 1999;9(2):187–196.

2. Vasanawala SS, Pauly JM, Nishimura DG. Linear combination steady-state free precession MRI. Magn Reson Med 2000;43:82–90

3. Lu A, Brodsky E, Grist TM, Block WF. Rapid fat-suppressed isotropic steady-state free precession imaging using true 3D multiple-half-echo projection reconstruction. Magn Reson Med 2005;53 (3):692–699.

4. Klifa CS, Shimakawa A, Siraj Z, Gibbs JE, Wilmes LJ, Partridge SC, Proctor E, Hylton NM. Characterization of breast lesions using 3D FIESTA and contrast-enhanced magnetic resonance imaging. J Magn Reson Imaging 2007;25(1):82–88.

5. Moran CJ, Kelcz F, Jung Y, Brodsky EK, Fain SB, Block WF. J Magn. Reson. Imaging 2009;30:134–144.[Epub head of print]

Diffusion Weighted Imaging of the Breast—Promises and Problems

Frederick Kelcz, PhD, MD
Department of Radiology, University of Wisconsin, Madison, USA 53792-3252

Introduction

The radiologist interpreting breast MRI is often faced with a multitude of enhancing breast lesions and must come to a conclusion as to their potential to represent malignancy. With the sensitivity of breast MRI, in most studies, well into the low to upper 90th percentile, missing an invasive cancer is very unlikely. However, as has often been stated, the specificity of breast MRI is significantly lower than the sensitivity and, in current practice, is likely in the 70–80% range. Problematic benign lesions include hormonally stimulated normal fibroglandular tissue, fibroadenoma and papilloma. Factors such as lesion morphology and the post gadolinium intensity curve (TIC) enter into the assignment of BI-RADS diagnostic category. For example, a mass displaying morphological signs of macrolobular border, nonenhancing septations and high, virtually "cyst-like" T2 signal intensity (SI) is likely a fibroadenoma. Moreover, if this mass lesion displays a Type I (persistent) TIC, this would further confirm benignity. However, in our experience some fibroadenomas may display borderline morphological characteristics, be only mildly T2 intense and even display Type II (plateau) or Type III (washout) TIC's, which are, respectively, indeterminate or suggestive of malignancy. We have similarly observed that in some younger patients regions of hormonally stimulated normal glandular tissue may display Type II and Type III curves as well. If focal, such a finding could also result in a false positive result.

Diffusion Weighted Imaging (DWI)

DWI has been in use in other parts of the body, in particular, in neurological imaging for some time and has only recently been applied to breast imaging (1–6). DWI measures the mobility of water molecules within a matrix of tissue, thus indirectly providing information regarding that tissue. If the tissue is made up of tightly packed to cells (as is a cancer), water diffusion is decreased. In benign processes, water diffusion is less restricted.

Diffusion images are produced by imposing strong gradients (with strength measure by the "b-value" [sec/mm^2]) before and after the 180 degree rephasing pulse during an echoplanar imaging (EPI) sequence. These pulses will counteract each other so that water molecules that do not move will retain their full signal intensity after both pulses, while water molecules that diffuse away from their original position will lose signal. The loss of signal will be proportional to the diffusion. Diffusion images are produced in pairs with b-values typically being 0 and 1,000 s/mm^2 for breast applications. The loss of signal between the b=0 and b=1,000 images can be expressed as an Apparent Diffusion Coefficient (ADC). The formula for calculating ADC value is:

$$ADC = (1/b) \times ln(S_o/S_d);\ where\ b = diffusion\ pulse,$$

$$S_o = SI\ with\ b = 0,\ and\ S_d = SI\ with\ b = 1000$$

Although we have used dedicated software (Functool© GE Healthcare, Waukesha, WI, USA) to calculate ADC values and to generate images called ADC maps, the radiologist without access to software can calculate ADC of specific lesions using a simple scientific calculator, measuring SI of the lesion in question, from the PACS station and entering values into the formula above. As an example, the ROI of a mass in the b=0 image might be 750 arbitrary units and in the b=1,000 image, 150 units. The formula above would indicate: $ADC = 1/1000 \times \ln(750/150) = 1.61 \times 10^{-3}\text{mm}^2/\text{sec}$. This would be a value typically associated with a fibroadenoma.

The ADC map is typically quite noisy and is viewed in conjunction with the diffusion and contrast-enhanced images. Diffusion imaging is very rapid, typically requiring less than 1 min per breast, and so, can be incorporated into a busy clinical practice with little table time burden.

MR Protocol

We perform DWI at 1.5 T (GE Healthcare, Waukesha, WI, USA) in the sagittal plane to conform to the existing breast MRI protocol. Technical factors: TR=3,000 ms/TE: min=79.3 ms; FOV=24×24 cm; Slice=5 mm, skip 1 mm; Matrix=128×128; Nex=2; b values=0, 1,000 s/mm^2. All three diffusion directions are averaged. Images are viewed on a commercial workstation with dedicated software (Functool©, GE Healthcare, Waukesha, WI, USA).

Looking at the Diffusion Images

Diffusion images are quite noisy compared to routine spin echo and gradient echo imaging, and are often associated with artifacts as will be discussed below. The diffusion images should be viewed as an image pair, observing what happens to the SI of lesions between the b=0 and b=1,000 images, and correlating this change to the ADC value. From work we presented at the ARRS in 2008 (7), we established an ADC value of $<1.2\times10^{-3}$ mm^2/s as being worrisome for malignancy. In that small retrospective study, the mean ADC of breast cancer was 0.98×10^{-3} mm^2/s; that of fibroadenomas was 1.72×10^{-3} mm^2/s and that of benign other lesions was 1.53×10^{-3} mm^2/s. We found that DWI was most useful a in confirming that lesions thought to be fibroadenomas, but somewhat atypical in appearance or enhancement, were indeed fibroadenomas. Figure 1 below shows the post Gd-enhanced images and ADC maps for a fibroadenoma and an invasive ductal cancer.

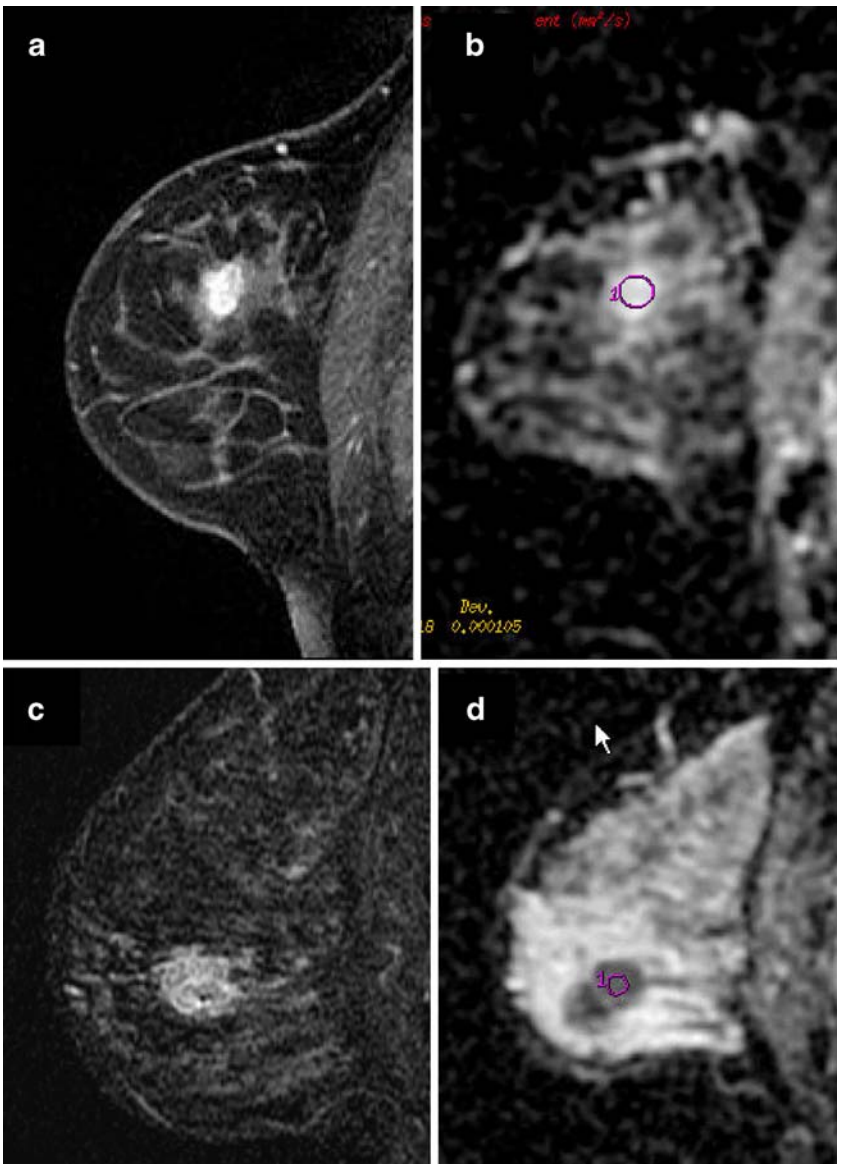

Figure 1: (a) Enhancing fibroadenoma in post-Gd image. (b) ADC map with ROI in place. The average ADC value was 2.07×10^{-3} mm^2/s, well above the threshold of 1.2×10^{-3} mm^2/s, below which we worry about malignancy. (c) Heterogeneously enhancing invasive ductal cancer. Note biopsy marking clip (tiny black focus) within the central inferior portion of the lesion. (d) ADC map with ROI in place. ADC was 0.91×10^{-3} mm^2/s, highly suggestive of malignancy. Tumor morphology on ADC map appears different due to partial volume effects from thicker DWI slice (6 mm between slices vs. 3 mm for image in (c)). Note that titanium clip did not affect quality of ADC map.

Before ADC values can be used to help make a diagnosis, the lesion must be reliably detected within the noisy ADC images. For the rather large lesions shown in Figure 1, this is not usually a problem, but for small lesions, comparable in size to the surrounding foci of fibroglandular tissue, this can be more challenging. There are several useful techniques that we have found to be helpful in correlating gadolinium-enhanced high spatial resolution imaging to low resolution, noisy DWI and ADC data: (a) use morphology and local topography within the breast to establish the correspondence (e.g. the lesion of concern is an ellipse and 1 cm from a 2 cm cyst, or is part of a triad of three lesions); (b) use software specifically meant to look at DWI data—our software package allows selected overlays of any other sequence to be viewed with the ADC map with manual control of transparency of one image relative to the other; (c) use the b=0 diffusion image, which corresponds closely to the fat suppressed

T2 image, which in turn, has similar spatial resolution to the contrast enhanced scan. Thus, once an enhancing lesion is confidently located within the T2 image, it can be located in the b=0 image, which, in turn virtually overlays the b=1,000 image (images shifts can occur, addressed, below).

Problem of Image Shift
Likely because the breasts are imaged off-axis, and EPI requires such a uniform magnetic field, there is a variable and non-linear image shift between the routine SPGR and spin-echo images and the EPI-based DWI images. This can lead to uncertainty as to which ADC value is associated with which lesion. *This shift may be the single greatest factor preventing incorporation of DWI into routine breast imaging* and will severely inhibit efforts to incorporate DWI into computer aided detection and diagnosis software. Using the techniques mentioned above will solve the problem in many cases, but in our initial retrospective study, image shift and the inability to be certain as to which lesion corresponded to which DWI map location caused us to discard a significant number of lesions.

Problems with Fat
Fat is dark on DWI imaging and as a result, partial volume effects between small lesions and surrounding fat may produce artifactually low ADC values. We do not recommend using ADC value to classify lesions under such circumstances.

Problems due to Blood/Proteinaceous material
Post biopsy coagulated blood or proteinaceous debris within normal ducts or a cyst can result in low ADC values and can easily be mistaken for malignancy. Always interpret DWI results in the context of pre-contrast T1 weighted and post-Gd enhanced imaging.

Hints for successful use of DWI in the breast

(a) Use the b=1000 image to *detect* lesions; use the ADC map to *characterize* lesions. Cancer is typically quite bright on a b=1,000 image (but watch out for false positive from shine through effects (see (d) below). Trying to detect cancer on an ADC map in a heterogeneous breast is extremely difficult as the low signal cannot be distinguished from low signal due to intermixed glandular tissue and fat.
(b) Always make sure to correlate DWI results and ADC measurements with *enhancing lesions*. This will avoid false positive results from blood or proteinaceous debris within benign cysts.
(c) Be very careful in determining which ADC value corresponds to which lesion. Use image overlay between ADC maps and subtracted, Gd-enhanced images to determine image shift. Until technical improvements in diffusion imaging such as implementation of non-echo planar techniques prove robust, the human eye may remain best at determining which ADC value to assign to an enhancing lesion.
(d) Shine through effects result from a lesion starting with unusually high SI on the b=0 image, and although dropping in SI significantly (implying a benign lesion), nevertheless retains sufficient signal to appear bright on the b=1,000 image. For larger lesions ADC can be used to differentiate true water diffusion restriction from shine through. For smaller lesions where ADC is of limited value due to partial volume effects, use your eye to compare the relative reduction in signal (or not) from the area of interest as compared to other surrounding breast tissue.

Conclusions
Image shift, image noise and distortion associated with currently used EPI-DWI will likely inhibit widespread adoption of this technique. However, after clinically using DWI for 3 years, we confirm that, carefully applied, DWI provides unique information orthogonal to contrast enhancement and can significantly increase confidence in distinguishing similarly appearing, enhancing benign and malignant lesions.

References
1) Guo Y, Cai YQ, Cai ZL, et. al. Differentiation of clinically benign and malignant breast lesions using diffusion-weighted imaging. J Magn Reson Imaging 2002;16:172–178.
2) Kinoshita T, Yashiro N, Ihara N, et. al. Diffusion-weighted half-Fourier single-shot turbo spin echo imaging in breast tumors: differentiation of invasive ductal carcinoma from fibroadenoma. J Comput Assist Tomog 2002:26:1042–1046.
3) Marini C, Iacconi C, Giannelli, et. al. Quantitative diffusion-weighted MR imaging in the differential diagnosis of breast lesion. Eur Radiol 2007;17:2646–2655.
4) Woodhams R, Matsunaga K, Iwasbuchi K, et. al. Diffusion-weighted imaging of malignant breast tumors: the usefulness of apparent diffusion coefficient (ADC) and ADC map for the detection of malignant breast tumors and evaluation of cancer extension. J.Comput.Assist.Tomogr 2005;29:644.
5) Rubesova E, Grell AS, De Maertelaer V, et. al. Quantitative diffusion imaging in breast cancer: a clinical prospective study. J Magn Reson Imaging 2007;24:319–324.
6). Yabuucchi H, Matsuo Y, Okafuji T, et. al. Enhanced mass on contrast-enhanced breast MR imaging: Lesion characterization using combination of dynamic contrast-enhanced and diffusion-weighted MR images. J Magn Reson Imaging 2008;28:1157–1165
7) F. Kelcz, R.A. Musack. Use of Diffusion Weighted Imaging to Improve Specificity in Diagnosis of Enhancing Breast Lesions detected during Breast MRI. Electronic Teaching poster—ARRS annual meeting, April 13–18, 2008. Washington, DC. Also selected for http://womensimagingonline.arrs.org

Do Advanced MR Methods Add Value to Routine Contrast-enhanced Breast MRI?

Frederick Kelcz, PhD, MD
University of Wisconsin, Madison 53792-3252, USA

Acknowledgements
The work presented here was possible due to the joint efforts of a collaboration between the Depts. of Radiology[1] and Medical Physics[2] involving the following individuals:
Catherine J. Moran[2], Karl Vigen[1], Garima Agrawal[1] and Walter F. Block[2]

Introduction
Breast MRI is so sensitive in the detection of invasive breast cancer (>92% in most studies) that that recent research has appropriately emphasized methods for improving specificity, which continues to be variable (1–3) and troublesome. False positive results are typically associated with fibroadenomas, polyps, and common benign nonmass areas of enhancement associated with fibrocystic change and sclerosing adenosis. The costs of follow-up imaging and/or biopsy for these benign lesions are especially troublesome to those advocating for increased use of MRI in the political setting of constraining health care costs.
Over the past decade several sophisticated techniques for improving breast MRI diagnosis have been proposed (4,5). However, in many scientific studies, a baseline standard and

complete breast MRI was not used as a basis of comparison to determine if there was any added value derived from these sometimes time-consuming techniques. We present preliminary results from an ongoing study that is meant to address this issue.

Methods

Patients were recruited from those in whom biopsy results were already known or biopsy was planned. To avoid ambiguities associated with measurement of lesions, only patients with suspected or known masses were recruited (i.e. those with clustered microcalcifications not associated with a mass were not offered entry into this study). Furthermore, a lesion size estimate of at least 1 cm was required to allow adequate data sampling. Patients with marking clips within a lesion were not offered entry unless the lesion was so large that at least 1 cm of tissue remained for measurements. If the radiologist performing core biopsy prior to imaging was approached early enough, he/she was asked to place the marking clip at the edge, rather than at the center of the lesion. With IRB approval, patients were asked to come on two separate days, at least 24 h apart (to allow for contrast agent washout), and no more than 7 days apart (to avoid true changes in the biology or size of the tumor). All imaging was performed at 1.5 T with an 8 channel receive coil (GE Healthcare, Waukesha, WI, USA). On the first day, a standard sagittal breast MRI was performed including T1 and T2 precontrast imaging followed by a 3D commercial sequence (Vibrant©, GE Healthcare) acquiring a 3D volume in 75 s for eight acquisitions. On the second day of the study, the standard 3D GRE sequence was replaced by a more rapid dynamic imaging technique (PR-TRICKS at first, then VIPR [6,7]) to determine the value of sub-minute temporal resolution. Diffusion Weighted Imaging (DWI), MR Spectroscopy (MRS) and blood oxygen level dependent (BOLD) imaging was performed on both days to confirm reproducibility. DWI used an Echoplanar technique with b=0, 1,000 s/mm^2. MRS was performed using a commercially available single voxel package (BREASE©—GE Healthcare, Waukesha, WI). BOLD imaging used a 16 echo T2*-measurement sequence with TE's varying form 6.7 to 41.2 ms.

Image Analysis

The BI-RADS interpretation criteria were used to assess the lesions viewed both on a clinical PACS system and using proprietary manufacturer software on a dedicated work station (Functool©, GE Healthcare, Waukesha, WI, USA). This software also permitted calculation of the Apparent Diffusion Coefficient (ADC) for DWI imaging and of tissue relaxation for BOLD imaging. As data collection is still in process a single radiologist (FK) viewed the images and, although usually blinded to pathology, was not blinded to imaging results from mammography, ultrasound and clinical MRI (if performed). After coming to a conclusion as to the probable diagnosis from the standard clinical MRI examination, the additional imaging data was viewed to determine if there appeared to be any discriminatory power that added value to that obtained during standard clinical MRI.

Results

Difficulties in recruitment occurred that were not anticipated—it was difficult to find women who could return for two MRI examinations with a week, especially if the presumed or known diagnosis was malignancy and research MRI competed with preparation for therapy. Furthermore, since some patients had already had a clinical MRI, they became difficult to recruit for a study that required yet two more MRI examinations, each requiring a contrast injection. As a result only eight patients have been recruited thus far. The diagnoses were:

Four malignant lesions: one invasive lobular cancer (ILC); one invasive ductal cancer (IDC); one mucinous adenocarcinoma (MUC) and one metastatic cancer (melanoma, [MET]).

Four benign lesions: three Fibroadenomas (Fb) and one probable Fb, (possible phylloides), for which excision was recommended by the pathologist, but the patient was lost to follow-up and did not complete her second research MRI examination.

The results are summarized in the following table:

Clin Hx/Dx	Size	Conv MRI	ADC Day 1/2	MRS Day 1/2	BOLD Day 1/2	Added value
20 yo Fb	1.5 cm	4a Fb	2.21/2.29	No Chol/No Chol	8.6/8.5	No
59 yo MET	0.8 cm	4b Macrolob TIC III	1.0/1.08	Failed/Failed	Lesion not seen/tech probl	No
47 yo Fb	3.2 cm	4a	1.69/no 2nd day	Mod +/ no 2nd day	Tech prob	Mild??
41 yo MUC	1.9 cm	4a	2.40/2.48	Equiv/Equiv	Wrong TE's/missing	No
43 yo Fb	2.2 cm	4a	1.37/1.95	Weak/Neg	Wrong TE/34.8	No
45 yo IDC	1.4 cm	5	1.04/1.01	Chol +/Chol +	Tech prob both days	No
66 yo ILC	2.0 cm	5	0.71/0.69	Chol ++/Chol ++	21.5/23.8	No
45 yo Fb	0.9	4a	1.42/1/44	Failed/Failed	36.2/38.5	No

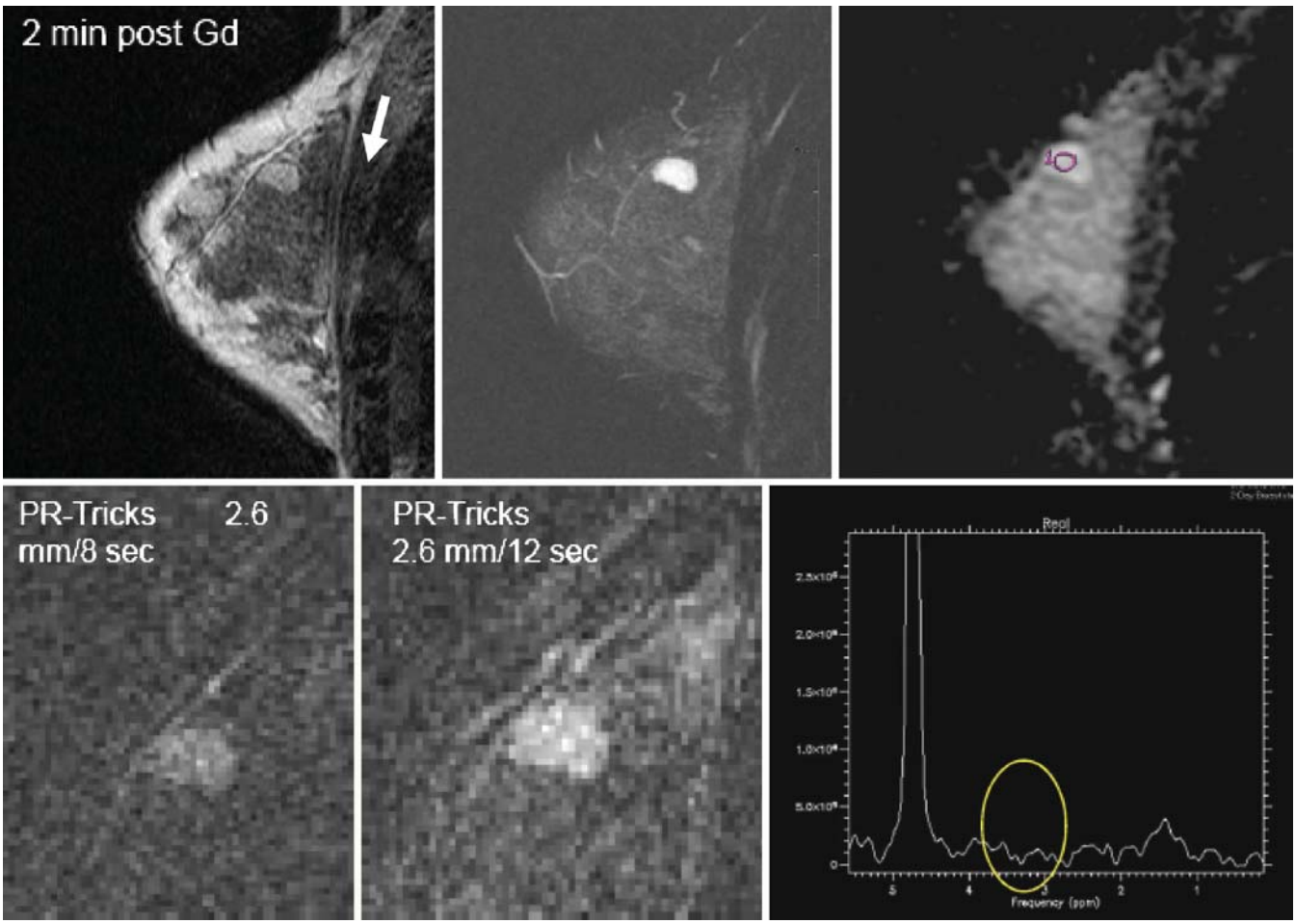

Example #1: 20 yo woman with Fibroadenoma Top row; left to right: [First Image]: frame from 2 min image of standard MRI displays well marginated macrolobulated lesion. [Second image]: high T2 SI typical of some fibroadenomas, and not typical of most breast malignancies. [Third image]: ADC map derived from diffusion series reveals high ADC value (mean for 2 days=2.25×10^{-3} mm^2/s). Bottom row; left to right: [First and second images]: frames from PR-Tricks high speed imaging at 8 s and 12 s after onset of enhancement displays no additional information. [Third image]: spectrum obtained from MRS sequence shows that no choline peak can be detected. Conclusion: Although additional information was concordant with diagnosis, most radiologists, given the conventional MRI findings, would easily conclude the mass was a fibroadenoma with high confidence. Thus, NO BENEFIT was the conclusion assigned to this case.

Discussion

Thus far, with only eight patients recruited, the advanced MR methods do not appear to significantly contribute to diagnosis arrived at by a conventional diagnostic breast MRI protocol. We summarize our early experience as follows:

DWI: Of the methods we have applied in this presentation, DWI seemed most reliable and consistent, correctly classifying seven of eight lesions. However, the high ADC value noted in one lesion may have lead to a delayed diagnosis of mucinous cancer. A recent publication (8) notes that the high ADC value of this type of tumor may be diagnostic and may offer reliable differentiation between fibroadenoma and mucinous neoplasm. Thus, correct use of ADC derived from DWI may require *two thresholds*, one below which breast cancer is suspected (e.g. 1.2×10^{-3} mm^2/s) and one above which mucinous malignancy is suspected (e.g. 2.3×10^{-3} mm^2/s). For most of the patients in our small study, DWI was only confirmatory, but for the time spent in

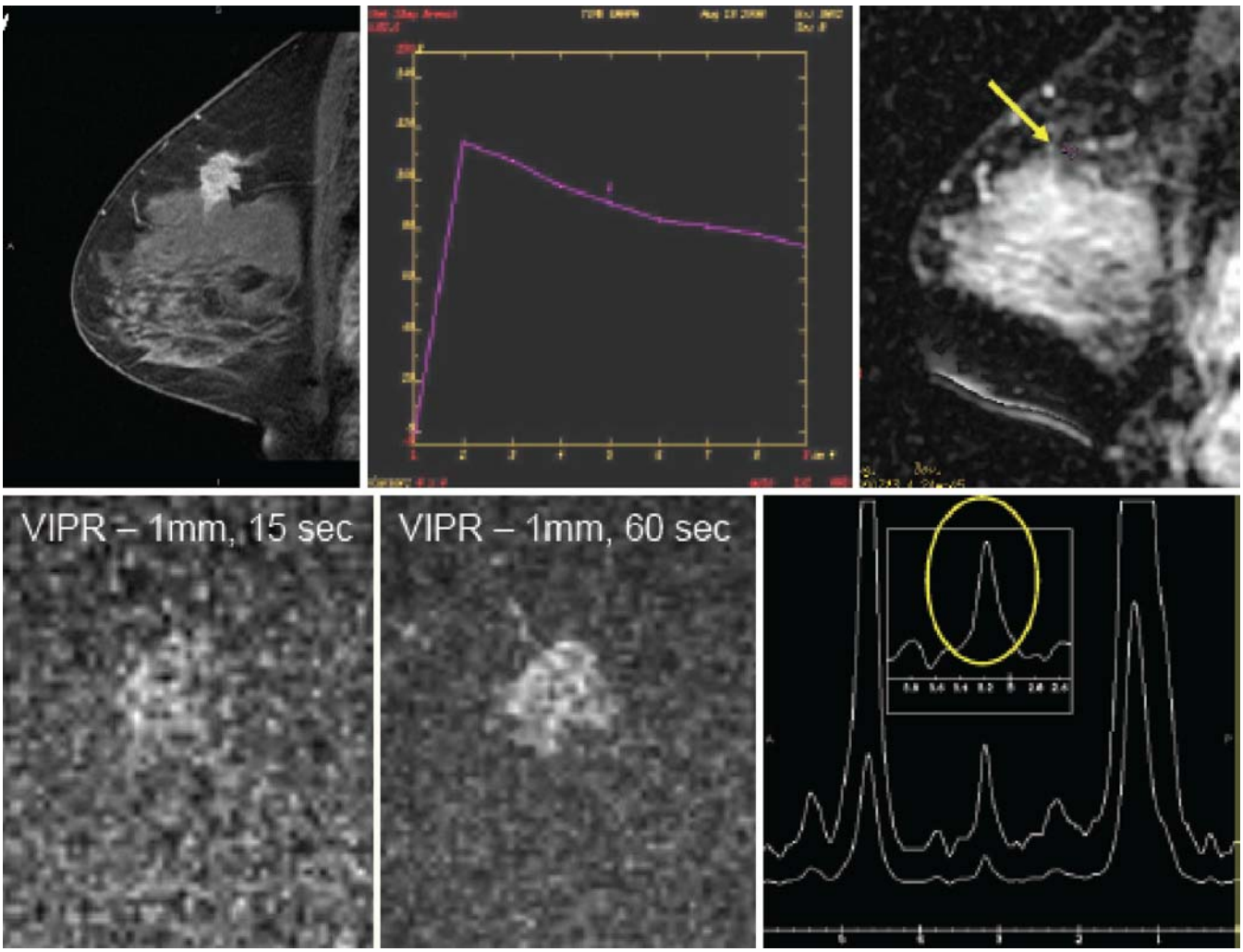

Example #2 66 yo woman with Invasive Lobular Cancer Top row; left to right: [First image]: image 7 min after gadolinium contrast injection from conventional breast MRI shows an enhancing spiculated lesion. [Second image]: time intensity curve reveals central washout, highly suspicious for malignancy. [Third image]: ADC map (third image) shows low ADC value typical of malignancy (mean for 2 days= 0.74×10^{-3} mm^2/s). Bottom row; left to right: [First and second image]: Two frames, at 15 and 60 s from VIPR high temporal resolution imaging showing no additional information—in fact, spicules are not well seen. [Third image]: Spectrum from MRS displays very strong choline peak typical of malignancy. Conclusion: Given the spiculated morphology and immediate strong enhancement and delayed washout TIC, most radiologists would assign a BI-RADS 5. Additional methods were confirmatory. Thus, NO BENEFIT was the conclusion assigned to this case.

obtaining the images, DWI offers a high return per added imaging time, and has potential for assisting in diagnosis of lesions in which conventional MR imaging is equivocal.

Rapid Imaging: Our experience with very rapid MRI imaging was based on the idea that morphological patterns seen during the earliest phases of enhancement might add a new dimension to MR diagnosis that is not being exploited by simple observation of time intensity curves. Yet, our initial experience was disappointing—as seen in the patients shown above, the early enhancement, using 8–15 s temporal resolution, did not add diagnostic value over the conventional criteria of lesion morphology and time intensity curves.

MRS: Of the methods used, MRS is probably the least useful for several reasons. First, the size of the lesions seems limiting. MRS failed completely to tune in two of our eight patients, whose tumors were smaller than 1 cm. This might be expected as the manufacturer recommended at least 1.5 cm diameter tumors when scanning at 1.5 T. Since the average size of breast

malignancies detected in our practice is approximately 1 cm, this implies that MRS could be applied less than half of our studies. Secondly, we have noted (outside of this study), that even some very large tumors could not be subjected to MRS, when tumor was intermixed with fatty breast tissue—thus the 1.5 cm recommendation requires 1.5 cm of *pure nonfatty tissue*. Furthermore despite the good results obtained elsewhere (5), it is hard to imagine a radiologist *not* biopsying a 2 cm mass only because MRS is negative for choline. Third, the time required for MRS, 5 min per scan, plus prescanning, (which failed approximately 25% of the time), was far greater than that of the other methods, and applied to only one region of interest. This would require live time monitoring of breast MRI, which is not practical in a busy clinical practice. Thus, at least for diagnostic purposes, and given the current limitations, it is hard to see a future for MRS solely applied to breast imaging for diagnostic purposes.

BOLD: Not much literature pertaining to use of BOLD imaging in the breast is available. BOLD imaging has been associated with applications associated with predicting radiotherapeutic response by indirect measurement of tissue oxygenation (9, 10). Our interest in BOLD imaging directed at the diagnostic value of the BOLD contrast mechanism. We did not employ carbogen modulated breathing (10) and used an admittedly naive approach with several technical problems marring data acquisition. Our table of results, above, shows the relaxation of the lesion; not listed, due to space limitation, was the relaxation of adjacent normal fibroglandular tissue. Although several lesions did stand out against the background on individual GRE images, we did not discern a contrast effect that promised effective diagnostic uses for this contrast mechanism as a means for detection or for differentiation of benign and malignant lesions within fibroglandular tissue.

Conclusions

The sensitivity of standard 3D contrast-enhanced breast MRI is already so high that additional MR methods added to a standard technique are unlikely to improve on this aspect of imaging. Improvement in the specificity of selecting how which enhancing lesions are truly concerning is still required. Of the advanced methods we employed, and for the small patient population thus far imaged, no significant benefit was realized from addition of advanced breast evaluation techniques over the basic breast MRI clinical sequences. Nevertheless, of all the methods, DWI, the incorporation of which added only 2 min to overall imaging, appears to offer the greatest potential for improving differentiation of benign from malignant lesions in that subset of lesions with overlapping characteristics on conventional imaging.

References

1. Bazzocchi M, Zuiani C, Panizza P, et al. Contrast-enhanced breast MRI in patients with suspicious microcalcifications on mammography: results of a multicenter trial. AJR Am J Roentgenol 2006;186:1723–1732
2. Berg WA, Gutierrez L, NessAiver MS, et. al. Diagnostic accuracy of mammography, clinical examination, US, and MR imaging in preoperative assessment of breast cancer. Radiology 2004;233:830–849
3. Kriege M, Brekelmans CT, Boetes C et. al. Efficacy of MRI and mammography for breast-cancer screening in women with a familial or genetic predisposition. N Engl J Med 2004;351–427
4. Marini C, Iacconi C, Giannelli et. al. Quantitative diffusion-weighted MR imaging in the differential diagnosis of breast lesion. Eur Radiol 2007;17:2646–2655
5. Bartella L, Morris EA, Dershaw DD et. al. Proton MR spectroscopy with choline peak as malignancy marker improves positive predictive value for breast cancer diagnosis: preliminary study. Radiology 2006;239:686–692
6. Vigen KK, Peters DC, Grist TM, Block WF Mistretta CA. Undersampled projection-reconstruction imaging for time-resolved contrast-enhanced imaging. Mag Reson Med 2000;43:170–176
7. Barger AV, Block WF, Toropov Y, Grist TM, Mistretta CA. Time-resolved contrast-enhanced imaging with isotropic resolution and broad coverage using an undersampled 3D projection trajectory. Magn Reson Med 2002;48:297–305
8. Woodhams R, Matsunaga K, Iwabuchi, K et. al. Diffusion-weighted imaging of mucinous carcinoma of the breast: evaluation of apparent diffusion coefficient and signal intensity in correlation with histologic findings. AJR AmJ Roentgenol. 2009;193:260–266.
9. Alonzi R, Padhani AR, Allen C. Dynamic contrast enhanced MRI in prostate cancer. Eur J Radiol 2007;63:335–350.
10. Taylor NJ, Baddeley H, Goodchild KA, et. al. Bold MRI of human tumor oxygenation during carbogen breathing. J Magnetic Reson Imag 2001;14:156–163

Molecular ultrasound imaging: Principles and potential application in diagnosis and therapy monitoring of breast cancer

Moritz Palmowski MD[1,2], Wiltrud Lederle PhD[1], Jessica Bzyl[1], Jessica Gaetjens PhD[1], Fabian Kiessling MD[1]
[1]Institute of Experimental Molecular Imaging, Medical Faculty, RWTH Aachen University, Germany
[2]Department of Diagnostic Radiology, Medical Faculty, RWTH Aachen University, Germany

Correspondence author:
Prof. Dr. Fabian Kiessling, MD, Institute of Experimental Molecular Imaging, RWTH-Aachen University, Pauwelsstrasse 30, 52074 Aachen, Germany, Tel.: +49 241 80 36124, Fax: +49 241 80 82442, E-mail: fkiessling@ukaachen.de

Introduction

In the past decades, significant advances have been made in the diagnosis of breast cancer. In addition to the considerable technical improvements of dynamic contrast enhanced (DCE) magnetic resonance imaging (MRI) [1], ultrasound has undergone revolutionary changes that have improved its spatial and temporal resolution and enhanced its soft tissue contrast [2]. In today's breast imaging, ultrasound provides valuable morphologic information and a recent study has demonstrated the advantage of ultrasound for diagnosis of breast cancer when being combined with conventional mammography [3].
Furthermore, the development of contrast sensitive imaging techniques enables us to gain insight into dynamic physiologic and pathophysiologic processes such as blood flow, tissue perfusion or blood volume [2]. Recent studies have demonstrated the value of contrast-enhanced ultrasound not only for diagnosis of breast cancer [4] but also for monitoring antiangiogenic treatment effects [5–6].
Another recent advancement of ultrasound has been the ability to analyze disease associated endothelial receptors, a technique known as molecular ultrasound imaging [2, 7]. The fundamental principles of this modality are based on the improvement of contrast specific imaging techniques and on the development of target-specific ultrasound contrast agents. In preclinical studies, molecular ultrasound imaging has demonstrated its ability to

diagnose and characterize tumor tissues [8–12]. Today, molecular contrast agents are evaluated for clinical approval and are expected to be available soon [13].
This abstract will give a brief introduction into the principles of ultrasound contrast agents and targeting of microbubbles. Furthermore, we will introduce into different imaging strategies for molecular ultrasound. Finally, we will discuss recent literature focussing on the potential of molecular ultrasound imaging in oncology.

Principles of ultrasound contrast agents and strategies for targeting

Ultrasound contrast agents consist of stabilized gas-filled bubbles with a mean diameter of 1–3 μm. Depending on their shell composition, microbubbles can be divided into softshell (e.g. stabilized by phospholipid) or hardshell (e.g. stabilized by a polymer) bubbles. Due to the encapsulated gas core, microbubbles (especially softshell bubbles) are more compressible by several orders of magnitude when compared to blood or tissue and the bubbles are smaller than the wavelength of a diagnostic ultrasound pulse. Thus, oscillation occurs with compression (during the pressure peak of the pulse) and expansion (during the pressure nadir) [2]. This vibration produces an acoustic backscatter, which can be detected by ultrasound devices. Firstly, at a very low energy level, insonation leads to reflection of the ultrasound pulse without changing the overall pulse spectrum (linear signal). At higher pulse energy levels at the bubble-specific resonance frequency, they also produce harmonic signals (non-linear signals) since the gas within the microbubble can only be compressed to a limited extent. Today, non-linear signals enable sensitive detection of ultrasound contrast agents by the use of contrast-specific pulse sequences [14]. An alternative way of visualizing gas-filled microbubbles is to destroy the bubbles with a high-energy ultrasound pulse. This imaging approach is frequently applied for detection of hardshell bubbles which provide lesser harmonic signals as compared to softshell contrast agents. Upon disruption the gas of the cracked microbubble expands and creates a very strong echo of a free gas bubble, which can easily be detected in color and power Doppler modes, determined as "Stimulated Acoustic Emission (SAE)" [15, 16].
Microbubbles remain within the blood for several minutes until they are cleared by the lung, liver and spleen [17]. Due to their size in the range of micrometers, ultrasound contrast agents hemodynamically behave like red blood cells and remain strictly intravascular [2, 3]. Thus, they serve as blood pool enhancers for the assessment and characterization of tissue perfusion. Molecular ultrasound imaging is based on a modification of the microbubble shell, which leads to a selective adhesion within the vasculature of the affected tissue. In general, the target affinity is achieved by the non-covalent or covalent attachment of target-specific ligands to the microbubble surface [2–3]. Usually, antibodies or small peptides are used as target molecules. The specific ligands can either be directly connected to the surface of the microbubbles. Alternatively, linking molecules like streptavidin-biotin can be used (Figure 1). Covalent coating with streptavidin creates a microbubble with several thousand binding sites for biotinylated ligands. This strategy allows an easy attachment of different antibodies and is advantageous for preclinical testing of suitable molecular targets. However, streptavidin can cause an unwanted immune response. Therefore, other coupling strategies such as covalent binding have to be used when considering a potential application of the desired probe in humans [13].

Imaging strategies

The accumulation of targeted microbubbles can be assessed by several strategies. Predominantly, the relative contrast enhancement within a two-dimensional ultrasound image is measured after the freely circulating microbubbles have been cleared from the blood (usually after few minutes) (Figure 2) [9]. Using contrast sensitive pulse sequences, this technique can easily be translated into the clinics. A disadvantage is the fact that, up to now, only two-dimensional ultrasound images can be acquired.
Besides this "non-destructive" imaging approach, which is suited for detection of softshell microbubbles, "destructive" imaging techniques can be used for the quantification of contrast agents with a hard shell. The disintegration of the microbubbles causes a signal (stimulated acoustic emission; SAE) which can be detected in Doppler-mode. However, in this context it is important to note that it is difficult to distinguish whether the signal within a voxel originates from only one or from several microbubbles. Thus, a saturation of the Doppler-signal is reached very fast which denies a reliable quantification of the amount of stationary microbubbles. This problem is particularly relevant for molecular ultrasound imaging where intense local accumulation of microbubbles can occur. With the aim of allowing better quantification of stationary microbubbles within a three-dimensional object, "sensitive particle acoustic quantification (SPAQ)" was developed [16] (Figure 3).
SPAQ is based on the micrometer-wise, motor-driven movement of the ultrasound transducer after a destructive Doppler scan. During the first destructive scan microbubbles are destroyed in a broad slice, but after moving several micrometers forward, new microbubbles can only be destroyed in the non-overlapping distance. Thus, a volumetric scan of the object with (virtually) very thin slices can be performed in which single microbubbles are detected [16]. A mathematical correction enables to determine the microbubble concentrations in a tissue volume [18]. The principle of SPAQ might be easily implemented in existing ultrasound breast scanners [19]. Thus, volumetric imaging of the entire breast with assessment of targeted ultrasound contrast agents should be feasible.

Tumor angiogenesis and molecular targets

The development of a malignant tumor can be divided into two major phases: the early "avascular phase" and the advanced "vascularized phase". The avascular phase is characterized by a limited tumor growth, up to a size of 1–2 mm. Up to this diameter, the tumor cells are sufficiently supplied with nutriments by diffusion and do not require direct vascular supply. Beyond this size, diffusion alone does not suffice, and the innermost tumor cells become hypoxic [20]. They respond by expressing pro-angiogenic factors which stimulate the surrounding blood vessels. Consequently, angiogenic sprouting occurs (partially mediated by the vascular endothelial growth factor, VEGF) with development of an activated "tumor" vasculature [21] (Figure 4). The newly formed angiogenic vessels allow invasive tumor growth and the generation of metastases in other organs. The activated endothelial cells in the tumor vasculature express characteristic marker molecules (e.g. VEGFR2, CD105, avb3-Integrin), which are not expressed constitutively by quiescent endothelial cells. These markers can therefore be used as targets for the specific imaging of the tumor vasculature. Also in breast cancer several factors have been identified as promoters of angiogenesis. Next to the ones mentioned above stromal PDGF and its receptors are associated with estrogen receptor negativity and correlate with shorter survival [22]. There is evidence that

PDGFR is also expressed by endothelial cells [23] and thus may serve as a molecular target for imaging tumor vasculature of breast carcinomas and to determine tumor aggressiveness.

Imaging of angiogenesis and monitoring of anticancer therapies

The most recognized angiogenic marker molecule is the vascular endothelial growth factor receptor-2 (VEGFR-2), which has been extensively studied as a target for molecular ultrasound imaging [8–10, 12, 17]. It has been reported that microbubbles conjugated to antibodies against VEGFR-2 accumulate within various subcutaneously implanted tumor models significantly more than unspecific control microbubbles. Despite the high retention in the tumor tissue, no relevant accumulation of tumor-specific microbubbles was observed in healthy tissue, underlining the potential diagnostic impact of targeted ultrasound contrast agents (Figure 5).

Beyond the diagnosis of cancer it has further been demonstrated that "highly invasive metastatic" and "non-metastatic" breast cancer models can be differentiated by the binding characteristics of VEGRF-2 specific microbubbles [24]. This demonstrates the capacity of targeted ultrasound to characterize the angiogenic activity and to predict the degree of malignancy.

For these initial results, most research groups used high-frequency ultrasound devices dedicated for small animal imaging in a semi-quantitative, two-dimensional, single-slice technique. In a recent study, Korpanty and colleagues used a clinical ultrasound system for the assessment of anti-angiogenic treatment effects [12]. They used (1) an antibody against the VEGF/VEGF-receptor complex in an orthotopic model of pancreatic cancer and (2) antibodies against VEGFR-2 and/or against CD105 (endoglin) in two subcutaneous models of pancreatic cancer during anti-angiogenic treatment. They detected decreasing marker densities after tumor-suppressive therapy, which correlated with the observed effects of treatment. Korpanty and co-workers used a "non-destructive" imaging technique to acquire several two-dimensional slices throughout the tumor in order to assess its representative volume. In one group of subcutaneously implanted tumors, they performed multi-marker imaging, assessing two markers (VEGFR-2 and CD105) during the same examination session. Long intervals between the subsequent scans (~1 h) were necessary to ensure passive clearance of targeted microbubbles from the marker molecule before subsequent microbubbles could be administered.

Two additional studies report on the assessment of treatment effects [8, 25]. Instead of adopting the two-dimensional approach of assessing multiple slices like Korpanty and coworkers, they used a three-dimensional imaging technique (SPAQ) [16]. Using SPAQ, all stationary microbubbles within a tumor are actively destroyed during a scanning procedure, enabling the sequential administration of different charges of specific microbubbles over short time intervals. Thus, assessment of multiple angiogenic markers was possible and enabled the molecular profiling of angiogenesis during tumor progression and treatment. One study thereby demonstrated an upregulation of VEGFR-2 and of $\alpha_v\beta_3$ integrin during tumor progression, and a downregulation of both markers after anti-angiogenic therapy [8]. The other SPAQ-study used molecular ultrasound imaging to intra-individually track changes in angiogenic marker expression after carbon ion irradiation in experimental tumors [25]. They observed that carbon ion irradiation upregulates the inflammatory marker ICAM-1 and the angiogenic marker $\alpha_v\beta_3$ integrin in the tumor neovasculature. These results clearly demonstrate that molecular ultrasound does not only enhance the diagnosis of malignoma but also may help to characterize and monitor the angiogenic profile of a tumor.

Outlook

Contrast-enhanced ultrasound imaging of the breast has already been established in clinical practice. Based on the encouraging results obtained by molecular ultrasound imaging in different preclinical studies, we expect that this technique will find its way into the clinics soon. The necessary imaging technology is already available in the clinics and novel three-dimensional imaging techniques will be established for breast imaging soon. Suitable target-specific ultrasound contrast agents are on the verge of being carried into the clinics. In this regard, ultrasound, and especially reproducible three-dimensional imaging techniques, may be used as a considerable supplement to DCE MRI and mammography for diagnosis or therapy monitoring of breast cancers. Moreover, targeted ultrasound may support treatment control and the characterization of disease state during interventional procedures.

References

1. Kaiser WA (2007) Breast magnetic resonance imaging: principles and techniques. Semin Roentgenol 42:228–35
2. Kiessling F, Huppert J, Palmowski M (2009) Functional and molecular ultrasound imaging: concepts and contrast agents. Curr Med Chem 16:627–42
3. jBerg WA, Blume JD, Cormack JB et al (2008) Combined screening with ultrasound and mammography vs mammography alone in women at elevated risk of breast cancer. JAMA 299:2151–63
4. Balleyguier C, Opolon P, Mathieu MC et al (2009)New potential and applications of contrast-enhanced ultrasound of the breast: Own investigations and review of the literature. Eur J Radiol 69:14–23
5. Palmowski M, Huppert J, Hauff P et al (2008) Vessel fractions in tumor xenografts depicted by flow-or contrast-sensitive three-dimensional high-frequency Doppler ultrasound respond differently to antiangiogenic treatment. Cancer Res 68:7042–9
6. Pamowski M, Lederle W, Gaetjens J et al. Comparison of conventional time–intensity curves versus maximum intensity over time for post processing of dynamic contrast-enhanced ultrasound. Submitted
7. Dayton PA, Rychak JJ (2007) Molecular ultrasound imaging using microbubble contrast agents. Front Biosci 12:5124–42
8. Palmowski M, Huppert J, Ladewig G, et al (2008) Molecular Profiling of Angiogenesis with Targeted Ultrasound Imaging: Early Assessment of Anti-Angiogenic Therapy Effects. Molecular Cancer Therapeutics 7:101–9
9. Willmann JK, Paulmurugan R, Chen K et al (2008) US imaging of tumor angiogenesis with microbubbles targeted to vascular endothelial growth factor receptor type 2 in mice. Radiology 246:508–18
10. Rychak JJ, Graba J, Cheung AM (2007) Microultrasound molecular imaging of vascular endothelial growth factor receptor 2 in a mouse model of tumor angiogenesis. Mol Imaging 6:289–96
11. Weller GE, Wong MK, Modzelewski RA et al (2005) Ultrasonic imaging of tumor angiogenesis using contrast microbubbles targeted via the tumor-binding peptide arginine-arginine-leucine. Cancer Res 6:533–9
12. Korpanty G, Carbon JG, Grayburn PA et al (2007) Monitoring response to anticancer therapy by targeting microbubbles to tumor vasculature. Clin Cancer Res 13:323–30
13. Pochon S, Tardy-Cantalupi I, Messager T (2008) US Angiogenesis Imaging with KDR-Targeted Microbubbles. World Molecular Imaging Congress. Book of Abstracts p:
14. Burns PN (2000) Pulse inversion imaging of liver blood flow: improved method for characterizing focal masses with microbubble contrast. Invest Radiol 35:58–61

15. Uhlendorf V, Hoffmann (1994) Nonlinear acoustical response of coated microbubbles in diagnostic ultrasound. IEEE Ultrason Symp 1559
16. Reinhardt M, Hauff P, Briel A et al (2005) Sensitive particle acoustic quantification (SPAQ): a new ultrasound-based approach for the quantification of ultrasound contrast media in high concentrations. Invest Radiol 40:2–7
17. Palmowski M, Morgenstern B, Hauff P et al (2008) Pharmacodynamics of streptavidin-coated cyanoacrylate microbubbles designed for molecular ultrasound imaging. Invest Radiol 43:162–169
18. Siepmann M, Palmowski M, Kießling F et al (2008) "Statistical Corrections for the Precise Estimation of Cyanoacrylate Microbubble Concentration in Targeted Imaging," Proc IEEE Ultrasonics Symposium p:993–996
19. Kotsianos-Hermle D, Hiltawsky KM, Wirth S et al (2009) Analysis of 107 breast lesions with automated 3D ultrasound and comparison with mammography and manual ultrasound. Eur J Radiol 71:109–15
20. Folkman, J (2006) Angiogenesis. Annu Rev Med 57:1–18
21. Yancopoulos GD, Davis S, Gale NW et al (2000) Vascular-specific growth factors and blood vessel formation. Nature 407:242–8
22. Paulsson J, Sjöblom T, Micke P et al (2009) Prognostic significance of stromal platelet-derived growth factor ß-receptor expression in human breast cancer. Am J Pathol 175:334–341
23. Vrekoussis T, Stathopoulos E.N, Kafousi M et al (2007) Expression of endothelial PDGF receptors α and ß in breast cancer: Up-regulation of endothelial PDGF receptor ß. Oncology reports 17:1115–1119
24. Lyshchik A, Fleischer AC, Huamani J et al (2007) Molecular imaging of vascular endothelial growth factor receptor 2 expression using targeted contrast-enhanced high-frequency ultrasonography. J Ultrasound Med 26:1575–86
25. Palmowski M, Peschke P, Huppert J et al (2008) Molecular ultrasound imaging of early vascular response in prostate carcinoma irradiated with heavy ions. Neoplasia. In press.

Figures:

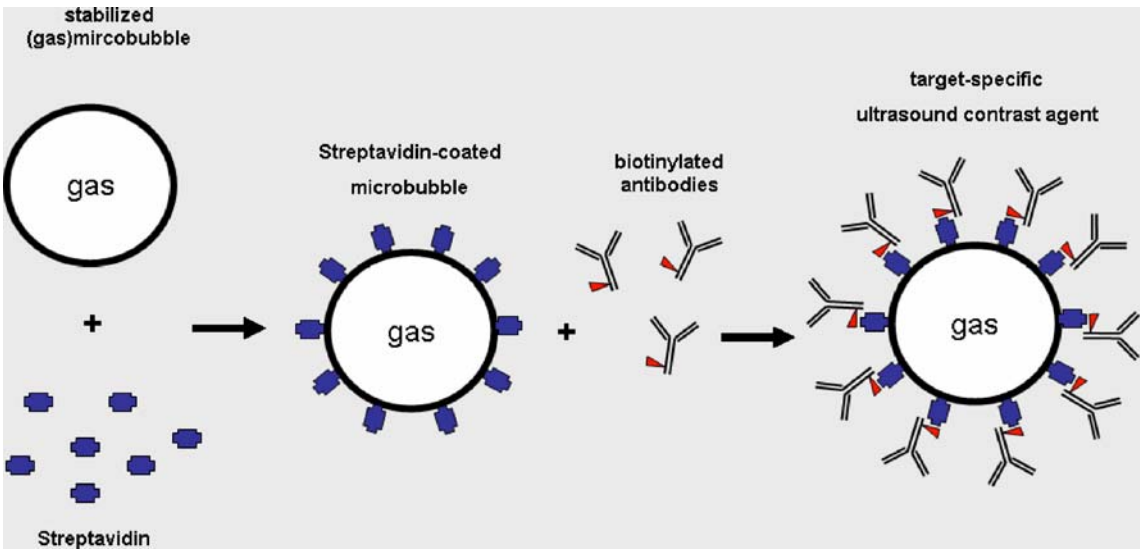

Figure 1: Synthesis and characterization of target specific microbubbles.

Cyanoacrylate microbubbles are synthesized by polymerization of butyl-2-cyanoacrylate. In a second step, streptavidin molecules are linked covalently to the surface, producing a streptavidin coated microbubble. Finally, biotinylated ligands/antibodies can be connected via streptavidin-biotin binding systems, resulting in target specific microbubbles.

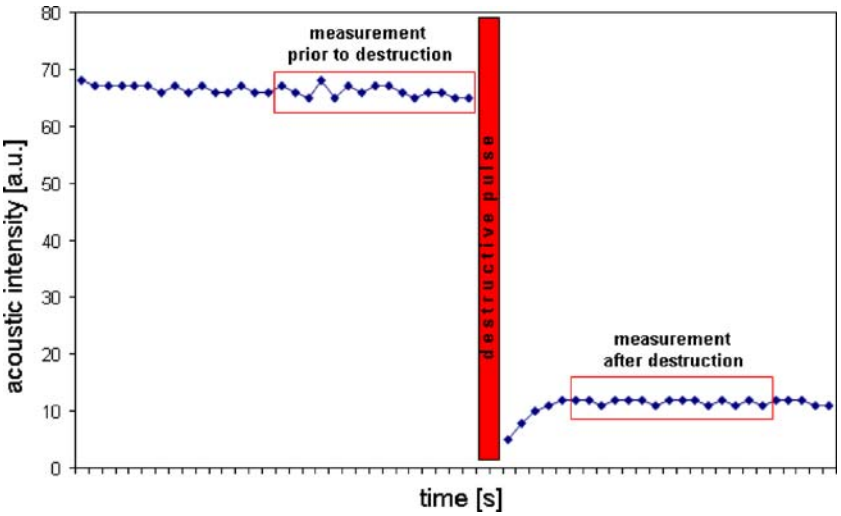

Figure 2: Two-dimensional technique to determine the retention of targeted microbubbles.

The figure shows a representative time–intensity curve of a tumor acquired several minutes after administration of targeted microbubbles. Prior to a destructive ultrasound pulse, the acoustic intensity has three components: (1) echoes from stationary microbubbles, (2) echoes from microbubbles which are still in the circulation and (3) echos from the tumor tissue (very low when using contrast sensitive imaging techniques). After digital subtraction of post-destruction values from pre-destruction values, the resulting echos represent the targeted microbubbles [9].

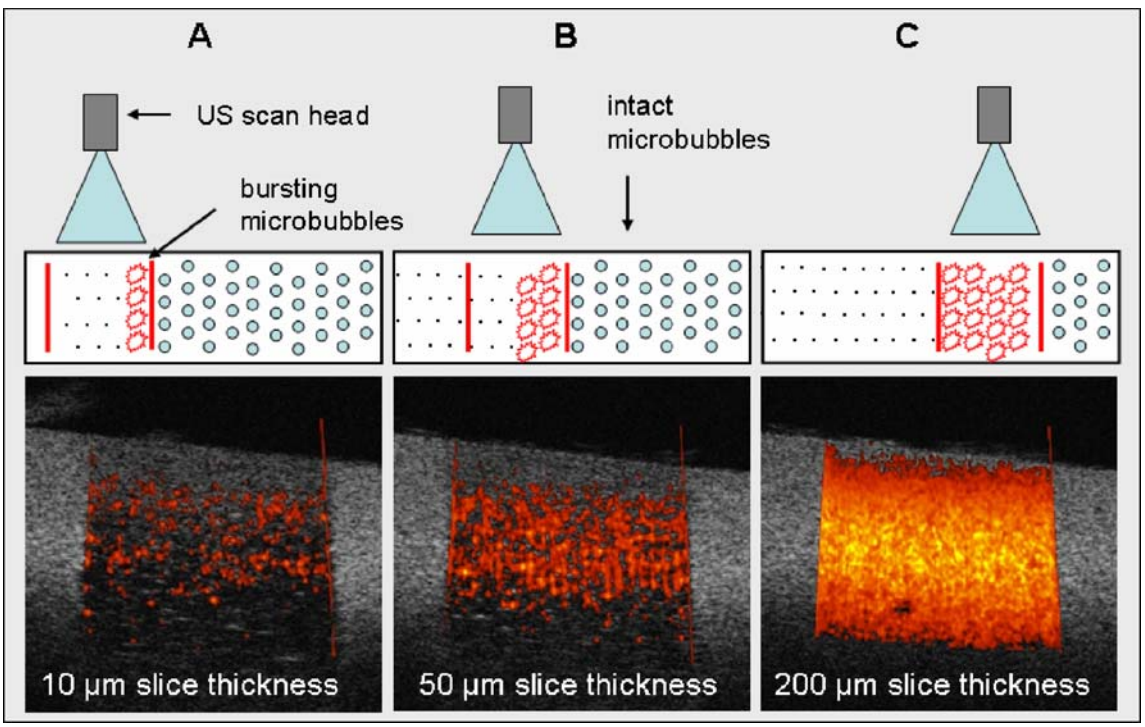

Figure 3: Three-dimensional quantification of stationary contrast agents using the sensitive particle acoustic quantification technology (SPAQ [16]).

Drawings illustrate the principle of SPAQ. If an ultrasound transducer moves over an object (here: agar phantom containing microbubbles), the ultrasound beam destroys the microbubbles within the acoustic field. (**A**) Low frame-to-frame displacement between the single ultrasound pulses results in a high SPAQ resolution providing good discrimination of single signals. (**B** and **C**) Higher displacements (=larger SPAQ-slices) produce lower SPAQ resolutions finally resulting in an overlay of single SAE signals. "Proof-of-principle" in an agar phantom filled with microbubbles.

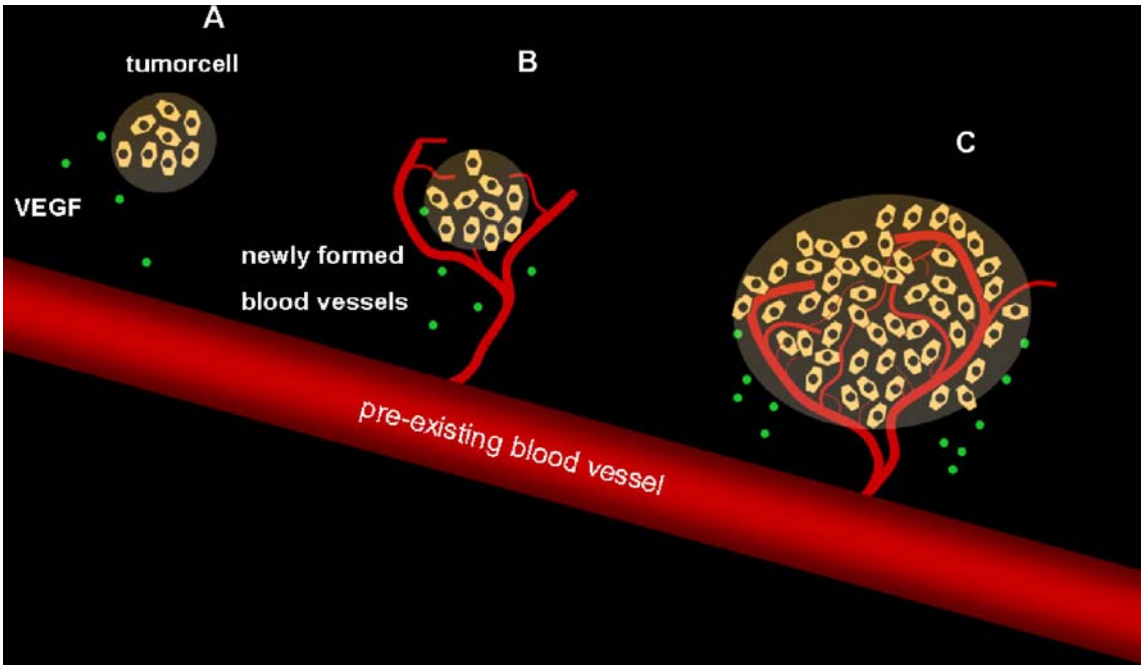

Figure 4: Onset of angiogenesis in tumors.

A: During early tumor growth, the tumor cells are sufficiently supplied with nutriments by diffusion and do not require a direct vascular supply. Reaching a critical size, diffusion alone does not sufficiently supply all tumor cells. They respond by expression of pro-angiogenic factors (e.g. VEGF, symbolized as green dots).
B: The pro-angiogenic growth factors stimulate the surrounding endothelial cells. Consequently, angiogenic sprouting occurs with development of activated blood vessels.
C: The newly formed vessels enable further invasive growth of the tumor. These vessels express disease associated molecular markers (e.g. growth factor receptors) which can be targeted by specific ultrasound contrast agents.

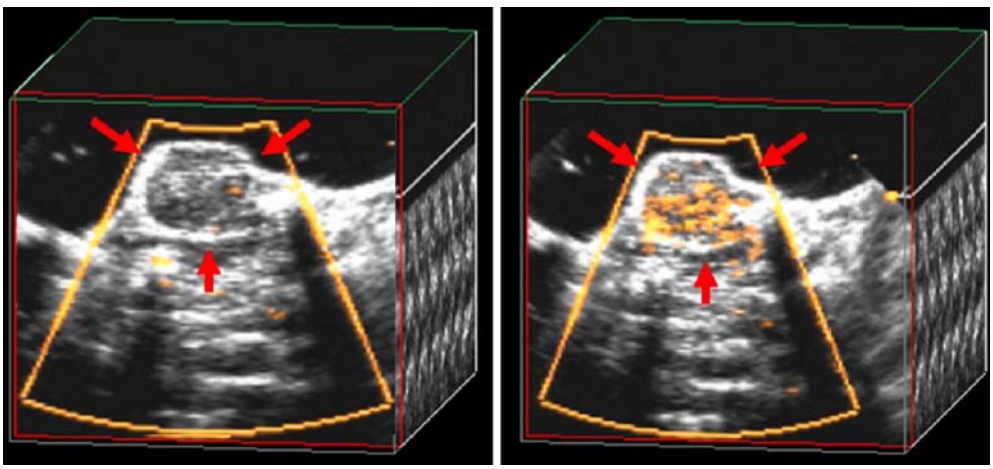

Figure 5: Molecular ultrasound imaging using microbubbles targeted to vascular endothelial growth factor receptor-2 (VEGFR-2).

All panels show three-dimensional data sets of a skin carcinoma xenograft (red arrows) implanted subcutaneously on the hind limb of a nude mouse. Data sets were acquired with the sensitive particle acoustic quantification method (SPAQ). (left image) The tumor after administration of streptavidin-coated polycyanoacrylate microbubbles. Only isolated Doppler signals (yellow dots) are visible within the tumor. (right image) After conjugation of biotinylated antibodies (against VEGFR-2) to the streptavidin-coated microbubble-shell, strongly increased binding of microbubbles occurs (bar: 5 mm).

Magnetic resonance guided focused ultrasound treatment of tumors

Walter Kucharczyk, MD, FRCPC
University of Toronto, Canada

The purpose of this paper is to discuss the science of magnetic resonance guided focused ultrasound (MRgFUS), the method of performing MRgFUS, and the use and results of MRgFUS in the treatment of breast cancer. My own personal experience with THE MRgFUS treatment of breast cancer is extremely limited. Thus I am very grateful to Dr. Hidemi Furasawa for his generous provision to me of his MRgFUS breast cancer treatment results and illustrative cases that are shown in this paper.

MRgFUS is a treatment that incorporates MR imaging with an efficient tumor ablative method - focused ultrasound. MRgFUS has been proved effective as a minimally invasive treatment method to achieve thermal ablation in a wide variety of benign and malignant tumor processes in the human body (1–4). Two distinct advantages of this system are the accurate tumor delineation with three-dimensional treatment planning provided by using MR imaging and continuous temperature mapping in the treatment zone (MR thermography). The combination of these two features allows accurate targeting of the tumor and immediate determination of temperatures achieved in the treated zone (5). Studies have demonstrated MR imaging–guided focused ultrasound to be an effective, well-tolerated treatment for uterine leiomyomas, with minimal morbidity (6, 7). Treatment of neoplastic processes in the brain, liver, and other organs with MR imaging-guided focused ultrasound are presently being evaluated (8–10). Recent studies have also suggested that MR imaging–guided focused ultrasound may become a viable alternative treatment in the palliation of painful bone metastases (13, 27).

The thermal effect of high-energy focused ultrasound waves on human tissue has been documented in the literature as long as fifty years ago (14, 15). These early studies (16, 17) demonstrated the ability of high-energy focused ultrasound waves to induce thermal necrosis. Cell death and tissue coagulation necrosis occurs due to protein denaturation when the temperature of the cell is raised to above 56°C for at least 1 second (18, 19). More recent studies (20–22) have clearly established the accuracy of MR thermographic sequences in the estimation of temperature changes in human tissues following treatment with focused ultrasound energy. Integration of a focused ultrasound therapeutic system with MR thermographic imaging (MRgFUS) allows the operator to accurately target and treat a focal pathologic lesion while obtaining real-time temperature measurements of the treated and adjacent tissues. This technologic development allows a true “closed loop” monitoring of the treatment in real time, hence allowing more efficient and safer ablation procedures. As previously documented in the literature by other investigators using the MRgFUS system, individual sonications (focused ultrasound energy delivered to the pathologic lesion) are immediately assessed for accurate targeting and theoretical temperature achieved in the treated tissue, and sonications are performed until total ablation of the pathologic lesion is completed (3, 23, 24).

MRgFUS has several advantages compared with other thermal ablation techniques that are presently available. Unlike most other ablation technologies that utilize heat or cold (interstitial laser therapy, radiofrequency ablation, microwave ablation, and cryoablation), MRgFUS ablation does not require the insertion of a probe or thermal-conducting needle into the patient, hence making the procedure less invasive and eliminating the need for image-guided interventional skills.

There are different methods of performing MRgFUS. The method used by this author and by Furasawa et al is based on consecutive point sonications (ExAblate System, Insightec, Israel). Other MRgFUS methods heat larger areas, but with all MRgFUS methods, the operator is able to alter the treatment according to the thermal feedback information obtained from the MR thermographic sequences. If adequate thermal elevation has not been achieved at a presumed site of ablation, the same region can be immediately re-treated, and incomplete ablation procedures can be avoided. The fact that each sonication results in only a small area of ablation is also advantageous with respect to adverse events. If the feedback imaging results suggest poor targeting for a particular sonication, immediate correction can be made to avoid destruction of large amounts of normal tissue in proximity to the pathologic entity. This is in direct contrast to most catheter or needle insertion–type ablation procedures in which immediate thermal feedback is unavailable and follow- up imaging studies with infusion are utilized to assess if ablation was successful. Some radiofrequency ablation probes do provide temperature information to the operator, but this information does not immediately influence treatment decisions. This lack of closed loop feedback does not allow one to detect faulty catheter or needle placement, possibly resulting in some destruction of normal tissue and increasing the risk of procedure morbidity.

Some of the earliest trials of treating breast cancer with MRgFUS were published by Gianfelice at el (2, 3, 24). Today, the world’s greatest cumulative experience is with Furasawa et al (25, 26). Furasawa published an MRgFUS safety and effectiveness study for the ablation of breast carcinomas in 2006 (25). In this study, 30 women with biopsy-proved breast cancer underwent MRgFUS treatment. Gadolinium-enhanced MR images were used for treatment planning and post-treatment radiologic assessment of treated tissue. Temperature-sensitive MR images provided real-time treatment monitoring. After MRgFUS, all 30 women underwent wide excision or mastectomy. The extent of thermal ablation was assessed with tumor histology. Treatment was well tolerated, with a minimum of adverse effects, especially when performed under local anesthesia. On pathologic examination, mean necrosis of the targeted breast tumors was 96.9% (range 78% to 100%) of tumor volume. Fifteen (53.5%) of 28 evaluable patients had 100% necrosis of the ablated tumor; only 3 patients (10.7%) had less than 95% necrosis. In 28 (93.3%) patients, 100% of the malignancy was within the treatment field, and 98% and 95% of tumor lay within the treatment field in 2 remaining patients. Retrospective analysis in two patients with residual tumor showed treatment was not delivered to the full recommended area, reaffirming the need for precise localization and the value of contrast-enhanced images for treatment planning.

Furasawa’s paper in 2007 described 21 women with core biopsy proven ductal carcinoma of the breast treated by MRgFUS (26). The median diameter of the tumor was 15 mm (range: 5–50 mm). Seventeen patients were treated once, and 4 patients twice, with a median followup of 14 months (range: 3–26 months). One case of recurrence of pure mucinous carcinoma was experienced. There

was no evidence of recurrence in any of the other 20 cases. They concluded that MRgFUS is a good means of local control of breast cancer, but acknowledged that longer followup and a larger series is required to draw more definitive conclusions.

References

1. Jolesz FA, Hynynen K, McDannold N, Tempany C. MR imaging-controlled focused ultrasound ablation: a noninvasive image-guided surgery. Magn Reson Imaging Clin N Am 2005;13 (3):545–560.
2. Gianfelice D, Khiat A, Boulanger Y, Amara M, Belblidia A. Feasibility of magnetic resonance imaging-guided focused ultrasound surgery as an adjunct to tamoxifen therapy in high-risk surgical patients with breast carcinoma. J Vasc Interv Radiol 2003;14(10):1275–1282.
3. Gianfelice D, Khiat A, Amara M, Belblidia A, Boulanger Y. MR imaging-guided focused US ablation of breast cancer: histopathologic assessment of effectiveness—initial experience. Radiology 2003;227(3):849–855.
4. Hynynen K, Pomeroy O, Smith DN, et al. MR imaging–guided focused ultrasound surgery of fibroadenomas in the breast: a feasibility study. Radiology 2001;219(1):176–185.
5. Moonen CT, Quesson B, Salomir R, et al. Thermal therapies in interventional MR imaging: focused ultrasound. Neuroimaging Clin N Am 2001;11(4):737–747.
6. Stewart EA, Gedroyc WM, Tempany CM, et al. Focused ultrasound treatment of uterine fibroid tumors: safety and feasibility of a noninvasive thermoablative technique. Am J Obstet Gynecol 2003;189(1):48–54.
7. Hindley J, Gedroyc WM, Regan L, et al. MRI guidance of focused ultrasound therapy of uterine fibroids: early results. AJR Am J Roentgenol 2004;183(6):1713–1719.
8. Ram Z, Cohen ZR, Harnof S, et al. Magnetic resonance imaging-guided, high-intensity focused ultrasound for brain tumor therapy. Neurosurgery 2006;59(5):949–955.
9. Kopelman D, Inbar Y, Hanannel A, et al. Magnetic resonance-guided focused ultrasound surgery (MRgFUS): ablation of liver tissue in a porcine model. Eur J Radiol 2006; 59(2):157–162.
10. Kopelman D, Inbar Y, Hanannel A, et al. Magnetic resonance-guided focused ultrasound surgery (MRgFUS). Four ablation treatments of a single canine hepatocellular adenoma. HPB (Oxford) 2006;8(4):292–298.
11. Ripamonti C, Fulfaro F. Malignant bone pain: pathophysiology and treatment. Curr Rev Pain 2000;4(3):187–196.
12. Mercadante S. Malignant bone pain: pathophysiology and treatment. Pain 1997;69(1–2):1–18.
13. Catane R, Beck A, Inbar Y, et al. MR-guided focused ultrasound surgery (MRgFUS) for the palliation of pain in patients with bone metastases: preliminary clinical experience. Ann Oncol 2007;18(1):163–167.
14. Ballantine HT Jr, Hueter TF, Nauta WJ, Sosa DM. Focal destruction of nervous tissue by focused ultrasound: biophysical factors influencing its application. J Exp Med 1956;104(3):337–360.
15. Lele PP. A simple method for production of trackless focal lesions with focused ultrasound: physical factors. J Physiol 1962; 160:494–512.
16. Sapareto SA, Dewey WC. Thermal dose determination in cancer therapy. Int J Radiat Oncol Biol Phys 1984;10(6):787–800.
17. Fry WJ. Intense ultrasound in investigations of the central nervous system. Adv Biol Med Phys 1958;6:281–348.
18. Jolesz FA, Hynynen K. Magnetic resonance image-guided focused ultrasound surgery. Cancer J 2002;8(suppl 1):S100–S112.
19. Chung AH, Jolesz FA, Hynynen K. Thermal dosimetry of a focused ultrasound beam in vivo by magnetic resonance imaging. Med Phys 1999;26(9):2017–2026.
20. McDannold N, King RL, Jolesz FA, Hynynen K. The use of quantitative temperature images to predict the optimal power for focused ultrasound surgery: in vivo verification in rabbit muscle and brain. Med Phys 2002; 29(3):356–365.
21. Hindman JC. Proton resonance shift of water in the gas and liquid states. J Chem Phys 1966;44(12):4582–4592.
22. Ishihara Y, Calderon A, Watanabe H, et al. A precise mapping using proton chemical shift. Magn Reson Med 1995;34(6):814–823.
23. Cline HE, Hynynen K, Watkins RD. Focused US system for MR imaging-guided tumor ablation. Radiology 1995;194 (3):731–737.
24. Khiat A, Gianfelice D, Amara M, Boulanger Y. Influence of post-treatment delay on the evaluation of the response to focused ultrasound surgery of breast cancer by dynamic contrast enhanced MRI. Br J Radiol 2006; 79(940):308–314.
25. Furusawa H, Namba K, Thomsen S, et al. Magnetic Resonance–Guided Focused Ultrasound Surgery of Breast Cancer: Reliability and Effectiveness. J Am Coll Surg 2006;203:54–63.
26. Furusawa H, Kiyoshi K, Hiroshi Nakahara H, et al. The Evolving Non-Surgical Ablation of Breast Cancer: MR Guided Focused Ultrasound (MRgFUS). Breast Cancer 14:55–58, 2007.
27. Gianfelice D, Gupta C, Kucharczyk W, et al. Palliative Treatment of Painful Bone Metastases with MR Imaging– guided Focused Ultrasound. Radiology; 249(1): 356–363: October 2008.

Nephrogenic Systemic Fibrosis (NSF)—Is the danger real?

Walter Kucharczyk
Departments of Medical Imaging and Surgery (Neurosurgery), University of Toronto, Toronto, Canada

NSF is a very rare systemic disease characterized by formation of connective tissue in the skin which becomes thickened, coarse and hard, sometimes leading to contractures and joint immobility. It was first described in the literature in 2000 with the first report dating back to 1997. The relationship to gadolinium contrast agents was not recognized until several years later.

Patients with NSF can also have involvement of other organs including the lungs, liver, muscles and heart. NSF may develop over a period of a few days or several weeks or months. Five percent of patients have a rapidly progressive and fulminant course. Aside from one to two cases in patients going into acute renal failure, the disease has only been reported in patients with severe (GFR<30 ml/min) or end-stage renal disease (GFR< 15 ml/min). About 90% of all NSF cases have occurred in patients with GFR<15, and the majority of these were on dialysis. The association between NSF and gadolinium-based contrast agents (GBCA) was first described in 2006. Skin biopsy is required in make a definitive diagnosis.

The risk of developing NSF is related to type and dose of GBCA, and the degree of renal failure. The largest number of cases have been reported with Omniscan, with Magnevist being the second most frequently associated agent. Both of these are “linear” GBCA chelates. The incidence per administered dose with the macrocyclic agents has been far less, even allowing for their less frequent use. The number of cases classified by agent, and whether confounded or not confounded, is shown in the table below, excerpted from a presentation by Tim Leiner at the ISMRM annual meeting in May 2008.

Overall Number of Cases with Different Agents

Gd-based CA	Number of reports[1,2]	Unconfounded Cases[1,2]	Confounded Cases[1,2]	Estimated number of administrations[3]
Omniscan®	369	327	42	>40 Million
Magnevist®	125	43	82	>90 Million
Optimark®	20	9	11	> 6 Million
MultiHance®	7	0	7	> 4 Million
ProHance®	8	1	7	>13 Million
Dotarem®	1	0	1	> 10 Million
Vasovist®	1	0	1	< 1 Million
Gadovist®	1	0	1	> 3 Million
Primovist®	0	0	0	< 1 Million

(1) Penfield et al, Sem Dialysis 2008;21:129-84; (2) Personal communications with GE, Bracco, Bayer-Schering Pharma and Covidien; (3) Arlington Medical Resources Database | www.amr-data.com (accessed april 2008)

The recognition of the association between renal failure, GBCA type, and GBCA dose in 2006 was widely disseminated through the medical community leading to appropriate modifications of indications, contra-indications, agent and dose for CEMRI in renally impaired patient. The incidence of new cases of this disease fell dramatically in 2007 and at the time of this writing, no newly diagnosed confirmed cases have occurred in 2008. The data "by date of diagnosis" (*not* "by date reported" to the company) is shown for Omniscan.

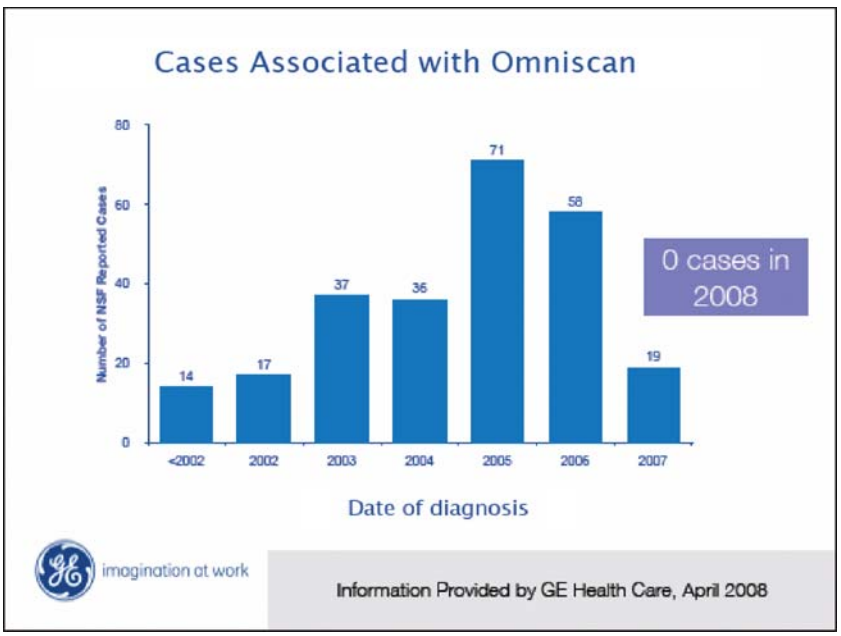

The down-side to these otherwise entirely appropriate actions is that many mildly to moderately renally impaired patients might have been denied the diagnostic benefit of a CEMRI exam for the potential avoidance of an extremely rare disease. This presentation will summarize the existing data, discuss the selection of appropriate diagnostic imaging tests, and provide suggestions for risk avoidance and risk–benefit analysis.

Estimation of tumour growth rates based on sequential MRI and X-ray mammography measurements of high risk women enrolled in breast cancer screening studies – Consequences for follow ups

Martin O. Leach, Inge-Marie Obdeijn, Wim C. J. Hop, Petrina A. Causer, Ellen Warner, Linda Pointon, Kimberley Hill, Jan G. M. Klijn, Ruth M.L. Warren, Fiona J. Gilbert, Madeleine M. A. Tilanus-Linthorst. (The IMMRIS collaboration)

Cancer Research UK and EPSRC Centre for Cancer Imaging, Institute of Cancer Research and Royal Marsden NHS Foundation Trust, Downs Road, Sutton, Surrey, SM2 5PT, UK. (see reference 1 for full address information)

In sequential screening studies, it is possible to examine scans prior to screen detected or interval detected cancers, to identify earlier evidence of cancer not detected during screening examinations, or to estimate the maximum size of disease that would be likely to be undetected. By taking account of the size of disease at detection, the interval between detection and prior measurements (whether tumour is seen or not seen) and the actual size (or assumed maximum possible non-detectable size), it is possible to estimate the minimum likely growth rate of breast tumours(1).

In this study, images and clinical data for women enrolled in the United Kingdom (2), Dutch (3) and Canadian (4) screening trials for women at familial risk of breast cancer were examined to identify women with invasive cancer in whom there were previous MRI and/or X-ray mammography measurements, measuring tumour size at diagnosis and at preceding visits. Tumour doubling time was assessed in 100 women.

Measurements were performed in 43 women with a BRCA1 mutation, 16 women with a BRCA2 mutation and 41 women at high risk without an identified mutation.

Tumour growth rate reduced as age increased (P=0.004). The tumour doubling time in BRCA1/2 mutation carriers diagnosed at ages ≤40, 41–50, >50 years was 28, 68 and 81 days respectively, compared with 83, 121 and 173 days for the high risk group. Compared with high risk women, growth was twice as fast in BRCA1 (P=0.003) and BRCA2 (P=0.03) mutation carriers. The pathological size of detected disease decreased with increasing age (P=0.001), with a median size of 9 mm in women >40 years, and 15 mm for women ≤40 years (P=0.003). The tumours were seen to be larger in young women with BRCA1 mutations.

This study indicates that age and mutation status are important factors in growth rate, with implications for the design of screening procedures.

References

1. Madeleine M.A. Tilanus-Linthorst, Inge-Marie Obdeijn, Wim C.J.Hop, Petrina A.Causer, Martin O. Leach, Ellen Warner, Linda Pointon, Kimberley Hill, Jan G.M. Klijn, Ruth M.L. Warren, and Fiona J. Gilbert
BRCA1 Mutation and Young Age Predict Fast Breast Cancer Growth in the Dutch, United Kingdom, and Canadian Magnetic Resonance Imaging Screening Trials
Clin Cancer Res 2007;13(24) 7357–62

2. Leach MO, Boggis CR, Dixon AK, et al.; MARIBS study group. Screening with magnetic resonance imaging and mammography of a UK population at high familial risk of breast cancer: a prospective multicentre cohort study (MARIBS).
Lancet 2005;365:1769–78.

3. Kriege M, Brekelmans CTM, Boetes C, et al.
Efficacy of MRI and mammography for breast-cancer screening in women with a familial or genetic predisposition.
N Engl J Med 2004;351:427–37.

4. Warner E, Plewes DB, Hill KA, et al.
Surveillance of BRCA1 and BRCA2 mutation carriers with magnetic resonance imaging, ultrasound, mammography and clinical breast examination.
JAMA 2004;292: 1317–25.

Evaluation of density in relation to genetic mutations

Martin O Leach, Deborah Thompson, Gek Kwan-Lim, Simon A Gayther, Susan J Ramus, Iqbal Warsi, Fiona Lennard, Michael Khazen, Emilie Bryant, Caroline Boggis, Sadie Reed, D Gareth Evans, Ros Eeles, Douglas Easton, Ruth Warren, on behalf of The UK study of MRI screening for breast cancer in women at high risk (MARIBS).

Cancer Research UK and EPSRC Centre for Cancer Imaging, Institute of Cancer Research and Royal Marsden NHS Foundation Trust, Downs Road, Sutton, Surrey, SM2 5PT, UK. (see reference 5 for full address information)

Mammographic density is an independent risk factor for breast cancer, resulting in an increase in risk of 4–6 fold in women with dense breast compared with those with fatty breasts (1). Mammographic breast density is usually assessed by visually, in some cases using a scoring scheme, or using two-dimensional interactive computer programs such as CUMULUS (2) that calculate percentage mammographic density and dense breast area. These methods are based on assessment of the 2D projection mammograms. We have developed a method of assessing the proportion of water based tissue in the breast based on 3D images obtained in MRI breast assessment using MRIBview software (3). The method utilises a high resolution 3D T1 weighted MRI image obtained prior to contrast injection, together with a proton density weighted image that enables a uniformity correction. These formed part of the MARIBS study acquisition protocol (4). The MR density measurement utilises a computer tool that interactively segments water and fat based tissue and incorporates a visual check of accuracy of segmentation.

In a pilot study the MR densities obtained with this tool were compared with mammographic density, calculated by CUMULUS and also evaluated by visual inspection using a 21 point scale. This assessment was performed in 138 subjects who were imaged with both MRI and mammography during the MARIBS study. Comparison of the percent dense (water based) volume on MRI compared with the percent dense area calculated using CUMULUS in 264 breast measurements from 137 women resulted in a correlation factor r=0.78, with a slope of 0.56 (95% CI interval 0.48–0.63, P<0.001). Thus the density values measured by MRI were some 56% of those measured from X-ray mammograms. Comparison of MRI density and percentage area mammographic density assessed visually on a 21 point scale also gave a similar relationship with a slope of 0.56 (95% CI interval 0.47–0.64, P<0.001).

To provide information on the reproducibility of the techniques the percent density for left and right breasts were compared within both modalities. The correlation coefficient for MRI density was 0.95, and for mammography was 0.84. These were not significantly different (P=0.16).

Building on this pilot study, this MRI based density assessment technique, together with the visual and CUMULUS techniques using mammography, has been applied to a larger cohort of 665 MRI images and 607 mammography images obtained during the MARIBS study (5). In this study we compared the techniques, assessed consistency of reading for the techniques, related density measurements to anthropomorphic and hormonal factors known to be associated with breast cancer risk. We also investigated the relationship of density measures with breast cancer mutation status (BRCA1, BRCA2) based on clinical testing, or research testing based on anonymised blood samples. The probability of carrying BRCA1 and BRCA2 gene mutations for the cohort, including women with uninformative BRCA1 or BRCA2 test results, or not tested for BRCA1 or BRCA2, but with family history pedigrees, was assessed using the Boadicea computer program (6).

There was a positive correlation between percent dense volume measured by MRI and percent dense area as measured by the CUMULUS program (correlation coefficient=0.76). Both CUMULUS percent dense area and MRI dense volume were negatively associated with BMI, weight, hip, waist, and chest circumferences, parity and WHR. MRI also showed a possible negative association with previous oral contraceptive use. Mammographic percent dense area was lower in BRCA1 mutation carriers (p=0.001) as was MRI percent dense volume (p=0.010). There was no association with BRCA2 carrier status. Women with absolute MRI dense volume in the higher 50% of the distribution had double the risk of those in the lower 50% (p=0.009). No significant association between density and the presence of a range of single nuclear polymorphisms was seen.

References

1. McCormack VA, Dos SSI. Breast density and parenchymal patterns as markers of breast cancer risk: a meta-analysis. *Cancer Epidemiol Biomarkers Prev* 2006;15:1159–69.

2. Byng JW, Yaffe MJ, Jong RA, et al. Analysis of mammographic density and breast cancer risk from digitized mammograms. *Radiographics* 1998;18:1587–98.

3. Khazen M, Warren RM, Boggis CR, Bryant EC, Reed S, Warsi I, Pointon LJ, Kwan-Lim GE, Thompson D, Eeles R, Easton D, Evans DG, Leach MO: A pilot study of compositional analysis of the breast and estimation of breast mammographic density using three-dimensional T1-weighted magnetic resonance imaging. *Cancer Epidemiol Biomarkers Prev* 2008, 17: 2268–2274.

4. Brown J, Buckley D, Coulthard A, et al. Magnetic resonance imaging screening in women at genetic risk of breast cancer: imaging and analysis protocol for the UK multicentre study. *Magn Reson Imaging* 2000;18:765–76.

5. Deborah Thompson, Martin Leach, Gek Kwan-Lim, Simon A Gayther, Susan J Ramus, Iqbal Warsi, Fiona Lennard, Michael Khazen, Emilie Bryant, Caroline Boggis, Sadie Reed, D Gareth Evans, Ros Eeles, Douglas Easton, Ruth Warren, on behalf of The UK study of MRI screening for breast cancer in women at high risk (MARIBS)[1]. Assessing the usefulness of a novel MRI-based breast density estimation algorithm in a cohort of women at high genetic risk of breast cancer (the UK MARIBS study). *Cancer Epidemiol Biomarkers Prev.* Submitted 2009.

6. Antoniou AC, Cunningham AP, Peto J, Evans DG, Lalloo F, Narod SA, Risch HA, Eyfjord JE, Hopper JL, Southey MC, Olsson H, Johannsson O, Borg A, Pasini B, Radice P, Manoukian S, Eccles DM, Tang N, Olah E, Anton-Culver H, Warner E, Lubinski J, Gronwald J, Gorski B, Tryggvadottir L, Syrjakoski K, Kallioniemi OP, Eerola H, Nevanlinna H, Pharoah PD *et al.*: The BOADICEA model of genetic susceptibility to breast and ovarian cancers: updates and extensions. *Br J Cancer* 2008, 98: 1457–1466.

New Methods in Breast Imaging: PET/CT, Positron Emission Mammography, Scintimammography and Other Molecular Imaging Techniques

Jessica W.T. Leung, M.D.[1,2], Randall A. Hawkins, M.D., Ph.D.[2]
[1]Breast Health Center, California Pacific Medical Center, San Francisco, CA
[2]Department of Radiology and Biomedical Imaging, University of California, San Francisco, School of Medicine

While breast imaging focuses on the detection of breast cancer with appropriate screening, diagnostic, and biopsy methods based on mammography, ultrasound and magnetic resonance imaging (MRI), "functional" or "molecular" imaging methods are showing promise as adjuncts to standard methods for lesion characterization and, perhaps more importantly, for tumor staging and treatment monitoring. These techniques include positron emission tomography-computed tomography (PET/CT), positron emission mammography (PEM), scintimammography, and novel molecular imaging techniques.

Positron emission tomography (PET), including PET/CT and PEM, employ positron-emitting radiopharmaceuticals such as 2-[F-18]-fluoro-2-deoxy-D-glucose (FDG) to generate qualitative images as well as quantitative estimates of biochemical processes. Because most aggressive neoplasms (including invasive breast cancers) have high glucose metabolic rates, PET FDG imaging has emerged as a widely utilized method for tumor detection, staging, and treatment monitoring. However, the relatively limited spatial resolution of PET compared to mammography, ultrasound, and MRI has limited its role in breast cancer detection and diagnosis, although PET FDG imaging has proven to be very useful as a whole body tumor staging and treatment monitoring technique. In an effort to improve the resolution of PET and its potential utility for imaging lesions within the breast itself, dedicated PET breast imaging devices (PEM systems), with smaller fields-of-view than standard whole body PET and PET/CT systems, are now in commercial production.

Paralleling the development of PET and PEM with FDG imaging, investigators have utilized gamma camera technology using the single photon radiotracer Tc-99m sestamibi to detect primary breast cancers. This method, often referred to as "molecular breast imaging" (MBI) takes advantage of the biochemical affinity of breast cancers for Tc-99m sestamibi. This agent is a substrate for the multi-drug resistant (MDR) transport system, and it is actively taken up by breast cancer cells. However, sestamibi uptake, like FDG uptake, is not specific for breast cancer; other pathological as well as physiological processes will result in visible regions of tracer uptake. Similar to the development of PEM systems for dedicated imaging of the breast with PET techniques, smaller dedicated gamma-camera-based imaging systems for MBI imaging are now commercially available, including single and dual detector systems that produce a combination of either planar or tomographic images.

These smaller dedicated gamma camera technology breast imaging devices, like PEM systems, have the advantage of improved resolution because of the small field-of-view and

detector design compared to standard whole body systems. Additionally, because the smaller systems require fewer or smaller detectors than larger systems, they are less expensive than standard systems. However, balanced against the improved resolution and cost effectiveness of these dedicated radioisotope breast imaging devices is the fundamental question: where do these methods fit in the overall management of breast lesions? Is there a role for these methods in the initial detection of breast cancers, interdigitated into the mammography/ultrasound/MRI algorithm, or are they primarily useful in detecting disease recurrence, staging and monitoring treatment responses?

While most of the studies to date with MBI have focused on breast cancer detection, and most of the work with whole body PET/CT deals primarily with disease recurrence and mapping the extent of metastases, both gamma camera and PET methods, using Tc-99m sestamibi and FDG, respectively, can be targeted within the breast specifically or optimized to whole body exams. The ultimate determinant of the utility of these methods will be the emerging data demonstrating the accuracy, sensitivity, and specificity of the methods relative to well established clinical endpoints in managing breast cancer.

Beyond PET FDG and gamma camera sestamibi imaging, there is very active research and development in a wide range of molecular imaging probes which have the potential to more specifically bind to breast cancer cells and to characterize molecular features of the disease (such as estrogen receptor status), which have relevance to disease management. These efforts include: (a) positron emitting radiopharmaceuticals such as F-18 fluoroestradiol for in-vivo characterization of estrogen receptor status (1), F-18-3'-deoxy-3'-fluoro-1-thymidine (F-18 FLT) for evaluation of cancer cell proliferation rates (2), and other radiopharmaceuticals for PET imaging, (b) single photon tracers including labeled monoclonal antibodies (3) for gamma camera and SPECT imaging, and (c) receptor targeted nanoparticles and other agents for breast cancer imaging with optical and MRI techniques (25).

PET Imaging of Breast Cancer: Methods and Detection of Primary Tumor

The tracer FDG is transported across cell membranes by the GLUT transporter system and is then phosphorylated by hexokinase into FDG-6-PO_4. FDG-6-PO_4 is then trapped within the cell associated with mitochondria. Tracer kinetic models of FDG transport and phosphorylation produce estimates of the glucose metabolic rate based upon PET measurements of the total F-18 activity in tissue as represented by PET cross sectional images. Because full quantification of glucose metabolic rates in units of μmol/min/g of tissue using the PET FDG method require kinetic (dynamic) images of a given body region together with blood samples of F-18 to measure the plasma time activity concentration ("input function"), standard clinical studies are usually performed in a "static" mode approximately 40–60 min after the injection of FDG (4).

The total F-18 signal activity (voxel concentration of F-18 on a PET image) is proportional to the glucose metabolic rate at a given point in time, and for simplicity most clinical applications of the PET FDG method produce static images of a given body region (e.g. breast and thorax) or whole body images. With this technique, rather than measuring the absolute value of the glucose metabolic rate with the PET FDG model, the commonly used quantitative index is the "standardized uptake value" (SUV). While the SUV is proportional to the absolute value of glucose metabolism, it is not equal to it. Additionally, because the SUV varies in proportion to the total tissue F-18 concentration, it is actually a function of time (SUV(t)). Most centers do not take into account the time dependency of the SUV index because the F-18 tissue (and tumor) concentration is usually reasonably stable during static image acquisition. Nevertheless, this approximation remains a source of error in routinely performed SUV measurements.

Another source of error in the SUV is the partial volume effect. The SUV values of smaller lesions (in the order of 1–2 cm and smaller) will be underestimated because of signal averaging with background tissue. While both timing and partial volume errors in SUV measurements can be corrected with more rigorous data acquisition and analysis methods, this is usually not done in clinical exams. Therefore, SUV indices must be interpreted with caution (4).

Because aggressive neoplasms (including invasive breast cancers) generally have high glycolytic rates compared to normal tissues, they will appear on a PET FDG scan as a "hot" region, with proportionately high SUV values compared to background tissue. Because the conspicuity of a lesion is a function of both its size and the signal/background ratio in a given image, both the tumor FDG uptake (SUV value) and the background tissue metabolic rate (FDG uptake) will affect PET FDG tumor detection rates. Fat, for example, has lower baseline FDG uptake values than heart, skeletal muscle, or brain. Therefore, primary breast cancers can be detected with PET FDG imaging.

FDG uptake is also increased in sites of inflammation and in other disease states. In some cases, distinguishing cancers from sites of inflammation, particularly recurrent neoplasms following surgery, can be problematic. The primary challenge in detecting primary breast cancers with PET, however, is usually not inflammatory conditions but the relatively small size of the lesions.

Whole body PET and PET/CT systems have a sensitivity of 64%–96%, specificity of 73%–100%, positive predictive value of 81%–100%, and negative predictive value of 81%–100% for detecting primary breast cancers (5) [Figure 1]. However, the sensitivity is lower for smaller lesions (<1 cm), and therefore whole body PET/CT systems are not used to routinely detect primary breast cancers, although these lesions may be detected incidentally in the course of whole body PET imaging if they are sufficiently large. In contrast, PEM systems can detect smaller primary breast cancers because of their improved resolution and sensitivity compared to whole body systems (6) [Figure 2]. In the series by Berg et al., PEM detected 10 of 11 in-situ and 33 of 37 (89%) invasive breast cancers, including one of two T1a and four of six T1b tumors. PEM systems capable of being utilized for biopsies have also been developed (7).

PET and PET/CT in Breast Cancer Staging, Detection of Recurrence, and Treatment Monitoring

Rather than the detection of primary cancers within the breast, the current primary use of PET/CT in imaging breast cancer is whole body imaging for staging and treatment monitoring (4, 8, 9). In this context, whole body PET/CT imaging, usually with multi-detector CT components ranging from 16 to 64 slices, is the dominant device.

No in-vivo technique has a higher sensitivity than sentinel lymph node guided biopsy methods because of the ability of the latter technique to detect micrometastatic nodal involvement. Nevertheless, the specificity of PET imaging for axillary nodal disease in breast cancer patients is high. In a prospective multicenter trial of 360 women with newly diagnosed invasive breast cancer who underwent FDG PET/CT imaging (10), the sensitivity of nodal involvement was 61%, the specificity was 80%, and the positive and negative predictive values were 62% and 79%, respectively. However, when a quantitative SUV-lean (numerical value corrected for lean body mass) threshold of 2.0 was used, the specificity increased to 99%, although the sensitivity was lowered to 25%. The sensitivity for PET FDG imaging was significantly higher for invasive ductal carcinoma than for invasive lobular carcinoma.

Another prospective study (11) demonstrated positive predictive values of PET FDG imaging for axillary involvement of greater than 98%, leading to the suggestion than in some patients sentinel node biopsies may be unnecessary. However, because of the high sensitivity and diagnostic accuracy of sentinel lymph node guided biopsies, it is very likely that this procedure will remain the appropriate nodal staging tool in the majority of breast cancer patients.

A particular strength of FDG PET/CT imaging is identifying distant metastases and disease recurrence. In brief, PET/CT is generally more sensitive than the combination of plain films, ultrasound, and bone scans for detection of metastases and disease recurrence (4). Lytic osseous lesions in particular tend to be highly FDG avid, and in this context PET/CT can be both more sensitive and more specific than nuclear medicine bone scans in detecting osseous metastases. Blastic osseous metastases often have lower FDG avidity than lytic lesions. In breast cancer patients, lytic lesions become sclerotic during healing, in which case FDG uptake also decreases.

Another important application of FDG PET/CT is mapping the response to neoadjuvant and other forms of chemotherapy. Serial decreases in SUV indices in primary tumors and metastases correlate well with clinical responses to treatment. Kim et al. (12) demonstrated a sensitivity of 85% and 82%, respectively, in differentiating neoadjuvant therapy responders from non-responders using a criterion of a 79% decrease in the SUV to make this distinction. Other series have also demonstrated the utility of serial changes in SUV values of metastases in distinguishing responders from non-responders to systemic chemotherapy (4, 8, 9). While encouraging, these results are complicated by methodological issues encountered in accurately measuring SUV values in a reproducible fashion as discussed previously. More prospective trials are needed that will help both standardize methods of data analysis and generate numerical criteria that will more accurately distinguish between responders and non-responders.

Sestamibi Breast Imaging

Technetium (Tc)-99m labeled sestamibi is a cationic compound that is internalized in a variety of tumor cells and normal tissues. Clinicians use it as a SPECT myocardial perfusion agent for detection of coronary artery disease because of its flow dependent tissue uptake, and it is also useful to detect parathyroid adenomas. Of specific relevance to breast cancer, sestamibi is internalized in many types of cancer cells, and it is also a substrate for the membrane associated permeability glycoprotein (P-glycoprotein), which is a key component of the multi-drug resistance (MDR) external transporter system (13, 14, 15).

These biochemical characteristics of sestamibi explain a potential inverse correlation between Tc-99m sestamibi uptake in breast cancer cells and the level of membrane-associated P-glycoprotein. Mubashar et al (16) demonstrated the potential use of Tc-99m sestamibi imaging in patients treated with a modulator of the MDR system (toremifene) as a practical method to identify the presence or absence of a functioning MDR system in breast cancer patients prior to chemotherapy. While this remains an intriguing potential application of Tc-99m sestamibi imaging, the large clinical experience with the method is now focused on detection of primary breasts cancers [Figure 3]. The relatively complex biodistribution of Tc-99m sestamibi outside of the breast has limited its use as an agent to detect distant metastases and to measure treatment responses, unlike the experience with PET FDG imaging.

Most of the current clinical experience with single head dedicated gamma camera breast imaging devices is based on planar images acquired in the craniocaudal and mediolateral oblique projections to facilitate comparison with mammography. Potential advantages of Tc-99m sestamibi scintimammography compared to mammography are: (1) independence from breast density in depicting lesions; (2) no need for significant compression during image acquisition. Hruska et al. (17) found that Tc-99m sestamibi scintimammography ("Molecular Breast Imaging" or MBI) consistently identified mammographically occult lesions with a false positive rate lower than mammography. They also demonstrated a high concordance in 47 of 48 patients undergoing both MRI and MBI at the Mayo Clinic. In one patient in their series, two cancers were detected with MRI that were missed with MBI. In a retrospective review of 146 patients, Brem et al. (18) correctly identified cancers in 80 of 83 malignant lesions (96.4% sensitivity). The smallest invasive cancer and smallest DCIS lesion were 1 mm in size. Additionally, they identified occult cancers not seen at mammography or ultrasound in 6 patients. They detected five of six in situ carcinomas less than 1 cm, and 16 of 18 invasive cancers (89%) less than 1 cm. These investigators employed a single detector dedicated breast imaging device, resulting in images they referred to as "breast-specific gamma imaging" (BSGI). Acquired in a planar imaging format, this commercially available system has consistently demonstrated a high sensitivity, but relatively low specificity, for detection of primary breast cancers.

In another retrospective study, Brem et al. (19) evaluated 20 women with 22 biopsy-proven DCIS lesions. Seven patients (with eight biopsy proven DCIS foci) also underwent MRI. The histologic size of DCIS ranged from 2 mm to 21 mm. The overall sensitivity for DCIS was 82% for mammography, 91% for BSGI, and 88% for MRI, although no statistically significant difference between the three modalities was seen. The same investigators also demonstrated a similar trend of higher sensitivity of BSGI compared to mammography, ultrasound, and MRI (without statistically significant differences) in a series of 26 women with 28 biopsy proven invasive lobular carcinomas (20).

As an alternative to BSGI utilizing a single head gamma detector system, dual head dedicated gamma camera breast imaging systems are becoming available (21). These systems have the advantage of improved energy and spatial resolution compared to the single detector BSGI systems. In a direct comparison of the single versus dual detector approach in a series of 150 patients with suspicious lesions measuring less than 2 cm at mammography or ultrasound, 128 cancers in 88 patients were identified (21). The sensitivity for detection of cancers less than 1 cm was 82% (50/61) for the dual detector system compared to 68% (41/61) for the single head system.

New Optical and MRI Methods

There is great interest in evolving optical and MRI methods directed at breast cancer detection and characterization. While these methods remain investigational at this time, they show promise for the future both because of the low risk of the methods (no ionizing radiation) and because of potentially unique tissue characterization capabilities.

Tromberg et al. recently reviewed the potential of diffuse optical imaging technologies for breast cancer management (22, 23). These optical imaging methods, using near-infrared light to image the optical properties of deep tissues (such as the breast), have the potential to assist in distinguishing between benign and malignant breast lesions. It is also a potential tool for evaluating the effects of neoadjuvant chemotherapy.

Beyond the now widely utilized and evolving use of gadolinium enhanced MRI using 1.5 T and 3.0 T systems in breast cancer patients, there are two additional MRI applications which are now largely in the pre-clinical investigation stage. These applications have the potential to further refine detection and tissue

characterization in breast cancer patients. These include MR spectroscopy (MRS) (24) and targeted contrast agents, such as nanoparticles (25). Of these two general approaches, MRS is more likely to be clinically applicable in the near future because it utilizes standard 1.5 T or 3.0 T systems now in production with an approved contrast agent (gadolinium). New contrast agents, such as nanoparticles and other molecular MRI probes, must first navigate through a more complex regulatory approval process prior to clinical implementation. When administered in pharmacologic doses required to generate a useful MR signal, such contrast agents may potentially induce side effects, such as nephrogenic systemic fibrosis syndrome which is now recognized as a potential complication with gadolinium contrast in patients with compromised renal function (26).

Conclusions

New breast imaging methods must develop in a challenging imaging environment already populated by the successful imaging combination of mammography, ultrasound, and MRI for breast cancer detection and diagnosis. While PET and gamma camera based technologies are now approved for clinical use and are increasingly utilized, their precise role in the detection and diagnosis of breast cancer remains to be more precisely defined. While whole body PET/CT imaging has now become a standard method for detecting distant metastases in breast cancer patients, both PET methods (PEM) and gamma camera based breast imaging methods such as MBI need further clinical validation before becoming standard clinical tools. At this point, both PEM and MBI show promise as adjunct methods in subsets of patients with non-diagnostic mammograms (e.g. dense breasts), and also may be more specific than MRI in some patient groups.

Now largely in preclinical studies, optical and new MR methods (MRS and novel contrast agents) also appear promising, but they are not yet at the point of multi-center clinical trial implementation that will be necessary to define their clinical role in breast imaging. Nevertheless, these emerging techniques will likely herald the advent of tumor-specific molecular imaging of the breast.

References

1. Dehdashti F, Mortimer JE, Siegel BA, et al. Positron tomographic assessment of estrogen receptors in breast cancer: comparison with FDG-PET and in vitro receptor assays. J Nucl Med 36:1766–1774, 1995.
2. Direcks WG, Berndsen SC, Proost, et al. F-18 FDG and F-18 FLT uptake in human breast cancer cells in relation to the effects of chemotherapy: an in vitro study. Br J Cancer 99:481–487, 2008.
3. McLarty K, Cornelissen B, Zhongli C, et al. Micro-SPECT/CT with In-111-DTPA-Pertuzamab sensitively detects Trastuzumab-mediated HER2 downregulation and xenografts. J Nucl Med 50: 1340–1348, 2009.tumor response in athymic mice bearing MDI-MB-361 human breast cancer
4. Franc BL, Hawkins RA. Positron emission tomography, positron emission tomography-computed tomography, and molecular imaging of the breast cancer patient. Semin Roentgenol 4: 265–279, 2007.
5. Scheidhauer K, Walter C, Seemann MD. FDG PET and other imaging modalities in the primary diagnosis of suspicious breast lesions. Eur J Nucl Med Mol Imaging 31(suppl 1): S70–S79, 2004.
6. Berg WA, Weinberg IN, Narayanan D, et al. High-resolution fluoro-deoxyglucose positron emission tomography with compression (positron emission mammography) is highly accurate in depicting primary breast cancer. Breast J 12:309–323, 2006.
7. Raylman RR, Majewski S, Smith MR et al. The positron emission mammography/tomography breast imaging and biopsy system (PEM/PET): design, construction and phantom-based measurements. Phys Med Biol 53: 637–653, 2008.
8. Lee JH, Rosen EL, Mankoff DA. The role of radiotracer imaging in the diagnosis and management of patients with breast cancer: Part 1—Overview, detection, and staging. J Nucl Med 50: 569–581, 2009.
9. Lee JH, Rosen EL, Mankoff DA. The role of radiotracer imaging in the diagnosis and management of patients with breast cancer: Part 2—response to therapy, other indications, and future directions. J Nucl Med 59: 738–748, 2009.
10. Wahl RL, Siegel BA, Coleman RE, et al. Prospective multicenter study of axillary nodal staging by positron emission tomography in breast cancer: a report of the staging breast cancer with PET study group. J Clin Oncol 22: 277–285, 2004.
11. Gil-Rendo A, Zoroze A, Garcia-Velloso MJ, et al. Fluorodeoxyglucose positron emission tomography with sentinel lymph node biopsy for evaluation of axillary involvement in breast cancer. Br J Surg 93: 707–712, 2006.
12. Kim SJ, Kim SK, Lee ES, et al. Predictive value of FDG PET for pathological response of breast cancer to neoadjuvant chemotherapy. Ann Oncol 15: 1352–1357, 2004.
13. Scheper RJ, Broxterman HJ, Scheffer GL, et al. Overexpression of a M(r) 110,000 vesicular protein in non-P-glycoprotein-mediated multidrug resistance. Cancer Res 53:1475–1479, 1993.
14. Chen CJ, Chin JE, Ueda K, et al. Internal duplication and homology with bacterial transport proteins in the ndr1 (P-glycoprotein) gene from multidrug-resistant human cells. Cell 47: 381–389, 1986.
15. Piwnica-Worms D, Rao VV, Kronauge JF et al. Characterization of multidrug resistance P-glycoprotein transport function with an organo-technetium cation. Biochemistry 34:12210–12220, 1995.
16. Mubashar M, Harrington KJ, Chaudhary KS, et al. Tc-99m sestamibi imaging in the assessment of toremifene as a modulator of multidrug resistance in patients with breast cancer. J Nucl Med 43:519–525, 2002).
17. Hruska CB, Boughey JC, Phillips SW, et al. Scientific Impact Recognition Award: molecular breast imaging: a review of the Mayo Clinic experience. The American Journal of Surgery 196: 470–476, 2008.
18. Brem RF, Floerke AC, Rapelyea JA, et al. Breast-specific Gamma Imaging as an adjunct imaging modality for the diagnosis of breast cancer. Radiology 247:651–657, 2008.
19. Brem RF, Fishman M, Rapelyea JA. Detection of ductal carcinoma in situ with mammography, breast specific gamma imaging, and magnetic resonance imaging: a comparative study. Academic Radiology 14:945–950, 2007.
20. Brem RF, Ioffe M, Rapelyea JA, et al. Invasive lobular carcinoma: detection with mammography, sonography, MRI and breast-specific gamma imaging. AJR 192:379–393, 2009.
21. Hruska CB, Phillips SW, Whaley DH, et al. Molecular breast imaging: use of a dual-head dedicated gamma camera to detect small breast tumors. AJR 191: 1805–1815, 2008.
22. Tromberg BJ, Pogue BW, Paulsen KD, et al. Assessing the future of diffuse optical imaging technologies for breast cancer management. Med Phys 35: 2443–24451, 2008.
23. Chung SH, Cerussi AE, Clifa C, et al. In vivo water state measurements in breast cancer using broadband diffuse optical spectroscopy. Phys Med Biol 53: 6713–6727, 2008.
24. Sardanelli F, Fausto A, Leo G, et al. In vivo proton MR spectroscopy of the breast using the total choline peak integral as a marker of malignancy. AJR 192: 1608–1617, 2009.
25. Yan L, Peng X-H, Wang YA, et al. Receptor-targeted nanoparticles for in vivo imaging of breast cancer. Clin Cancer Res 14: 4722–4732, 2009.
26. Morris MF, Zhang Y, Zhang H, et al. Features of nephrogenic systemic fibrosis on radiology examinations. AJR 193: 61–69, 2009.

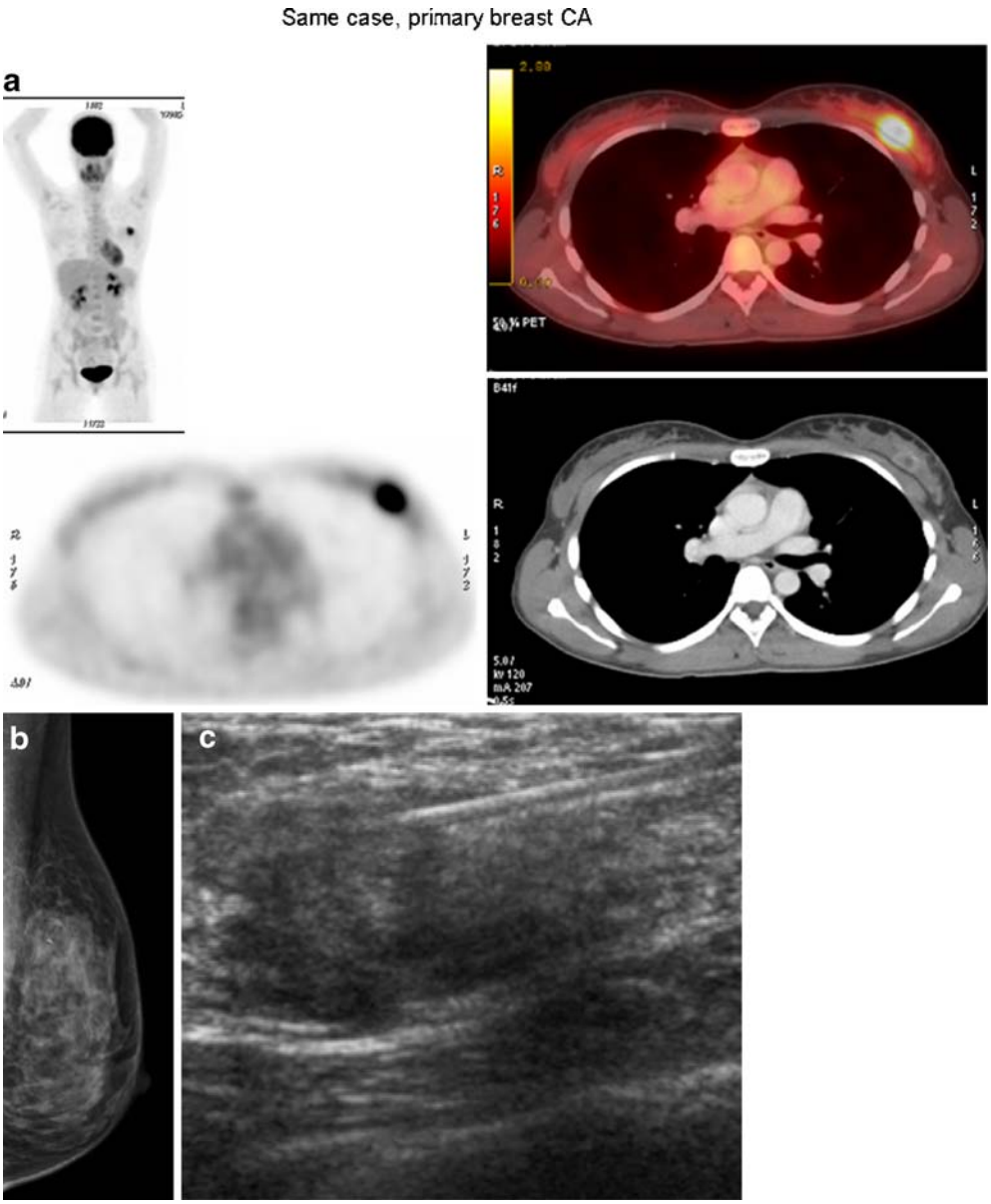

Figure 1: Biopsy-proven invasive ductal carcinoma, occult at mammography but seen at PET-CT and ultrasound A. PET-CT images in axial and coronal projections demonstrate focus of increased uptake in left breast. B. Ultrasound shows an ill-defined hypoechoic mass. Ultrasound-guided core biopsy reveals invasive ductal carcinoma. C. Post-biopsy mammogram in lateral projection shows presence of the biopsy clip, but no mammographic sign of cancer is seen. This invasive ductal carcinoma is occult at mammography.

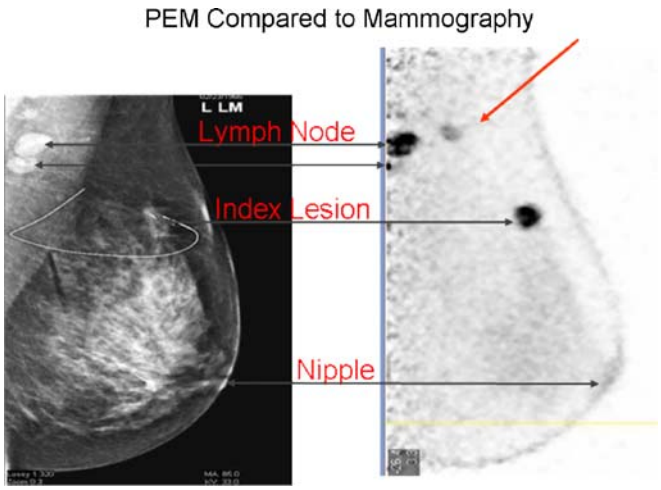

Figure 2 Positron emission mammogram (PEM) shows the presence of a second site of cancer in patient with known primary site of cancer. This second cancer is not detected at mammography. (Images in figure 2 courtesy of Naviscan)

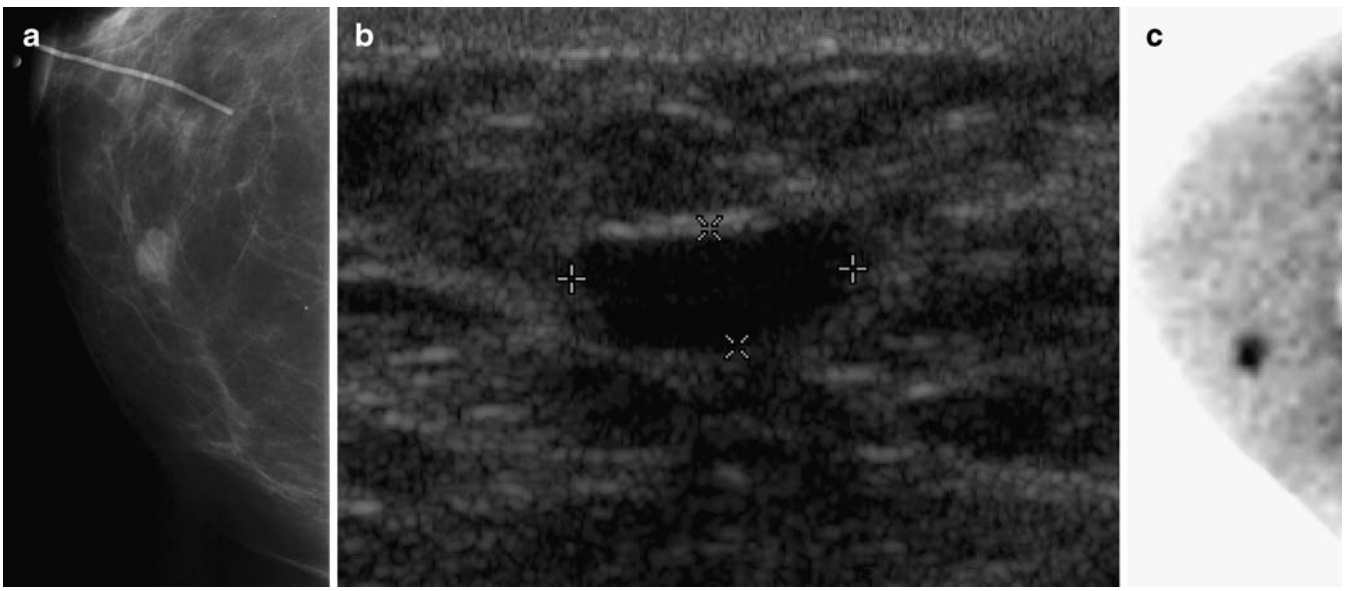

Figure 3: Biopsy-proven low-grade ductal carcinoma in-situ, in which sestamibi scintimammogram is more accurate than ultrasound. A. Mammogram in craniocaudal projection shows an ovoid mass in the inner aspect. B. Ultrasound shows an anechoic ovoid mass consistent with a benign cyst. C. Sestamibi scintimammogram in the craniocaudal projection shows an ovoid focus of increased uptake. (Images in figure 3 courtesy of Dilon)

Lessons from a surgeon: MRS on Fine Needle Biopsy (FNA): Clinical Application in the Diagnosis and Staging of Breast Cancer

Peter Malycha[1] AM FRACS FRCS, and Carolyn Mountford[2] DPhil
[1]Department of Surgery, Royal Adelaide Hospital, North Terrace, Adelaide 5000, Australia.
[2]Centre for Clinical Spectroscopy, Department of Radiology, Brigham & Women's Hospital, Harvard Medical School, Brigham Circle, BC-3-010-CC, and Boston, MA 02120, USA

With current developments there is a good chance that magnetic resonance spectroscopy (MRS), used to analyze fine needle aspirate from the breast, will change the way in which we manage this disease (1–3). MRS, the first of the molecular imaging techniques, has been slow to be accepted into routine clinical practice. There are several reasons for this. The first is the lack of a robust and automated MR system that could be used by hospital technicians. This problem has been recently overcome by the Liposciences Group (4) in their quest for an automated measurement of serum lipoproteins. We now are attempting to emulate this development for the breast biopsy program. This project is underway and is one of several programs aimed at using MRS of specimens to provide predictive information not available by any other method. Another example comes from our colleagues in Canada who have used MRS to analyze stool and, when combined with appropriate data analysis methodology, has the potential to detect colorectal neoplasia accurately and reliably (5).

The success of the breast method depends upon an ability to obtain approximately 1×10^6 cells that are representative of the tumor. Depending upon the country in question this may be undertaken by the surgeon, radiologist or cytologist. A quality FNA from the breast lesion is needed and this can be achieved using a 23 gauge needle and the use of ultrasound guidance. Some groups now use MRI guided biopsy procedures. In those countries where a core is preferred by the pathologist the FNA needs to be taken prior to the core.

The original research, performed in Australia between 1996 and 2006 (1–3), was directed towards showing that a malignant breast cancer spectrum, which differed from a benign spectrum, could be used to diagnose breast cancer, at 8.5 Tesla, by comparing the ratio of the choline to creatine resonances at 3.23: and 3.05 (3). This provided an accuracy of 96% (Figure 1).

It was recognized that there were many chemical species appearing and altering during the transition from benign to malignant including going through the various categories of DCIS (Figure) 2 (6). These changes were often subtle and many occurred at the same time. Also in any one specimen there could be several categories present at any one time. This provided a dilemma for the interpretation of the data since if there was less than 5% of a clinically important pathology could it be recognized by the human eye from a spectrum.

Over the next 10 years a self propagating computer generated algorithm was developed from 40 plus chemical species available for interrogation. The pattern recognition method called "Statistical Classification Strategies" (SCS) was developed in collaboration with Ian Smith and his colleagues at the National Research Council of Canada (7–9). The pattern recognition method took MRS from being subjective to objective and did not rely on prior knowledge for spectral analysis. Clinically this opened many more opportunities.

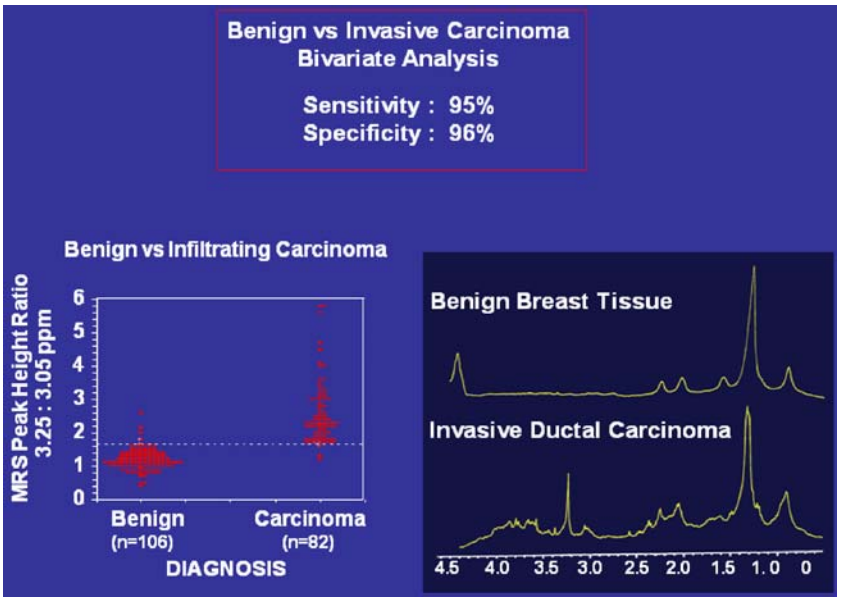

Figure 1. Right ^{1}H MR spectra (8.5T, 37°C) of breast fine needle aspiration biopsies (FNA) with SNR>10. A) Malignant; B) Benign. Spectra were acquired over a sweep width of 3,597 Hz, 8,192 data points, 256 accumulations and a relaxation delay of 2 s. A plot of the ratio of choline to creatine. Reprinted from Radiology (2) with permission.

The SCS method confirmed that reported by the visual interpretation of the spectra and showed the MRS method to distinguish between benign and malignant breast disease with the same accuracy of 96% (10). However SCS was also able to identify which cancers had already metastasized to axillary lymph nodes (1). MRS/SCS predicted the presence of nodal metastases, sensitivity 96% and specificity 94%. The obverse held by predicting node negativity, sensitivity 94%, specificity 96%.

MRS/SCS was also able to assess lymphovascular invasion and oestrogen and progesterone receptor status with a lesser but impressive accuracy. Similarly MRS/SCS was able to distinguish the degree of invasion of tumors and also identify in situ disease.

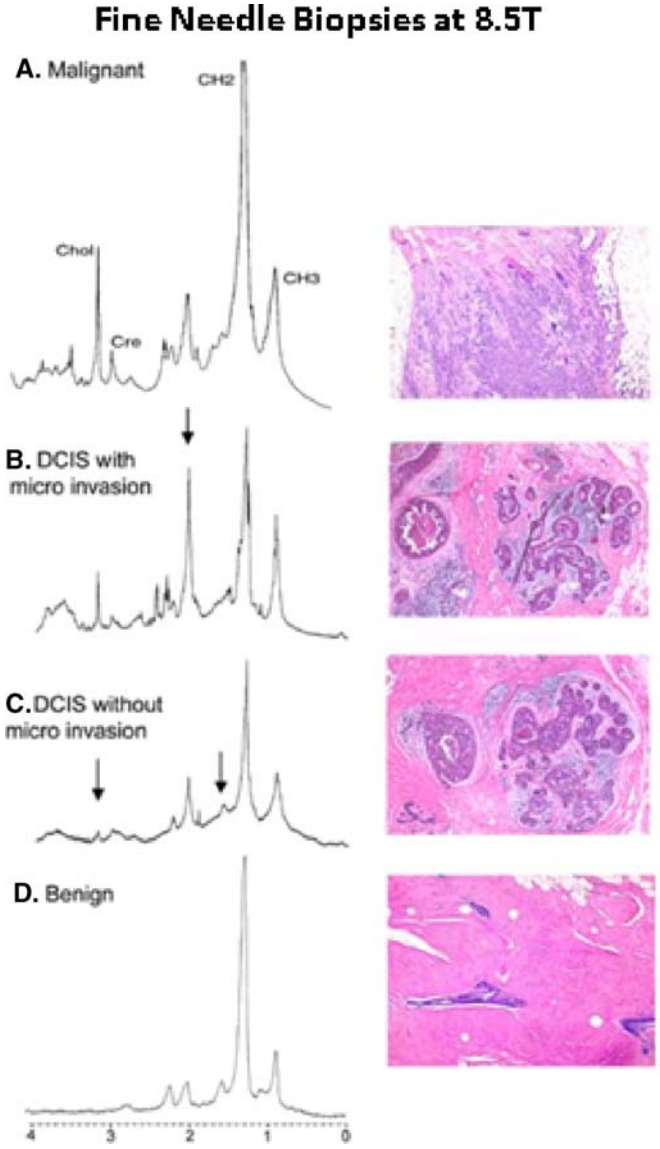

Figure 2 Spectra of in situ and invasive cancer obtained by FNA. MRS/SCS provides much more information than visual inspection 1H MRS of FNA specimens obtained in an 8.5 T Bruker MR spectrometer. SW 3597 Hz, 8192 data points, NS=256 and a TR of 2 s.
A. malignant tissue;
B. DCIS with microinvasion;
C. DCIS without microinvasion;
D. benign control tissue.
Spectra are on the left, and correlation histology is on the right. Difference in 1H MR spectra at 8.5 T predicts the histology. Taken from British Journal of Surgery 2001:88:1234–40, with permission from John Wiley & Sons Ltd.

The accuracy of the MRS/SCS method relied upon detailed histopathology and clinical documentation. The surgical and pathology teams were integral to the success of the method. The correlative pathology was achieved by providing the pathologist with the tissue around the end of the needle track for serial sectioned pathology. Fine needle aspiration samples and a 2×2×1 mm piece of corroborative breast cancer tissue were taken at operation with both specimens stored in liquid nitrogen before being sent MRS and histopathology. The remainder of the breast cancer tissue was sent for standard paraffin section histopathology where type, size, grade, the presence of lympho-vascular invasion and nodal status were reported in the synoptic format recommended by the National Breast Cancer Centre. The initial work was done before we adopted sentinel node biopsy (SNB) as our recommended axillary surgery for early breast cancers.

While this presentation will review the history of MRS of FNA of the breast it will also focus on the role of the new platform being prepared for use in hospitals and pathology laboratories. MS Cognosis is a clinical development arm that has been established to move MRS for breast lesions into clinical practice***. The use of the MS Cognosis technology will involve the radiologist or surgeon taking a FNA sample before any other invasive procedure is performed, expelling the small amount into a vial and then placing it in liquid nitrogen for transport to the vertical bore magnet. The spectral information can be obtained within 10 min, the SCS applied and a report provided. It is envisaged that a report that will state whether benign or malignant, the axillary nodal status and comment on lympho-vascular invasion and receptor status. Included will be an analysis of its accuracy, crispness and predictive value which can then be used alongside other clinical material upon which decision making depends.

If MR Cognosis can be developed as expected, axillary surgery will be performed only when this and perhaps other clinical factors indicate. Sentinel node biopsy would become redundant. Her 2 and modern hormone receptor analyses that are now used in breast cancer will need to be incorporated in the new classifiers. Finally this method lends itself to assisting the surgeon during surgery by providing an immediate report on the margins of the tumor to ensure complete removal of the tumor.

*** Neither of the authors have a shareholding in the company Cognosis nor have ownership of the related patents. Both are on the Scientific Advisory Board.

References

1. Lean C, Doran S, Somorjai RL, Malycha P, Clarke D, Himmelreich U, Bourne R, Dolenko B, Nikulin AE, Mountford C. Determination of grade and receptor status from the primary breast lesion by magnetic resonance spectroscopy. Technology in Cancer Research & Treatment 2004;3(6):551–556.
2. Mackinnon WB, Barry PA, Malycha PL, Gillett DJ, Russell P, Lean CL, Doran ST, Barraclough BH, Bilous M, Mountford CE. Fine-needle biopsy specimens of benign breast lesions distinguished from invasive cancer ex vivo with proton MR spectroscopy. Radiology 1997;204(3):661–666.
3. Mountford CE, Somorjai RL, Malycha P, Gluch L, Lean C, Russell P, Barraclough B, Gillett D, Himmelreich U, Dolenko B, Nikulin AE, Smith IC. Diagnosis and prognosis of breast cancer by magnetic resonance spectroscopy of fine-needle aspirates analysed using a statistical classification strategy. Br J Surg 2001;88(9):1234–1240.
4. Liposcience. NMR LipoProfile: uncover the unseen risk. Volume 2002: Liposcience.
5. Bezabeh T, Somorjai R, Dolenko B, Bryskina N, Levin B, Bernstein C, Jeyarajah E, Steinhart A, Rubin D, Smith I. Detecting colorectal cancer by 1H magnetic resonance spectroscopy of fecal extracts. NMR in biomedicine 2009;22(6):593–600.

6. Mountford C, Lean C, Malycha P, Russell P. Proton spectroscopy provides accurate pathology on biopsy and in vivo. Journal of Magnetic Resonance Imaging 2006;24(3):459–477.
7. Lean CL, Somorjai RL, Smith ICP, Russell P, Mountford CE. Accurate diagnosis and prognosis of human cancers by proton MRS and a three stage classification strategy. In: Webb G, editor. Annual Reports NMR Spectroscopy. Volume 48. Guildford: Academic Press; 2002. p 71–111.
8. Somorjai R, Dolenko B, Baumgartner R. Class Prediction and Discovery Using Gene Microarray and Proteomics Mass Spectroscopy Data: Curses, Caveats, Cautions. Bioinformatics 2003;19(12):1484–1491.
9. Somorjai RL, Alexander ME, Baumgartner R, Booth S, Bowman C, Demko A, Dolenko B, Mandelzweig M, Nikulin AE, Pizzi NJ, Pranckeviciene E, Summers AR, Zhilkin P. A Data-Driven, Flexible Machine Learning Strategy for the Classification of Biomedical Data. In: Dubitzky W, Azuaje F, editors. Artificial Intelligence Methods and Tools for Systems Biology. Boston: Springer and Kluwer; 2004.
10. Mackinnon WB, Delbridge L, Russell P, Lean CL, May GL, Doran S, Dowd S, Mountford CE. Two-dimensional proton magnetic resonance spectroscopy for tissue characterization of thyroid neoplasms. World Journal of Surgery 1996;20(7):841–847.

Spectroscopy at 3T: Potential and Pitfalls

Carolyn Mountford DPhil, Saadallah Ramadan PhD, Alex Lin PhD RT, Lisa Bussolari, BSc RT, Tuan Luu BSc RT, Aida Farier RT, Wendy Canty RT, Eva Gombos MD, Peter Stanwell RT PhD. Centers for Clinical Spectroscopy and Breast Imaging, Department of Radiology, Brigham & Women's Hospital, Harvard Medical School, Brigham Circle, BC-3-010-CC, and Boston, MA 02120, USA.

The Potential of Breast Spectroscopy

One dimensional spectroscopy: The potential is for the non invasive and unambiguous diagnosis of breast pathology and the capacity to monitor therapy using one dimensional (1D) magnetic resonance spectroscopy (MRS). The challenge is to generate spectra, as close as possible, to the spectral quality obtained from cell suspensions and fine needle aspirates (FNA) (2). If this can be done then examination of the choline to creatine ratio will distinguish between malignant and benign lesions with an accuracy of approximately 96% (2). The ability to resolve these resonances *in-vivo* is heavily reliant on obtaining high quality localized homogeneity. There are several controllable limiting factors in achieving the required homogeneity that include; the magnet (e.g. ability to minimize the effect of tissue susceptibility through shimming), the breast coil and the operator. With each optimized there are a series of diagnostic resonances available for inspection (Figure 1).

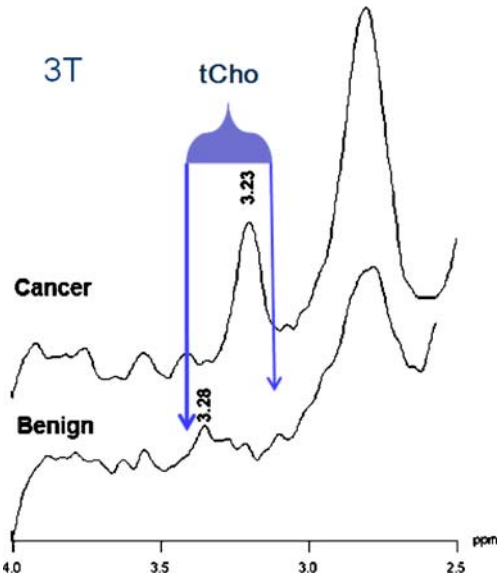

Figure 1. In vivo single voxel spectra (3T, PRESS, TE=135 ms/TR=2,000 ms, 192 signal averages). Spectra are processed as described (1) and were referenced to the methylene resonance of lipid at 1.33 ppm and water at 4.74 ppm. In the spectrum from the cancer bearing patient (top) the resonance is at 3.23 ppm and consistent with phosphocholine. In the spectrum from the fibroadenoma (bottom) the resonance is centred at 3.28 ppm. These spectra were collected using a Siemens Trio with a 4 channel breast coil

Two dimensional spectroscopy: Two dimensional (2D) magnetic resonance spectroscopy (MRS) allows those resonances that are composite in a one dimensional spectrum, to be examined usually as individual components, in a second frequency. The 2D method has allowed the assignment of molecules, that are both diagnostic and prognostic, in the spectra from breast cell lines, tissues(3) and now in vivo Figures 2 and 3. The in vivo 2D spectrum of a healthy breast is shown in Figure 5 (Unpublished data). Cross peaks denoted A–G are from the lipid molecules (some fat and some diagnostic when in a carcinoma) as shown in Structure 1 (4).

An in vivo 2D COSY spectrum, obtained from a malignant breast lesion, is shown in Figure 3. Again the cross peaks denoted A–G are from the lipid molecules as shown in Structure 1 are apparent, however there are clearly multiple types of lipid present as

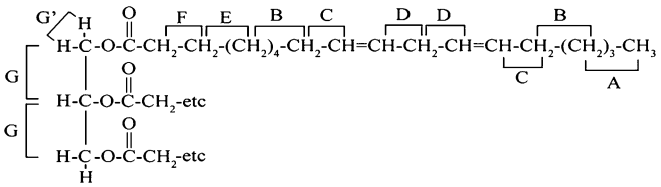

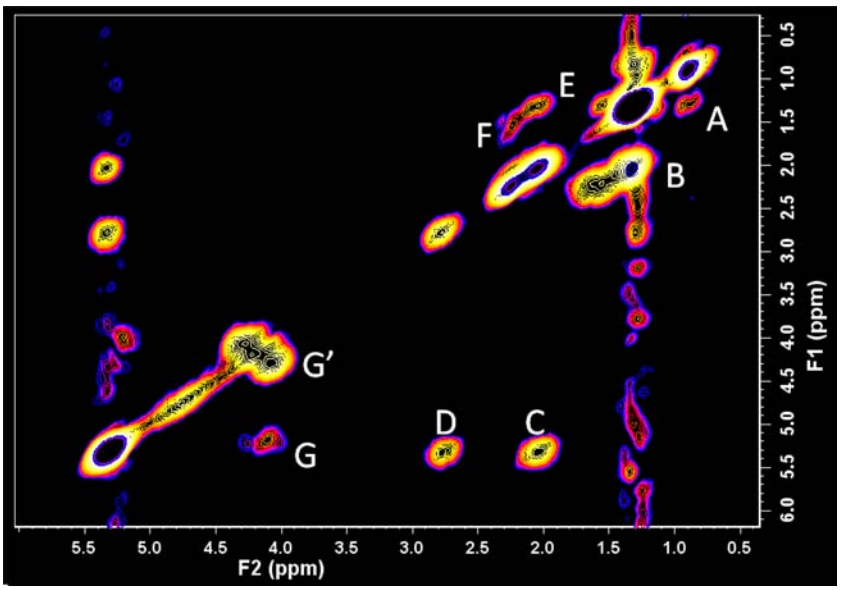

Figure 2. COSY spectrum from a healthy breast. Voxel size: 15×15×15 mm^3. Data was acquired with 4 averages per increment; 96 increments;$TE_{initial}$=30 ms; increment size of 0.8 ms; F2 spectral width: 2,000 Hz; F1 Spectral width: 1250 Hz; TR: 1.5 s; total exp time: 9.6 minutes; acquired points 512; acquisition duration: 256 ms; no water suppression, coil: 16 channel breast coil.

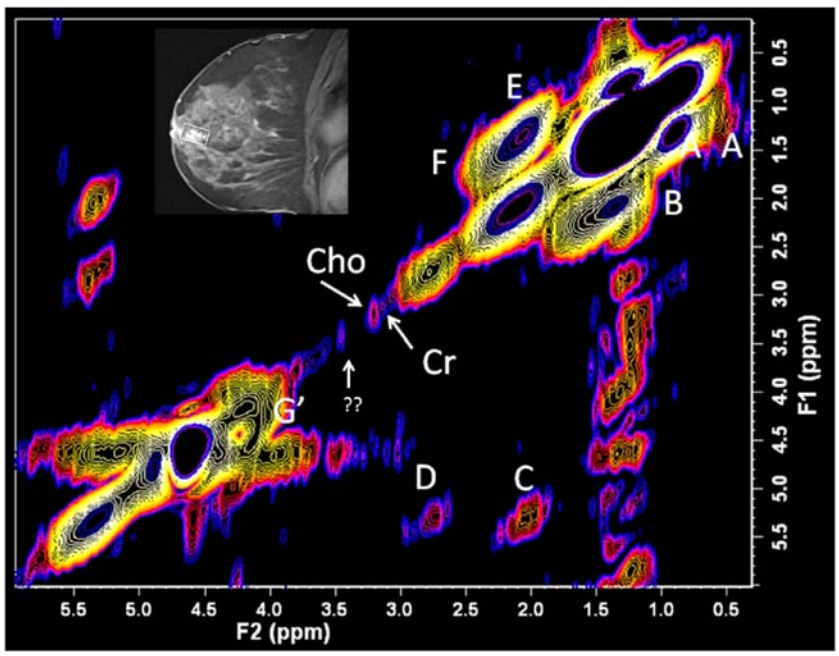

Figure 3. COSY spectrum acquired from a malignant lesion (voxel placement shown top). Experimental parameters: voxel size: 15×15×15 mm^3; 4 averages per increment; 55 increments; TEinitial=30 ms; increment size: 0.8 ms; F2 spectral width: 2,000 Hz; F1 Spectral width: 1,250 Hz; TR: 1.5 s; total exp time: 5.5 min; acquired points 512; acquisition duration: 256 ms, water suppression ON, coil: 7 channel coil.

denoted by the multiple crosspeaks C and D. Of particular interest are the diagonal resonances from choline at 3.23, creatine at 3.05 and an as yet unassigned resonance at 3.40 ppm. The use of the COSY method has overcome the problem of false negatives by resolving the choline and creatine resonances from under the broad fat spectrum. This should now increase the accuracy of the method but this awaits a clinical study. The volume of each of these diagonal species can be measured as previously described (5). This COSY method is still under development and it is expected that the lipid can be further reduced in intensity by adding a further acquisition filter (6).

Current Pitfalls of In Vivo Breast Spectroscopy

In a busy hospital clinic the 1D MRS methods has to be accurate and the data accrued in less than 10 min. If the operator of the scanner is a PhD spectroscopist *and* a trained technologist the result will be diagnostic and accurate. Unfortunately such people are rare and the accuracy of breast spectroscopy today remains site dependent.

The quality of the spectra currently depend upon a series of factors. The size and cellularity of the tumour; whether it is pre or post biopsy (bruising and haematoma generate their own spectrum); magnet frequency; the type of coil i.e. 4, 7 or 16 channel and very importantly, the capacity of the operator to shim the magnet. However with these bases covered at 3 T and using a 7 channel breast coil the choline and creatine resonances are separate entities in tumors above 1 cm in size. For tumours less than a centimeter it is necessary to acquire considerably more data in order for the signal to noise to be adequate for diagnostic information to be recorded. Parameters that need to be taken into consideration for tumors 1 cm and above are described in Stanwell (7).

Breast Coils and Resonance Assignments

At 3 T, using either a 7 or 16 channel breast coil, the data can be accrued with increased SNR per unit time leading to a concomitant reduction in scan time. Using the 7 channel breast coil increased SNR allows for the distinction to be made between resonances at 3.05 ppm (creatine), 3.23 ppm (choline), 3.28 ppm (unassigned) and 3.40 ppm (unassigned). This is in contrast to using the 4 channel coil where 3.05 ppm (creatine) and 3.23 ppm (choline) appear as one resonance but the unassigned resonance at 3.28 pp is separate (Unpublished data).

Why are these distinctions important? The presence of the choline resonance is diagnostic for a malignant tumor (8). In contrast the unassigned resonance at 3.28 ppm is found in some lactating mothers and some healthy women during the menstrual cycle. The presence of a resonance "around 3.2 ppm" is thus not good enough for diagnostic purposes. This means that the spectra have to be very carefully referenced. The water resonance should be at 4.73 ppm and the methylene of the lipid at 1.33 ppm. Incorrect referencing will result in either a false positive or false negative. There are papers in the literature that show spectra that are clearly incorrectly referenced and hence the incorrect diagnosis was reported.

Correlation with Histopathology

Correlation of the spectroscopy data with the general histopathology report is often inadequate. In our studies in Australia the surgeons would be sent an image of the voxel location overlaid on the "best" contrast-enhanced image. An intra operative biopsy would then be obtained for histological correlation with the MRS. This is probably the most difficult part of the study.

Histological correlation for validation of the spectroscopy result by radiological methods is again not trivial . It requires clear knowledge and statement of side, location including quadrant or clockwise location and distance from the nipple as well as exact size of the targeted abnormality. If the lesion is seen by mammography and ultrasound, core biopsy or localization can be performed and specimen radiography or specimen sonography can identify the lesion within the excised tissue. Pathology correlation of lesions detected by MRI only may be quite difficult or in some cases impossible. When spectroscopy examination performed immediately prior to the MR guided biopsy direct correlation can be made with good accuracy.

"Total Choline" a Misnomer

The initial studies introducing MRS to interrogate the pathology of malignant breast lesions was at 1.5 T (9) and one very broad resonance was recorded around 3.2 ppm. Despite the increase in magnet field strength and improved coil technology the term "total choline" is still in use. Unfortunately, its continued use and the lack of attention to shimming and spectral referencing, the reported accuracy of the MRS method is seen as lower than it really should be. In some situations, for example, monitoring therapy, the choline resonance will decrease but other resonances in the region will increase thus negating the recording of the perceived response (10). With the currently available 3 T technology the accuracy of the method will become obvious when all of the resonances in the spectrum are interrogated and carefully correlated with pathology and clinical outcomes.

References

1. Stanwell P, Gluch L, Clark D, Lean C, Giuffre B, Malycha P, Tomanek B, Mountford C. Specificity of choline metabolites for in vivo diagnosis of breast cancer using 1H MRS at 1.5T. European Radiology 2005;15(5):1037–1043.

2. Mackinnon WB, Barry PA, Malycha PL, Gillett DJ, Russell P, Lean CL, Doran ST, Barraclough BH, Bilous M, Mountford CE. Fine-needle biopsy specimens of benign breast lesions distinguished from invasive cancer ex vivo with proton MR spectroscopy. Radiology 1997;204(3):661–666.

3. Ramadan S, Mountford C. Two-Dimensional Magnetic Resonance Spectroscopy on Biopsy and In Vivo. In: Webb GA, editor. Annual Reports on NMR Spectroscopy. Volume 65. Burlington: Academic Press; 2009. p 161–199.

4. May GL, Wright LC, Holmes KT, Williams PG, Smith IC, Wright PE, Fox RM, Mountford CE. Assignment of methylene proton resonances in NMR spectra of embryonic and transformed cells to plasma membrane triglyceride. Journal of Biological Chemistry 1986;261(7):3048–3053.

5. Lean CL, Mackinnon WB, Delikatny EJ, Whitehead RH, Mountford CE. Cell-surface fucosylation and magnetic resonance spectroscopy characterization of human malignant colorectal cells. Biochemistry 1992;31(45):11095–11105.

6. Holmes K, Williams P, Bloom M, Dyne M, Mountford C, King N, Karaman M, Ninham B, Blanden R. Magnetic resonance study of lymphocytes stimulated with concanavalin A. Magnetic Resonance in Medicine & Biology 1988;1:75–79.

7. Stanwell P, Mountford C. In vivo proton MR spectroscopy of the breast. Radiographics 2007;27:S253–S266.

8. Aboagye EO, Bhujwalla ZM. Malignant Transformation Alters Membrane Choline Phospholipid Metabolism of Human Mammary Epithelial Cells. Cancer Research 1999;59:80–84.

9. Roebuck JR, Cecil KM, Schnall MD, Lenkinski RE. Human Breast lesions: Characterization with Proton MR Spectroscopy. Radiology 1998;209:269–275.

10. Baek H-M, Chen J-H, Nie K, Yu HJ, Bahri S, Mehta RS, Nalcioglu O, Su M-Y. Predicting Pathologic Response to Neoadjuvant Chemotherapy in Breast Cancer by Using MR Imaging and Quantitative 1H MR Spectroscopy. Radiology 2009;251(3):653–662.

Michael T. Nelson, M.D.
Professor of Radiology, University of Minnesota Medical Center–Fairview, Minneapolis, MN 55455

Breast MRI is extremely sensitive for breast cancer, but specificity can depend on the magnet, coils, sequences, and personal experience of the radiologist. Breast cancer metabolites can be measured as a biomarker by measuring decrease in tCho after chemotherapy and an increase in tCho in a positive tumor diagnosis seen on MRI and measured by MRS.

We have performed spectroscopy on normal breast tissue at 3 T, 4 T, and 7 T using laser technique with single voxel spectroscopy. Normal breast tissue as well as benign lesions do have normal choline within the tissue; however, cancers metabolites have elevated choline. The tCho can be measured in MLM/kg. Elevated tCho >1.5 means cancer 90% of the time when one has good signal to noise ratio during spectroscopy.

Does MRI spectroscopy help the radiologist in diagnosis breast cancer? To answer this question we did an ROC analysis with expert readers reading blinded MRI/MRS breast cancer studies. The results showed that all expert radiologist readers improved their ROC curves when the tCho of each lesion was presented to them as an addition to normal DCE curves and morphology of breast cancer lesions. These results are encouraging and if tCho could easily (12 min scan) be obtained, it may become a common measurement to help decrease unneeded breast biopsies.

The ability to measure tCho in large tumors undergoing neoadjuvant chemotherapy helps oncologist decide if the chemotherapy is working by measuring tCho at 24-h after the first dose of chemotherapy. If tCho decreases over the baseline (before chemo) then 80% of patients will respond to the chemotherapy regimen (responder). If the tCho is increased or the same, then the chemotherapy is not working and this patient will be a non-responder. Oncologist could use this biomarker measurement to decide which chemotherapy regimen works on each tumor. If the patient is a non-responder then the chemotherapy can be switched by the Oncologist 8–10 weeks before there is a response in size of volume of the tumor. This has lead to a multi-institutional study of ACRIN 6657-I-SPIE to see if these methods will work in multiple platforms (vendors). The study will be 150 patients and include multiple measurements over time (including volume and also biomarkers).

In conclusion MRI/MRS choline measurements will help the radiologist and oncologist improve the diagnosis and treatment of breast cancer.

High Field 3T/4T/7T MRI/MRS in the Diagnosis and Treatment of Breast Cancer

Michael T. Nelson, M.D.
Professor of Radiology. University of Minnesota, Minneapolis, MN, USA

Introduction

In *vivo* proton magnetic resonance spectroscopy (^{1}H MRS) is being used as a clinical tool for diagnosing and characterizing breast cancer. Alterations of the levels of choline containing metabolites, are associated with malignancy and is becoming an important biomarker. High field MRI scanners at 3 T, 4 T, 4 T, and 7 T have been used to evaluate the role of ^{1}HMRS measurement of total choline containing compounds in patients with breast cancer. Newer development in high field MR scanning and quantitative MRS may help breast imagers improve sensitivity and specificity in diagnosing and treating breast cancer.

In *vivo* breast MRS shows a resonance at ~3.2 ppm that is associated with malignancy. A This 3.2 ppm peak includes contributions from choline, phosphocholine, glycerophosphocholine, and several other metabolites. All of these metabolites are called total choline or tCho. This tCho is increased in breast malignancies and this aberrant increase in tCho concentration parallels tumorigenesis with high grade breast cancers associated with increased phosphocholine concentration.

The use of tCho as a diagnostic biomarker in breast cancer has been successfully shown at many institutions using 1.5 T MR. The studies on 1.5 T scanners have not measured Quantitative tCho measurement but have only detected the tCho 3.2 peak, under the assumption that a detectable tCho peak indicates a malignancy. MRS tCho measurements are improved or higher field scanners (3 T and above). The increased sensitivity and greater spectral resolution improves the detectability and quantitation of tCho. The ability to detect in smaller lesions is enhanced at higher field strength.

The quality of MRS measurement depends on MR sensitivity, spectral resolution, voxel localization and elimination of artifacts. Sensitivity increases linearly with voxel volume, Bo field strength, and the square root of the number of averages acquired in the MRI/MRS sequence.

Commercial breast coil design shows a large variation in sensitivity. Commercial breast coils continue to improve with better S/N and will allow better MRI/MRS imaging. The majority of breast MRS quantification has been performed using single voxel spectroscopy (SVS) with localization techniques such as LASER, PRESS or STEAM. These SVS methods are good for MRS of a single breast tumor but will not cover the entire breast.

Clinical Applications of MRI/MRS

Diagnostic MRS

The most widely used application of breast MRS is for diagnosing suspicious breast lesions which enhance on MRI. There has been multiple publications from 1.5 T showing sensitivities of 70–100% and specificities of 67–100%. A retrospective review of five out of eight studies showed an average sensitivity of 83% and specificity of 85%. The ability of clinicians to achieve these results with various MRI/MRS systems and different measuring techniques demonstrates that breast MRS is clinically practical and useful to a breast imager. A recent report compared breast MRI/MRS at 3 T and 1.5 T and reported that tCho could be detected in smaller cancers at 3 T than 1.5 T. At extreme field strength (7 T) tCho can be detected in normal breast tissues.

ROC Analysis

A study by Meisamy et al showed that by adding in Vivo quantitative 1H MR spectroscopy, there was improved diagnostic accuracy of the breast MR interpretation by all expert radiologists in an observer performance (ROC) study at 4 T. The study shows the ability to improve the diagnosis of breast cancer and decrease benign breast biopsies. With the improvement in field strength, breast coils software, and faster computer aided detection, MRI/MRS will become useful as an adjunct to all breast MRI studies.

Monitoring treatment response

Breast MRI/MRS can be used to evaluate treatment response to chemotherapy. The clinical analysis shows that increased tCho reflects aberrant metabolism of tumor cells and cell viability. A decrease in tCho shows that the chemotherapy is effective. This decreased tCho within 24–48 h after chemotherapy shows that the patient will have a positive response to the selected chemotherapy.

Meisamy et al. study showed MRS decreased tCho at 24 h after chemotherapy showing these patients would be “responders” to the course of chemotherapy (10–12 weeks). This is before any change in size of the breast cancer (longest diameter or volume). A total responder to chemotherapy, may show no tCho measurement and no contrast uptake.

ACRIN6657 is a multi-institutional study presently underway to test the single voxel MRS tCho measurement as a biomarker. The ability to measure decreased tCho decreases as tumors shrink. As the tumor decreases in size during chemotherapy, it will cause difficulty in measurement of tCho due to (1). Variation in voxel placement, (2). Partial volume averaging of adipose tissue becomes more of a problem.

Ultra High Field MRS

Higher field MRI scanners (7 T) can increase sensitivity and spectral resolution. The sensitivity of ^{1}H MRS increases linearly with increased field strength so smaller voxel can be obtained. With new bo shimming techniques, higher field gives increased spectral resolution allowing many more chemical resonance (biomarkers) to be resolved. There are multiple problems associated with higher field strengths: (1). Bo shimming is more difficult, (2). Radiofrequency B1 inhomogeneities make coil designs more complicated, (3). Relaxation contents change, (4). Longer T1 value require longer TR's at 4 T, 7 T normal breast tissue choline can be detected and therefore quantitative tCho will be required for evaluating breast cancer detection and treatment.

Conclusion

Proton spectroscopy can provide useful clinical information for patients with breast cancer. Multiple biomarkers including MRI/MRS tCho, DCE, and diffusion imaging all provide new clinical information to clinicians. With further research improved magnets, coils and software, the era of personalized medicine and metabolic imaging has arrived.

Acknowledgement

We would like to acknowledge the following grants from NIH (Grants CA92004. CA120509, RR08079, and RR00400) and the DOD Breast Cancer Research program (DAMD 17-01-1-0331).

References

1. Reis LAG, Eisner MP, Kosary CL, et al. (eds): SEER Cancer Statistics Review 1975–2002. National Cancer Institute: Bethesda, MD. http://seer.cancer.gove/csr/1975_2002/, based on November 2004 SEER data submission, posted online 2005.
2. Aboagye EO, Bhujwalla ZM: Malignant transformation alters membrane choline phospholipid metabolism of human mammary epithelial cells. Cancer Res. 59(1):80–84, 1999
3. Podo F: Tumour phospholipid metabolism. NMR Biomed. 12 (7): 413–439, 1999.
4. Vaughan JT, Garwood M, Collins CM, et al: 7T vs 4T: RF power, homogeneity, and signal-to-noise comparison in head images. Magn. Reson. Med. 46(1): 24–30, 2001.
5. Gruetter R, Weisdorf SA, Rajanayagan V, et al: Resolution improvements in in vivo 1H NMR spectra with increased magnetic field strength. J Magn. Reson. 135: 260–264, 1998.
6. Meisamy S. Bolan PJ, Baker EH, et al: Neoadjuvant chemotherapy of locally advanced breast cancer: predicting response with in vivo 1H Mr spectroscopy: a pilot study at 4T. Radiol 233(2): 424–431, 2004
7. Meisamy S. Bolan PJ, Baker EH, et al: Additin in vivo quantitative 1H MR spectroscopy to improve diagnostic accuracy of breast MR imaging: preliminary results of observer performance study at 4T. Radiol 236(2): 465–475, 2005

Evaluation of Axillary Lymph Nodes: A Challenge?

Gillian M Newstead MD
Clinical Breast Imaging, The University of Chicago, Chicago, USA

Introduction

Axillary lymph node status is an essential prognostic factor in the evaluation of patients with a newly diagnosed breast cancer [1–3]. Fine needle aspiration [FNA] is typically performed for assessment of clinically palpable axillary lymph nodes. Axillary lymph node dissection [ALND] has served as the reference standard for determining lymph node metastasis. A relatively high morbidity is associated with lymph node dissection, and complications such as lymphedema, numbness and limited shoulder movement have been reported [4, 5]. In recent years, up to 70% of patients with breast cancer are shown to be histopathologically node negative at diagnosis largely due to early diagnosis resulting from population-based screening with mammography [6–8]. A newer, less invasive sentinel lymph node biopsy technique has been introduced (SLNB) and is now widely accepted as an alternative to ALND. This technique, although less invasive is time-consuming, requiring surgeons to spend a considerable amount of time in the operating room in order to harvest the nodes, and when frozen section is requested, to wait for pathologists to render an intra-operative histologic diagnosis [9–11]. SLNB however is not perfect, the radioactive tracer injection for SLNB has a variable time-course of biologic distribution, and a small number of patients experience failure to elucidate a sentinel lymph node. More than three sentinel lymph nodes may be detected on occasion (12). A noninvasive technique that could accurately identify metastases in nonpalpable axillary lymph nodes would be beneficial for patients. Various imaging techniques—ultrasonography (US)—magnetic resonance (MR) imaging and computed tomography (CT) and positron emission tomography (PET) have been used for visualization and characterization of non-palpable axillary lymph nodes [5–20]. If reliable, these techniques could provide an alternative diagnostic method to surgical lymph node assessment and avoid the morbidity associated with SLNB. Pre-operative lymph node staging could obviate the need for time-consuming SLNB and allow surgeons to perform ALND directly when positive nodal status can be ascertained pre-operatively (11, 15–23).

Ultrasound

The preoperative imaging assessment of axillary lymph node metastases is currently based mainly on measurements of nodal morphology. Of the various possible imaging modalities, ultrasound has been the most widely used (15–20). Ultrasound is the most useful because of its convenience, general availability, good morphologic visualization of small lesions, and its ability to evaluate blood flow and distribution. Several investigators have reported varying sensitivity of pre-operative ultrasound, with ranges from 35% to 95%, (11, 16, 17, 20–22). Positive indicators for nodal metastasis include cortical thickening, large nodal size, and lobulated shape. A study by Abe et al. (23) suggests that non hilar blood flow (NHBF) may be an important additional indicator for nodal metastasis. Nodal infiltration of metastatic disease, with increased blood flow, probably results in engorged pre-existing peripheral vessels, which are present in perinodal capsular connective tissue around the cortex. Disruption of the hilar blood supply is thought to result from neo-angiogenesis, stimulated by metastases embedded in the small vessels at the cortical periphery (26–28). The presence of NHBF is not a specific characteristic for nodal metastasis and may be seen in other pathologic conditions such as inflammatory processes and reactive nodes. A positive predictive value of 78% (52/67) for nodal metastasis, has been reported when this finding is detected in one or more axillary lymph nodes of patients with known ipsilateral primary breast cancer (23). Other useful findings include absence of the nodal fatty hilum and thickening of the cortex. Deurloo et al. suggested that cortical thickening of at least 23 mm is a good predictor of lymph node metastasis with sensitivity 95% and specificity 44% reported (20). A relative thickness measure of the cortex to the short axis of the lymph node has been proposed, as an alternative to measures of absolute cortical thickness alone. Using this criterion in combination with positive NHBF, higher positive predictive values for nodal metastases (81%) have been reported (23).

Ultrasound-guided Intervention

Some investigators have reported high sensitivity and specificity (sensitivity: 62–86%, specificity: 99–100%) for preoperative lymph node staging using ultrasonography in combination with fine needle aspiration (FNA) (11, 19–23). FNA is often performed as a method of cytologic confirmation of suspicious axillary lymph nodes, as well as for evaluation of supraclavicular and internal mammary chain nodes. The advantage of using FNA for both palpable and nonpalpable node assessment is that the procedure is less invasive, lower risk, cheaper and faster. FNA is more convenient for the patient than core needle biopsy, and multiple nodes may more easily be sampled. FNA techniques however require operator expertise and the cooperation of experienced cytologists, not readily available in many institutions. FNA is most efficacious when a cytologist is available to perform an instant reading on the retrieved material, thereby reducing the likelihood of insufficient or inadequate sampling.

Core needle biopsy is a standard procedure, available at most institutions in the U.S, and is less operator-dependent than FNA in terms of obtaining a good sample. The main concern in performing core needle biopsy within the axilla is to avoid damaging major vessels and nerves because lymph nodes are often located near those structures. Core needle biopsy for axillary lymph node assessment can be done quickly and safely and could become a standard method for preoperative nodal diagnosis. In a study by Abe et al. [23] axillary lymph node biopsy was performed under ultrasound guidance, for 68 patients with breast cancer using a 14 G Achieve needle, yielding a sensitivity of 94% (64/68), with no significant complications. In this study, for the majority (62%) of patients with positive results, the need for a SLNB procedure was obviated. Those patients with a negative core biopsy result however still underwent a SLNB. The axillary node core biopsy technique is not limited to breast cancer cases, and can be used to stage metastases from other carcinomas or lymphomas. A limitation of US-guided core biopsy is that direct correlation between core-biopsied nodes and surgically removed nodes cannot always be made, so it may be uncertain that the node sampled is truly a sentinel node.

MRI

Traditionally, radiologists evaluate MRI and US images of axillary nodes independently, as part of a preoperative imaging protocol. In our practice, all patients with newly diagnosed breast cancer undergo bilateral diagnostic mammography, ultrasound of the ipsilateral breast and axilla, and most patients also receive MR imaging. MRI has the advantage of accurately assessing the size and morphology and location of axillary lymph nodes, which are well seen on T2-weighted 3D non fat-suppressed acquisitions. Normal nodes are visualized at MRI, with fatty hila, smooth margins, and a homogeneous signal. MRI has the capability of showing morphological changes in the lymph node cortex and sinus, which could allow for discrimination between benign and malignant nodes (24, 25). There are very few studies reported in the literature, however Mortellaro et al evaluated the axillary lymph node status in a cohort of 56 patients with breast cancer (26). MR images were evaluated prior to axillary sampling. All SLNB positive patients 27% (15/56), underwent completion axillary dissection. The number of axillary nodes, contrast kinetics, and number of nodes without fatty hilum were recorded. Data were analyzed in the context of final breast pathology, sentinel lymph node status, and axillary nodal status. In this study, the presence of any axillary lymph node without a fatty hilum and the number of nodes without a fatty hilum on MR imaging significantly correlated with pathologic node positivity ($P=0.04$); whereas the kinetic data, number and size of the nodes did not correlate with histology.

Contrast Agents

A lymph node-specific class of MR contrast agents, collectively known as ultrasmall superparamagnetic iron oxide (USPIO) agents have been developed but are not yet approved by the Federal Drug Administration in the United States. These MR contrast agents reportedly allow the identification of malignant nodal infiltration, independently of lymph node size. These agents are classified as nanoparticles (mean diameter, 30 nm), and are composed of an iron oxide core coated with low-molecular-weight dextran. MR imaging is performed before, and within 24–36 h after, intravenous administration of the USPIO contrast agent. Initial data suggests that non-metastatic lymph nodes generally exhibit uptake of contrast material, resulting in decreased signal intensity (SI) on T2-and T2*-weighted MR images. Metastatic lymph nodes generally do not exhibit any uptake, and SI remains unchanged. The lack of change of signal intensity in metastatic lymph nodes has been attributed to replacement of macrophages by metastatic cells which lack reticuloendothelial activity and show no USPIO contrast uptake. Studies of patients with head and neck, urologic, rectal, prostate and breast cancers using USPIO contrast agents, have confirmed the potential for improved detection of lymph node metastases when compared with standard gadolinium-enhanced MRI examinations. Memarsadeghi et al reported on a study of 22 women receiving unenhanced and enhanced UPSIO MR imaging, (27), finding sensitivity, specificity and accuracy of 100%, 98% and 98% respectively, for the 133 nodes evaluated with the UPSIO contrast agent. Further study is needed however before this promising technique gains clinical acceptance.

Can MRI provide prognostic information?

Breast MR imaging provides a measure of tumor angiogenic activity. Routine clinical breast MR image interpretation involves assessment of the kinetic behavior of suspicious enhancing lesions, and classification of the enhancement using standard assessment of the time course curves [28]. It is generally accepted that angiogenesis is required to support cancer growth and metastasis, therefore consideration could be given to the hypothesis that the higher the degree of angiogenesis within a given tumor, the more likely that there will be spread of cancer cells to the draining lymph nodes. Montemurro et al reported that invasive breast cancers with higher angiogenesis are more likely to have positive nodes [29]. Tuncbilek et al have shown correlation between lymph nodes metastasis and washout slope of the primary tumor [30]. Evaluation of a cohort of 62 patients by Bahri et al, found that although the angiogenic activity of breast cancer evaluated by DCE-MRI was significantly higher in node positive compared to node negative patients, it could not predict the nodal status accurately [31].

In the past few years, commercial computer-assisted software, has been widely used by radiologists in order to streamline image analysis. Since automated computerized analysis of medical images generates quantitative indices for characterization, it is expected that such indices will reduce inter-and intra-observer variation by providing a more objective evaluation of the images. In addition, complex algorithms may glean unique information from lesions that might be difficult to assess visually by a radiologist. The ability of imaging to describe the prognosis of a breast cancer lesion could influence possible treatments as well as provide insight into biologic factors governing the varying metastatic potential of individual tumors. DCE-MRI has emerged as an effective modality for characterizing malignant lesions, and computer-assisted diagnostic methods have been developed to automate this task. Textural, morphological, kinetic, and spatial enhancement variance features could be extracted form the kinetic data, in an effort to distinguish between invasive cancers

with positive and negative lymph nodes. It is expected that the role of computer-aided diagnosis will evolve from malignant vs. benign classification to characterization of the metastatic potential of index cancers.

Summary

At present, ultrasound and ultrasound-guided interventions are the primary methods used in clinical practice, for evaluation of lymph nodes for metastases. In the future, advanced MR image quantification methods might allow the radiologist to incorporate prognostic factors such as expected histological grade, receptor profiles and likelihood of lymph node involvement, into the radiology report. The output from such quantitative image analysis will potentially be useful in the data-mining of lesion characteristics with clinical, histopathological, and genomic data. This ongoing research may well expand the role of breast MRI imaging from diagnosis to prognosis and therapy assessment, thus contributing to "personalized medicine" for each individual patient.

References

1. Banerjee M, George J, Song EY, Roy A, Hryniuk W. Tree-based model for breast cancer prognostication. J. Clin Oncol 2004; 22: 2567–2575
2. Cianfrocca M, Goldstein LJ. Prognostic and predictive factors on early-stage breast cancer. Oncologist 2004; 9: 606–616
3. Krag D, Weaver D, Ashikaga T, et al. The sentinel node in breast cancer. A multicenter validation study. N Engl J Med 1998; 339: 941–946
4. Reynolds C, Mick R, Donohue JH, et al. Sentinel Lymph Node Biopsy With Metastasis: Can Axillary Dissection Be Avoided in Some Patients With Breast Cancer? J Clin Oncol, 1999; 17: 1720.
5. Lovrics PJ, Chen V, Coates G, et al. A Prospective Evaluation of Positron Emission Tomography Scanning, Sentinel Lymph Node Biopsy, and Standard Axillary Dissection for Axillary Staging in Patients with Early Stage Breast Cancer. Ann Surg Oncol 2004; 11: 846–853
6. Siegel BM, Mayzel KA, Love SM. Level I and II axillary dissection in the treatment of early-stage breast cancer. An analysis of 259 consecutive patients. Arch Surg 1990; 125: 1144–1147.
7. Swenson KK, Nissen MJ, Ceronsky C, Swenson L, Lee MW, Tuttle TM. Comparison of Side Effects Between Sentinel Lymph Node and Axillary Lymph Node Dissection for Breast Cancer. Ann Surg Oncol 2002; 9: 745–753
8. Mincey BA, Bammer T, Atkinson EJ, Perez EA. Role of Axillary Node Dissection in Patients With T1a and T1b Breast Cancer. Mayo Clinic Experience. Arch Surg. 2001;136:779–782
9. Fraile M, Rull M, Julian F J, et al. Sentinel node biopsy as a practical alternative to axillary lymph node dissection in breast cancer patients: an approach to its validity. Ann Onc 2000; 11: 701–705
10. McMasters KM., Giuliano AE., Ross MI., et al. Sentinel-Lymph-Node Biopsy for Breast Cancer—Not Yet the Standard of Care. N Engl J Med 1998; 339:990–995
11. de Kanter AY, van Eijck, van Geel AN, et al. Multicentre study of ultrasonographically guided axillary node biopsy in patients with breast cancer. Br J Surg 1999; 86: 1459–1462
12. Kumar R, Jana S, Heiba S, et al. Retrospective analysis of sentinel node localization in multifocal, multicentric, palpable, or nonpalpable breast cancer. JNM 2003; 44: 7–10
13. Murray AD, Staff RT, Redpath TW, et al. Dynamic contrast enhanced MRI of the axilla in women with breast cancer: comparison with pathology of excised nodes. Br J Radiol 2002; 75: 220–228
14. Ohta M, Tokuda Y, Saitoh Y, et al. Comparative efficacy of positron emission tomography and ultrasonography in preoperative evaluation of axillary lymph node metastases in breast cancer. Breast Cancer 2000; 7: 99–103
15. Michel SCA, Keller TM, Fröhlich JM, et al. Preoperative Breast Cancer Staging: MR Imaging of the Axilla with Ultrasmall Superparamagnetic Iron Oxide Enhancement. Radiology 2002; 225: 527–536.
16. Vaidya JS, Vyas JJ, Thakur MH, et al. Role of ultrasonography to detect axillary node involvement in operable breast cancer. Eur J Surg Oncol 1996; 22: 140–143
17. Yang W, Ahuja A, Tang A, et al. High resolution sonographic detection of axillary lymph node metastasis in breast cancer. J Ultrasound Med 1996; 15: 241–246
18. de Freitas R Jr, Costa MV, Schneider SV, Nicolau MA, Marussi E. Accuracy of ultrasound and clinical examination in the diagnosis of axillary lymph node metastases in breast cancer. Eur J Surg Oncol 1991; 17: 240–244
19. Tate JJ, Lewis V, Archer T, Guyer PG, Royle GT, Taylor I. Ultrasound detection of axillary lymph node metastases in breast cancer. Eur J Surg Oncol 1989; 15: 139–141
20. Deurloo EE, Tanis PJ, Gilhuijs KGA, et al. Reduction in the number of sentinel lymph node procedures by preoperative ultrasonography of the axilla in breast cancer. Eur J Cancer 2003; 39: 1068–1073
21. van Rijk MC, Deurloo EE, Nieweg OE, et al. Ultrasonography and fine-needle aspiration cytology can spare breast cancer patients unnecessary sentinel lymph node biopsy. Ann Surg Oncol 2006; 13: 31–35
22. Bedrosian I, Bedi D, Kuerer HM, et al. Impact of clinicopathological factors on sensitivity of axillary ultrasonography in the detection of axillary nodal metastases in patients with breast cancer. Ann Surg Oncol 2003; 10: 1025–1030
23. Abe H, Schmidt RA, Kulkarni K, Sennett CA, Mueller JS, Newstead GM, Axillary lymph nodes suspicious for breast cancer metastasis: sampling with US-guided 14-gauge core-needle biopsy—clinical experience in 100 patients. Radiology. 2009 Jan; 250(1): 41–9
24. Luciani, A., E. Itti, et al. (2006). Lymph node imaging: basic principles. Eur J Radiol **58**(3): 338–44.
25. Rety, F., O. Clement, et al. (2000). MR lymphography using iron oxide nanoparticles in rats: pharmacokinetics in the lymphatic system after intravenous injection. J Magn Reson Imaging **12**(5): 734–9.
26. Mortellaro VE, Marshall J, Singer L, Hochwald SN, Chang M, Copeland EM, Grobmyer SR. Magnetic resonance imaging for axillary staging in patients with breast cancer. J Magn Reson Imaging. 2009 May 22
27. Memarsadeghi M, Riedl CC, Kaneider A, Galid A, Rudas M, Matzek W, Helbich TH. Axillary Lymph Node Metastases in Patients with Breast Carcinomas: Assessment with Nonenhanced versus USPIO-enhanced MR Imaging. Radiology 2006;241:367–377.
28. American College of Radiology. Breast Imaging Reporting and Data System Atlas (BI-RADS atlas). Reston, VA: American College of Radiology, 2003.
29. Montemurro F, Martincich L, Sarotto I, et al. Relationship between DCE-MRI morphological and functional features and histopathological characteristics of breast cancer. Eur Radiol. 2007;17:1490–1497.
30. Tuncbilek N, Karakas HM, Okten OO. Dynamic magnetic resonance imaging in determining histopathological prognostic factors of invasive breast cancers. Eur J Radiol. 2005 Feb;53(2):199–205

31. Bahri S, Chen JH, Yu HJ, Kuzucan A, Nalcioglu O, Su MY. Can dynamic contrast-enhanced MRI (DCE-MRI) predict tumor recurrence and lymph node status in patients with breast cancer? Ann Oncol. 2008 Apr;19(4):822–4.

Coil for localization of lesions in MR mammography in comparison to other biopsy coils

PD Dr. S. Obenauer
UMG, Department of Diagnostic Radiology, Robert-Koch-Str. 40, 37099 Goettingen, Germany, obenauerheuser@yahoo.de

With the use of diagnostic MR imaging of the breast MR guided minimal invasive interventions are increasingly needed to obtain histologic proof of lesions, that are occult at mammography and ultrasound. The first attempts to perform MR-guided localization were " free-handed techniques" with cutaneous markers positioned on the skin for orientation. All devices for MR guided interventions use perforated plates for breast compression. The systems differ in the positioning of the patient. MR guided interventions are time consuming and expensive. Therefore it is necessary to insure, that the diagnostic MR examination of the referring institution establishing the indication for biopsy is of high quality. Different MR compatible biopsy needles are used (Vacora, Mammotome, ATEC) with different needle gauges. Up to now the imaging of the biopsy procedure itself is not really possible due to a lack of compatibility of the biopsy needle. Careful reviewing of imaging and pathologic findings is therefore recommended. A consensus about quality assurance of MR-guided vacuum-assisted breast biopsy (VAB) was achieved based on the existing literature and experience of an interdisciplinary group comprising European specialists in breast imaging and VAB. The essentials of this consensus were: "Full imaging work-up must be completed according to existing standards before an indication for MR-guided VAB is established. The procedure should be reserved for lesions demonstrable by MRI alone. Acquisition of >24 cores (11-Gauge) should be routinely attempted, with the intention of sufficiently removing small lesions for accurate diagnosis. Following biopsy the patient should be re-imaged to demonstrate the biopsy site and its proximity to the lesion and hence the likely accuracy of the sampling. All patients should be discussed in a regular interdisciplinary conference and a documented consensus reached regarding patient management. Regular audit and review of all MR-guided VAB results and subsequent follow-up are recommended. This consensus 2008 does not replace official recommendations for percutaneous biopsy." Furthermore, Gossmann et al reported 2008 about real-time magnetic resonance (MR) imaging–guided wire localization of suspicious breast lesions. Needle placement was monitored in 30 women by using a dynamic balanced gradient-echo sequence with a temporal resolution of 0.5 second. In all patients, the tip of the needle was clearly identified during placement. Results show that real-time MR-guided wire localization permits correction of the needle position during placement and reduces the interventional procedure time.

We use in Göttingen a dedicated device integrated into a customary commercial surface coil which allows interventions in supine position developed by Fischer et al. ("Göttinger device") and the commercial INVIVO breast coil with the "post and pillar" biopsy device. Here the patient is in prone position with the biopsy device from laterally for MR-guided interventions (Figure 1–4). Furthermore results of the literature and currently accepted methods for MR-guided tissue sampling will be reviewed (Table 1+2).

In conclusion, MR-compatible devices enable MRI-guided breast interventions, including preoperative lesion localization and minimally invasive biopsy. For the evaluation of additional enhancing lesions in patients with breast carcinoma referred for operation the preoperative wire localization is remaining a widespread safe and simple method. This could either be done in prone or supine position of the patient. Assuming accurate patient selection percutaneous MR vacuum-assisted biopsy is a safe and accurate method for the evaluation of even small enhancing breast lesions.

Table 1: Results of MR-guided wire localizations

Author	Number	Benign	Malignant	Interruption
Heywang-Köbrunner 1994	11	3 (27%)	7 (64%)	1
Orel 1994	11	7 (64%)	4 (36%)	–
Fischer 1994	28	16 (57%)	12 (43%)	2
Kuhl 1997	97	44 (45%)	53 (55%)	–
Fischer 1998	132	68 (52%)	64 (48%)	–
Kuhl 2002	138	69 (50%)	69 (50%)	–
Liberman 2002	100	75 (75%)	25 (25%)	–
Morris 2002	101	70 (70%)	31 (30%)	–
UMG 1997–2005	275	150 (55%)	125 (45%)	2
UMG 2005–2007	71	48 (67%)	23 (33%)	–

Table 2: Results of MR-guided biopsies

Author	Number pat./biop.	Histology			Accur.	Discordant	Time	Compl.
		Malig.	Border.	Ben.				
Liberman 2005	106/112	25%	20%	55%	97%	12%	33 min	5,3%
Orel 2006	75/85	61%	21%	18%	98%	NR	30–60 min	0% (major)
Perlet 2006	538/538	27%	3%	70%	96%	16%	70 min	< 1%
Viehweg 2007	39/53	26%	4%	70%	100%	12%	60 min	NR
Kuhl, Schrading 2007	200/316	43%	5%	52%	99%	NR	62 min	3%
Fischer 2009	365/389	27%	13%	60%	99%	0,5%	43,2 min	< 1%

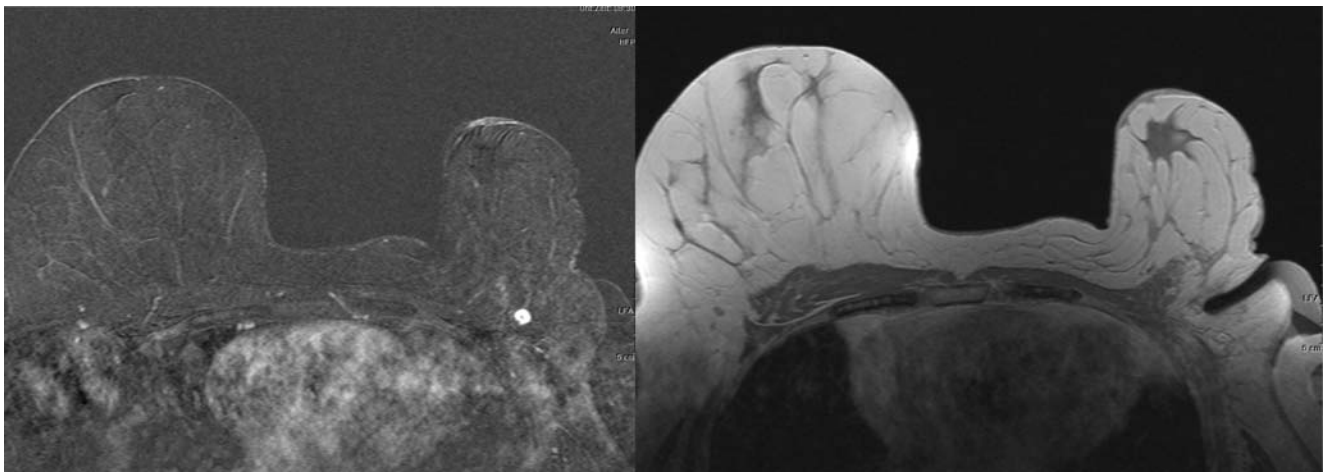

Figure 1: Hypervascularized lesion in the left breast near the thoracic wall without correlation in ultrasound, second-look ultrasound and mammography. Therefore MRI-wire localization with the INVIVO breast coil and the “post and pillar” device has been done. Histology: Lymph node without suspicious of malignancy.

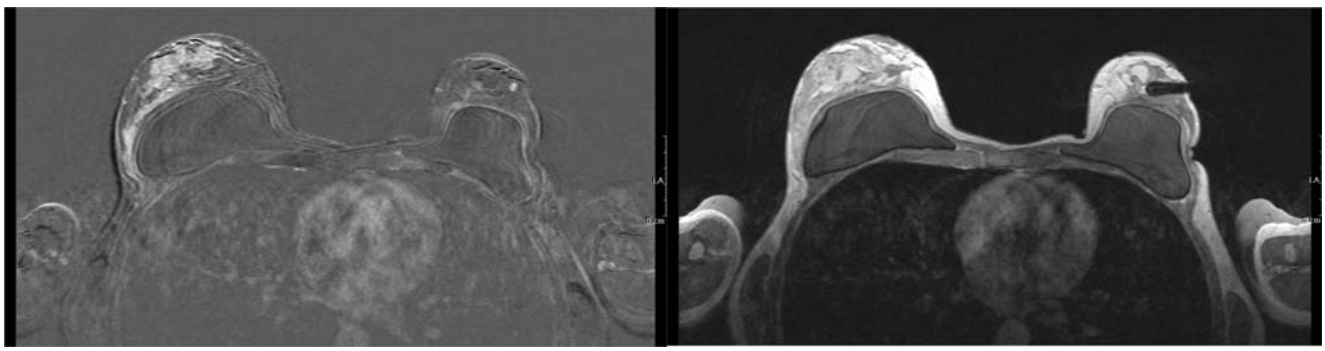

Figure 2: Hypervascularized lesion in the left breast with histological proven diffuse ductal carcinoma in situ (high grade DCIS with necrosis) in the right breast. Bilateral breast prosthesis. MRI-wire localization of the left side was done from laterally with the INVIVO breast coil with a “post and pillar” device while mastectomy of the right side was done. Histology: On the right side invasive ductal carcinoma with intraductal component (high-grade DCIS). On the left side fibroadenoma.

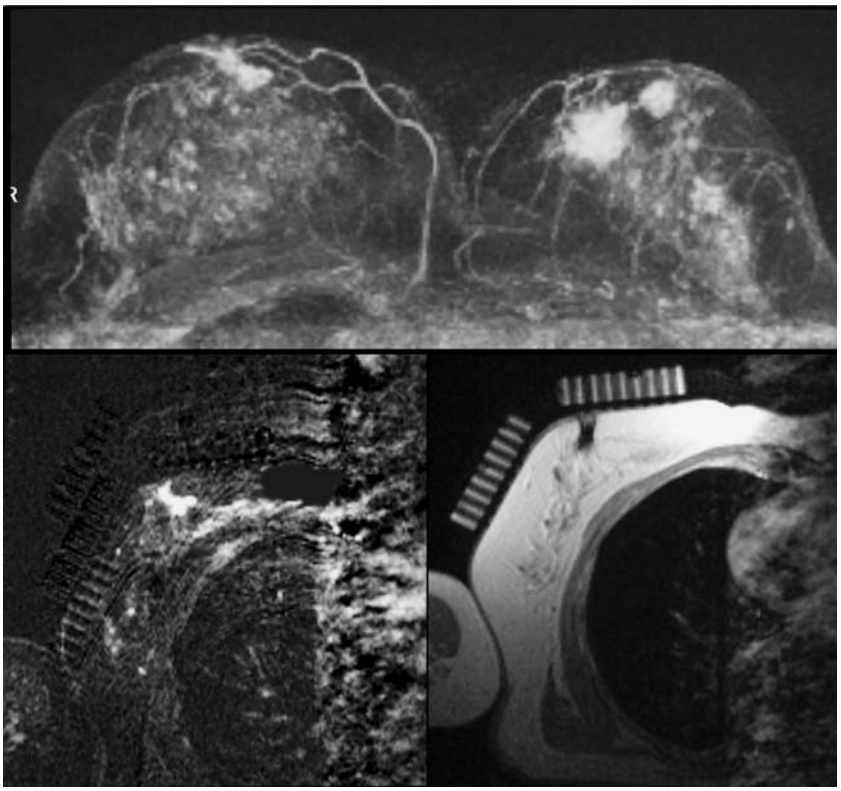

Figure 3: Patient with histological proven multicentric tumor in the left breast. In the right breast perimamillary a hypervascularized lesion was seen in MRI. Therefore MRI-localization of the lesion in the right breast was done before surgery of the left breast with the "Göttinger" biopsy device in supine position of the patient. Histology: Invasive ductal carcinoma of the right side (pT1b), Invasive lobular carcinoma of the left side (pT2N1).

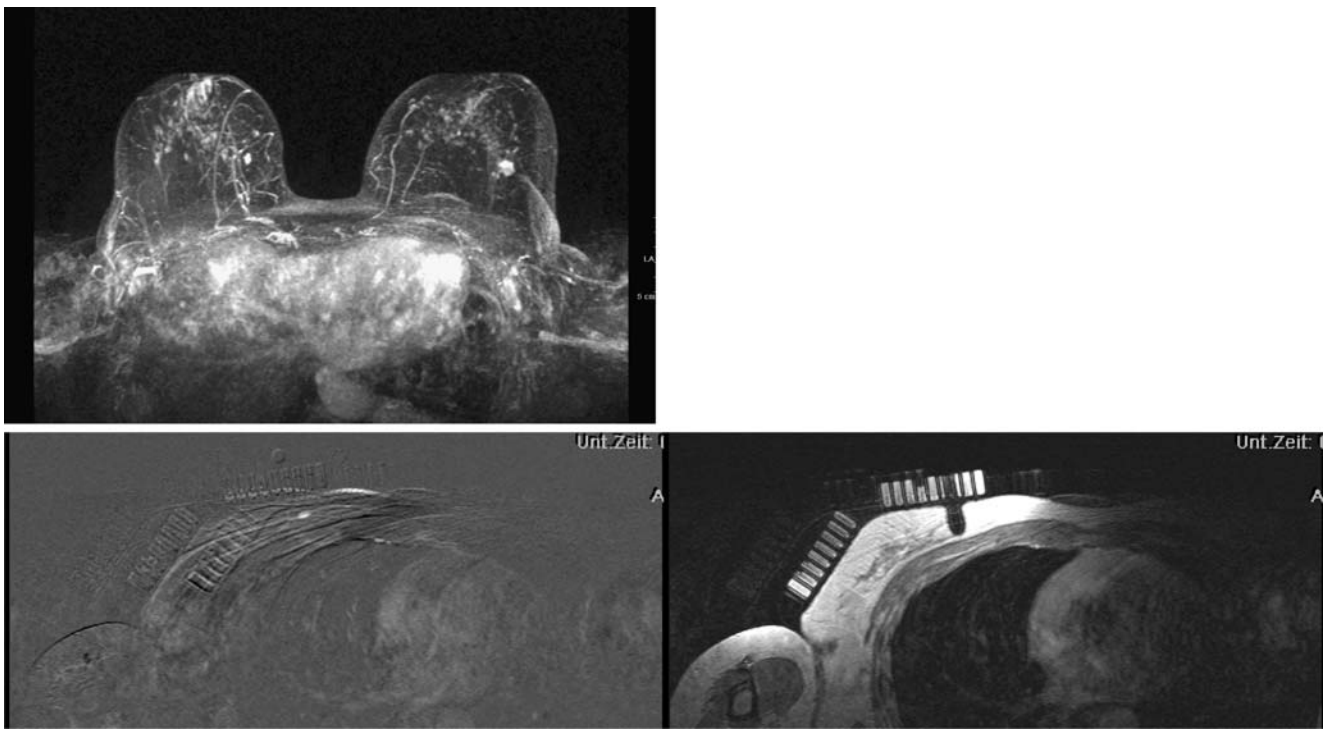

Figure 4: Histologically proven IDC in the left breast with extensive intraductal component. In the right breast MRI shows a hypervascularized lesion in the medial quadrant with diffuse contrast media enhancement to the nipple. Therefore MRI localization of the lesion in the right breast in supine position was done before surgery of the left breast. Histology of the right side reveals fibroadenoma and sclerosing adenosis without malignancy. In the left breast histology was IDC pT1b.

References
Fischer U, Vosshenrich R, Döler W, et al. MR imaging guided breast intervention: experience with two systems. Radiology 1995; 195:533–8.
Fischer U, Schwethelm L, Baum FT, Luftner-Nagel S, Teubner J. Effort, Accuracy and Histology of MR-Guided Vacuum Biopsy of Suspicious Breast Lesions—Retrospective Evaluation after 389 Interventions. Rofo 2009 Jul 6. [Epub].
Gossmann A, Bangard C, Warm M, Schmutzler RK, Mallmann P, Lackner KJ. Real-time MR-guided wire localization of breast lesions by using an open 1.0-T imager: initial experience. Radiology 2008 May; 247(2):535–42.
Heywang-Köbrunner SH, Heinig A, Pickuth D, et al. Interventional MRI of the breast: lesion localisation and biopsy. Eur Radiol 2000; 10:36–45.
Heywang-Köbrunner SH, Sinnatamby R, Lebeau A, Lebrecht A, Britton PD, Schreer I; Consensus Group. Interdisciplinary consensus on the uses and technique of MR-guided vacuum-assisted breast biopsy (VAB): Results of a European consensus meeting. Eur J Radiol 2008 Aug 23. [Epub ahead of print]
Kuhl CK, Elevelt A, Leutner CC, et al. Interventional breast MR imaging: clinical use of a stereotactic localization and biopsy device. Radiology 1997; 204: 667–75.
Liberman L. Clinical management issues in percutaneous core breast biopsy. Radiol Clin North Am 2000; 38: 791–807.
Morris EA, Liberman L, Dershaw DD, Kaplan JB, LaTrenta LR, Abramson AF, Ballon DJ. Preoperative MR imaging-guided needle localization of breast lesions. AJR Am J Roentgenol 2002 May;178(5):1211–20.
Orel SG, Schnall MD, Newman RW, Powell CM, Torosian MH, Rosato EF. MR imaging-guided localization and biopsy of breast lesions: initial experience. Radiology 1994; 193: 97–102.
Perlet C, Heinig A, Prat X, Baath L, Sittek H, Stets C, Lamarque JM, Andersson I, Schneider P, Taourel P, Reiser M, Heywang-Köbrunner SH. Multicenter study for the evaluation of a dedicated biopsy device for MR-guided vacuum biopsy of the breast. Eur Radiol 2002; 12: 1463–1470.
Siegmann KC, Gorriz C, Xydeas T, et al. Preoperative magnetic resonance imaging-guided localization of 131 breast lesions with modified embolization coils. Invest Radiol 2005; 40: 368–77.
Viehweg P, Heinig A, Lampe D et al. Retrospective analysis for evaluation of the value of contrast-enhanced MRI in patients with breast conservative therapy. MAGMA 1998; 7: 141–152.

MRI evaluation for eligibility to partial breast irradiation

Roberto Orecchia
Department of Radio-Oncology, European Institute of Oncology, Milan, Italy
& University of Milan School of Medicine, Milan, Italy
& CNAO Foundation, Pave, Italy
Correspondence address:
Istituto Europeo di Oncologia, Dipartimento di Radioterapia, via Ripamonti 435, 20141 Milano, Italia, e-mail: roberto.orecchia@ieo.it, phone: +39-02-57489037, fax: +39-02-94379227

Introduction

Breast-conserving surgery (BCS), which classically consists of the surgical removal of the tumor mass plus a margin, followed by post-operative whole breast irradiation (WBI), is considered the current standard approach for most women with early stage breast cancer. This combined treatment has indeed shown results equivalent to those of mastectomy in terms of local control and survival rates in women with comparable tumor size and stage. Post-operative radiation therapy (RT) includes the irradiation of the whole breast, up to a dose of 45–50 Gy delivered over 5–6 weeks. In most patients, a boost dose of 10–15 Gy to the tumor bed is added, further prolonging the treatment time of additional 1 or 2 weeks. In the last meta-analysis of the most relevant randomised trials, which included more than 7,000 patients treated by BCS with or without RT, a significant difference in local recurrences was observed at 5-year (7% versus 26%) with a reduction of 19% in favour of RT (1). Comparable relevance was also noted in terms of reducing the 15-year breast cancer mortality (30.5% versus 35.9%, with a gain of 5.4%) and the overall mortality, with a similar rate of gain. The greatest benefit was obtained in the group of patients with positive axillary nodes, with the reduction of 7.1% at 15 years on the breast cancer mortality risk. In spite of these excellent data, in the last years, several institutions are trying to revisit the adjuvant radiation treatment setting, especially with regard to possible changes in both the overall treatment time and the target volume. This concept has been developed mainly by the clinical application of the modern philosophy of partial breast irradiation (PBI) (2). PBI, which consists of the irradiation of the site of tumor excision and adjacent tissues only, can be realised using different approaches, including brachytherapy techniques, intra operative RT (IORT), and high precision external beam RT (3). All these techniques generally provide shorter schedule of fractionation (no more than 10 fractions), with the extreme case of the one single dose for IORT (4).
Up to date, no conclusive data are available on the possible role of PBI with respects to proper patient selection and best technical approach (5). Also the results in terms of safety and effectiveness should be managed with caution. These uncertainties are mainly due to the too short follow-up time of some institutional experiences, and the need to wait the definitive results of several large randomised trials that are still currently ongoing.
The goal of this paper is to shortly review the rationale and the research currently being undertaken within the framework of PBI, trying to focus on the possible contribution of new imaging modalities, and mainly MRI, in order to optimise patients selection and treatment procedures.

Rationale for combining MRI and PBI in selecting patients

Whether the entire breast needs to be irradiated or not after BCS is actually the key issue on which are based the new perspectives in terms of PBI. The rationale for the use of this segmental irradiation in place of WBI can be sustained by the results of some long term studies reporting that local relapses, after BCS with/without WBI, occur at the original tumour site at a rate of 85% or more, as, for instance, in the Milan III trial (6). On the contrary, there are also data suggesting that the extent and the amount of multifocal cancer in the vicinity of the primary tumor could vary from patients to patients, with the risk of an incidence of elsewhere failure higher than those reported in the previous trials. For example, in one study it has been reported that only 56% of the local recurrences occurred in or close the primary tumor bed (7). These results seem to be corroborated by the pathological findings classically reported by Holland in mastectomy specimens of large size primary tumor, according to which only 39% of the cases showed no evidence of micro-foci beyond the primary lesion and 41% of the cases had residual cancer cells situated remote from the index quadrant, 2 cm and more (8). A recently reported series, focusing on women with stage I and II tumours who underwent a re-excision after lumpectomy as part of their BCS, has shown more encouraging results, with only 9% of the patients having pathological evidence of disease at more than 15 mm from the initial lumpectomy cavity (9). In addition to histopathological studies another concern is raised by MRI studies that have detected microscopic foci outside the tumour beds in a significant percentage of patients. MRI performed in women newly diagnosed identifies such missed lesions by conventional imaging in more than 20% of cases (10,11). Even

though the clinical relevance of these wide-spread and occult multifocal/multicentric malignant foci in other quadrants is not totally clear, these data suggest to apply strict eligibility criteria for PBI. The use of MRI in patients eligible for PBI can facilitate the proper selection of these cases, in which patterns and rates of breast tumor recurrence over time should be the different from patients submitted to WBI. In addition MRI can also detect occult malignancies within the contralateral breast (3–5% of cases). All these additional information can more correctly tailor the patient management, especially when, as the case of PBI, established selection criteria are not yet validated in current clinical practice.

Rationale for combining MRI and PBI in treatment planning

PBI can be carried out with several different techniques. At least three main approaches are most currently used in clinical setting: IORT, brachytherapy and external beam RT (2–5).

With IORT the entire dose must by necessity be delivered in a single fraction. Many, different sized applicators permit to place all the tissue to be irradiated at the same distance and therefore allow a uniform dose distribution. Applicators are tried to find the one that best fits on the surgical bed or in the cavity. Target identification is made on the patient breast by direct visualisation of together the surgeon and radiation oncologist.

Brachytherapy has been used for more than 30 years as a boost to complete WBI. More recently it has been used as sole modality in many PBI trials. Technically we can distinguish catheter based and balloon based approaches. In the former many catheters are inserted (usually in two or more parallel planes), either during surgery or in a subsequent phase. This procedure needs to create a 3D CT-based optimization of the dose distribution, which allows covering a target regardless of its more or less regular shape. Imaging and/or surgical clips can help to identify target volume.

External beam RT must of course be targeted to a single quadrant. This can be implemented with different techniques ranging from 3D-conformal RT to Intensity Modulated RT to proton beams. The target volume is contoured by the radiation oncologist on a simulation CT scan. All external beam techniques allow a more flexible choice of volumes to be irradiated and grant a more homogeneous dose distribution. Some special issues that may lead to a geographic miss must be addressed: it may be difficult to precisely individuate the target volume and organ motion may play a relatively greater role (12). The surgical cavity/tumor bed are not so evident on the CT scan after more than ten days from the operation, and even clips inserted during surgery may migrate within the remaining breast (13,14). Organ motion due to respiratory activity is of course present also during WBI, but the target is bigger and so adding geometrical margins results in a relatively smaller increase in irradiated volume. In PBI adding margins to the smaller CTV can produce an excessive increase in irradiated volume. The use of 4D planning with respiratory gating or customized tray on which the patients lays prone allows to manage or reduce the impact of organ motion (15). An other problem is due to the fact that compared to the single fraction approach of IORT, all the brachytherapy and external beam RT techniques offer a wider fractionation range, varying from to 10 fractions of 4 Gy each in 10 days, to 10 fractions of 3.4 Gy each in 5 days to 7 fractions to 5.2 Gy in 4 days, and many others. This means that image guidance is necessary not only for identifying the target but also for guaranteeing the daily reproducibility of the set-up, allowing the appropriate full dose is effectively given.

Preliminary results

In spite of the strong rationale for image guided localisation of the breast target before and during the treatment, especially when PBI is delivered, few data are available on the literature on the impact of new imaging modality, and especially for MRI, both in terms of clinical outcomes and cost/effectiveness. All the studies are observational, with small sample sizes, and therefore subject to selection bias. Also in the ongoing randomised comparisons between standard breast conserving treatment and PBI (GEC-ESTRO, NSABP B39/RTOG 0413, ELIOT, TargIT, and others) there no selection criteria based on imaging. At the same time no recommended image guided protocols exist to delineate the breast target for RT planning.

Multifocality

A recent publication described no benefit in the use of MRI at initial diagnosis for improving outcome after BCS with WBI, but stated that it may be valuable for selecting patients for accelerated partial breast irradiation (16). Breast MRI may provide benefit by potentially refining criteria for selecting patients with its ability to detect multifocality and additional tumor sites away from the tumor bed. Among eligibility criteria for PBI, which currently include age 50+ years, histology non-lobular carcinoma, without DCIS, tumor size up to 25–30 mm, nodal stage N0 (micrometastasis), free surgical margins and tumor location 5 mm under skin surface, the unifocal disease is the most quoted. With regard to this point a very interesting study from the MD Anderson Cancer Center showed a high percentage of multicentric cancers in 284 patients with T1–T2, N0–N1, M0 breast disease (17). Pathology of the mastectomies showed that 60 patients (21%) had multicentric breast cancers, 30 patients (11%) had two lesions, 13 patients (5%) had three lesions, and 17 patients (6%) had four or more lesions. This group of patients would be eligible for treatment with PBI by most of the applied selection criteria.

The role of breast MRI in selecting patients who are theoretically eligible for accelerated partial breast radiation therapy has been described in few studies. In one retrospective series on 79 such patients, physical examination and conventional imaging with mammography and sonography were found to be insufficient to exclude additional occult lesions, whereas MRI was more revealing (18). Additional foci of cancer were detected at final pathology in 38% of patients, all of which were also seen on MRI. In 10% of total patients, additional sites of disease were observed away from the index tumor. If these cases, which were clinically assessed and imaged by conventional means, had been considered appropriate for PBI; with the addition of the MRI, these patients would be considered ineligible and might have been converted to mastectomy.

In an other retrospective study, since 2002 MRI was used nonselectively for the staging of patients with nonmetastatic breast cancer (19). Of 450 consecutive patients with invasive breast cancer, 110 patients who were eligible for PBI were identified by using criteria outlined by NSABP B39/RTOG 0413 trial based on mammography, ultrasonography, and initial pathology. In that trial, patients were randomized to receive either WBI or PBI. MRI reports were reviewed to determine whether MRI identified secondary lesions within the same quadrant (multifocal), in a different quadrant (multicentric), or in the contralateral breast. These lesions were pathologically proven carcinoma and would have rendered the patient ineligible for PBI. In terms of results MRI identified secondary lesions in 10% of patients. Multifocal disease was identified in 3.6%, multicentric disease was identified in 4.5%, and contralateral disease was identified in 1.8%. The proportion of patients with false-positive MRI findings was 4.5%. The positive predictive value of MRI was 72.2%. These data suggest that MRI should be considered to assess PBI eligibility to minimize potential local failures.

A total of 260 patients met eligibility criteria for NSABP B-39/RTOG 0413 and evaluated also with MRI has been retrospectively reviewed (20). DCIS was present in 63 patients, and invasive breast cancer was found in 197 patients. MRI identified

suspicious lesions in 35 ipsilateral breasts (13%) and in 16 contralateral breasts (6%). Mammographically occult, synchronous ipsilateral foci were found by MRI in 11 patients (4.2%), and in the contralateral breast in 4 patients (1.5%). By univariate analysis, lobular histology, pathologic T2, and AJCC stage II were significantly associated with additional ipsilateral disease. Of patients with lobular histology, 18% had ipsilateral secondary cancers or DCIS, compared with 3% in the remainder of histologic subtypes (P=.004). No patient older than 70 years had synchronous cancers or DCIS detected. Based on these data breast MRI was able to identify synchronous mammographically occult foci in 5.8% of early breast cancer patients who would otherwise be candidates for APBI.

Localisation of the tumour bed after BCS

The current standard for tumour bed localisation includes preoperative imaging, clinical examination, surgical findings, fiducial markers and sometimes postoperative ultrasound and/or CT scan. None of these methods is totally satisfactory for accurate treatment plannings. High resolution 3D ultrasound allows good spatial orientation, but its limited application in breast RT planning is due to difficulties in achieving accurate co-registration between ultrasound and CT, particularly in a mobile structure such as the breast. Metal clips supplement the information provided by CT imaging alone. However the clips only identify a limited number of points and their position may change over time during radiation therapy due to deformation of the excision area. One of the limitations of CT is its limited soft tissue contrast, making it difficult to differentiate normal breast tissue from the tumor bed. MRI provides better soft tissue contrast. In a very recent study using titanium clips and fused images from CT and MRI in the prone position showed discordances in tumour excision cavity volumes compared to titanium clips/CT in a prospective series of 30 women managed by BCS, WBRT and boost irradiation (21). In 28/30 cases the supplementation of CT data by MR increased the tumour excision cavity volume. CTV values on CT and on MR correlated well (Pearson correlation coefficient 0.957, $p<0.001$). The conformity index between CT and MR was relatively low for the tumour bed (0.53) but substantially higher for the CTV (0.87) and for the planning target volume (PTV) (0.92). The higher conformity for the CTV and PTV between MR and CT is explained by the size of the margin in relation to the size of the discordance and to the constraints on expansion caused by the skin, chest wall and breast tissue boundaries. For most patients the addition of MR to CT/clip information produced target volumes which were satisfactorily covered by tangential partial breast irradiation fields based on CTV (CT). In only 4/30 cases was coverage inadequate. It is likely that MR based tumour excision cavity overestimates the real size of the cavity by including haemorrhage and haematoma that does not necessarily lie within the excision cavity.

Conclusions

Over the past few years an increasing number of papers have appeared in peer-reviewed journals detailing various approaches of PBI, utilizing fractionated external beam or single dose intraoperative or brachytherapy techniques. The concept of PBI has been often associated with the use of accelerated schedules of fractionation. The comparison between the current standard for early stage breast cancer with early data coming from PBI techniques poses a dilemma as to when preliminary results are sufficiently mature to allow practitioners and patients to consider a new treatment approach as safe.

The use of PBI in place of the WBI in properly selected patients may represent the possibility of overcoming some constraints such as the accessibility to the centres of radiotherapy, the socio-economic impact on the working life and on the personal habits of the patient. Another important advantage is the avoidance of the interactions with the systemic therapy, that may determine delays in the initiation or in the carrying out of the conventional treatment. These potential benefits must be balanced with the potential risk of recurrence within the untreated breast tissue in the breast receiving PBI. Significant practical considerations also include the precise choice of technique. Patient selection remains uncertain, including questions regarding age exclusions, applicability with various primary tumor sizes, histopathologic features (lobular, EIC and DCIS), tumor-free margin and amount of tumor near the margins, and negative (including micrometastasis) or positive axillary lymph node status (up to three or more). For this reason, proper selection and management should be improved. The impact of new emerging image modality on PBI should be addressed. The high negative predictive value of MRI has the potential to ameliorate selection of patients, reducing the risk to include cases with multifocal or multicentric diseases, or with contralateral lesions. Also the issues of target volume definition and daily reproducibility may be considered. In general, when compared with mammography or ultrasound, breast MRI could be superior in pathological correlation. However the efficacy of MRI with respect to clinically relevant end-point has to be addressed and defined from analyzing the results of randomized trials. Second generation randomized trials on PBI appear necessary to consolidate our expertise and try to assess the impact of the image guidance on clinical outcomes.

References

1. Clarke M, Collins R, Darby S, on behalf of Early Breast Cancer Trialists' Collaborative Group (EBCTCG). Effects of radiotherapy and of differences in the extent of surgery for early breast cancer on local recurrence and 15-year survival: an overview of the randomised trials. Lancet 2005; 366: 2087–106.
2. Walner P, Arthur D, Bartelink H, et al. Workshop on partial breast irradiation: state of the art and the science. J Natl Cancer Inst 2004; 96: 175–84.
3. Bernier J, Viale G, Orecchia R, et al. Partial irradiation of the breast: old challenge, new solutions. Breast 2006; 15: 466–75.
4. Orecchia R, Veronesi U. Intraoperative electrons. Semin Radiat Oncol 2005; 15: 76–83.
5. Orecchia R, Fossati P. Partial breast irradiation: ready for routine? Breast 2007; 16(S2): 89–97.
6. Veronesi U, Marubini E, Mariani L, et al. Radiotherapy after breast-conserving surgery in small breast carcinoma: long-term results of a randomized trial. Ann Oncol 2001; 12: 997–1003.
7. Bartelink H, Horiot JC, Poortmans P, et al. Recurrence rates after treatment of breast cancer with standard radiotherapy with or without additional radiation. N Engl J Med 2001; 345: 1378–87.
8. Holland R, Veling SH, Mravunac M, et al. Histologic multifocality of Tis, T1-2 breast carcinomas. Implications for clinical trials of breast-conserving surgery. Cancer 1985; 56: 979–90.
9. Vicini FA, Kestin LL, Goldstein NS. Defining the clinical target volume for patients with early-stage breast cancer treated with lumpectomy and accelerated partial breast irradiation: a pathologic analysis. Int J Radiat Oncol Biol Phys 2004; 60:722–30.
10. Patani N, Mokbel K. The utility of MRI for the screening and staging of breast cancer. Int J Clin Pract 2008; 62: 450–3.
11.Lehman CD, DeMartini W, Anderson BO, et al. Indications for breast MRI in the patient with newly diagnosed breast cancer. J Natl Compr Canc Netw 2009; 7: 193–201.

12. Landis DM, Luo W, Song R et al. Variability among breast radiation oncologists in delineation of the postsurgical lumpectomy cavity. Int J Rad Oncol Biol Phys 2007; 67: 1299–1308.
13. Harris EJ, Donovan EM, Yarnold JR, et al. Characterization of target volume changes during breast irradiation using implanted fiducial markers and portal imaging. Int J Rad Oncol Biol Phys 2009; 73:: 958–66.
14. Hassan Y, Kim L, Martinez A, et al. Image guidance in external beam accelerated partial breast irradiation: comparison of surrogates for the lumpectomy cavity. Int J Rad Oncol Biol Phys 2008; 70: 619–25.
15. Moran JM, Ben-David MA, Marsh RB, et al. Accelerated partial breast irradiation: what is the dosimetric effect of advanced technology approaches? Int J Rad Oncol Biol Phys 2009; Jun 17 (Epub ahead of print).
16. Solin LJ, Orel SG, Hwang W, et al. Relationship of breast magnetic resonance imaging to outcome after breast-conservation treatment with radiation for women with early-stage invasive breast carcinoma or ductal carcinoma in situ. J Clin Oncol 2008; 26: 386–391.
17. Vlastos G, Rubio IT, Mirza NQ, et al. Impact of multicentricity on clinical outcome in patients with T12, N0-1, M0 breast cancer. Ann Surg Oncol 2000; 7: 581–7.
18. Godinez J, Gombos EC, Chikarmane SA, et al. Breast MRI in the evaluation of eligibility for accelerated partial breast irradiation. AJR Am J Roentgenol 2008; 191: 272–7.
19. Al-Hallaq HA, Mell LK, Bradley JA, et al. Magnetic resonance imaging identifies multifocal and multicentric disease in breast cancer patients who are eligible for partial breast irradiation. Cancer 2008; 113: 2408–14.
20. Tendulkar RD, Chellman-Jeffers M, Rybicki LA, et al. Preoperative breast magnetic resonance imaging identifies in early breast cancer patients: implications for partial breast irradiation. Cancer 2009; 115: 1621–30.
21. Kirby AM, Yarnold JR, Evans PM, et al. Tumor bed delineation for partial breast and breast boost radiotherapy planned in the prone position: what does MRI and to X-ray localisation of titanium clips placed in the excision cavity wall? Int J Rad Oncol Biol Phys 2009; 74: 1276–82.

Breast MRI in the cancer of unknown primary (CUP-Syndrome)

Pietro Panizza, Isabella Fedele, Claudio Losio, Alessandro Del Maschio.
Breast Imaging, Department of Radiology, Vita-Salute University, San Raffaele Hospital, Milano Italy

CUP is the acronym for Carcinoma of Unknown Primary; we can consider this syndrome when we find metastases but we are not able to identify the primary cancer. This condition creates a dilemma with regard to treatment and feeling of the patient. Histopathologic assessment of metastases allows to suspect the origin of the cancer but in case of adenocarcinoma we have to consider more than one site, as breast, thyroid, lung, gastric, pancreatic, colon, ovary and kidney cancer [1–4]. Estrogen and progesterone receptor analysis suggests a breast origin, but estrogen receptor protein as been shown also in carcinoma of the colon, malignant melanoma, papillary ovarian cancer, endometrial tumors and renal carcinomas [5]. On the opposite, not all breast cancers are positive at hormonal receptor studies. Other immunohistochemical analysis [6], as gross cyst disease fluid protein, may suggest a breast origin.

The frequency of occult breast carcinoma is less than 1% (0.3–0.8) of all the breast carcinomas[10]. In these case the patient presents metastatic disease, often with axillary nodes involvement, but clinical evaluation, mammography and sonography are not able to identify the primary cancer.

Treatments reported in literature in those patients are very different, ranging from mastectomy to quadrantectomy, radiotherapy on the breast and the axilla or watchful waiting; today the suggested intervention is axillary dissection and breast radiotherapy [6–11]. In fact in case of mastectomy the pathologist find cancer only in the 45 to 75% of the breast [12]; for these reason it is very important to visualize the lesion and proceed to a correct therapy. The survival for patients with axillary node metastases and unknown primary malignancy is at least comparable with that for stage II breast cancer and it is quite the same in case of breast-conserving therapy or mastectomy [13,14].

Due to the high sensitivity of dynamic breast MRI in the depiction of breast cancer, greater than that of mammography, some authors [15–23] studied with this technique patients with CUP syndrome with a suspected breast origin; results of those studies are reported in Table 1.

In our experience we studied 39 patients with diagnosis of adenocarcinoma metastases suspected for breast primary, with negative clinical examination, mammography and sonography, that underwent breast MRI.

At MRI we found suspicious enhancing areas in 22 out of 39 patients (56.4%). Among the 22 positive MRI breast cancer has been confirmed in 13 at histology and 1 at cytology; 4 disappeared after chemotherapy and 1 patient died without diagnosis (Figures 1–2); three cases were negative for malignancy at histology (false positive MRI findings—FP) (Figure 3). Eight out of 13 malignant lesions were in the upper lateral quadrant, one was in the center of the breast behind the nipple, four were multicentric and underwent mastectomy. The remaining patient with positive MRI has been treated with chemotherapy and the lesion disappeared at MRI follow up. Positive predictive value in detecting unknown cancer of suspected breast origin was 85.7%.

Among the 17 of 39 patients with negative MRI (43.6%), three underwent upper-lateral quadrantectomy and no lesions were found at histology (Figures 4–5); the remaining 14 patients were treated with axillary dissection and radio/chemotherapy; no lesions have been demonstrated at long follow-up (4–12 yrs, mean 8.5 yrs).

The MRI capability to visualize breast cancer in CUP syndrome is quite different in the literature, ranging from 25 to 86% [15–23]. Our experience is similar to that of Schorn [18] and Buchanan [23]; we found cancer in the 49% of the cases and in patients with negative MRI no cancers appeared during follow-up or at surgical operation (Negative predictive value of 100%).

On the basis of literature and our results, we can conclude that in case of metastases suggestive of breast origin in which the primary cancer is occult at traditional investigative methods, MRI is the last chance, often able to visualize and stage cancer, allowing the right surgical treatment, conservative or radical depending on the number and site of lesions.

When MRI is negative, breast surgery is not indicated. However, Buchanan [23] found two carcinomas in eight mastectomies after negative MRI; looking at these results we can conclude that in case of negative MRI surgery is not indicated but breast radiotherapy and clinical treatment are necessary.

In our long follow-up experience, in agreement with literature results, after radiotherapy and/or clinical treatment no primary cancer appeared in the breast and in other organs.

In case of metastases of unknown primary, suspicious to be of breast origin, MRI should follow clinical examination, mammography and sonography before definitely classify breast cancer as occult.

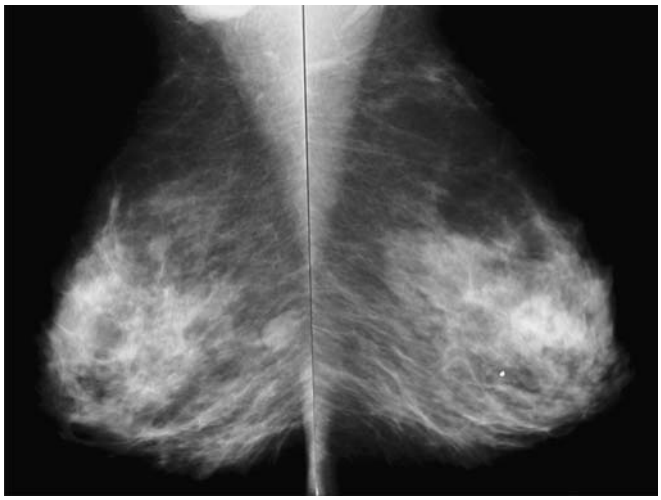

Fig. 1. Patient with lymph node metastases in the right axilla. Mammography is negative.

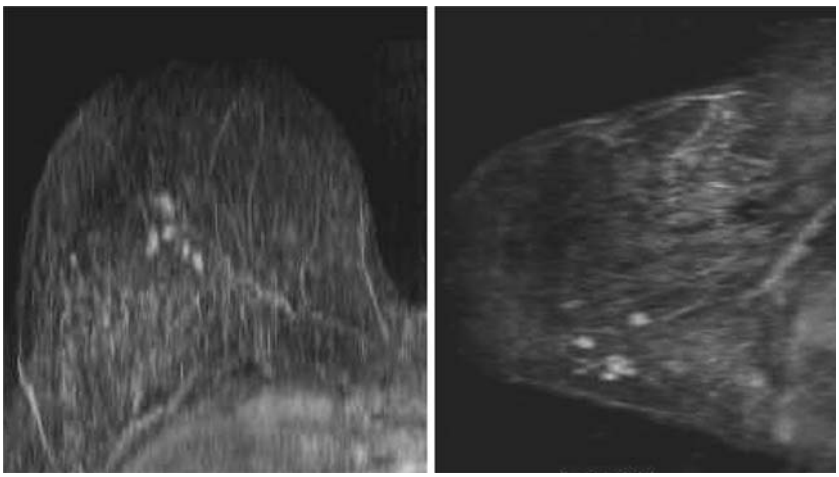

Fig. 2. Same patient. MRI shows five focal enhancing areas, between the inferior quadrants, suspicious for malignancy. IDC at histology

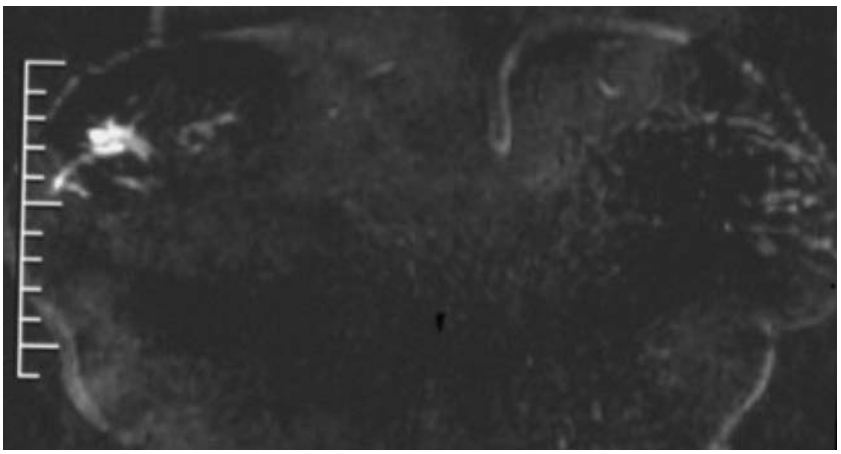

Fig. 3. Patient with axillary lymph node metastases, suspicious to be of breast origin. Traditional examinations were negative. The focal enhancement at MRI in the upper lateral quadrant of the right breast is a false positive finding. It was a sclerosing adenosis at histology.

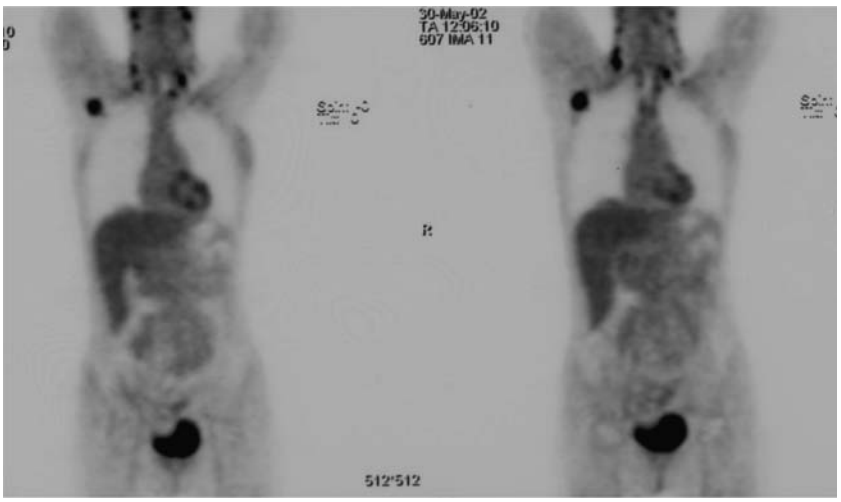

Fig. 4. In this patient PET demonstrated right axillary, sovra-clavicular and latero-cervical lymph node metastases. At histology the axillary one was suspicious for breast origin.

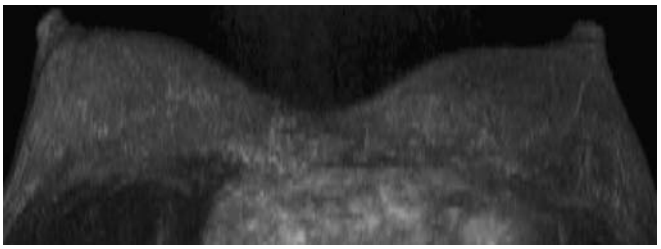

Fig. 5. Same patient of Fig. 4. Clinical evaluation, mammography, US were negative. MRI does not show any breast lesion.

References

1. Chorost MI, Lee MC et al (2004) Unknown Primary. Journal of Surgical Oncology 87:191–203
2. Van De Wouw AJ, Jansen RLH et al. (2003) The unknown biology of the unknown primary tumor: a literature review. Annals of Oncology 14:191–196
3. Haupt HM, Rosen PP, Kinne DW (1985) Breast carcinoma presenting with axillary lymph node metastases. Am J Surg Pathol 9:165–175
4. Van Ooijen B, Bontenbal M, Henzen-Logmans SC et al (1993) Axillary nodal metastases from an occult primary consistent with breast carcinoma. Br J Surg 80: 299–1300
5. Bhatia SK, Saclarides TJ, Witt TR et al (1987) Hormone receptor studies in axillary metastases from occult breast cancers. Cancer 59:1170–1172
6. Brown RW, Campagna LB, Dunn JK et al (1997) Immunohistochemical identification of tumor markers in metastatic adenocarcinoma. A diagnostic adjunct in the determination of primary site. Am J Clin Pathol 107(1):12–19
7. Knapper WH (1991) Management of occult breast cancer presenting as axillary metastases. Semin Surg Oncol 7:311–313
8. Jackson B, Scott-Conner C, Moulder J (1995) Axillary metastasis from occult breast carcinoma: diagnosis and management. Am Surg 61(5):431–434
9. Merson M, Andreola S, Galimberti V et al (1992): Breast carcinoma presenting as axillary metastases without evidence of a primary tumor. Cancer 70:504–508
10. Galimberti V, Bassani G, Monti S et al (2004) Clinical experience with axillary presentation breast cancer. Breast Cancer Res Treat 88:43–47
11. Kemeny MM, Rivera DA, Terz JJ et al (1986) Occult breast adenocarcinoma with axillary metastases. Am J Surg 152:43–47
12. Niu Y, Fan Y, Fu X (1995) Whole organ subserial section examination of occult breast carcinoma. Chung Hua Chung Liu Tsa Chih 17(4):298–300
13. Patel J, Nemoto T, Rosner D, et al (1981) Axillary lymph node metastasis from an occult breast cancer. Cancer 47:2923–2927
14. Hortobagyi GN, Buzdar AU (1995;) Current status of adjuvant systemic therapy for primary breast cancer: progress and controversy. CA Cancer J Clin 45:199–226
15. Brenner RJ, Rothman BJ (1997) Detection of primary breast cancer in women with known adenocarcinoma metastatic to the axilla: use of MRI after negative clinical and mammographic examination. J Magn Reson Imaging 7(6):1153–1158
16. Morris EA, Schwartz LH, Dershaw DD et al (1997) MR imaging of the breast in patients with occult primary breast carcinoma. Radiology 205: 437–440

17. Tilanus-Linthorst MM, Obdeijn AI, Bontenbal M et al (1997) MRI in patients with axillary metastases of occult breast carcinoma. Breast Cancer Res Treat 44(2):179–182
18. Schorn C, Fischer U, Luftner-Nagel S et al (1999) MRI of the breast in patients with metastatic disease of unknown primary. Eur Radiol 9:470–473
19. Orel SG, Weinstein SP, Schnall MD et al (1999) Breast MR imaging in patients with axillary node metastases and unknown primary malignancy. Radiology 212:543–549
20. Stomper PC, Herman S, Klippenstein DL et al (1995) Suspect breast lesions: findings at dynamic gadolinium-enhanced MR imaging correlated with mammographic and pathologic features. Radiology 197:387–395
21. Obdeijn IM, Brouwers-Kuyper EM, Tilanus-Linthorst MM et al (2000) MR imaging-guided sonography followed by fine needle aspiration cytology in occult carcinoma of the breast. AJR 174(4):1079–1084
22. Olson JA Jr, Morris EA, Van Zee KJ et al (2000) Magnetic resonance imaging facilitates breast conservation for occult breast cancer. Ann Surg Oncol 7(6):411–415
23. Buchanan CL, Morris EA, Dorn PL at al (2005) Utility of Breast Magnetic Resonance Imaging in patients with occult primary breast cancer. Ann Surg Oncol 12:1045–1053

Table 1. Literature: results of breast MRI in Cup Syndrome

Year/author	Identified/CUP Breast cancer/ examinated	% Breast cancer found
1997 Morris	9/12	75%
1997 Tilanus–Lindthorst	4/4	100%
1999 Schorn	6/14	43%
1999 Orel	19/22	86%
1999 Stomper	2/8	25%
2000 Obdeijn	8/20	40%
2000 Olson	28/40	70%
2005 Buchanan	33/69	48%

CAD: is it really helpful?

Federica Pediconi, Valeria Dominelli.
Department of Radiological Sciences, "Sapienza", University of Rome, Rome, Italy

Breast Magnetic Resonance Imaging (MRI) is creating a revolution in breast diagnosis and intervention. In the last decade, breast MRI has evolved from being an investigational technique to a clinically valuable tool for breast cancer detection and diagnosis.

Because of its high sensitivity and effectiveness in dense breast tissue, MRI can be a valuable additional to the diagnostic work up of a patient with a breast abnormality or biopsy-proven cancer.

There are a number of clinical indications for which breast MRI is believed to add value to the conventional clinical and diagnostic work up, including evaluation of patients with axillary carcinoma and negative mammographic and clinical findings (Cup Syndrome), evaluation of women with questionable mammographic findings and previous breast surgery to distinguish post-surgical scar from recurrent carcinoma and staging of the extent of a cancer diagnosed by percutaneous needle biopsy.

The sensitivity of MRI to breast carcinoma and its high staging accuracy, has lead to the emerging role of MRI in breast cancer screening for women identified to be at high risk and to the current use for assessing tumor response to neo-adjuvant chemotherapy.

Breast MRI has not achieved widespread use in clinical practice because of its high cost and extensive time required by both the technologist and the radiologist in image acquisition, processing and interpretation.

Over the last years or so, many investigators have carried out basic studies and clinical applications toward the development of modern computerized schemes for detection and characterization of lesions in radiological images, based on computer vision and artificial intelligence. These methods and techniques are generally called computer-aided diagnosis (CAD) schemes and they provide the use of computerized image analysis in interpreting an imaging. Computer-aided diagnosis assist the interpreter by drawing attention to areas in the image that might have been overlooked, and by giving probability of malignancy estimates for regions of interest. It provides a second opinion with the potential to improve the diagnostic accuracy and efficiency of breast MR imaging interpretation.

Most of the FDA-approved breast MRI CAD commercially available supports evaluation of dynamic MR data acquired during contrast administration [e.g. CADstream® (Confirma), DynaCAD® (Invivo), 3TP® (formerly CADsciences, now ICad), AW & Functool ® (GE Medical)].

CAD softwares load a complete MRM study and automatically perform the necessary post-processing operations such as image subtraction, contrast adjustment and eventually image realignment.

Each image in each post-contrast sequence is previously realigned (registered), if necessary, to the corresponding image in the pre-contrast (basal) sequence, in order to reduce movement artefacts. The realigned images are then automatically subtracted in order to enhance only contrast agent related differences.

A significant enhancement threshold is defined on the basis of a global breast volume enhancement evaluation, in order to automatically identify all suspected lesions that could also be seen by the human eye.

For all the pixels above threshold in the subtracted images a SI/T curve is extracted and partitioned in a three linear piece-wise segmentation. According to the combination of angular coefficients of each of the three linear segments, the SI/T curve is associated with one (or none) of the typical SI/T trends. Thus, each pixel is color coded where red hues are associated with type III SI/T curve (more frequently in malignant lesions), while green ones are associated to type I (more frequently in benign lesions).

In 2005, Pediconi et al assessed the efficacy of a new software for the characterization of breast MR lesions [1]. They preoperatively evaluated 36 consecutive women with suspected breast cancer

based on mammography and sonography. Images were analyzed with the CAD software package and separately with a standard display method. A total of 68 lesions were detected at final diagnosis in the 36 evaluated patients and all were assessed histologically.

All 68 (100%) lesions were detected with both methods and good correlation with histopathologic specimens was obtained. Confidence for both detection and characterization was significantly (P=0.025) better with the color-coded method, although no difference (P= 0.05) between the methods was noted in terms of the sensitivity, specificity, and overall accuracy for lesion characterization. Excellent agreement between the two methods was noted for both the determination of lesion size (kappa=0.77) and determination of SI/T curves (kappa=0.85) (fig. 1).

The semiautomatic pixel by pixel analysis of the ROI makes the procedure largely operator independent and can help radiologists distinguish different patterns inside a single lesion, maybe allowing to reduce false negative evaluation.

Lehman et al. in 2006 evaluated thirty-three consecutive lesions (nine malignant, 24 benign) seen only on MRI with and without an automated software. They recorded the automated analyses of kinetic enhancement for each lesion at 50%, 80% and 100% enhancement threshold [2].

All malignant lesions showed significant enhancement at all thresholds. In comparison with the unassisted interpretations, the computer-assisted analyses yielded false-positive rates that were reduced by 25% at a 50% threshold, 33% at an 80% threshold (p=0.05) and 50% at 100% threshold for enhancement (p<0.01). Lehman did not observed significant differences between enhancement profile of benign and malignant lesions.

This latter issue was recently examined by Williams and her group [3]. They retrospectively determined the sensitivity of kinetic features measured with computer-aided evaluation in discriminating benign from malignant lesions, with histopathologic findings as reference standard. In the evaluation of 154 lesions (41 malignant, 113 benign), the presence of threshold enhancement at computer-aided evaluation was sensitive for malignancy, with 38 of 41 (93%) malignant lesions demonstrating enhancement at both the 50% and 100% thresholds. The discrimination between benign and malignant lesions was improved by the absence of threshold enhancement at computer-aided evaluation compared with that at initial interpretation by the radiologists. Therefore false-positive rates were reduced by 8.8% at the 50% enhancement threshold (not significant) and by 23.0% at the 100% enhancement threshold (p=0.02) when compared with that at initial interpretation.

They concluded that computer-aided evaluation has the potential to improve the discrimination of benign from malignant breast lesions at MR imaging but, given the presence of false-negative cases, it should be always used as a tool to supplement the radiologist's subjective interpretation.

While manual placement of a region of interest provides kinetic information only for portions of a given lesion, computer-aided evaluation generates detailed data for all pixels in the lesion. Furthermore, several studies demonstrated that there is high degree of variability in curve shape estimates from manually-placed ROIs. The radiologists agreement rate improve from 60% to 73% when ROIs are automatically selected using breast MRI CAD systems.

In addition to improving specificity, automated software programs should contribute to the field of breast MRI by providing more objective and detailed information regarding MR examinations and lesions. Computed-aided evaluation could decrease heterogenicity of interpretations across radiologist of varying levels of experience in breast MRI interpretations. A full automated system has also the potential to decrease the amount of time required for image processing.

In 2005 Demartini et al analyzed the utility of CAD applied to breast MRI in 15 patients undergoing neo-adjuvant chemotherapy for 16 newly diagnosed advanced breast cancers [4]. Following chemotherapy, 7/16 showed no residual significant enhancement but all had residual disease at pathology. Furthermore they observed that radiologist-measured tumor sizes demonstrated better correlation with sizes at pathology compared with CAD generated tumor size. CAD may be helpful in assessing changes in MRI enhancement profiles of tumors following chemotherapy. However, CAD-assessed significant enhancement following chemotherapy can be falsely negative for residual malignancy, and CAD tumor sizes are less accurate than those measured by the radiologist in predicting size of residual malignancy. CAD may complement but should not replace the radiologist's assessment of tumors in this patient population.

Commercial breast MRI CAD systems rely primarily on kinetics analysis for detecting suspicious regions but there is clinical need for including morphology analysis into CAD systems to assist radiologists in the detections of cancers and differentiation of benign from malignant lesions.

Another serious problem is observer variability in evaluation of lesion morphology. Fully automated computer-generated features have no user variability which increase objectivity and reproducibility and simplifies MRI analysis.

In the last years different CAD systems and new algorithms have been developed in order to employ morphology to analyze margin sharpness and to determine the degree of lesion vascularization. These systems are particularly helpful for identifying cancers that fail to exhibit cancer-like kinetics, such as many invasive lobular carcinomas and some ductal carcinomas in situ (DCIS).

ONCAD® (Penn Diagnostic) is the first FDA-cleared, morphology-based CAD system designed for contrast-enhanced MR. Analyzing MR results with morphology, ONCAD® highlights regions with suspicious margins.

In a multicentric study published in 2006, Penn et al. presented a fully automated method of identifying and classifying margin sharpness of breast lesions on MR that can be used to direct radiologists' attention to lesions with suspicious morphologies [5]. In particular they demonstrated the effectiveness of morphological blooming both for the identification of cancers with benign-like kinetics and the discrimination of normal tissues that exhibit cancer-like enhancement curves.

In the last year, we tested the utility and the diagnostic accuracy of a new investigational CAD system (not yet commercially available), CAREBOX® (Bracco Imaging, Spa), that integrate morphologic and dynamic information in order to better differentiate between malignant and benign lesions.

To assess the efficacy of the new software for the detection and characterization of MR breast lesions, we retrospectively evaluated 60 consecutive patients who underwent breast MRI examination from September 2007 to January 2009 for whom histological reports or follow-up at 12 months were available.

Images were analyzed with the new software and separately with the standard method by an expert radiologist. Statistical comparison was performed for diagnostic accuracy in lesion detection and characterization, on lesion and patient basis, and compared with histopathologic findings or follow-up.

A total of 118 lesions (73 malignant and 45 benign) were detected at final diagnosis in the 60 evaluated patients and all were assessed histologically or with a follow-up. CAD detected 67 of the 73 malignant lesions (sensitivity 92%) and, among these lesions, 57 were correctly classified as malignant (sensitivity 85%) (fig. 2, fig. 3). Regarding benign lesions the CAD system identified 42/45 benign lesions (sensitivity 93%) and 29/42 were correctly classified as benign (specificity 70%).

Breast MRI CAD workstations automate post-processing of acquired breast MRI exams and offer software to further analyze suspicious lesions. Analysis systems can make interpretation of breast MRI exams faster and, in some cases, more reliable than interpretation from PACs or film.

The introduction of CAD systems in the diagnostic routine will definitely help radiologists who has a short-time experience by giving them a second opinion [5]. CAD evaluation will also be a valuable tool for expert radiologists since it will bring a remarkable speed-up of their work especially when the new softwares, with morphological information included, will be fully integrated with any MRI scanner and PACS.

Nowadays, because of the presence of false positive or false negative findings in some cases, CAD systems should be always used only as a supplement to the radiologist's subjective interpretation.

Additional studies are being performed to evaluate more clearly the ability of software programs to address challenges that delay more widespread dissemination of breast MRI in appropriate clinical populations.

References

1) Pediconi F, Catalano C, Venditti F, Ercolani M et al. Color-coded automated signal intensity curves for detection and characterization of breast lesions: preliminary evaluation of a new software package for integrated magnetic resonance-based breast imaging. Invest Radiol 2005; 40 (7): 448–57

2) Lehman CD, Peacock S, Demartini WB, Chen X. A new automated software system to evaluate breast MR examinations: improved specificity without decreased sensitivity. AJR 2006; 187 (1) 51–6

3) Williams TC, Demartini WB, Partridge SC et al. Breast MR imaging: computer-aided evaluation program for discriminating benign from malignant lesions. Radiology 2007; 244(1):94–103

4) Demartini WB, Lehman CD, Peacock S, Russell MT et al. Computer-aided detection applied to breast MRI: assessment of CAD-generated enhancement and tumor sizes in breast cancers before and after neoadjuvant chemotherapy. Acad Radiol. 2005 12(7): 806–14

5) Penn Al, Thompson SF, Brem RF, Lehman et al. Morphologic blooming in breast MRI as a characterization of margin for discriminating benign from malignant lesions. Academic Radiology 2006; 13:1344–1354

6) Veltman J, Mann RM, Meijer FJA et al. The additional value of three time point color coding in dynamic contrast-enhanced MRI of the breast for inexperienced and experienced readers. Eur J Radiol 2009, in press

Figures

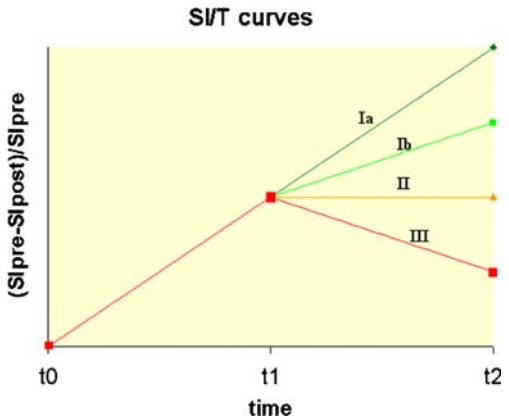

Fig.1: SI/T types: Ia, Ib = benign lesion, II = borderline, III = malignant lesion

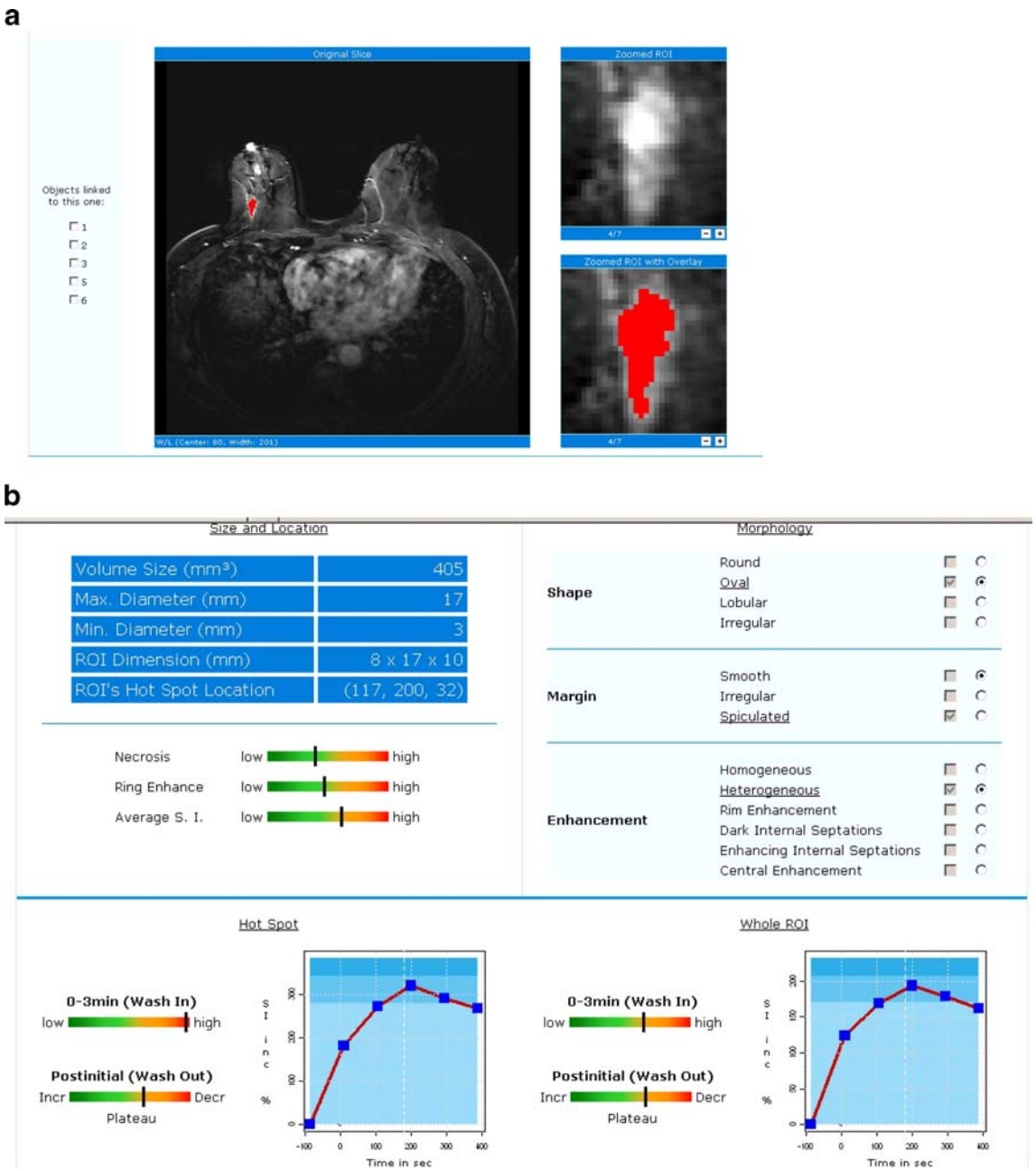

Fig.2: Breast MRI identified an irregular enhancing mass classified at pathology as an ILC. This lesion were identified on CAREBOX® (A), and correctly classified in the report (B).

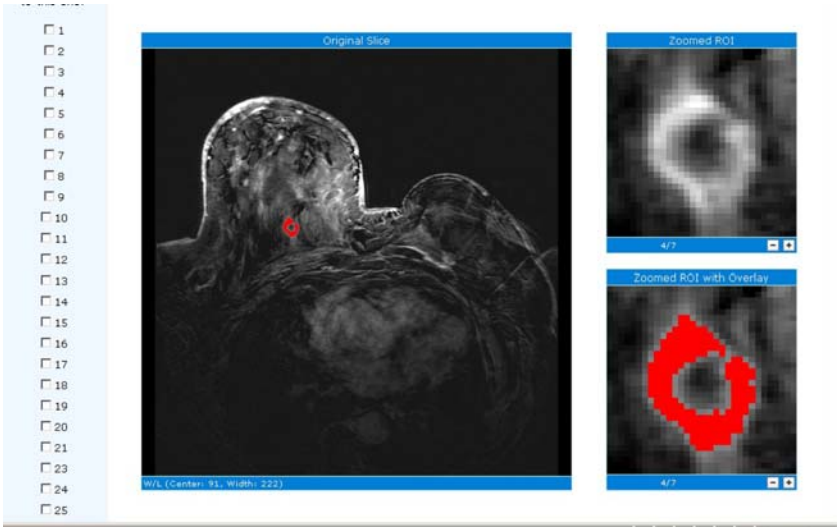

Fig.3: Typical "rim enhancement" in malignant lesion (IDC) correctly evaluated by CAD system.

Adaptive 3D K-Space Sampling with Compressed Sensing for Breast MRI

Chan R, Marshall H, Ramsay E, Plewes DB
Imaging Research, Sunnybrook Health Sciences Centre, University of Toronto, Canada

Introduction

Women who carry the BRCA1/2 gene mutations have an elevated lifetime risk (>80%) of breast cancer[1]. Unlike conventional mammography, dynamic contrast-enhanced magnetic resonance imaging (MRI) has a high sensitivity (71–100%)[2] for detecting cancers in this population. However, current DCE-MRI methods have a more modest positive predictive value of approximately 45%[2] reflecting the challenge of consistently distinguishing malignant cancers from benign tumours. Without improvement, a percentage (approximately 3–5%) of screened patients will continue to undergo unnecessary and invasive breast-biopsy procedures for benign lesions[2]. The differentiation of malignant and benign lesions can be improved by having images of high spatial resolution, to visualize morphological features of the tumour, together with images of high temporal resolution to probe lesion pharmacokinetics. However, conventional Cartesian sampling methods are capable of producing only one type of image, with a specific spatio-temporal resolution balance. Thus the ideal goal of achieving both high temporal and high spatial resolution bilateral imaging for each patient, may require two MRI contrast-enhanced examinations with the concomitant increase in cost, complexity and patient anxiety.

Adaptive Sampling

As an alternative to conducting prescribed scans of a known spatial-temporal resolution, an adaptive sampling of k-space data[3] can be considered. This approach allows either high-temporal-resolution or high-spatial-resolution images to be retrospectively reconstructed from the same dataset with the advantage that multiple images sets can be produced, each with a different spatial-temporal balance. The high spatial resolution images show details of breast morphology but use data acquired over a long time, while the high temporal resolution images from the same scan provide information on contrast uptake, but rendered with reduced spatial resolution.

Initial approaches of adaptive sampling using 2D radial imaging[4,5] (or stacks of 2D planes to perform volumetric imaging) were restricted to discrete resolutions due to the commensurate nature of the radial spokes that were chosen. A more flexible golden-angle 2D-radial-sampling method has been developed[6] that eliminates the need to reconstruct at discrete resolutions. This method achieves this by incrementing each successive spoke from the last by the golden angle $(\sqrt{5}-1)/2*180° \approx 111.25°$. An important property is that any consecutive set of spokes is relatively well-distributed, regardless of the number of spokes in the set. The added flexibility of this approach allows imaging to be truly adaptive (in 2D), since image reconstruction can be performed at any spatio-temporal resolution, using any number of spokes to create a 2D image. Recently, we have extended this approach to volume acquisition with 3D radial sampling of k-space using multidimensional golden means (MGM) based on a general formulation of the Fibonacci sequences[7]. In this application, we use two-dimensional golden means (rather than the golden angle from [6]) and a method to transform the resulting sampling pattern to generate radial spokes in 3D k-space. This allows various images to be reconstructed in 3D with an arbitrary spatio-temporal resolution balance.

Having extra flexibility of reconstruction in 3D is potentially important for several reasons. As the enhancement profile for any patient is unknown prior to imaging, we cannot predict at what point in the enhancement process will yield maximum contrast. With an adaptive method, reconstruction can be carried out to reconstruct data at any time, and over any temporal window to ensure maximum tumour contrast. As a result, we anticipate the potential for optimizing lesion conspicuity on a patient specific basis. Furthermore, being able to adjust the temporal resolution of the reconstructed image allows a more accurate assessment of the start of enhancement, potentially improving the accuracy of pharmacokinetic modeling of contrast kinetic uptake.

Reconstruction of Adaptive Data

One drawback of all of these techniques is that the high-temporal-resolution (dynamic) images suffer from under-sampling aliasing artifacts which present as well-defined streaks in the image domain. One very simple approach to remove these artifacts is through a KWIC reconstruction as proposed by Song[8]. In this method, data from different radial samples are used to fill k-space with an approximately uniform sampling density. As the periphery of k-space will require more radial samples, the data must be drawn from greater number of samples which are

acquired over a longer duration. As such, while KWIC images show excellent suppression of aliasing artifacts, they exhibit a spatial-frequency-dependent temporal resolution which makes the enhancement of the lesion somewhat size-dependent. Another approach is based on a constrained reconstruction approach such as HYPR and its variants as proposed by Mistretta[9]. Originally developed for MRA applications where the objects of interest are sparse in space. In principle HYPR can be applied to reconstruct objects that are not sparse but imposes the physiologically unrealistic constraint that tumours enhance in a spatially uniform manner. Alternatively, one can apply imaging processing technique to remove aliasing artifacts. We have shown that independent components analysis (ICA), can remove streaks from 2D images when obtained with under-sampled radial data[10,11]. While the resulting images are visually improved, they are not quantitatively reliable. A general and potentially more robust approach of reducing aliasing artifacts is through the use of reconstruction methods based on regularization and iterative minimization techniques[12].

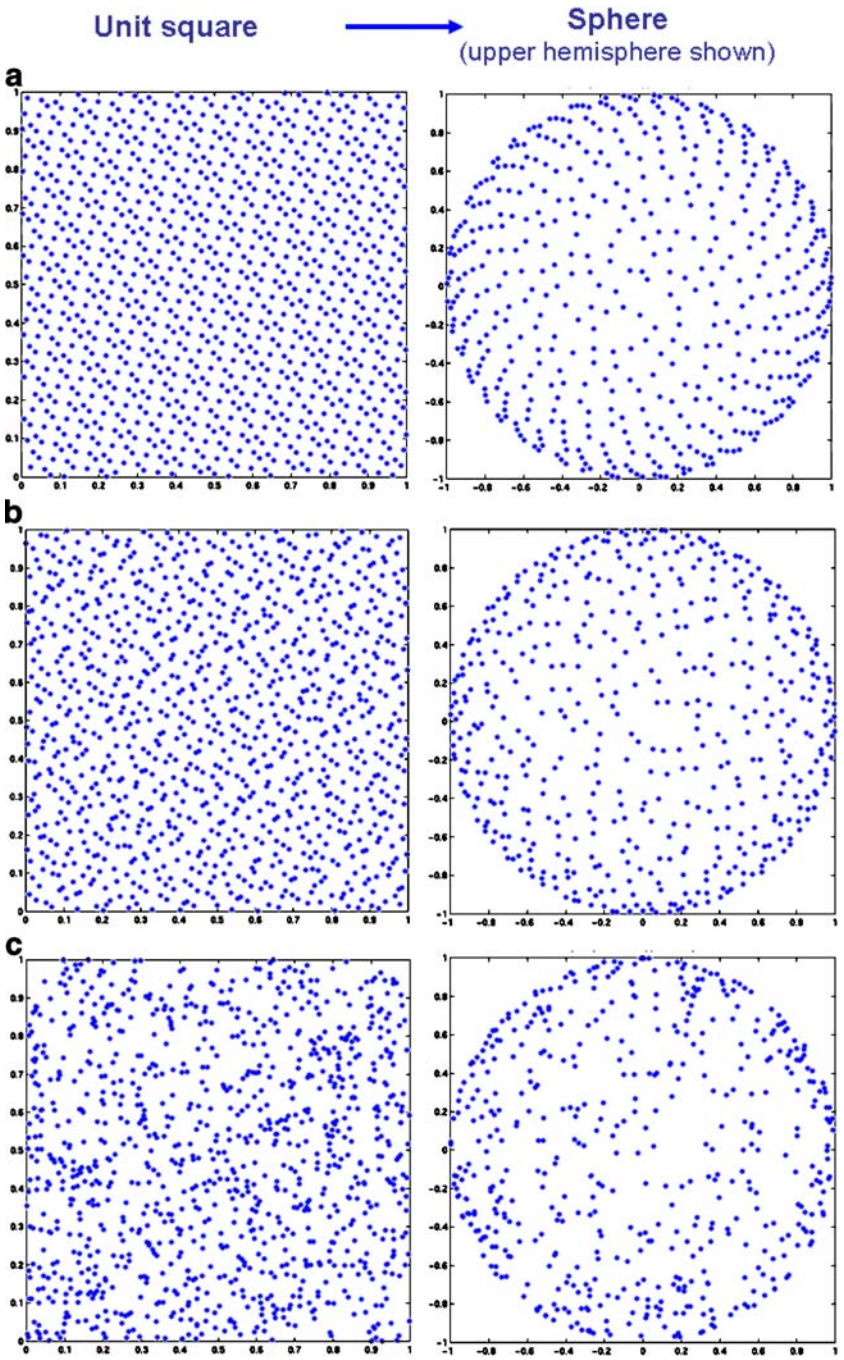

Figure 1. Sampling patterns: Sample points generated from 3 different sampling schemes (a) multidimensional golden means (MGM), (b) Halton sequences and (c) random sampling are shown. One hundred sample points on a unit square (on the left column) are transformed to a spherical geometry (shown on the right column, of upper hemisphere only, as seen from above) for 3D radial sampling.

These methods work by adding a-priori knowledge or imposing additional constraints into the reconstruction process which fundamentally reduces the amount of data needed to reconstruct the desired image. As a result, the magnitude of aliasing artifacts can be dramatically reduced. Operationally, this is done by seeking an image which is consistent with both the data we measure and any a-priori assumptions we can realistically make about the object. More specifically, this is done using penalty terms to an objective function *f(x)* that is to be minimized: $f(x) = \|Ax - y\|_2^2 + \lambda R(x)$, where x is the image we want to reconstruct, *R(x)* is the penalty function, *A* is the forward physics of the MR imaging system (in this case a Fourier Transform operator), and *y* is the under-sampled k-space data. The choice of λ, the regularization parameter, influences the final image by balancing its consistency with the measured data against obeying our a-priori assumptions.

If the image is sparse in some domain and incoherent sampling is used, as in the case of certain adaptive sampling methods, then L1-norm regularization can be used to perform compressed sensing[13,14] on MRI data[15]. Compressed sensing is capable of exactly recovering sparse data from very few samples. In compressed sensing, the regularization terms are typically of the form $R(x)=\|Wx\|_1$, where $\|\cdot\|_1$ is the L1-norm of a vector and *W* is some sparsifying transform. By incorporating compressed sensing methods into our adaptive reconstruction, we can reduce unwanted aliasing artifacts from our dynamic images, using a non-linear conjugate gradient minimization algorithm[15].

We have studied the sparse properties of the image data using a wavelet transform. This is consistent with the property of adaptive sampling which exhibits a level of incoherence in the k-space sampling which is a necessary for the success of a compressed sensing reconstruction. We also explored different 3D adaptive sampling techniques that may be better suited for sparse reconstruction. Specifically, we have compared the point-spread-function characteristics of MGM sampling with that that of Halton sampling[16] and found that Halton sampling appears to offer more advantageous data incoherence compared to that of MGM or random sampling[17] with a reduction in aliasing artifacts in 3D.

This is illustrated in Figure 1 where three different sampling schemes: MGM, Halton sampling, and random sampling are compared. On panels a, b and c, we illustrate the sampling properties of the three approaches in a unit square. In this representation, the ordinate (y value) and abscissa (x value) represent the values of a two-dimensional adaptive sample. For example, in panel c, each point is determined by a pair of random numbers between 0 and unity. The distribution of points is truly random in the unit square and shows regions where tight clustering of data points can occur as well as regions were adjacent data points are sparsely distributed. In the corresponding panel on the right, this unit square is mapped onto the surface of a unit hemisphere with each point representing the tip of a radial k-space sampling trajectory. In this case, we see large regions that are poorly sampled, which results in large aliasing artifacts and thus reduced image quality. However, when compared MGM, we find more coherent aliasing artifacts that result from the spiraling pattern of samples seen towards poles of the sphere (Figure 1a). We have shown that Halton sampling (Figure 1b) provides a good compromise between MGM (Figure 1a) and random sampling (Figure 1c), yielding more incoherent aliasing artifacts and thereby striking a balance between the liabilities of increase aliasing artifacts while maintaining data incoherency to exploit in compressed sensing reconstruction.

Summary

We present the combination of compressed sensing and multi-dimensional incoherent adaptive-sampling methods to achieve a flexible image acquisition with arbitrary spatio-temporal resolution while offering the potential for controlling aliasing artifacts through compresses sensing algorithms. The combination of these approaches could potentially improve image quality in adaptive DCE-MRI and possibly enhance the differentiation of malignant versus benign lesions in breast MRI screening in the future.

References

1. Ford D, et al. Am J Hum Genet 1998. 62: p.676–689.
2. DeMartini W, et al. Acad Radiol 2008; 15:408–416
3. Song HK, et al. Magn Reson Med 2001;46:503–509.
4. Du J, et al. Magn Reson Med 2002; 48:516–522.
5. Ramsay E, et al. Magn Reson Med 2006; 24:617–624.
6. Winkelmann S, et al. IEEE Trans Med Imaging 2007;26:68–76.
7. Chan RW, et al. Magn Reson Med 2009; 61:354–363.
8. Song HK et al, MRM, 2000, 52, 815–824,
9. Mistreeta C. et al, MRM 2006,55(10): 30–40
10. Martel AL, et al. Magn Reson Med 2008;59 :874–884.
11. Martel AL, et al. ISMRM Workshop on Data Sampling and Image Reconstruction, Sedona 2009. Poster #18.
12. Block KT et al, MRM2007, 57, 1086–1098.
13. Candes E, et al. IEEE Trans Information Theory 2006;52:489–509.
14. Donoho D. IEEE Trans on Information Theory 2006;52:1289–1306.
15. Lustig M, et al. Magn Reson Med 2007; 58:1182–1195.
16. Halton JH. Numerische Mathematik. 1960;2:84–90.
17. Chan RW, et al. ISMRM Workshop on Data Sampling and Image Reconstruction, Sedona 2009. Poster #34.

Hyperpolarized ^{13}C NMR for Cancer Imaging

Cunningham CH, Chen AP, Plewes DB
Imaging Research, Sunnybrook Health Sciences Centre, University of Toronto, Canada

Introduction

In clinical practice, the detection, diagnosis and staging of cancer remains a primary challenge. All primary modalities can, with the addition of appropriate contrast agents, provide anatomic demarcation and in the case of MRI offer excellent definition of the extent of breast cancers. MRI contrast agents such Gd-DTPA have simple structures that operate on the basis of well know mechanisms to alter relaxation times. In spite of their biological simplicity, these agents have proven to be extremely valuable with breast DCE-MRI being an excellent example. In this case, contrast enhancement resolves factors related to tumour blood flow, microvascular permeability, extravascular–extracellular distribution spaces and microvascular architecture. Taken together, Gd-DTPA as a contrast agent for DCE-MRI is a simple, yet reliable contrast agent for sensitive detection of early breast cancer.

Recently there is a growing interest in molecular imaging methods which promise a class of agents that are targeted to, and in some cases, activated by a specific biological mechanism. Such agents must meet daunting challenges for human application, including that they exhibit adequate molecular specificity, appropriate sensitivity to permit detection by human scale imaging machines such as CT, ultrasound or MRI, are easily delivered, while at the same time being cost effective and posing negligible toxicity. Of course, isotopic imaging methods and in

particular ^{18}FDG-PET imaging represents one of the few examples of such an agent that is widely available for clinical use. In particular,^{18}FDG-PET has recently gained acceptance for its ability to detect and diagnose cancer by virtue of the fact that ^{18}FDG mimics glucose and as such reports glucose transport. ^{18}FDG is metabolized into 3-deoxyglucose-6-phosphate, which becomes trapped inside a glucose consuming cell thereby rendering it detectable under PET. As such, ^{18}FDG-PET images indicate areas of high glucose transport and a high rate of aerobic glycolysis[1], known as the Warburg effect[2]. While not seen in all cancers, it appears to be a common feature in rapidly growing tumours[3] with energy production in many tumours being as much as 400 fold greater than the energy demands of normal biosynthesis[4].

Recently an alternate approach for assessing metabolism and associated diseases manifesting the Warhburg effect has been proposed in the form of metabolic imaging with dynamic nuclear polarization (DNP)[5,6]. This new class of MR imaging appears to address the challenges of specificity, sensitivity and toxicity and may provide an alternate approach to ^{18}FDG PET imaging. The technique operates to generate an injectable solution that is "hyperpolarized", or exhibits a degree of spin alignment that is up to 5 orders of magnitude higher than that at normal conditions within a standard 3T MRI system. Unlike ^{18}FDG PET imaging, this large increase in magnetic signal offers the potential to conduct metabolic imaging on a very short time scale and offers the potential to track the time constants and reaction rates of key metabolites in a chosen biochemical pathway. Various spin-1/2 nuclei can be hyperpolarized using this method, but the majority of work done thus far using ^{13}C-labeled pyruvate[7] that enables imaging of enzymatic reactions involved in cellular metabolism *in vivo*. The fact that pyruvate is at the root of major energy-generating metabolic pathways suggest that altered pyruvate dynamics will be a sensitive indicator to differentiate normal from cancerous cells. It has been shown that injected hyperpolarized pyruvate in cancer cells is avidly exchanged with lactate[8,9] and alanine[10]. This makes ^{13}C-DNP a promising candidate as a new tool in cancer diagnosis and treatment monitoring. In this lecture, we present an overview of the operation of a DNP polarizer, the logistics of metabolic imaging experiments using hyperpolarized [1-^{13}C] pyruvate, current work with tumor models in vivo, and the potential applications to breast cancer imaging using hyperpolarized substrates.

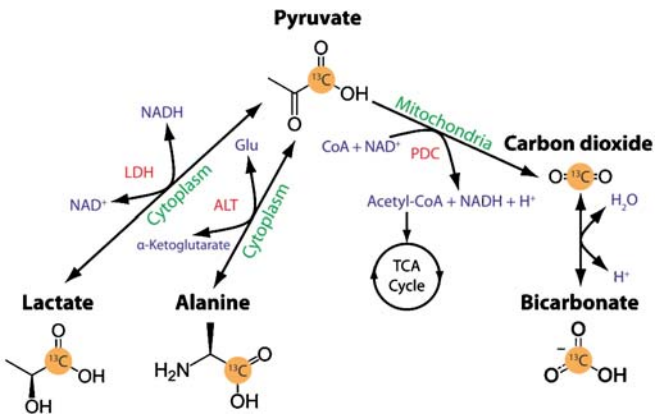

Figure 1. The metabolic reactions that can be probed by the injection of hyperpolarized pyruvate in vivo.

Operation of a DNP-Dissolution System

A DNP-dissolution system consists of vertical-bore superconducting magnet equipped with a cylindrical variable-temperature insert (VTI) containing a microwave chamber at the center of the magnet. By pumping the liquid He bath in the VTI down to low pressure, the temperature within the liquid He can be lowered to ~1 K. The only polarizer currently available commercially (HyperSense, Oxford Instruments) operates at a field strength of 3.35 T and a temperature of 1.4 K.

A small sample (e.g. 50 μL) of a purified substrate labeled with a spin-1/2 nucleus, such as [1-^{13}C] pyruvate, is doped with mM concentrations of a stable organic free radical and placed within the microwave chamber and cooled to the operating temperature of the polarizer over several minutes. Microwave irradiation at a frequency near the electron spin resonance (94.1 GHz at 3.35 T) mediates a transfer of polarization from the highly polarized electrons provided by the free radical to the spin-1/2 nuclei, with the polarization buildup taking place over about 1 hour until it reached equilibrium.

In order to create an injectable solution of the desired substrate, the sample must be thawed to room temperature. This is done by heating a buffered solvent (~5 mL) to high temperature and pressure, and then releasing the solvent so that it rapidly mixes with the frozen sample. This dissolution takes place in seconds, and forces the diluted sample out of the polarizer magnet and through a transfer line and into a collection vessel outside of the polarizer. If this dissolution is sufficiently rapid, the result is a hyperpolarized solution that is ready for injection *in vivo*.

***In vivo* Experiments with Hyperpolarized Pyruvate**

Hyperpolarized pyruvate is typically dissolved to a concentration of 80 mM for small animal applications. The T1 of the magnetization in solution, which determines the decay rate of the hyperpolarization, depends on the local magnetic environment but is on the order of 60 seconds at 3T. This necessitates rapid transfer of the solution to the injection site. For rat experiments, a 2 mL injection can be administered through an extension tube attached to a tail vein catheter. The injection is delivered as a bolus over ~10 seconds.

A ^{13}C spectrum acquired several seconds after the injection will contain peaks corresponding to the injected pyruvate, but also from products of the reaction between pyruvate and several enzymes involved in cell metabolism. These other peaks are shifted in frequency due to the change in the molecular structure surrounding the ^{13}C nucleus after the corresponding reaction. The products of these biochemical reactions can be seen *in vivo* after the injection of hyperpolarized pyruvate, as shown in Fig. 1.

The data acquisition in a ^{13}C exam consists of conventional proton imaging for anatomical reference, followed by acquisition of ^{13}C spectroscopic (frequency-resolved) data containing information about the relative heights of the various peaks. This spectroscopic acquisition can take several forms ranging from a dynamic acquisition (see Fig. 2) in which spectroscopic data with poor spatial localization (e.g. data from an entire slice) are acquired every 2 or 3 seconds for several minutes, to an

imaging acquisition in which a snapshot of the spatially-resolved peaks heights is taken over a smaller time window, as indicated by the imaging window shown in Fig. 2.

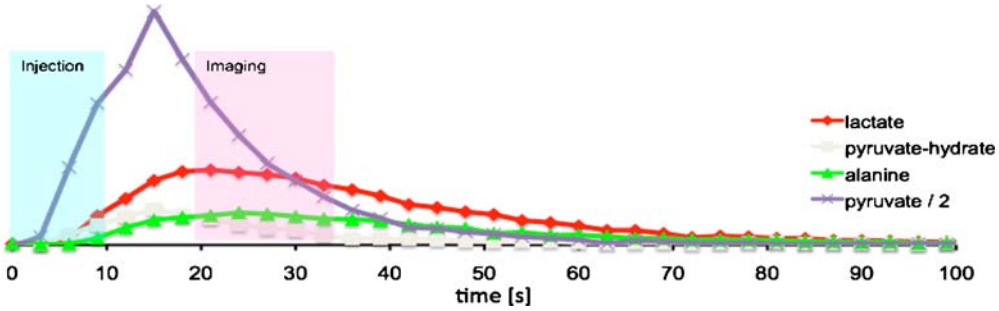

Figure 2 A dynamic 13C acquisition results in a time-course for the injected substrate as well as the products resulting from the associated enzymatic reactions. Such a time course can be used to model the kinetics of these reactions, giving a measure of enzyme activity, or can be used to measure the appropriate timing for an 13C spectroscopic imaging acquisition as shown in Fig. 3.

Elevated Lactate in Cancer

Hyperpolarized ^{13}C studies have shown promise as new tool in the management of cancer due to the fact that certain cancers are known to display abnormal metabolism associated with the Warburg Effect. This is characterized by the effect that most tumors produce energy predominantly by glycolysis, producing lactate, as opposed to normal oxidation of pyruvate within the mitochondria as in most normal cells. This phenomenon is seen as an elevated lactate-to-pyruvate ratio in the tumor region when compared to spectra outside the tumor where lactate levels are much reduced as seen as shown in the central panel of Fig. 3.

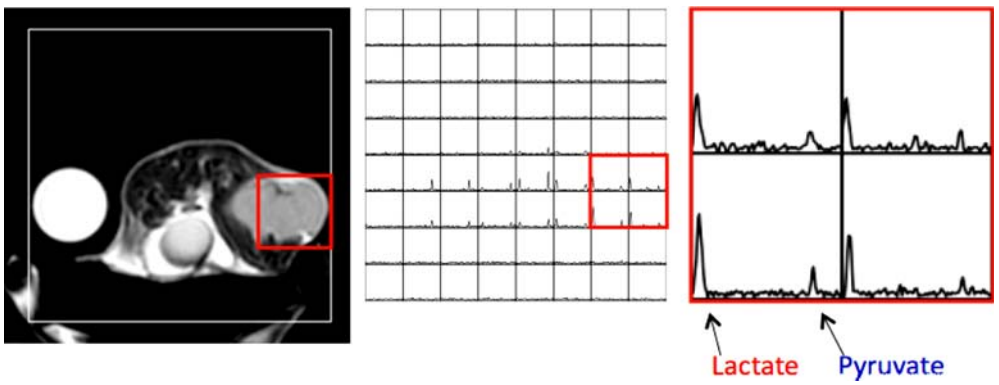

Figure 3: *Hyperpolarized 13C study of an MDA-231 breast cancer xenograft in the mouse hind limb. (Left) The T2-weighted anatomical image is used as a reference for the spatially-resolved 13C spectroscopic imaging data. (Middle) The 3D spectroscopic imaging acquisition results in a grid of spectra with each grid element corresponding to the different spatial locations within the white box shown on the anatomical image. (Right) The voxels within the tumor, which correspond to the red box on the anatomical image (Left) and the grid of spectra (Middle) displays a lactate-to-pyruvate ratio higher than any other location, indicating an aggressive cancer.*

Applications to Human Breast Cancer

The studies outlined above were all in animal models and illustrate the potential of elevated lactate/pyruvate ratios to identify cancer. However, in order for these to be applied to human applications, the processing of the pyruvate sample must be altered to remove the mM concentration of the free-radial which was introduced for the generation of electron spin polarization that was transferred to the ^{13}C nuclear spins. This filtering must be done in such a way to ensure the sample sterility and is a topic of active research[11]. Given the success of this development, one can anticipate a number of interesting applications of ^{13}C-Pyruvate hyperpolarized MRI in breast cancer. In particular, ^{13}C NMR spectroscopy has been used to assess choline transport in breast cancer cell lines[12] which is a similar finding to that offered by proton spectroscopy[13]. As pyruvate transformation into lactate appears to be elevated in cancer cells and thus resolved by hyperpolarized ^{13}C-labelled pyruvate, one can anticipate that this technique could find application in assessing the efficacy of neo-adjuvant therapy in locally advanced breast cancer patients parallel to the findings of proton spectroscopy. Similarly, such a technique may find application in the detection of early indicator of breast cancer recurrence. Unlike proton MRS, the lack of large background solvent signal (water and fat) in ^{13}C spectra may allow detection

of smaller region of residual / recurrence disease. While the obvious application as an aid in differentiating lesion characterization may be feasible, competitive and less complex alternatives such as diffusion imaging or proton spectroscopy would appear more attractive. The future of the technology will depend on the critical step of demonstrating achieving safe and effective human studies which are in the planning phase for application in the prostate[14]. Given a positive and cost effective outcome with these studies, applications in breast cancer may not be far behind.

References

1. Board M et al, Biochem J, 1990: 265: 503–509.
2. Xu RH et al, Cancer Res 2005: 65: 613–621.
3. Dastidar SG et al, Exp Cell Biol 1989; 57: 159–164.
4. Newsholme EA et al, Adv Enzyme Regul, 1991; 31: 225–246.
5. Golman K et al, Proc Natl Acad Sci USA, 2003;100:10435–10439.
6. Ardenkjaer-Larsen JH, Proc Natl Acad Sci USA, 2003: 100: 10158–63.
7. Golman K et al , Cancer Research 2006(20),10855–60
8. Koukourakis MI et al Neoplasia 2005; 7:1–6
9. Golman K et al, Proc Natl Acad Sci USA 2006; 103: 11270–11275.
10. Day, S.E. et al Nat Med 2007;13(11):1382–1387
11. Vigneron DB, 17th Scientific Meeting and Exhibition of the International Society of Magnetic Resonance in Medicine, lecture 51, April 18–24, 2009, Honolulu, Hawaii.
12. Katz-Brull R. et al, Cancer Research, 62, 1966–1970, 2002
13. Bolan, P.J. et. al. MagnReson Med. 2003 Dec;50(6):1134–43
14. Kurhanewicz J., 17th Scientific Meeting and Exhibition of the International Society of Magnetic Resonance in Medicine, lecture 770, April 18–24, 2009, Honolulu, Hawaii.

Surprising results in the other breast!

D.M. Renz[1], J. Böttcher[1], T. Vag[1], A.B. Herzog[1], M. Gajda[2], O. Camara[3], I.B. Runnebaum[3], W.A. Kaiser[1]
[1]Institute of Diagnostic and Interventional Radiology, Friedrich Schiller University Jena, Germany
[2]Institute of Pathology, Friedrich Schiller University Jena, Germany
[3]Clinic of Gynaecology, Friedrich Schiller University Jena, Germany

Introduction

Magnetic resonance mammography (MRM) has become a well-established method in the diagnosis of invasive breast carcinoma (1–3). In the pretherapeutic staging of invasive breast cancer, MRM is the most accurate imaging modality in determining tumour size and in depicting multifocality and multicentricity (4–6). Magnetic resonance imaging (MRI) has also the potential to visualize by X-ray mammography or ultrasonography missed contralateral breast malignancies in patients with primary breast cancer; the published detection rate for otherwise occult contralateral carcinomas ranged up to 24% (4, 7–11).

Women with unilateral, i.e. primary index, breast cancer reveal an increased risk of developing an additional contralateral breast carcinoma. Indeed, the most common second malignant tumour for patients with unilateral breast carcinoma is cancer in the contralateral breast (12, 13). To our knowledge, a comparison of the MRI appearance of the primary index versus the contralateral carcinomas, has not been analysed in detail. The purpose of this study was to describe MRI characteristics of the bilateral carcinomas, considering dynamic and morphologic parameters in T1- and T2-weighted sequences, and to compare the tumour appearances of the corresponding bilateral carcinomas. The further aim was to compare histologic findings and the main localization of the primary index versus the contralateral carcinomas.

Patients and Methods

The observation period of our investigation was extended with a nearly duration of 12 years. All evaluated MRI examinations were performed at our radiological institute from December 22nd, 1994 to October 16th, 2006 using standardized MRI conditions. Only MR mammographies with subsequent histology were included. To achieve reliable data for histology (i.e. same pathologist), exclusively patients from the clinic of gynaecology at our university hospital were enrolled. In the observation period, 1345 patients with histologically verified 917 malignant and 586 benign lesions fulfilled the inclusion criteria. The 917 malignant lesions were seen in 875 women: 833 subjects presented a unilateral breast carcinoma, and 42 women showed besides the primary index a contralateral breast carcinoma. Thus, contrast-enhanced MR mammography revealed in 42 of 875 patients (4.8%), who suffer from a primary index breast carcinoma, a contralateral cancer. The ages of these 42 women ranged from 33 to 87 years (mean=62.9±11.6 years). All of the 42 primary index carcinomas could be detected by X-ray mammography and ultrasonography alone or by both imaging modalities. The 42 subjects received MR mammography for pretherapeutic staging. However, only 20 of 42 contralateral breast carcinomas (47.6%) could be visualized by X-ray mammography and/or ultrasonography. Thus, MRM had the potential to detect 22 of 42 (52.4%) on X-ray mammography and ultrasonography occult malignant lesions. In 875 patients, MRI therefore identified 22 (2.5%) otherwise missed breast cancers.

All MRI examinations were performed with two technically comparable imaging protocols. Firstly, the images were performed by a 1.5-T Gyroscan ACSII-scanner (Philips Healthcare, Hamburg, Germany). For the dynamic study, multi-slice 2D fast-field-echo axial T1-weighted sequences were obtained with the parameters as follows: repetition time TR 97 ms; echo time TE 5.0 ms; matrix 205×256; flip angle 80°; slice thickness 4.0 mm; field of view 350 mm. Axial T2-weighted turbo-spin-echo images (TR 4,000 ms; TE 300 ms; matrix 193×256; flip angle 90°; field of view 350 mm) were obtained in identical slice positions. Secondly, the images were obtained by a 1.5-T Siemens system (Symphony; Siemens Medical Solutions, Erlangen, Germany). For the dynamic study, multi-slice 2D FLASH (fast low-angle shot) axial T1-weighted sequences were acquired with the following parameters: TR 113 ms; TE 4.6 ms; matrix 384×384; flip angle 80°; slice thickness 3.0 mm; field of view 350 mm. Axial T2-weighted turbo-spin-echo images (TR 8,900 ms; TE 207 ms; matrix 512×512; flip angle 90°; field of view 350 mm) were performed in identical slice positions. In both technical protocols, 0.1 mmol/kg body weight gadopentetate dimeglumine (Magnevist; Bayer Schering Pharma, Berlin, Germany) was intravenously administered as a rapid bolus followed by 20 ml saline flush after acquisition of a native T1-weighted sequence. Thirty seconds after contrast media and saline injection, dynamic MRM was continued with the same

sequence parameters and under identical tuning conditions at 1-min intervals up to 7 min. The native unenhanced images were subtracted from postcontrast dynamic images.

Results

Nearly all of the primary index carcinomas were histologically confirmed as invasive tumours; only two of 42 primary cancers were histopathologically verified as ductal carcinomas in situ (DCIS). In comparison, eight of 42 contralateral carcinomas were proven as in-situ carcinomas at histology. Considering all 42 bilateral breast carcinomas, the histologic tumour type (i.e. ductal, lobular, mucinous or tubular invasive carcinoma as well as DCIS) of the bilateral cancers was the same at the two breasts in 54.8%. Correlation analyses were performed for assessing similarities between all evaluated characteristics of the corresponding bilateral carcinomas. Regarding the histologic tumour type, the correlation coefficient Cramer's V was 0.436 ($p<0.05$).

Thirty-three subjects showed masses in both breasts on MR mammography. In 75.8%, the initial signal increase (i.e. <100% or >100%) of the bilateral masses, and in 66.7%, the postinitial curve types (i.e. continuous increase, plateau phenomenon or wash-out sign) were the same between the primary index and the corresponding contralateral carcinomas. The correlation coefficient Phi for the comparison of the dichotomous variable initial signal increase and the correlation coefficient Cramer's V for the comparison of the postinitial curve types reached both a statistically significant level ($p<0.05$).

Based on the BI-RADS criteria (14), the shape (i.e. round/oval, lobulated or irregular). and the margin (i.e. smooth, irregular or spiculated) of the detected masses were in more than half of the cases the same between the primary index and the corresponding contralateral carcinomas; the bilateral congruence regarding the shape was 51.5%, the congruence of the margin was 60.6%. In 81.8%, the masses of both breasts showed identical signal intensity (i.e. hypointense, isointense or hyperintense) in the T2-weighted images. The correlation coefficients Cramer's V reached statistical significance for the variables shape, margin and T2-signal intensity of the masses ($p<0.05$).

Blooming sign means that 1 minute after bolus injection a fast enhancing lesion shows a sharply configurated border; the lesion's rim becomes more and more unsharp up to 7 min after contrast media administration. In 69.7%, the blooming sign could be synchronously detected in the masses of the primary index and their corresponding bilateral cancer or could not be observed in neither of the bilateral masses. The correlation coefficient Phi was 0.465 ($p<0.05$).

The primary index carcinomas as well as the contralateral carcinomas most frequently occurred in the upper outer as the main quadrant. In 26 of 42 subjects (61.9%), the primary index and their corresponding contralateral cancers had the identical main tumour quadrant. The main tumour localization (i.e. retromamillar, central or dorsal) of the corresponding bilateral carcinomas was the same in 28 of 42 subjects (66.7%).

Conclusion

In patients with a primary index cancer, MR mammography has a remarkable potential to detect contralateral carcinomas, which could not be visualized by X-ray mammography and/or ultrasonography at time of diagnosis. The contralateral carcinomas frequently reveal identical histological tumour type and main localization as well as dynamic and morphologic MR imaging parameters compared with the corresponding primary index cancer.

References

1. Orel SG, Schnall MD (2001) MR imaging of the breast for the detection, diagnosis, and staging of breast cancer. Radiology 220:13–30
2. Kuhl CK (2007) Current status of breast MR imaging. Part 2. Clinical applications. Radiology 244:672–691
3. Kaiser WA, Zeitler E (1989) MR imaging of the breast: fast imaging sequences with and without Gd-DTPA. Preliminary observations. Radiology 170:681–686
4. Fischer U, Kopka L, Grabbe E (1999) Breast carcinoma: effect of preoperative contrast-enhanced MR imaging on the therapeutic approach. Radiology 213:881–888
5. Boetes C, Mus RD, Holland R, Barentsz JO, Strijk SP, Wobbes T, Hendriks JH, Ruys SH (1995) Breast tumors: comparative accuracy of MR imaging relative to mammography and US for demonstrating extent. Radiology 197:743–747
6. Sardanelli F, Giuseppetti GM, Panizza P, Bazzocchi M, Fausto A, Simonetti G, Lattanzio V, Del Maschio A (2004) Sensitivity of MRI versus mammography for detecting foci of multifocal, multicentric breast cancer in fatty and dense breasts using the whole-breast pathologic examination as a gold standard. AJR Am J Roentgenol 183:1149–1157
7. Lee SG, Orel SG, Woo IJ, Cruz-Jove E, Putt ME, Solin LJ, Czerniecki BJ, Schnall MD (2003) MR imaging screening of the contralateral breast in patients with newly diagnosed breast cancer: preliminary results. Radiology 226:773–778
8. Liberman L, Morris EA, Kim CM, Kaplan JB, Abramson AF, Menell JH, Van Zee KJ, Dershaw DD (2003) MR imaging findings in the contralateral breast of women with recently diagnosed breast cancer. AJR Am J Roentgenol 180:333–341
9. Slanetz PJ, Edmister WB, Yeh ED, Talele AC, Kopans DB (2002) Occult contralateral breast carcinoma incidentally detected by breast magnetic resonance imaging. Breast J 8:145–148
10. Rieber A, Merkle E, Böhm W, Brambs HJ, Tomczak R (1997) MRI of histologically confirmed mammary carcinoma: clinical relevance of diagnostic procedures for detection of multifocal or contralateral secondary carcinoma. J Comput Assist Tomogr 21:773–779
11. Lehman CD, Gatsonis C, Kuhl CK, Hendrick RE, Pisano ED, Hanna L, Peacock S, Smazal SF, Maki DD, Julian TB, DePeri ER, Bluemke DA, Schnall MD (2007) MRI evaluation of the contralateral breast in women with recently diagnosed breast cancer. N Engl J Med 365:1295–1303
12. Jobsen JJ, van der Palen J, Ong F, Meerwaldt JH (2003) Synchronous, bilateral breast cancer: prognostic value and incidence. Breast 12:83–88
13. Heron DE, Komarnicky LT, Hyslop T, Schwartz GF, Mansfield CM (2000) Bilateral breast carcinoma: risk factors and outcomes for patients with synchronous and metachronous disease. Cancer 88:2739–2750
14. American College of Radiology (2003) Breast imaging reporting and data system (BI-RADS) atlas. 4th edn. American College of Radiology, Reston, VA

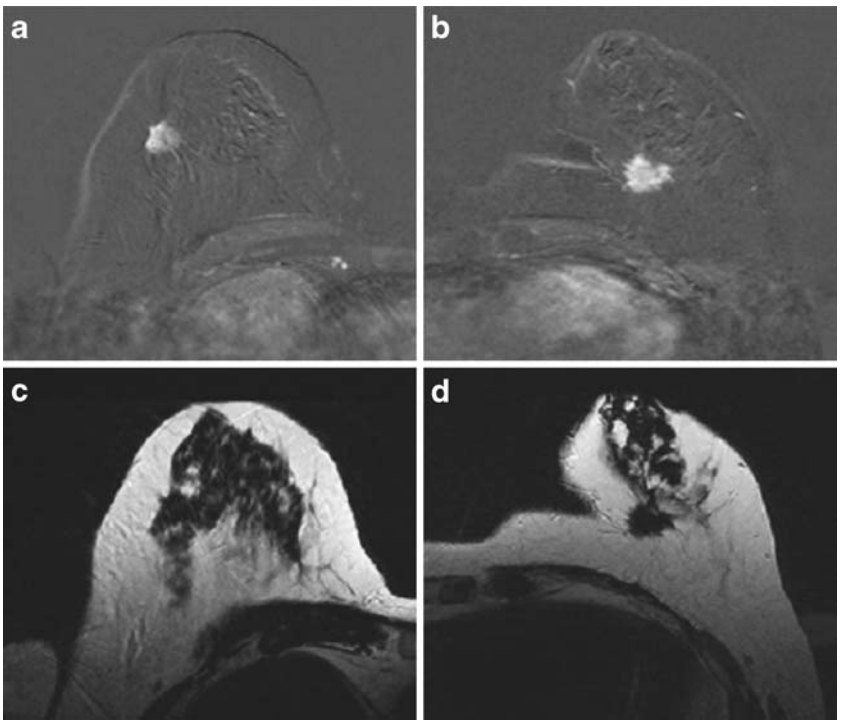

Figures A to D: Bilateral invasive ductal carcinomas. Both cancers had the upper outer as the main quadrant. Both masses present an irregular shape in the subtraction images 1 min. after bolus injection (Fig. A, B). The cancer of the right breast (Fig. A) shows an irregular margin, the carcinoma of the left breast (Fig. B) a spiculated margin. In the T2-weighted images, the bilateral masses are hypointense (Fig. C, D).

Clinical relevance of disseminated and circulating tumor cells in breast cancer patients

Sabine Riethdorf, Harriet Wikman, and Klaus Pantel
Institute of Tumor Biology, University Medical Center Hamburg-Eppendorf, Hamburg, Germany
Correspondence to:
Dr. Sabine Riethdorf, Institute of Tumor Biology, University Medical Center Hamburg-Eppendorf, Martinistr. 52, 20246 Hamburg, Germany, Tel.: +49-40-7410-52628, Fax: +49-40-7410-56546, E-Mail: s.riethdorf@uke.uni-hamburg.de

Summary
Breast cancer is one of the leading causes of cancer-related death in women. Most breast cancer patients undergo a complete resection (R0) of their primary tumor but they still harbor a considerable risk to die from subsequent metastatic relapse caused by minimal residual disease (MRD) not being eliminated by primary surgery, radio-or chemotherapy. The occurrence of distant metastases mainly determining the prognosis of patients with primary breast cancer is due to clinically occult micrometastasis present in secondary organs at primary diagnosis. To prove this early spread of tumor cells undetectable even by high resolution imaging technologies, sensitive and specific immunocytochemical and molecular assays have been developed to identify disseminated tumor cells (DTC) in the bone marrow (BM) and circulating tumor cells (CTC) in the peripheral blood at the single cell level among millions of normal cells (1, 2). Bone marrow plays the most prominent role among the distant organs as indicator organ for minimal residual disease (MRD), because it is easily accessible by aspiration through the iliac crest and it appears to be a common homing organ for DTC derived from various types of epithelial tumors (3). While the prognostic impact of DTC in BM has been demonstrated for primary breast cancer patients, less is known about the clinical relevance of CTC in these patients. However, sequential peripheral blood analyses are more convenient for patients than BM analyses and many research groups are currently evaluating the clinical utility of CTC for assessment of prognosis and monitoring of systemic therapy. This article will focus on the relevance of DTC in BM and CTC in blood in breast cancer patients. Current findings suggest that DTC/CTC are capable to survive chemotherapy and persist in a dormant non-proliferating state over many years. The presented currently available methods for the detection and characterization of DTC/CTC provide the potential to monitor systemic tumor cell dissemination in BM and blood as one of the first crucial steps in the metastatic cascade. Furthermore, we will discuss the clinical relevance of DTC/CTC detection with regard to an improved individualized management of cancer patients.

Cytometric and molecular detection of DTC/CTC

Because of the low concentration of DTC/CTC (1×10^{-5}–10^{-6}) in BM and blood, direct detection of these cells is usually not feasible without a prior enrichment step (e.g., gradient centrifugation through Ficoll-Paque; size-based enrichment by membrane filter devices such as ISET (isolation by size of epithelial tumor cells (4)); MEMS (micro electro-mechanical system)-based microfilter approaches (5) or immunomagnetic bead separation performed either as positive selection of DTC using

epithelium-specific antibodies (e.g., anti EpCAM) or negative depletion of hematopoetic cells (e.g., by antibodies against the common leukocyte antigen CD45). The advantages and disadvantages of these enrichment methods have been discussed elsewhere (6, 7).

Current methods to screen BM aspirates or peripheral blood for DTC/CTC after enrichment can be classified into cytometric/immunological and molecular approaches (1, 8).

Among the cytometric methods immunocytochemistry (ICC) is the most widely used approach (3, 8) having the advantage to facilitate characterization of both cell size and shape as well as the nucleus–plasma relation of each individual event. Thereby illegitimate expression of the protein of interest in BM cells can be excluded as far as possible. Because of the absence of tumor-specific target antigens, monoclonal antibodies against various epithelium-specific antigens such as cytoskeleton-associated cytokeratins, surface adhesion molecules, or growth factor receptors are applied for the detection of DTC/CTC (1, 8). The most commonly used antibodies, like A45-B/B3 and AE1/AE3, are directed against various intracellular cytokeratins (CK), which are intermediate filament proteins that are expressed in epithelial cells but usually not in haematopoietic cells. The detection rates of DTC/CTC in BM and blood from non-metastatic breast cancer patients vary considerably reflecting the different sensitivity but also specificity of the numerous detection methods and antibodies used thus far (for review see (2, 9). To overcome these problems and to provide a basis for future multicentric clinical trials, a consensus concept for the detection and enrichment of DTC in BM, but not yet for blood has been proposed (10). Criteria to evaluate morphology and staining results after automatic microscopic screening using sophisticated imaging approaches have also been defined to avoid false-positive and false-negative results (10–12).

Flow cytometry-based methods have also been used for the detection of CTC/DTC (13–15). However, very few studies have been conducted on larger patient cohorts. Because of the lower sensitivity of flow cytometry as compared to other methods it has mainly been described for analysis of BM or blood taken from advanced stage cancer patients with overt metastases.

With the EPISPOT (epithelial immunospot) technique, discrimination between viable and apoptotic DTC/CTC is facilitated. This approach allows detecting viable DTC/CTC by their ability to secrete individual proteins after short term culture (48 hours). In a recently published study, Muc-1 and/or CK19 secreting DTC could be demonstrated in BM samples of breast cancer patients with (90%) and without (50%) over metastases, but not from healthy controls (16). Furthermore, the detection of full-length CK19 releasing cells by this technique correlated with the presence of overt metastasis and a reduced survival of breast cancer patients (17).

Several new techniques have been developed and applied for CTC detection in the peripheral blood. Progress towards a standardized method for CTC detection was reached through the introduction of the CellSearch system (Veridex, Warren, NJ, USA), an automated enrichment and immunostaining device that has been cleared by the US. food and drug administration for the detection of CTC in peripheral blood of patients with metastatic breast cancer (18, 19). Recently, Nagrath et al. presented a "CTC"-chip", a microfluid platform which consists of an array of anti-EpCAM antibody-coated microposts capable to capture CTC from unfractionated blood under precisely controlled laminar flow conditions (20). CTC counts 2–3 log units higher than those found by other groups using FDA-approved methods were reported by Pachmann et al. in nearly 100% of breast cancer patients using the MAINTRAC^{TM} assay (21). Furthermore, ultra-speed automated digital microscopy fibre-optic array scanning technology (FAST) and laser printing techniques have been developed to excite 300.000 cells per second (22–24). Very recently, Talasaz presented a new sample preparation technology, the MagSweeper, an automated immunomagnetic separation technology that gently enriches CTC from blood (25).

Measurements of epithelium-specific or rather organ-specific transcripts such as CK19 and 20, HER2 or mammaglobin by RT (reverse transcriptase)-PCR have been proven as promising to detect DTC/CTC (for review see (2, 9)). The main drawback of RT-PCR approaches using surrogate tissue-specific markers are false positive results due to illegitimate low-level of epithelial-or tissue-related transcription in normal cells (26). Moreover, heterogeneity in the expression levels of a particular target transcript cannot be predicted. Nevertheless, several studies provided evidence for a clinical relevance of DTC/CTC detected by RT-PCR (for review see (2, 9)).

Phenotypic and molecular characterization of DTC/CTC

Previous reports indicated that DTC might be genomically instable and heterogeneous (27) and capable to disseminate in a less progressed genomic state, acquiring genomic alterations typical for fully metastatic cells later (28). DTC are heterogeneous regarding the expression of growth factor receptors, adhesion molecules, proteases and their inducer and receptors, major histocompatibility complex antigens, signaling kinases, melanoma associated antigens (MAGE) or telomerase activity (for review see (1, 3). Of particular importance is the epidermal growth factor receptor HER2, the expression of which in primary tumors is essential for Trastuzumab treatment decisions of breast cancer patients (29, 30). HER2 overexpression on DTC in BM was predictive for a poor clinical outcome of stage I–III breast cancer patients (31). In the study of Vincent-Salomon et al. (32), in the majority of the cases the HER2 status remained stable between DTC and the corresponding primary tumors. However, there is also evidence for discrepancies between the HER2 status in primary tumors and DTC in BM and CTC in blood (31, 33, 34) and CTC in blood (35–37). Although HER2 expression was heterogeneous in DTC from individual patients, HER2-positive DTC might identify additional patients who can benefit from Trastuzumab therapy (34). Further studies are ongoing to verify whether HER2-positive DTC/CTC have predictive value for an improved response of the patients to Trastuzumab treatment.

Negativity for Ki-67 staining suggests that the vast majority of DTC persists in a non-proliferating dormant state (33, 38, 39), which might also be responsible for their partial resistance to adjuvant chemotherapy in high risk breast cancer patients (40).

There is first evidence for a molecular signature of primary tumors spreading early into BM (41, 42); however, information about global gene expression of DTC is still limited. Bos et al. provided evidence for organ-specific metastatic extravasation of breast cancer cells into brain, lung and bone marrow with the later one being a relatively permissive process owing to the fenestrated endothelium lining the sinusoid capillaries (43). For CTC isolated from blood of patients with metastatic breast cancer, global gene expression profiles could be defined and a list of CTC-specific genes was obtained, which might be useful to distinguish normal donors from cancer patients (44). TWIST1, a transcription factor that plays a pivotal role in metastasis by promoting epithelial-mesenchymal transition (45, 46), was part of the gene expression signature identified in EpCAM-enriched cells from BM of breast cancer patients after chemotherapy (47). Moreover, TWIST1 expression was associated with occurrence of distant metastasis and local progression (47).

Whether DTC possess stem or progenitor cell features enabling them to both self-renew and differentiate is currently under debate. Positivity of CD44 and absent/weak expression of CD24,

or expression of ALDH-1 seem to be characteristic for breast cancer initiating cells with a high capacity to form tumors in immunosuppressed mice (48–50). Recently, by gene expression analysis of $CD44^{+}/CD24^{-/low}$ cells separated from breast cancer tissue, a 186 gene "invasiveness gene signature" was published, which was significantly associated with a reduced overall and metastasis-free survival of the breast cancer patients analyzed (51). First hints for stem cell features of DTC in BM were provided by Balic et al. and Alix-Panabieres et al. who demonstrated a significant number of DTC from BM of breast cancer patients with either $CD44^{+}/CD24^{-/low}$ or $CK19^{+}/Muc\text{-}1^{-}$ stem cell-like phenotypes (16, 52). Resistance to systemic chemotherapy and the long term persistence of DTC in BM of cancer patients is also consistent with their putative stem cell phenotype (40, 53, 54).

Prognostic and therapeutic relevance of DTC/CTC

Today the overall survival of breast cancer patients is relatively high (80–90%–5 year, 70–80% 10 year), however, a considerable fraction of nodal negative patients still relapse (25–30% and 15–50%) and this can often take place many years (>10 years) after the removal of the primary tumor (55). The detection of DTC in BM is still not part of the routine tumor staging in the clinical practice; however, emerging data anticipate a future role of DTC detection for risk stratification and therapeutic monitoring of breast cancer patients (56). The size of the patient cohorts analyzed and the applied detection methods in numerous studies investigating the presence and clinical relevance of DTC in BM of breast cancer patients vary considerably. In studies detecting cytokeratins or mucin (Muc-1), the prevalence of DTC in early-stage disease ranges between 15–40%, whereas in patients with metastatic breast cancer the rate increases up to 70% (for review see (2, 9)).

Braun et al., published a meta-analysis evaluating results of 4703 breast cancer patients in which the presence of DTC in BM was not only predictive of the development of skeletal metastases but also predicted the development of metastases in other organs (56). Detection of DTC has already been introduced in international tumor staging systems (57, 58), and in 2007 DTC and CTC (circulating tumor cells) were mentioned for the first time in the American Society of Oncology (ASCO) recommendations on tumor markers (59).

Besides their presence at primary diagnosis and surgery, DTC have been described to survive chemotherapy and hormonal therapy (38, 40) and they can persist in BM over many years post-surgery. This persistence is also linked to an increased risk of late metastatic relapse (53, 54, 60). For example, in high-risk breast cancer patients (>3 involved axillary lymph nodes or extensive invasion of cutaneous lymph vessels), the presence of tumor cells after therapy was associated with an extremely poor prognosis (40). A European pooled analysis involving 696 breast cancer patients confirmed these findings. Here, 16% of breast cancer patients had tumor cell persistence in BM, and their presence was an independent prognostic factor for subsequent reduced breast cancer survival (61, 62).

Very recently, Bidard et al. reported about the prognostic relevance of DTC detection in stage I to III breast cancer patients. They identified 15% of 621 breast cancer patients as DTC-positive (63). As also published by Bidard et al., the presence of DTC in BM may be associated with a different pattern of locoregional cancer cell dissemination and might influence locoregional recurrence-free survival. Systemic hormone therapy and radiotherapy could help to prevent reseeding of the primary tumor area by DTC (64).

Repeated BM sampling seems to be difficult to introduce in the clinical management of patients with solid tumors. Therefore, sequential peripheral blood analyses are more convenient and many research groups are currently assessing the clinical utility of CTC. Thus far, only few studies have directly compared BM and blood analyses in the same patients (38, 65, 66). Wiedswang et al. published the largest study on 341 patients with stage I–IV breast cancer and showed that the detection of DTC in BM had superior prognostic significance over CTC measurements in stage M_0-patients (65). By contrast, Bidard et al. reported a superior significance of the CTC counts but they analyzed only patients with metastatic breast cancer (66). Thus far, these findings do not support the use of CTC from blood to replace DTC from BM as a prognostic indicator in breast cancer and only studies on larger cohorts of patients may help to clarify this important issue.

Many research groups are assessing the clinical value of CTC analyses for therapy monitoring that have provided significant prognostic information in metastatic breast cancer. Cristofanilli et al. showed that the number of CTC before treatment and at the first follow up visit after initiation of therapy is an independent predictor of progression-free and overall survival in patients with metastatic breast cancer (18). Moreover, results by Hayes et al. indicated that the absence or presence of CTC in peripheral blood of metastatic cancer patients at any time during therapy is a direct reflection of the patient's response, or lack of response, respectively, to therapy (67) and seems to be superior or additive to conventional imaging methods for response evaluation such as radiologic assessment including computed tomograms (CT scans) (20, 68, 69). However, despite these promising data the recent ASCO guidelines have stated that even the use of the recently FDA-cleared CellSearch assay in patients with metastatic breast cancer cannot be recommended until further validation confirms the clinical value of this test (59). The clinical utility of CTC measurements in metastatic breast cancer patients is now being prospectively addressed in a randomized trial SWOG S0500 led by the Southwest Oncology group (Treatment decision making based on blood levels of tumor cells in women with metastatic breast cancer receiving chemotherapy, www.cancer.gov/clinicaltrials/SWOG-S0500, last modified 10/23/2008 (70) expecting to enroll 500 patients with metastatic breast cancer.

The most important challenge of new DTC/CTC technologies is to monitor MRD in patients without signs of overt metastasis. Pierga et al. monitored CTC counts in 118 patients with large operable or locally advanced breast cancer before and after neoadjuvant chemotherapy. In a phase II trial (REMAGUS 02), the authors showed that the presence of CTC after a short follow-up time of 18 months was an independent prognostic factor for reduced metastasis-free survival (71). Interestingly, they did not find a significant correlation for response of the primary tumor to chemotherapy, which is usually used as an indicator for treatment response.

Pachmann et al. analyzed 91 non-metastatic primary breast cancer patients and reported that a greater than 10-fold increase in CTC counts compared to marginal changes in CTC numbers and marginal changes to decreased CTC numbers at the end of adjuvant chemotherapy were correlated with a significantly reduced relapse-free survival of the patients ($p<0.01$) (72).

Follow up analyses of two German trials using the CellSearch technology—the GEPARQuattro trial focusing on neoadjuvant chemotherapy and additionally—if indicated—Trastuzumab treatment and the SUCCESS trial focusing on adjuvant chemotherapy—are still ongoing and will show whether the observed decreases in CTC rates will be associated with an improved survival rate (73, 74). Preliminary results from the SUCCESS trial in which blood samples from 1,500 node-positive and high risk node-negative breast cancer patients before and after

adjuvant taxane-based chemotherapy were analyzed, demonstrate a prognostic relevance of CTC detected in about 10% of patients after chemotherapy (74). In patients treated within the GeparQuattro trial, CTC were detected in about 20% of patients prior to neoadjuvant chemotherapy with CTC incidence decreasing significantly to 10% of patients after neoadjuvant chemotherapy. This decrease, however, was not associated with the tumor response to the neoadjuvant therapy. The GeparQuattro study incorporated three chemotherapeutic arms and Trastuzumab treatment for patients with HER2-positive primary tumors. Measurement of HER2 expression of CTC within this study reveled that the HER2 status of CTC not necessarily reflects that of the primary tumor. Whether CTC detection in the context of this study will have prognostic relevance has to be demonstrated in follow-up observations of these patients (73). In a very recent publication, Xenidis et al. described 32.7% of 437 patients with early breast cancer as CTC-positive by CK19-RT-PCR after completion of adjuvant chemotherapy. Patients with detectable CK19 mRNA postchemotherapy showed a significantly reduced overall and disease-free survival (75).

Conclusions

The reliable detection of DTC in BM and of CTC in blood of breast cancer patients years before the occurrence of distant overt metastases is facilitated by several rare cell detection techniques. This information may be used to assess the individual prognosis of cancer patients and to stratify the patients at risk to systemic adjuvant or neoadjuvant therapies aimed to prevent recurrences and metastatic relapses. However, for the future implementation of DTC/CTC detection into clinical routine practice reliable standardized methods with a high degree of reproducibility have to be established.

DTC in BM have been detected not only in breast cancer, but also in other solid tumor types suggesting that the BM might be a preferred reservoir for blood-borne DTC. The BM environment may allow these cells to persist over many years and to disseminate into other organs. However, it cannot be excluded that BM is simply a convenient indicator organ and that early DTC are also present in other organs such as lung or liver which are less easily accessible than BM. Recent data support the hypothesis that the BM provides a reservoir out of which DTC might disseminate also in other organs such as lung, liver and brain (76).

Several studies found DTC in BM even many years after surgery and adjuvant therapy and the presence of these DTC was associated with an increased risk for metastatic relapse (53, 54, 60). These results demonstrate that DTC can reside in a dormant state before they grow out into overt skeleton metastases. To understand this dormant stage together with the identification of the initiating cells of overt metastases are some of the most challenging areas of basic research on the biology of DTC. In this context, the development of appropriate mouse models, which mimic MRD, are of utmost importance to perform functional studies for validation of the descriptive findings observed in cancer patients.

Sequential peripheral blood drawings in particular for real-time monitoring of MRD in cancer patients undergoing systemic therapies (e.g., chemotherapy, hormonal therapy or antibody therapy) should be more acceptable than repeated BM aspirations. To answer the question if CTC measurements could replace the examination of BM, many research groups are currently assessing CTC in clinical studies with encouraging results (for review, see (1)). Implementation of CTC/DTC measurements into clinical trials has the potential to obtain an important future biomarker for real-time monitoring of the efficacy of systemic adjuvant therapy in individual cancer patients.

References

1. Pantel K, Brakenhoff RH, Brandt B (2008) Detection, clinical relevance and specific biological properties of disseminating tumour cells. Nat Rev Cancer 8:329–340.
2. Pantel K, Alix-Panabières C, Riethdorf S (2009) Cancer micrometastasis. Nat Clin Pract Oncol Apr 28:
3. Pantel K, Brakenhoff RH (2004) Dissecting the metastatic cascade. Nat Rev Cancer 4:448–456.
4. Pinzani P, Salvadori B, Simi L, Bianchi S, Distante V, Cataliotti L, Pazzagli M, Orlando C (2006) Isolation by size of epithelial tumor cells in peripheral blood of patients with breast cancer: correlation with real-time reverse transcriptase-polymerase chain reaction results and feasibility of molecular analysis by laser microdissection. Hum Pathol 37:711–718.
5. Zheng S, Lin H, Liu JQ, Balic M, Datar R, Cote RJ, Tai YC (2007) Membrane microfilter device for selective capture, electrolysis and genomic analysis of human circulating tumor cells. J Chromatogr A 1162:154–161.
6. Zach O, Lutz D (2006) Tumor cell detection in peripheral blood and bone marrow. Curr Opin Oncol 18:48–56.
7. Alix-Panabieres C, Riethdorf S, Pantel K (2008) Circulating tumor cells and bone marrow micrometastasis. Clin Cancer Res 14:5013–5021.
8. Lacroix M (2006) Significance, detection and markers of disseminated breast cancer cells. Endocr Relat Cancer 13:1033–1067.
9. Riethdorf S, Wikman H, Pantel K (2008) Review: Biological relevance of disseminated tumor cells in cancer patients. Int J Cancer 123:1991–2006.
10. Fehm T, Braun S, Muller V, Janni W, Gebauer G, Marth C, Schindlbeck C, Wallwiener D, Borgen E, Naume B, Pantel K, Solomayer E (2006) A concept for the standardized detection of disseminated tumor cells in bone marrow from patients with primary breast cancer and its clinical implementation. Cancer 107:885–892.
11. Borgen E, Beiske K, Trachsel S, Nesland JM, Kvalheim G, Herstad TK, Schlichting E, Qvist H, Naume B (1998) Immunocytochemical detection of isolated epithelial cells in bone marrow: non-specific staining and contribution by plasma cells directly reactive to alkaline phosphatase. J Pathol 185:427–434.
12. Borgen E, Pantel K, Schlimok G, Muller P, Otte M, Renolen A, Ehnle S, Coith C, Nesland JM, Naume B (2006) A European interlaboratory testing of three well-known procedures for immunocytochemical detection of epithelial cells in bone marrow. Results from analysis of normal bone marrow. Cytometry B Clin Cytom 70:400–409.
13. Cohen SJ, Alpaugh RK, Gross S, O'Hara SM, Smirnov DA, Terstappen LW, Allard WJ, Bilbee M, Cheng JD, Hoffman JP, Lewis NL, Pellegrino A, Rogatko A, Sigurdson E, Wang H, Watson JC, Weiner LM, Meropol NJ (2006) Isolation and characterization of circulating tumor cells in patients with metastatic colorectal cancer. Clin Colorectal Cancer 6:125–132.
14. Garcia JA, Rosenberg JE, Weinberg V, Scott J, Frohlich M, Park JW, Small EJ (2007) Evaluation and significance of circulating epithelial cells in patients with hormone-refractory prostate cancer. BJU Int 99:519–524.
15. Wang L, Wang Y, Liu Y, Cheng M, Wu X, Wei H (2009) Flow cytometric analysis of CK19 expression in the peripheral blood of breast carcinoma patients: relevance for circulating tumor cell detection. J Exp Clin Cancer Res 28:57.
16. Alix-Panabieres C, Vendrell JP, Pelle O, Rebillard X, Riethdorf S, Muller V, Fabbro M, Pantel K (2007) Detection and characterization of putative metastatic precursor cells in cancer patients. Clin Chem 53:537–539.

17. Alix-Panabieres C, Vendrell JP, Slijper M, Pelle O, Barbotte E, Mercier G, Jacot W, Fabbro M, Pantel K (2009) Full length cytokeratin-19 is released by human tumor cells: a potential role in metastatic progression of breast cancer. Breast Cancer Res 11: R39.
18. Cristofanilli M, Budd GT, Ellis MJ, Stopeck A, Matera J, Miller MC, Reuben JM, Doyle GV, Allard WJ, Terstappen LW, Hayes DF (2004) Circulating tumor cells, disease progression, and survival in metastatic breast cancer. N Engl J Med 351:781–791.
19. Riethdorf S, Fritsche H, Muller V, Rau T, Schindlbeck C, Rack B, Janni W, Coith C, Beck K, Janicke F, Jackson S, Gornet T, Cristofanilli M, Pantel K (2007) Detection of Circulating Tumor Cells in Peripheral Blood of Patients with Metastatic Breast Cancer: A Validation Study of the CellSearch System. Clin Cancer Res 13:920–928.
20. Nagrath S, Sequist LV, Maheswaran S, Bell DW, Irimia D, Ulkus L, Smith MR, Kwak EL, Digumarthy S, Muzikansky A, Ryan P, Balis UJ, Tompkins RG, Haber DA, Toner M (2007) Isolation of rare circulating tumour cells in cancer patients by microchip technology. Nature 450:1235–1239.
21. Pachmann K, Clement JH, Schneider CP, Willen B, Camara O, Pachmann U, Hoffken K (2005) Standardized quantification of circulating peripheral tumor cells from lung and breast cancer. Clin Chem Lab Med 43:617–627.
22. Krivacic RT, Ladanyi A, Curry DN, Hsieh HB, Kuhn P, Bergsrud DE, Kepros JF, Barbera T, Ho MY, Chen LB, Lerner RA, Bruce RH (2004) A rare-cell detector for cancer. Proc Natl Acad Sci U S A 101:10501–10504.
23. Curry DN, Krivacic RT, Hsieh HB, Ladanyi A, Bergsrud DE, Ho MY, Chen LB, Kuhn P, Bruce RH (2004) High-speed detection of occult tumor cells in peripheral blood. Conf Proc IEEE Eng Med Biol Soc 2:1267–1270.
24. Hsieh HB, Marrinucci D, Bethel K, Curry DN, Humphrey M, Krivacic RT, Kroener J, Kroener L, Ladanyi A, Lazarus N, Kuhn P, Bruce RH, Nieva J (2006) High speed detection of circulating tumor cells. Biosens Bioelectron 21:1893–1899.
25. Talasaz AH, Powell AA, Huber DE, Berbee JG, Roh KH, Yu W, Xiao W, Davis MM, Pease RF, Mindrinos MN, Jeffrey SS, Davis RW (2009) Isolating highly enriched populations of circulating epithelial cells and other rare cells from blood using a magnetic sweeper device. Proc Natl Acad Sci U S A 106:3970–3975.
26. Ring A, Smith IE, Dowsett M (2004) Circulating tumour cells in breast cancer. Lancet Oncol 5:79–88.
27. Klein CA, Blankenstein TJ, Schmidt-Kittler O, Petronio M, Polzer B, Stoecklein NH, Riethmuller G (2002) Genetic heterogeneity of single disseminated tumour cells in minimal residual cancer. Lancet 360:683–689.
28. Schmidt-Kittler O, Ragg T, Daskalakis A, Granzow M, Ahr A, Blankenstein TJ, Kaufmann M, Diebold J, Arnholdt H, Muller P, Bischoff J, Harich D, Schlimok G, Riethmuller G, Eils R, Klein CA (2003) From latent disseminated cells to overt metastasis: genetic analysis of systemic breast cancer progression. Proc Natl Acad Sci U S A 100:7737–7742.
29. Piccart-Gebhart MJ, Procter M, Leyland-Jones B, Goldhirsch A, Untch M, Smith I, Gianni L, Baselga J, Bell R, Jackisch C, Cameron D, Dowsett M, Barrios CH, Steger G, Huang CS, Andersson M, Inbar M, Lichinitser M, Lang I, Nitz U, Iwata H, Thomssen C, Lohrisch C, Suter TM, Ruschoff J, Suto T, Greatorex V, Ward C, Straehle C, McFadden E, Dolci MS, Gelber RD (2005) Trastuzumab after adjuvant chemotherapy in HER2-positive breast cancer. N Engl J Med 353:1659–1672.
30. Steeg PS (2006) Tumor metastasis: mechanistic insights and clinical challenges. Nat Med 12:895–904.
31. Braun S, Schlimok G, Heumos I, Schaller G, Riethdorf L, Riethmuller G, Pantel K (2001) ErbB2 overexpression on occult metastatic cells in bone marrow predicts poor clinical outcome of stage I–III breast cancer patients. Cancer Res 61:1890–1895.
32. Vincent-Salomon A, Pierga JY, Couturier J, d'Enghien CD, Nos C, Sigal-Zafrani B, Lae M, Freneaux P, Dieras V, Thiery JP, Sastre-Garau X (2007) HER2 status of bone marrow micrometastasis and their corresponding primary tumours in a pilot study of 27 cases: a possible tool for anti-HER2 therapy management? Br J Cancer 96:654–659.
33. Pantel K, Schlimok G, Braun S, Kutter D, Lindemann F, Schaller G, Funke I, Izbicki JR, Riethmuller G (1993) Differential expression of proliferation-associated molecules in individual micrometastatic carcinoma cells. J Natl Cancer Inst 85:1419–1424.
34. Solomayer EF, Becker S, Pergola-Becker G, Bachmann R, Kramer B, Vogel U, Neubauer H, Wallwiener D, Huober J, Fehm TN (2006) Comparison of HER2 status between primary tumor and disseminated tumor cells in primary breast cancer patients. Breast Cancer Res Treat 98:179–184.
35. Meng S, Tripathy D, Shete S, Ashfaq R, Haley B, Perkins S, Beitsch P, Khan A, Euhus D, Osborne C, Frenkel E, Hoover S, Leitch M, Clifford E, Vitetta E, Morrison L, Herlyn D, Terstappen LW, Fleming T, Fehm T, Tucker T, Lane N, Wang J, Uhr J (2004) HER-2 gene amplification can be acquired as breast cancer progresses. Proc Natl Acad Sci U S A 101:9393–9398.
36. Wulfing P, Borchard J, Buerger H, Heidl S, Zanker KS, Kiesel L, Brandt B (2006) HER2-positive circulating tumor cells indicate poor clinical outcome in stage I to III breast cancer patients. Clin Cancer Res 12:1715–1720.
37. Riethdorf S, Loibl S, Komor M, Houber J, Schrader I, Conrad U, Untch M, von Minckwitz G, Pantel K, Muller V (2007) Incidence and kinetics of circulating tumor cells in breast cancer patients treated with primary systemic therapy including trastuzumab for patients with HER2-positive tumors—a translational project within the study "GeparQuattro". Breast Cancer Res Treat 106 (S1):Abstract 5025.
38. Muller V, Stahmann N, Riethdorf S, Rau T, Zabel T, Goetz A, Janicke F, Pantel K (2005) Circulating tumor cells in breast cancer: correlation to bone marrow micrometastases, heterogeneous response to systemic therapy and low proliferative activity. Clin Cancer Res 11:3678–3685.
39. Wikman H, Vessella RL, Pantel K (2008) Cancer micrometastasis and tumor dormancy. APMIS in press:
40. Braun S, Kentenich C, Janni W, Hepp F, de Waal J, Willgeroth F, Sommer H, Pantel K (2000) Lack of effect of adjuvant chemotherapy on the elimination of single dormant tumor cells in bone marrow of high-risk breast cancer patients. J Clin Oncol 18:80–86.
41. Woelfle U, Cloos J, Sauter G, Riethdorf L, Janicke F, van Diest P, Brakenhoff R, Pantel K (2003) Molecular signature associated with bone marrow micrometastasis in human breast cancer. Cancer Res 63:5679–5684.
42. Naume B, Zhao X, Synnestvedt M, Borgen E, Giercksky Russnes H, Lingjorde OC, Stromberg M, Wiedswang G, Kvalheim G, Karesen R, Nesland JM, Borresen-Dale A-L, Sorlie T (2007) Presence of bone marrow micrometastasis is associated with different recurrence risk within molecular subtypes of breast cancer. Molecular Oncology 1:160–171.
43. Bos PD, Zhang XH, Nadal C, Shu W, Gomis RR, Nguyen DX, Minn AJ, van de Vijver MJ, Gerald WL, Foekens JA, Massague J (2009) Genes that mediate breast cancer metastasis to the brain. Nature 459:1005–1009.

44. Smirnov DA, Foulk BW, Doyle GV, Connelly MC, Terstappen LW, O'Hara SM (2006) Global gene expression profiling of circulating endothelial cells in patients with metastatic carcinomas. Cancer Res 66:2918–2922.
45. Rosivatz E, Becker I, Specht K, Fricke E, Luber B, Busch R, Hofler H, Becker KF (2002) Differential expression of the epithelial-mesenchymal transition regulators snail, SIP1, and twist in gastric cancer. Am J Pathol 161:1881–1891.
46. Lo HW, Hsu SC, Xia W, Cao X, Shih JY, Wei Y, Abbruzzese JL, Hortobagyi GN, Hung MC (2007) Epidermal growth factor receptor cooperates with signal transducer and activator of transcription 3 to induce epithelial-mesenchymal transition in cancer cells via up-regulation of TWIST gene expression. Cancer Res 67:9066–9076.
47. Watson MA, Ylagan LR, Trinkaus KM, Gillanders WE, Naughton MJ, Weilbaecher KN, Fleming TP, Aft RL (2007) Isolation and molecular profiling of bone marrow micrometastases identifies TWIST1 as a marker of early tumor relapse in breast cancer patients. Clin Cancer Res 13:5001–5009.
48. Sheridan C, Kishimoto H, Fuchs RK, Mehrotra S, Bhat-Nakshatri P, Turner CH, Goulet R, Jr., Badve S, Nakshatri H (2006) CD44+/CD24− breast cancer cells exhibit enhanced invasive properties: an early step necessary for metastasis. Breast Cancer Res 8:R59.
49. Fillmore C, Kuperwasser C (2007) Human breast cancer stem cell markers CD44 and CD24: enriching for cells with functional properties in mice or in man? Breast Cancer Res 9:303.
50. Ginestier C, Hur MH, Charafe-Jauffret E, Monville F, Dutcher J, Brown M, Jacquemier J, Viens P, Kleer C, Liu S, Schott A, Hayes D, Birnbaum D, Wicha MS, Dontu G (2007) ALDH1 is a marker of normal and malignant human mammary stem cells and a predictor of poor clinical outcome. Cell Stem Cell 1:555–567.
51. Liu R, Wang X, Chen GY, Dalerba P, Gurney A, Hoey T, Sherlock G, Lewicki J, Shedden K, Clarke MF (2007) The prognostic role of a gene signature from tumorigenic breast-cancer cells. N Engl J Med 356:217–226.
52. Balic M, Lin H, Young L, Hawes D, Giuliano A, McNamara G, Datar RH, Cote RJ (2006) Most early disseminated cancer cells detected in bone marrow of breast cancer patients have a putative breast cancer stem cell phenotype. Clin Cancer Res 12:5615–5621.
53. Wiedswang G, Borgen E, Karesen R, Qvist H, Janbu J, Kvalheim G, Nesland JM, Naume B (2004) Isolated tumor cells in bone marrow three years after diagnosis in disease-free breast cancer patients predict unfavorable clinical outcome. Clin Cancer Res 10:5342–5348.
54. Janni W, Rack B, Schindlbeck C, Strobl B, Rjosk D, Braun S, Sommer H, Pantel K, Gerber B, Friese K (2005) The persistence of isolated tumor cells in bone marrow from patients with breast carcinoma predicts an increased risk for recurrence. Cancer 103:884–891.
55. Lang JE, Hall CS, Singh B, Lucci A (2007) Significance of micrometastasis in bone marrow and blood of operable breast cancer patients: research tool or clinical application? Expert Rev Anticancer Ther 7:1463–1472.
56. Braun S, Vogl FD, Naume B, Janni W, Osborne MP, Coombes RC, Schlimok G, Diel IJ, Gerber B, Gebauer G, Pierga JY, Marth C, Oruzio D, Wiedswang G, Solomayer EF, Kundt G, Strobl B, Fehm T, Wong GY, Bliss J, Vincent-Salomon A, Pantel K (2005) A pooled analysis of bone marrow micrometastasis in breast cancer. N Engl J Med 353:793–802.
57. Hermanek P, Hutter RV, Sobin LH, Wittekind C (1999) International Union Against Cancer. Classification of isolated tumor cells and micrometastasis. Cancer 86:2668–2673.
58. Singletary SE, Greene FL, Sobin LH (2003) Classification of isolated tumor cells: clarification of the 6th edition of the American Joint Committee on Cancer Staging Manual. Cancer 98:2740–2741.
59. Harris L, Fritsche H, Mennel R, Norton L, Ravdin P, Taube S, Somerfield MR, Hayes DF, Bast RC, Jr. (2007) American Society of Clinical Oncology 2007 update of recommendations for the use of tumor markers in breast cancer. J Clin Oncol 25:5287–5312.
60. Slade MJ, Singh A, Smith BM, Tripuraneni G, Hall E, Peckitt C, Fox S, Graham H, Luchtenborg M, Sinnett HD, Cross NC, Coombes RC (2005) Persistence of bone marrow micrometastases in patients receiving adjuvant therapy for breast cancer: results at 4 years. Int J Cancer 114:94–100.
61. Janni W, Wiedswang G, Fehm T, Jueckstock J, Borgen E, Rack B, Braun S, Sommer H, Solomayer E, Pantel K, Nesland JM, Genss E, Friese K, Naume B (2006) Persistence of disseminated tumor cells (DTC) in bone marrow (BM) during follow-up predicts increased risk for relapse up-date of the pooled European data. Breast Cancer Res Treat 100 (suppl 1) abstr 18:
62. Naume B, Fehm T, Wiedswang G, Jückstock J, Borgen E, Rack B, Synnestvedt M, Braun S, Sommer H, Solomayer E, Pantel K, Friese K, Janni W (2008) Persistence of isolated tumor cells in the bone marrow of breast cancer patients predicts increased risk for relapse—a European pooled analysis. SABCS 2008 #304:
63. Bidard FC, Vincent-Salomon A, Gomme S, Nos C, De Rycke Y, Thiery JP, Sigal-Zafrani B, Mignot L, Sastre-Garau X, Pierga JY (2008) Disseminated tumor cells of breast cancer patients: a strong prognostic factor for distant and local relapse. Clin Cancer Res 14:3306–3311.
64. Bidard FC, Kirova YM, Vincent-Salomon A, Alran S, de Rycke Y, Sigal-Zafrani B, Sastre-Garau X, Mignot L, Fourquet A, Pierga JY (2009) Disseminated tumor cells and the risk of locoregional recurrence in nonmetastatic breast cancer. Ann Oncol
65. Wiedswang G, Borgen E, Schirmer C, Karesen R, Kvalheim G, Nesland JM, Naume B (2006) Comparison of the clinical significance of occult tumor cells in blood and bone marrow in breast cancer. Int J Cancer 118:2013–2019.
66. Bidard FC, Vincent-Salomon A, Sigal-Zafrani B, Dieras V, Mathiot C, Mignot L, Thiery JP, Sastre-Garau X, Pierga JY (2008) Prognosis of women with stage IV breast cancer depends on detection of circulating tumor cells rather than disseminated tumor cells. Ann Oncol 19:496–500.
67. Hayes DF, Cristofanilli M, Budd GT, Ellis MJ, Stopeck A, Miller MC, Matera J, Allard WJ, Doyle GV, Terstappen LW (2006) Circulating tumor cells at each follow-up time point during therapy of metastatic breast cancer patients predict progression-free and overall survival. Clin Cancer Res 12:4218–4224.
68. Budd GT, Cristofanilli M, Ellis MJ, Stopeck A, Borden E, Miller MC, Matera J, Repollet M, Doyle GV, Terstappen LW, Hayes DF (2006) Circulating tumor cells versus imaging—predicting overall survival in metastatic breast cancer. Clin Cancer Res 12:6403–6409.
69. De Giorgi U, Valero V, Rohren E, Dawood S, Ueno NT, Miller MC, Doyle GV, Jackson S, Andreopoulou E, Handy BC, Reuben JM, Fritsche HA, Macapinlac HA, Hortobagyi GN, Cristofanilli M (2009) Circulating tumor cells and [18F] fluorodeoxyglucose positron emission tomography/computed tomography for outcome prediction in metastatic breast cancer. J Clin Oncol 27:3303–3311.
70. Treatment decision making based on blood levels of tumor cells in women with metastatic breast cancer receiving chemotherapy. SWOG-S0500. www.cancer.gov/clinicaltrials

71. Pierga JY, Bidard FC, Mathiot C, Brain E, Delaloge S, Giachetti S, de Cremoux P, Salmon R, Vincent-Salomon A, Marty M (2008) Circulating tumor cell detection predicts early metastatic relapse after neoadjuvant chemotherapy in large operable and locally advanced breast cancer in a phase II randomized trial. Clin Cancer Res 14:7004–7010.
72. Pachmann K, Camara O, Kavallaris A, Krauspe S, Malarski N, Gajda M, Kroll T, Jorke C, Hammer U, Altendorf-Hofmann A, Rabenstein C, Pachmann U, Runnebaum I, Hoffken K (2008) Monitoring the response of circulating epithelial tumor cells to adjuvant chemotherapy in breast cancer allows detection of patients at risk of early relapse. J Clin Oncol 26:1208–1215.
73. Muller V, Riethdorf S, Loibl S, Komor M, Houber J, Schrader I, Conrad U, Untch M, von Minckwitz G, Pantel K (2007) Prospective monitoring of circulating tumor cells in breast cancer patients treated with primary systemic therapy—A translational project of the German breast Group study GeparQuattro. J Clin Oncol 25 (18S):Abstract 21085.
74. Rack BK, Schindlbeck C, Schneeweiss A, Hilfrich J, Lorenz R, Beckmann MW, Pantel K, Lichtenegger W, Sommer HL, Janni WJ (2008) Prognostic relevance of circulating tumor cells (CTCs) in peripheral blood of breast cancer patients before and after adjuvant chemotherapy: The German SUCCESS-Trial. J Clin Oncol 28 (S):Abstract 503.
75. Xenidis N, Ignatiadis M, Apostolaki S, Perraki M, Kalbakis K, Agelaki S, Stathopoulos EN, Chlouverakis G, Lianidou E, Kakolyris S, Georgoulias V, Mavroudis D (2009) Cytokeratin-19 mRNA-positive circulating tumor cells after adjuvant chemotherapy in patients with early breast cancer. J Clin Oncol 27:2177–2184.
76. Gnant M, Mlineritsch B, Schippinger W, Luschin-Ebengreuth G, Postlberger S, Menzel C, Jakesz R, Seifert M, Hubalek M, Bjelic-Radisic V, Samonigg H, Tausch C, Eidtmann H, Steger G, Kwasny W, Dubsky P, Fridrik M, Fitzal F, Stierer M, Rucklinger E, Greil R, Marth C (2009) Endocrine therapy plus zoledronic acid in premenopausal breast cancer. N Engl J Med 360:679–691.

3D ultrasound computer tomography (USCT)

N.V. Ruiter, M. Zapf, T. Hopp, R. Dapp, G. Göbel,
and H. Gemmeke
Forschungszentrum Karlsruhe, Institute for Data Processing and Electronics, Karlsruhe, Germany, nicole.ruiter@ipe.fzk.de

Abstract
Ultrasound computer tomography (USCT) is an imaging method aimed at early breast cancer diagnosis. It is capable of producing 3D images with sub-millimeter resolution and high signal-to-noise ratio. In this paper exemplary results of the first experimental setup for a full 3D USCT are presented and discussed, and an outlook for a clinically applicable system is given.

Introduction
For further improvement of breast cancer diagnosis a new imaging method should ideally have high sensitivity by providing high image quality at sub-millimeter resolution in 3D. Additionally, high specificity should be available by providing a combined view on different tissue properties altered by cancer. Furthermore, the method should be inexpensive for screening, and apply no harm to the screened population.

We are developing a new imaging method for breast cancer diagnosis, ultrasound computer tomography (USCT), recording of 3D images with sub-millimeter resolution. The typical speckle noise of ultrasound images is reduced to the background noise and the typical shadowing is significantly lowered. Additionally, measurements of other tissue parameters, i.e. speed of sound and attenuation, are possible in millimeter resolution. Furthermore, the USCT images can be easily registered to MRI (Magnetic Resonance Imaging) volumes, due to imaging the undeformed breast in prone position in 3D. This combination may support early breast cancer diagnosis by providing complementary information about the tissue properties. Additionally Doppler, elastography and functional imaging with contrast agents are possible.
The methodology is characterized and tested with an experimental 3D setup (3D USCT, see Fig 1.). In this paper the results of our experimental 3D USCT are presented and discussed. Based on these results the necessary steps for a clinically applicable USCT system in 3D are described.

Methodology
The principle of imaging with USCT is given in Fig. 2 simplified in 2D. The object is surrounded by ultrasound transducers. One by one each transducer emits an approximately unfocused spherical wave, until the object was insonified from all directions. During each shot, all other transducers receive the transmitted, scattered and reflected signals.
Our approach to USCT combines two basic concepts: synthetic aperture imaging for post beam forming and ultrasound emission and reception from many different directions (spatial compounding).
Conventional ultrasound transducers use phased arrays for imaging. Thus many small emitters are combined to create one scan line focused to one point; the second focus dimension, the elevation plane, is usually fixed by an acoustic lens. During reception beam forming is carried out. As result of the single focus during emission the image lines show only the highest resolution in the vicinity of this focal point.
Synthetic aperture bases on the idea to combine many low resolution images to one high resolution image. Ultrasound is sequentially emitted from small elements as unfocused spherical wave. The received signals are combined by post beam forming, so that the image information can be optimally focused at any image point, increasing the overall image resolution and decreasing the spatial variability of the point spread function (PSF). In Fig. 3 simulated distribution of the PSF of the current 3D USCT setup is given, for details refer to [1]. With an appropriate sensor configuration the post beam forming can also be done in the elevation plane resulting in optimal focused images in 3D. Mathematically, beam forming with phased arrays and post beam forming are equivalent [2]. For example post beam forming is equivalent to focusing a phased array to each image point. In practice this is not done due to the real time requirements of manually operated ultrasound transducers.
Ultrasound emission from many directions increases the signal-to-noise ratio and decreases the speckle noise. Additionally, the shadowing effects of attenuating objects are reduced, so that the outlines of the objects become visible in 3D. When used with a manual operated ultrasound transducer or with a positioning device, the resolution is decreased by inaccuracies in assumed transducer position and deformation of the breast. If the position is known accurately, as for a fixed setup like in USCT, the overall resolution is even increased.

Surrounding the breast with ultrasound transducers in a fixed setup has further advantages: with the same image acquisition step data for reflection and transmission tomography is recorded, enabling the reconstruction of three different tissue properties, which are perfectly registered. Additionally, imaging of an undeformed breast in 3D allows the registration of the images with other modalities and earlier images of the same modality for follow up.

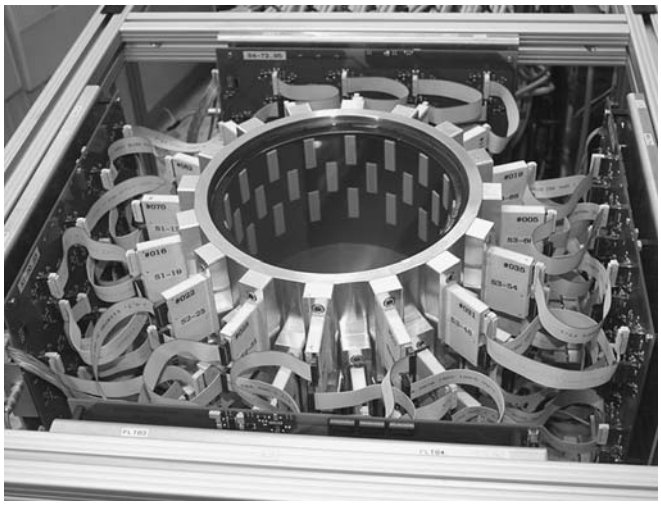

Figure 1: *Experimental 3D USCT*. The cylindrical configuration has a diameter of 18 cm and a height of 20 cm. The cylinder is filled with water and holds the object to be imaged. 384 emitters and 1,536 receivers are available. Currently, volumes are acquired with six different motor positions, resulting in 2,304 virtual emitting and 9,216 virtual receiving positions.

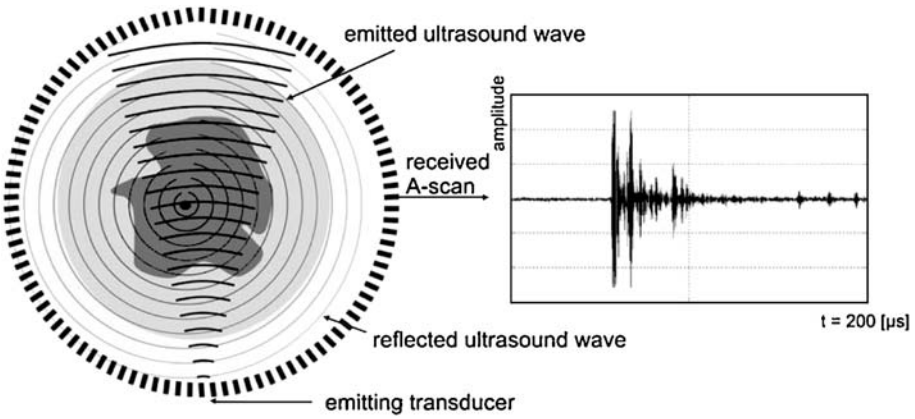

Figure 2: *The principle of imaging with USCT*. Left: A single transducer emits a spherical wave front; all other transducers receive the transmitted, scattered, and reflected ultrasonic waves. Right: Received ultrasound signal (A-scan) at one exemplary receiver.

Our current setup groups 384 emitters and 1,536 receivers on a cylindrical surface with 18 cm diameter and 20 cm height. The volumes are acquired at six different motor positions, resulting in 2304 virtual emitting and 9216 virtual receiving positions. The transducers have a resonance frequency of 2.7 MHz and a bandwidth of 50%. To increase the emitted sound pressure and the sensitivity of the recording for the experimental setup, the transducers as point sources are only approximated. The −6dB opening angle in 3D is ±15°, which limits the optim0ally insonified volume to a sphere with radius 2.5 cm in the center of the USCT. All image content outside this sphere will have less contrast and higher noise level. The excitation of the emitters can be arbitrarily programmed. The experiments described in the result section were carried out using frequency coded chirps to increase the signal-to-noise ratio of the recorded pressure over time signals (A-scans).

For one breast volume 3.5 Mio A-scans are recorded, resulting in 20 GB of raw data. For this purely experimental setup imaging phantoms, long data acquisition times were acceptable to decrease the costs, therefore imaging of one volume in full data acquisition mode takes about 8 h.

3D reflectivity imaging of a whole breast volume at the current wavelength with a full aperture would require more than 100,000 transducer positions, which is not feasible with today's technology. To enable synthetic aperture imaging in 3D, the data acquisition is carried out on a so-called sparse aperture, i.e. fewer A-scans are recorded as required by the sampling theorem. In ultrasound imaging this creates 'grating lobes', i.e. PSF of one point scatterer cannot be safely approximated to be local. For example a strong point scatterer will not only result in high grey values in the vicinity of the point's position, but result in a global artifact pattern of high grey values.

The reconstruction algorithm for reflectivity images applied here is a synthetic aperture focusing technique (SAFT), see [3] for details. SAFT calculates at each image point the mean of all reflections which might originate from this position. Norton and Linzer [4] showed that for ideal conditions, i.e. continuous aperture, isotropic point scatterers, no attenuation, SAFT solves the inverse problem of calculating the local impedance differences. For the simplest reconstruction the average speed of sound may be assumed to be constant, e.g. the speed of sound of water at the temperature measured during image acquisition. For more advanced reconstruction the speed of sound maps can be applied to correct the travel time. We apply also a phase aberration correction using an optimal scaled pulse to cope for additional deviations in travel time, e.g. small temperature gradient in the surrounding water. To suppress the artefacts caused by the grating lobes, a local median filter is applied during the SAFT reconstruction, refer to [3] for details.

Speed of sound and qualitative absorption volumes are reconstructed by evaluating the time and amplitude of the transmitted pulse and using the Feldkamp–Davis–Kress (FDK) algorithm for inverse Radon projection in a cone beam geometry, refer to [5] for details.

Results

A number of different phantoms have been imaged with the experimental 3D USCT. In the following three examples for reflectivity imaging with increasing complexity are described. The complexity for the reflectivity imaging is currently given rather by the contrast, overall size and attenuation of the objects than by the size of the smallest content.

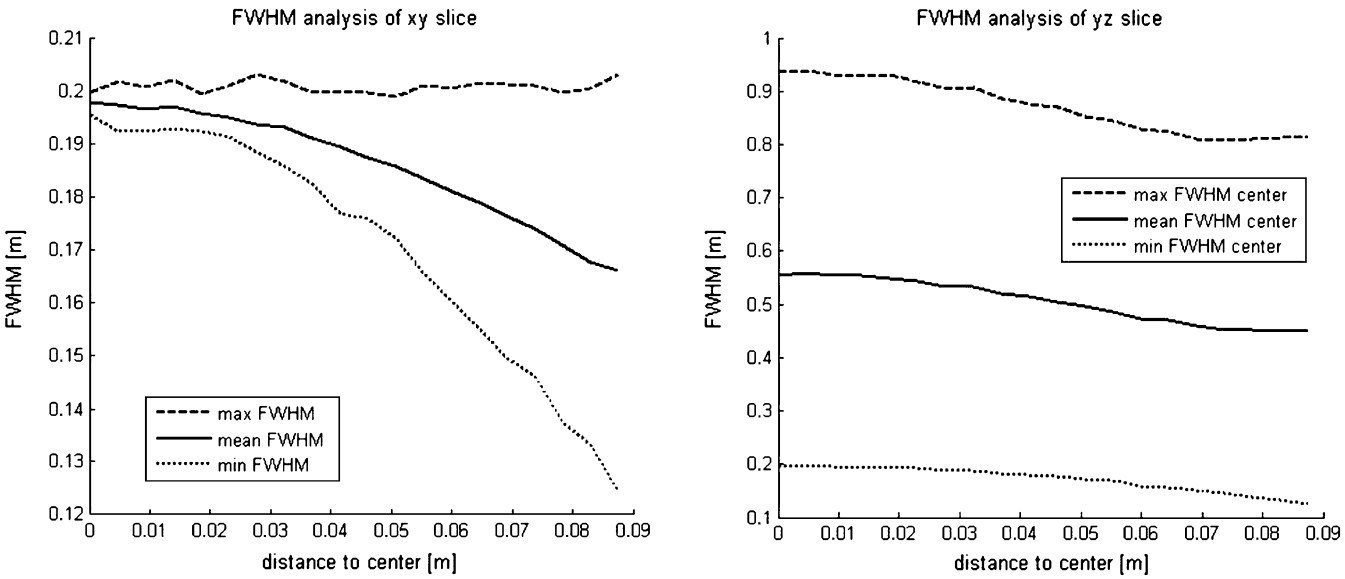

Figure 3: *Simulated distribution of the point spread function over space*. Top: Full width half maximum (FWHM) over distance from center of xy plane at half height. Bottom: FWHM over distance from center of yz plane. In [m].

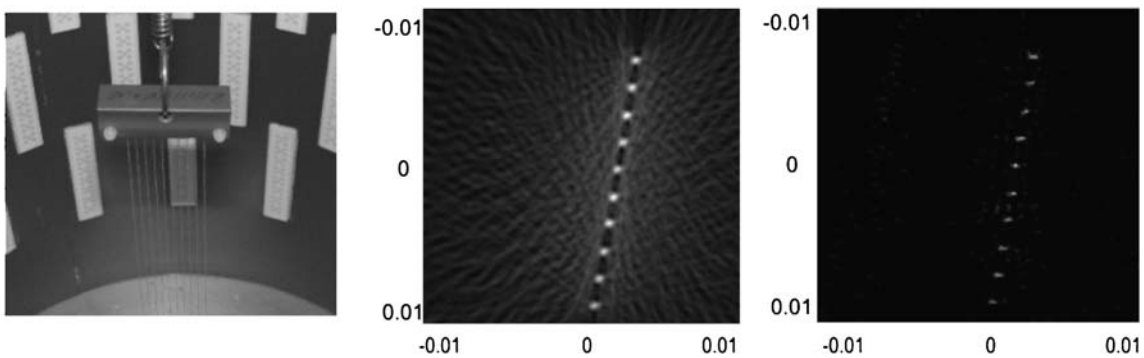

Figure 4: *Nylon thread phantom*. Left: photo of experiment. Right top: slice reconstruction using phase aberration correction (FWHM 0.63 mm, SDNR 11). Right bottom: slice reconstruction with additional grating lobe suppression (FWHM 0.24 mm, SDNR 36). In [mm].

Nylon thread phantom

The least complex phantom consists of ten nylon threads with a diameter of 0.2 mm each and a distance of 2 mm, see Fig. 4. The diameter equals the theoretical highest resolution of the system in xy slice at the center of the USCT (see Fig. 3). The nylon threads have high contrast, behave approximately like point scatterers in the xy plane and are located in the center of the imaging volume. The nylon threads were embedded in water, and the temperature of the water was recorded during the measurement (28° to 29°C).

The two example reconstructions given in Fig. 4 show (top right image) the reflectivity reconstruction with phase aberration correction and (bottom right) reconstruction with additional grating lobe suppression. The edge lengths of the slices are 2.3 cm and the pixel size is 23 μm.

The known ground truth of the phantom allows quantitative assessment of the reconstruction quality by measuring the resolution in terms of FWHM (*f*ull *w*idth of the PSF at *h*alf *m*aximum amplitude), and the image contrast in terms of SDNR (*s*ignal *d*ifference to *n*oise *r*atio, difference between mean of signal and mean of background, normalized by standard deviation of background). The first reconstruction resulted in a FWHM of 0.62 mm and a SDNR of 11 (compared to SDNR 0.5 of simple envelope reconstruction). Still side and grating lobes are visible and degrade the image. The second results in a resolution near the optimum with FWHM of 0.24 mm and a high contrast of 36. The side and grating lobes are sufficiently suppressed.

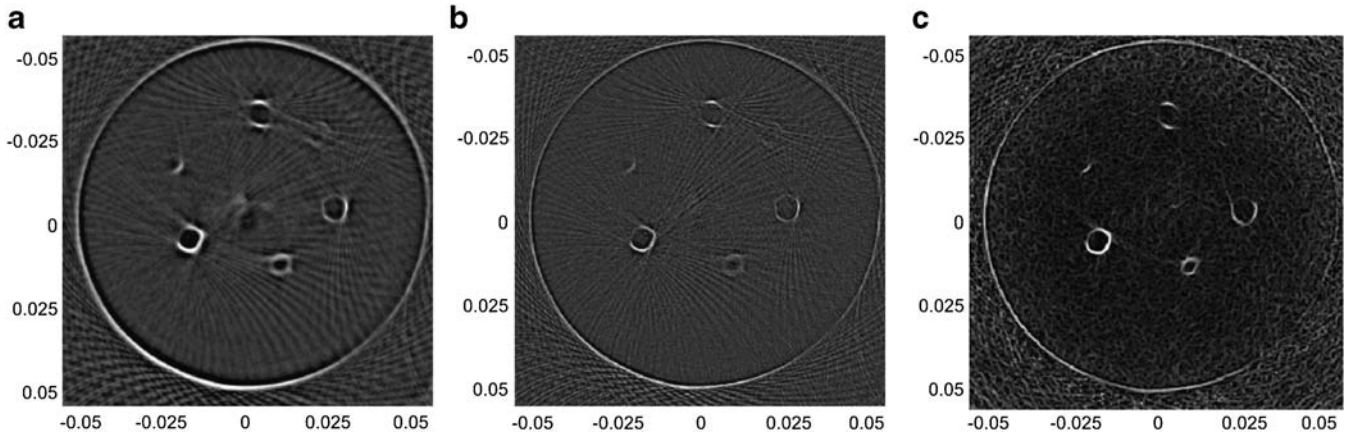

Figure 5: *MRI phantom*. Left slice reconstruction using envelope reconstruction (a), middle phase aberration correction (b), and right additional grating lobe reduction (c). In [m].

MRI Phantom

The second phantom, reflectivity reconstructions see Fig. 5, has higher complexity. It is a commercial MRI biopsy phantom (Radiological Diagnostic Products, Inc., USA) and consists of gelatin (speed of sound approx. 1,520 m/s with low attenuation) with cyst like lesions of approx. 1 cm diameter. It is cylindrical with a diameter of 10 cm and narrows at the top to a hemisphere. The cyst like structures' reflection behavior is approx. comparable to diffusely scattering surfaces and they strongly dampen the signal in transmission.

The phantom was imaged with a chirp excitation (2.4 MHz, 6.4 μs duration). The water temperature was stable at 27°C. The image area is $(11.2\ \text{cm})^2$ and the pixel area is $(180\ \mu\text{m})^2$. For all reconstructions the same subset of A-scans was used.

In Fig. 5 the left image shows a slice reconstructed using the envelop transformation of the original signal (5.a); speed of sound correction was applied. The middle image was reconstructed using phase aberration correction (5.b). Both resulting images were filtered with a local 2D median filter and this filtered image was subtracted from the original image to remove low frequencies. In the right image grating lobe reduction was added (5.c).

As the exact ground truth of the phantom is not known, only a qualitative evaluation could be carried out: in the envelope image (5.a) the image detail is degraded by application of the envelop transformation to the signal. The grating lobes are clearly visible as arched beams originating on the outer and inner surfaces of the phantom. Some parts of the surfaces have lower contrast than others, e.g. left and right part of the cyst like structure at 12 o'clock. This is partly due to the inhomogeneous illumination and partly due to a defect emitter at 10 o'clock. The effect of the non-uniform illumination is worsened by the limitation of the reflection directions due to the diffuse scattering surfaces instead of ideal point scatterers. Cyst like structures in other parts of the phantom create artifacts in the slice image (1, 5 and 10 o'clock) due to grating lobes in 3D and the currently non-uniform resolution.

Image 5.b shows the phantom in sharper detail due to the application of the optimal pulse. The grating lobes and illumination inhomogeneities are still visible. The contrast of the phantom cysts is reduced, but they are still visible. In 5.c grating lobe reduction is applied. The current algorithm operates in 2D and ignores 3D effects. The grating lobes are significantly suppressed, especially in the center of the phantom. The lateral image parts, especially outside the phantom, still show artifacts.

CIRS Triple Modality Biopsy Phantom

The most complex phantom presented here is a triple modality biopsy phantom (CIRS Incorporated, USA). The phantom is breast shaped (approx. $12\times8\times10\ \text{cm}^3$, see Fig. 6, top left photo) and contains cancer and cyst mimicking masses of 2 to 10 mm in diameter. Its physical characteristics resemble at mean a 50% glandular breast. The damping of the main material is approx. 0.5 dB/cm at 2.4 MHz for transmission. The average speed of sound is approx. 1,450 m/s. The material shows typical speckling texture in conventional ultrasound (Fig. 6, top right). The lesions'

reflection behavior is also similar to diffuse scattering surfaces. The cancer mimicking lesions contain a large number of strongly scattering objects, which are approx. point scatterers.

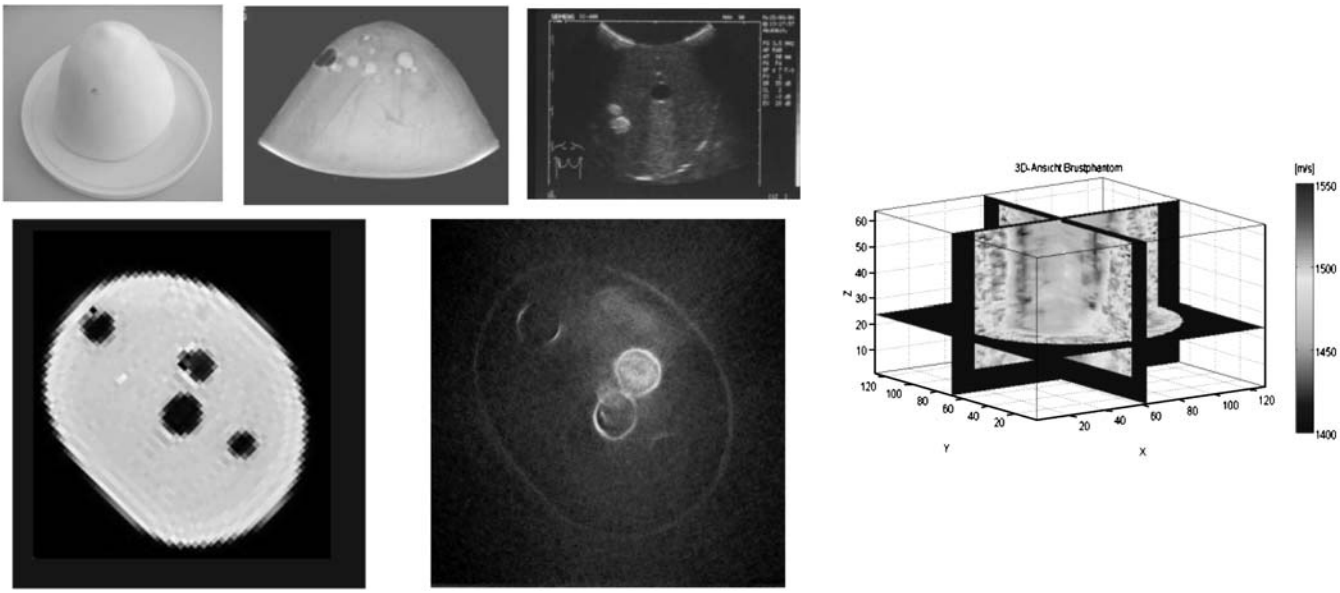

Figure 6: *CIRS Triple Modality Biopsy Phantom*. Top row, left to right: photo of phantom, X-ray mammogram, B-scan with conventional US scanner. Bottom row: MRI slice (left) and USCT slice (right). Right image: 3D view of speed of sound reconstruction.

An X-ray mammogram, B-scans with a conventional ultrasound scanner and a MRI volume of the phantom were available for comparison (Fig. 6, top middle and right, bottom left).
Again chirp excitation was applied. The water temperature during data acquisition ranged from 20 to 23°C, corresponding to a speed of sound range from of 1481 to 1,490 m/s. The reconstruction (Fig. 6, bottom right image) uses phase aberration and grating lobe reduction. The image area is $(11.2\ \mathrm{cm})^2$, the pixel area is $(180\ \mu\mathrm{m})^2$. The largest diameter of the phantom in this slice is approx. 7 cm. In Fig. 6, right image, a 3D depiction of the speed of sound map of the phantom is given.
All lesions depicted in the MRI slice are visible in the USCT image. The depiction of the lesions in the USCT image has smoother surfaces. The grating lobes are significantly suppressed, but the overall appearance of the USCT image is noisy, similar to the artifacts in Fig. 5.3. Very promising is the significant differentiation between 'cyst' and 'cancer' mimicking lesions in the USCT slice image.

Discussion and Conclusion

This first experimental full 3D USCT showed the potential of synthetic aperture imaging with spatial compounding in 3D for breast cancer diagnosis. Volumes of reflectivity with sub-millimeter resolution can be reconstructed for a breast in prone position. The spatial compounding reduces the speckle to the image background noise. Additionally, volumes of the speed of sound and (qualitative) absorption can be reconstructed. They are used for correction of the reflectivity images, and can be applied as two additional perfectly registered modalities for diagnosis.
The limitations of the purely experimental system are long data acquisition time, inhomogeneous illumination, spatially varying and anisotropic PSF and appearance of grating lobes due to the sparse aperture approach. To overcome these limitations and move towards a system for clinical tests, 3D USCT II is currently built.
Based on simulations of PSF, image contrast and illumination, a more optimal aperture in form of a semi-ellipsoid is proposed for the next generation 3D USCT [6], see Fig. 7. The optimized semi-ellipsoidal aperture will be equipped with 640 emitters and 1,440 receivers. The aperture can be rotated and lifted in almost arbitrary steps.
The new system offers fast data acquisition with comparable or larger number of virtual transducers. The mean resolution, measured by the size and deformation of the spatially varying PSF, is improved by 62% by the new aperture. The illumination within breast volume will be homogeneous and is approx. three times higher than for the current cylindrical aperture.
The contrast reduction by the grating lobes will be decreased by 23%. Additionally, the adapted reconstruction algorithms show first positive results and will be developed further.
To enable imaging of living tissue, the new data acquisition hardware will provide an overall data acquisition time below 3 min.

References

[1] G. F. Schwarzenberg, R. Stotzka, M. Zapf, H. Gemmeke, N. V. Ruiter: *Resolution assessment of a 3D Ultrasound Computer Tomograph using Ellipsoidal Backprojection*, Proc. IEEE UFFC, 2006.
[2] F. Anderson, F. Morgan, *Active imaging analysis via ellipsoidal projection*, Acoust. Imag., 21, pp. 171–181, 1995.
[3] N.V. Ruiter, G.F. Schwarzenberg, M. Zapf, H. Gemmeke: *Conclusions from an Experimental 3D Ultrasound Computer Tomograph,* Proc. IEEE NSS/MIC, 2008.

[4] S.J. Norton, M. Linzer: Ultrasonic reflectivity imaging in three Dimensions: exact inverse scattering solutions for plane, cylindrical and spherical apertures, IEEE Trans. Biomed. Engin., 28(2), 1981.
[5] N.V. Ruiter, R. Schnell, M. Zapf, H. Gemmeke: *Phase aberration correction for 3D Ultrasound Computer Tomography Images*, Proc. IEEE UFFC, 2007.
[6] G.F. Schwarzenberg, M. Zapf, N.V Ruiter: *Aperture Optimization for 3D Ultrasound Computer Tomography*, Proc. IEEE UFFC, 2007.

Figure 7: *Current status 3D USCT II.* The semi-ellipsoidal configuration has a diameter of 28 cm and a height of 18 cm. The lower image shows the first batch of the new ultrasound transducer systems.

Matching Mammography and MR-Mammography—Where exactly is microcalcification in MRM?

T. Hopp[1], N.V. Ruiter[1], M. Dietzel[2], P. Baltzer[2], W.A. Kaiser[2]
[1]Institute for Data Processing and Electronics, Forschungszentrum Karlsruhe
[2]Institute of Diagnostic and Interventional Radiology, Friedrich Schiller University Hospital Jena
{torsten.hopp, nicole.ruiter}@ipe.fzk.de
{matthias.dietzel, pascal.baltzer, werner.kaiser}@med.uni-jena.de

Abstract
X-ray mammography is the standard screening method for early breast cancer diagnosis, however it has limited contrast for tumors within glandular tissue and only produces two-dimensional projections of a deformed breast. MRI offers high contrast of soft tissue and high diagnostic accuracy. As microcalcifications are displayed in X-ray mammograms exclusively, it is of interest to correlate both modalities for diagnosis. The correlation is challenging, as in X-ray mammography the breast is compressed and only 2D projections are shown while in MRI an undeformed breast is imaged in 3D. For matching both modalities, a patient specific biomechanical model is built. The compression during mammography is applied to this model using a FEM simulation. First results with clinical data show displacements of less than 5 mm in most cases.
In a clinical study, which is currently carried out, the methodology is evaluated with higher number of datasets to analyze the accuracy and clinical applicability for breast cancer diagnosis. The matching software was extended to deal with variations in clinical data. The study design consists of a two-step approach, which first evaluates the accuracy of the matching and second evaluates the clinical applicability.
The matching is expected to give radiologists a beneficial assistance for the multimodal diagnosis of breast cancer in an early stage as e.g. the position of microcalcification can be located in MRI volumes.

I. Introduction

X-ray mammography is the most widely used imaging method for early breast cancer detection. It provides 2D projections of a deformed breast and has limited contrast for tumors within glandular tissue. Breast MRI (Magnetic Resonance Imaging) offers excellent soft tissue contrast and high diagnostic accuracy [1].
While in MRI the morphology and angiogenesis of a tumor is described accurately, microcalcifications are displayed in X-ray tomography, exclusively. As certain types of microcalcifications can be associated with invasive carcinoma or preinvasive breast cancer, it is of interest to correlate both modalities for diagnosis. In earlier works of Ruiter et al. [2], [3] a model based matching of X-ray mammograms and MRI volumes was presented. It allows automatic localization of the position of a lesion in 3D in a MRI based image given the position of a lesion in a 2D mammogram. Vice versa, the position of a lesion in the 2D mammogram can be calculated given the position in a MRI image. In first evaluations with clinical datasets, this method showed promising results. Displacements of the matching could be accounted to be lower than 5 mm, which is applicable for early breast cancer diagnosis [2].
In clinical practice, this matching methodology may help predicting the position of microcalcification in an MRI volume and therefore delivering information of the exact position within the breast. The matching of the images results in additional information for radiologists and images benefiting of the advantages of both modalities.
In a next step, further enhancements of the method and the matching software had to be carried out as preparation of a clinical evaluation, as the algorithms have only been tested with few datasets. Within a project of the Institute of Diagnostic and Interventional Radiology (IDIR) at Friedrich Schiller University Hospital Jena and the Institute of Data Processing and Electronics (IPE) at Forschungszentrum Karlsruhe, a clinical study is currently realized. The challenge is to apply the image matching to up to 1,000 datasets to show the quality of matching and measure the effect of this method for breast cancer diagnosis.
In this paper, we present the methodology and first results with clinical datasets. Based on this we focus on recent developments to extend the matching software and the design of the clinical study. Finally, a conclusion is given and future work is presented.

II. Matching of X-ray mammograms and MRI volumes

A) Methodology

The matching of X-ray mammograms and MRI volumes is challenging as compression is mandatory for every conventional mammography, whereas breast MRI is performed without compression. The breast consists of deformable, mobile and inhomogeneous tissue, which results in variations of the deformation [3]. The approach for the matching applies a model of the deformable behavior of the breast. Based on the 3D volume of MRI, a simulation deforms this model according to the deformation of the breast during mammography (Figure 1).

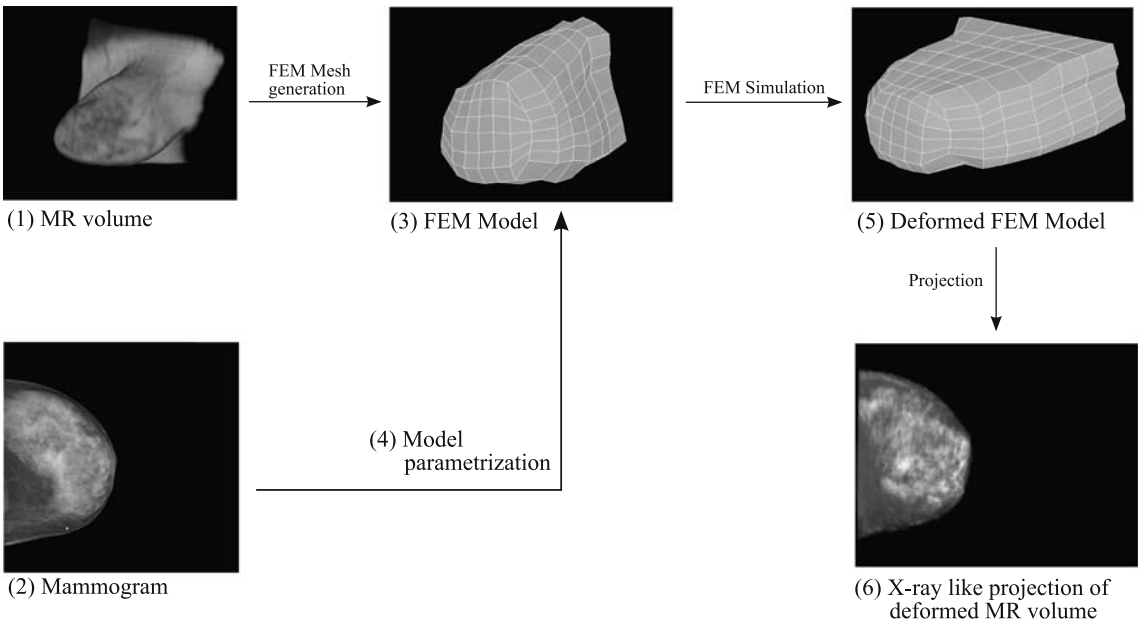

Figure 1: Matching process: the MRI volume (1) and the X-ray mammogram (2) are used to generate a patient specific finite element mesh (3). Tissue properties and deformation process are formulated (4) and the FEM simulation is carried out. The generated MRI image of the deformed breast (5) is used for the subsequent X-ray like projection (6).

The model is based on every individual MRI volume. The breast tissue is estimated as imaged in the MRI by a segmentation algorithm. Upon this estimation, a finite element model (FEM) is built. By identifying boundary conditions the model is refined. An appropriate non-linear, incompressible tissue model is applied. Resulting equations are solved using solution methods for large deformations in Ansys [4], a commercial software to solve FEM simulations. The deformation is mimicked by a plate compression formulated as FEM. For this, the projection angle of the mammogram has to be estimated as well as the compression ratio of the breast during mammography and the amount of tissue imaged. In a second step, the simulated deformation is applied to the MRI volume to estimate the deformed breast during mammography.

The matching ensures direct comparability: the deformed breast in the simulation is an approximation of the compressed breast in the mammogram. The result of the FEM simulation is used for the generation of artificial MRI projections, comparable to the mammogram both in spatial configuration and simulated X-ray attenuation. Additionally, the information about the deformation connects both modalities, which allows the calculation of positions of lesions in the MRI given the position in two X-ray mammograms.

B) First results

The described methodology was applied to six datasets including X-ray mammograms and MRI of each patient. For the evaluation, all datasets included lesions in both the mammograms and the corresponding MRI images. The positions of the lesions were marked by a radiologist. Thus, the simulated location and the real location could be compared [2]. The distance of the center of the lesion and the overlapping area respectively volume are given in Table 1 and Table 2. Figure 2 shows resulting images.

Dataset	Center displacement	Overlap (in %)
1	3.7 mm	40.7
2	4.3 mm	85.7
3	5.0 mm	100
4	2.3 mm	100
5	4.0 mm	86.7
6	4.2 mm	84.6

Table 1: Results of lesion localization in the mammograms: Center displacements and overlap of the lesions' area.

Dataset	Center displacement	Overlap (in%)
1	4.6 mm	88.9
2	3.2 mm	99.6
3	5.4 mm	58.9
4	1.6 mm	100
5	6.2 mm	100
6	2.2 mm	100

Table 2: Results of lesion localization in the MRI images: Center displacements and overlaps of the lesions volume.

The mean displacement of the center of a lesion is 4.3 mm (standard deviation±1 mm) for predicting the lesion in mammograms, and 3.9 mm (standard deviation±1.7 mm) for predicting the lesion in MRI images. In more than three quarters, the center distance is well below 5 mm, which is applicable for clinical usage, as structures become just visible at this size.
The results are very promising and it is assumed that the combination of both modalities may result in a more effective diagnosis of breast cancer in an early stage. Thus, in the following we will present the recent development and the design of a clinical study to evaluate this assumption.

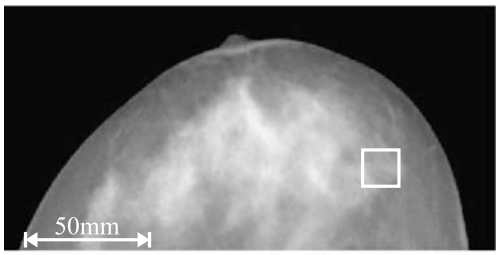

Cranio-caudal X-ray mammogram

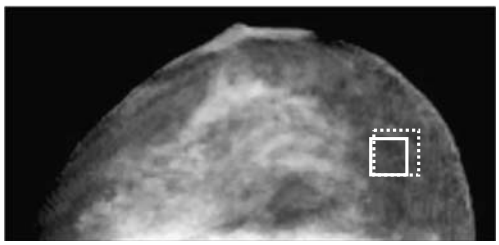

X-ray like projection of deformed MRI

Figure 2: Dataset 2, estimated and original lesion position in the cranio-caudal X-ray mammogram. Top: Cranio-caudal X-ray mammogram. The real lesion position is given as a solid boundary box. Bottom: Projection of the MRI volume after matching. The boundary box of the projected MRI lesion is given as dotted line and the original position as a solid line. The center lesion distance is 4.3 mm and the area overlap amounts to 86%.

III. Software extension

Due to the small number of clinical datasets for the first evaluation of the methodology in earlier work, it was assumed, that the results may be only valid for the given datasets used to build the model [2]. Clinical data varies in quality and patient individual attributes, therefore, the software was enhanced to increase the robustness for a clinical study, where images and patients show a wide range of characteristics.

The software has to deal with images in different formats, as the DICOM standard [5] varies slightly for different imaging devices. Therefore the software was extended by an abstraction layer reading data from DICOM folders automatically and converting it in appropriate formats for the matching process.
Essential for the generation of the FEM mesh is a smooth and accurate segmentation of the image data. As experiments showed, the simulation is very sensitive to uncontinuous edges of the segmentation of the breast. Therefore, the former segmentation method based on thresholding and morphological operations was extended by the approach of Chan and Vese [6] using active contours without edges.
As by now the software was used mainly manually by a scientist, the effort for the matching of a single dataset was accordingly high. This was improved by the automation of the software following Figure 3, which is necessary for the use with a large number of datasets. Furthermore, for a faster execution of the evaluation of numerous datasets, the software will be adapted for parallel execution on multiple workstations.

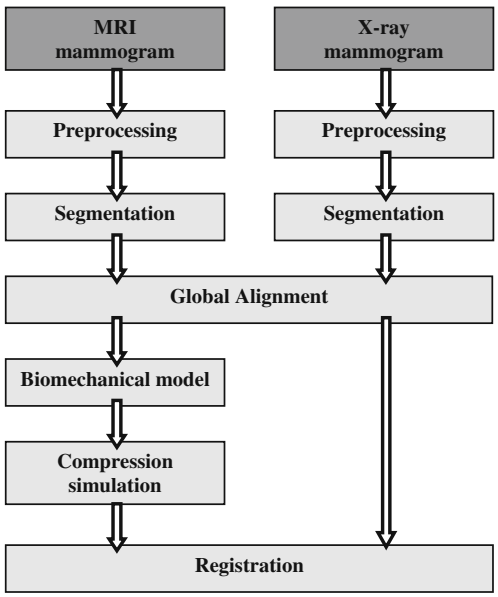

Figure 3: Workflow of the matching software for X-ray mammograms and 3D MRI mammograms

IV. Clinical study

The aim is first to evaluate the matching approach with a large number of datasets and second to examine the applicability of the software for usage in breast cancer diagnosis.
In the pre-study-phase clinical datasets for retrospective studies were gathered by the radiologists of IDIR. The dataset of one patient consists of images of both modalities including varying diagnostic findings. They are made anonymous and transferred to a central database. After the matching is done, resulting images and metadata are available for diagnostic findings by the radiologists. Therefore, a diagnosis software was implemented which allows the presentation of the clinical datasets and matching results according to the study design. The diagnosis software also includes functionality for the marking of lesions, as these marks are essential for the evaluation of the matching quality. Furthermore, the diagnosis of the radiologists can be

submitted via a consistent mask, including medical findings using BI-RADS classification. All information is kept in the central database and will be used for statistical analysis.
The design of the first clinical study is divided into two parts:
First, a retrospective accuracy study is currently carried out. For the evaluation of the quality of the matching, 50 datasets including benign, calcified and non-calcified lesions are used, as the lesions are clearly visible in both modalities. Afterwards 50 datasets with partial calcified adenomas are used for further optimization of the matching software. The first retrospective study concludes with up to 500 datasets with cysts or adenomas for statistical significance. The results are expected to show the accuracy of the matching and identify criterions for datasets to be included or excluded in the next part of the study. The coherencies between different parameters for X-ray mammography (e.g. compression ratio, type of mammographic device), MRI (e.g. effect of motion artifacts) and patients (e.g. age, size and density of the breast) will be analyzed.
Second, the retrospective clinical study will be carried out including a large dataset with focal findings and with non-nodular accumulation of contrast agent. The results will be passed to three radiologists for independent anonymous diagnosis, for which the merged datasets are once considered and once not. The results will be used to measure the benefit of the image matching for clinical usage, as the medical findings with and without merged data can be compared. Also the comparison with histological diagnostic findings of the corresponding patient is expected to give information about the usability of the method.
Based on the two-step clinical study presented, a second therapy referred study will be carried out. Its purpose is to find out the influence of the merged data for further therapies. Finally, a prospective workflow study will evaluate the feasibility of the image matching in clinical routine. Analyses of the expenditure of time, the technical availability and sources of errors have to be done.
Parallel to the clinical study, the enhancement of the matching software will be further adapted to react on upcoming problems and to increase the robustness for a wide range of patient and image characteristics.

V. Conclusion and Outlook

In this paper we presented a model based method to register mammograms and MRI images using patient specific biomechanical models. This takes in account the deformation of the breast during mammography and creates directly comparable projection images. Furthermore, lesions can be localized in the MRI image given the positions in two standard X-ray mammograms. First results are very promising. The average center displacement of lesions marked in images of both modalities is 4.3 mm for predicting the lesions in mammograms and 3.9 mm for predicting the lesion in MRI images.
This approach is expected to give radiologists a beneficial assistance for the multimodal diagnosis of breast cancer in an early stage as e.g. the position of microcalcification can be located in MRI volumes. Possible advantages for clinical practice are expected to be a more confident diagnosis and a more specific localization of lesions. This would result in a higher certainty for breast-preserving surgery.
To evaluate this, a clinical study is carried out. We presented enhancements to the matching software, which are essential to increase the robustness, as the clinical study includes a wide range of patient and image characteristics. To allow a fast execution of the software, it was automated and prepared for parallel execution.
The clinical study is designed to evaluate the quality of the matching process and the applicability of the merged images in clinical usage. It will include up to 1,500 datasets in a two-step approach: first, the accuracy of the matching is measured; afterwards, the benefit of the method is evaluated by the independent medical finding of radiologists with and without merged images.
In future work, we are about to analyze the results of the clinical study statistically, using the central database. The image matching software will be extended to a tool for the matching of different modalities like 3D Ultrasound Computer Tomography [7], X-ray Computer Tomography or Tomosynthesis. This will allow the comparison of the image quality and specificity of the modalities. Furthermore, the results can be used for multimodal diagnosis. For a better estimation of the breast characteristics, the material model of the biomechanical model for the deformation simulation will be extended. Texture based recognition may help localizing tumors in the merged images.

Acknowledgement

This work is supported by the German Research Society under grants no. KA 293/8-1 and RU 1547/1-1.

References

[1] W. DeMartini, C. Lehmann. *A review of current evidence-based clinical applications for breast magnetic resonance imaging*, Top Magn Reson Imaging 2008; Vol. 19, pp. 143–150
[2] N. V. Ruiter, R. Stotzka, T. O. Müller, H. Gemmeke, J. R. Reichenbach, W. A. Kaiser. *Model-based registration of X-ray mammograms and MR images of the female breast*, IEEE Transactions on Nuclear Science, Vol. 53, No.1, February 2006, pp. 204–211
[3] N. V. Ruiter, R. Stotzka, T. O. Müller, J. R. Reichenbach, S. Wurdinger, H. Gemmeke, W. A. Kaiser. *Model Based Fusion of X-ray Mammograms and MR Volumes of the Female Breast*. MRM—Congress on MR-Mammography 2003, pp. D65–D67
[4] Ansys Inc. Software Products, website http://www.ansys.com/products/default.asp
[5] National Electrical Manufacturers Association. Digital Imaging and Communications in Medicine (DICOM). 2008. available online at ftp://medical.nema.org/medical/dicom/2008/
[6] T. Chan & L. Vese. *Active contours without edges*. Image Processing, IEEE Transactions on, 2001, 10, 266–277
[7] H. Gemmeke, N. V. Ruiter. *3D ultrasound computer tomography for medical imaging*. Nuclear Instruments and Methods in Physics Research A, 550(2007) S.1057–65.

Software solutions in evaluation of dynamic MRI of the breast

Andreas Saleh, MD, MBA[1], Kathinka D. Kurz, MD[2]
[1]Institute of Radiology, Düsseldorf University Hospital, Moorenstr. 5, 40225 Düsseldorf, Germany
[2]Department of Radiology, Stavanger University Hospital, Postboks 8100, 4068 Stavanger, Norway

Magnetic resonance imaging (MRI) of the breast is the most sensitive tool for the detection and characterization of breast cancer. This is based on the fact that nearly all invasive breast cancers do enhance contrast material. The characterization of enhancing lesions as benign or malignant remains a challenge. The specificity of MR imaging of the breast has been reported to be between 20% and 100%. There is increasing evidence, that the integration of architectural features and signal intensity time course data is the most effective way to reduce false-positive results of breast MRI. Time signal intensity curves are usually obtained on the basis of manually defined regions of interest (ROIs) led by intensity increased areas within subtraction images. Limitations of ROI analysis include the fact that only subjectively selected areas are examined and that the pixel measurements of

the chosen regions are averaged. The dynamic breast MRI scan contains much more data compared to the information shown in the subtraction images. This additional information can be visualized by using a software program that produces parametric color overlays on all image slices to identify areas of significant enhancement. The definition of "significant enhancement" is user defined. Pixel values at the unenhanced and contrast-enhanced series are compared. If the pixel value increases an user defined threshold (e.g. 100%) the pixel will be shown in color. If the pixel value fails to increase by the established threshold, no color overlay will be made. For the interpretation of the examination all enhancing areas decreasing a defined threshold are "eliminated" from analysis. To further improve specificity without decreasing sensitivity the program assigns a specific color to each pixel that meets the threshold for significant enhancement. The color assigned depends on the change in the pixel values between the initial contrast-enhanced series and the following contrast-enhanced series. If the pixel value on the following series decrease by a user defined value (e.g. 20%) that pixel is color coded red, representing a washout curve. If the pixel value does not change in either direction by more than a user defined value, it is color-coded yellow for plateau enhancement. If the pixel value increases by more than a user defined value (e.g. 10%) it is color-coded blue, indicating persistent enhancement (Fig. 1).

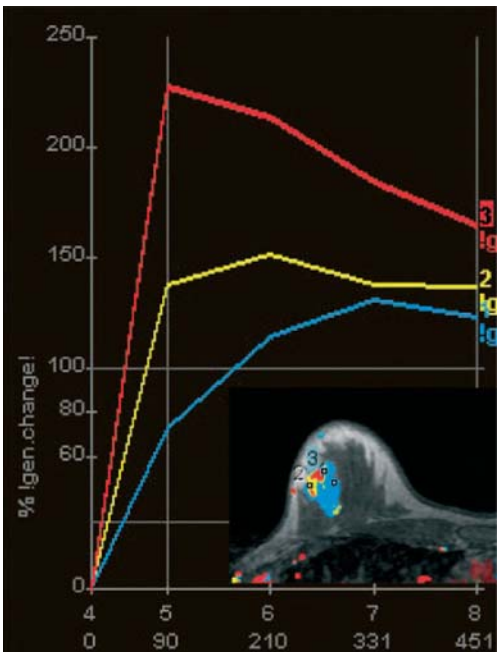

Fig.1 The blue line represents a ROI that did increase to level of significant enhancement and continued to increase on following series to a value more than 20% higher than its value on immediate contrast-enhanced series. The yellow line represents a ROI that increased to level of significant enhancement and did not change in either direction by more than 20%, indicating plateau enhancement. The red line represents a ROI that increased to level of significant enhancement and then decreased by more than 20% on following contrast enhanced scans, indicating washout enhancement. All grey pixels do not increase to level of significant enhancement and are therefore not color-coded.

In order to preserve the possibility of a semiquantitative assessment of the intensity of contrast enhancement the program should be able to produce image modulated overlays. That means that the hue of the color pixel is influenced (modulated) by the brightness of the underlying grey pixel. The parametric images are easier to read and less noisy when the smallest color-coded area consists of more than one pixel (the amount is user defined, e.g. 3×3).

In breasts with multiple areas of contrast enhancement, often seen in young patients, by fibrocystic changes in the breasts or in patients treated with hormone replacement therapy it can be

extremely difficult to distinguish benign from malignant lesions by visual inspection of the subtraction images but may be not by using parametric images (Fig. 2).

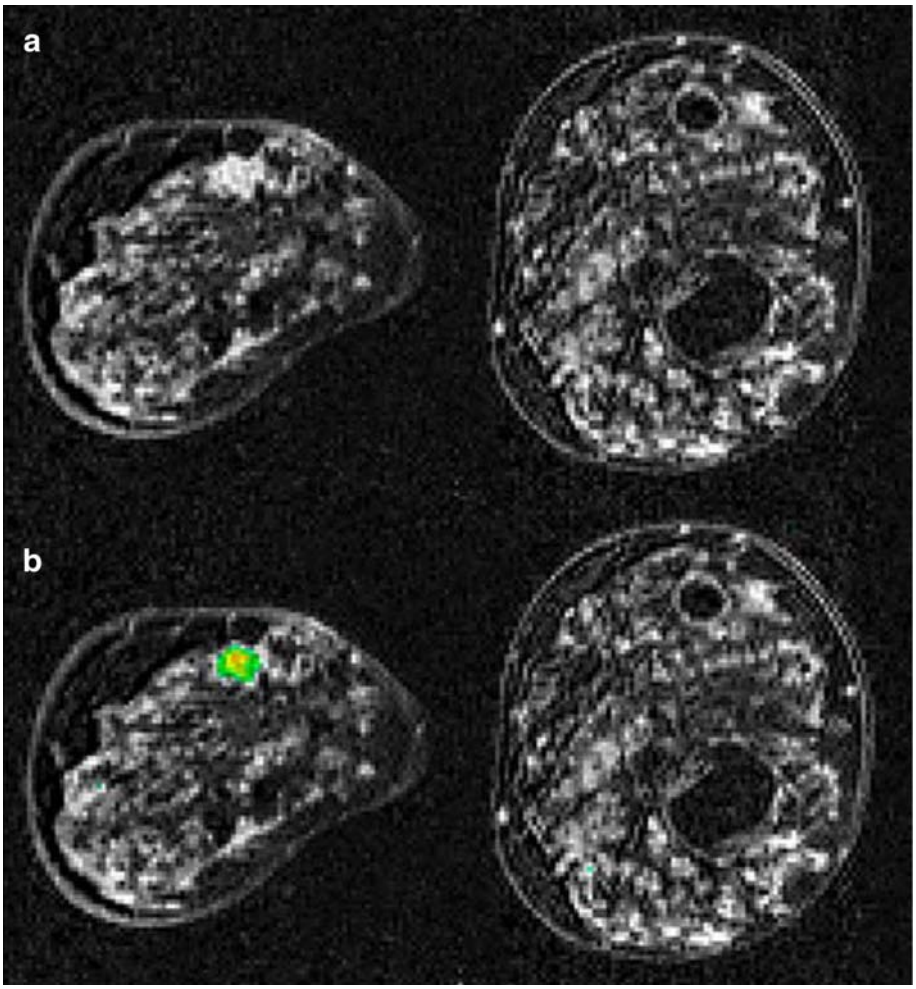

Fig. 2 A 9-mm invasive ductal carcinoma at 12 o'clock in the right breast and distinctive partially enhancing fibrocystic changes in both breasts. a) shows the early subtraction image, b) the parametric overlay. The carcinoma is labelled whereas the multiple enhancing benign areas are not indicated with color-coded overlay. The patient was treated with breast-conserving therapy and radiation of the right breast. There were no signs of recurrent disease in the follow-up MRI 28 months later.

Summary
Parametric image overlay visualizes more information out of the dynamic breast MRI data set than subtraction images combined with ROI measurements and has therefore the potential to increase specificity without decreasing sensitivity. These programs may decrease the amount of time required for image interpretation.

Split dynamics with combined perfusion analysis and dynamic MRI of the breast

Kathinka D. Kurz, MD[1], Andreas Saleh, MD, MBA[2], Kjell Inge Gjesdal, PhD[3]
[1] Department of Radiology, Stavanger University Hospital, Postboks 8100, 4068 Stavanger, Norway
[2]Institute of Diagnostic Radiology, Düsseldorf University Hospital, Moorenstr. 5, 40225 Düsseldorf, Germany
[3]Sunnmøre MR-klinikk, Langelandsveg 15, 6010 Ålesund, Norway

Introduction
Dynamic contrast enhanced magnetic resonance imaging (=DCE MRI) of the breast has become an important tool to detect and characterize breast diseases. DCE MRI of the breast offers a

higher sensitivity compared to mammography and ultrasonography. For DCE MRI of the breast, a T1-weighted series prior to contrast agent injection in a cubital vein is obtained, followed by several (usually six or more) series after contrast agent injection. This in combination with fast MR scan techniques allows the study of signal changes in various tissue types over time. The shape of the time intensity curves (TIC) from regions of interest (ROI) serves as one of the important diagnostic criteria. The temporal resolution of DCE MRI of the breast is usually between one and two minutes. The main drawback of DCE MRI is the limited specificity, reported to be between 37% and 100% in the literature.

Several studies of perfusion MRI of the breast for further characterization of enhancing lesions have been performed. The studies show, that analysis of perfusion has the potential to enhance the specificity of MRI. Perfusion imaging has a temporal resolution of only a few seconds with the technique available today, however, the spatial resolution of the perfusion images is too low for diagnostic evaluation of the morphology of lesions. Therefore, patients have to undergo two contrast enhanced examinations on separate days, which is not optimal in respect to patient friendliness or health care costs. The reluctance to adopt perfusion imaging for breast diseases has probably been further reinforced by the increasing awareness about gadolinium associated nephrogenic systemic fibrosis. Therefore, in contrast to MR imaging of other tumors, like gliomas in the central nervous system or soft tissue sarcomas, perfusion studies of breast tumors are not widely used in clinical practice today.

We have developed a scanning protocol, "split dynamic imaging," for performing DCE MRI and perfusion MRI after a single intravenous contrast bolus. The perfusion images obtained have a temporal resolution of only 2.7 s, and the dynamic scan a high enough spatial resolution for morphologic analysis. The aim of this study is to analyze if split dynamic imaging allows more accurate differentiation of benign from malignant lesions in the breast than DCE MRI.

Material and Methods

50 female patients at least one solid mass in the breast were prospectively included in the study between March 2008 and July 2009. Informed consent was collected from all patients as well as approval of the institution's review board for clinical research.

Half of the patients had benign solid masses in the breast, while the other half had malignant tumors. Definitive cytological or histopathological diagnosis was available for all patients. In 22 patients the benign lesions were fibroadenomas, in two patients intraductal papilloma without atypia and in one patient an intramammary benign lymph node. Eighteen patients had invasive ductal carcinoma, while invasive lobular carcinoma, mucinous carcinoma, and tubular carcinoma, were found in three, two and one patient respectively. One patient had an inflammatory carcinoma. Three patients were excluded as histological analysis revealed complex sclerosing lesion in one patient and adenosis two patients. Two patients were excluded because of severe motion artifacts.

All investigations were performed on a Philips Intera 2.2 MR scanner operating at 1.5 Tesla (Philips Medical Systems, Best, The Netherlands). The patients were placed in prone position on the magnetic bore, with the breasts positioned in a 7 channel dedicated double breast coil (Invivo, Orlando, Florida, US). The study protocol comprised an axial T2-weighted series and a fat suppressed T2-weighted series with fat suppression by inversion recovery in the coronal plane. A T1-weighted 3D fat suppressed fast spoiled gradient echo sequence in the axial plane was obtained before and six times after contrast agent injection. Between each sequence a T1-weighted gradient echo perfusion series in the axial plane was performed, for 80 s during contrast bolus injection and for 10 s between each dynamic scan. After the last dynamic scan, perfusion series was performed for 153 s. The scan parameters for the T2-weighted series in the axial plane were: TR=4,200 ms, TE=90 ms, slice thickness 5 mm. The scan parameters for the fat suppressed T2-weighted series in the coronal plane: TR=9128 ms, TE=60 ms, IR=150 ms, slice thickness 5 mm. The scan parameters for the T1-weighted 3D fat suppressed series were TR=6.9 ms, TE=3.4 ms, inversion time 90 ms, total scan duration 7 min and 16 s, per dynamic scan 1 min and 12 s. The parameters for the perfusion series in the axial plane was TR=42 ms, TE=2.9 ms, total scan duration 3 min and 27 s, per dynamic scan 2.7 s.

Gadobenate dimeglumine (Multihance, Schering AG, Berlin, Germany) 0.1 mmol per kg body weight of was injected as a bolus at 5 ml per second into a forearm vein. After the preliminary unenhanced T1-weighted 3D fat suppressed fast spoiled gradient echo sequence, the contrast bolus was given. Ten seconds later, the T1-weighted perfusion imaging begun and lasted for additional 70. Thereafter the first contrast enhanced 3D T1-weighted fat suppressed fast spoiled gradient echo sequence was obtained followed by perfusion imaging for 10 s. T1-weighted and perfusion images were thus alternately repeated five more times. The last perfusion series was obtained over 153 s.

The perfusion data were exported to a workstation running a commercially available perfusion analysis software (nordicICE, NordicNeuroLab, Bergen, Norway). Regions of interest (ROI) around the solid lesion were drawn on images from one of the early contrast enhanced 3D T1w fat suppressed series. The ROIs will then be transposed on the corresponding images from the perfusion series, ROIs in parenchyma without focal lesions in the same breast served as controls. Preliminary variables selected for analysis are: Mean transit time (MTT), extravascular-extracellular volume (Ve) and inhomogeneity of tumor blood volume. All other of images were analyzed with software bundled with the MR scanner.

Results

As the analysis of the data was not completed at the time of abstract submission, the following images are provided instead to illustrate the analysis performed. Results from the study will be presented in detail at the congress.

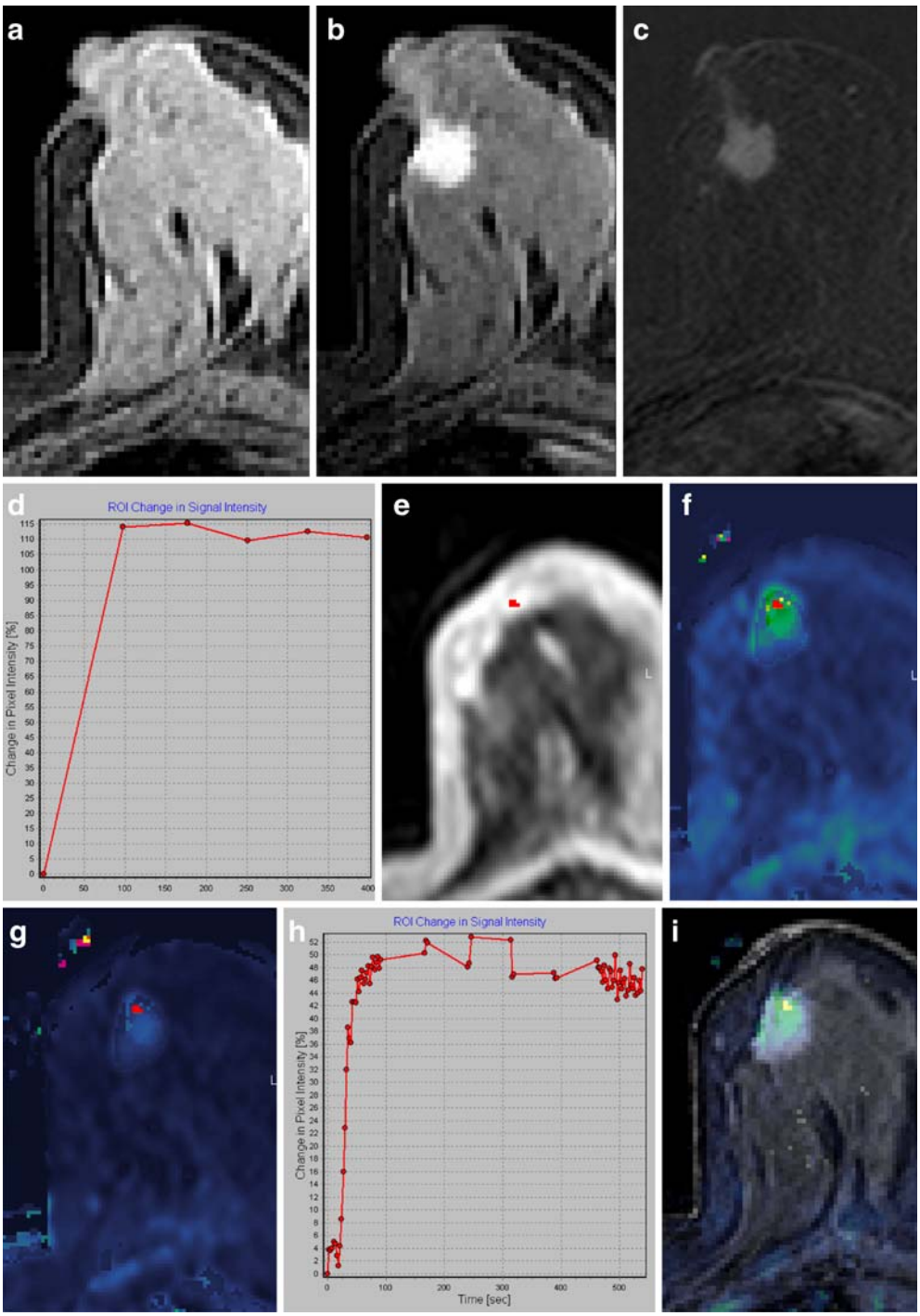

Figure 1.

55 year old patient with an architectural distortion in the right breast on the screening mammogram (not shown). Clinical examination was unremarkable. Histology showed a 27 mm invasive ductal carcinoma, grade 2.
a) Unenhanced T1-weighted 3D fat suppressed fast spoiled gradient echo series.
b) T1-weighted 3D fat suppressed fast spoiled gradient echo image 2 min after intravenous contrast agent injection. A round mass with spiculated margins is seen in the anterior third of the breast slightly lateral to the retromamillary line.
c) Early subtraction series demonstrates the contrast enhancing mass.

d) Time intensity curve from the dynamic scans. The signal intensity rises fast in the initial phase with plateau in the delayed phase (type 2 curve).
e) T1-weighted image of perfusion series in the first minute after contrast agent injection.
f) K trans parametric image calculated from the perfusion series (K trans=capillary permeability).
g) K ep parametric image calculated from the perfusion series (K ep=wash out)
h) Time signal intensity diagram from the perfusion series.
i) Result of fusion image of a T1-weighted 3D fat suppressed fast spoiled gradient echo image obtained 2 min after contrast injection with a parametric map of distribution volume from the perfusion series. The overlay of parametric images from the perfusion series over the dynamic series, facilitates spatial orientation of the perfusion dataset.

Discussion
Our results demonstrate that it is feasible to combine perfusion imaging with conventional DCE MRI of the breast after a single bolus of intravenous contrast with split dynamic scanning. By eliminating the need for a second contrast enhanced study on another day, the imaging protocol presented above could encourage the adoption of perfusion MRI for the investigation of breast diseases. It may perhaps be pertinent to note, that in the absence of an alternative, a software developed for analyzing perfusion of the brain was used in our study. While it served the purpose, the development of similar software customized for breast MRI would be of great advantage.

Summary
We present a protocol for combining dynamic contrast enhanced MRI with perfusion MRI of the breast using only one dose of a contrast agent. The protocol overcomes the principal drawback of perfusion breast imaging as performed today, and hence has the potential to accelerate the adoption of perfusion MRI of the breast.

Breast MR imaging for screening women at high risk

Francesco Sardanelli[1], Luca Carbonaro[1], Filippo Santoro[2], Franca Podo[2]
[1]Università degli Studi di Milano, Dipartimento di Scienze Medico-Chirurgiche, IRCCS Policlinico San Donato, Milan, Italy
[2] Istituto Superiore di Sanità, Dipartimento di Biologia Cellulare e Neuroscienze, Rome, Italy

1. Women at high risk for breast cancer
Approximately 5% of all breast cancers occur in women with hereditary predisposition even though a relevant familial clustering can be found for other 5% to 10% of breast cancers. BRCA1 and BRCA2 are the most frequently implicated genes when deleterious mutations are found, with a further small percentage occurring in women with TP53 mutations (Li-Fraumeni syndrome) or other rare mutations [1]. BRCA mutation carriers or untested first degree relatives of BRCA mutation carriers should be considered at high risk of breast cancer, a category implying a 20–25% or greater lifetime risk according to the American Cancer Society [2]. Women at high risk of breast cancer are also those who underwent mantle radiotherapy under 30 years of age for Hodgkin's disease [2]. An intermediate risk (15–20% lifetime) is given by other factors such as family history, previous diagnosis of breast invasive cancer or DCIS, papilloma, atypical ductal hyperplasia, lobular intraepithelial neoplasia, heterogeneously or extremely dense breast at mammography [2].
Note that the general female population has a lifetime mean risk under 15% (12.7% in USA [http://www.cancer.gov/cancertopics/factsheet/Detection/probability-breast-cancer], 12.5% in Europe [https://oraweb.cern.ch/pls/ttdatabase/docs/F14740/Flyers.pdf], up to 14.3% in The Netherlands [3].
While some women at high risk opt for bilateral mastectomies which gives about 90% reduction in risk [4], a larger proportion prefer to undertake screening of their breasts in an attempt to detect the disease at an early stage to prevent mortality. The rationale for this choice is the extrapolation of the advantage in terms of mortality reduction obtained with the early diagnosis by means of screening mammography of over 50 year old general female population, calculated to be about 30% [5]. Interestingly, two recent case–control studies also showed that breast cancer mortality associated with screening invitation was reduced by 25% [6] or 35% [7]; however, breast cancer mortality for actually screened women was reported to be reduced by 45% [6] or even 48% [7].

2. The evidence in favor of annual MRI screening of high risk women
The high sensitivity of magnetic resonance imaging (MRI) in detecting breast cancer compared to conventional imaging techniques in high risk women was demonstrated in several prospective cohort studies carried out in The Netherlands [8], Canada [9], United Kingdom [10], Germany [11], Italy [12], United States [13, 14], Norway [15], and Austria [16]. A meta-analysis of five of these [8–12] on 3,571 women with 9,652 rounds found 168 patients with breast cancer and the pooled analysis has shown that MRI detected 81% of breast cancer compared to mammography and ultrasonography detecting 40% and 43% respectively, with only 19% of the invasive cancers having nodal involvement [17]. Pooling the data of all the eight prospective studies including the still unpublished final results of the Italian study, we obtain about 5,000 screened women (36% of them being BRCA mutation carriers), 12,800 rounds, a mean age at entry of 42 years ranging from 18 to 80, 2.6 rounds per woman, 243 screen-detected cancers, 18 interval cancers (7%), total annual cancer rate 2.0%, tumor size ≤1 cm 45%, invasive cancers 79%, grade 3 at pathology 57%, positive nodal status compared to invasive cancers 22%.
However, all these studies were observational cohort studies and not randomized controlled trials. This means that an estimate of benefit for mortality reduction should use surrogate endpoints. These indirect indicators suggest a probable positive impact on patients outcome. In particular, the low rate of lymph node involvement (which is comparable to population mammography screening studies) suggests the MRI screening may be beneficial. A limitation to the use of these surrogate endpoints may derive from the poor prognosis of small-size triple negative (ER^-, PgR^-, $HER2^-$) breast cancers without nodal involvement, which are frequently diagnosed in BRCA1 mutation carriers [18].
A particular concern is the radiation dose in the young women with BRCA mutation where the breast tissue is believed to be more sensitive [19]. In fact, mammography should be avoided up to 34 years of age as there is no evidence that the benefits outweigh the radiation risks from mammography [20,21].
In high-risk women in whom a suspicious lesion is found on MRI, a second look targeted ultrasonography (US) can localize the abnormality allowing a core needle biopsy to be undertaken. A familial high-risk cohort of 43 women with 48 suspicious lesions on MRI, had a second look ultrasonography. The lesion was identified and US-guided biopsy undertaken in 67% of cases. In 11/12 cancers, ultrasonography correctly identified the lesion [22].

In women who are unable to tolerate MRI or have contraindication to the examination itself or to the gadolinium-based contrast agent administration, bilateral whole breast ultrasonography should be considered alone until 35 years of age and as an adjunct to mammography after 35 years of age. The rationale is given by the ability of this technique to detect cancer in high-risk women (ranging from 33% to 65%, and 43% overall, in three studies [17]). In a larger view, we can take into account that in women younger than 50 years with dense breasts and negative mammogram, ultrasonography yielded an additional 0.4% cancer rate [23].

3. Conclusions and research perspectives

There is a large body of evidence in favor of annual MRI screening of women at high risk of breast cancer starting from 25–30 years of age, including women at high risk who have been already diagnosed and treated for breast cancer [24]. However, relevant open questions are the following:

- models for calculating individual risk of breast cancer are not sufficiently developed and tested on a large scale (family and individual history should be integrated with data from individual breast density);
- MRI screening should be organized and controlled like mammographic screening, including woman's informed consent and accurate quality check of equipments and diagnostic performance with particular reference to MRI sensitivity and positive predictive value (monitoring carefully the number of interval cancers and the number of needle biopsies prompted by MRI for false positive findings);
- the real need of mammography also after 35 years of age (for the possible detection of MR-undetected cancers) should be investigated;
- definition of upper limit of age for non enrolling women or discontinuing annual MRI should be investigated, too.

References

1. Easton DF, Eeles RA (2008) Genome-wide association studies in cancer. Hum Mol Genet 17(R2):R109
2. Saslow D, Boetes C, Burke W, et al; American Cancer Society Breast Cancer Advisory Group (2007) American Cancer Society guidelines for breast screening with MRI as an adjunct to mammography. CA Cancer J Clin 57:75–89
3. Paap E, Broeders MJ, van Schoor G, Otten JD, Verbeek AL (2008) Large increase in a Dutch woman's lifetime risk of developing breast cancer. Eur J Cancer 44:1485–1487
4. Hartmann LC, Sellers TA, Schaid DJ, et al (2001) Efficacy of bilateral prophylactic mastectomy in BRCA1 and BRCA2 gene mutation carriers. J Natl Cancer Inst 93:1633–1667
5. International Agency for Research on Cancer (2002) Breast Cancer Screening. Lyon: IARC Press
6. Puliti D, Miccinesi G, Collina N, et al; IMPACT Working Group (2008) Effectiveness of service screening: a case–control study to assess breast cancer mortality reduction. Br J Cancer 99:423–427
7. Allgood PC, Warwick J, Warren RM, Day NE, Duffy SW (2008) A case–control study of the impact of the East Anglian breast screening programme on breast cancer mortality. Br J Cancer 98:206–209
8. Kriege M, Brekelmans CT, Boetes C, et al (2004) Efficacy of MRI and mammography for breast-cancer screening in women with a familial or genetic predisposition. New Engl J Med 351:427–437
9. Warner E, Plewes DB, Hill KA, et al (2004) Surveillance of BRCA1 and BRCA2 mutation carriers with magnetic resonance imaging, ultrasound, mammography, and clinical breast examination. JAMA 292:1317–1325
10. Leach MO, Boggis CR, Dixon AK, et al (2005) Screening with magnetic resonance imaging and mammography of a UK population at high familial risk of breast cancer: a prospective multicentre cohort study (MARIBS). Lancet 365:1769–1778
11. Kuhl CK, Schrading S, Leutner CC, et al (2005) Mammography, breast ultrasound, and magnetic resonance imaging for surveillance of women at high familial risk for breast cancer. J Clin Oncol 23:8469–8476
12. Sardanelli F, Podo F, D'Agnolo G, et al (2007) Multicenter comparative multimodality surveillance of women at genetic-familial high risk for breast cancer (HIBCRIT study): Interim results. Radiology 242:698–715.
13. Lehman CD, Blume JD, Weatherall P, et al; International Breast MRI Consortium Working Group (2005) Screening women at high risk for breast cancer with mammography and magnetic resonance imaging. Cancer 103(9):1898–1905
14. Lehman CD, Isaacs C, Schnall MD, et al (2007) Cancer yield of mammography, MR, and US in high-risk women: prospective multi-institution breast cancer screening study. Radiology 244:381–388
15. Hagen AI, Kvistad KA, Maehle L, et al (2007) Sensitivity of MRI versus conventional screening in the diagnosis of BRCA-associated breast cancer in a national prospective series. Breast 16:367–374
16. Riedl CC, Ponhold L, Flory D, et al (2007) Magnetic resonance imaging of the breast improves detection of invasive cancer, preinvasive cancer, and premalignant lesions during surveillance of women at high risk for breast cancer. Clin Cancer Res 13:6144–6152
17. Sardanelli F, Podo F (2007) Breast MR imaging in women at high-risk of breast cancer. Is something changing in early breast cancer detection? Eur Radiol 17:873–887
18. Fatouros M, Baltoyiannis G, Roukos DH (2008) The predominant role of surgery in the prevention and new trends in the surgical treatment of women with BRCA1/2 mutations. Ann Surg Oncol 15:21–33
19. Broeks A, Braaf LM, Huseinovic A, et al (2007) Identification of women with an increased risk of developing radiation-induced breast cancer: a case only study. Breast Cancer Res 9: R26
20. Sardanelli F, Podo F (2007) Management of an inherited predisposition to breast cancer. N Engl J Med 357:1663.
21. Berrington de Gonzalez A, Berg CD, Visvanathan K, Robson M (2009) Estimated risk of radiation-induced breast cancer from mammographic screening for young BRCA mutation carriers. J Natl Cancer Inst 101:205–209
22. Sim L, Hendriks J, Bult P, Fook-Chong S (2005) US correlation for MRI-detected breast lesions in women with familial risk of breast cancer. Clin Radiol 60:801–806
23. Corsetti V, Houssami N, Ferrari A, et al (2008) Breast screening with ultrasound in women with mammography-negative dense breasts: evidence on incremental cancer detection and false positives, and associated cost. Eur J Cancer 44:539–544
24. Sardanelli F, Podo F (2005) Women with history of breast cancer excluded from screening programs: is it the right choice? Radiology 234:971

The complexity of DCIS

Francesco Sardanelli
Università degli Studi di Milano, Dipartimento di Scienze Medico-Chirurgiche, IRCCS Policlinico San Donato, Milan, Italy

1. DCIS (and LIN)

Ductal carcinoma in situ (DCIS) is a challenging diagnosis in breast imaging. Its importance is related to the currently favored hypothesis that invasive ductal carcinoma (IDC) evolves progressively through sequential stages, usually from ductal hyperplasia without cellular atypia to atypical ductal hyperplasia, to DCIS, and, eventually, to IDC [1, 2]. This biological evolution may produce branches and dead ends, so that many lesions may arrest or even regress [1]. Even though this conceptual framework holds also for lobular neoplasms, lobular carcinoma in situ (LCIS) has been recently defined only as a high-risk lesion and grouped with atypical lobular hyperplasia into the so-called *lobular intraepithelial neoplasia* (LIN). The risk for invasive breast cancer is estimated to be six to ten times higher for patients with LCIS [3, 4] and eight to ten times higher for patients with DCIS [5, 6].

DCIS is a complex pathological entity in which malignant breast epithelial cells arise and proliferate inside the ducts but do not invade the surrounding stroma [7]. It is a heterogeneous disease with several morphological variants that markedly differ in gross pathological appearance, growth pattern, and cytological features. In fact, a number of classification schemes exist for DCIS [7].

On the other hand, LIN is pathologically characterized by a solid proliferation of loosely cohesive, uniform, small cells that fill and distend the acini of one or more terminal duct lobular units, ranging from minimal intralobular proliferation to maximum filling of acini in several lobular units. According to the World Health Organization, LIN includes—as already mentioned—both atypical lobular hyperplasia and LCIS and LCIS was excluded from the list of true malignancies, even though the correct definition and treatment of this type of lesions is still debated [7−9]. The prevalence of DCIS at autopsy ranges from 0.2% to 16% [10−14]. The prevalence of LCIS appears to be lower, although few data are available [12]. DCIS accounts for 15–20% of all cases of breast cancer [14].

This paper is focused on the role of magnetic resonance imaging (MRI) in the diagnosis of DCIS. It can be found as pure lesion or as a component associated with an invasive cancer, within the primary tumor, clearly extending beyond the infiltrating margin of the primary tumour, or present in grossly normal adjacent breast tissue. This associated entity is called extensive intraductal component (EIC) and practically defined by the presence of DCIS occupying 25% or more of the area encompassed by the infiltrating tumor [15].

2. DCIS: MRI versus mammography and MRI features

Mammography is commonly considered highly sensitive for DCIS due to the frequent association with microcalcifications and the increasing use of screening mammography, which explains its increase in incidence [16−21]. Gd-enhanced MRI is considered highly sensitive for invasive breast cancer, with a sensitivity of 95–100% [22−30], but less sensitive for DCIS, with a reported sensitivity ranging from 20% to 95% [22–26, 28−41]. According to some old studies, MRI may be more sensitive for DCIS compared with mammography but lacks of specificity and may miss small lesions [22, 32]. However, most studies on diagnostic accuracy of DCIS have a heavy selection bias due to inclusion on the basis of mammographic detection, without considering DCIS missed with both techniques.

Radiologists should be aware of the peculiar characteristics of DCIS on MRI. According to BI-RADS MRI descriptors, we can detect lesions as foci (spot enhancement less than 5 mm in diameter), mass-like lesions (3D space-occupying lesion, usually round, oval, or irregular in shape), or non-mass-like lesions (enhancement of an area that is not a mass, which is the presentation of 30% of DCIS) [42]. Thus, it is important not to forget that about 70% of DCIS present as mass-like lesions. Non-mass-enhancement are subdivided as follows:

– linear (a line that may not conform to a duct);
– ductal (a line that may have branching, conforming to a duct);
– segmental (a triangular area of enhancement, apex pointing to the nipple, suggesting a duct or its branches)
– regional (enhancement in a large volume of tissue not conforming to a ductal distribution, geographic);
– focal (enhancement in a confined area, less than 25% of quadrant).

Attention should be paid to these non-mass-like morphologies, reported as possible presentation of DCIS [42–46].

3. Using the whole breast as a pathological standard of reference

A different approach for evaluating sensitivity for DCIS consists in comparing mammography and MRI using the whole-breast examination as a pathological reference standard [47]. We reviewed the results of a multicenter prospective study [48] that had enrolled patients with proven breast cancer and a planned unilateral or bilateral mastectomy. Pathological examination covered the entire excised breast with slices of 5 mm. Of a total 90 patients available for evaluation, we had 9 bilateral synchronous breast cancers, providing a total of 99 breasts for analysis. Pathology revealed 26 pure DCIS disease in 14 breasts of 14 patients, two multifocal and five multicentric DCIS, for a total of seven multifocal or multicentric DCIS in 14 breasts (50%). Mammography detected nine DCIS: four masses, two masses with microcalcifications, two clusters of microcalcifications not associated with a mass and one architectural distortion. Two other masses were detected, but misdiagnosed as benign or probably benign. MRI detected ten lesions, all judged as malignant. The morphological appearance was equally distributed between round, oval, or lobular (6/10) and linear, dendritic, or stellate (4/10); moreover, 90% (9/10) of the MR-detected lesions demonstrated an early enhancement >100%, whereas 80% (8/10) of them presented a washout kinetic pattern. The sensitivity for DCIS of mammography and MRI was 35% (9/26) and 38% (10/26), respectively, without significant difference. A significant difference in size was found between the group of four lesions detected by both modalities and measured at pathology (median 4.6 mm) versus that of the ten lesions missed by both modalities and measured at pathology (median 20 mm).

The combined sensitivity of mammography and MRI for the 26 DCIS of this series was 46% (12/26). Thus, 54% (14/26) of DCIS remained undetected at both mammography and MRI. The mean diameter at pathology of the 10 missed DCIS measured at pathology was 4.2±1.9 mm (median 4.6 mm). The sensitivity of mammography and MRI did not significantly differ in the two groups of fatty or nonfatty breasts. This study showed that if the pathological examination of the whole breast is used as a reference standard, a low sensitivity for DCIS is found for both mammography (35%) and MRI (38%), as well as for the two modalities in combination (46%).

Multifocal and multicentric DCIS is another important issue in clinical practice. Whereas Holland et al. found that most cases of DCIS are not multicentric (only one multicentric lesion in their

radiologic-pathologic correlation study of 119 mastectomy specimens from patients with DCIS) [49], other authors reported percentages of multicentric or multifocal DCIS in breast specimens between 8% and 36% [50, 51]. In our series, 50% (7/14) of patients and breasts had multifocal (2/14, 14%) or multicentric (5/14, 36%) DCIS. Our results are therefore similar to those obtained by Hwang et al (37% of multicentric DCIS) in a similar clinical setting (mastectomy specimens of patients with invasive cancers) [52].

4. Size factor and microcalcifications

Pathological lesion size is probably one point that explains DCIS detectability by both mammography and MRI. In fact, whereas in our study mentioned above, median lesion size at pathology was 5 mm, other studies reported series of larger lesions, which can explain the possibility to obtain higher levels of sensitivity [14, 21, 22, 23, 31, 41]. For example, Shiraishi et al. described a series of DCIS with a mean diameter of 55.1 mm, reporting a sensitivity of 87% for MRI and 77% for mammography [14], whereas Gilles et al. reported an early contrast enhancement in 34 of 36 DCIS studied with MRI, with a mean lesion size of 45 mm [31].

For DCIS, the sensitivity of mammography is considered to be between 27% and 78% and that of MRI between 20% and 95%, although in most studies, detection by imaging modalities is not defined on the basis of a whole-breast histopathology as a reference standard [16–21, 22–26, 28–41, 51, 53]. At mammography, microcalcifications are commonly advocated as a characteristic finding for DCIS [54, 55], allowing a higher sensitivity in comparison with MRI. However, using the whole breast as a pathological reference standard, microcalcifications did not make the difference.

5. Other factors influencing MRI sensitivity for DCIS

Several other factors should be taken in account for the depiction of DCIS on MRI: spatial resolution and scan plane, enhancement morphology and distribution (pattern), and enhancement kinetics (related to angiogenesis).

Orel et al. reported a relatively high detection rate of DCIS with breast MRI, with 70% of DCIS seen on mammography identified at MRI with a high-resolution, inversion-recovery-prepared pulse sequence [22]. According to other authors, DCIS may be accurately depicted by MRI in 95% of cases, compared with 70% on mammography, using a high-resolution dedicated sequence, i.e. rotating delivery of excitation off resonance [32]. Good results may be expected with a high-resolution technique, such as reported by Menell et al with a 2-mm slice thickness [53]. High spatial resolution also appears to be preferable to define the various enhancement patterns reported for a relevant number of DCIS: focal, diffuse, segmental (homogeneous or dotted/granular), clumped, ductal, linear, branching. Moreover, axial or also sagittal scan planes should be preferred to axial planes for depicting ductal enhancement, a typical distribution of DCIS [56].

Enhancement kinetics of DCIS is another factor to be considered. Bluemke et al reported only a 20% MRI sensitivity for DCIS using the presence of washout (type 3 curve); however, sensitivity increased to 60% when the plateau (type 2 curve) was included [57]. Gilles et al. demonstrated contrast enhancement in 34 of 36 DCIS of 4–75 mm in diameter. The level of enhancement was associated with lesion size and density packing of DCIS-involved ducts, and the two MR-undetected cases were pathologically demonstrated to have weak tumor angiogenesis around the ducts involved by the DCIS [31]. An earlier study demonstrated that the mean microvessel size was higher in DCIS tissue than in normal gland tissue, suggesting the possibility that contrast enhancement be related to tumor angiogenesis in stroma surrounding DCIS-involved ducts [58].

6. When mammographic detection is not the entry criteria of DCIS

Another interesting viewpoint for MRI detection of DCIS is given by the performance in high-risk women. Pooling together the 31 DCIS detected in six prospective studies in high-risk women [59−64], we have a sensitivity of 17/31 (55%) for mammography versus 20/31 (65%) for MRI [65]. In three studies in which clinical breast examination, mammography, ultrasonography, and MRI were used [56, 58, 59], only three of 83 cancers were detected solely by mammography (4%), all of them being DCIS. In the study by Kuhl et al on high-risk women [63], 8/9 DCIS were diagnosed with MRI (the false negative was detected but misdiagnosed as probably benign), 3 with mammography and none with ultrasonography.

In other words, when entry criteria other than mammographic detection are used, the sensitivity of mammography decreases. This has been strongly confirmed by the large observational study by Kuhl et al considering 167 women who had undergone mammography and MRI and received a final diagnosis of pure DCIS [66]. Mammography diagnosed 93 (56%) of these cases, MRI 153 (92%). Moreover, of the 89 high-grade DCIS, 43 (48%) were missed at mammography but diagnosed with MRI; on the other hand, MRI diagnosed 87 (98%) high-grade DCIS, the two missed cases having been diagnosed by mammography.

7. The extensive intraductal component (EIC) and DCIS size assessment

MRI also proved to be able to detect EIC associated with invasive cancers, an issue clearly related to the use of preoperative MRI for local staging. Confirming what we know for detection and size estimate of pure DCIS, a number of studies showed that EIC may partly be visible by mammography only, partly by both and partly by MRI alone.

Nakayama et al [67] studied one hundred patients with breast cancer using a 3D-VIBE sequence and reported only a 52% accuracy for the evaluation of ductal tumor spread. Ikeda et al [68] studied 93 women with breast cancer using a 3D fat-suppressed technique with magnetization transfer. In tumors with microlobulated or spiculated borders, tumor size tended to be underestimated on MR images. Fifty-nine patients (63%) had pathologically confirmed EIC; 42 of them (71%) had ductal continuous enhancement from the main tumor to the nipple or segmental enhancement surrounding the main tumor on MR images. Sensitivity, specificity, and accuracy of MR imaging in detecting EIC were 71%, 85%, and 76%, respectively.

Van Goethem et al [69] studied the prediction of EIC in 209 invasive cancer. At pathology they found 50 cancers with EIC, 49% of them predicted by mammography, by ultrasonography in 32%, and by MRI in 68%. MRI was also best in tumor size assessment. Typical MRI findings predictive of EIC were ductal or linear enhancement, long spicules, a regional enhancing area or nodules adjacent to a mass.

Schouten van der Velden et al [70] recently reported a correlation of radiological versus pathological size higher for MRI (r=0.65) than for mammography (r=0.20) in a small sample of patients with EIC (mammography, n=21; MRI, n=23). Mammography underestimated pathological tumor size in 62%. MRI over-or underestimated tumor size in 22% and 30% of the cases, respectively. MRI adequately estimated the extent more often in poorly differentiated EIC than in moderately differentiated EIC (60% versus 25%, respectively).

Regarding DCIS size assessment, a recent contribution by Kim et al [71] showed that of 72 DCIS, 68 (94%) were detected by MRI and 62 (86%) were detected by mammography. Moreover, correlation of the radiological size with pathology was significantly higher for MR (r=0.786) than for mammography (r= 0.633). However, MRI underestimated the size by more than 1 cm (including false negative examination) in 12 patients (17%), was accurate in 52 patients (72%), and overestimated the size by more than 1 cm in eight patients (11%) whereas the same data for mammography were 25 (35%), 31 (43%), and 16 (22%). MRI, but not mammography, showed significant correlation for the assessment of the size in noncomedo DCIS. Size assessment by MRI was affected by the nuclear grade and the presence of comedo necrosis, but not by the breast density or microinvasion. Summarizing studies which focused on the accuracy of assessing size of DCIS and EIC, MRI was shown to give a correct assessment in 48–76% of cases, resulting more accurate than mammography (27–49%), but neither method can today be considered completely reliable for DCIS size assessment. Over- and underestimates have been reported for MRI ranging from 11–22% and 17–30%, respectively.

7. Conclusions

In contrary to initial assumptions [72], MRI also proved to be able to detect DCIS and extensive EIC. Breast radiologists should be aware of the possible peculiar MRI characteristics of DCIS, different from those of IDC in terms of morphology and kinetics of contrast enhancement. At any rate, not all the DCIS can be detected with MRI and, in particular, low-grade DCIS may be entirely occult if characterized by low angiogenesis. This complexity limits also detection and size estimate of EIC associated with invasive cancers, even though MRI probably performs better than any other modality in this setting.

However, the biological significance and the overdiagnosis of DCIS (either detected or undetected with MRI) remain open problems that deserve further investigation. The use of MRI in order to get prognostic information on DCIS and to follow-up low-grade DCIS as an alternative to surgical and/or radiation therapy might be explored in future studies

References

1. Arpino G, Laucirica R, Elledge RM (2005) Premalignant and in situ breast disease: biology and clinical implications. Ann Intern Med 143:446–457
2. Lakhani SR (1999) The transition from hyperplasia to invasive carcinoma of the breast. J Pathol 187:272–278
3. Ottesen GL, Graversen HP, Blichert-Toft M et al (1993) Lobular carcinoma in situ of the female breast. Short-term results of a prospective nationwide study. The Danish Breast Cancer Cooperative Group. Am J Surg Pathol 17:14–21
4. Haagensen CD (1986) Lobular neoplasia. lobular carcinoma in situ. In: Haagensen CD, ed. Diseases of the breast. 3rd ed. Philadelphia, PA: Saunders: 192–241
5. Leonard GD, Swain SM (2004) Ductal carcinoma in situ, complexities and challenges. J Natl Cancer Inst 96:906–920
6. Collins LC, Tamimi RM, Baer HJ et al (2005) Outcome of patients with ductal carcinoma in situ untreated after diagnostic biopsy: results from the Nurses' Health Study. Cancer 103:1778–1784
7. Tavassoli FA, Devilee P (2003) Tumours of the breast and female genital organs. IARC Press—World Health Organization.
8. Chuba PJ, Hamre MR, Yap J et al (2005) Bilateral risk for subsequent breast cancer after lobular carcinoma-in-situ: analysis of surveillance, epidemiology, and end results data. J Clin Oncol 23:5534–5541
9. Bibeau F, Borrelly C, Chateau MC et al (2005) Recent data on lobular neoplasia of the breast: the pathologist's opinion. Bull Cancer 92:453–458
10. Bartow SA, Pathak DR, Black WC et al (1987) Prevalence of benign, atypical, and malignant breast lesions in populations at different risk for breast cancer. A forensic autopsy study. Cancer 60:2751–2760
11. Alpers CE, Wellings SR (1985) The prevalence of carcinoma in situ in normal and cancer-associated breasts. Hum Pathol 16:796–807
12. Colleau M, Magalon G, Bonnier P (2005) Breast carcinoma diagnosed from surgical specimens. Retrospective study on three years. Ann Chir Plast Esthet 50:127–133
13. Welch HG, Black WC (1997) Using autopsy series to estimate the disease ''reservoir'' for ductal carcinoma in situ of the breast: how much more breast cancer can we find? Ann Intern Med 127:1023–1028
14. Shiraishi A, Kurosaki Y, Maehara T et al (2003) Extension of ductal carcinoma in situ: histopathological association with MR imaging and mammography. Magn Reson Med Sci 2:159–63
15. Hurd TC, Sneige N, Allen PK, et al (1997) Impact of extensive intraductal component on recurrence and survival in patients with stage I or II breast cancer treated with breast conservation therapy. Ann Surg Oncol 4:119–124
16. Ernster VL, Barclay J (1997) Increases in ductal carcinoma in situ (DCIS) of the breast in relation to mammography: a dilemma. J Natl Cancer Inst Monogr 22:151–156
17. Ernster VL, Ballard-Barbash R, Barlow WE et al (2002) Detection of ductal carcinoma in situ in women undergoing screening mammography. J Natl Cancer Inst 94:1546–1554
18. Feuer EJ, Wun LM (1992) How much of the recent rise in breast cancer incidence can be explained by increases in mammography utilization? A dynamic population model approach. Am J Epidemiol 136:1423–1436
19. Ward BA, McKhann CF, Ravikumar TS (1992) Ten-year follow-up of breast carcinoma in situ in Connecticut. Arch Surg 127:1392–1395
20. Bush DS, Remington PL, Reeves M, Phillips JL (1994) In situ breast cancer correlates with mammography use, Wisconsin: 1980–1992. Wis Med J 93:483–484
21. Stomper PC, Connolly JL, Meyer JE, Harris JR (1989) Clinically occult ductal carcinoma in situ detected with mammography: analysis of 100 cases with radiologic-pathologic correlation. Radiology 172:235–241
22. Orel S, Medonca MH, Reynolds C et al (1997) MR imaging of ductal carcinoma in situ. Radiology 202:413–420
23. Gilles R, Guinebretiere JM, Lucidarme O et al (1994) Nonpalpable breast tumors: diagnosis with contrast-enhanced subtraction dynamic MR imaging. Radiology 191:625–631
24. Gilles R, Meunier M, Lucidarme O et al (1996) Clustered breast microcalcifications: evaluation by dynamic contrast-enhanced subtraction MRI. J Comput Assist Tomogr 20:9–14
25. Harms SE, Flamig DP, Hesley KL et al (1993) MR imaging of the breast with rotating delivery of excitation off resonance: clinical experience with pathologic correlation. Radiology 187:493–501
26. Stomper PC, Herman S, Klippenstein DL et al (1995) Suspect breast lesions: findings at dynamic gadolinium-enhanced MR imaging correlated with mammographic and pathologic features. Radiology 197:387–395
27. Hulka CA, Smith BL, Sgroi DC et al (1995) Benign and malignant breast lesions: differentiation with echo-planar MR imaging. Radiology 197:33–38
28. Bone B, Aspelin P, Bronge L et al (1996) Sensitivity and specificity of MR mammography with histopathological correlation in 250 breasts. Acta Radiol 37:208–213

29. Fobben ES, Rubin CZ, Kalisher L et al (1995) Breast MR imaging with commercially available techniques: radiologic-pathologic correlation. Radiology 196:143–152
30. Teifke A, Hlawatsch A, Beier T et al (2002) Undetected malignancies of the breast: dynamic contrast enhanced MR imaging at 1.0 T. Radiology 224:881–888
31. Gilles R, Zafrani B, Guinebretiere JM et al (1995) Ductal carcinoma in situ: MR imaging—histopathologic correlation. Radiology 196:415–419
32. Soderstrom CE, Harms SE, Copit DS et al (1996) 3D RODEO breast MRI of lesions containing ductal carcinoma in situ. Radiology 201:427–432
33. Boetes C, Strijk SP, Holland R et al (1997) False-negative MR imaging of malignant breast tumors. Eur Radiol 7:1231–1234
34. Viehweg P, Lampe D, Buchmann J, Heywang-Kobrünner SH (2000) In situ and minimally invasive breast cancer: morphologic and kinetic features on contrast enhanced MR imaging. MAGMA 11:129–137
35. Heywang-Kobrunner SH, Viehweg P et al (1997) Contrast-enhanced MRI of the breast: accuracy, value, controversies, solutions. Eur J Radiol 24:94–108
36. Tesoro-Tess JD, Amusoro A, Rovini D et al (1995) Microcalcifications in clinically normal breasts: the value of high field, surface coil, Gd-DTPA enhanced MRI. Eur Radiol 5:417–422
37. Neubauer H, Li M, Kuehne-Heid R et al (2003) High grade and non-high grade ductal carcinoma in situ on dynamic MR mammography: characteristic findings for signal increase and morphological pattern of enhancement. BJR 76:3–12
38. Fischer U, Westerhof JP, Brinck U et al (1996) Ductal carcinoma in situ in dynamic MR-mammography at 1.5. Rofo 164:290–294
39. Fischer U, Kopka L, Grabbe E (1999) Breast carcinoma: effect of the preoperative contrast-enhanced MR imaging on the therapeutic approach. Radiology 231:881–888
40. Zuiani C, Francescutti GE, Londero V et al (2002) Ductal carcinoma in situ: is there a role for MRI? J Exp Clin Cancer Res 21(suppl 3):89–95
41. Bazzocchi M, Zuiani C, Panizza P et al (2006) Contrast-enhanced breast MRI in patients with suspicious microcalcifications on mammography: results of a multicenter trial. AJR 186:1723–32
42. Raza S, Vallejo M, Chikarmane SA, Birdwell RL (2008) Pure ductal carcinoma in situ: a range of MRI features. AJR Am J Roentgenol 191:689–699
43. Liberman L, Morris EA, Dershaw DD et al (2003) Ductal enhancement on MR imaging of the breast. AJR 181:519–525
44. Liberman L, Morris EA, Lee M et al (2002) Breast lesions detected on MR imaging: features and positive predictive value. AJR 179:171–178
45. Van Goethem M, Schelfout K, Kersschot E et al (2005) Comparison of MRI features of different grades of DCIS and invasive carcinoma of the breast. JBR-BTR 88:225–232
46. Morakkabati-Spitz N, Leutner C, Schild H et al (2005) Diagnostic usefulness of segmental and linear enhancement in dynamic breast MRI. Eur Radiol 15:2010–2017
47. Sardanelli F, Bacigalupo L, Carbonaro L, et al (2008) What is the sensitivity of mammography and dynamic MR imaging for DCIS if the whole-breast histopathology is used as a reference standard? Radiol Med 113:439–451
48. Sardanelli F, Giuseppetti GM, Panizza P et al (2004) Sensitivity of MR vs. mammography for detecting foci of multifocal/multicentric breast cancer in fatty and dense breasts using the whole breast pathologic examination as a gold standard. AJR183:1149–1157
49. Holland R, Hendriks JH (1994) Microcalcifications associated with ductal carcinoma in situ: mammographic-pathologic correlation. Semin Diagn Pathol 11:181–192
50. Elling D, Vesper AS, Fiedler B et al (2001) Intraductal component in invasive breast cancer: analysis of 250 resected surgical specimens. Breast 10:405–410
51. Berg WA, Gutierrez L, NessAiver MS et al (2004) Diagnostic accuracy of mammography, clinical examination, US, and MR imaging in preoperative assessment of breast cancer. Radiology 233:830–849
52. Hwang ES, Kinkel K, Esserman LJ et al (2003) Magnetic resonance imaging in patients diagnosed with ductal carcinoma-in-situ: value in the diagnosis of residual disease, occult invasion, and multicentricity. Ann Surg Oncol 10:381–388
53. Menell JH, Morris EA, Dershaw DD et al (2005) Determination of the presence and extent of pure ductal carcinoma in situ by mammography and magnetic resonance imaging. Breast J 11:382–390
54. Dershaw DD, Abramson A, Kinne DW (1989) Ductal carcinoma in situ: mammographic findings and clinical implications. Radiology 170:411–415
55. Evans A, Pinder S, Wilson R et al (1994) Ductal carcinoma in situ of the breast: correlation between mammographic and pathologic findings. AJR 162:1307–1311
56. Kuhl C (2007) The current status of breast MR imaging. Part I. Choice of technique, image interpretation, diagnostic accuracy, and transfer to clinical practice. Radiology 244:356–378
57. Bluemke DA, Gatsonis CA, Chen MH et al (2004) Magnetic resonance imaging of the breast prior to biopsy. JAMA 292:2735–2742
58. Ottinetti A, Sapino A (1988) Morphometric evaluation of microvessels surrounding hyperplastic and neoplastic mammary lesions. Breast Cancer Res Treat 11:241–248
59. Tilanus-Linthorst MM, Obdeijn IMM, Bartels KC et al (2000) First experiences in screening women at high risk for breast cancer with MR imaging. Breast Cancer Res Treat 63:53−60
60. Kriege M, Brekelmans CT, Boetes C et al (2004) Efficacy of magnetic resonance imaging and mammography for breast cancer screening in women with a familial or genetic predisposition. N Engl J Med 351:427−437
61. Warner E, Plewes DB, Hill KA et al (2004) Surveillance of BRCA1 and BRCA2 mutation carriers with magnetic resonance imaging, ultrasound, mammography, and clinical breast examination. JAMA 292:1317−1325
62. Leach MO, Boggis CR, Dixon AK et al (2005) Screening with magnetic resonance imaging and mammography of a UK population at high familial risk of breast cancer: a prospective multicentre cohort study (MARIBS). Lancet 365:1769−1778
63. Kuhl CK, Schrading S, Leutner CC et al (2005) Mammography, breast ultrasound, and magnetic resonance imaging for surveillance of women at high familial risk for breast cancer. J Clin Oncol 23:8469–8476
64. Sardanelli F, Podo F, D'Agnolo G et al (2007) Multicenter comparative multimodality surveillance of women at genetic-familial high risk for breast cancer (HIBCRIT Study): Interim Results. Radiology 242:698–715
65. Sardanelli F, Podo F (2007) Breast MR imaging in women at high risk of breast cancer. Is something changing in early breast cancer detection? Eur Radiol 17:873–887
66. Kuhl CK, Schrading S, Bieling HB, et al (2007) MRI for diagnosis of pure ductal carcinoma in situ: a prospective observational study. Lancet 370:485−492
67. Nakayama S, Kakizaki D, Kaise H, et al (2004) Three-dimensional volumetric interpolated breath-hold magnetic resonance imaging for the diagnosis of breast tumors. Nippon Rinsho 62(4):790–798

68. Ikeda O, Nishimura R, Miyayama H, et al (2004) Magnetic resonance evaluation of the presence of an extensive intraductal component in breast cancer. Acta Radiol 45:721–725
69. Van Goethem M, Schelfout K, Kersschot E, et al (2007) MR mammography is useful in the preoperative locoregional staging of breast carcinomas with extensive intraductal component. Eur J Radiol 62:273–282
70. Schouten van der Velden AP, Boetes C, Bult P, Wobbes T (2009) Magnetic resonance imaging in size assessment of invasive breast carcinoma with an extensive intraductal component. BMC Med Imaging 7;9:5.
71. Kim do Y, Moon WK, Cho N, et al (2007) MRI of the breast for the detection and assessment of the size of ductal carcinoma in situ. Korean J Radiol 8:32–39
72. Westerhof JP, Fischer U, Moritz JD, Oestmann JW (1998) MR imaging of mammographically detected clustered calcifications: is there any value? Radiology 207:675–681

Comprehensive staging in breast cancer by whole-body MRI

Gerwin P Schmidt, MD
Institute for Clinical Radiology, University Hospitals Grosshadern, Ludwig-Maximillians-University Munich, Germany.
Correspondence address:
Gerwin Paul Schmidt, MD, Institute for Clinical Radiology, University Hospitals Grosshadern, Ludwig-Maximilians-University of Munich, Research focus: whole-body imaging, Marchioninistr. 15, 81377 München, Tel.: 0049 89 7095-0, Fax: 0049 89 7095-8832, e-mail: gerwin.schmidt@med.uni-muenchen.de

Introduction

Breast cancer is the most frequent malignancy and the most common cause of cancer-related death in women worldwide with approximately 500,000 deaths each year. Approximately 30% of all patients diagnosed with breast cancer are at risk of developing tumor recurrence at some time within the course of their disease. Therefore, early diagnosis and accurate restaging of recurrent breast cancer is important to define appropriate therapeutic strategies or to identify patients with limited disease who potentially could benefit from curative treatment. The basic imaging approach in the follow-up of breast cancer to date consists of regular mammography and clinical examinations as well as symptom-orientated multi-modal imaging strategies[1]. This procedure by large is based on the assumption, that an intensified after-care does not necessarily correlate with an increased survival benefit, issued from studies performed in the early 90's[2,3]. Unfortunately, this approach mainly comprises modalities with known poor sensitivity (e.g. chest radiographs), examinations with strong examiner-dependent variation of sensitivity (e.g. abdominal ultrasound) or procedures with limited specificity, like bone scintigraphy[4]. Especially in the last 10 years numerous promising concepts have been developed for the therapy of metastasized breast cancer, including hormonal drugs and immune therapy, which indicate an improvement in patients' progression-free survival[5,6,7]. New surgical and interventional techniques for the management of unifocal metastases have demonstrated effectiveness of local therapeutic approaches and reported promising survival rates. Against this background, whole-body imaging modalities such as positron emission tomography-computed tomography (PET-CT) or whole-body MRI (WB-MRI) appear as new promising tools to detect tumor recurrence with high accuracy in its initial stage and provide more effective therapeutic strategies to the patient.

Technical developments for WB-MRI

MRI, with its lack of ionizing radiation, high soft tissue contrast and spatial resolution is a useful application for tumor detection and staging of malignant disease. A high sensitivity has been reported for the detection of organ metastases, especially for tumors frequently metastasizing to the liver, bone or the brain, like breast cancer[8,9]. However, different requirements in coil setup, sequence design and slice positioning as well as time-consuming patient repositioning procedures in the past have delayed the realization of WB-MRI as a clinical application. Improvements in hardware and software, including dedicated rolling platforms with integrated surface coils facilitated WB-MRI and for the first time allowed whole-body imaging within less than one hour. However, with this technique considerable compromises in spatial resolution, especially in peripheral body regions like the head/neck and lower extremities, had to be taken in account[10]. Finally, multi-channel whole-body scanners, using a system of multiple phased-array coils covering the whole body like a matrix were introduced, which allowed WB-MRI without compromises in spatial resolution and made MRI a promising candidate for whole-body tumor imaging. Especially the combination of free table movement with parallel imaging acquisition techniques (PAT) has resulted in substantially shorter room time and enabled dedicated assessment of individual organs with various soft tissue contrast, image orientation and contrast media dynamics combined with whole-body anatomic coverage[11,12]. A "state of the art" whole-body MRI (WB-MRI) protocol should imply T1-weighted and STIR-imaging, which has proved highly efficient for the assessment of soft tissue-and bone structures, fast high resolution imaging of the lung (e.g. HASTE), as well as static and dynamic contrast-enhanced studies of the abdominal organs and brain. Using PAT acceleration, whole-body STIR-imaging is possible within 10:46 min and T1-weighted-imaging within 16:09 min at a 1.8×1.3 mm and 1.3×1.1 mm in-plane-resolution, respectively. Figure 1 gives a schematic overview of a proposed WB-MRI protocol for oncologic screening.

Recently, approved clinical multi-channel whole-body MR systems with field strength of 3 Tesla have become available. The potential two-fold gain in signal-to-noise ratio at 3 T can be used for either acquisition acceleration or increased spatial resolution, or for a compromise of both, which results in even shorter total room time, increased patient comfort and acceptance. Yet, only few scientific studies have described the use of high-field systems large field-of-view imaging, including the chest, abdomen or even as a whole-body application[13,14,15].

Finally, a promising new technique for WB-MRI in near future will be continuously moving table image acquisition ("move during scan"). Initial results for 3D whole-body continuous data acquisition as new potential strategy for WB-MRI, especially for large FOV-imaging in short bore systems, have been reported[16].

WB-MRI for the detection of breast cancer recurrence

In a recent study conducted by the Institute for Clinical Radiology Munich-Grosshadern, 33 women post breast cancer with either clinical symptoms or a suspicious imaging finding indicating tumor recurrence were examined with both WB-MRI on a 1.5 or 3 Tesla unit and FDG-PET-CT for comparison of diagnostic performance. In this analysis we found a high prevalence of recurrent disease (61%) and both FDG-PET-CT and WB-MRI showed a persuasive overall diagnostic accuracy (each 91%) for lesion-by-lesion detection of tumor recurrence. Sensitivity was 91% and 93%, specificity 90% and 86%, respectively. Both scanners reliably detected two local tumor recurrences. FDG-PET-CT showed advantages for the detection of lymph node involvement (accuracy for PET-CT 96%, WB-MRI 75%). Here

the problem of lymph node staging based on size criteria alone becomes evident: false-positive findings due to enlarged nodes in inflammatory processes or normal-sized nodes harboring micro-metastases often impair sensitivity and specificity of MRI and CT. The functional information of PET-CT obviously facilitates both localization and characterization of equivocal lymph nodes. However, new solutions to overcome these limitations have been introduced for total body MRI, e.g. with the introduction of whole-body diffusion-MRI for improved display and detection of pathologic lymph nodes on the basis of fat suppressed STIR echo-planar imaging (DWIBS)[17].

Due to its excellent contrast in soft tissue and parenchymal structures, the main performance of WB-MRI certainly lies within the detection of distant metastatic disease, especially in abdominal organs, the brain and bone, which represent frequent routes of metastasis in breast cancer. Although both modalities performed very reliable for the detection of organ metastases, WB-MRI showed a higher diagnostic accuracy of 94% versus 90% for PET-CT. Sensitivity of PET-CT can be impaired, especially for smaller bone marrow-or liver lesions showing no visible morphologic changes in CT or no significant tracer uptake. This may be especially the case for lesions below double the size of the spatial resolution of the PET-scanner, which usually is 6 mm. In the mentioned study indeed more small lesions (<5 mm) were detected by WB-MRI. Surprisingly, WB-MRI and FDG-PET-CT showed an even performance for the detection of lung metastases. Implementation of fast HASTE imaging in combination with PAT has minimized limitations in the assessment of lung pathologies, now enabling the detection of small lung nodules down to size of 7 mm, coming close to resolution achieved with a conventional spiral-CT-scanner. Considering the full field-of-view of a WB-MRI examination, covering the body from head to the calves, a total of 11 additional focal malignant foci were found in 5 patients, amongst previously unknown brain-and bone metastases. Total acquisition time for WB-MRI was further reduced from 51 min at 1.5 Tesla down to 43 min at 3 Tesla using identical resolution parameters.

Based on these promising initial results an extended study is currently performed in cooperation with the Department of Clinical Chemistry, Internal Medicine, Obstetrics and Gynecology focusing on an intensified aftercare in asymptomatic breast cancer patients with newly occurred significant tumor marker increase (CA 15-3, CEA) during follow-up of the disease. The main purpose will be to filter out patients with early or limited recurrent disease who potentially may benefit from adapted and individualized therapeutic strategies.

In summary, WB-MRI shows a robust performance similar to PET-CT and may significantly improve diagnostic accuracy in breast cancer patients with suspicion of recurrence and represent a promising alternative to multi-modality algorithms. As a consequence patients might benefit from earlier and more accurate tumor detection and improved therapeutic options.

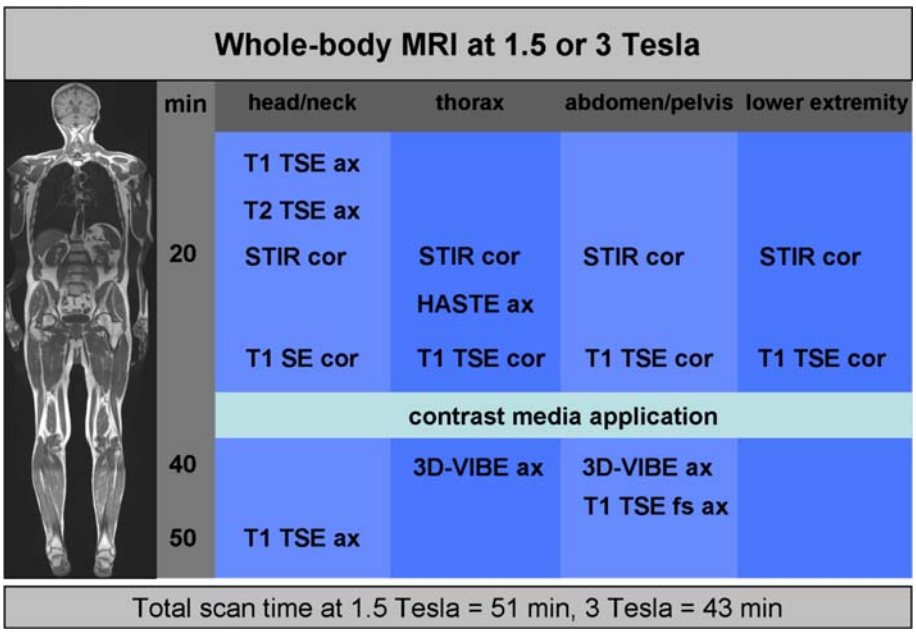

Figure 1: Whole-body MRI protocol for oncologic imaging on matrix coil multi-channel MRI systems (Magnetom Avanto and Tim Trio, Siemens Medical Solutions, Erlangen Germany).

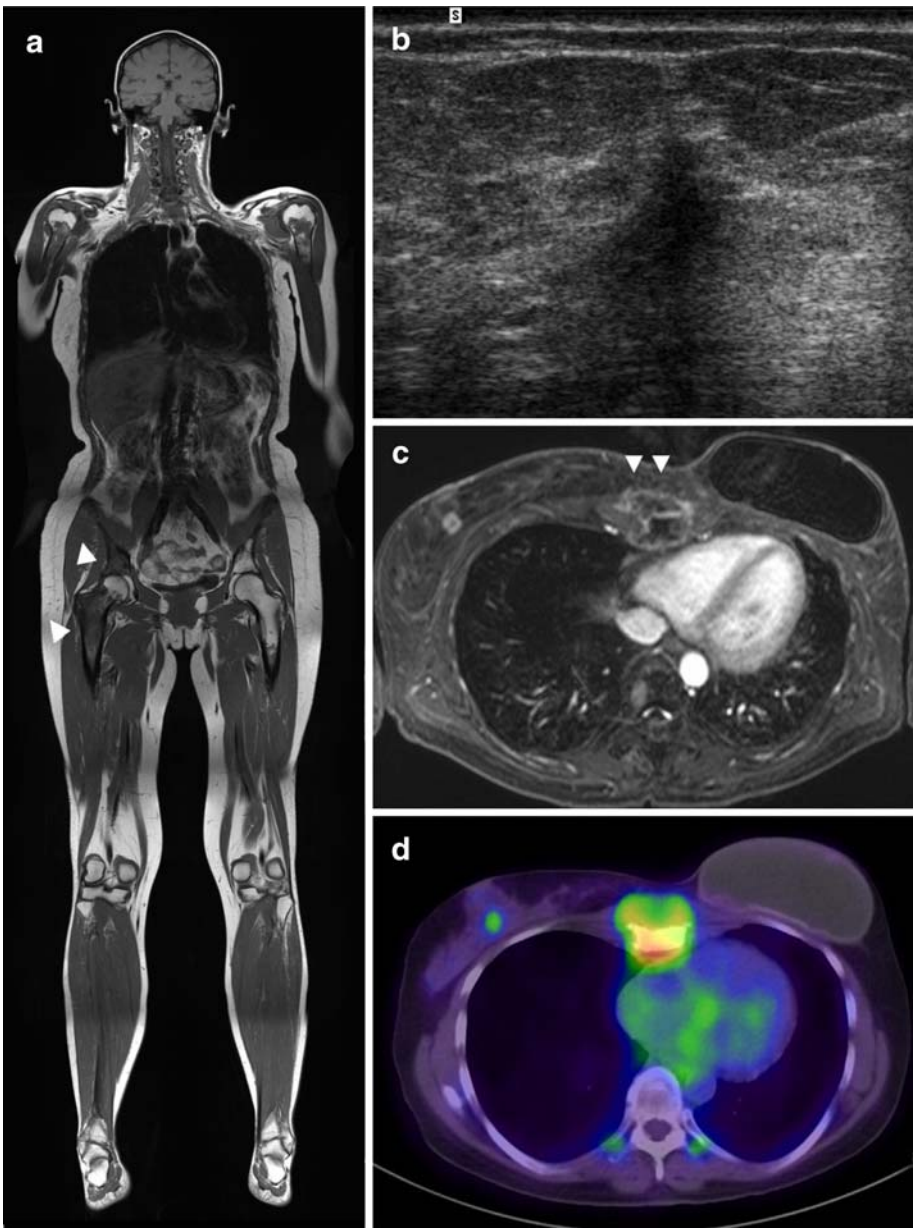

Figure 2: 45-year old woman with breast cancer and suspicion of tumor recurrence in breast radiographs/ultrasound during routine screening. A) Coronal whole-body T1w-TSE-imaging on four body levels at 1.5 Tesla shows large hypointense bone marrow lesions indicating bone metastases in the right proximal femur and acetabulum (arrowheads). B) Previous breast ultrasound showed an ill-defined hypoechogenic lesion (18 mm), suspicious of tumor recurrence of invasive-ductal carcinoma. C) 3D-VIBE-MRI in late venous phase at the anatomic level of the breast depicts an enhancing mass in the right breast indicating contralateral tumor recurrence. Additionally, a large sternal bone metastasis is described (arrowheads). D) PET-CT correlation of the thorax reveals pathologic FDG-uptake in the right breast lesion (SUV 3.2) as well as the sternal mass, confirming malignancy. Bilateral uptake in the facet joints is of degenerative nature.

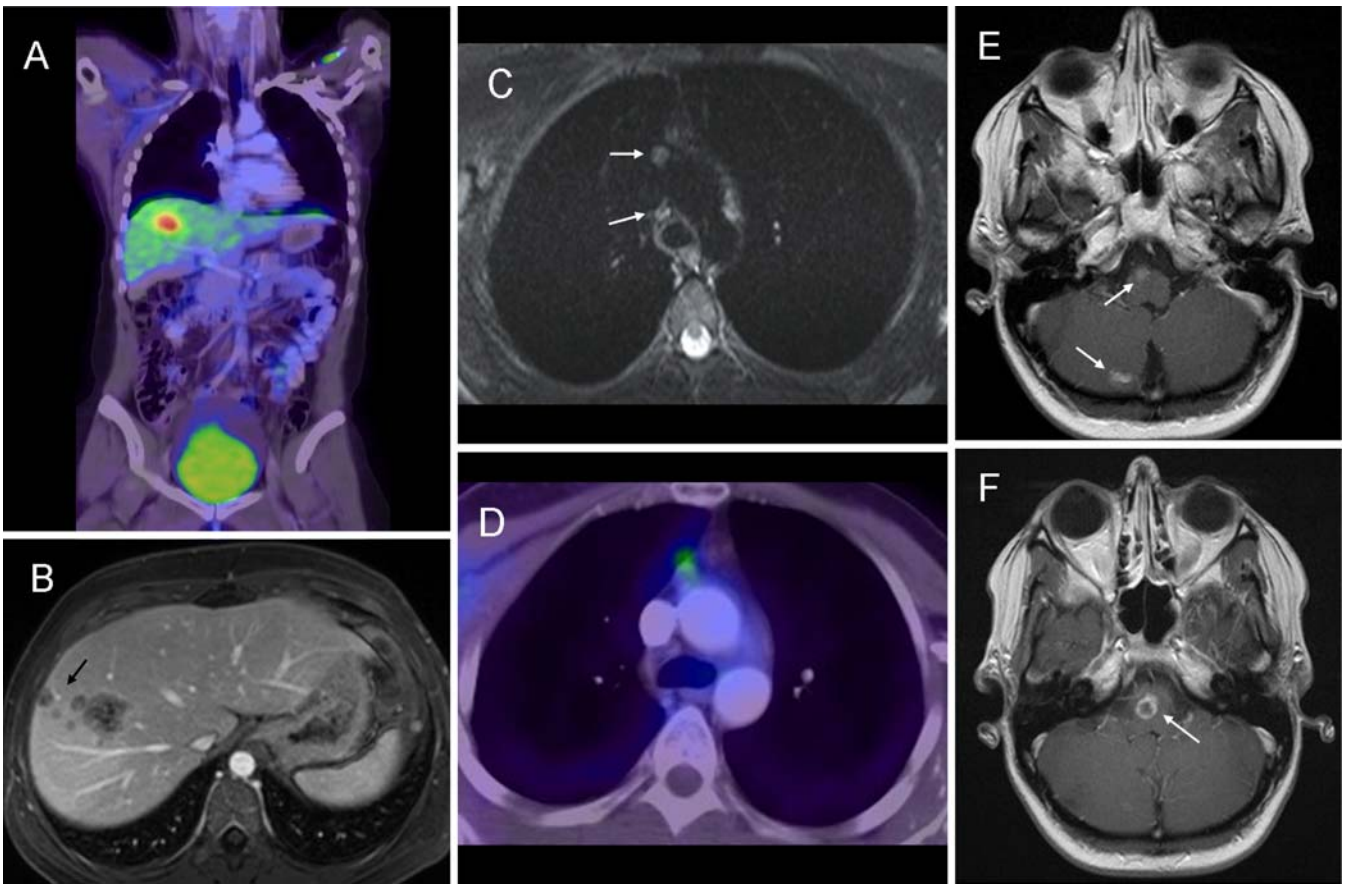

Figure 3: 40-year old woman with increased liver enzymes and suspicious mass in abdominal ultrasound. A) Whole-body PET-CT shows a focal liver metastasis with increased FDG-uptake. B) 3D-VIBE-MRI (1.5 Tesla) of the liver in portal venous phase confirms a large liver metastasis and shows additional multiple small satellite lesions (arrow). C) In a different patient axial STIR-imaging of the lung shows a round hyperintense structure in the upper ventral mediastinum, which is indicative of a lymph node, but difficult to distinguish from a vessel or pulsation artifact. Another hyperintense structure in the pre-tracheal region is hardly interpretable. D) PET-CT reveals a pathologic tracer uptake only in the ventral lymph node (SUV 3.0) confirmed as a lymph node metastasis in follow-up, the pretracheal node shows no significant uptake and was benign. In the same patient axial T1-weighted TSE-imaging of the brain post contrast shows well-defined multi-focal small brain metastases in the medulla, right cerebellum (E, arrows) and pons (F, arrow).

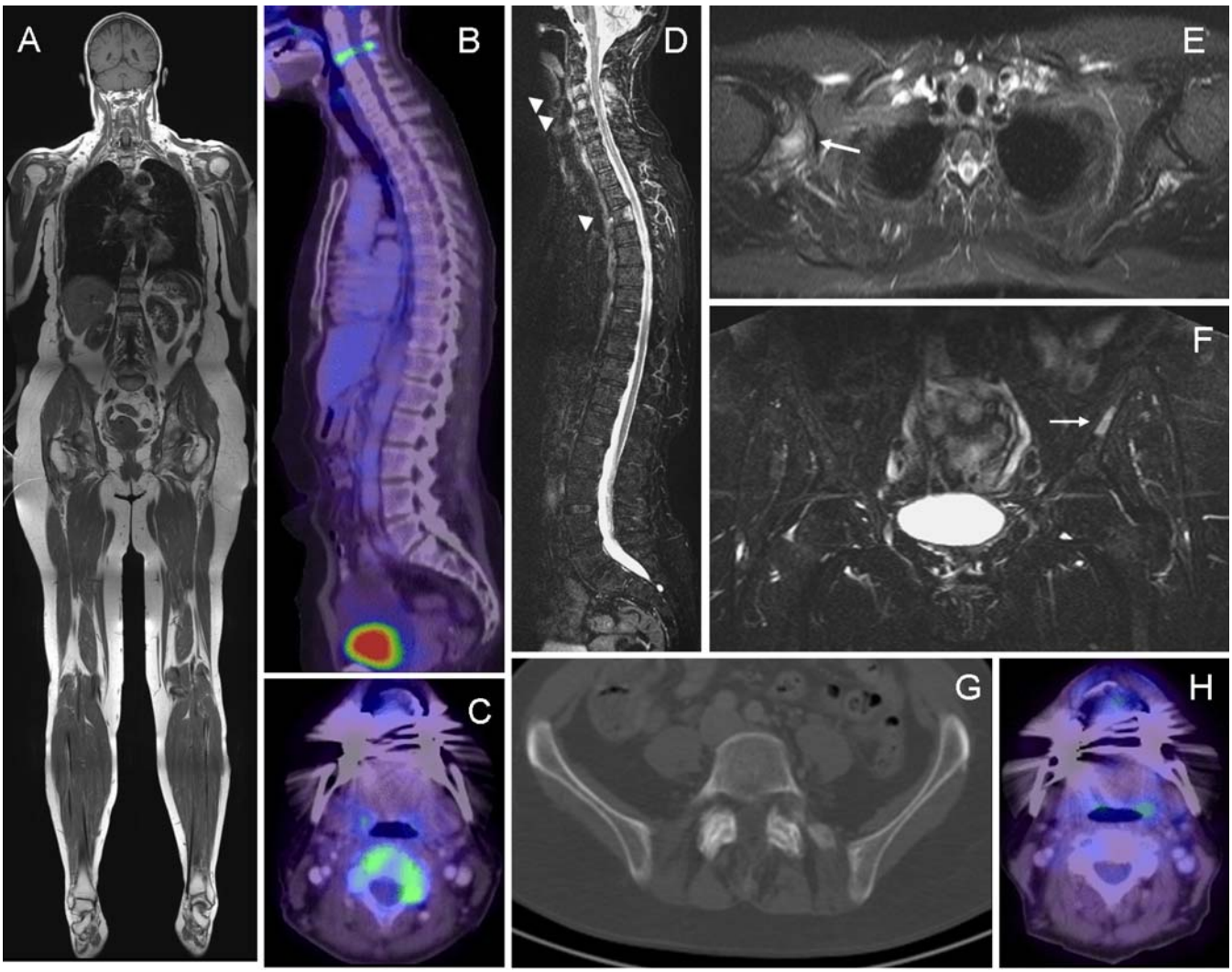

Figure 4: A) T-weighted TSE WB-MRI at 1.5 Tesla. B+C) Sagittal PET-CT correlation of the spine depicts a singular, extensive bone metastasis (SUV 5.0) in C3. D) WB-MRI shows multiple bone metastases in C3, C4 and TH5. E+F) More malignant lesions are found in the right coracoid and left iliac bone. G) CT-correlation of the pelvis is morphologically inconspicuous. H) PET-CT follow-up of the spine after 2 months radiation therapy shows a significant decrease in FDG-uptake by 50% (SUV=2.5), indicating therapy response.

References

1. Deutsche Krebsgesellschaft e.V.: Kreienberg R, Kopp I, Lorenz W, et al. (2004) S3-Leitlinie Diagnostik, Therapie und Nachsorge des Mammakarzinoms der Frau. pp. 42–44.
2. The GIVIO investigators (1994) Impact of follow-up testing on survival and health-related quality of life in breast cancer patients. A multicenter randomized controlled trial. JAMA 271: 1587–92.
3. Rosselli del Turco M, et al (1994) Intensive diagnostic follow-up after treatment of primary breast cancer. A randomized trial. National research council project on breast cancer follow-up. JAMA 271: 1593–7.
4. Schaner EG, Chang AE, Doppman JL, Conkle DM, Flye MW, Rosenberg SA (1978) Comparison of computed and conventional whole lung tomography in detecting pulmonary nodules: a prospective radiologic-pathologic study. AJR 131:51–54
5. O'Shaughnessy J, et al (2002) Superior survival with capecitabine plus docetaxel combination therapy in anthracycline-pretreated patients with advanced breast cancer: phase III trial results. J Clin Oncol 20: 2812–23.
6. Vlastos G, et al (2004) Long-term survival after an aggressive surgical approach in patients with breast cancer hepatic metastases. Ann Surg Oncol 11: 869–74.l
7. Mack MG, et al (2004) Breast cancer metastases in liver: laser-induced interstitial thermotherapy–local tumor control rate and survival data. Radiology 233: 400–9.
8. Engelhard K, Hollenbach HP, Wohlfart K, von Imhoff E, Fellner FA. (2004) Comparison of whole-body MRI with automatic moving table technique and bone scintigraphy for screening for bone metastases in patients with breast cancer. Eur Radiol. 2004 Jan;14(1):99–105.
9. Lauenstein TC, Goehde SC, Herborn CU, Goyen M, Oberhoff C, Debatin JF (2004) Whole-body MR imaging: evaluation of patients for metastases. Radiology 233: 139–48.
10. Lauenstein T, Freudenberg L, Goehde S, Ruehm G, Goyen M, Bosk S, et al (2002) Whole body MRI using a rolling table platform for the detection of bone metastases. Eur Radiol 12: 2091–2099.
11. Schlemmer HP, Schäfer J, Pfannenberg C, Radny P, Korchidi S, Müller-Horvat C (2005) Fast whole-body assessment of metastatic disease using a novel magnetic resonance imaging system: initial experiences. Invest Radiol 40: 64–71.
12. Schmidt GP, Baur-Melnyk A, Herzog P, Schmid R, Tiling R, Reiser MF, et al (2005) High-resolution whole-body MRI tumor staging with the use of parallel imaging versus dual modality PET-CT: experience on a 32-channel system. Invest Radiol 40: 743–753.
13. De Balzaire CM, Duhamel GD, Rofsky NM, Alsop DC (2004) MR imaging relaxation times of abdominal and pelvic tissues measured in vivo at 3.0 T: preliminary experience. Radiology 230: 652–659.
14. Fink C, Puderbach M, Biederer J, Fabel M, Dietrich O, Kauczor HU (2007) Lung MRI at 1.5 and 3 Tesla: observer preference study and lesion contrast using five different pulse sequences. Invest Radiol 42: 377–83.
15. Schmidt GP, Wintersperger B, Graser A, Baur-Melnyk A, Reiser MF, Schoenberg SO (2007) High-resolution whole-body magnetic resonance imaging applications at 1.5 and 3 Tesla: a comparative study. Invest Radiol: 449–59.
16. Zenge MO, Ladd ME, Vogt FM, Brauck K, Barkhausen J, Quick HH (2005) Whole-body magnetic resonance imaging featuring moving table continuous data acquisition with high-precision position feedback. Magn Reson Med 54: 707–711.
17. Takahara T, Imay Y, Yamashita T, Yasuda S, Nasu S, Van Cauteren M. (2004) Diffusion weighted whole body imaging with background body signal suppression (DWIBS): technical improvement using free breathing, STIR and high resolution 3D display. Radiat Med 22: 275–282.

Do we need MR-Mammography in Screening?

R. Schulz-Wendtland
University of Erlangen, Institute of Radiology, Gynaecological Radiology, Erlangen, Germany

What is screening? According to the statement of the WHO screening is defined as an organised, population-based program that achieves a high participation rate (over 70% attending in a given round) using an invitation addressed to each individual women in the eligible target population [1].

The guidelines (Breast MRI) of the European Society of Breast Imaging (EUSOBI) [2] include the following indications:

- Problem solving in case of inconclusive findings on conventional imaging.
- Screening of the contralateral breast in women with histological evidence of unilateral breast cancer.
- Evaluation of the breasts in case of metastases of an unknown primary carcinoma.
- Evaluation of therapy response in patients treated with neoadjuvant chemotherapy.
- Exclusion of local recurrence after breast-conserving therapy.
- Screening of women with lifetime risk of 20% or more to develop breast cancer, including mutation carriers.

In contrast of these indications the guidelines of the American Cancer Society (ACS) [3] for Breast Screening with MRI may systematically exclude MRI screening for many women who have a substantial risk for BRCA mutation - there is a necessity for greater awareness of breast cancer risk factors in the screening mammography population, so that high-risk women can be identified and given access to genetic testing and counseling regarding all risk-reducing interventions.
The high sensitivity for cancer makes breast MRI a desirable technique for screening purposes.
Therefore, many countries have performed screening studies in high-risk populations. As the most important of these studies were all performed in Europe (e.g. the Dutch MRISC study, the UK-based MARIBS study, the German single-center study and the Italian HIBCRIT study) [2], the ACS recommendations apply mostly to the European situation. The overall sensitivity for breast cancer in these high-risk populations is between 71 and 100% for MRI compared to 16–40% for mammography. The specificity ranges from 81 to 99% for MRI and 93 to 99% for mammography, which is illustrative for the higher detection rate of MR and the (almost two times) higher recall rate that unfortunately complicates MR screening.
There is evidence for the value of annual MR screening in BRCA gene mutation carriers, their first degree, untested relatives and all women with a lifetime risk of 20–25% according to models that depend largely upon family history.
Currently there is not sufficient evidence to recommend MRI or not in women with a lifetime risk of 15–20% and those with heterogeneously or extremely dense breasts.
Women with a lifetime risk of less than 15% should currently not be enrolled in MR screening programs.
It is still unclear when to start screening. In most high-risk patients starting at the age of 30 will probably be sufficient. However, in families where the first carcinomas presented at younger ages, the screening needs to start earlier as well. It seems advisable to follow the guidelines

for mammography in this aspect and start screening at an age 5 years younger than the youngest relative that presented with cancer. It is also unclear for how long screening with MR should be continued; in older women the breast density decreases significantly, and the added value of MR might thus decrease. However, at every age, the sensitivity for breast cancer of MRI is higher than that of mammography [4].

Mammography screening can reduce deaths from breast cancer. The available evidence on breast cancer screening was evaluated in Lyon by a Working Group convened by the International Agency for Research on Cancer (IARC) of the World Health Organisation (WHO), from 5–12 March 2002. The group, consisting of 24 experts from 11 countries, concluded that trials have provided sufficient evidence for the efficacy of mammography screening of women between 50 and 69 years. The reduction in mortality from breast cancer among women who chose to participate in screening programmes was estimated to be about 35%. For women aged 40–49 years, there is only limited evidence for a reduction. The quality of the trials that were used to make these evaluations was carefully assessed. The working group found that many of the earlier criticisms were unsubstantiated, and the remaining deficiencies were judged not to invalidate the trials' findings.

The effectiveness of national screening programmes varies due to differences in coverage of the female population, quality of mammography, treatment and other factors. Organised screening programmes are more effective in reducing the rate of death from breast cancer than sporadic screening of selected groups of women. The working group also concluded that there is insufficient evidence that clinical breast examination or self-examination reduce mortality from breast cancer. The detection rate for DCIS represent 20% - the largeness of the microcalcifications is approximately 130 microns [5,6].

Breast MR is an imaging method, which has high sensitivity (in invasive carcinoma 95–100%) and relatively low specificity (40–80%). The problem with the significance of dynamic contrast enhanced MRI in patients with suspicious microcalcifications of the breast is still being discussed [7]. Of course MRI is unable to image microcalcifications of the breast [8]. Its great importance is in the imaging of mammographically occult microcalcifications lesion of breast. Clustered malignant microcalcifications are the most common presentation of DCIS in mammography.

In MRI a very typical morphological feature for high but also for low DCIS is ductal pattern of enhancement [9–11]. Usually it is clumped, and the heterogeneous or homogeneous enhancement sometimes can be of branching appearance and follows the course of the duct [12]. The enhancement can also have a non regular stippled, spotty and micronodular appearance. Segmental and linear character of this enhancement is described and this morphological finding was assessed to have high PPV for DCIS lesions [9,13]. It was assessed that MRI morphologic features of DCIS can reflect differences in biology and pathology of these tumours [14]. The region of interest (ROI) which is necessary to gain relevant quantitative and qualitative evaluation of enhancement must be very small in this ductal pattern of enhancement to obtain the most accurate measurement. The ROI must cover only part of the lesion, and should be placed in the region of strongest enhancement on the first contrast – enhanced image. When the ROI is randomly placed in the mass, the enhancement curve may be variable and yield lower specificity [9].

However, regarding the detection of ductal carcinoma in situ (DCIS), the sensitivity of MRI varies between 70% and 100% according to the latest studies [11,15–18,19]. Breast MRI was significantly more sensitive than mammography in DCIS detection [10]. It was shown that, MRI had relatively high sensitivity for **high grade DCIS** which often showed rapid initial rise and 2 or 3 of enhancement pattern and thus resembles invasive carcinoma by its characteristics [20]. **Low grade DCIS** had often quite nontypical form of enhancement pattern and initial rise was usually lower and is of course difficult to differentiate it from benign proliferative processes that often enhance on MRI [21–24]. To Mariano et al. [17] study contrast-enhanced MRI using parametric mapping technique was useful in identifying all **intermediate and high grade DCIS** lesion. Regarding the kinetic curve assessment of DCIS, the rapid initial peak of enhancement was found in almost 77% and washout pattern of enhancement in nearly 54% of women [15]. As with MRI enhancement features, noted **differences** between the **low grade and high grade DCIS** ($p = 0.021$) and low grade and high grade DCIS with microinvasion, ($p = 0.006$) were found.

According to the statement of the WHO and the European guidelines for quality assurance in breast cancer screening and diagnosis [1,5,6] there exists no screening with MRI but there is evidence for the value of annual MR screening in BRCA gene mutation carriers, their first degree, untested relatives and all women with a lifetime risk of 20–25% according to models that depend largely upon family history [4]. However, at every age, the sensitivity for breast cancer of MRI is higher than that of mammography [4,6].

For screening as an organised, population-based program that achieves a high participation rate (over 70% attending in a given round) using an invitation addressed to each individual women in the eligible target population [1], we have to make the following conclusions:

MRI cannot considered a diagnostic tool for evaluating micro-calcifications (approximately 130 microns).

The sensitivity of MR imaging for DCIS detection is lower than achieved for invasive cancer [1, 5–7].

The results for DCIS in MRI are inhomogenous. It is, however, useful for identifying DCIS with more aggressive histological grades [8] - low grade DCIS have often quite nontypical form of enhancement pattern and initial rise is usually lower and is of course difficult to differentiate it from benign proliferative processes that often enhance on MRI [21–24].

The problem in DCIS is the histological diagnosis: only under the precondition of the European guidelines [4] that the histology will be made with a maximum thickness of 100 μm or thinner it is possible to diagnose a pure DCIS (low/intermediate/high grade) or micro-invasive cancer – this is important to detect and establish MRI criterias for DCIS [7] for a differentiation from benign proliferative processes to reduce an unnecessary higher recall rate.

After this, the next step will be to establish MRI in a selected screening region where all women (clients) receive Mammography and MRI.

References

1.Schulz-Wendtland R, Becker N, Bock K, Bautz W. Mammographiescreening. Der Radiologe 2007; 47:359–370.

2.Mann RM, Kuhl CK, Kinkel K, Boetes C. Breast MRI: guidelines from the European Society of Breast Imaging. EJR 2008; 18:1307–1318.

3.Murphy CD, Lee JM, Drohan B, et al. The American Cancer Society Guidelines for Breast Screening with Magnetic Resonance Imaging. Cancer 2009; 113:3116–3120.

4.Schrading S, Kuhl CK. Mammography, US and MR imaging phenotypes of familial breast cancer. Radiology 2008; 246:58–70.

5.Perry N, Broeders M, de Wolf C, et al. European guidelines for quality assurance in breast cancer screening and diagnosis. Fourth edition – summary document. Ann Oncol 2008; 19:614–622.

6.Schulz-Wendtland R. Mammakarzinom 2008 – State of the Art, Trends, Kontroversen: Aus der Sicht des Diagnostikers. GebFra 2008; 68:708–716.

7.Schulz-Wendtland R, Wenkel E, Bautz W. Who is best in detection DCIS: X-ray or MRM? EJR 2006; 16:92–93
8.Cilotti A, Iacconi C, Marini C, et al. Contrast-enhanced MR imaging in patients with BI-RADS™ 3–5 microcalcifications. Radiol Med 2007; 112:272–286.
9.Katarzyna J, Ouwerkerk R, Jacobs M, et al. Patterns of enhancement on breast MR images: Interpretation and Imaging Pitfalls. RadioGraphics 2006; 26:1719–1734.
10. Menell JH, Morris EA, Dershaw DD, Abramson AF, Brogi E, Liberman L. Determination of the presence and extent of pure ductal carcinoma in situ by mammography and magnetic resonance imaging. Breast 2005; 11:382–390
11.Van Goethem M, Schelvout K, Kersschot E, et al. Comparison of MRI features of different grades of DCIS and invasive carcinoma of the breast. JBR-BTR 2005; 88:225–232.
12.Ikeda O, Nishimura R, Miyayama H, et al. Magnetic resonance evaluation of the presence of an extensive intraductal component in breast cancer. Acta Radio 2004; 45:721–725.
13.Morakkabati-Spitz N, Leutner C, Schild H, Traeber F, Kuhl C. Diagnostic usefulness of segmental and linear enhancement in dynamic breast MRI. Eur Radiol 2005; 15:2010–2017.
14.Esserman LJ, Kumar AS, Herrera AF, et al. Magnetic resonance imaging captures the biology of ductal carcinoma in situ. J Clin Oncol 2006; 24:4603–4610.
15.Bazzocchi M, Zuiani C, Panizza P, et al. Contrast-enhanced breast MRI in patients with suspicious microcalcifications on mammography: results of a multicenter trial. AJR 2006; 186:1723–1732.
16.Kneeshaw PJ, Lowry M, Manton D, Hubbard A, Drew PJ, Turnbull LW. Differentiation of benign from malignant breast disease associated with screening detected microcalcifications using dynamic contrast enhanced magnetic resonance imaging. Breast 2005; 15:29–38.
17.Mariano MN, van den Bosch MA, Daniel BL, et al. Contrast-enhanced MRI of ductal carcinoma in situ: characteristic of a new intensity – modulated parametric mapping technique correlated with histopathologic findings. J Magn Reson Imaging 2005; 22:520–526.
18.Shiraishi A, Kurosaki Y, Maehara T, Suzuki M, Kurosumi M. Extension of ductal carcinoma in situ: histopathological association with MR imaging and mammography. Magn Reson Med Sci 2003; 2:159–163.
19.Zuiani C, Francescutti GE, Konsero V, Zunnui I, Bazzocchi M. Ductal carcinoma in situ: is there a role for MRI? J Exp Clin Cancer Res 2002; 21:89–95.
20.Kuhl CK, Schrading S, Bieling HB et al. MRI for diagnosis of pure ductal carcinoma in situ: prospective observational study. Lancet 2007; 370:485–492.
21.Jansen SA, Newstead GM, Abe H et al. Pure ductal carcinoma in situ: kinetic and morphologic MR characteristics compared with mammographic appearance and nuclear grade. Radiology 2007; 245:684–691.
22.Kumar AS, Chen DF, Au A, et al. Biologic significance of false-positive magnetic resonance imaging enhancement in the setting of ductal carcinoma in situ. Am J Surg 2006; 192:520–524.
23.Liberman L, Mason G, Morris EA, Dershaw DD. Does size matter? Positive predictive value of MRI detected breast lesions as a function of lesion size. AJR Am J Roentengenol 2006; 186:426–430.
24.Riedl CC, Ponhold L, Fuchsjäger M, Helbich Th, et al. Magnetic resonance imaging of the breast improves detection of invasive cancer, preinvasive cancer and premalignant lesions during surveillance of women at high risk for breast cancer. Clin Cancer Res 2007; 13:6144–6152.

Challenges in routine application of MR-Mammography

M. Shapiro Feinberg[1], E. Eyal[2], D. Badikhi[2], T. Golan[3], D. Grobgeld[2], E. Furman Haran[2] and H. Degani[2]
[1] Department if Imaging, Meir Medical Center, Israel
[2] Department of Biological Regulation, Weizmann Institute of Science, Israel
[3] Department of Oncology, Chaim Sheba Medical Center, Israel

Breast MR imaging has been around for more than two decades. The introduction of contrast agents to breast MRI had a seminal effect on the clinical application and has resulted in the start of a new era termed Dynamic contrast enhanced MRM. The ability to obtain high spatial resolution as well as temporal resolution provided both detailed morphological features and kinetic parameters of vascular function. Today, both MRS methods for detecting choline metabolites, as well as imaging water diffusion are adding possible new approaches for improving breast imaging.
In general MRM is currently indicated for specific groups of patients. The more general group includes patients with a 20–25% risk of developing breast cancer, such as: i. BRCA 1 or BRCA 2 gene mutation. ii. 1st degree relatives (not having had a genetic test). iii. Individuals with a history of mantle radiation for Hodgkin's disease and had radiation to chest between the ages of 10 to 30 years. iv. Individuals with Li-Fraumeni, Cowden or Bannayan Riley-Ruvalcaba syndrome. v. Patients with a new breast malignancy for screening the contra lateral breast cancer. In addition, it is applied to evaluate the extent of the disease and presence of multifocality and multicenttricity as well as for additional evaluation of equivocal clinical or imaging findings and in patients with breast augmentation. Despite the high sensitivity and specificity for the detection of breast cancer, which was achieved over the past few years in many clinical centers, MRM is facing several critical challenges that need to be addressed in order to be used routinely in clinical practice as a diagnostic tool. These challenges can be divided into technical/clinical and economic challenges. The technical/clinical challenges are:

1. Standardization of: Acquisition technique and protocol
   Analysis and interpretation
   Terminology of reporting –BIRADS for MRM
2. Increasing specificity and reducing false positive rate, including improvement and development of new fast scanning and processing techniques, as well as CAD.
3. Developing easy to implement biopsy devices.

The economic challenge of reducing the cost is linked to our ability to meet the technical/clinical challenges.
In the context of standardization of the technical requirements for Breast MRM a dedicated breast coil and the administration of a contrast agent is required. To standardize the protocol it is now accepted that both breasts should be simultaneously scanned. The minimum requirements for a diagnostic breast MRI are the following series of images: T2-weighted images, T2 Stir images for assessment of morphology and highlighting fluid in the breast, and finally T1 weighted pre-contrast and post contrast at a defined temporal resolution, with active or passive fat-suppression.
Adding additional scanning protocols should be justified by showing improved diagnostic accuracy. New methods such as diffusion weighted imaging, including ADC mapping is

relatively fast and appears to be adding information useful for improved diagnosis. Recent development of diffusion tensor imaging for tracking the mammary ducal trees have shown exciting prospects for detecting intra-ductal pathologies. MR spectroscopy of lesions can increase the specificity of diagnosis but it is still time consuming and limited to lesions of ≥1 cm. Although the standardization of the protocols can allow for variations depending on the MRI scanner capabilities and the reader's experience, it is important to still strive for full standardization of the analysis, interpretation and terminology used in reporting.

The analysis of breast MRI protocols can be divided into two main categories: Analysis of the morphological and of the dynamic features. Currently the morphological features are predominantly assessed by the reader and influenced by his experience, although attempts were made to use objective computer aided tools for morphological assessment, particularly of the lesion boundaries. In contrast, analysis of the dynamic datasets requires an image processing approach in order to extract the relevant information from the large amount of the data. Overall analysis of the DCE datasets uses: i. Evaluation of empirical parameters such as initial enhancement rate, time to maximum and wash-in/ wash out patterns of enhancement (persistent wash-in no washout, plateau or fast washout). 2. Evaluation based on fitting the data or simulating the data to a physiological model and obtaining parametric images of the fitted parameters and 3. Evaluation by model free methods, such as principal component analysis, that can objectively and rapidly interpret the overall dynamic behavior per pixel. Clearly the interpretation of the dynamic data using model based or model free methods of analysis can achieve high standardization of interpretation, which are based on quantification. This may help increasing the specificity of diagnosis and reducing the false positive interpretations, to an acceptable level.

In addition to the ability of MRM to detect and diagnose breast lesions it has the potential to be applied for assessment of prognosis and for predicting and monitoring response to Therapy. These challenges require further technique development and possibly expanding to new areas of molecular and metabolic MRI.

In conclusion, by meeting the challenges which currently face us in MRM it should be possible to make this highly advanced method of imaging more accessible to a large fraction of women, as well as highly helpful for the management of the surgical and treatment protocols.

Breast MRI in the neoadjuvant setting. What sensitivity for assessment of treatment efficacy? A tool to predict survival ?

F Thibault, A Tardivon, L Ollivier, C El Khoury

Corresponding author:
Fabienne Thibault, MD, Department of Medical Imaging, Institut Curie, 26 Rue d'Ulm, 75005 Paris, France, Tel. +33 1 44 32 42 00 Fax +33 1 44 32 40 15, fabienne.thibault@curie.net

Keywords: breast cancer, chemotherapy response, MRI, survival

In operable breast cancer patients, the main established benefit of neoadjuvant chemotherapy (NAC) is to increase the rates of breast conserving surgery (BCS) in patients not initially amenable to this option. The final decision to undertake BCS rather than mastectomy depends on the volume of residual disease relative to that of the breast. The first radiologist's task, hence, is to assess tumour response and determine the three-dimentionnal extent of final residual disease, a condition to minimise the rate of re-excision surgery and improve the therapeutic local control.

Several studies have shown that dynamic MR imaging is more accurate than conventional imaging and clinical examination for this purpose. However, depending on the pattern of histological changes induced by chemotherapy and on functional impact of drugs on neovasculature, the ability of dynamic MRI to detect residual malignancy may be reduced. Characterisation of a significant enhancement at the initial tumour site may be difficult in cases showing very low contrast uptake after NAC (Figure 1). By visual assessment, persistent disease may, therefore, be under-(rather than over)-estimated (1–5). In this respect, Chen et al (5) used the criterion of complete or probably complete MR response on post-treatment imaging when weaker or comparable enhancement relative to normal glandular tissue was found at the tumour site. They studied 25 HER-2 positive and 26 HER-2 negative tumours. MR identification of complete pathologic response appeared significantly higher in the HER-2 positive compared with the HER-2 negative group. A 31% false negative rate was found in HER-2 negative patients, showing scattered cells or small malignant foci at pathology, versus 4% in HER-2 positive patients. The accuracy of MRI also decreased in the patients who received antiangiogenic therapy.

Other relevant information potentially linked to the level of response shown by early MR assessment after one or two cycles of NAC, is the prediction of ultimate pathologic response, specifically complete response. The finding of a pathologic complete response to neoadjuvant chemotherapy (no evidence of residual invasive cancer in the breast and lymph nodes at the time of surgical resection) has been shown to correlate with improved survival. The prediction of complete remission could guide clinicians in medical treatment decisions. Conversely, early identification of poor responders could avoid ineffective treatment. The predictive role of MRI to this respect has not yet been addressed by specific prospective studies.

Recently, Loo et al (6) used a combination of morphology (extent) and kinetics (late tumour enhancement shown 450 seconds after contrast injection) to assess response before the third cycle of NAC in 54 patients. Reduction of less than 25% in largest diameter of late enhancement was found to predict residual tumour at pathology with 95% specificity, while about half of the patients with a larger response at imaging had complete remission at pathology.

A current research avenue for breast MR imaging in the neoadjuvant setting is the identification of features indicative of long-term clinical outcome. Pickles et al. (7) studied the ability of dynamic MR-derived parameters to predict disease free and overall survivals in 54 patients prior to NAC. Prognostic indicators such as tumour size, TNM stage, histological grade and type, hormonal receptor status obtained prior to treatment were included in the survival analysis and their value compared with that of the imaging parameters. These were pharmacokinetic parameters (i.e., quantitative model-based) and empirical enhancement parameters provided by time/intensity curves (a representation of tumour perfusion and neovessel permeability). All patients underwent subsequent surgery and adjuvant radiotherapy alone or in conjunction with hormonal and/or chemotherapy with the median follow-up time for disease free and overall survivals being close to 4 years. Multivariate analysis showed that empirical parameters had the highest predictive value for disease free and overall survivals, with a high level of neoangiogenesis resulting in lower disease free and overall survivals.

Such functional information may also be obtained using PET imaging and Proton MR spectroscopy.

This presentation points out the main clinical issues currently under investigation. When these primarily deal with local-regional therapeutic control, they also involve the medical oncologists' concern to tailor chemotherapy for each individual patient. From the radiologist's standpoint, morphology as well as several dynamic characteristics contain useful information already shown on breast MR images.

References

1. Rieber A, Zeitler H, Rosenthal H, Görich J, Kreienberg R, Brambs HJ, Tomczak R (1997) MRI of breast cancer: influence of chemotherapy on sensitivity. Br J Radiol 70:452–458
2. Balu-Maestro C, Chapellier C, Bleuse A, Chanalet I, Chauvel C, Largillier R (2002) Imaging in evaluation of response to neoadjuvant breast cancer treatment benefits of MRI. Breast Cancer Res Treat 72:145–152
3. Wasser K, Sinn HP, Fink C, Klein SK, Junkermann H, Lüdemann HP, Zuna I, Delorme S (2003) Accuracy of tumor size measurement in breast cancer using MRI is influenced by histological regression induced by neoadjuvant chemotherapy. Eur Radiol 13:1213–1223
4. Bhattacharyya M, Ryan D, Carpenter R, Vinnicombe S, Gallagher CJ (2008) Using MRI to plan breast-conserving surgery following neoadjuvant chemotherapy for early breast cancer. Br J Cancer 98 (2):289–93
5. Chen JH, Feig B, Agrawal G, Yu H, Carpenter PM, Mehta RS, Nalcioglu O, Su MY (2008) MRI evaluation of pathologically complete response and residual tumors in breast cancer after neoadjuvant chemotherapy. Cancer 112(1):17–26
6. Loo CE, Teertstra HJ, Rodenhuis S, van de Vijver MJ, Hannemann J, Muller SH, Peeters MJ, Gilhuijs KG (2008) Dynamic contrast-enhanced MRI for prediction of breast cancer response to neoadjuvant chemotherapy: initial results. AJR Am J Roentgenol 191(5):1331–8
7. Pickles MD, Manton DJ, Lowry M, Turnbull LW (2008) Prognostic value of pre-treatment DCE-MRI parameters in predicting disease free and overall survival for breast cancer patients undergoing neoadjuvant chemotherapy. Eur J Radiol Jun20[Epub ahead of print]

Figure 1a

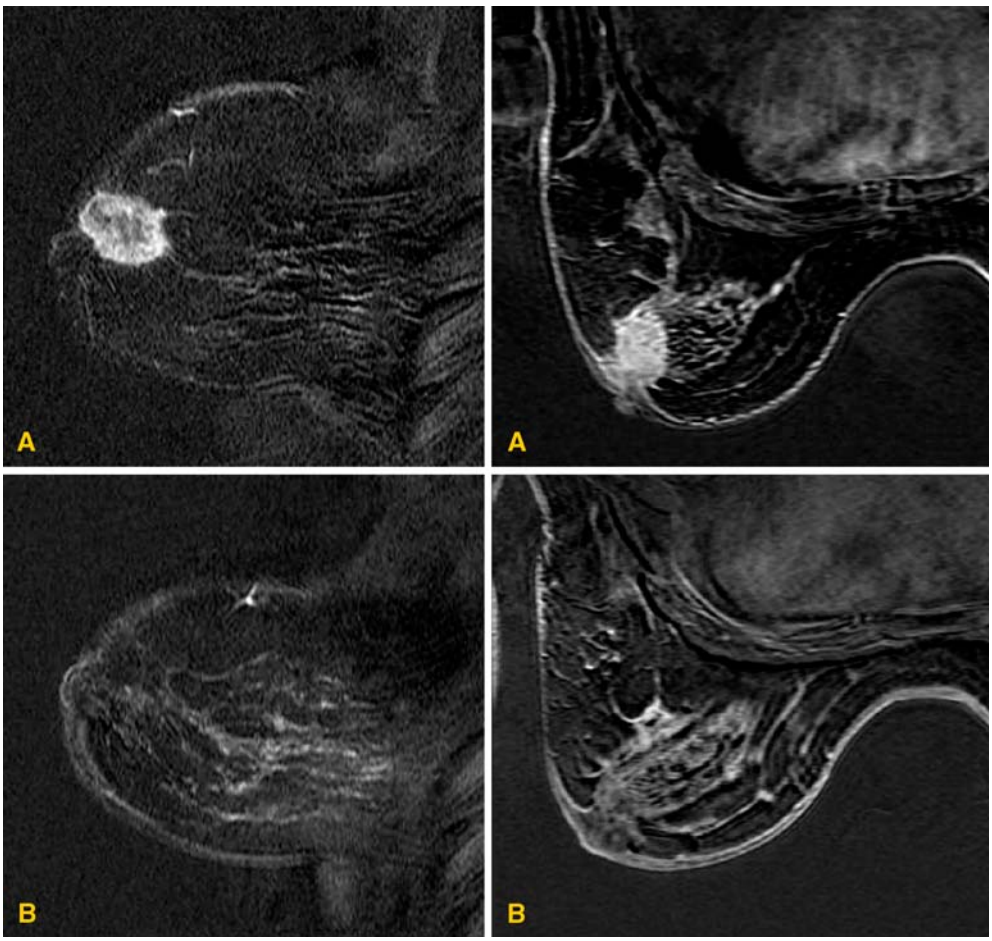

Example of a false negative MRI assessment of tumour response Forty-two years-old women with a supra-areolar 4.5-cm palpable tumour in left breast. Histology showed a grade 2 (Elston Ellis) invasive ductal carcinoma with hormonal receptor-negative and HER2 positive status. Clinical response to NAC was considered complete with only a vague supra-areolar resistance that was not measurable. There was no measurable lesion either on the mammogram, but a 1.5-cm nodule at breast ultrasound (not shown). **A**- Pre-chemotherapy MR scan (subtractions) showed an intensely enhancing tumour. **B**- Post-chemotherapy MR scan (subtractions) found no residual enhancement at the lesion site. Response was considered complete.

Figure 1b

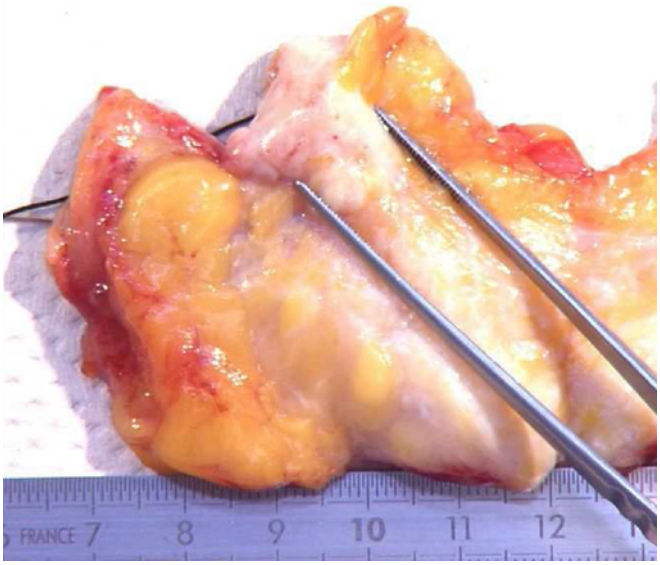

A- Surgical lumpectomy specimen Growth pathology showed a 1.5-cm residual tumour, which was almost exclusively composed of fibrous tissue.

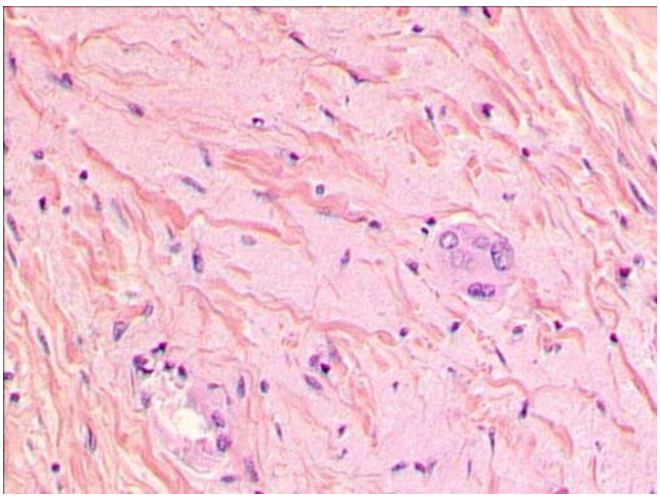

B- Microscopy (HES staining) At histogy, only sparse invasive tumour cells without any mitosis were visible. In situ carcinoma was found in some ductal sections. This finding was considered a major response. No residual metastatic lymph node was found at axillary dissection.

Categorization of Enhancing Breast Lesions

Mitsuhiro Tozaki
Division of Breast Imaging, Breast Center, Kameda Medical Center, Kamogawa, Chiba, Japan

Introduction

Breast MRI has shown diagnostic sensitivity of 94–99% for invasive breast cancer, whereas varying specificity has been reported. To improve specificity, detailed assessment of lesion morphology using three-dimensional (3D) MR imaging and of kinetic patterns using dynamic protocols has been reported useful. Several recent studies have reported diagnostic criteria combining the morphologic and kinetic characteristics [1–3].

Recently, the potential role of diffusion-weighted imaging (DWI) in characterizing breast lesions has been reported [4–6]. The apparent diffusion coefficient (ADC) value may be an effective parameter in distinguishing between benign and malignant breast lesions because tumor cellularity has a significant influence on the ADC values. However, there were no reports that specificity of DWI is higher than that of contrast-enhanced MRI among the patients with suspicious lesions.

The purpose of this study was to assess a new categorization of enhancing breast lesions, and to determine whether DWI might be useful tool for characterizing breast lesions.

Materials and Methods

Patients

One hundred sixty-five patients (age range, 16 to 89 years; mean, 49 years) who had 171 suspicious or highly suspicious lesions classified as Breast Imaging Reporting and Data System (BI-RADS)-MRI category 4 (n=112) or 5 (n=59) [7] and who had a biopsy performed after MR examinations were analyzed.

MR Imaging

MRI was performed using a 1.5-T system (Avanto; Siemens Healthcare, Erlangen, Germany). Before the administration of contrast material, bilateral sagittal fat-suppressed T2-weighted images and coronal T1-weighted images were obtained. In addition, coronal DWI were acquired with a spin-echo-type single-shot echo-planar imaging sequence incorporating the generalized auto-calibrating partially parallel acquisition (GRAPPA) algorithm for parallel acquisition. The parameters were as follows: TR/TE, 8000/96; field of view, 33 cm; matrix, 110×110; receiver bandwidth, 1684 Hz/pixel; parallel acquisition factor, 2.0; slice thickness, 3 mm; and time of acquisition, 2.5 minutes. Motion-probing gradient pulses were applied along the X, Y, and Z directions with b values of 500, 1000, 1500, 2000 and 3000 s/mm^2. Spectrally adiabatic inversion recovery (SPAIR) was used for fat suppression.

Dynamic MRI using a 3D fat-suppressed volumetric interpolated breath-hold examination (VIBE) sequence with parallel acquisition was obtained before and three times after the bolus injection of 0.1 mmol Gd-DTPA/kg at a rate of 2 mL/sec, followed by a 20-mL saline flush using an automatic injector. Both breasts were examined in the coronal plane on the first-, second-, and third-phase dynamic images, acquired at 30 seconds, 1.5 minutes, and 4.5 minutes, respectively. The dynamic MRI parameters were as follows: TR/TE, 5.2/2.3; flip angle, 12°; field of view, 33 cm; matrix, 448×318; receiver bandwidth, 430 Hz/pixel; interpolated slice thickness, 0.9 mm; partition, 144; and time of acquisition, 60 seconds. The right and left breasts were examined sagittally using the VIBE sequence without parallel acquisition at 2.5 minutes and 3.5 minutes, that is, between the second- and third-phase images, respectively (TR/TE, 4.0/2.2; flip angle, 15°; field of view, 16 cm; matrix, 256×256; receiver bandwidth, 390 Hz/pixel; interpolated slice thickness, 1.2 mm; partition, 80; and time of acquisition, 60 seconds).

Image Interpretation

For diagnostic interpretation, the BI-RADS MRI lexicon [7] was used. Initial-enhancement patterns were evaluated using the first- and second-phase dynamic images, and delayed-enhancement patterns were assessed using the third-phase dynamic images.

Lesions were categorized using the interpretation flowcharts of Tozaki et al. [2] and Fischer's score [8] for mass and focus and the interpretation method proposed by Tozaki et al. [9] for non-mass-like enhancement. In our prospective MR diagnosis, category 4 was subdivided into categories 4a and 4b (Table 1).

DWI: two-step evaluation for mass lesion

We previously reported the clinical usefulness of DWI using a two-step evaluation to detect rectal cancer [10]; we are testing a similar approach for breast mass lesions.

First, high b value (b=1500 s/mm^2) images were assessed visually. Next, ADC values of mass lesions were calculated among the patients with positive results on DWI. The highest signal portion of the lesion was visually identified on high b value images, and a circular region of interest (ROI) was placed manually on that portion of the lesion. We set 5-mm ROIs for mass lesions and 2-mm ROIs for focal lesions. ADC values (mm^2/s) were calculated according to the following equation:

$$ADC = 1/b_2 - b_1 \times ln[IS(b_1)/IS(b_2)],$$

where IS(b_1) and IS(b_2) are the signal densities resulting from two different gradient factors, b_1=500 s/mm^2 and b_2=1500 s/mm^2.

ADC measurements are not performed for non-mass-type lesions because it is sometimes impossible to identify the highest signal portion at one location in the lesions.

Results

Categorization

The lesion was classified as a mass lesion in 124 cases, non-mass-type lesion in 44 cases and focal lesion in three cases. All 171 lesions were included in Category 4a (n=22), Category 4b (n=90) or Category 5 (n=59). The rates of malignancy in the Category 4a, Category 4b and Category 5 lesions were 18%, 34%, and 95%, respectively.

DWI

All of the cases of invasive carcinoma and mass-forming DCIS were diagnosed, whereas eight non-mass-type DCIS could not be diagnosed. With the use of the two-step method of visual assessment of high b value images and a cutoff ADC value of 1.13×10^{-3} mm^2/s, we achieved a specificity of 67% (43/64) and sensitivity of 97% (61/63) for mass lesions, regardless of the lesion size (Figs 1,2). The 21 false-positive mass lesions were histologically characterized as intraductal papilloma (n=9), ductal adenoma (n=2), fibroadenoma (n=6), benign proliferative disease (n=1), radial scar (n=1), lymph node (n=1), and abscess (n=1).

Using this cutoff value (1.13×10^{-3} mm^2/s), only mucinous carcinoma was misclassified. Mucinous carcinoma consists of pure and mixed variants. Therefore, mucinous carcinoma with dominant mucus lakes would have high ADC values, and must be diagnosed despite the high ADC values. Micropapillary carcinoma also had a high ADC value (1.06×10^{-3} mm^2/s). This tumor was histologically characterized by a proliferation of tumor cell clusters within empty stromal spaces. We speculate that the water in the empty spaces could move more randomly as compared with that in the interstitium of invasive ductal carcinoma.

Conclusion

Our categorization of enhancing breast lesions is thought to be useful. DWI may be helpful in reducing the number of unnecessary biopsies following categorization into BI-RADS-MRI 4 or 5 lesions. However, this modality still has potential pitfalls in relation to the diagnosis of non-mass-type breast lesions. We believe that non-mass-type lesions should be evaluated by morphological characteristics.

References

1) Kinkel K, Helbich TH, Esserman LJ, et al. Dynamic high-spatial-resolution MR imaging of suspicious breast lesions: diagnostic criteria and interobserver variability. AJR Am J Roentgenol 2000;175: 35–43
2) Tozaki M, Igarashi T, Fukuda K. Positive and negative predictive values of BI-RADS-MRI descriptors for focal breast masses. Magn Reson Med Sci 2006;5:7–15
3) Schnall MD, Blume J, Bluemke DA, et al. Diagnostic architectural and dynamic features at breast MR imaging: multicenter study. Radiology 2006;238:42–53
4) Sinha S, Lucas-Quesada FA, Sinha U, DeBruhl N, Bassett LW. In vivo diffusion-weighted MRI of the breast: potential for lesion characterization. J Magn Reson Imaging 2002;15:693–704
5) Guo Y, Cai YQ, Cai ZL, et al. Differentiation of clinically benign and malignant breast lesions using diffusion-weighted imaging. J Magn Reson Imaging 2002;16:172–178
6) Rubesova E, Grell AS, De Maertelaer V, Metens T, Chao SL, Lemort M. Quantitative diffusion imaging in breast cancer: a clinical prospective study. J Magn Reson Imaging 2006;24:319–324
7) American College of Radiology. Breast imaging reporting and data system (BI-RADS), 4th ed. Reston, VA: American College of Radiology, 2003
8) Fischer U, Kopka L, Grabbe E. Breast carcinoma: effect of preoperative contrast-enhanced MR imaging on the therapeutic approach. Radiology 1999;213: 881–888
9) Tozaki M, Fukuda K. High-spatial-resolution MRI of non-masslike breast lesions: interpretation model based on BI-RADS MRI descriptors. AJR Am J Roentgenol 2006;187:330–337
10) Hosonuma T, Tozaki M, Ichiba N, et al. Clinical usefulness of diffusion-weighted imaging using low and high b-values to detect rectal cancer. Magn Reson Med Sci 2006;5:173–177

Table 1. Categorization of Breast Lesions on Contrast-Enhanced MRI

Mass lesion
Category 5
Spiculated margin
Irregular lesion: rapid washout pattern and rim enhancement
Category 4b
Irregular lesion
Smooth margin: washout pattern
Category 4a
Smooth margin: nonwashout and initial rapid rise
Category 3
Smooth margin: neither washout nor initial rapid rise
Non-mass-type lesion
Category 5
Segmental distribution and clustered ring enhancement
Category 4b
Segmental distribution
Branching ductal pattern
Clustered ring enhancement
Clumped architecture
Category 4a
Linear ductal pattern
Category 3
Not showing the characteristics of category 4 or 5

Fucos (less than 5 mm)
Category 4a
Rapid washout pattern
Category 3
Without rapid washout pattern

Figure Legends

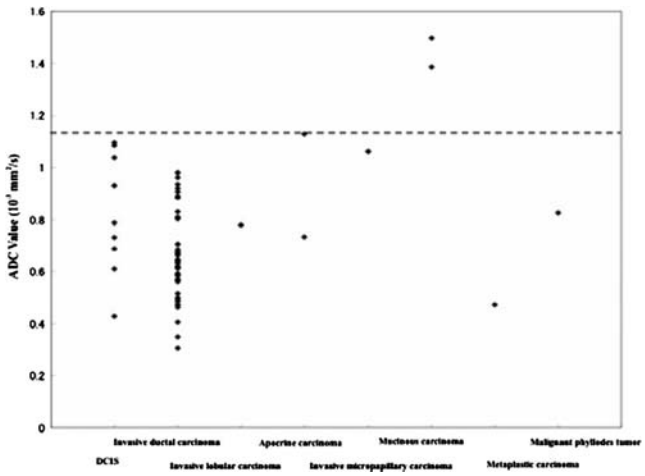

Fig. 1 The ADC of malignant tumors: Except for the case with mucinous carcinoma, the maximum ADC values of the malignant tumors was 1.13×10^{-3} mm^2/s.

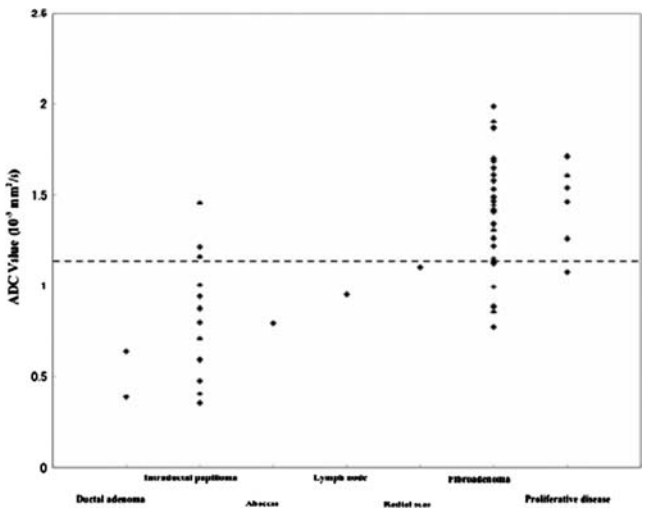

Fig. 2 The ADC of benign masses: With the use of the two-step method of visual assessment of high b value images and a cutoff ADC value of 1.13×10^{-3} mm^2/s, a specificity of 67% (43/64) and sensitivity of 97% (61/63) for mass lesions was obtained.

What is best for early response to chemotherapy: size, curve, diffusion, spectroscopy, PET?

Mitsuhiro Tozaki
Division of Breast Imaging, Breast Center, Kameda Medical Center, Kamogawa, Chiba, Japan

Introduction

Neoadjuvant chemotherapy has been one of the standard therapies for the treatment of stage II and III breast cancer. One of the current purposes of imaging during- neoadjuvant chemotherapy is to try to predict the pathological response early after the initiation of treatment. In the recently published breast MRI guidelines from the European Society of Breast Imaging [1], three MR examinations (before the start of chemotherapy, approximately half way during the course of chemotherapy and after the final course of chemotherapy) are recommended for breast cancer patients receiving neoadjuvant chemotherapy. The purpose of the second MRI is to evaluate the effect of the chemotherapy on the tumor [1].

Recently, several studies have indicated that proton MR spectroscopy (MRS) of the breast may be suitable for use as a surrogate measure of early chemotherapeutic efficacy in the patients with breast cancer [2–6]. In addition, FDG-PET is demonstrating great promise in the early evaluation of the effects of chemotherapeutic agents [7].

The purpose of this study was to assess the efficacy of MRI (size, curve, diffusion and quantitative MRS) and PET/CT to evaluate the early responses, after the second cycle of treatment, to neoadjuvant chemotherapy in breast cancer patients.

Materials and Methods

Patients

The eligibility criteria were as follows: patients who received neoadjuvant chemotherapy with an anthracycline-based regimen, underwent surgery after four cycles of chemotherapy, and underwent MRI, quantitative MRS and PET/CT before and after the second cycle of chemotherapy. Sixteen patients met the criteria to be included in the analysis.

MR Imaging

MRI was performed using a 1.5T system (Avanto; Siemens Medical Solutions, Erlangen, Germany). A double breast coil (breast matrix coil; Siemens Medical Solutions, Erlangen, Germany) was used for both MRI and MR spectroscopy. Before the administration of contrast material, bilateral sagittal fat-suppressed T2-weighted images and coronal T1-weighted images were obtained. In addition, coronal DWI were acquired with a spin-echo-type single-shot echo-planar imaging sequence incorporating the generalized auto-calibrating partially parallel acquisition (GRAPPA) algorithm for parallel acquisition. The parameters were as follows: TR/TE, 8000/96; field of view, 33 cm; matrix, 110×110; receiver bandwidth, 1684 Hz/pixel; parallel acquisition factor, 2.0; slice thickness, 3 mm; and time of acquisition, 2.5 minutes. Motion-probing gradient pulses were applied along the X, Y, and Z directions with b values of 500, 1000, 1500, 2000 and 3000 s/mm^2. Spectrally adiabatic inversion recovery (SPAIR) was used for fat suppression.

Dynamic MRI using a 3D fat-suppressed volumetric interpolated breathhold examination (VIBE) sequence with parallel acquisition was obtained before and three times after the bolus injection of 0.1 mmol Gd-DTPA/kg at a rate of 2 mL/sec. Both breasts were examined in the coronal plane on the first-, second-, and third-phase dynamic images, acquired at 30 seconds, 1.5 minutes, and 4.5 minutes, respectively. The

right and left breasts were examined sagittally using the VIBE sequence without parallel acquisition at 2.5 minutes and 3.5 minutes; that is, between the second- and third-phase images, respectively.

^{1}H MR Spectroscopy

After all of the MRI sequences had been performed, single-voxel MRS was performed using a point-resolved spectroscopy sequence (PRESS). The parameters of MRS were TR/TE=1620/270; voxel size= 15×15×15 mm^3; acquisitions= 256; spectral width= 1,000 Hz; data points= 1,024; and the time of acquisition was 7 minutes.

Shimming was performed automatically first, followed by manual shimming on the water resonance for optimization of the homogeneity in each volume of interest. After the shimming procedure, spectra were acquired with water suppression by applying three chemical-shift selective (CHESS) excitation pulses. By spectral suppression using dual band-selective inversion with gradient dephasing (BASING), the transverse magnetization was selectively dephased before and after the second spin-echo pulse.

Normalizing the Cho signal using an external standard method

A cylindrical bottle phantom with a height of 4.0 cm and a diameter of 2.5 cm was inserted behind the breast coil and fixed in position. The phantom was filled with 1.25 g of $NiSO_46H_2O$ per 1,000 g of H_2O. In each patient, ^{1}H MR spectroscopy of the phantom was performed immediately after the MR spectroscopy examination of the breast lesion. The scan was performed without water suppression. The voxel size was 7×7×15 mm^3, and the time of acquisition was 4 seconds.

The scaling factor was calculated according to the following formula:

$$scalingfactor = (106/MWH2O) \times (nH2O/nCho) \times (fT1H2O/fT1Cho) \times (fT2H2O/fT2Cho) \times (voxelH2O/voxelCho) \times (coilsensH2O/coilsensCho)$$

$$f_{T1} = 1 - \exp(-TR/T1), f_{T2} = \exp(-TE/T2)$$

where n_{Cho} and n_{H2O} are the numbers of ^{1}H nuclei for each molecule, respectively. The scaling factor can be changed to molar concentration by correcting for the number of ^{1}H nuclei per molecule and the molecular weight of the solvent (MW_{H2O}). The f_{T1} and f_{T2} relaxation factors were corrected using the equation for relaxation times.

Data Processing and Spectral Interpretation

The spectroscopic data processing protocol was saved and linked with the measurement protocol within the syngo software (Siemens Medical Solutions, Erlangen, Germany) to ensure that data processing was identical for each measurement. A Hanning filter with a window width of 400 ms was applied, and the Fourier vector was zero-filled up to 2048 time points. A scaling factor was 12096. We fitted the peaks of Cho and water with a Gaussian function, from 3.18 to 3.32 ppm for Cho, and at 4.7 ppm for water.

Phase correction was done manually. Using the residual water signal as a reference (4.7 ppm), the frequency of any detected resonance in the 3.00–3.50 ppm spectral region was recorded. If a peak at 3.21–3.23 ppm assigned to phosphocholine (PC) was clearly identifiable, water subtraction and baseline correction with a sixth-order polynominal fit were applied to obtain the flat baseline of an MR spectrum. Then the normalized Cho signal, which was calculated automatically, was recorded. In cases negative for Cho, the numerical value of Cho was defined as zero.

Tumor Size

The tumor size was measured using coronal and sagittal contrast-enhanced MR images and transverse multiplanar reconstruction of contrast-enhanced MR images.

Kinetic Curve

Initial-enhancement patterns (rapid, medium or slow) were evaluated based on the first- and second-phase dynamic images, and delayed-enhancement patterns (washout, plateau or persistent) were assessed based on the third-phase dynamic images [8].

Diffusion-weighted imaging (DWI)

The highest signal portion of the lesion was visually identified on high-b-value images (1500 s/mm^2), and a circular region of interest (ROI) was placed manually on that portion of the lesion. ADC values (mm^2/s) were calculated according to the following equation:

$$ADC = 1/b_2 - b_1 \times ln[IS(b_1)/IS(b_2)],$$

where IS(b_1) and IS(b_2) are the signal densities resulting from two different gradient factors, b_1=500 s/mm^2 and b_2=1500 s/mm^2.

PET/CT

Patients received a total of 4.3 MBq/kg of ^{18}F-FDG by intravenous administration. Imaging data were obtained with a PET/CT scanner (Discovery St with Dimension Console; GE Medical Systems) that produced transaxial, coronal, and sagittal reconstructions of CT, PET, and fusion PET/CT data for interpretation. This system consists of a 16-detector-row CT scanner and a PET scanner with a 3D image-acquisition algorithm. The PET camera produces 47 slices, each 3.27 mm thick, along a 157-mm axial field of view.

A circular ROI with a diameter of 5 to 10 mm was placed manually on any PET/CT image revealing a breast tumor. From these ROIs, the SUV was calculated according to the following formula: SUV = activity/mL tissue (decay corrected)/injected dose/body weight. Maximum SUV was recorded as peak SUV.

Results

The ΔCho_{2nd} (reduction rates of the normalized Cho signal after the second cycle of chemotherapy) and the ΔSUV_{2nd} were statistically significantly different between the pathological responders and non-responders ($p<0.01$; Mann-Whitney U-test), whereas the changes of the kinetic curve pattern, the ΔLS_{2nd} and the ΔADC_{2nd} were not significantly different between the two groups (Fig 1).

Conclusion

The changes in Cho on MRS and SUV on PET/CT after the second cycle of chemotherapy may be more sensitive to changes in the tumor size, kinetic curves, or ADC values to predict the pathological response.

References

1) Mann RM, Kuhl CK, Kinkel K, Boetes C. Breast MRI: guidelines from the European Society of Breast Imaging. Eur Radiol 2008; 18:1307–1318.

2) Jagannathan NR, Kumar M, Seenu V, et al. Evaluation of total choline from in-vivo volume localized proton MR spectroscopy and its response to neoadjuvant chemotherapy in locally advanced breast cancer. Br J Cancer 2001:84:1016–1022.
3) Meisamy S, Bolan PJ, Baker EH, et al. Neoadjuvant chemotherapy of locally advanced breast cancer: predicting response with in vivo (1)H MR spectroscopy–a pilot study at 4 T. Radiology 2004;233:424–431.
4) Kumar M, Jagannathan NR, Seenu V, Dwivedi SN, Julka PK, Rath GK. Monitoring the therapeutic response of locally advanced breast cancer patients: sequential in vivo proton MR spectroscopy study. J Magn Reson Imaging 2006;24:325–332.
5) Tozaki M, Sakamoto M, Oyama Y, et al. Monitoring of early response to neoadjuvant chemotherapy in breast cancer with 1H MR spectroscopy: comparison to sequential 2-[18F]-fluorodeoxyglucose positron emission tomography. J Magn Reson Imaging 2008; 28:420–427.
6) Baek HM, Chen JH, Nie K, et al. Predicting pathologic response to neoadjuvant chemotherapy in breast cancer by using MR imaging and quantitative 1H MR spectroscopy. Radiology 2009;251:653–662.
7) Rousseau C, Devillers A, Sagan C, et al. Monitoring of early response to neoadjuvant chemotherapy in stage II and III breast cancer by [18F]fluorodeoxyglucose positron emission tomography. J Clin Oncol 2006;24:5366–5372.
8) American College of Radiology. Breast imaging reporting and data system (BI-RADS), 4th ed. Reston, VA: American College of Radiology, 2003

Figure Legends

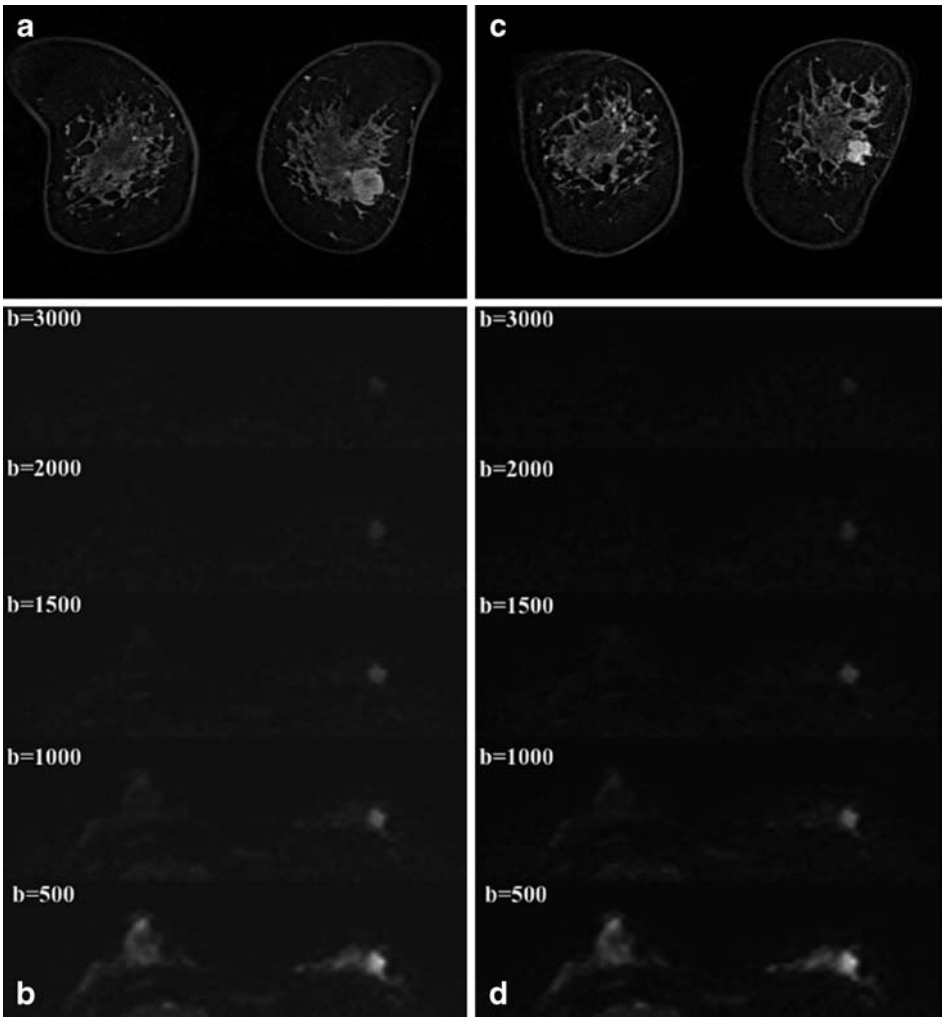

Fig. 1 Coronal 3D fat-suppressed MR images before (A) and after (C) the second cycle of chemotherapy show an enhancing breast cancer. Transverse multiplanar reconstruction of diffusion-weighted images before (B) and after (D) the second cycle of chemotherapy shows high-signal-intensity mass. Despite the decrease in tumor size due to the chemotherapeutic effect, the lesion after the second cycle of chemotherapy had a low ADC values (0.73×10^{-3} mm^2/s) similar to the pre-therapy value (0.81×10^{-3} mm^2/s).

COMICE Trial: Is MRM really useful?

LW Turnbull[1*], SR Brown[2], C Olivier[2], I Harvey[1], J Brown[2], P Drew[3], A Hanby[4], A Manca[5], V Napp[2], M Sculpher[5], L G Walker[6], S Walker[5] on behalf of the COMICE Trial Group
1 Centre for MR Investigations, University of Hull and Hull and East Yorkshire Hospitals NHS Trust
2 Clinical Trials Research Unit, University of Leeds, Leeds
3 Hull York Medical School
4 Leeds Teaching Hospitals Trust, Leeds
5 Centre for Health Economics, University of York, York
6 Institute of Rehabilitation and Oncology Health Centres, University of Hull and Hull and East Yorkshire Hospitals NHS Trust

** Author for correspondence:
Professor L Turnbull
Centre for Magnetic Resonance Investigations
Hull Royal Infirmary
Anlaby Road
Hull
HU3 2JZ
Tel: 01482 674082
Email: l.w.turnbull@hull.ac.uk
ISRCTN: 57474502
The trial was funded by grants from the NIHR Health Technology Assessment Programme, project number 99/27/05.

Introduction
The main objective of the COMICE trial was to determine if the addition of magnetic resonance (MR) imaging of the breast to current patient evaluation by triple assessment (clinical, radiological and pathological) would aid the localisation of tumour within the breast and hence reduce the re-operation rate in women with primary tumours scheduled for wide local excision.

Design
COMICE was a multi-centre, randomised, controlled, open, fixed sample, parallel group trial with equal randomisation, in women with biopsy-proven primary breast cancer who were scheduled for wide local excision following triple assessment. Patients were randomised to receive MR imaging or no further investigations. A pragmatic approach to trial design was chosen so that results could be generalisable in clinical practice and to reduce unnecessary protocol-driven trial costs.

Participants
Women aged 18 years or over who had undergone X-ray mammography and ultrasound scanning during the current episode, with pathologically documented primary breast carcinoma and who were scheduled for wide local excision and capable of providing written informed consent were recruited. Patients who were medically unstable, had a known contraindication to MR scanning or to the use of a paramagnetic contrast agent; had renal failure; had undergone chemotherapy/ hormonal therapy in the previous 12 months or had had previous surgery, radiotherapy or serious trauma to the ipsilateral breast; were pregnant or breast feeding; or had a disability preventing prone scanning were excluded. This study took place at 45 hospital-based research centres throughout the UK.

Methods
Patients were randomised to receive MR imaging or no MR imaging. Randomisation was performed using minimisation incorporating a random element. The following minimisation factors were incorporated: Consultant Breast Surgeon, patient's age (<50 years vs. ≥50 years) and breast density (ACR BIRADS pattern 1 vs. ACR BIRADS pattern 2, 3 or 4).
MR imaging was performed at 1.5T with a dedicated bilateral breast surface coil. Dynamic contrast-enhanced MR imaging utilized a T1-weighted, 3D fast spoiled gradient echo sequence (temporal resolution 45 seconds) was acquired following intravenous injection of contrast agent (0.1 mmol Gd-DTPA/ kg body weight), and high resolution (0.7 mm×0.9 mm in plane) fat-suppressed T1-weighted 3D SPGR images were acquired for lesion morphology. Data analysis included evaluation of the signal intensity time curves and lesion morphology.
The primary endpoint of the COMICE trial was the rate of repeat operation or mastectomy at further operation, or pathologically avoidable mastectomy at initial operation. The rate of re-operation was defined as the number of patients in each arm experiencing a repeat operation or mastectomy further to initial surgery, within six months of randomisation, plus the number of patients who had undergone a pathologically avoidable mastectomy at initial operation in each arm divided by the total number of patients in each arm.
Secondary outcome measures included: factors associated with discrepancy between imaging findings and histopathology; the effectiveness of imaging; change in clinical management following MR imaging; the clinical significance of MR-only detected lesions and the ipsilateral tumour recurrence rate.

Results
In total 1623 patients were consented and randomised between December 2001 and January 2007 (816 MR imaging, 807 no MR imaging). No differences in the re-operation rate were found between the two groups of patients (MR imaging patients 18.75%, No MR imaging patients 19.33%, difference= 0.58%, 95% confidence interval (CI) [-3.24%, 4.40%]), and the addition of MR imaging to conventional triple assessment alone was not found to be statistically significantly associated with a reduced re-operation (odds ratio =0.96, 95% CI=[0.75, 1.24], p=0.7691). Sixteen patients in the MR imaging arm (2.0%) underwent a pathologically avoidable mastectomy at initial surgery.
Overall the best agreement between all imaging modalities and histopathology, with respect to tumour size and extent of disease, was found in patients who were over 50, had ductal tumours NST and who were lymph node negative. Considering the effectiveness of imaging, the sensitivity and positive predictive values of MR imaging (with regard to determining patient management) were 50.0% (95% CI [42.65, 57.35]) and 61.8% (95% CI [53.87, 69.74]) respectively, and of the 58 patients undergoing a mastectomy, in the MR imaging arm, 16 (27.6%) were classed as being pathologically avoidable. The agreement between imaging methods and pathology, as assessed by weighted kappa statistics, ranged from 0.3803 for ultrasound to 0.4767 for MR imaging.
None of the 25 patients with MR-only detected <5 mm lesions had a clinically significant lesion evident at their 12-month repeat MR imaging scan. Of the 66 patients with MR-only detected ≥5 mm biopsy negative lesions, only three had potentially clinically significant lesions at their 12-month repeat MR imaging scan, however this was based on overall lesion score as these lesions were not biopsied.
Kaplan Meier estimates of the local recurrence-free interval rate were 99.87% (95% CI [99.05%, 99.98%]) for patients randomised to MR imaging, compared to 99.73% (95% CI [98.93%, 99.93%]), for

patients randomised to no MR imaging. No differences in QoL were seen between the two groups of patients.

Conclusions

The results of this study show that the addition of MR imaging to X-ray mammography and ultrasound does not reduce the re-operation rate. Indeed over the time-span of the trial despite advances in both mammographic and ultrasound technologies and out with the context of this trial, the re-operation rates reported for the UK for screen-detected breast cancer increased from 14.2% to 17.0%.

The possible effect of surgical expertise to assimilate and appropriately use the additional information provided by MR imaging was investigated, but no statistically significant association between consultant surgeon and re-operation rate was identified, although there was a trend towards lower re-operation rates for those consultant surgeons with the greatest experience.

The rate of pathologically avoidable mastectomy at initial operation was incorporated into the primary endpoints of this study, as it was thought possible that MR imaging could over-estimate the size and extent of disease, and thus result in an inappropriate recommendation for mastectomy. The results showed that 7.1% of patients underwent a mastectomy at initial operation, in the MR imaging arm. Of these, 2.0% of all MR imaging patients underwent a pathologically avoidable mastectomy at initial operation, and 0.3% of patients underwent a mastectomy through patient choice. Since the COMICE trial only considers those women already scheduled to receive WLE, identified via triple assessment, comparison with the rate of pathologically avoidable mastectomies as a consequence of triple assessment alone with that for MR imaging was not possible. It is essential that biopsy of additional MR only detected lesions be performed, prior to alteration in surgical management, to minimise the risk of avoidable mastectomy. It is important to note however that 4.8% of patients correctly underwent a mastectomy at initial operation, as a result of the MR imaging findings. Nonetheless, this did not result in a significant reduction in the rate of repeat operation or mastectomy at further operation in this arm.

No statistically significant association between ACR BI-RADS classification and re-operation rate was identified. However the patient's age was found to be highly statistically significant, indicating that patients aged 50 years or over were less likely to undergo re-operation than those aged less than 50 (OR=0.64, 95% CI=[0.48, 0.87], p=0.0041). The reasons associated with these findings are unclear.

Surgical techniques for the loco-regional treatment of malignancy have changed little since wide local excision replaced mastectomy as the procedure of choice for tumours stage II or less. Optimal excision of tumour is dependent on the ability of the surgeon to utilise the imaging information provided and to palpate the lesion in its entirety during surgery to allow complete excision. This is very demanding and consideration must be given to the investigation of alternative treatments, namely image-guided ablation, for the treatment of small tumours.

Diffusion changes in chemotherapy of breast cancer: the earliest sign?

Lindsay W. Turnbull1, Bing Ma2, Charles R. Meyer2, Martin D. Pickles1, Thomas L. Chenevert2, Peyton H. Bland2, Craig Galban2, Alnawaz Rehemtulla3, and Brian D. Ross2

1Centre for Magnetic Resonance Investigations, Division of Cancer, Postgraduate Medical School, University of Hull, HU3 2JZ Hull, UK

2Department of Radiology, University of Michigan Medical School,

3Department of Radiation Oncology, University of Michigan Medical School,

Author for correspondence:
Dr Bing Ma
Department of Radiology, University of Michigan Medical School, Ann Arbor, MI, 48109, USA
bingm@umich.

Abstract

Diffusion-weighted (DW) imaging provides a new contrast mechanism for evaluation of tumors. By imaging alterations in microscopic motion of water molecules secondary to changes in microcirculation and water diffusivity, DW imaging yields new qualitative and quantitative information about tumors that can be used to improve tumor detection, characterise some tumors, and monitor and predict response to chemotherapy. Neoadjuvant chemotherapy (NAC) is currently employed for patients with locally advanced breast cancer to achieve tumor shrinkage, allowing breast conservation surgery for a proportion of the patients. Unfortunately 20–25% of all breast cancer patients do not respond to chemotherapy. Identification of surrogate biomarkers that can predict therapeutic outcome earlier or more accurately than current methods would be valuable to tailor treatment to individual patients and would allow cost-effective use of resources.

The primary aim of this study was to use voxel-based analysis of changes in the apparent diffusion coefficient (ADC) of water to assess therapeutic response in primary breast cancers. Functional diffusion maps (fDM) which represent a voxel-by-voxel scatter plot of the registered pre- vs. post-therapy ADC values were created for all patients. A prerequisite for proper fDM analysis using pre- and post-therapy breast examinations is that the corresponding pre- and post-treatment image voxels contain similar cellular partial volume contributions. Mutual information based image registration algorithms were applied to align the pre- and post-treatment scans. Tumor volumes of interest were drawn on the high resolution post-contrast anatomical image volumes and were warped onto the pre-treatment diffusion volumes. Subsequent registrations between the pre- and post-treatment diffusion scans are also warped to account for repositioning deformations to the breast as well as any compartmental changes to the tumor.

14 patients with biopsy-proven breast cancer were scanned prior to and after the first, second and fourth cycle of NAC. All were deemed to have responded to treatment based on RECIST criteria. Treatment cycles consisted of epirubicin and cyclophosphamide administered at 3 week intervals. Patients were scanned either on a 3.0 or 1.5T scanner (GE Healthcare, Milwaukee, WI, USA) in combination with dedicated bilateral breast coils. Diffusion weighted MRI was acquired axially with a water-only excitation, single-shot, dual spin-echo EPI sequence with the following parameters: TR, 4000 ms, fractional TE, 74 ms (3.0 T) or 98 ms (1.5 T); FOV, 340×340 mm; matrix, 128×128; slice, 5 mm; gap, 1 mm; 10 averages; b values, 0 and 700 s =mm2, applied in all three orthogonal directions. A dual spin-echo EPI sequence was utilized since this sequence reduces eddy currents and therefore image distortions.

The first post-therapy data acquisition took place within 2–12 days after the initiation of the first cycle of treatment. The second post-therapy data acquisition took place within 11–19 days after the initiation of the second cycle of treatment and within 32–39 days after the initiation of the first treatment cycle. To study the role of ADC changes between pre- and post-therapy examinations as an early indicator of treatment effectiveness, we focused on the

relationship between ADC changes and time intervals after initiation of treatment. In this study post-treatment scans included the diffusion scans obtained after both the first and the second cycle of treatment. Linear regression analysis showed a correlation between ADC changes and interval lengths after the initiation of treatment, with p-value 0.03. We clearly observed that examinations at five weeks post-treatment exhibited a larger effect size in ADC change compared to the one week post-chemotherapy counterparts. Logistic regression analysis was performed to further examine the correlation of ADC changes during treatment with clinical outcomes. A logistic regression fit with $p=0.009$ at five weeks post-treatment, demonstrated that the probability of response to NAC is strongly associated with increased ADC values. We observed 1 false positive and 1 false negative, resulting in a sensitivity of 90% and a specificity of 75%. Logistic regression at one week post-treatment showed no capability of separating responders from non-responders.
In this preliminary study changes in ADC have potential for use in assessing NAC effectiveness and are likely to be an increasing function of the temporal interval after the initiation of treatment with, as yet, an unknown time limit. Logistic regression analysis has further revealed that ADC changes at five weeks post-NAC are highly correlated with treatment response.

Evaluation of Cancer Aggressiveness using Magnetic Resonance Mammography

Tibor Vag, MD, PhD [1], Pascal A.T. Baltzer [1], MD, Matthias Dietzel, MD [1]; Mieczyslaw Gajda, MD [2]; Oumar Camara, MD [3]; Christian Freiberg [1]; Sebastian Beger [1]; Werner A. Kaiser, MD, MS [1]
1 Institute of Diagnostic and Interventional Radiology, Friedrich-Schiller-University Jena, Erlanger Allee 101, D-07740 Jena, Germany
2 Institute of Pathology, Friedrich-Schiller-University Jena, Ziegelmühlenweg 1, D-07740 Jena, Germany
3 Clinic of Gynecology, Friedrich-Schiller-University Jena, Bachstr. 18, D-07740 Jena, Germany

Objective:
Dynamic contrast enhanced magnetic resonance mammography (MRM) is a well established method in the diagnosis of invasive breast cancer. Distinction between benign and malignant lesions in MRM is possible by evaluating their morphology and enhancement pattern. A strong initial signal increase, followed by a plateau or washout curve is regarded as indicative for malignancy whereas a slow initial enhancement and a persistent curve type are thought to be associated with benign lesions.
The aim of this study was to correlate these kinetic features of invasive breast carcinomas with histologic prognostic factors using a computer aided evaluation software.

Material and Methods:
128 patients (age between 30 and 82 years with a mean of 60 years) with 145 invasive breast carcinomas underwent dynamic MR-mammography. Different kinetic features from the invasive breast lesions were obtained using a commercially available software able to automatically assess enhancement characteristics of a given lesion. Findings were correlated with histologic prognostic factors determining tumor aggressiveness (tumor size, lymph node status, estrogen/progesterone receptors [ER/PR] status, HER-2/neu status and tumor grade) using a nonparametric rank test (two-sided Mann-Whitney-U) and a two-sided chi-square test, respectively.

Results:
Significant correlations were found between positive lymph node status and washout enhancement curve type ($p<0.05$). Furthermore, lesions with negative ER and PR status exhibited a significantly higher contrast washout rate in the delayed dynamic phase compared to ER/PR positive lesions ($p<0.05$). PR-negative lesions additionally displayed a significantly stronger initial contrast enhancement rate compared to PR-positive lesions ($p<0.05$). On the other hand, no statistical significance could be observed between histological tumor grading or HER-2/neu status and kinetic features.

Conclusion:
Breast cancer exhibiting a washout enhancement curve with strong initial contrast enhancement and strong washout rate in the delayed phase tends to be more aggressive than lesions lacking these features.

Enhancing nodules in preoperative MR - What should we do?

M. Van Goethem, K Schelfout, I Verslegers, I Biltjes, L Hufkens, P Parizel

Introduction.
MR Mammography is superior in detection of breast cancer, but the problem with MR Mammography remains its lack of specificity.
For this reason, Magnetic Resonance Imaging (MRI) may only be performed for the right indications. An important indication is locoregional staging of patients with breast carcinoma. Especially in these cases, enhancement of benign lesions is a problem, and that is the reason that the use of preoperative MR is still controversial. Surgeons and gynaecologists are afraid that the use of MR leads too often to mastectomies, where there is no proof that the survival will be better for these patients.
The use of the BI-RADS classification could make it possible to give unambiguous MR reports. But especially in the BI-RADS 3 group, the probably benign lesions, the positive predictive value will be low.

Why staging of tumor extent within the breast and exclusion of multifocality, multicentricity in the same or contralateral breast.

In the majority of breast cancer patients diagnosed today, disease-free and overall survival are similar after breast conserving therapy when compared to mastectomy. Breast cancer recurrence after breast conserving surgery is reported in 3 to 19% of patients and is mostly due to incomplete resection or multifocality (1). Furthermore, breast tumor recurrence is a risk factor for distant metastasis and mortality. Therefore, good preoperative staging before planning breast conserving surgery is important.
Reports have demonstrated that MR detects **multifocal/multicentric** carcinoma in up to 37% of breast cancer patients. But 20% false positive additional enhancing lesions are reported, which can lead to unnecessary wider excision or mastectomy (2).

Synchronous bilateral breast cancer accounts for 3–6% of breast cancers. The reported rates of MRI-demonstrated but mammographically and clinically occult contralateral breast cancer varies between 5.7–24%.
A literature search performed by the Blue Cross and Blue Shield Association

Technology Evaluation Center (TEC)(3) identified studies using contrast-enhanced breast MRI in patients with localized breast cancer. They considered 18 studies (n=1401) confirming that MR has a better sensitivity for identifying multicentric breast tumors compared to conventional staging. Studies demonstrated sensitivity of 75–100% and specificity of 82–100% for multicentric tumor foci and a PPV of 50–100%, the 3 most representative studies had a PPV of 67–100%. Due to the moderate specificity and relatively low PPV, presurgical biopsy of additional lesions should be performed before changing conservative therapy to mastectomy. Approximately 2% to 15% of women who appear eligible for breast conserving therapy have multicentric disease, detected on MRI. The presence of multicentric disease appears somewhat higher in patients with ductal carcinoma in situ (DCIS) (20–28%) or infiltrating lobular carcinoma (ILC) (17–40%).

The results of more recent clinical studies, showed again the superior role of MRI to detect additional lesions occult on other imaging methods. A large prospective, multicenter trial involving 426 women with confirmed breast cancer was performed at 15 institutions in the US, Canada, and Germany (4). Women underwent mammography and MRI prior to biopsy of the suspicious index lesion. MRI had a significantly higher yield of confirmed cancer incidental lesions than mammography. They concluded that consideration needs to be given to the integration of breast MRI into the pretreatment evaluation of women seeking breast conservation therapy.

Due to its growth pattern, invasive lobular carcinoma is often difficult to detect on clinical examination, mammography and US. Moreover, patients with invasive lobular carcinoma (ILC) are reported to have a relatively high frequency of multifocal, multicentric or bilateral breast cancer (14–31%) (5). Even if one ILC in a patient is detected, additional lesions may potentially be occult on the routine imaging examination. Several studies of the role of MRI in ILC are published, the number of patients varied between 20 and 32. The conclusion was that MRI is superior to mammography in determining the extent of ILC, including the presence of multifocal/multicentric disease (16–50%).

MRI detected lesions. Problems.

Of the additional enhancing lesions reported in literature, up to 20% are false positive, this can lead to unnecessary wider excision or mastectomy(2).

In our study of 204 patients with a breast carcinoma, sixty five additional foci were considered malignant on MRI. Ten of these lesions corresponded with benign breast changes or normal breast parenchyma. Histopathological examination confirmed 45 additional invasive cancers and 10 additional pure DCIS foci in 33 patients (6). Of the benign lesions, 12 were considered BI-RADS 3, 12 BI-RADS 4 and none BI-RADS 5.

Two lesions classified as BI-RADS 3 turned out to be malignant.

In another study we performed, in 101 of 297 malignant lesions there was enhancement around or adjacent to the tumor. Enhancing areas including long spicules, ductal pattern, noduli or a zone with enhancement surrounding a carcinoma correlated in 89,1% (respectively 92,5%, 89%, 84% and 100%) with invasive or in situ extension of the carcinoma (7). However, seventeen lesions showed an overestimation of more than 1 cm, 11 of them of more than 2 cm.

Solutions?

To reduce false positive enhancement, MRI mammography may only be performed between day 7 and 14 of the menstrual cycle. This is however impossible if patients have a suspicious lesion.

Image guided biopsies must be done of all enhancing lesions that are probably malignant, before change in therapy is performed.

All patients with suspect lesions detected on MRI must have a review of the mammography and a second look ultrasound with knowledge of the MR images and with special attention for the additional enhancing lesions.. If a corresponding lesion is seen on ultrasound, core biopsy can easily be performed under ultrasound. If a lesion is seen on mammography, stereotactic guided biopsy can be performed.

If on MRI additional enhancing lesions are detected, ultrasound has to be performed, if the lesion is detected on ultrasound also, the likelihood of carcinoma seems higher than for lesions without ultrasound correlate (8).

If there is no corresponding lesion on mammography or ultrasound, MRI guided biopsy must be performed if the lesion on MR is suspect.

If **small homogeneous enhancing nodules** of less than 5 mm are seen, and cannot be detected on ultrasound and/or mammography, they are probably benign and no change in therapy planning needs to be done.

Enhancement adjacent to a malignant mass is in 89,1% due to invasive or in situ extension of the carcinoma. If the diameter of the whole enhancing lesion, mass and surrounding enhancing area, is significantly larger than that measured on mammography or ultrasound, biopsies should be performed in the peripheral borders of the enhancing surrounding area, to prevent unnecessary wider excision.

Contralateral breast

If benign appearing enhancing lesions are seen in the other breast and the MRI was not performed in the right period of the menstrual cycle, control MRI in another period of the menstrual cycle must be done. When probably benign lesions are seen on MRI in the contralateral breast, and not on a second look ultrasound, MR has to be repeated after 6 months.

Round foci of less than 5 mm may be interpreted as benign lesions, especially if the enhancement is contnous in time or with a late maximum.

1 Schnall MD, Blume J, Bluemke DA, Deangelis GA, Debruhl N, Harms S, et al. MRI detection of distinct incidental cancer in women with primary cancer studied in IBMC 6883. J Surg Oncol. 2005;92(1):32–8

2 Schelfout K, Van Goethem M, Kersschot E, et al. Preoperative breast MRI in patients with invasive lobular breast carcinoma. Eur Radiol. 2004;14(7):1209–16.

3 Schelfout K, Van Goethem M, Kersschot E, et al Contrast-enhanced MR imaging of breast lesions and effect on treatment. Eur J Surg Oncol. 2004;30:501–7.

4 Van Goethem M, Schelfout K, Kersschot E, et al. Enhancing area surrounding breast carcinoma on MR mammography: comparison with pathological examination. Eur Radiol. 2004;14:1363–70.

5 LaTrenta LR, Menell JH, Morris EA, Abramson AF, Dershaw DD, Liberman L.Breast lesions detected with MR imaging: utility and histopathologic importance of identification with US. Radiology. 2003;227:856–61.

DNA and protein chip technologies in oncology - from research to diagnosis

Core Unit Chip Application, Institute of Human Genetics, Jena University Hospital
Ferdinand von Eggeling, Günther Ernst, Christian Melle

Biomarkers, especially for diagnostic use, have applications in a wide range of diseases. In the oncology field, most markers are lacking in sensitivity and specificity and/or in their ability to detect tumors in the early stages. However, in nearly all neoplasias, early detection is of high importance for appropriate therapy and ultimately for the patients' survival. The survival rate when treated in stage I is in some malignancies nearly 100%. However, it can decrease finally nearly to zero in stage IV. Thus, there are major efforts to identify highly specific, early biomarkers, which are also economical to apply in screening or in routine diagnostic testing. In this talk, we will present some possible attempts, which lead us from tumor research to potential diagnostic markers. These attempts include the separation of functional tissue areas by laser-based microdisssection and DNA and Protein chips for the analysis of differentially expressed genes and proteins.

B-catenin Mediated Radiation Resistance of Mammary Gland Progenitors and Breast Cancer Tumor-initiating Cells

Wendy A. Woodward,[1] Mercy S. Chen[2], Frances Kittrel[2] and Jeffrey M. Rosen[2]
Department of Radiation Oncology, The University of Texas M.D. Anderson Cancer Center, Houston, TX[1] and Department of Molecular and Cellular Biology, Baylor College of Medicine, Houston, TX[2]

Address correspondence to:
Wendy A. Woodward, M.D. Ph.D
Department of Radiation Oncology
The University of Texas M.D. Anderson Cancer Center
1515 Holcombe Blvd., Box 1202
Houston, TX 77030
Email: wwoodward@mdanderson.org
Tel: (713) 563–8481
Fax: (713) 563–6940
Running head: Breast Cancer TIC's
Keywords: Tumor- initiating Cells, Breast cancer, Radiation, Wnt/ β-catenin
Nonstandard abbreviations used: TICs, Tumor-initiating cells; CD, COMMA-D; MECs, mammary epithelial cells; Sca1$^+$, stem cell antigen-1 positive; Sca1$^-$, stem cell antigen-1 negative; SP, side population; MSCV, murine stem cell virus; GFP, green fluorescent protein; MIN, mammary intraepithelial neoplasia; Gy, Gray (1 Gy=100 rads).

Abstract:
The existence of adult stem cells in mammary tissue was elegantly demonstrated many decades ago through limiting dilution transplantation experiments. Prospective identification of these normal mammary gland stem cells and similarly multipotent cells from human breast cancer capable of initiating tumor growth in dilution transplantation experiments has catapulted the field into a new era of research and discovery. In normal and tumor tissue, progenitors and tumor initiating cells (TICs) appear resistant to clinically relevant doses of radiation, a phenomenon mediated in part by stem cell survival pathways such as the Wnt/β-catenin pathway. Stabilization of the Wnt/β-catenin pathway in murine mammary Comma-D cells increases mammary gland outgrowth from cells transplanted into cleared mammary fatpads, and increases survival of murine mammary gland progenitors after in vivo radiation. Human breast cancer cell line progenitors are more resistant to radiation than non-progenitors and selectively re-localize activated β-catenin to the nucleus in response to radiation. We propose Wnt/β-catenin may be an attractive pathway to selectively target breast cancer TICs.

Introduction:
"Every animal appears as a sum of vital units, each of which bears in itself the complete characteristics of life"

Rudolf Virchow, Cellular Pathologie, 1858

In 1858, pathologist Rudolf Virchow postulated the existence of stem cells in adult organs that are capable of recapitulating the entire organ [1]. By definition, an adult stem cell is a cell from a given organ that is capable of indefinite replicative potential and that possesses the ability to both self-renew and differentiate into the cellular components of that organ. The existence of adult stem cells in mammary tissue was elegantly demonstrated many decades ago through limiting dilution transplantation experiments, in which clonal progenitors generated complete, functional mammary outgrowths containing ductal, alveolar, and myoepithelial cells when transplanted into the cleared mammary fat pads of recipient mice [2]. Subsequently, other researchers extended this idea by demonstrating that samples taken from any portion of the mammary gland were able to give rise to mammary epithelial outgrowths, with complete developmental capacity, independent of age and developmental stage [3]. This impressive renewal capacity has been ascribed to the function of a multipotent mammary gland stem cell population that resides and persists throughout the mammary parenchyma. This normal stem cell population serves three important functions: to give rise to the tissues of the adult mammary gland during development, to serve as a reserve for repair in the event of tissue damage, and to allow for the enormous tissue expansion and remodeling that occurs in the mammary gland during multiple cycles of pregnancy, lactation and involution.

Prospective identification of normal and cancer stem cells

The identity of at least one group of cells in this stem cell population was revealed when Stingl and his colleagues isolated single mouse mammary epithelial cells with CD45$^-$Ter119$^-$CD31$^-$Sca-1^{low}-CD24^{med}CD49f^{high} mark, which are able to regenerate an entire mammary gland within 6 weeks in vivo while simultaneously executing up to ten symmetrical self-renewal divisions [4]. At the same time, Shackleton and colleagues showed that a single mouse mammary gland cell with Lin$^-$CD29^{hi}CD24$^+$ mark can generate a functional mammary gland [5]. Zhang et al expanded this work in the normal murine mammary gland to mammary tumors using the P53-null murine mammary cancer model. Based on limiting dilution transplantation assays they report that cells with Lin$^-$CD29^{Hi}CD24^{Hi} mark were more tumorigenic than whole population [6]. Breast cancer tumor-initiating cells (TICs) have been isolated from human breast cancer as well. Al-Hajj and colleagues purified a subpopulation of breast cancer cells with CD44$^+$ CD24$^{-/low}$Lineage$^-$ mark from patient samples and demonstrated that 100 cells from this subpopulation generated a tumor in nude mice compared to 1 million cells from the whole population [7]. Dontu and colleagues took this work a step further and found that breast cancer cells with both CD44$^+$ CD24$^{-/low}$Lineage$^-$ mark and aldehyde dehydrogenase activity assayed using a flow cytometry assay were more tumorigenic [8] and cells with either mark alone. Twenty cells with both CD44$^+$ CD24$^{-/low}$Lineage$^-$ and aldehyde dehydrogenase activity generated tumors in nude mice.

Clinical evidence of radiation resistance of TIC's

The enormous interest in the existence of TICs hinges in part on the hypothesis that these cells represent a small population of the total tumor which is responsible for tumor recurrence. The implication is that these cells existing in the bulk tumor at the time of treatment are resistant to therapy in patients who experience disease recurrence, and that targeted therapies against these cells may be more effective than current therapies that target the unselected tumor bulk (Figure 1). Examination of clinical outcome data grouped by biologic subtype supports this assertion. Analysis of gene array data from human breast tumor tissue has shown that tumors can be grouped according to similarity in expression profiles to the various cell types in normal breast tissue including the most undifferentiated basal cells [9]. Furthermore, clinical outcome correlated with the cell of origin with patients with basal tumors having the lowest overall survival in spite of optimal treatment [10]. Clinically, this suggests that the undifferentiated, basal tumors are the most resistant to therapy. Clinical data examining cohorts of patients specifically resistant to radiation are consistent with this observation. In a retrospective analysis of 470 patients with locally advanced breast cancer treated with mastectomy, axillary lymph node dissection, doxorubicin based chemotherapy and radiation, recursive partitioning analysis revealed that the highest rates of local recurrence in spite of maximal therapy were predicted by estrogen receptor (ER) negative status [11]. In patients with early stage breast cancer and low risk of local recurrence after breast conserving therapy (lumpectomy + radiation, BCT) the risk of local recurrence was higher among women with tumors of basal or Her-2-neu + cell of origin[12]. A similar analysis of 1000 patients from the Danish randomized trials which showed post-mastectomy radiation improved overall survival in high risk women, demonstrated that the survival benefit from radiation was limited to patients with receptor positive disease [13]. Thus, there is a clinical correlation that tumors without markers of luminal differentiation are clinically resistant to radiation, and numerous reports have suggested that mammary gland stem cells and cancer stem cells lack markers of luminal differentiation (reviewed in [14]).

Pre-clinical evidence of radiation resistance of TIC's

Pre-clinical data supporting the hypothesis that TICs are resistant to relevant therapies and that stem cell survival factors can mediate this resistance now extend from normal murine mammary gland progenitors to murine tumor models to human breast cancer. Understanding the signaling pathways involved in the self-renewal of both normal and cancer stem cells is an important first step towards anti-cancer therapies targeting cancer stem cells. Studies of hematopoietic, intestinal, muscle, and embryonic stem cell models have identified several key signaling pathways involved in self-renewal and maintenance of the stem cell pool (review [15]). Unsurprisingly, many of these pathways have been implicated in cancer, which is consistent with the hypothesis that dysregulation of normal stem cell self-renewal can lead to cancer initiation.

Inhibition of ß-catenin signaling in mammary alveolar progenitors leads to the inhibition of mammary development and pregnancy-induced proliferation implicating ß-catenin as a stem cell survival factor in the mammary gland [16]. We hypothesized that if Wnt/ß-cat signaling functions as a stem cell survival factor, stabilized ß-cat might enhance mammary outgrowths from transplanted cells, while inhibition of ß-cat signaling through expression of the dominant-negative construct ß-eng might inhibit or delay outgrowth. To examine the effect of the ß-cat signaling on the ability to form outgrowths, CD cells were transduced with the ß-galactosidase (control), stabilized ß-cat, and ß-eng constructs cloned into pS2 vectors previously described[16] and transplanted into the cleared fat pads of 3 week-old Balb/c mice. Eight fat pads (4 mice) were transplanted per construct. An initial biopsy (n=2 per construct) was taken for whole mount staining at 8 weeks. All mice were sacrificed by 28 weeks and all outgrowths were imbedded for pathology. All slides were reviewed with a breast pathologist with expertise in mouse mammary development.

Although small numbers, outgrowths from mice transplanted with ß-cat-transduced cells were consistently more prominent and filled a larger percentage of the fat pad (eight-week outgrowths, Figure 2). A small number of tumors developed from cells transduced with each of the three constructs by twenty weeks, however ß-cat-derived outgrowths which produced tumors developed consistently invasive, high-grade tumors, and all ß-cat derived outgrowths after 8 weeks demonstrated evidence of mammary intraepithelial neoplasia (MIN, Figure 2 - ß-cat H&E inset). In preliminary experiments, an increased survival fraction was observed in irradiated cells derived from ß-cat-induced tumors as compared to those from the control ß-galactoside transduced CD cells (data not shown).

We subsequently demonstrated that progenitor cells in the mammary gland are more resistant to clinically relevant doses of radiation than are non-progenitors, which constitute the bulk of the mammary gland, and that overexpression of the Wnt/ß-catenin pathway can enhance the radioresistance of progenitor cells [17]. In wildtype mice, this effect varies by mouse strain and is most pronounced in the radiosensitive Balb/c strain where enrichment of the progenitor population is statistically significant at 2 Gy. These experiments also demonstrate that radiation resistance in primary MECs can be altered through manipulation of the Wnt/ß-catenin stem cell survival pathway [17]. Understanding the mechanisms of resistance in normal MECs is an important step towards designing novel therapies for tumor progenitor cells.

Additional studies of the mouse mammary gland have confirmed the repopulating ability in additional populations of cells selected for expression of Stem Cell Antigen-1 (Sca1, [18, 19]) within a "side population": the latter is a flow cytometry based assay to select for stemness in cells that extrude Hoechst 33342 via a cell membrane pump [20, 21]. It can be concluded that these populations are enriched for mammary gland repopulating units. We have shown that therapeutic doses of irradiation of normal mammary epithelial cells enriched for side population and $Sca1^+$ cells, but not $lin^-CD24^+CD29^+$ cells. This suggests that the $Sca1^+$ and side population cells are resistant to radiation as selective enrichment following irradiation was a function of cell death of unmarked populations and these were observed to decrease with increasing doses of radiation (and to exhibit increased foci of DNA damage; see below) when compared to $Sca1^+$ cells [17]. In Sca1 + cells from the weakly tumorigenic murine cell line Comma-D, this effect was related to increased localization of β-catenin to the nucleus of Sca1 + cells in decreased persostance of DNA damage foci [22].

Similar findings of radiation resistance have been reported using the estrogen receptor positive breast cancer cell line MCF-7 [23]. Breast cancer cells were radiated at different doses and cultured in tumorsphere culture, in which stem/progenitor cells are preferentially selected to survive and form tumorospheres [24]. After 10–14 days, tumorspheres are counted and a survival curve is plotted. This "clonogenic assay" is the gold standard approach to assess resistance of single cells measured through the retained ability to proliferate. These authors report that MCF-7 spheres cultured in mammosphere media were enriched for $CD44^+CD24^{lo}$ marked cells and were more resistant than cells cultured in conventional adherent culture to single dose and fractionated radiation therapy based on clonogenic assays

[23]. The latter is particularly important since radiation is delivered in the clinic in fractionated doses to limit normal tissue toxicity. We have also shown that MCF-7 cells cultured as spheres and passaged to further enrich for self-renewing cells increases the radioresistance of these cells further supporting the conclusion that this is not an effect of growth factors or sphere formation alone (unpublished data). Similar to studies in murine mammary progenitors, MCF-7 progenitors (assayed as side population, SP, vs. non-side population, NSP) demonstrate marked relocalization of β-catenin after radiation selectively n progenitor cells (Figure 3).

Additional clonogenic data have been described using in vitro and in vivo murine models. Using the murine p53 null mammary gland tumor model, Zhang et al report that secondary mammospheres formed from the tumorigenic $Lin^{-}CD29^{H}CD24^{H}$ subgroup are enriched in the $Lin^{-}CD29^{H}CD24^{H}$ tumor-initiating cells, whereas cells cultured on plastic with serum are not, and treatment with increasing doses of radiation up to 6 Gy, a lethal dose for the bulk of the p53-null mammary tumor cells when plated with serum on plastic, suggested that mammospheres displayed radiation resistance[6].

Conclusion:

In conclusion, decades of data have described the existence of stem cells in the mammary gland, and recent prospective studies have identified these cells in the normal breast and breast cancer. This has greatly facilitated the study of these cells including radioresistance and targeting. We and others have demonstrated radioresistance of progenitor cells in the mouse mammary gland and TICs in human breast cancer cell lines. On the basis of our findings, we suggest that the Wnt/ß-catenin signaling pathway may be an attractive target for directed anti-stem cell therapeutics. These studies underscore the potential for treatment strategies that target pathways such as Wnt/ß-catenin that are responsible for self-renewal.

Methods:

Retroviral Transduction of CD cells

Stabilized ß-cat [25] and ß-eng constructs were cloned into the pS2 retroviral backbone (kindly provided by Aguilar-Cordova, Baylor College of Medicine, Faustinella et al., 1994) as described in Tepera et al [16]. Stabilized ß-cat and ß-eng were also cloned into the pMSCV-IRES-GFP retroviral backbone (kindly provided by Dr. Greg Hannon, Cold Spring Harbor, NY. 293T cells (ATCC) grown in Dulbecco's modified Eagles' medium (DMEM, JRH Biosciences) supplemented with 10% fetal bovine serum (JRH Biosciences), 2 mM glutamine (Sigma), and 0.05 mg/ml gentamycin (Sigma) were used as packaging cells by transiently transfecting pMSCV-ß-cat or pMSCV-ß-eng with pCL-Eco construct (Imgenex Corp). Transfection was accomplished using FuGene (Roche) according to the manufacturer's guidelines. CD cells were plated in 60 mm or 100 mm tissue culture plates. Forty-eight hrs after transfection (day 3), medium was collected from transfected 293T cells, filtered through 0.22 mm syringe filter, and applied to CD cells in a 1:1 ratio (1 plate 293T to 1 plate CD), CD cells were spun at 3,000 g in a Marathon 6K clinical centrifuge (Fisher Scientific) on a swinging platform rotor for 30 min. The retroviral supernatant was removed from CD cells and replaced with CD media: DMEM/F12 (JRH Biosciences) supplemented with 2% fetal bovine serum, 5 µg/ml gentamycin (Sigma), 10 µg/ml Insulin (Sigma), 5 µg/ml epidermal growth factor (Invitrogen). 10% fetal bovine serum, 2 mM glutamine (Sigma), 0.05 mg/ml gentamycin (Sigma), 5 mg/ml insulin (Sigma), and 0.01 mg/ml epidermal growth factor (Invitrogen). CD cells were grown for 48 hrs after transduction before harvesting. Irradiation of samples was performed 24 hrs prior to flow cytometry analysis unless otherwise stated. Cell passage was planned such that cells were 50–75% confluent at the time of irradiation. In experiments using constructs in MSCV vectors, GFP positive cells were sorted by flow cytometry into CD culture media on day 5 and subsequently passaged to obtain appropriate cell numbers for further experiments. In transplantation experiments using constructs in PS2 vectors, on day 5, cells were harvested using trypsin (5x) with EDTA for 20 min and resuspended in phosphate buffered saline (1×10^6 cells/ml) using trypan blue to exclude dead cells. 10,000 cells/per fat pad were injected into the cleared fat pads of Balb/c mice as previously described [19]. Whole mounts of mammary outgrowths from transplants were fixed with 4% paraformaldehyde and stained overnight with Carmine Alum (Sigma).

Immunofluorescence. MCF7 cells were cultured and prepared for flow cytometry using Hoescht-33342, resuspended in $HBSS^{+}$, and filtered through a 0.45-µm cell filter into polypropylene tubes (Fisher) containing 0.5 µg/mL of propidium iodide (Sigma) to exclude dead cells. Analysis and sorting were performed on a triple laser MoFlo (Cytomation, Fort Collins, CO). The Hoechst dye was excited at 350 nm, and its fluorescence measured at 450 nm/20BP filter blue and 675 nm EFLP optical filter red, as described previously [26]. Characteristic SP vs. NSP populations were sorted onto slides. The sorted cells were fixed in 4% paraformaldehyde for 15 min and stained with phospho-H2AX antibody (1:200) and a secondary fitc-conjugated anti-rabbit antibody (Molecular Probes, Carlsbad, CA). Activated ß-catenin was measured using the anti-non-phospho-ß-catenin antibody, clone 8E7 (Upstate Cell Signaling Solutions, Charlottesville, VA) and texas-red conjugated secondary. Nuclei were counterstained with 4'',6-diamidino-2-phenylindole, dihydrochloride (Vector, Burlingame, CA), and coverslips were mounted with a SlowFade light antifade kit (Molecular Probes). Images were captured at 100x using a Zeiss CCD camera.

Acknowledgements:

Frances Kittrel for expertise and assistance in mammary gland transplants and Li "Jessica" Li for immunoflurescence assistance. The Morgan Welch Inflammatory Breast Cancer Research Program and Clinic; The State of Texas Grant for Rare and Aggressive Cancers; The American Airlines Komen Foundation Promise Grant KGO81287; The University of Texas Institutional Research Grant, K12–5611B through the University of Texas Health Sciences Center from the National Institute of Health; R01CA138239–01; IRG The University of Texas M.D. Anderson Cancer Center.

References:

[1] Wilson EB. The Cell in Development and Heredity. New York: The MacMillan Company, 1928.

[2] Deome KB, Faulkin LJ, Jr., Bern HA, Blair PB. Development of mammary tumors from hyperplastic alveolar nodules transplanted into gland-free mammary fat pads of female C3H mice. Cancer Res 1959;19(5):515–20.

[3] Smith GH, Medina D. A morphologically distinct candidate for an epithelial stem cell in mouse mammary gland. J Cell Sci 1988;90 (Pt 1):173–83.

[4] Stingl J, Eirew P, Ricketson I, et al. Purification and unique properties of mammary epithelial stem cells. Nature 2006;439 (7079):993–7.

[5] Shackleton M, Vaillant F, Simpson KJ, et al. Generation of a functional mammary gland from a single stem cell. Nature 2006;439 (7072):84–8.

[6] Zhang M, Behbod F, Atkinson RL, et al. Identification of tumor-initiating cells in a p53-null mouse model of breast cancer. Cancer Res 2008;68(12):4674–82.
[7] Al-Hajj M, Wicha MS, Benito-Hernandez A, Morrison SJ, Clarke MF. Prospective identification of tumorigenic breast cancer cells. Proc Natl Acad Sci U S A 2003;100(7):3983–8.
[8] Ginestier C, Hur MH, Charafe-Jauffret E, et al. ALDH1 is a marker of normal and malignant human mammary stem cells and a predictor of poor clinical outcome. Cell Stem Cell 2007;1(5):555–67.
[9] Sorlie T, Perou CM, Tibshirani R, et al. Gene expression patterns of breast carcinomas distinguish tumor subclasses with clinical implications. Proc Natl Acad Sci U S A 2001;98 (19):10869–74.
[10] Shin BK, Lee Y, Lee JB, et al. Breast carcinomas expressing basal markers have poor clinical outcome regardless of estrogen receptor status. Oncology reports 2008;19(3):617–25.
[11] Woodward WA, Strom EA, Tucker SL, et al. Locoregional recurrence after doxorubicin-based chemotherapy and postmastectomy: Implications for breast cancer patients with early-stage disease and predictors for recurrence after postmastectomy radiation. International journal of radiation oncology, biology, physics 2003;57 (2):336–44.
[12] Nguyen PL, Taghian AG, Katz MS, et al. Breast cancer subtype approximated by estrogen receptor, progesterone receptor, and HER-2 is associated with local and distant recurrence after breast-conserving therapy. J Clin Oncol 2008;26(14):2373–8.
[13] Kyndi M, Sorensen FB, Knudsen H, Overgaard M, Nielsen HM, Overgaard J. Estrogen receptor, progesterone receptor, HER-2, and response to postmastectomy radiotherapy in high-risk breast cancer: the Danish Breast Cancer Cooperative Group. J Clin Oncol 2008;26 (9):1419–26.
[14] Regan J, Smalley M. Prospective isolation and functional analysis of stem and differentiated cells from the mouse mammary gland. Stem cell reviews 2007;3(2):124–36.
[15] Yamashita YM, Fuller MT, Jones DL. Signaling in stem cell niches: lessons from the Drosophila germline. J Cell Sci 2005;118(Pt 4):665–72.
[16] Tepera SB, McCrea PD, Rosen JM. A beta-catenin survival signal is required for normal lobular development in the mammary gland. J Cell Sci 2003;116(Pt 6):1137–49.
[17] Woodward WA, Chen MS, Behbod F, Alfaro MP, Buchholz TA, Rosen JM. WNT/beta-catenin mediates radiation resistance of mouse mammary progenitor cells. Proc Natl Acad Sci U S A 2007;104 (2):618–23.
[18] Welm B, Behbod F, Goodell MA, Rosen JM. Isolation and characterization of functional mammary gland stem cells. Cell Prolif 2003;36 Suppl 1:17–32.
[19] Welm BE, Tepera SB, Venezia T, Graubert TA, Rosen JM, Goodell MA. Sca-1(pos) cells in the mouse mammary gland represent an enriched progenitor cell population. Dev Biol 2002;245(1):42–56.
[20] Hirschmann-Jax C, Foster AE, Wulf GG, et al. A distinct "side population" of cells with high drug efflux capacity in human tumor cells. Proc Natl Acad Sci U S A 2004;101(39):14228–33.
[21] Kondo T, Setoguchi T, Taga T. Persistence of a small subpopulation of cancer stem-like cells in the C6 glioma cell line. Proc Natl Acad Sci U S A 2004;101(3):781–6.
[22] Chen MS, Woodward WA, Behbod F, et al. Wnt/beta-catenin mediates radiation resistance of Sca1 + progenitors in an immortalized mammary gland cell line. J Cell Sci 2007;120(Pt 3):468–77.
[23] Phillips TM, McBride WH, Pajonk F. The response of CD24(-/low)/CD44 + breast cancer-initiating cells to radiation. Journal of the National Cancer Institute 2006;98(24):1777–85.
[24] Dontu G, Abdallah WM, Foley JM, et al. In vitro propagation and transcriptional profiling of human mammary stem/progenitor cells. Genes Dev 2003;17(10):1253–70.
[25] Montross WT, Ji H, McCrea PD. A beta-catenin/engrailed chimera selectively suppresses Wnt signaling. J Cell Sci 2000;113 (Pt 10):1759–70.
[26] Goodell MA, Brose K, Paradis G, Conner AS, Mulligan RC. Isolation and functional properties of murine hematopoietic stem cells that are replicating in vivo. J Exp Med 1996;183(4):1797–806.

Figure Legends:

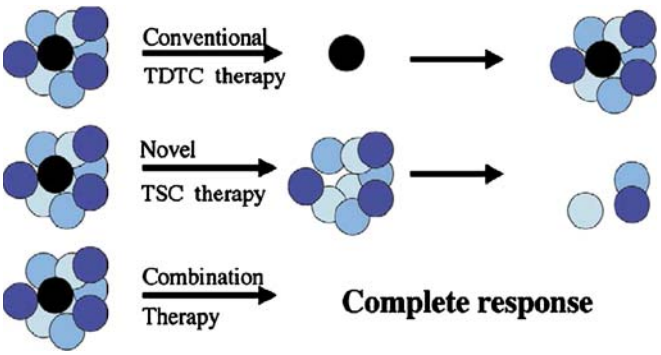

Figure 1.

Cancer therapy that does not kill tumor stem cells may provide gratifying initial results but ultimately result in recurrence. Conventional therapies target proliferating, terminally differentiated cells, may leave tumor stem cells, which could lead to recurrence. Ideally, tumor stem cell therapies would specifically target tumor stem cells, and used alone might lead to tumor regression, but may not dissolve tumor bulk leading to questions regarding response rates and potentially untreated tumor-related symptoms. Combining conventional therapy with treatment targeting tumor stem cells may lead to effective elimination of both tumor bulk as well as tumor stem cells that might otherwise lead to recurrence. (Reprinted with permission from [22]).

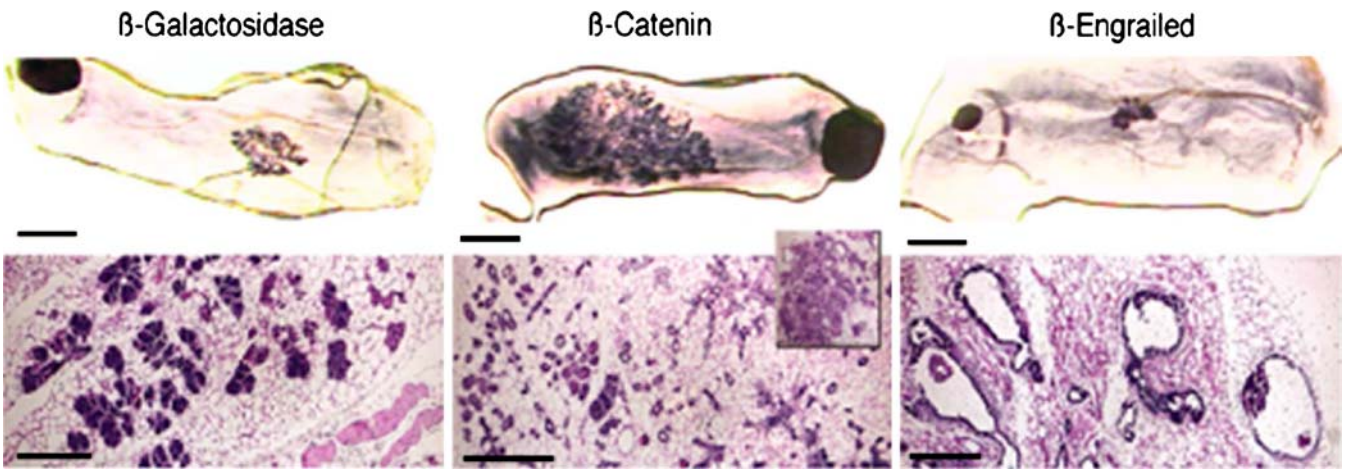

Figure 2.

Stabilized ß-catenin expression promotes mammary outgrowths from transplanted CD cells. (A) CD cells transduced with ß-galactosidase (control), ß-catenin, or ß-engrailed were transplanted into cleared mammary fat pads of Balb/c mice. Outgrowths were taken from two glands per group, stained for whole mounts with Carmine Alum (top, scale bar= 5 mm.) and stained for pathology with hemotoxylin and eosin (bottom).

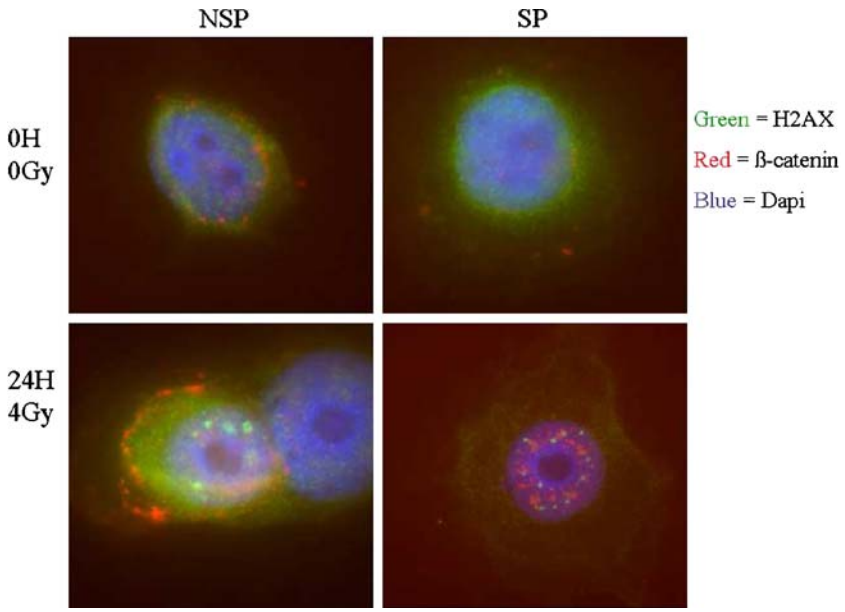

Figure 3.

Differences in ß-catenin localization between SP and NSP subpopulation. Immunostaining for active, non-phosphorylated ß-catenin in SP and NSP cells 24 hours after 0 Gy (mock radiation) and 4 Gy. ß-catenin is visualized in red, and the nuclei are stained with DAPI in blue. DNA double strand break foci are visualized in green with γ-H2AX antibody. Images were captured by deconvolution microscopy using a Zeiss AxioVert S100 TV microscope and a DeltaVision restoration microscopy system (Applied Precision, Inc.).

BI-RADS 3 – probably benign lesions on MR-Mammography in genetic high-risk women

Wunderlich P.
Department of Diagnostic Radiology, Technical University, Dresden, Germany

Purpose: Lifetime risk for developing breast cancer is significantly increased among women with an inherited predisposition to breast cancer. For these women surveillance programs including annual mammography and MR imaging are meanwhile recommended management options. MR-mammography is a very sensitive method that can detect cancers that are otherwise occult. However use of

breast MR imaging can cause disadvantageous effects like benign biopsies. Furthermore it may lead to short-term follow up examinations of MR-detected probably benign findings, which causes anxiety, takes time and costs. Purpose of our study was the evaluation of findings scored as BI-RADS 3 (probably benign) on MR-Mammography in an intensified breast cancer screening program for women at risk of familial breast cancer.

Material und Methods: Our prospective trial included 75 asymptomatic women within the observation period, from November 1, 1999 through October 31, 2007. The population included women with proven mutation of the BRCA 1-gene (n=13), BRCA 2-gene (n =5), heterozygous risk of ≥ 20% or lifetime risk for developing breast cancer of ≥ 30% (n=57), respectively. The study protocol consisted of 6-monthly clinical examination as well as ultrasound and yearly mammography and contrast enhanced MR-mammography. In the program surveillance is offered to women at an age of 25 years or at an age 5 years younger than that at which the youngest family member was found to have breast cancer, but mammography not before age 30. MR-mammography in general stops at an age of 55 years; the mammographic parenchymal density was recorded almost entirely fatty (type 1) or mildly dense (type 2), respectively. These criteria are established by the German Consortium for Hereditary Breast and Ovarian Cancer. We reviewed the examinations of 67 eligible women, in whom MR imaging was as an integrated part of the surveillance program. MR-mammography examinations were performed with the patient prone in a 1,5 T system using a dedicated bilateral surface breast coil. Our imaging sequence includes T2-weighted sequence, followed by a dynamic T1-weighted three dimensional gradient-echo sequence with an intravenous administration of gadolinium-containing contrast medium (0,1 mmol/kg body weight). Menopausal status was premenopausal in 57 and postmenopausal in 10 women. Mean age at first screening round was 40±10 years. Whenever possible, the examination was performed between day 6 and 16 of the menstrual cycle. Based on personal history four women were under HRT, in whom cessation of medication was performed 4–6 weeks before MR imaging. The results of MR imaging were scored in a standardized way, according the Breast Imaging Reporting and Data System (BI-RADS®) classification. For each imaging method we used a cut-off level of BI-RADS 4. Results were scored positive, when the finding was classified BI-RADS 4 or higher.

Results: On MR-Mammography probably benign abnormalities were found in 23 of 67 (34%) women. Detection rate of BI-RADS 3 findings were highest in the first screening round. The majority of the findings were characterized as foci or small (≤ 10 mm), well-circumscribed homogeneous masses. No lesion exhibited wash-out on kinetic analysis. Ultrasound revealed correlate findings in four cases, which were scored just as probably benign. In our evaluation none of the probably benign MR findings exhibited a correlate on mammography or ultrasound that was scored positive. Furthermore results of clinical examination were negative in the correlating area. One woman had a subsequent percutaneous biopsy. Histology revealed fibrocystic changes with fibroadenomatosis. In this case and all remaining women follow up studies were performed at a median of 26 months (range, 6–78). No cancer was found in an area previously interpreted as probably benign during the observation period. No finding showed progression during follow-up. Five lesions resolved on subsequent examinations, all in premenopausal women, interpreted as hormonal changes.

Conclusion: MR-mammography is a valuable method in screening genetic high-risk women, but it can generate short term examinations and benign biopsies due to probably benign findings. As expected, prevalence of probably benign findings was highest in the first screening round lacking previous imaging. Premenopausal status is a factor associated with probably benign findings due to variable, hormone induced enhancement. Biopsy rate was low and no lesion turned out to be cancer on biopsy or follow-up. Based on our data also in genetic high-risk women short term follow-up seems to be reasonable for probably benign MR findings, provided clinical examination, mammography and ultrasound are scored negative.

Indication and value of additional MRM in a big routine clinic in China

Fan Yang, Xiang-Quan Kong, Gan-Sheng Feng
Radiology Department, Union Hospital Wuhan, 430022/ Wuhan, China

Background
The mortality and incidence of breast cancer are high in Western countries and relatively low in China and other parts of Asian countries. In China the mortality of breast cancer has gradually been increasing, and is much higher in urban areas than in non-urban areas. Due to the double effects of both increasing risk factors and population growth and ageing, breast cancer will be one of the most extensively increasing cancers in Chinese women. The prevention and control of breast cancer will be of great emphasis for future. MR-Mammography (MRM) is becoming recognized as an indispensable adjunct to mammography and ultrasound. It has been available for over a decade in most Chinese big Clinics.

Purpose
To evaluate the indication and value of MRM in Chinese patients.

Methods and Material
This retrospective study included a total of 376 patients (mean age, 46.0 years ± 13.6 [SD]; range, 19–78 years) who had MRM examination(s) in our hospital from 2007 to 2009. Among them 125 patients were confirmed by histology. MRM examinations were performed on 1.5 T systems by using the standard dedicated bilateral breast coils. The MRM protocols included dynamic T1WI series and a T2WI TSE sequence. Indications for MRM fall into the following categories: screening, diagnosis, staging of carcinoma, treatment monitoring and evaluation of augmented breast.

Result
Index tumor was identified in 122/125 patients. Sensitivity in detection of index lesion was 98% for MRM. There were 23 patients(6.1%) for screening examination(8 patients at high risk and 15 asymptomatic patients). 210(55.9%) patients with suspicious lesion at other examinations underwent MRM for diagnosis issue, most of these patients were with dense breasts or suspicious calcification lesions. 39 patients(10.4%) with new diagnosis of breast cancer were evaluated for the extent of tumor involvement or multifiocal lesions. 59 patients (15.7%) on neoadjuvant chemotherapy came to monitor response the chemotherapy. 45(12.0%) patients came for augment evaluation.

Conclusions
MRM is now a clinical reality in China. It can contribute valuable and decisive information to the evaluation of breast disease. This is particularly true in dense breasts which were the common breast pattern of Chinese women. The high cost of MRM and limited adoption of breast conserving therapy were the main limitations for MRM practice in China.

Can MR imaging rule out malignancy associated with borderline (B3) lesions diagnosed at core needle biopsy?

Chiara Zuiani, Anna Linda, Viviana Londero, Massimo, Bazzocchi

Core needle biopsies (CNB) using stereotactic mammography or ultrasound guidance are commonly performed as the initial diagnostic approach to nonpalpable breast lesions. Although the subsequent management of patients with invasive cancer, ductal carcinoma in situ (DCIS), and most benign lesions diagnosed on CNB specimens is straightforward, certain nonmalignant lesions – borderline lesions or lesions of uncertain malignant potential (B3 core histology) pose dilemmas with regard to the most appropriate clinical management following CNB (1–5).

Borderline histology spectrum is a heterogeneous group of lesions which includes papillary lesions (PL), lobular neoplasia (LN), atypical ductal hyperplasia (ADH), radial sclerosing lesions (RSL), fibroepithelial lesions, mucocele-like lesions and columnar cells lesions (6). The frequency of B3 core histology has been increasing over the last several years as a result of the widespread diffusion of screening programs, availability of imaging techniques able to detect very subtle findings, and extensive use of percutaneous CNB for the initial evaluation of clinically occult breast lesions. B3 core needle histology accounts for about 4–9% of all CNB results, according to recent reports (5, 7–10). The distribution of lesion categories within the borderline spectrum varies between institutions; however, ADH, LN, PL and RSL are those that are more frequently encountered (7–10). These lesions are considered unreliable percutaneous diagnoses because of the risk of being upgraded to malignancy at surgical excision. In a large, comprehensive series, (7) about one-third of borderline lesions on CNB proved to be malignant (35.1% or 29.9%, based on excision histology or based on excision or follow-up, respectively). In addition, the Authors of this report made the point that lesion-related likelihood of malignancy is variable: lesions categorized on CNB as ADH or LN are associated with a significantly higher probability of cancer as an outcome relative to PL and RSL. A more recent paper reported a 20% malignancy underestimation rate among 523 B3 lesions detected by mammographic screening (10). However, most of articles regarding these lesions reported very variable overall and specific underestimation rates an are based on small, single-institution studies that are retrospective and have inherent built-in selection bias.

Therefore, at present there are insufficient data to draw any definitive conclusions on the appropriate management (surgical excision versus follow-up) of these lesions.

As a consequence, the treatment of patients with these lesions varies even within patients of the same hospital and institution depending on the respective physicians (11).

The major advantage of surgical excision over follow-up is that it provides immediate definitive diagnosis; however, it is more expensive and it causes scarring on subsequent mammograms. On the other hand, the potential disadvantage of follow-up is that the patients might be lost.

Several authors have tried to identify imaging and histopathological features useful to predict the likelihood of malignancy, in order to select cases in which surgical excision may not be necessary (12–15). However, no clinical nor imaging nor biopsy feature alone or in combination has been demonstrated to correctly identify borderline lesions with less than 2% chance of carcinoma at surgical excision, which, according to the American College of Radiology recommendations (16) can be managed with short-term follow up.

MR imaging is a powerful tool in breast imaging, that is now used in academic centers as well as community hospitals. Breast MRI has very high sensitivity for the detection both of invasive (17) and non-invasive breast carcinomas (18–21). It is well known that some cancers may not be visualized readily because they are very small in size or because of a diffuse pattern of spread; however, because of improvement in spatial resolution (high spatially resolved dynamic protocols, 3T magnetic fields) and increasing awareness of non-classic malignant patterns shown by some tumor histotypes (non-mass-like enhancement, progressive enhancement), many cancers occult at MRI in the past may be more easily detected today. This results in improvement in the negative predictive value of breast MRI in the clinical practice.

As lack of enhancement has been shown to be a strong predictor of benignity (22), it might be assumed that breast MRI can be of value in the evaluation of B3 lesions, in particular in excluding the association with malignant foci.

Before discussing the possible applications of breast MRI to this clinical setting, we will review the MRI appearances of the most frequently encountered borderline lesions (papillomas, LN, ADH and RSL) when they are not associated with malignancy, based on the few reports published in the literature and on our own experience.

MRI APPEARANCE OF BORDERLINE LESIONS

MRI patterns of presentations of papillomas have been well described (23–26). In particular, Daniel and coworkers (23) revealed three MRI appearances for papillomas. These include: 1) “small lumenal mass” papillomas, which are small, smooth enhanced masses that are connected to the nipple by an enlarged duct (**Fig. 1a**); 2) “tumor-like” papillomas, which have morphologic findings that are suspicious of invasive malignancy (ie, irregular margins, rim enhancement, spiculation, and/or suspicious dynamic enhancement) (**Fig. 1b**); 3) “MRI-Occult” papillomas, which are invisible on MRI.

In breast MR imaging, as in mammography, there is no finding that is specific for LN and that would allow the prospective diagnosis of LN. Although little has been published about the appearance of LN on MRI (27), this lesion may appear as clumped or patchy foci of enhancement or as non-mass-like enhancement with ductal distribution, just as mastopathic changes, focal adenosis, or DCIS (**Fig.2**). The presence of mass-like enhancement should raise the suspicion of association with an invasive component.

As well as LN, ADH appearance on MRI has been poorly described (27). ADH may have MR imaging findings indistinguishable from cancer, just as it can have mammographic patterns indistinguishable from those of malignancy (**Fig.3**). According to Liberman and coworkers (27), ADH constitutes 9% of suspicious linear ductal enhancement.

RSL can show variable appearances on MRI, as well on mammography and sonography, ranging from occult lesions to spiculated lesions indistinguishable from carcinoma (28–30). In our experience, RSL visible on MRI can present as non-enhancing “architectural distortions”, reflecting their mammographic appearance (**Fig.4a**), or as spiculated, intensely enhancing masses (**Fig.4b**), overlapping invasive carcinomas.

BREAST MRI IN THE MANAGEMENT OF B3 LESIONS

Because of its capability in the identification of breast cancer and its high negative predictive value for malignancy (NPV) (22), we hypotesized that breast MRI might be able to assess the malignant potential of borderline (B3) lesions diagnosed at CNB, thus identifying those women with borderline lesions with extremely low risk of harbouring malignancy.

We performed a retrospective analysis of 3920 CNB performed in our institute over a seven-year period and identified 275 lesions diagnosed as B3. Of these B3 lesions, 94 lesions in 92 women (age range, 38–83 yr) had been assessed with MRI (1.0 or 1.5 T) within two weeks before (n=48) or after (n=46) CNB and were surgically confirmed (n=80) or followed-up for at least 24 months (n =14). These lesions constituted our study population.

Breast MR images were reviewed by two experienced breast radiologists and findings were classified using a robust multimodality score, the Fischer-Baum score (31). Lesions included in groups I, II and III were interpreted as "non-suspicious", while those in groups IV and V were considered as "suspicious", with respect to the harbouring of malignant disease. The results of histological analysis and follow-up (malignant versus benign) were considered the gold standard for comparison with the MRI findings.

Of 80 surgically excised lesions, 10 proved to be malignant, while none of the lesions that were followed-up showed interval changes. Overall, the prevalence of cancer was 10/94 (10.6%). While 9 (33.3%) of the 27 lesions classified as suspicious on MRI were malignant, only one (1.5%) of the 67 lesions classified as non-suspicious was malignant. This was the case of a 6-mm low-grade DCIS, diagnosed as an ADH at CNB, that was included in Fischer-Baum group III ("probably benign") at MRI evaluation.

Breast MRI provided a sensitivity of 90.0%, a specificity of 78.6%, a positive predictive value of 33.3% and a negative predictive value of 98.5%.

Due to its very high NPV for malignancy, breast MRI can be very useful in excluding the presence of associated malignancy in this setting. A correct identification of B3 lesions that are not associated with malignancy could direct the patients towards an imaging follow-up rather than surgical excision, thus reducing both patient's anxiety and costs related to the surgical procedure. Another advantage would be to avoid the surgical scarring, which can alter the interpretation of the following imaging studies.

Our preliminary experience indicates a potential new approach in the management of women with B3 lesions: breast MRI may identify patients with extremely low risk of harbouring malignancy for whom surgical excision could be avoided.

Prospective studies of MRI following B3 diagnosis are warranted to support these results (32).

References

1. Parker SH, Burbank F, Jackman RJ, et al. Percutaneous large-core breast biopsy: a multi-institutional study. Radiology. 1994;193:359–64.
2. Berg WA. Image-guided breast biopsy and management of high-risk lesions. Radiol Clin North Am. 2004;42:935–46.
3. Bazzocchi M, Zuiani C, Degano GP, et al. The use of automatic devices for ultrasonography-guided histologic biopsy of breast lesions. Radiol Med. 1993;86:599–602
4. Ellis IO, Humphreys S, Michell M, et al. Best Practice No 179. Guidelines for breast needle core biopsy handling and reporting in breast screening assessment. J Clin Pathol. 2004;57:897–902.
5. Schueller G, Jaromi S, Ponhold L, et al. US-guided 14-gauge core-needle breast biopsy: results of a validation study in 1352 cases. Radiology. 2008;248:406–13.
6. Jacobs TW, Connolly JL, Schnitt SJ. Nonmalignant lesions in breast core needle biopsies: to excise or not to excise? Am J Surg Pathol. 2002;26:1095–110.
7. Houssami N, Ciatto S, Bilous M, et al. Borderline breast core needle histology: predictive values for malignancy in lesions of uncertain malignant potential (B3). Br J Cancer. 2007;96:1253–7.
8. Zuiani C, Londero V, Bestagno A, et al. Proliferative high-risk lesions of the breast: contribution and limits of US-guided core biopsy. Radiol Med. 2005;110:589–602.
9. Linda A, Zuiani C, Bazzocchi M, et al. Borderline breast lesions diagnosed at core needle biopsy: can magnetic resonance mammography rule out associated malignancy? Preliminary results based on 79 surgically excised lesions. Breast. 2008;17:125–31.
10. El-Sayed ME, Rakha EA, Reed J, et al. Predictive value of needle core biopsy diagnoses of lesions of uncertain malignant potential (B3) in abnormalities detected by mammographic screening. Histopathology. 2008;53:650–7.
11. Lawton TJ, Georgian-Smith D. Excision of high-risk breast lesions on needle biopsy: is there a standard of core? AJR Am J Roentgenol. 2009;192:W268.
12. Shin HJ, Kim HH, Kim SM, et al. Papillary lesions of the breast diagnosed at percutaneous sonographically guided biopsy: comparison of sonographic features and biopsy methods. AJR Am J Roentgenol. 2008;190:630–6.
13. Londero V, Zuiani C, Linda A, et al. Lobular neoplasia: core needle breast biopsy underestimation of malignancy in relation to radiologic and pathologic features. Breast. 2008;17:623–30.
14. Ko E, Han W, Lee JW, et al. Scoring system for predicting malignancy in patients diagnosed with atypical ductal hyperplasia at ultrasound-guided core needle biopsy. Breast Cancer Res Treat. 2008;112:189–95.
15. López-Medina A, Cintora E, Múgica B, et al. Radial scars diagnosed at stereotactic core-needle biopsy: surgical biopsy findings. Eur Radiol. 2006;16:1803–10.
16. ACR breast imaging reporting and data system, breast imaging atlas. Reston (VA): American College of Radiology; 2003.
17. Peters NH, Borel Rinkes IH, Zuithoff NP, et al. Meta-analysis of MR imaging in the diagnosis of breast lesions. Radiology. 2008;246:116–24.
18. Bazzocchi M, Zuiani C, Panizza P, et al. Contrast-enhanced breast MRI in patients with suspicious microcalcifications on mammography: results of a multicenter trial. AJR Am J Roentgenol. 2006;186:1723–32.
19. Zuiani C, Francescutti GE, Londero V, et al. Ductal carcinoma in situ: is there a role for MRI? J Exp Clin Cancer Res. 2002;21:89–95.
20. Kuhl CK, Schrading S, Bieling HB, et al. MRI for diagnosis of pure ductal carcinoma in situ: a prospective observational study. Lancet. 2007;370:485–92.
21. Schouten van der Velden AP, Schlooz-Vries MS, Boetes C, Wobbes T. Magnetic resonance imaging of ductal carcinoma in situ: what is its clinical application? A review. Am J Surg. 2009 Apr 16.
22. Schnall MD, Blume J, Bluemke DA, et al. Diagnostic architectural and dynamic features at breast MR imaging: multicenter study. Radiology. 2006;238:42–53.
23. Daniel BL, Gardner RW, Birdwell RL, et al. Magnetic resonance imaging of intraductal papilloma of the breast, Magn Reson Imaging. 2003;21:887–92.
24. Krämer SC, Rieber A, Görich J, Aschoff AJ, et al. Diagnosis of papillomas of the breast: value of magnetic resonance mammography in comparison with galactography. Eur Radiol. 2000; 10:1733–6.
25. Francis A, England D, Rowlands D, et al. Breast papilloma: mammogram, ultrasound and MRI appearances. Breast. 2002;11:394–7.
26. Rovno HD, Siegelman ES, Reynolds C, et al. Solitary intraductal papilloma: findings at MR imaging and MR galactography. AJR Am J Roentgenol. 1999;172:151–5.
27. Liberman L, Morris EA, Dershaw DD, et al. Ductal enhancement on MR imaging of the breast. AJR Am J Roentgenol. 2003;181:519–259.

28. Pediconi F, Occhiato R, Venditti F, et al. Radial scars of the breast: contrast-enhanced magnetic resonance mammography appearance. Breast J. 2005;11:23–8.
29. Perfetto F, Fiorentino F, Urbano F, et al. Adjunctive diagnostic value of MRI in the breast radial scar. Radiol Med. 2009 May 30.
30. Kuhl CK. Concepts for differential diagnosis in breast MR imaging. Magn Reson Imaging Clin N Am. 2006;14:305–28.
31. Baum F, Fischer U, Vosshenrich R, et al. Classification of hypervascularized lesions in CE MR imaging of the breast. Eur Radiol. 2002;12:1087–92.
32. Sardanelli F, Houssami N. Evaluation of lesions of uncertain malignant potential (B3) at core needle biopsy using magnetic resonance imaging: a new approach warrants prospective studies. Breast. 2008;17:117–9.

IMAGE LEGEND

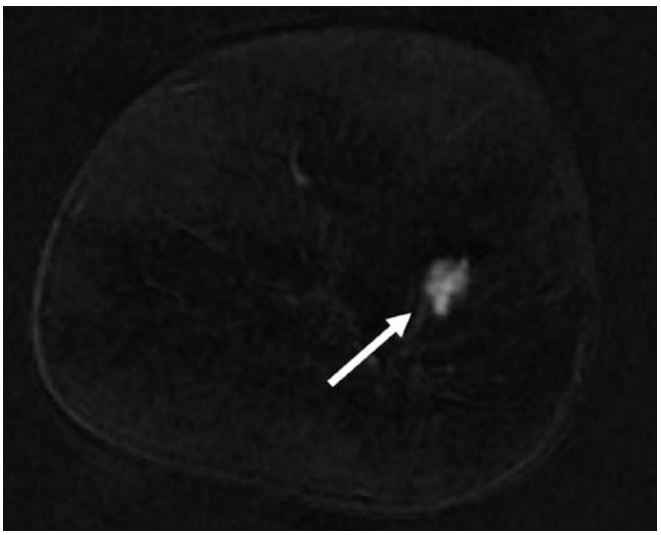

b)FLASH T1 enhanced MRI subtracted image demonstrates an irregular intensely enhancing mass in the outer quadrants of the left breast (arrow). Sonographically-guided core-needle-biopsy diagnosis was benign papilloma and it was confirmed at surgical excision.

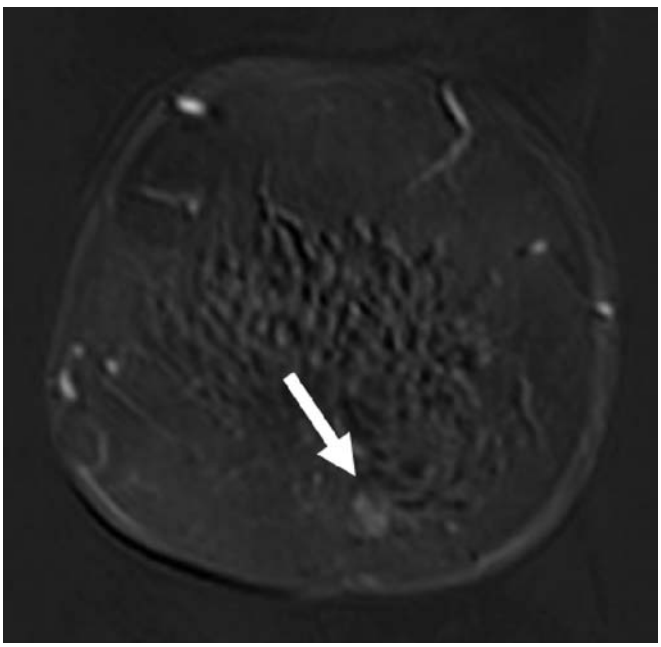

Figure 1. Benign papillomas. a)FLASH T1 enhanced MRI subtracted image demonstrates a small well-defined slightly enhancing mass in the lower quadrants of the left breast (arrow). Sonographically-guided core-needle-biopsy diagnosis was benign papilloma and it was confirmed at surgical excision.

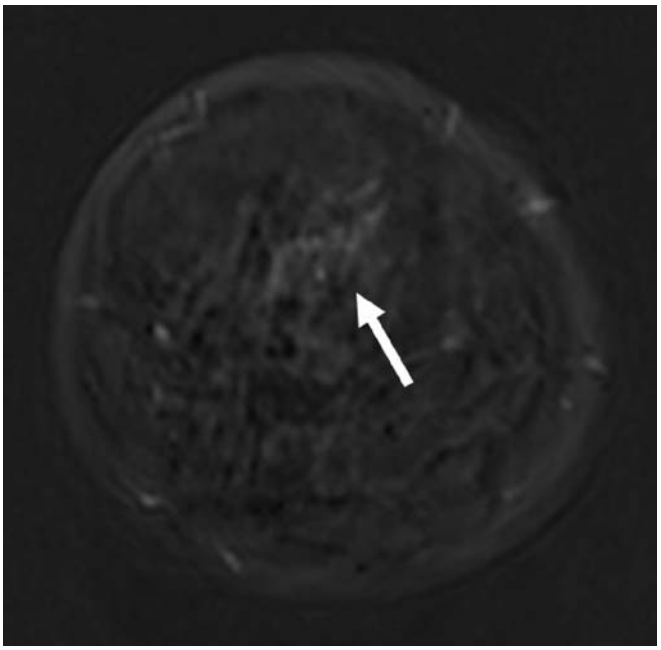

Figure 2. Lobular neoplasia.FLASH T1 enhanced MRI subtracted image shows mild, non-mass-like enhancement in the upper quadrants of the left breast (arrow). Sonographically-guided core-needle-biopsy demonstrated lobular neoplasia. The diagnosis was confirmed at subsequent surgical excision.

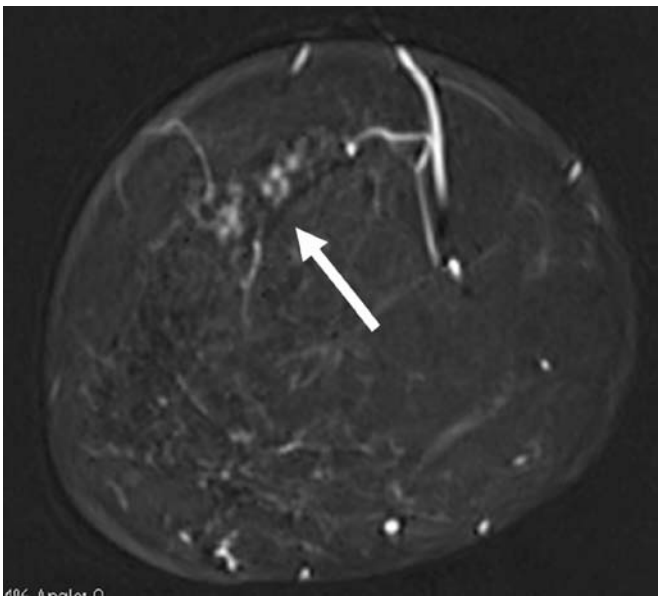

Figure 3. Atypical ductal hyperplasia.FLASH T1 enhanced MRI subtracted image shows clumped, non-mass-like enhancement in the upper-outer quadrant of the right breast (arrow). Stereotactically-guided vacuum assisted biopsy of powdery calcifications in the same area demonstrated atypical ductal hyperplasia. The diagnosis was confirmed at subsequent surgical excision.

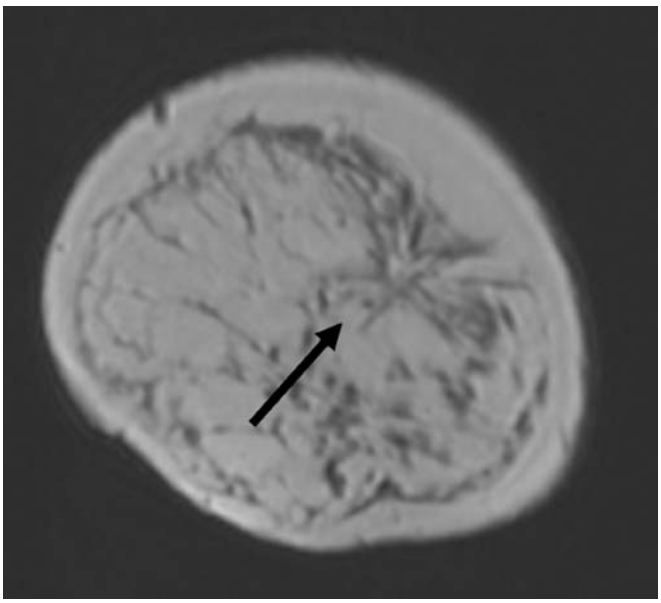

Figure 4. Radial sclerosing lesions. a) FLASH T1 non-enhanced MRI image demonstrates an area of architectural distortion in the upper-outer quadrant of the left breast (arrow). Stereotactically-guided vacuum-assisted biopsy diagnosis was radial sclerosing lesion and it was confirmed at surgical excision.

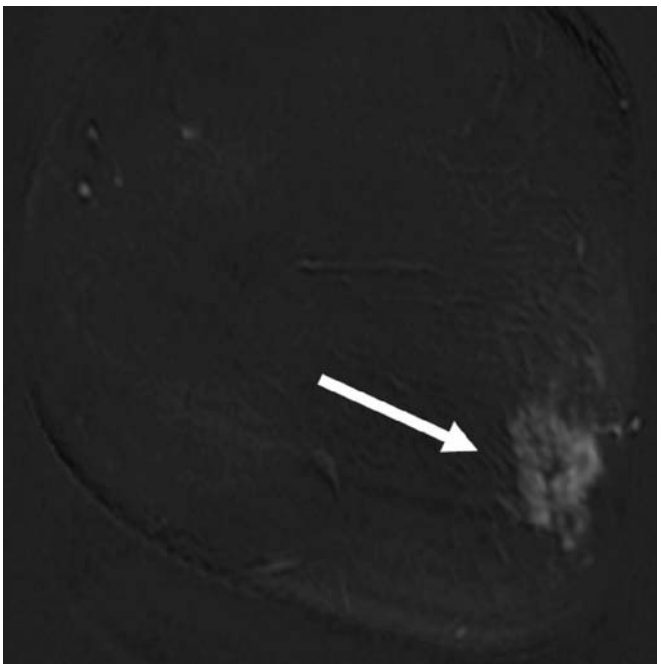

b) FLASH T1 enhanced MRI subtracted image demonstrates an area of irregular, heterogeneously and intensely enhancement in the lower-outer quadrant of the left breast (arrow). Sonographically-guided core-needle-biopsy diagnosis was radial sclerosing lesion and it was confirmed at surgical excision.

POSTER

Impact of CAD in Breast MRI: Prediction of disease-free Nipple–Areola Complex in Patients with extended DCIS

A Artmann[1], N A Böhm[1], I Lämmer-Skarke[1], S Paepke[2], M Kiechle[2], E J Rummeny[1]
[1]Department of Diagnostic Radiology—Section Breast Imaging, Technical University Munich, Germany
[2]Department of Obstetrics and Gynecology, Technical University Munich, Germany

Correspondence author:
Dr. Almut Artmann, MD, Institute for Diagnostic Radiology, Imaging and Interventional Breast Diagnosis, Klinikum r.d.Isar, TU München, Ismaningerstr. 19, 81675 Munich, Tel. +49 89 4140 6731, Fax +49 89 4140 6732, almut.artmann@lrz.tum.de

key words: Breast cancer, DCIS, MRI, CAD, skin-sparing mastectomy

Purpose
An important assumption for skin-sparing mastectomy (SSM), a surgical option in selected patients with extended ductal carcinoma in situ (DCIS) is a disease-free nipple–areola complex (NAC). Breast MRI can be used to exclude patients with disease in ductal tissue behind the NAC. The purpose of this study was to evaluate the impact of computer-aided detection (CAD) as an additional diagnostic tool in the prediction of preoperative tumour extension with respect to the NAC.

Method and Materials
41 patients with extended DCIS underwent 3D (Gd)-enhanced 1.5T MR mammography preoperatively using a T1-w FLASH pulse sequence. Two radiologists assessed the images in consensus reading for non-mass enhancement with segmental or ductal distribution. According to the enhancement distance towards the NAC 3 groups were defined: (1) NAC reached; (2) ≥4–6 mm (intraoperative assessment of surgical margins required); (3) ≥6 mm (disease-free). Histopathological analysis served as standard of reference.

Results
Contrast uptake was ductal in 81% and segmental in 19%. Without CAD 3 false-positive cases for retroareolar tumour involvement were found in group (1). Disease-free NAC was found in 10/41 (2); 28/41 were categorized in group 3. With additional CAD 21/41of this subgroup was classified as (2). The CAD findings evaluated more accurate the tumour extension and diameters in correlation with the microscopic margins of resection.

Conclusion
Preoperative MRI including CAD enables detailed evaluation of the subnipple ductal tissue and prediction of disease-free NAC. This breast imaging modality is important for the preoperative decision making between prophylactic mastectomy and skin sparing mastectomy in patients with extended DCIS.

Clinical Relevance/Application
For the oncological safety of SSM Breast MRI with additional CAD can show NAC involvement, an important assumption of surgical planning in breast cancer patients.

A new signal enhancement index for DCE-MRI and methods for its implementation in breast imaging at 3T

C.A. Azlan, T.S. Ahearn, P. Di Giovanni, S.I. Semple, F.J. Gilbert, T.W. Redpath
Aberdeen Biomedical Imaging Centre, University of Aberdeen, Scotland, UK, azlan.ahmad@abdn.ac.uk

Purpose
To develop and evaluate a new method of measuring signal enhancement due to contrast agent uptakes that is independent of native-T1 (T_{10}) and to assess its implementation methods in breast dynamic contrast-enhanced (DCE)-MRI at 3T.

Methods and Materials
We introduced a new enhancement index (ER_{PD}) which is normalised to the pre-contrast proton density signals (S_{PD}), $ER_{PD}=(S_{POST}-S_{PRE})/S_{PD}$, where S_{PRE} and S_{POST} are pre and post-contrast signal intensities in the tissue. The index was compared with common index in DCE-MRI i.e. enhancement ratio (ER) [$ER=(S_{POST}-S_{PRE})/S_{PRE}$]. To minimise the effect of B1 transmission-field inhomogeneity at 3T, a saturation recovery snapshot-FLASH (SRSF) sequence was employed. We used computer simulations and phantom experiments to evaluate this new technique.

Results
It was found that ER is significantly influenced by T_{10}. However, ER_{PD} is much less influenced by this factor. By using FLASH, ER_{PD} is affected by B1-field inhomogeneity. This effect was reduced when SRSF was employed.

Conclusion
ER_{PD} is much less affected by T_{10} as the ER. This new index may provide better representation of contrast agent uptake in DCE-MRI of the breast. ER_{PD} errors due to B1 transmission-field inhomogeneity at 3 T can be minimised by using SRSF sequence.

Assessment of Image Registration for Follow-up MR Mammography

Tobias Böhler[1], Ulrich Bick[2], Horst K. Hahn[1]
[1]Fraunhofer MEVIS, Universitätsallee 29, 28359 Bremen, Germany
[2]Charité Universitätsmedizin, Institut für Radiologie, 10098 Berlin, Germany

Introduction
Joint analysis of MRI and additional sequences acquired after a specific period of time is still a novel field of research. Commonly, such an analysis is referred to as follow-up analysis. While short dynamic sequences already allow an estimation of lesion malignity through the observation of contrast-agent enhancement or fat-saturated images, the ambition of follow-up imaging goes beyond that. In particular, follow-up analysis might be useful for the detection of malignant cancers when they are graded as "probably benign", or when uncertainty with respect to grading remains. Typically, these are classified as BI-RADS category 3 [2, 7]. Consequently, the number and costs of unrequired biopsies might be reduced if the follow-up diagnostics allow successful detection by regular surveillance [2, 3, 7]. However, breast biopsy remains the ultimate investigative procedure for suspicious lesions [11].
For conventional X-ray mammography (MG), the study of short-term follow-up images after 12-month intervals was shown to have a rather low sensitivity compared to other diagnostic examinations [1]. However, there is no general protocol for such examinations, e.g., the temporal intervals might vary in length [1–2]. As opposed to X-ray mammography, the role of diagnostic follow-up imaging for breast MRI remains an open question. Follow-up MRI have been used complementarily to MG for long-term classifications of lesions over several years time [4], or to detect potential recurrent diseases [6]. Short-term analysis of MRI has been regularly applied to the assessment of interventional or medicamentous treatment of lesions [5, 10, 14]. Employing retrospective follow-up imaging, it was shown that additional MRI examination allow the detection of contralateral breast cancers [13] and for early-cancer patients might even lead to changes in treatment planning and management [12]. Moreover, a review of different follow-up schedules has been published [15].
The three-dimensional acquisition of MR images allows to establish accurate spatial correlation between images. Whereas it is often tedious to relate image regions between follow-up X-ray mammographies, region-correlations can be computed automatically for MR images, for instance to compensate patient motion [8]. Such methods are potentially capable to establish correspondence between images at substantially different time points in follow-up diagnostics. Furthermore, since MR images retain the full 3-D spatial information, these images might even be co-registered to other mammographic modalities, such as ultrasound or conventional MG. Inter-modality analysis was found to be highly beneficial if employed for instance in a screening setting for high-risk patients [9, 10].

In contrast to diagnostics, the automatic deformable image registration of follow-up breast MR images is still an unresolved issue. In this paper, we overview the challenges and potential solutions, and discuss image registration results.

Methods

Application of follow-up image registration is a sequential procedure including various subtasks. The MRI data was acquired on four different MR systems (Siemens Magnetom and Symphony Vision, Avanto, Sonata). For some datasets, different scanners and protocols for the original and follow-up images have been employed, therefore fields-of-view (FOVs) and parametric settings varied immensely, along with signal-to-noise-ratios, coil inhomogeneities and presence of MR artifacts. For example, some images focused only on selected FOVs, while other images covered the whole breast. Overall 20 breast image registrations were performed with follow-up data from 17 patients.

As a precursor to registration, the left and right breasts were separated to allow independent and larger displacements and deformations. For the initial assessment, we divided each MR image by splitting along the image centerline. While less accurate than dedicated cropping [16], such a division proved to be sufficient during our preliminary evaluation and first, qualitative assessment. As the reference for our registration, we selected the follow-up image, whereas the original image was taken as the template image to register and transform.

Besides local tissue variations, the images were generally considerably dislocated with respect to MRT device coordinates, resulting from a different placement of the patient at both acquisitions. This issue was more prominent when different MR scanners had been employed for the acquisition. Consequently, after cropping the images an initial linear image registration was performed, incorporating translation, rotation and non-isotropic scaling. No shear component of the affine-linear transformation was computed in order to avoid geometric distortions. Registration was achieved by minimizing the normalized cross-correlation coefficient using a Levenberg–Marquardt optimizer [17]. Purpose of the linear registration was the adjustment of initial positions and compensation of substantial volume differences.

Subsequently, a linear-elastic image registration was performed on the pre-registered images to compensate for tissue variations caused by unequal compression and patient movement [8]. Template and reference images were selected identically to the linear registration. An intensity-based sum-of-squared distances measure was selected in order to achieve maximum correspondence of image intensities [17]. Explicit linear-elastic regularization was performed in each iteration. Unlike motion correction for dynamic MRI, we employed smaller regularization kernels and no volume-constraint in order to compensate larger deformations.

Results

For the preliminary assessment, registration results were compared qualitatively using an overlay of reference and template images in different color schemes. In addition, an alternating, checkerboard-like view was employed.

Visual inspection of our registration results revealed that the proposed procedure is able to successfully co-register follow-up and original time points, and the registration converged for all 20 cases. However, registration results for individual datasets were considerably different: For two cases, substantial tissue deformation and increase in volume had taken place during the follow-up interval, so that the linear image registration failed to correctly estimate the displacement. As a consequence, the elastic correction was mislead by a wrongly placed initial positioning and therefore matched uncorrelated breast regions.

On the other hand, the proposed method produced promising results for different datasets, even for pronounced large deformations. The non-linear image registration successfully compensated major elastic tissue deformations, facilitating a comparison of images.

Discussion

Our initial assessment demonstrated the applicability of the proposed combination of methods for follow-up registration. In particular, the individual linear registration of breasts proved to be often already sufficient to establish rough spatial correspondence between images. This technique might be exploited in order to synchronize diagnostic hangings. On the other hand, the linear registration failed for a some images, rendering the elastic registration invalid as well. Probably the major challenge of follow-up registration is the adjustment of the elastic transformation to sufficiently compensate breast deformations and retain diagnostically significant tissue changes. In addition, implementation issues concerning the cropping of breasts and the application of multiple image transformations need to be engaged.

On summary, automated image registration of follow-up data is feasible using customized image processing and registration methods. Our evaluation indicates that linear image registration alone already reduced the predominant image displacements. Subsequent non-linear image registration further reduced tissue deformations and allowed an accurate comparison of images. We are currently investigating breast deformation characteristics and corresponding biomechanical models in order to improve understanding and compensation of local tissue changes, as well as quantitative evaluation methods.

References

[1] E. J. Aiello Bowles et al.: Accuracy of Short-Interval Follow-Up Mammograms by Patient and Radiologist Characteristics, AJR, vol. 190(5), pp. 1200–1208, 2008.

[2] X. Varas, F. Leborgne, J. H. Leborgne: Nonpalpable, Probably Benign Lesions: Role of Follow-Up Mammography, Radiology, vol. 184(2), pp. 409–41, 1992.

[3] E. A. Sickles: Periodic Mammographic Follow-up of Probably Benign Lesions: Results in 3,184 Consecutive Cases, Radiology, vol. 179(2), pp. 463–468, 1991.

[4] C. K. Kuhl et al.: Dynamic Breast MR Imaging: Are Signal Intensity Time Course Data Useful for Differential Diagnosis of Enhancing Lesions?, Radiology, vol. 211(1), pp. 101–110, 1999.

[5] C. K. Kuhl et al.: Breast MR Imaging Screening in 192 Women Proved or Suspected to be Carriers of a Breast Cancer Susceptibility Gene: Preliminary Results, Radiology, vol. 215(1), pp. 267–279, 2000.

[6] A. Rieber et al.: Value of MR Mammography in the Detection and Exclusion of Recurrent Breast Carcinoma, Journal of Computer Assissted Tomography 1997, vol. 21(5), pp. 780–784.

[7] X. Varas et al.: Revisiting the Mammographic Follow-Up of BI-RADS Category 3 Lesions, AJR, vol. 179(3), pp. 691–695, 2002.

[8] T. Boehler, and H.-O. Peitgen: A Combined Algorithm for Breast MRI Motion Correction, SPIE Medical Imaging, 65141R-1, 2007.

[9] E. Warner et al.: Comparison of Breast Magnetic Resonance Imaging, Mammography, and Ultrasound for Surveillance of Women at High Risk for Hereditary Breast Cancer, Journal of Clinical Oncology, vol. 19(15), pp. 3524–3531, 2001.

[10] C. K. Kuhl, Mammography, Breast Ultrasound, and Magnetic Resonance Imaging for Surveillance of Women at High Familial Risk for Breast Cancer, Journal of Clinical Oncology, vol. 23(33), pp. 8469–8476, 2005.

[11] Bluemke et al.: Magnetic Resonance Imaging of the Breast Prior to Biopsy, JAMA, vol. 292(22), pp. 2735–2742, 2004.
[12] Wiener et al.: Assessment of Suspected Breast Cancer by MRI: A Prospective Clinical Trial Using a Combined Kinetic and Morphologic Analysis, AJR, vol. 184(3), pp. 878–886, 2005.
[13] C. D. Lehman et al.: MRI Evaluation of the Contralateral Breast in Women with Recently Diagnosed Breast Cancer, The New England Journal of Medicine, vol. 356(13), pp. 1295–1303, 2007.
[14] P. Viehweg et al.: MR Imaging of the Contralateral Breast in Patients after Breast-Conserving Therapy, European Radiology, vol. 14(3), pp. 402–408, 2004.
[15] D. A. Montgomery, K Krupa, and T. G. Cooke: Alternative Methods of Follow Up in Breast Cancer: A Systematic Review of the Literature, British Journal of Cancer, vol. 96, pp. 1625–1632, 2007.
[16] M. Koenig, S. Kohle, and H.-O. Peitgen: Automatic Cropping of Breast Regions for Registration in MR Mammography, SPIE Medical Imaging, pp. 1563–1570, 2005.
[17] J. Modersitzki: Numerical Methods for Image Registration, Oxford Press, 2004.

Does breast density have an impact on the indications for MRI?

S Cagioli MD; F Pediconi, MD; V Dominelli, MD; ML Luciani, MD; V. Casali, MD; C Catalano, MD; R Passariello, MD
University of Rome "La Sapienza", Department of Radiology, Rome, Italy

Purpose
Mammographic density is the third largest risk factor for DCIS and invasive breast cancer. Our purpose was to establish the value of breast MRI compared to X-ray mammography and ultrasound for breast cancer evaluation in women with dense breast parenchyma.

Materials and Methods
Between October 2002 and October 2006, 598 subjects underwent breast MRI at our institution because of suspicious or inconclusive findings on clinical examination, ultrasound and X-ray mammography. Of these 598 subjects 238 had dense breast parenchyma and were included in the present retrospective evaluation. Breast MRI was performed at 1.5 T before and after administration of 0.1 mmol/kg of c.a. Lesions considered malignant (BI-RADS 4 or 5) on X-ray mammography and/or ultrasound and as BI-RADS 3, 4 or 5 on MRI were evaluated histologically. Other lesions were followed up at 6 months. The diagnostic performance of each technique was determined and compared using a general linear mixed model with appropriate correction for multiplicity.

Results
At final diagnosis 121/238 (50.8%) women had one or more confirmed malignant lesions, whereas 117(49.2%) had benign lesions or no lesions. Among 97 women who underwent all three techniques more lesions (malignant and benign) were detected with breast MRI (n=135) than with X-ray mammography (n=85) or ultrasound (n=107) and diagnostic confidence was greater. In terms of patient-based diagnostic accuracy breast MRI was significantly (p<0.0001) superior to both X-ray mammography and ultrasound (96.9% accuracy for MRI vs. 60.8% for mammography and 66.0% for US). Malignant lesions were histologically confirmed in 55/97 women who underwent all three techniques. Breast MRI detected more cases of multifocal, multicentric and contralateral disease and fewer misdiagnoses occurred. Overall, breast MRI led to a modification of the surgical approach for 28 (23.1%) of the 121 women with diagnosed malignant disease.

Conclusion
Breast MRI should be considered for routine breast cancer evaluation in women with dense breast parenchyma.

Clinical relevance/application
Breast MRI should be considered for routine breast cancer evaluation in women with dense breast parenchyma.

Incidental Enhancing Lesions Found on preoperative Breast MRI: management and role of Second Look Ultrasound

S. Cagioli MD; F. Pediconi, MD; V. Dominelli, MD; ML Luciani, MD; V. Casale; C. Catalano, R. Passariello, MD
University of Rome "La Sapienza", Department of Radiology, Rome, Italy

Purpose
To investigate the role of second look high resolution ultrasound (US) for the evaluation of incidental enhancing lesions detected on preoperative breast magnetic resonance imaging (MRI) that have no correlation on X-ray mammography and first look ultrasound.

Method and Materials
Between November 2004 and March 2007, 182 patients with suspected breast cancer based on conventional imaging modalities and confirmed by pathology underwent breast MRI with 0.1 mmol/kg o c.a. for staging. Patients with additional incidental lesions on breast MRI thereafter underwent a second look high resolution US examination directed specifically at the site of the incidental finding. Correlation of enhancement patterns (mass vs non-mass) between MR and US was performed. Images were evaluated in consensus and comparison was performed for diagnostic performance. Final diagnosis was based on biopsy or follow up.

Results
Breast MRI detected 55 additional lesions in 46/182 patients that were not seen on X-ray mammography or initial whole-breast US. Of these 55 lesions, 42 corresponding lesions were subsequently detected on second-look US in 38/46 patients. Twenty-four of the 42 lesions with a US correlate were confirmed as malignant compared with seven of 13 lesions without a US correlate. Second-look US depicted 8/9 BI-RADS five lesions, 16/22 BI-RADS four lesions and 18/24 BI-RADS three lesions. The ability of second look US to identify incidental lesions was higher for mass than for non-mass enhancement. Sensitivity, specificity, accuracy, PPV and NPV for the differentiation of malignant from benign lesions was 100%, 88.9%, 94.5%, 90.3% and 100%, respectively, for MRI and 90.5%, 61.9%, 76.2%, 70.4% and 86.7%, respectively, for second-look US.

Conclusion
Direct second look US is a feasible confirmatory method for incidental findings in breast MRI. Directed second-look US is potentially a cheap and readily available technique for localization and biopsy of suspicious incidental lesions detected on MRI alone.

Clinical Relevance/Application
Directed second-look US offers a means to confirm the presence of incidental enhancing lesions detected on MRI and to aid differentiation of benign from malignant lesions. Directed second-look US is potentially a cheap and readily available technique for localization of suspicious incidental lesions detected on MRI alone that require biopsy. Lesions detected at breast MRI that can be depicted with directed US, it may be amenable to US-guided percutaneous biopsy which may spare the patient a surgical biopsy or MR-guided biopsy if the procedure subsequently yields benign results.

Contrast-enhanced Magnetic Resonance Mammography (MRM): Improvement in Breast Lesion Detection and Characterization with Gadobenate Dimeglumine (Gd-BOPTA) Compared to Gadopentate Dimeglumine (Gd-DTPA)

V. Dominelli, MD, F Pediconi, MD; S. Cagioli, MD; ML Lucani, MD; F. Vasselli; C Catalano, MD; R Passariello, MD
University of Rome "La Sapienza", Department of Radiology, Rome, Italy

Purpose
To prospectively and intra-individually compare 0.1 mmol/kg doses of gadobenate dimeglumine and gadopentetate dimeglumine for contrast-enhanced breast MRI.

Method and Materials
Forty-seven women (mean age: 50.8±12.9 years) with breast lesions classified as BI-RADS 3, 4 or 5 for suspicion of malignancy underwent two identical MR examinations at 1.5 T separated by 48–72 h. T1w gradient-echo images were acquired pre-dose and at 2 min intervals after the randomized injection of gadopentetate dimeglumine or gadobenate dimeglumine at 2 ml/s. Two blinded readers evaluated randomized image sets for lesion detection and differentiation as benign or malignant compared to histology. McNemar's Exact test and the Generalized Estimating Equation (GEE) were used to compare lesion detection rates and diagnostic performance in terms of sensitivity, specificity, accuracy and positive and negative predictive values (PPV and NPV).

Results
Histopathology data were available for 78 lesions. Significantly more lesions overall (75/78 [96%] vs. 62/78 [79%]; $p=0.0002$) and significantly more malignant lesions (49/50 [98%] vs. 38/50 [76%]; $p=0.0009$) were detected with gadobenate dimeglumine. All detected malignant lesions were correctly diagnosed with both agents. More detected benign lesions were correctly diagnosed with gadobenate dimeglumine (20/26 [77%] vs. 17/24 [71%], respectively). Differentiation of lesions was significantly ($p=0.0001$) better with gadobenate dimeglumine. Significantly better diagnostic performance was noted with gadobenate dimeglumine for sensitivity (98.0% vs. 76.0%; $p=0.0064$), accuracy (88.5% vs. 69.2%; $p=0.0004$), PPV (86.0% vs. 76.0%; $p=0.0321$) and NPV (95.2% vs. 57.1%; $p=0.0003$).

Conclusion
Lesion detection and malignant/benign differentiation is significantly better with 0.1 mmol/kg gadobenate dimeglumine compared to 0.1 mmol/kg gadopentetate dimeglumine.

Clinical Relevance/Application
Gadobenate dimeglumine at a standard dose of 0.1 mmol/kg bodyweight is potentially the contrast agent of choice for breast MRI.

Preoperative Magnetic Resonance Imaging Of The Breast: Does It Affect Local Recurrence Rate?

V. Dominelli MD; F. Pediconi MD; S. Cagioli MD; ML Luciani MD; F. Vasselli; C. Catalano MD; R. Passariello MD
University of Rome "La Sapienza", Department of Radiology, Rome, Italy

Purpose
To evaluate the benefit of preoperative MRI for patients with breast cancer in terms of local recurrence rates after the surgical treatment of the primary carcinoma.

Materials and Methods
We retrospectively evaluated 49 patients with histologically-proven local breast cancer recurrence detected between 7 and 47 months after initial surgical treatment of the primary carcinoma. The surgical treatment of the primary carcinoma was mastectomy in 14 patients, quadrantectomy in 30 patients and lumpectomy in four patients; in all cases surgical treatment removed the entire tumor with margins free of disease. All patients underwent the same types of systemic treatment after breast surgery. All patients underwent follow-up breast MRI to evaluate the extent of the relapse. The patients were differentiated into two groups: group A which comprised 10/49 patients who had preoperative contrast-enhanced breast MRI before surgery and group B which comprised 39/49 patients that did not have a breast MRI examination before surgery. The chi-square test was used for statistical evaluation.

Results
The surgical treatment for the primary carcinoma was mastectomy in 14 patients (six in group A and eight in group B), quadrantectomy in 30 patients (three in group A and 27 in group B), lumpectomy in five patients (one in group A and four in group B). There were 28 (57%) cases of recurrence in the same breast after breast conserving surgery (4/10 [40%] in group A vs 24/39 [61%] in group B), five (10%) cases of local recurrence after mastectomy (4/10[40%] in group A vs 1/39 [3%] in group B) and 16 (33%) cases of contralateral disease (2/10 [20%] in group A vs 14/39 [36%] in group B). Metachronous contralateral carcinoma and local recurrence in the ipsilateral breast were significantly ($p<0.001$) more frequent in patients without preoperative local MR staging (88% and 85% respectively) compared to those with breast carcinoma who underwent MRI before primary therapy (12% and 14%, respectively).

Conclusion
Preoperative local MR staging allows a significant reduction of ipsilateral recurrences and contralateral cancer at follow-up. Breast MRI is recommended in patients with histologically proven breast cancer for better evaluation of the extent of disease.

Clinical Statement
Preoperative breast MRI is a reliable technique for the staging of breast carcinoma and allows reduction of local recurrence rates.

Excitation independent bilateral breast asymmetry analysis using contrast-enhanced MR Mammography: Preliminary results

Ertas G. and Leach MO.
Cancer Research UK and EPSRC Cancer Imaging Centre, Institute of Cancer Research and Royal Marsden NHS Foundation Trust, Sutton, Surrey, SM2 5PT, UK

Purpose
To develop an excitation independent method for bilateral breast asymmetry analysis using contrast-enhanced MR Mammography.

Materials and Methods
The study dataset comprises dynamic images of 40 women acquired using a pre-determined 3D T1-weighted sequence in 14 centres during the UK multi-centre study of MRI screening for breast cancer (MARIBS) ($1.33\times1.33\times2.5$ mm^3 spatial and 90 s temporal resolutions, Gd-DTPA dose of 0.2 mmol/kg bodyweight, five post-contrast acquisitions). There are 20 normal and 20 abnormal cases (11 benign and nine malignant lesions in a range of sizes).
The left and the right breasts are first segmented on pre-contrast images using a semi-automated bias corrected fuzzy c-means clustering based algorithm that we have developed. Segmentation results are inspected visually and some manual corrections are performed to completely cover the axilla if necessary. For each voxel inside a segmented breast, an intensity vector is formed using the pre and post-contrast images and centred using the *prototype vector determined for fat.* Principal components analysis is applied to the centred vectors and the first components are used to construct a histogram with optimal bin width determined by Scott's method. The absolute entropy difference (AED) of the histogram pair and the residual AED of the Gaussian curve fit subtracted histogram pair for the left and the right breasts are calculated. The algorithm was implemented using IDL 7.0 (ITT Visual Information Solutions, USA). The significance and accuracy of each feature in detection of abnormality and in diagnosis of breast cancer were statistically analyzed using SPSS 15 (SPSS Inc., USA). Significance of the features were tested using independent samples t-test with either a pooled or a separate variance as determined by the Levene's test for equality of variances. A P-value of <0.05 is considered statistically significant. Diagnostic accuracy was assessed for the significant features using the area under the receiver operating characteristic curve (Az).

Results
There are no significant differences between the normal and abnormal cases for the absolute entropy difference (0.12 ± 0.08 and 0.19 ± 0.14, $P=0.08$) and the residual absolute entropy difference (0.19 ± 0.17 and 0.24 ± 0.18, $P=0.31$). In discrimination of benign or normal cases from malignant cases, absolute entropy difference is significant and shows good accuracy (0.12 ± 0.08 and 0.27 ± 0.15, $P=0.02$, $Az=0.79$) while residual absolute entropy difference is insignificant (0.19 ± 0.15 and 0.29 ± 0.22, $P=0.14$). Principal component based analysis of multi-centre contrast enhanced MR mammography is shown to be feasible in bilateral breast asymmetry analysis for cancer diagnosis.

Conclusion
The bilateral asymmetry analysis method introduced is efficient and in this pilot study accurately identifies the presence of breast cancer using MR Mammography. We hope that it will facilitate breast examination and improve the detection of lesions, simplifying clinical evaluations.

Acknowledgment
This work was supported by EPSRC (EO35736/1) and also by Cancer Research UK (C1060/A10334).

Full-automatic Detection of Fiducial Markers in Breast MRI for MR-guided Intervention

Konstantions Filippatos[1], Tobias Böhler[2], Benjamin Geisler[2], Harald Zachmann[1], Thorsten Twellmann[1]
[1]MeVis Medical Solutions AG, Bremen, Germany
[2]Fraunhofer MEVIS, Bremen, Germany

Introduction
With its remarkable sensitivity, DCE-MRI has become one of the first-line tools for detection and diagnosis of breast cancer, particularly in dense breasts. Many findings however require a histological work-up, but cannot be depicted by targeted ultrasound during biopsy. In this situation, MRI-guided biopsy procedures offer several advantages regarding precision and clinical workflow and is increasingly used in clinical practice [1, 2].
Part of the MR-guided biopsy workflow is the alignment of the patient position and navigation grid with the preoperative MR images. In these images, the location and orientation of the navigation grid is indicated by a number of fiducial markers.
In this study, we propose and evaluate a multivendor-capable method for accurate localization of the fiducial markers. After choosing the navigation grid model, the method detects full-automatically the fiducial markers in the 3D image data, on which basis a virtual navigation grid can be subsequently placed in the images in order to compute the parameters for needle navigation.

Materials
During MR guided breast interventions the patient is usually placed in a prone position on a breast coil array with mediolateral as well as craniocaudal access to the breast. Localization units, mounted on the coil, facilitate breast immobilization and stereotactic, computer assisted guidance of surgical instrumentation, either horizontal (grid localization unit) or inclined (post pillar localization unit).
The key challenge during MR-guided breast interventions is the intraoperative determination of the coordinates of the lesion by means of the localization unit. This can be achieved after establishing a spatial correlation between patient and unit coordinate systems, assigned by an affine transformation. For its computation, center point coordinates of corresponding fiducial markers in both coordinate frames are used. The fiducial markers are designed as cylindrical containers on the localization device, filled with dilute contrast agent for high MR signals. Using the determined affine transformation, every interesting point in the MR image can be expressed in localization unit coordinates. Thus, the precise insertion point on the breast skin as well the insertion direction and distance to the lesion can be computed relatively to the localization device.

Method
For localization of the fiducial centers, we propose a full-automatic method based on generic image processing algorithms for fiducial detection. In addition, we apply template matching [3,4] for distinction and labeling of various forms of fiducials in a single image and for center

point optimization. Hence, the geometry of every present fiducial is required as a priori knowledge. This information is stored in form of model specific parameter files, which are created once a new grid model is adopted, and is used to define a fiducial template.

The detection algorithm is based on the determination of connected components of high intensity and defined shape in the image background. First, a noise model of the particular image is determined and an adequate intensity threshold is computed for air–breast separation. After histogram analysis of the air region, only voxels in an empirically determined high quantile of the histogram distribution are considered for further processing. These voxels constitute a number of connected structures representing fiducial candidates.

Because in practice fiducials are frequently not uniformly filled or contaminated with contrast agent at the breech, they may not always emerge with a uniform signal and expected geometry in the image. Therefore, the original image voxels around each candidate are again retrieved. Subsequently, the main axis of the fiducial template, which is based on the stored geometry information, is approximately aligned to the particular candidate and an advanced registration is performed [3, 4]. Thus, a linear transformation of the fiducial template is computed, in order to match the rigid-body fiducial to each of the candidates. Only candidates with a low resulting matching error are labeled as fiducial markers. The center of gravity of the registered template is returned. In this way, centers of e.g. partially filled fiducials, which are represented by a partially defined cylinder, can be correctly localized, guaranteeing an accurate intervention.

Results

The developed approach has been evaluated in 25 clinical cases, during which patients underwent biopsy using three different models of localization units. The fiducial containers varied in dimensions between 5.8 mm×2.4 mm and 40 mm×1.25 mm for length and radius respectively, whereas at most two different fiducials where present in the same image. The images varied in resolution of 0.58×0.58×3, 0.91×0.91×1.3, and 0.68×0.68×3.3.

An expert radiologist defined ground truth fiducial centers and ranked all fiducials in three classes by means of the degree of filling with contrast. 27% were fully filled with contrast, 30% partially and 43% had not been filled above one third.

Out of 109 fiducial markers, 105 were successfully localized, yielding a detection success rate of 0.96. A false positive rate of 0.44 per image, arising from fiducial-like tools or artifacts, or included breast skin parts, was additionally observed. The average distance deviation of all detected fiducials to the ground truth center points was 0.93 mm. By means of the visibility classes, the first class averaged to 0.61 mm, the middle one to 0.93, and the worse one to 1.39 mm of distance deviation. Summarizing, 16 out of 25 interventions could be executed without further user interaction for selection or modification of fiducials, or elimination of false positive structures. Only in 4 of the rest cases however, the users would have to perform the time consuming step of retrieving lost fiducials.

Conclusion

Accurate and reliable biopsy or resection of small lesions is an important aspect of a MRI-based clinical workflow for breast cancer diagnosis. We developed a novel method for detection and center point determination of fiducial markers on breast coil arrays to assist the precise intraoperative navigation during breast interventions. The full-automatic method determines all information for accurate placement of a preselected localization unit, eliminating the time consuming and often inaccurate step of manual definition of the fiducial positions, and leading to more precise and faster interventions with fewer MR control scans.

Acknowledgment

We would like to thank Volker Diehl of "Klinikum Bremen Mitte" Hospital, MR-and PET/CT Center and Dr. med. Pascal A. T. Baltzer of "Universitätsklinikum Jena" Hospital, Institute for Diagnostic and Interventional Radiology for data acquisition and support.

References

1. H. Mahnken, R. Jens Ricke CT-and MR-Guided Interventions in Radiology, Springer-Verlag Berlin Heidelberg, 2009.
2. D.D. Dershaw, Imaging-Guided Interventional Breast Techniques, Springer-Verlag New York, Inc., 2003.
3. J. Modersitzki: Numerical Methods for Image Registration, Oxford Press, 2004.
4. J. V. Hajnal, D. L. G. Hill, D. J. Hawkes (editors): Medical Image Registration, CRC Press, 2001.

Histologic findings of breast cancer after cryotherapy.

[1]Gajda M., [2]Baltzer P. A. T., [2]Pfleiderer S. O. R., [3]Camara O., [3]Runnebaum I. B., [2]Kaiser W. A. and [1]Petersen I.
[1]Institute of Pathology, [2]Institute of Diagnostic und Interventional Radiology,
[3]Clinic of Gynecology
University hospital Jena, Germany

Introduction

Breast cancer is the most frequent cancer in women. In Germany, more than 47.000 women have newly diagnosed breast cancer each year, out of them 20.000 patients younger than 69 years old (1).

Breast conservative treatment (BCT) is nowadays a standard therapeutic approach on breast cancer with equal outcome compared to mastectomy. Improvement of diagnostic imaging modalities lead to detection of early breast cancer stages (2–8).

Consequently, there is a trend towards minimal invasive procedures for breast cancer therapy. Thermical procedures dominate percutaneous therapy options. Interstitial laser therapy (ILT), radiofrequency ablation (RFA) or highly focused ultrasound (HIFU) destroy malignant tissue due to heat development. On the other hand, cryotherapy destroys tumor cells by rapid cooling of a probe down to −180°C (9–20).

Up to now, cryotherapy was mainly used for treatment of neoplastic liver lesions as well as prostate carcinoma (21). In the last years, some reports on cryotherapy of breast cancer and fibroadenoma were published (19, 20). In this study, therapy effects of cryotherapy was assessed histologically regarding tissue specimen obtained by open surgery after percutaneous cryotherapy of breast cancer.

Materials and Methods

Between 1999 and 2007, 53 patients (mean age 61 years, range 38–81 years), 53 malignant breast lesions (39 invasive ductal cancers, six invasive lobular cancers, two mixed invasive ductal and lobular cancers, three invasive tubular cancers one adenocystic cancer and two DCIS) were treated by percutaneous cryotherapy. Mean tumor size obtained by ultrasound was 15.3 mm with a range between 5 and 37 mm.

Following local anesthesia, an Argon based cryotherapy probe was placed inside the tumor under ultrasound guidance. The therapy protocol consisted of two freezing cycles of 7 and 10 min, each followed by passive thawing periods, the first limited to 5 min, the second until complete thawing of the resulting ice ball. Ice ball size was measured every minute using ultrasound. After 1 to 35 days, cryotherapy was followed by open surgery. Post therapeutic tissue specimens were worked up histological.

Work up of biopsy cylinders as well as surgery specimens was performed according to international standards as well as the German S3 guidelines giving special attention to the exact topographic marking of slice preparations. In every biopsy, the percentage of positive tumor cell nuclei for estrogen as well as progesterone receptors and the her2/neu status were assessed. Mastectomy specimens are marked in two planes; segment or quadrant resections are mostly marked in three planes by string markings. After fixation in acid free 4% formalin, approximately 5 mm slices were cut along the longest specimen axis. In 26 cases, also ipsilateral lymph nodes (mean number: 11) could be assessed. In 27 patients, the sentinel lymph node method was performed.

Results

In all cases, the cryotherapy probe was placed successful under ultrasound guidance. In two patients, the procedure was stopped premature due to technical failures. Complete cryotherapy was performed in 51 cases. Sonographical measured ice ball size was between 21.7 and 39.5 mm (mean 31 mm). Macroscopic lesion sizes in surgical resections were found between 0 and 55 mm (mean 27.4 mm). A typical macroscopic appearance of post therapeutic specimens was found: the treated tumor showed a livid deep red zone due to therapy induced bleeding, necrosis and reparative processes. In the first 3 days, in all histological preparations distinct bleeding, necrosis and tumor cell shadows were found. In the next days, xanthogranulomatous inflammation and lymphatic plasma cellular infiltrations appear, from the second week on accompanied by varying degrees of fibrosis and granular tissue. Histological workup revealed in all cases at least partial tumor destruction. In 26 cases with a diameter of up to 19 mm before cryotherapy, complete tumor destruction could be verified. In 24 cases, residual tumor (14 invasive ductal cancers, one invasive ductal cancer with invasive lobular component, four invasive lobular cancers, one adenocystic cancer and four ductal carcinoma in situ (DCIS)) was found. Lymph node metastasis was found in five patients with residual cancer and three patients without residual cancer.

Discussion

The present study demonstrates the feasibility of local breast cancer treatment using cryotherapy (16, 17). Especially small tumors with a tumor diameter of 16 mm or less could be treated successfully with no incomplete treatment in this group. Of major importance is therapeutic experience as well as inclusion criteria. Between 1999 and 2001, 27 patients were treated by cryotherapy with only 5 tumor free cases in histopathology workup. By contrast, 26 patients were treated between 2002 and 2007 with residual tumor in only three cases and two lymph node metastases. In this cohort, one tumor was 30 mm in size, the others below 17 mm (22).

According to our experience, following inclusion criteria should be used for ultrasound guided cryotherapy after informed consent of the patient: ultrasound visible cancer stage T1 (≤15 mm), skin distance above 10 mm, localization outside the nipple region. DCIS as well as invasive lobular cancer seem to be less suitable for cryotherapy. According to the German S3 guidelines, sentinel lymph node biopsy is necessary in all patients with biopsy proven breast cancer.

Concluding, percutaneous, ultrasound guided cryotherapy is a simple and safe method for treatment of small breast cancer. However, larger studies with a higher number of cases as well as a clinical long term follow are needed to further evaluate the potential of cryotherapy for breast cancer treatment.

References

1. Fisher B, Redmond C, Poisson R, et al. (1989) Eight year results of a randomized clinical trial comparing total mastectomy and lumpectomy with or without irradiation in the treatment of breast cancer. N Engl J Med. 320:822–828.
2. Burak WE Jr, Agnese DM, Povoski SP, et al. (2003) Radiofrequency ablation of invasive breast carcinoma followed by delayed surgical excision. Cancer 98:1369–1376.
3. Dowlatshahi K, Francescatti DS, Bloom KJ. (2002) Laser therapy for small breast cancers. Am J Surg. 184:359–363.
4. Hayashi AH, Silver SF, van der Westhuizen NG, et al. (2003) Invasive breast carcinoma with ultrasound-guided radiofrequency ablation. Treatment of Am J Surg. 185:429–435.
5. Pfleiderer SOR, Reichenbach JR, Wurdinger S, et al. (2003) Interventional MR-mammography: manipulator-assisted large core biopsy and interstitial laser therapy of tumors of the female breast. Z Med Phys. 13: 198–202.
6. Boehm T, Malich A, Reichenbach JR, et al. (2001) Percutaneous radiofrequency (RF) thermal ablation of rabbit tumors embedded in fat: a model for RF ablation of breast tumors. Invest Radiol. 36:480–486.
7. Hilger I, Hiergeist R, Hergt R, et al. (2002) Thermal ablation of tumors using magnetic nanoparticles: an in vivo feasibility study. Invest Radiol. 37:580–586.
8. Gianfelice D, Khiat A, Amara M, et al. (2003) MR imaging-guided focused US ablation of breast cancer: histopathologic assessment of effectiveness initial experience. Radiology 227:849–855.
9. Hewitt PM, Zhao J, Akhter J, et al. (1997) A comparative laboratory study of liquid nitrogen and argon gas cryosurgery systems. Cryobiology 35:303–308.
10. Silverman SG, Tuncalli K, Douglass FA, et al. (2000) MR imaging-guided percutaneous cryotherapy of liver tumors: Initial experience Radiology 217:657–664.
11. Staren ED, Sabel MS, Gianakakis LM, et al. Cryosurgery of breast cancer. Arch Surg. 1997;132:28–33.
12. Rand RW, Rand RP, Eggerding FA, et al. Cryolumpectomy for breast cancer: an experimental study. Cryobiology. 1985;22:307–318.
13. Rabin Y, Julian TB, Olson P, et al. Long-term follow-up post-cryosurgery in a sheep breast model. Cryobiology. 1999;39:29–46.
14. Suzuki Y. Cryosurgical treatment of advanced breast cancer and cryoimmunological responses. Skin Cancer. 1995;10:19–26.
15. Tanaka S. Cryosurgical treatment of advanced breast cancer. Skin Cancer. 1995;10:9–18.
16. Pfleiderer SOR, Freesmeyer MG, Marx C, et al. (2003) Cryotherapy of breast cancer under ultrasound-guidance: initial results and limitations. Eur Radiol. 12:3009–3014.
17. Pfleiderer SOR, Marx C, Camara O, Gajda M, Kaiser WA (2005) Ultrasound-Guided, Percutaneous Cryotherapy of Small (≤ 15 mm) Breast Cancers. Investigative Radiology 40: 472–477.
18. Morin J, Traore A, Dionne G, Dumont M, Fouquette B, Dufour M, Cloutier S, Moisan C (2004) Magnetic resonance-guided percutaneous cryosurgery of breast carcinoma: technique and early clinical results. Can J Surg. 47:347–351.
19. Kaufman CS, Bachman B, Littrup PJ, et al. (2003) Office-based ultrasound guided cryoablation of breast fibroadenomas. Am J Surg. 184:394–400.

20. Kaufman CS, Bachman B, Littrup PJ, et al. (2004) Cryoablation treatment of benign breast lesions with 12-month-follow-up. Am J Surg. 188: 340–348.
21. Seifert JK, Morris DL. (1999) World survey on the complications of hepatic and prostate cryotherapy. World J Surg. 23:109–114.
22. Gajda M. Pfleiderer SOR, Camara O, Baltzer PAT, Böttcher J, Hilger I, Runnebaum IB, Kaiser WA, Petersen I. (2009) Histopathological study of breast cancer after cryotherapy ablation. Der Pathologe. Suppl. 1. 30: 13.

Assessment of Diagnostic Accuracy of Breast MRI in the Detection of Breast Cancer in Iranian Patients

Masoumeh Guity, Koosha Ghazi-Moghadam, Amirreza Azizian, Majid Shakiba, Elham Tahery
Tehran University of Medical Sciences, Tehran, Iran

Keywords: Breast cancer, contrast-enhanced breast MRI, BIRADS, ROC curve

Abstract
Background Breast MR imaging is a non-invasive imaging modality and has a high sensitivity and moderate specificity in the detection of breast cancer. In this study we aimed to assess the diagnostic accuracy of MRI in detecting breast malignancies in Iranian patients.
Method We reviewed MR images of 112 patients who either underwent biopsy or were followed by second MRI after 12 months. Images were reported based on MR Breast Imaging Reporting and Data System (BIRADS) lexicon and analyzed premised on Receiver Operating Characteristics (ROC) curves. Considering the first cut-off point of ROC curve, BIRADS 3 images were categorized as negative and BIRADS 4 or 5 images were classified as positive. BIRADS 3 or 4 images were considered as negative and BIRADS 5 images were grouped as positive for the second cut-off point.
Results The sensitivity and specificity of the first cut-off point are 97.9% and 47.2% and these figures are 25% and 99.4% for the second cut-off point, respectively. Negative predictive value (NPV) of BIRADS 3 is 98.6%, while positive predictive value (PPV) of BIRADS 5 is 92.3%. In addition, area under the ROC curve (AUC) or accuracy of MRI is 91%.
Conclusion MRI is a valuable modality in detecting breast cancer and it has high diagnostic accuracy. The BIRADS 4 results were not clear-cut and these must be evaluated more carefully. Regarding that unnecessary biopsies are suggested for patients in this category, it would be favorable to define subtypes in this group.

Texture-based characterization of breast cancer on contrast-enhanced MRI

Kirsi Holli [1,2,*], Anna-Leena Lääperi [1,3], Lara Harrison [2,3], Tiina Luukkaala [4,5], Pertti Ryymin[1]
Prasun Dastidar [1,2,3], Seppo Soimakallio [1,3], Hannu Eskola [1,2]
[1]Medical Imaging Centre, Tampere University Hospital, Tampere, Finland
[2]Department of Biomedical Engineering, Tampere University of Technology, Tampere, Finland
[3]Tampere Medical School, University of Tampere, Tampere, Finland
[4]Science Center, Pirkanmaa Hospital District, Tampere, Finland
[5]Tampere School of Public Health, University of Tampere, Tampere, Finland

Introduction
Texture is an important feature in image analysis, which is related to qualitative properties of surfaces and corresponds to both brightness value and pixel locations [1]. Texture analysis (TA) of magnetic resonance (MR) images is a quantitative method that can be used to quantify and detect structural abnormalities. One of the most common methods for TA is the grey level co-occurrence matrix first proposed by Haralick [2]. The co-occurrence matrix texture model has been widely applied in TA for identification of tissues to detect the abnormality within an organ tissue and identification of different pathological stages [3, 4, 5, 6]. Our previous study [7] showed that grey level co-occurrence matrix based texture features proved to be the most consistent in distinguishing between two histological types of breast cancer when comparing with other methods such as histogram, run-length matrix, the absolute gradient, and autoregressive model based features.

Purpose
Purpose of this study was to investigate differences in the texture features between invasive lobular and ductal breast cancer extracted from dynamic contrast enhanced magnetic resonance images (DCE-MRI), and to evaluate the effect of grade and size of cancer on the texture analysis.

Material and Methods
The database consisted of MR images from 20 patients (mean age 50.6±SD 10.6; range 37 to 70 years) with biopsy-proven breast cancer. Ten histopathologically typical invasive ductal cancers and ten typical invasive lobular cancers were included in this retrospective TA study. Imaging was performed on a 1.5 T MRI device using four channel breast array coil. The dynamic study consisted of six measurements, three-dimensional (3D) axial T1-weighted gradient echo sequence. The first frame (pre-contrast) was acquired before injection of paramagnetic contrast agent (Gd, 0.1 mmol/kg body, Dotarem®), followed by five measurements. The T1-weighted pre-contrast and first post-contrast series were chosen for TA. The image slice for feature measurements was chosen on the basis of optimal representation of the largest tumour area from both imaging series. Manually defined irregular regions of interests containing the tumour were defined in each image. Gray level co-occurrence matrix based texture features, which give information about the gray-level value distribution of pairs of pixels, were calculated in five distances (d=1, 2, 3, 4 and 5) with four directions (θ=0°, 45°, 90° and 135°) and tested with histology (Mann–Whitney test), grade of malignancy (median test) and lesion size (Spearman's rho).

Results
Texture feature *sum average* which is the average of normalized greytone image in the spatial domain (d=3, θ=45°) gained significantly higher value in invasive lobular breast cancer (p=0.035) in pre-contrast images. In post-contrast images feature *inverse difference moment*, which refers to the homogeneity of the image having larger value in a smooth image (d=4, θ=135°), was significantly higher (p=0.029) also in invasive lobular breast cancer. The grade of malignancy varied from 1 to 3. In pre-contrast images *inverse difference moment* features (d=3 and 4, θ=135°) were significantly higher (p=0.042) in grade 2 malignancy. In post-contrast images the *sum average* features (d=2, 3, 4, 5, θ=0°, 45°) were significantly higher in grade 2 malignancy (p value varying from 0.021 to 0.042).
The median lesion size was 25 mm (range, 7–60 mm). Most of the calculated texture features correlated with the lesion size in both pre-and post-contrast images. In both images positive correlation was observed in *entropy* and *sum entropy* (correlation coefficient r varying from 0.719 to 0.905, p<0.001) and negative correlation in *angular second momentum* (correlation coefficient r varying from −0.735 to −0.905, p<0.001) at any

given distance or direction. The feature *sum entropy* measures the randomness within an image and *entropy* is an indication of the complexity within an image, so a complex image produces a high *entropy* value. *Angular second moment* is a measure of homogeneity of an image and the higher value of this feature indicates that the intensity varies less in an image so it will be greater for the homogeneous image. We observed that in larger lesions the value of *entropy* and *sum entropy* was higher and the value of *angular second momentum* lower, indicating that the larger lesions appear more complex within the image than the smaller ones.

Conclusions

The results of this preliminary study indicate that texture features extracted from DCE-MRI can be used to distinguish between two histological types of breast cancer. Significant texture features could also be determined for different grades and different sizes of cancer. Future studies with larger database should focus on testing the acquired results and clinical applicability of TA in characterization of breast lesions in MRI.

References

[1] Tuceryan M and Jain AK (1998) Texture analysis. In: Chen CH, Pau LF, Wang PSP (eds.) The Handbook of Pattern Recognition and Computer Vision, 2nd edn. World Scientific Publishing Co. pp, 207–248.
[2] Haralick RM (1979) Statistical and structural approaches to texture. Proc IEEE 67:786–804.
[3] Mahmoud-Ghoneim D, Alkaabi MK, de Certaines JD et al (2008) The impact of image dynamic range on texture classification of brain white matter. BMC Medical Imaging 8:18
[4] Zhang J, Tong L, Wang L et al (2008) Texture analysis of multiple sclerosis: a comparative study. Magnetic Resonance Imaging 26:1160–1166.
[5] Chen W, Giger ML, Li H, et al. Volumetric texture analysis of breast lesions on contrast-enhanced magnetic resonance image. Magn Reson Med 2007; 58:562–571.
[6] Gibbs P, Turnbull LW (2003) Textural analysis of contrast-enhanced MR Images of the breast. Magn Reson Med 50:92–98.
[7] Holli KK, Lääperi A-L, Harrison L et al (2009) Characterization of breast cancer types by texture analysis of magnetic resonance images. Accepted 2009-07-10.

Value of normalized ADC in characterization of breast masses

Jena, Amarnath DNB (NM); Taneja, Sangeeta DNB (Radiodiagnosis); Sidhu Ramandeep MD (Radiodiagnosis)
Rajiv Gandhi Cancer Institute & Research Center, New Delhi, India

Introduction

The apparent diffusion coefficient (ADC) value of breast lesions in Diffusion-weighted MRI (DWI) has the potential of improving the specificity of routine DCE-MRI of the breast [(1)]. Improved specificity of calculated ADC has been reported by normalizing with respect to glandular tissue [(2)]. The purpose of this study is to assess role of calculated ADC normalized with an external reference in the characterisation of breast masses.

Materials and methods

64 women were evaluated with DCE-MRI of the breast done on 1.5 Tesla AVANTO (Siemens, Germany) using a dedicated dual breast coil. DWI was done using EPI-SPAIR sequences employing b values 0, 1,500 and an inline calculated ADC Map was obtained. Calculated ADC of the mass was obtained by drawing an ROI on the ADC Map corresponding to the enhancing region of the mass on DCE-MRI and showing restricted diffusion on DWI. Ratio of ADC of mass (ADC M) and values of ROI placed on the normal glandular tissue of opposite breast (GT) & over an external Reference (Ref) were taken for the calculation of normalized ADC M/GT and ADC M/Ref respectively. Statistical analysis was done using SPSS version 12 to calculate AUC, sensitivity, specificity, accuracy, PPV & NPV of ADC M, ADC M/GT and ADC M/Ref.

Results

Sixty six lesions (47 malignant; 19 benign) were detected in 64 women (Age group: 22–75 years; 41, pre/peri menopausal and 23, post menopausal). Average size of the lesion was 3.87 cm in the malignant group and 3.39 cm in the benign group. All the lesions could be identified on ADC-Map. In malignant tumors, the mean ADC was (mean±SEM) $0.769\pm0.022\times10^{-3}$ mm^2/second, and in benign tumors the mean ADC was $1.28\pm0.062\times10^{-3}$ mm^2/second. According to receiver operating characteristic (ROC) curves, we found a threshold of 0.967×10^{-3} mm^2/second which distinguished between malignant and benign lesions with highest sensitivity (91.5%) and specificity (94.7%) and an accuracy of 92.5% (P value<.001). A threshold value of 0.90×10^{-3} mm^2/second yielded 100% specificity however with reduced sensitivity (89.4%). ADC M/GT in our cases had a lower sensitivity and specificity (74.5 and 78.9%) compared to ADC M contrary to the values reported previously [(2)]. However, ADC M/Ref exhibited a better sensitivity, specificity and PPV of 89.4%, 94.7% and 97.7% respectively. 4/47 malignant lesion were false negative on ADC & ADC M/Ref. One lesion of the benign group was false positive.

Discussion

Our data supports the fact that calculated ADC may be used as a useful discriminator between malignant and benign lesions of breast [(3)]. The technique of using external reference for normalization of calculated ADC, as in our study, appears to not only limit the influence of imaging related variations, but also completely avoid any variations of hormone related ADC changes that may be present in glandular tissue of breast at the time of examination. Calculated ADC of mass or normalized ADC value with an external reference may prove as better parameter than ADC normalized with normal glandular breast tissue.

Two of our false negative lesions on ADC were non mass enhancements with wide variation of calculated ADC value. The other two false negative lesions showed rim enhancement with central area of necrosis which showed no restriction of diffusion and hence resulted in relatively higher ADC value. The single false positive lesion on ADC in our study was an intraductal papilloma. Similar finding has been reported previously by Woodhams, et al. in 2005[(4)].

Conclusion

DWI in conjunction with routine breast MRI may improve the specificity of DCE-breast MRI. Normalization of ADC with an external reference may serve as a better parameter for discriminating malignant from benign breast lesions.

References

1. F. P. Pereira, et al., 2008 Breast Cancer symposium. Abstract No: 75.
2. El-Khouli, et al., American Roentgen Ray society (ARRS) 2009 Annual meeting: Abstract 129.
3. Erika Rubesona, et al. Quantitative diffusion imaging in breast cancer: A clinical prospective study. Journal of Magnetic Resonance Imaging. 2006; 24: 319–324.

4. Woodhams, et al., ADC Mapping of benign and malignant breast tumors. Magnetic Resonance in Medical Sciences 2005; 4:35–42.

MR-guided interventions on only MR-detectable lesions in breast-MRI: a pathologic-radiologic comparison

Malich A; Kott A; Ulrich A; Feger J; MIkulik S
Institute for Radiology, Südharz-Krankenhaus Nordhausen, Nordhausen, Germany

Purpose
MR-guided interventions on mammographically and sonographically occult, MR-based enhancing lesions is still time consuming, depends critically on the experience of the radiologist and there is only limited access to this intervention. Study aimed to analyzed those lesions exclusively visible in MRI in order to prove the histopathological outcome, the imaging characteristics and the incidence of malignant findings in order to analyze the clinical relevance of MR-guided interventions of the female breast.

Methods
116/140 interventions between 12/06 and 10/08 were successfully performed, most common reasons of termination were no access to lesions located close to the chest wall (21%) and non enhancement of initially suspicious (non mass) lesions (51.7%). All cases were analyzed in retrospect regarding dynamic and morphological data, histopathology, size. All images were obtained using the same protocol (1.5 T Achiva, Philips; 0.1 mmol Gd-DTPA/kgbw; slice thickness 3 mm, dynamic analyses by CAD (Confirma®), intervention planning by SureLoc (Confirma)®, intervention positioning by Noras positioning aid®).

Results
35/106 interventionally biopsied lesions were histologically proven as B4/5 (30.3%), 18% as B3, and the remaining 51.7% as B2. Mean size was calculated (in mm) as 6×5 (B5); 8×7 (B4), 6×5 (B3) and 6×5 (B2), respectively. 38/60 (63%) B2 lesions are characterized by a sharp shape (vs. 11/35 within B4/5; 29%). 27/60 B2 lesions were hypointense in T2 vs. 19/35 B4/5 (45% vs. 54%). Perifocal edema occurred in 9/60 B2 lesions and 6/35 B4/5 lesions (15% vs. 17%). Spiculations were observed in 11/60 B2 and 15/35 B4/5 lesions (18% vs. 43%). Dynamic enhancement did not differ significantly among the different histological entities: strong initial wash in was observed (CAD-based) in 48/60 B2 (80%) and 32/35 B4/5 lesions (91%), wash out (>10%) was measured (CAD-based) in 40/60 B2 lesions (67%) and 28/35 B4/5 lesions (80%).
Most common benign lesions were proven as papillomata (9%) fibroadenoma (14%) and sclerosing adenosis (17%) whereas the most common malignant entity was DCIS (15%).
CAD-based planning of intervention access was reliable, differences to manual access calculation were <1 mm in each direction. No miscalculation occurred.

Conclusion
MR-guided biopsies are of increasing importance in the verification of only MR-detected breast lesions. Morphology is, despite the small mean size, a valuable parameter to take into account, because most B4/5 lesions are characterized by an irregular edge, spiculations and a hypointense signal in T2. The ratio of about 1/3 of B4/5 findings of only MR-detected breast lesions undergoing MR-guided biopsy support the clinical relevance of this intervention procedure even on subtle lesions. Due to the time and resource consuming technology, MR-guided interventions should be done only on those lesions being not otherwise visualizable.

Breast MRI Fusion Imaging: Techniques and Applications

Siegler P[1], Bevan PD[1], Holloway C[1], Thevathasan G[2], Ma K[2], Bluvol N[2], Sela G[2], Millot L[1], Plewes DB[1]
[1]Imaging Research, Sunnybrook Health Sciences Centre, University of Toronto, Canada
[2]Sentinelle Medical Limited, 555 Richmond Street, Toronto, Canada

1. Introduction
Routine clinical assessment of pathologies may use more than one imaging modality to aid in the detection, diagnosis or intervention of suspicious lesions. These various imaging procedures are routinely performed without any means to spatially correlate the image data. Instead, the radiologist uses her knowledge of anatomy to associate common anatomic features among imaging modalities. Only recently, systems have been developed which permit accurate co-registration of imaging to ensure alignment of lesion contrast. These include PET-CT[1] and more recently PET-MRI[2], both of which achieve image alignment by designing a patient transport device that permits accurate shuttling of the patient between the two calibrated imaging volumes. In these cases, it is assumed that the patient position is stable and predictable between the two imaging sessions. These applications are well suited to neurological applications by virtue of the relatively inflexible anatomy which ensures relatively accurate co-alignment. However, when applied to body imaging in general and breast imaging in particular, the issue of ensuring spatial alignment is substantially more challenging. Nevertheless, given a means to achieve some form of fixation of tissue, the options for registration of MRI data are numerous as summarized in Figure 1. For example, by conducting an MRI exam in a patient support structure that itself contains fiducial markers which can be resolved within the MR exam as well as via a second means, we create the framework for a "global reference frame". This second means might be resolved via optical or magnetic means in a dynamic manner after the MR exam has been completed. This could then be used to direct devices, such as pointers or virtual measuring devices that would allow the operator to manoeuvre through a virtual imaging volume spatially matched to the real anatomy. Alternatively one could use the global reference frame to direct another imaging device such as an ultrasound (US) probe which could then be placed in contact with the patient to generate co-registered US imagery[3]. Finally, one could envision that rather than placing fiducial markers on the patient transport device, one could attach the fiducial markers to the patient herself. In this case, we align the patient to the previously obtained MRI data. Given this, it would then be feasible to fuse a virtual MRI lesion with the patient anatomy in real-time. The global reference frame can then be seen as a vehicle that can be used to move from one imaging space or task to another. In this light, it is then feasible to envision a number of interesting possibilities to augment current breast MRI practices which combine the sensitivity of breast MRI

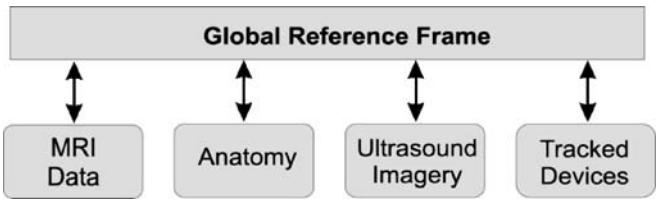

Figure 1. Data fusion options

with the strengths of other imaging or localization methods for interventional applications. In this presentation we will discuss possible co-registration arrangements and their potential applications to breast cancer which are abstracted in the following sections.

2. Applications to Breast MRI—Prone MRI

In the case of breast MRI, high quality imaging is performed with the patient in the prone position with her breasts pendant into appropriate breast coils. This configuration allows good RF loading of the coils with breast tissue and serves to minimize motion due to patient respiration as the patient is lying on her sternum and chest wall so that respiration motion takes place posterior of the breast tissue of interest. In order to achieve registration with other imaging applications, we have developed a special purpose patient transport system which incorporates breast coils mounted in moveable plates that provide gentle medial-lateral compression. This serves to immobilize the breast into an approximately rectangular format in the axial plane to minimize the amount of data (slices) needed to cover the breast. This system has been successfully used for breast biopsy[4] for a number of years in our ongoing screening of high risk patients.

However, this same system was designed to provide a large open space below and around the breasts so that other imaging procedures could be performed. It permits US imaging by tracking a set of optical fiducial markers mounted on specialized frames which were used to hold the MRI receiver coils in contact with the breast[5]. These fiducial markers were visible in the DCE-MRI data. Subsequent US imaging was performed by removing the MRI receiver coils and the US probe was coupled to the breast though a thin plastic membrane which served to maintain the breast shape in the same configuration as during the MRI examination. An example of this technique is shown in Figure 2, where a DCE-MRI exam (Fig. 2a) shows an enhancing lesion. During the subsequent US examination, the US image of this lesion (Fig. 2b) is co-registered with the pre-contrast MRI (Fig. 2c) so that the MRI is simultaneously presented to the examiner with same slice orientation as the actual US. The parenchymal patterns surround the MRI lesions are clearly seen and recognized in the US imaging, with the fat-fibroglandular contrast reversed. The dynamic correlation between the real-time US and the previous MRI was performed with a prototype co-registration package running under Aegis[6]. This approach is being studied as an approach for second-look ultrasound to improve the overall diagnostic accuracy of the MRI procedure.

3. Supine MRI

Another interesting example of this kind of co-registration is to provide a means for a surgeon to resolve the extent of disease as seen in DCE-MRI while in the operating room. This would form the basis for a surgical planning tool in which contrast enhanced MRI data would be presented to the radiologist co-registered to the patient herself. Again, appropriate fiducials and tracking methods would permit the alignment of the MRI data to the patient's breast position. However, in this case, prone MRI would not be appropriate as the breast configuration would be dramatically different than that seen in the OR setting. Rather, we would prefer to use breast MRI obtained in the supine position with the patient's arm associated with the involved breast abducted at 90° to the superior–inferior axis. Normal breast imaging is not performed in this way as the opportunity for optimal breast coils would be sacrificed. Furthermore, respiration and the associated motion artefacts could be problematic. While breath-hold procedures could be envisioned, it would require multiple repetitions during the course of a long (~10 min) contrast enhanced examination procedure which could be challenging for anxious breast cancer patients.

To address these issues, we have developed a specialized breast coil which is designed for breast MRI. It is a four coil array which is mounted on a surface which allows a degree of

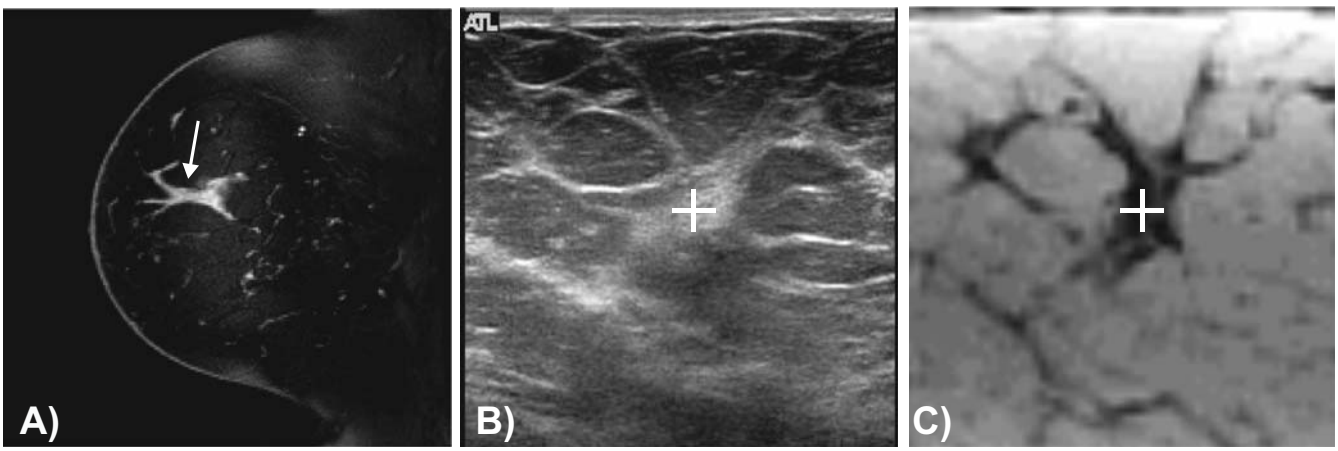

Figure 2. DCE-breast MRI (a) showing an enhancing lesion (arrow). Using optical co-registration, the subsequent ultrasound imaging of the same lesion (b) is aligned with the MRI without fat suppression (c).

independent positioning of each coil and the overall coil array[7]. This permits the coil shape and position to be altered to be close to the breast to maximize image SNR. The goal is to shape the coil to match the supine breast outline while not touching the breast to allow it to rest in its native supine configuration found immediately prior to breast surgery. An illustration of a prototype supine breast array is shown in Figure 3. In order to compensate for respiration artefacts, we have implemented a version of ZMART[8] which dynamically adjusts the k-space phase encoding in response to patient respiration as monitored by a respiration belt[9]. A typical volunteer non-contrast supine breast MR image with motion compensation acquired with the specialized coil array is shown in Figure 4. It was achieved with essentially no increase in scan time to provide motion compensation compared to the standard acquisition time.

In order to link this image data to the OR setting, this procedure will require placement of MRI visible fiducial markers distributed over the surface of the breast which can then be assessed subsequently via optical tracking. In a limited study, we have shown that the errors associated with repositioning of the breast can result in positional errors of approximately 3–5 mm depending on the location throughout the breast[10]. We are currently exploring methods to compensate for this error based on non-linear spatial transformations. Ideally, one should image the patient with her arm abducted at 90° to match the typical patient position during breast surgery. However, as most medical facilities have no open MR system available, we are exploring the effect of imaging without abduction and using non-linear spatial transformations for correction. Taken together, we hope to apply this method as a means for pre-surgical planning to define the extent of disease as an alternative for the current assessment of the surgical field which is frequently based on mammography.

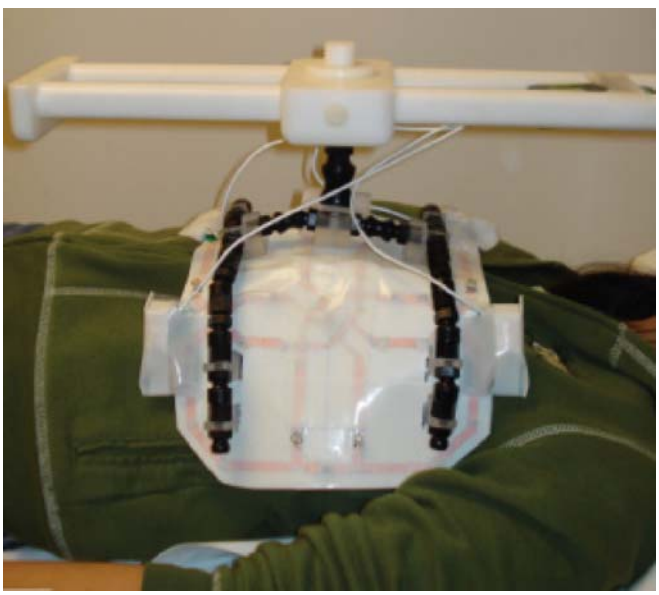

Figure 3. A prototype supine breast coil array suspended immediately above a volunteer's breast. Gimbaled joints allow control over coil orientation and shape.

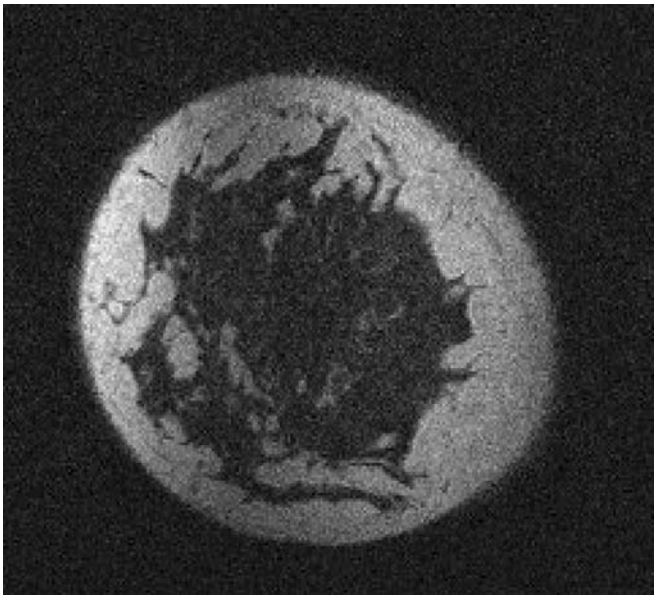

Figure 4. Non contrast breast MRI taken in the supine position with prototype breast coil array and motion compensation.

4. Prone to Supine Breast MRI

The use of a supine breast coil array can generate MR images which closely match the body position anticipated during a breast surgery. However, for other applications such as breast biopsy in the supine position, the use of *a-priori* MRI information to target a lesion would not likely be of sufficient accuracy for a confident biopsy procedure. Rather, including a co-registered ultrasound would be preferable to guide a free-hand biopsy procedure. We have been exploring the use of alternative MRI procedures based on alternative reference frames which will serve to jointly conform the breast into a shape consistent to the needs for high quality prone breast MRI, followed by subsequent ultrasound imaging in the supine position while ensuring a good correlation between the two imaging settings with dynamic lesion co-registration. Such an approach requires a unique coil shape which preserves the breast configuration between the acquisition of MRI data and subsequent US imaging. While at an early stage, we will review our experience with this configuration in phantoms and volunteer data.

5. Conclusion

Co-registration of breast MRI data can serve to augment the power of DCE-MRI into alternate applications and approaches for breast biopsy, surgical planning and perhaps surgical intervention. In each case, a global reference frame is needed to align and associate patient specific markers between the various imaging settings. If successful, this approach offers the option of reducing the number of MRI guided breast biopsy which permits the biopsy procedure to be performed by ultrasound which is a more familiar approach for most breast radiologists. An additional advantage would be to reduce pressure on MRI access by reducing the amount of time used for interventional applications, freeing time for breast MRI applications and potentially reducing the cost of an MRI initiated breast biopsy procedure. In application to surgery, the use of supine MRI could

serve as a tool for surgical planning. In this case, surface mapping and co-registration of the breast outline would likely be needed to ensure accurate breast tissue configuration arising from differences in patient position between MRI and the OR settings. Finally, these same methods which can be applied to breast imaging could be applied to other body MRI applications, such as co-registering MRI and microbubble enhanced liver ultrasound to improve lesion characterization.

References

1. Townsend DW, Beyer T. A combined PET/CT scanner: the path to true image fusion, Br. J. Radiol 2002;75:Spec No:S24–30.
2. Bolus NC, George R., Washington J, Newcomer BR. PET-MRI: The blended-modality choice of the future? J. Nucl. Med. Technol. 2009;7(2):63–71.
3. Piron CA, Causer P, Jong R, Shumak R, Plewes DB. IEEE Trans Med Imaging. 2003 Sep;22(9):1100–10.
4. Causer PA, Piron CA, Jong RA, Plewes DB. MR imaging-guided breast localization system with medial or lateral access. Radiology 2006;240:369–379.
5. Causer PA, Piron CA, Jong RA, Plewes DB. Preliminary in-vivo validation of a dedicated breast MRI and sonographic coregistration imaging system. Am J Roentgenol 2008;191:1203–1207.
6. Aegis is an open-source image display and registration software package distributed by Sentinelle Medical Inc, 555 Richmond Street, Toronto, Ontario, Canada.
7. Siegler P, Thevathsan G, Piron C, Marshall H, Devine P, Plewes DB. Flexible Four Element Phased Array Coil for Supine Breast MRI, 17th Scientific Meeting and Exhibition of the Society of Magnetic Resonance in Medicine, Hawaii, USA, 2009.
8. Huber ME, Hengesback D, Botnar FM, Kissinger KV, Boesigner P, Manning WJ, Stuber M. Motion artifact reduction and vessel enhancement for free-breathing navigator-gated coronary MRA Using 3D k-space reordering. Magn Reson Med 2001;45(4):645–652.
9. Siegler P, Holloway C, Causer P, Plewes DB. Modified ZMART for Supine Breast MRI, The 16th Scientific Meeting and Exhibition of the International Society of Magnetic Resonance in Medicine, Toronto, Ontario, Canada, 2008.
10. Siegler P, Holloway D, Causer P, Plewes DB. Positional Variations of the Breast in Supine Position between Two MR Scans, 15th Annual Meeting of the Internationals Society of Magnetic Resonance in Medicine, Berlin, Germany 2007.

Multimodality Breast Imaging Evaluation of Architectural Distortion with Emphasis on Utilization of Breast MRI and Pathological Correlation

Shaheen MD, Khosa MD, Stoddart MD, Rosen MD MPH, Slanetz MD MPH
Correspondence author:
Chief of Radiology & Director of Women's Imaging, Harrington Memorial Hospital, Instructor in Radiology-Harvard Medical School, e-mail: rshaheen@bidmc.harvard.edu

Purpose

To describe imaging appearances of architectural distortion (AD) on multiple modalities and to evaluate the role of breast MRI in the management of AD with pathological correlation.

Content or Organization

AD is the third most common appearance of breast cancer. AD can be primary or secondary. Primary AD is a rare finding that may represent breast cancer, DCIS, radial scar, complex sclerosing lesion, and fat necrosis. Secondary AD can be expected following breast biopsy, lumpectomy, breast reduction surgery, trauma, and infections. AD is a subtle finding on screening mammograms even in the era of digital mammography and CAD analysis. Once AD is questioned on mammography, it is often better characterized using multimodality imaging including ultrasound and MRI. Retrospective review of 16 breast MRIs performed for suspected AD on mammography have confirmed the presence of AD in 8/16 (50%). Seven of16 (44%) warranted intervention, of which Five of 16 (31%) underwent core or surgical biopsy and two patients (12%) were lost to follow up. One of eight (12%) had invasive ductal carcinoma and management changed from lumpectomy to mastectomy as AD was more extensive on MRI. Four of eight (50%) with suspicious AD on mammography and MRI had radial scars or complex sclerosing lesions (CSL) on surgical pathology. One of eight (12%) with history of breast trauma and prior pathology proven fat necrosis on core biopsy, had non-suspicious AD appearance on MRI and follow up imaging was recommended.

Conclusion

Familiarity with the spectrum of multimodality imaging appearances of AD and underlying pathology can impact management of this vague yet significant finding. Although MRI is sensitive in detection of AD and extent of disease, its ability to differentiate cancer from other benign diseases remains low, and therefore, MR does not obviate the need for tissue diagnosis. Radial scars and CSL can be highly suspicious on MRI warranting intervention.

Evaluation of 3D parametric analysis of MR-mammography for follow-up assessment of malignant lesions under primary systemic therapy

Umutlu L[1], Maderwald S[1], Heusner T[1], Kümmel S[2], Hauth EA[1], Forsting M[1], Lauenstein TC[1]
[1]University Hospital Essen, Department of Diagnostic and Interventional Radiology and Neuroradiology, Essen
[2] Department of Gynaecology and Obstetrics, University Hospital Essen;

Purpose

To evaluate a three-dimensional (3D) parametric analysis in dynamic MR mammography for (a) volume determination and analysis of (b) contrast kinetic and (c) pharmacokinetic changes of malignant lesions under neoadjuvant chemotherapy.

Material and Methods

85 patients with histopathologically proven breast cancer were studied. Breast MR examinations were performed in all subjects on a 1.5 T scanner (Magnetom Espree, Siemens Medical Solutions) (a) before and (b) on average 12 weeks after initiation of systemic chemotherapy. Dynamic T1w GRE sequences were collected at six different time points after intravenous contrast injection (Gadobutrol, 0.1 mmol/kg body weight). The contrast kinetics of all malignant lesions were analysed quantitatively on a pixel by pixel basis using a computer-aided detection system (iCAD). The signal enhancement pattern was coded by three color intensities and three color

hues. Pharmacokinetic changes were analysed based on the Tofts model including vascular permeability and extracellular volume fraction.

Results
In comparison to the baseline MR mammography, follow-up mammographies showed a significant tumor size reduction of 57% on average. The change of color hues and color intensities demonstrated a significant shift from malignant fast wash-out kinetics to progressive fibrotization and a decline of the inhomogeneous tumor configuration. The assessment of the pharmacokinetic changes under therapy revealed a statistically significant decrease of the vascular permeability ($p<0.05$). However, extracellular volume fraction changes revealed only a slight decrease under chemotherapy (mean decline of 21%).

Conclusion
The parametric analysis provides a reliable evaluation of tumor size, contrast kinetics, vascular permeability and extracellular volume fraction within less than 10 min. This analysis for treatment follow-up of malignant breast lesions enables the reader to easily evaluate early treatment response, in terms of tumor size reduction and change of kinetic behaviour.

Dynamic contrast enhanced breast MRI at 7T: a feasibility trial

Umutlu L[1,2], Maderwald S[1,2], Kraff O[1,2], Theysohn J[1,2], Kuemmel S[3], Hauth EA[1,2], Forsting M[1,2], Ladd ME[1,2], Quick HH[1,2], Lauenstein TC[1,2]
[1]Department of Diagnostic and Interventional Radiology and Neuroradiology, University Hospital Essen, Germany
[2]Erwin L. Hahn Institute for Magnetic Resonance Imaging, University Duisburg-Essen, Germany
[3]Department of Gynaecology and Obstetrics, University Hospital Essen; Germany;

Introduction
The aim of this study was to establish a specific breast examination protocol for a 7 T whole-body MRI system and assess the feasibility of dynamic contrast-enhanced (DCE) ultra high field breast imaging.

Material and Methods
A total of 15 subjects were examined on a 7 T whole-body MRI system (Magnetom 7 T, Siemens, Erlangen) using a unilateral linearly polarized single-loop coil (Rapid Biomedical, Würzburg, Germany). The study population included eight healthy subjects, two subjects with distinct cases of fibrocystic tissue changes and five patients with histopathologically proven breast cancer. Subjects were placed in prone position on a biopsy support system, with the coil placed directly below the region of interest. After sequence modification the examination protocol included the following sequences: (1) T2-weighted TSE sequence; (2) 6 dynamic T1-weighted spoiled gradient-echo sequences; (3) subtraction imaging. B1-Maps of a phantom and healthy volunteers were obtained.

Results
Contrast-enhanced T1-weighted imaging at 7T could be obtained at high spatial resolution with short acquisition times, providing high image accuracy and a conclusively good delineation of small anatomical and pathological structures. T2-weighted imaging could be obtained with high spatial resolution at adequate acquisition times. Due to coil limitations, four high field MR examinations showed decreased diagnostic value. Known inhomogeneities of the radiofrequency field could be verified by the obtained B1-Maps.

Conclusions
This first scientific approach of DCE breast MRI at 7 T demonstrates the feasibility and complexity of ultra high field breast MR imaging. The implementation of further advanced bilateral coil concepts could enable dedicated B1 shimming techniques and parallel imaging to ameliorate current limitations due to the coil and SAR restrictions at ultra high field magnetic strength.

Gadobutrol supported MR-Mammography of healthy volunteers. Pilot Study results from the population-based study.

Ungerer, S. [1], Hegenscheid, K. [1], Langner, S. [1], Ohlinger. R. [2], Hosten, N. [1], Puls, R. [1]
[1]Institute for Diagnostic Radiology and Neuroradiology, Ferdinand-Sauerbruch-Str. 1, 17487 Greifswald, Tel. +49 (0) 3834/867057
[2]Clinic of Gynaecology and Obstetrics, Wollweberstraße 1, 17457 Greifswald, Tel. +49 (0) 3834/866500

Purpose
Approximately 2,000 female volunteers will undergo a Gadobutrol supported MR-Mammography, included in a whole-body MRI protocol, within the next three years in the population-based Study of Health in Pomerania (SHIP). We present a pilot study conducted to determine the feasibility of breast MRI in a whole-body MR imagining (WB-MRI) protocol of a large-scale population based study. Further we will proof breast MRI-imaging as a screening method.

Material and Methods
Each participant gives his oral and written informed consent before examination. Because of time limitation of the examination protocol, only axial sequences are made. The protocol consists an axial T2-weighted fat saturated sequence (axial T2 TIRM, 34 slices, slice-thickness 4 mm, TR 5,800 ms, TE 56 ms, TI 170 ms), an axial T2-weighted-TSE sequence (36 slices, slice thickness 4 mm, TR 4,660 ms, TE 67 ms), a fat-saturated SE breast diffusion in axial planes (34 slices, slice-thickness 4 mm, TR 7,900 ms, TE 91 ms) and an axial T1-weighted 3D-FLASH dynamic sequence (128 slices, slice-thickness 1.5 mm, TR 8.86 ms, TE 4.51 ms) including the first plain measurement, five measurements after given an intravenous bolus of Gadobutrol (0.1 ml/kg/BW), with five automatically generated subtractions and additionally two maximal intensity projections.

Results
35 breast-scans were successfully completed in a mean scan time of 140 min for WB-MRI. Standard parameters of healthy breast tissue were calculated. Further on we had collated altogether seven results, two of them fibroadenoma, one lymph node in the breast tissue, one cyst, two obscure findings and one result, which had been high grade suspected of carcinoma. Though all three results had turned out as benign and finally could be classified as false-positive findings.

Conclusion
The preliminary results indicate that MR-Mammography in a large prospective, population-based study within the frame of a whole-body-protocol is feasible and references of normal beast tissue can be generated. A variety of positive findings provide valuable information on disease prevalence in this population. Further studies will show, if MR-Mammography is suitable for a screening method.